Characterisation of the earliest thalamocortical interaction *in vivo* and *in vitro*

Sara Bandiera

Balliol College

Department of Physiology Anatomy and Genetics

University of Oxford

Supervisor: Prof. Zoltán Molnár
Second Supervisor: Prof. William James

A thesis submitted for the degree of Doctor of Philosophy
Trinity Term 2023

Alla mia Elisabetta

Acknowledgements

I extend my deepest gratitude to my supervisor, Professor Zoltán Molnár, for his unwavering support, guidance, and inspiration throughout my research journey. His genuine passion for science, enthusiasm, and curiosity were contagious, fostering the best possible environment in which to begin my academic path. He believed in me even when I doubted myself, allowing me the freedom to explore, make mistakes, and learn through the process without judgment. His trust, encouragement, and ability to uplift me have shaped not only this dissertation but also the way I approach science more broadly. He will always remain a model for the kind of scientist and mentor I aspire to become.

I am equally grateful to my co-supervisor, Professor William James, and to the members of my thesis committee, Professor Nobuhiko Yamamoto and Professor Colin Akerman, for their constructive feedback and valuable suggestions, which greatly improved the quality of this work.

I would also like to acknowledge my peers for their camaraderie and the stimulating discussions that inspired me throughout my academic journey. Special thanks to Elise, who became a close friend from our very first day of the DPhil program and quickly proved to be the perfect companion for spontaneous and vaguely planned trips. To Florina, whose sharp mind and humble attitude taught me that brilliance and modesty can coexist effortlessly. And to Auguste, who first welcomed me into the lab and provided much-needed distractions beyond it—thank you for making the long days lighter and more enjoyable.

My sincere thanks to all my collaborators, both within and outside the UK. To Dr. Gavin Clowry and Dr. Faye McLeod, for guiding me virtually from my first year and later welcoming me in person to their lab (and home). Your constant support was fundamental in shaping this project. To Professor Chiaki Maruyama and her team, thank you for the insightful discussions over the years and for your enthusiasm in collaborating with me on this study and beyond.

A very special thanks goes to Professor Eri Kawashita. Working side by side with you in Oxford was, without doubt, the best time I spent in the lab during my DPhil. Your energy and positivity made every day a pleasure, and I am deeply grateful that our time as colleagues grew into a true friendship. I look forward to meeting you again in Japan.

My heartfelt gratitude also goes to my family. To my mum, the person who believed in me more than anyone else, from my very first day of school to my very last day of the DPhil. You taught me to be ambitious and to never let anyone stand in the way of my dreams, even when they seemed impossibly far away. Your love has shown itself in the most selfless way: by encouraging me to leave home and follow those dreams, even though I know how much you missed me. Thank you for your endless patience, for always waiting for me to come back, and for treasuring every small moment we have together. To my little *sorellina*, Carla, for keeping me sane throughout these years. Hearing my work described through your wonderfully unscientific translations always made this journey feel lighter and more grounded and helped me immensely whenever things grew heavy or obstacles arose. I sometimes wonder if your unconventional and inventive way of helping me prepare for my Developmental Neurobiology exam was what first sparked my passion for the topic I ended up studying throughout my DPhil. To my dad and Bea, for always knowing when I needed a break, and for giving me those moments of calm and laughter that helped me recharge and dive back in.

To my friends in the UK, who have been my constant anchors beyond the lab. To Alice, for being my unwavering mentor since the very first day I was your master's student. Even from overseas, you never stopped guiding and supporting me throughout my PhD—thank you for always being there, no matter the distance. To Giulia, who began her own journey alongside mine—you've been my reference point for laughter, a spare bed, and spontaneous tapas nights. Thank you for making everything more enjoyable, from PhD applications to moving and through the most demanding phases of this research. To Andrea, my acquired brother, who still refuses to listen to anything related to my work yet has never failed to show up when it truly mattered. We've been buddies since our undergraduate days in Italy and have never missed each other since. Thank you for celebrating my

achievements and comforting me during the rougher stretches of this path. To Chiara, for being a steady reference point since we met during our Master's. Thank you for choosing to move to the same side of the Channel as me, and for all our scientific and non-scientific chats over walks, coffees, and pints. Your resilience and professionalism are a true inspiration. And to Nick, who lifted my days in Oxford and taught me how to stay mentally strong when circumstances turned against me. Thank you for honking around with me and for being my home and family over these years.

To my friends back home in Italy, for believing I deserve a Nobel Prize every time I run a Western blot. Your enthusiasm for what I do, though so far from your own realities, means everything to me. Your friendship and support, from the days of primary school to high school and beyond, are something I will never take for granted.

I am also grateful for the many people I had the pleasure of meeting, inside and outside academia, during my DPhil years. Those spontaneous discussions and encounters enriched both my science and my life.

This thesis is dedicated to Elisabetta Caon, my "Betta", one of the brightest minds and kindest souls I have ever encountered in academia. You left us too soon, yet your light continues to shine within me. I will forever remember how to face every challenge in this career with a smile, just as only you could.

Abstract

My thesis investigates the cell types and the specific molecular mechanisms involved in the earliest interaction between thalamic axons and the developing cerebral cortex in the human fetal brain. Early thalamic afferents (TCA) provide a major source of extrinsic influence on the intrinsic programmes of cortical neurogenesis. To investigate the early cortical target(s) reached by TCA during human brain development, these events at their earliest stages, I first traced the early thalamic axons projecting toward the cortex by immunohistochemistry and with carbocyanine dyes in human *post-mortem* fetal brains. I showed that these axons exhibited a close anatomical relationship with the existing germinal compartments already at 13 post-conception week (PCW). By 17 PCW, TCA did not only reach the transient subplate, a well-known target for thalamic axons in the mammalian brain, but also projected towards the outer subventricular zone (OSVZ), the most expanded germinal compartment of the human cortex at this age, a phenomenon never observed in previous studies in rodents.

I identified VGF, a neurosecretory protein, as a promising molecule that might produced in the thalamus and secreted in the immature cortex upon regulated release. VGF has the potential to influence both post-mitotic subplate neurons and proliferating OSVZ progenitors through various neuroactive peptides resulting from its proteolytic processing. Initially, I evaluated VGF gene expression and protein distribution in the thalamus and key cortical areas of the human prenatal brain using various experimental methods. I confirmed that VGF is specifically expressed by mature excitatory neurons of the thalamus that project to the cortex in a region- and cell-restricted manner. Moreover, I demonstrated VGF protein presence not only in the thalamus, but also in the neocortex, suggesting transport to cortical areas by TCA. My data also suggests that VGF expression is not restricted to sensorial thalamic nuclei, as observed in the developing mouse brain, but is highly expressed by the

associative mediodorsal nucleus (MD) and consistently transported to the prefrontal cortex in human. This supports the hypothesis of an evolutionary repurposing of this conserved neurotrophin in the human developing brain.

Finally, I started investigating the consequences of VGF release by thalamic axons in the immature cortex. I showed that VGF application significantly increases the spontaneous activity of subplate neurons in organotypic slices obtained from a 13 PCW human frontal cortex. Conversely, full-size VGF did not alter mitotic rates of cortical progenitors in 2D induced human cortical cell cultures. As several effects attributed to VGF are mediated by its neuroactive peptides, I then investigated the potential proteases involved in VGF cleavage and their expression profiles in the developing human brain.

Collectively, my findings suggest a distinctive influence of thalamic axons on human cortical development, where they interact with unique target compartments of the developing cortex, such as the outer subventricular zone (OSVZ). This interaction could be partly mediated through paracrine mechanisms by secretion of VGF, along with its neuroactive peptides.

Statement of Authorship

I contributed to the design, performance, and analysis of the experiments for all results included in this thesis, unless otherwise stated. The exceptions and collaborations are listed below. My supervisor, Professor Zoltán Molnár, provided guidance and approved the experimental designs. He also assisted in the performance and analysis of the experiments.

During my research, Professor Eri Kawashita from the Department of Pathological Biochemistry, Kyoto Pharmaceutical University (Japan), visited the Laboratory of Professor Molnár. We collaborated on the design, performance, and analysis of the molecular experiments (qPCR and Western Blot) described in Chapters 4 and 5.

For the initial processing of human brain tissue, Professor Zoltán Molnár performed the sectioning into coronal slabs according to anatomical references, and the microdissection of brain regions from fresh-frozen tissue for RNA and protein extraction. I assisted Professor Molnár in this process. Additionally, Professor Molnár performed the placement of DiI crystals for axon tracing (Chapter 3) with my assistance.

I collaborated and received training from Doctor Becky Carlyle from the University of Oxford, Department of Physiology Anatomy and Genetics, for the proteomic analysis of human fetal neocortex described in Chapters 5 and 6. Laura Pearson, a visiting undergraduate student from the University of Manchester under Dr. Carlyle's supervision, was responsible for the maintenance, treatment, and image acquisition of iPSC-derived cortical cell cultures used in Chapter 6. The results are presented in Figure 6.2.

As part of a collaboration supported by the MRC, I visited the laboratory of Doctors Gavin Clowry and Faye McLeod at Biosciences Institute, Neuroscience, Neurodisability and Neurological Disorders, Newcastle University. I performed all the experiments with human organotypic cortical slices *in vitro* described in Chapter 6. Doctor McLeod was primarily responsible for tissue collection, processing, and culture maintenance *in vitro*. She provided extensive training and assistance with the experimental procedures, including performing calcium imaging. Colleagues in Doctor McLeod's

laboratory, who were experts in the technique and subsequent analysis, aided in the data analysis. The results are presented in Figures 6.3-6.6.

For advice on bioinformatic analysis of single-cell transcriptomics, I consulted with Doctor Kostantin Khodosevich from the Biotech Research & Innovation Centre (BRIC), University of Copenhagen.

All other experiments, including their design, performance, and analysis, were conducted solely by me with generous guidance from members of the Molnár laboratory and the wider scientific community.

All the human samples used in this work were generously collected and provided by the Human Developmental Biology Resource (HDBR) under approved project 200538 titled 'Early Thalamocortical Interactions.' The samples were transported to the laboratory in Oxford from the two HDBR centres in Newcastle (Newcastle University) and London (UCL) under the Material Transfer Agreement (MTA) entered with the two institutions. The personnel of the tissue bank conducted the initial screening of the samples to ensure they met the eligibility criteria for my project. Only necessary information, such as age and the absence of major neuropathologies that could impact the results and their interpretation, was disclosed regarding the identity of the samples.

Preliminary results from the axon tracing analysis (Chapter 3) have been discussed in a chapter of "The Cerebral Cortex and Thalamus," edited by Martin Usrey and Murray Sherman and published by Oxford University Press.

List of Abbreviations

3rd V = third ventricle

A

A / Ant = anterior

AChE= Acetylcholinesterase

AD = Alzheimer's Disease

Amy = amygdala

ANs = anterior nuclei (thalamus)

ASD = Autism Spectrum Disorders

B

BD = bipolar disorder

BDNF = brain derived neurotrophic factor

bRGC = basal radial glial cell

C

Ca = Caudate nucleus

Calb2 = calbindin 2

CalR = calretinin

CAPN = calpain

CBC= cerebellar cortex

CC= cortico-cortical or corpus callosum (according to context)

CGE = caudal ganglionic eminence

ChPl = Choroid Plexus

Cing = Cingulate

cKO= conditional knockout

Cl = Claustrum

CM = centromedial nucleus (thalamus)

CP= cortical plate

CRC = Cajal Retzius cell

CS = carniage stage

CT / CTA = corticothalamic (axons)

CTS= cathepsin

Cx = cerebral cortex

D

D = dorsal

DEG = differentially expressed gene

Die = diencephalon

DiI = 1,1′-dioctadecyl-3,3,3′,3′-tetramethylindocarbocyanine perchlorate

DIV = days *in vitro*

dLGN = dorsolateral geniculate nucleus

dlPFC = dorsolateral prefrontal cortex

DTB = diencephalic-telencephalic boundary

DTH/dTH = dorsal thalamus

E

E(11)= embryonic day

ECM= extracellular matrix

ELISA = enzyme-linked immunosorbent assay

ER = endoplasmic reticulum

F

FFPE = formalin-fixed paraffin-embedded

FPKM= fragments per kilobase of transcript per million

G

GADPH= glyceraldehyde-3-phosphate dehydrogenase

GAP43= Growth Associated Protein 43

GBX2= gastrulation brain homeobox 2

GE = ganglionic eminence

GFAP= glial fibrillary acidic protein

GO= gene ontology

H

HOPX= HOP homeobox

HP= hippocampus

Hypo= hypothalamus

I

IC= internal capsule

IF= immunofluorescence

IFL= inner fiber layer

IHC= immunohistochemistry

Ins= insula

IPC= intermediate precursor cell

iPSC= induced pluripotent stem cell

ISVZ= inner subventricular zone

IZ= intermediate zone

K

KO= knockout

kDa= kiloDalton

L

L / Lat = lateral

L(4) = layer 4

L1CAM= L1 Cell Adhesion Molecule

LC-MS/MS= liquid chromatography tandem mass spectrometry

LD= lateral dorsal nucleus (thalamus)

LDVC= large dense core vesicle

LGE= lateral ganglionic eminence

LMD= laser microdisected

LP= lateral posterior nucleus (thalamus)

LV= lateral ventral nuclei (thalamus)

M

M / Med= medial

M1 / M1C / Mot= motor cortex

MACC= multilaminar axonal-cell compartment

MB= midbrain

MD= mediodorsal nucleus (thalamus)

Mes= mesencephalon

MGE= medial ganglionic eminence

MGN= medial geniculate nucleus (thalamus)

MMP= Matrix Metallopeptidase (or metalloprotease)

mRNA= messenger Ribonucleic acid (RNA)

MS= Mass Spectrometry

MST= mitotic somal translocation

MZ= marginal zone

N

N1CAM= neuronal cell adhesion molecule 1

NCX= neocortex

NEC= neural epithelial cell

NGF= nerve growth factor

NGN1= neurogenin 1

NMDAR=N-methyl-D-aspartate receptor

NPC= neural progenitor (precursor) cell

NT3= neurotrophin 3

NTNG1=Netrin G1

Nurr1 / NR4A2 = Nuclear Receptor Subfamily 4 Group A Member 2

O

oRGC= outer radial glial cell

OSVZ= outer subventricular zone

P

P(21)= postnatal day

P / post= posterior

Par = parietal

PC / PCA= principal component (analysis)

PC / PCSK= pro-protein convertase (or pro-hormone convertase)

PCW = post conceptional week

PFC= prefrontal cortex

pSP= pre-subplate

PSPB= pallial-subpallial boundary

Pu = Putamen

Q

qPCR = quantitative polymerase chain reaction

R

RGC= radial glial cell

Rhomb= rhombencephalon

ROBO1= Roundabout Guidance Receptor 1

ROR-β / RORC= RAR-related orphan receptor β/C

RPKM= Reads Per Kilobase per Million mapped reads

S

S1 / SS= somatosensory cortex

SATB2= Special AT-rich sequence-binding protein 2

SC= spinal cord

SCGN= Secretagogin

scRNAseq= single cell RNA sequencing

SDS-PAGE= sodium dodecyl sulfate–polyacrylamide gel electrophoresis

SLC17A6= solute carrier family 17 member 6 (VGlut2)

SNAP25= Synaptosome Associated Protein 25

SP= subplate

SPN= subplate neuron

STR= striatum

SVZ= subventricular zone

T

TBP= TATA box-binding protein

TC = thalamocortical

TCA= thalamocortical afferents (axons)

TCF7L2= Transcription factor 7-like 2

Tel= telencephalon

Temp= temporal

tRGC= truncated radial glial cell

TrkB= Tropomyosin receptor kinase B

U

UMAP= uniform manifold approximation and projection

V

V = ventral

V1 / V1C= visual cortex

VB= ventrobasal nucleus (thalamus)

VGlut2= vesicular glutamate transporter 2 (SLC17A6)

VNs= ventral nuclei (thalamus)

VP = ventral posterior nucleus (thalamus)

VPL= ventro-posterior lateral nucleus (thalamus)

VPM= ventro-posterior medial nucleus (thalamus)

vRGC= ventricular radial glial cell

vTH= ventral thalamus

VZ= ventricular zone

W

WB=- Western Blot

Table of Content

Abstract……..……1

Statement of Authorship…….....3

Abbreviations……5

Table of Content…….…… 11

Chapter 1: Introduction…….…..…16

1.1 Cortical development in the human brain…….…….17

1.1.1 Developmental of the cerebral cortex in the human brain……..…17

1.1.2 The evolution of the germinal compartments and the subventricular zone (SVZ)…..... 22

Extrinsic factors shaping the SVZ …… 27

Clinical relevance of the human SVZ…… 29

1.1.3 The subplate zone……...30

The "waiting period" and early transient circuits established within the subplate……..33

Clinical relevance of the subplate……..35

1.1.4 Intrinsic and extrinsic mechanisms shaping cortical development and formation of the cortical maps…….....36

1.2 Development of the thalamocortical system……..…….42

1.2.1 Main events involved in the early development of the thalamocortical connection……..42

1.2.2 Dynamic functional interaction of eearly thalamic axons and the cortex……..….45

1.2.3 Interaction of thalamocortical axons and the cortical subventricular zone in primates.…48

1.2.4 Relevance of early thalamic axons in human cortical evolution and pathologies ……..…51

1.3 VGF as a thalamic modulator of cortical development…….52

1.3.1 VGF: expression, transport, and functional effects……52

VGF-derived peptides……53

VGF receptors and roles in neurophysiology……55

VGF in human neuropathologies…….……..56

1.3.2 VGF expression pattern and role in the thalamocortical system.…….……57

1.3.3 VGF processing enzymes……...61

RATIONALE AND AIMS OF THE STUDY…….……..63

Chapter 2: Material and Methods……65
2.1 Human brain samples……..…..65
2.1.1 Human fetal brain specimens…….……65
2.1.2 Human Tissue Storage…….…..68
2.1.3 Brain tissue sectioning…….…..68
2.2 Histological techniques……..…70
2.2.1 Carbocyanine dye (DiI) axonal tracing…….……70
2.2.2 Immunohistological staining ……70
2.2.2.1 Immunofluorescence staining (IF)……70
2.2.2.2 Immunohistochemistry staining (IHC)…….72
2.2.3 Cresyl Violet (Nissl) staining……74
2.2.4 Imaging…….…….75
2.2.4.1 Epifluorescence Microscopy…….……75
2.2.4.2 Confocal Microscopy……..……..75
2.2.4.3 Neurolucida……..……76
2.2.4.4 Image acquisition and from HDBR Digital Image Hub……..……..76
2.2.5 Anatomical annotation of the brain sections……...……..78
2.2.6 Semi-quantitative analysis of DiI-positive axonal signal (17 PCW cortex)……...…….. 81
2.3 Molecular biology techniques……..……82
2.3.1 RNA extraction…….…….82
2.3.2 Quantitative polymerase chain reaction (qPCR)…….……..84
Reverse Transcription…….……..84
Primer design…….……...84
qPCR ...……..……..84
2.3.3 Protein extraction…….…..87
2.3.3.1 Protein extraction from fresh-frozen brain tissue for Western Blot analysis……87
2.3.3.2 Protein extraction from PFA-fixed brain tissue for Western Blot analysis……...88
2.3.3.3 Protein extraction from fresh-frozen brain tissue for Mass Spectrometry……89
2.3.4 SDS-PAGE and Western Blot Analysis……90
2.3.5 Enzyme-linked immunosorbent assay (ELISA)……....92
2.4 Bioinformatics……...94
2.4.1 Bioinformatic analysis of Brainspan's datasets……..…94
2.4.2 Bioinformatic analysis of single-cell RNA sequencing datasets…….…..96
2.4.3 Bioinformatic prediction of VGF-processing enzymes using Proteasix…….……..99

2.5 *In vitro* techniques……...101

2.5.1 *In vitro* culture of human iPSC-derived cortical neurons……101

2.5.2 *In vitro* culture of human cortical organotypic slices……..103

2.5.3 *In vitro* application of recombinant human VGF……...…….104

CONTENT OF THE THESIS……...……...105

Chapter 3: Tracing of the earliest thalamocortical axons in the human fetal brain

Introduction……...……107

3.1 Time-course analysis of the earliest thalamic innervation of the human fetal cortex by immunohistochemistry (embryonic and early fetal periods)……...…..109

3.2 Carbocyanine dye-tracing of thalamic axons in the human fetal brain……..…...117

3.2.1 7 post-conception week (PCW) (Carniage Stage 21)……...…117

3.2.2 13 post-conception week (PCW)……...…...126

3.2.3 17 post-conception week (PCW)……...…...134

TCA trajectory from the internal capsule to the cortex…….……137
TCA innervate the subplate zone……...……...146
TCA interact with the OSVZ progenitors……..…….……...…150
Semi-quantitative analysis of DiI-labelled axons in the SP and OSVZ……...158

Conclusions……...…160

Discussion……...……162

Chapter 4: Expression of VGF by thalamocortical projecting neurons in the human fetal brain……170

Introduction……..…….…….. 170

4.1 VGF regional expression profiling in the human developing brain shows a high, sustained, and preferential thalamic expression of VGF……...172

4.1.1 VGF is differentially expressed in the human prenatal thalamus vs all brain regions (RNAseq data)……..…172

4.1.2 VGF is highly expressed in the human prenatal thalamus (RNAseq data)…….…...174

4.1.3 VGF is differentially expressed in the human prenatal thalamus vs all neocortical areas (RNAseq data)…….……...176

4.1.4 VGF is differentially expressed in the human prenatal thalamus vs all brain regions and neocortical areas (Exon Array data)…...…….….178

4.2 VGF sub-regional expression profiling in the human developing thalamus and neocortex reveals a different expression pattern than in the rodent developing brain……..…..…181

4.3 VGF single-cell expression profiling in the human thalamus identifies specific expression of VGF by mature excitatory thalamocortical projecting neurons……...187

4.4 Validation of the expression pattern of VGF by qPCR analysis……..……197

Conclusions……..200

Discussion…….201

Chapter 5: Thalamocortical projecting neurons produce and transport VGF protein to the developing human cortex……...……205

Introduction……...…205

5.1 Evaluation of VGF at Western Blot analysis in the human fetal cortex……....207

5.1.1 Distribution of VGF protein across brain regions (thalamus and neocortex)…….….207

Full-length VGF (~ 75 kDa) ……..……..…207

VGF as sum of its proteoforms…….……..……..…209

5.1.2 VGF protein is detected in PFA-fixed human brain tissue (17 PCW)…….….216

5.2 Immunohistochemical evaluation of VGF protein distribution in the human fetal brain 218

10 PCW human brain (medial coronal plane) ……..…..……219

13-17 PCW human frontal cortex (anterior coronal plane) ……..…..……221

16-17 PCW human brain (medial coronal plane) ……224

5.3 VGF detection in the human fetal cortex by Mass Spectrometry analysis……..……..230

5.3.1 Evaluation of the quality and reliability of the proteomic dataset (Gene Ontology Enrichment Analysis) ……..……..……231

5.3.2 Detection of VGF in the proteomic dataset of the human fetal cortex……..235

Conclusions…….……...237

Discussion…….……..238

Chapter 6: VGF functional effects and peptidases prediction……244
Introduction…….…….244
6.1 Functional validation of VGF in *in vitro* models……..……..……..…246
6.1.1 Effects of VGF application in iPSC-derived cortical cells *in vitro* ……248
6.1.2 Effects of VGF application in cortical organotypic slices from human fetal brain….251
6.1.2.1 Preliminary evaluation of the model……..……..…….…251
Immunofluorescence staining……..……..….252
Western Blot Analysis……..……..……..254
ELISA……..……..…..257
6.1.2.2 Effects of exogenous application of VGF in organotypic cortical slices……...259
6.2 Prediction and expression profiling of VGF enzymes ……..……..261
6.2.1 Bioinformatic prediction of VGF proteases by Proteasix……..……..262
6.2.2 Selection of predicted proteases to validate based on proteomic dataset…….....264
6.2.3 Expression profiling of the selected VGF proteases……..……..266
a. LMD microarrays (15-21 PCW) ……..……..……..267
b. Exon-array hbatlas.org (all developmental ages) ……..…….273
c. scRNAseq dataset (USCS Cell Browser) ……..……281
d. qPCR validation (13-20 PCW) ……..…….…..287
e. Western Blot validation (20 PCW) ……..……....293
Conclusions……...296
Discussion……...298

Chapter 7: General discussion and future perspectives of the study……305
7.1 General discussion on the study…….……..…305
General discussion on the main results of the study ……...305
Critical assessment of the results contradicting the working hypothesis of the study…….309
7.2 Future perspectives of the study……..……..…...311
7.3 Other future directions……..……...…314
7.4 Limitations of the study……..……..……315
Conclusive remarks……..……316

References……..……317
Supplementary Material……..…….

CHAPTER 1

Introduction

The mammalian cerebral cortex is responsible for sensory processing, motor control, cognitive abilities, and socio-emotional responses. The development of the neocortex follows stereotypical and conserved histogenic stages, including cell proliferation, production of neurons and glial cells, their differentiation and migration, as well as axon pathfinding and outgrowth and synaptogenesis (**Figure 1.1**). The cerebral cortex is organized according to a basic hexalaminar pattern across all mammalian brains, however, during evolution, this brain region has undergone a remarkable transformation in both size and complexity, culminating in human (**Figure 1.2**). These changes, are thought to underlie the divergence in sensorial specialization and cognitive abilities across species. While in rodent cortical development is completed within weeks after birth, in human the histogenic processes lasts for years, starting in the early first trimester of gestation and continuing until puberty. Over the last decades, researchers started unraveling the mechanisms behind the precise generation of neuronal types, the establishment of connectivity patterns, and the inter-relationship between intrinsic genetic factors and extrinsic environmental influences in shaping the different cortical areas. However, as the majority of the study has been conducted in animal models, our understanding of these event in the development and evolution of the human neocortex remain limited. Deciphering the intricate process of human cortical development would be essential to get an insight into the emergence of our unique cognitive abilities. Furthermore, it would shed lights on the pathophysiology of neurodevelopmental disorders arising from dysregulation of these crucial events, and open new avenues for therapeutic approaches. One of the greatest questions in developmental neuroscience is to understand how the cortex specialises into distinct cortical areas by starting from a relatively homogeneous and uniform structure. Is it due to strict inherent genetic signals? Are these specialisations imposed extrinsically by environmental factors? How is the environmental influence mediated to the developing cortex? How do extrinsic factors interact with intrinsic genetic

programmes in shaping the development of the cerebral cortex? My thesis is going to explore these exciting questions.

1.1 CORTICAL DEVELOPMENT IN THE HUMAN BRAIN

1.1.1 Developmental of the cerebral cortex in the human brain

The central nervous system starts to develop from a monolayer neural sheet, the neural plate, that invaginate to form the neural tube around 3 PCW (Nakatsu *et al.* 2000) (**Figure 1.1**). This structure further compartmentalises, and the rostral end will form the telencephalic vesicles that will give rise to the cerebral cortex. In these regions of the anterior neural tube, along the forming ventricles, lies a uniform layer of neuroepithelial cells adjacent to the lateral ventricles, the ventricular zone (VZ), while the basal membrane covers the surface adjacent to the pial surface. The ventricular zone is the site of neurogenesis. As organogenesis advances, the progenitor cells differentiate into ventricular radial glia (vRG), also known as apical progenitors. The vRG cells extend basal processes that span the entire thickness of the developing cortex, while their apical processes maintain contact with the VZ (Bystron *et al.* 2008; Lui *et al.* 2011). Initially, they primarily undergo symmetric cell divisions, expanding the pool of progenitors. Later during cortical development, vRG cells undergo asymmetric divisions to give rise to intermediate progenitor cells (IPCs) or neurons (Kelley *et al.* 2022). The regulation of the symmetric and asymmetric divisions and the divisions of the IPCs is key to determining the size of the cerebral cortex and the proportions of these divisions show considerable species variation. Differently from rodent RGC which express only classic marker vimentin, human RGC are also positive for glial fibrillary acidic protein (GFAP), and its expression can be detected throughout at least the final two-thirds of gestation (Choi 1986; Zecevic 2004).

As development progresses and progenitor cells accumulate, the **subventricular zone (SVZ)** emerges and continues to expand until mid-gestation, eventually forming the outer SVZ (OSVZ) (**Figures 1.1-1.4**). The OSVZ was first described by Smart and colleagues (Smart *et al.* 2002), and can be distinguished as a distinct layer of the developing human cortex from 12 PCW. This compartment represents a distinctive feature of large mammalian cortices and is composed of

intermediate precursor cells (IPC) and progenitors known as outer radial glia (oRG) or basal radial glia (bRGC) progenitors (Fietz *et al.* 2010; Hansen *et al.* 2010; Cadwell *et al.* 2019) (**Figure 1.4 C-D**). A more detailed description of this transient compartment is provided in the next paragraph.

The first cortical neurons are generated around 4.5 PCW in the human brain (Bystron *et al.* 2008; Lui *et al.* 2011; Marin-Padilla 2014; Kostovic *et al.* 2015). Their organization into a six-layered laminar pattern is established **inside-out migration process**, with deep layer neurogenesis preceding upper layer neurogenesis (Angevine *et al.* 1961; Sidman *et al.* 1973; Rakic 1974; Caviness *et al.* 1978; Marin-Padilla 1995; Nadarajah *et al.* 2003; Bystron *et al.* 2008; Lui *et al.* 2011; Ortega *et al.* 2018; Klingler *et al.* 2019). The formation of different neuronal subtypes in these layers occurs due to the combined expression of specific transcription factors during successive rounds of cell division and migration (Molyneaux *et al.* 2007; Kwan *et al.* 2012). These are instructed at the level of the progenitor cells, which progressively restrict their competence to produce specific subpopulations of neurons during neurogenesis (McConnell *et al.* 1991; Frantz *et al.* 1996; Lukaszewicz *et al.* 2005). Simultaneously to the radial migration of neurons generated within the cortical VZ and SVZ, tangential migration of the interneurons that are generated subcortically also occurs (Letinic *et al.* 2002; Ma *et al.* 2013). As the cortical plate grows, the cortex enlarges, and the process of gyrification begins (Kostovic *et al.* 2010; Andescavage *et al.* 2017).

Three key features of human cortical development are noteworthy: the evolutionary expansion and specialization of the subventricular zone, particularly of its outer portion (OSVZ); the enlargement of the human cortical subplate; and the later overgrowth of the upper cortical layers 2/3 (Kelley *et al.* 2022) (**Figure 1.3**). Interestingly, the first two compartments are the closest cortical layer to the ingrowing TCA, and they reach their maximum expansion in concomitance with the arrival of these axons in substantial numbers during mid-gestation. A detailed introduction is provided for these two specific transient layers, which will be the main target of investigation within the cortex in the Results chapters of this Thesis. The upper cortical layers 2 and 3 on the other hand are crucial for cortico-cortical connections, thus underlying the emergence of higher brain functions in humans (Rakic 2009; Zecevic *et al.* 2011; Malik *et al.* 2013).

Figure 1.1

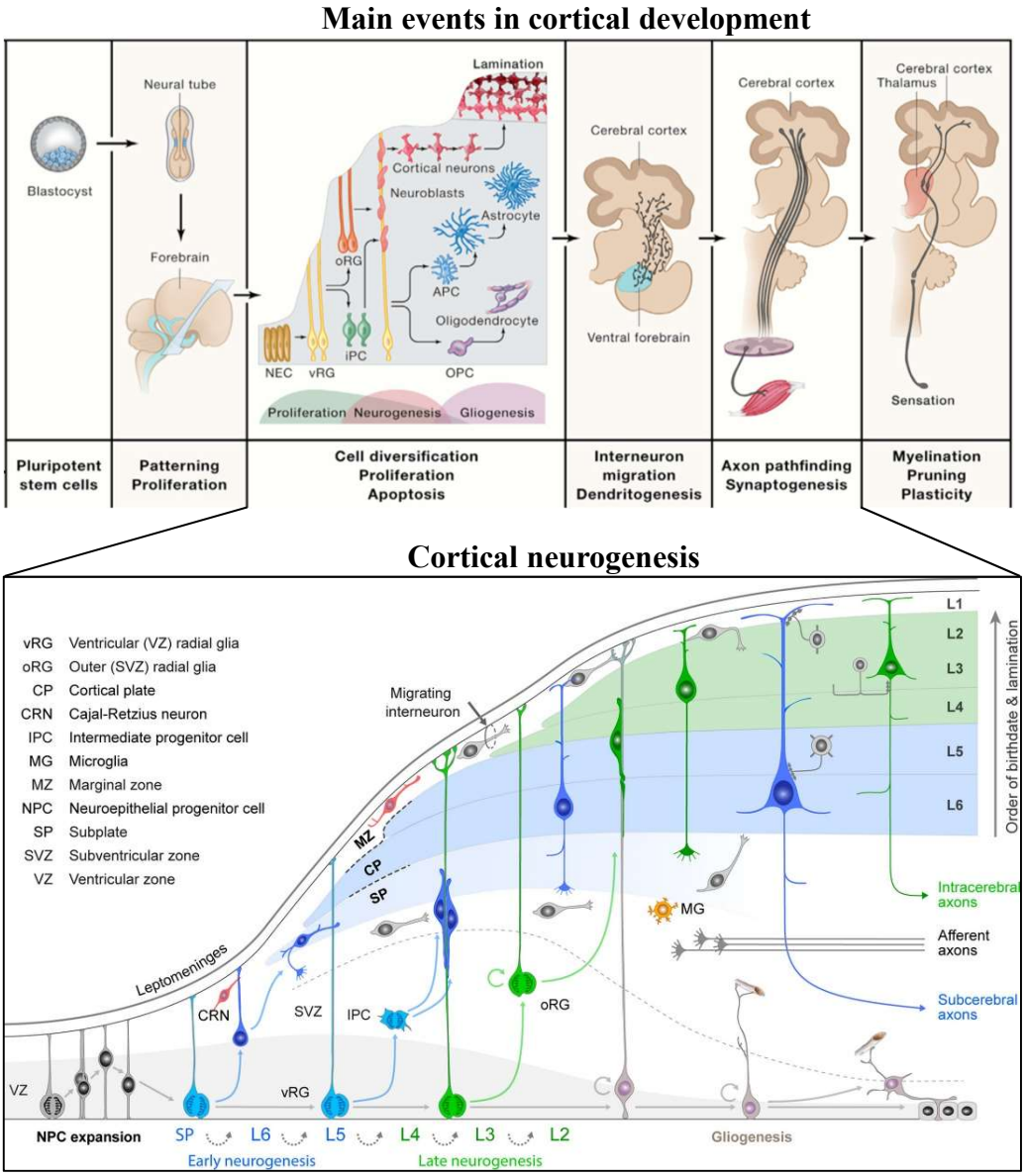

Figure 1.1: Schematic illustration of the major event of human cortical development
The formation of the neural tube starts in human around 3 PCW. After the initial patterning, the generation of the cerebral cortex begins in the rostral part of the forebrain. The major histogenic events at this stage start from a uniform sheet of neural epithelial cells (NEC) cells lining the ventricles that turn into proliferating progenitors. The first progenitors committed to the neural lineage are referred to as ventricular radial glia (vRG) within the ventricular zone (VZ). Later, other progenitors will be produced, the outer RG cells (oRG) and the intermediate precursors cells (IPC), which do not have contact with the ventricular side and reside in the subventricular zone (SVZ). Post-mitotic cortical neurons originates from the germinal compartments and migrate radially toward the pial surface where they give rise to the prospective cortical layers. At the end of neurogenesis, gliogenesis starts to produce oligodendrocytes and astrocytes. Interneurons that are produced in the ventral telencephalon migrate tangentially to populate the developing cortex. At the same time, neurons mature and their processes acquire specialized dendrites. Other major events occurring beyond the production of cortical neurons include the outgrowth of axonal projections, their pathfinding, and the establishment of synaptic connections once they reach their interacting partners. At later stages, axons will be wrapped by myelin sheet, synapses will be pruned, and connections will be further refined.

Adapted from Kelley and Pasca (2021) (top) and from Kwan et al. (2012) (bottom).

Figure 1.2

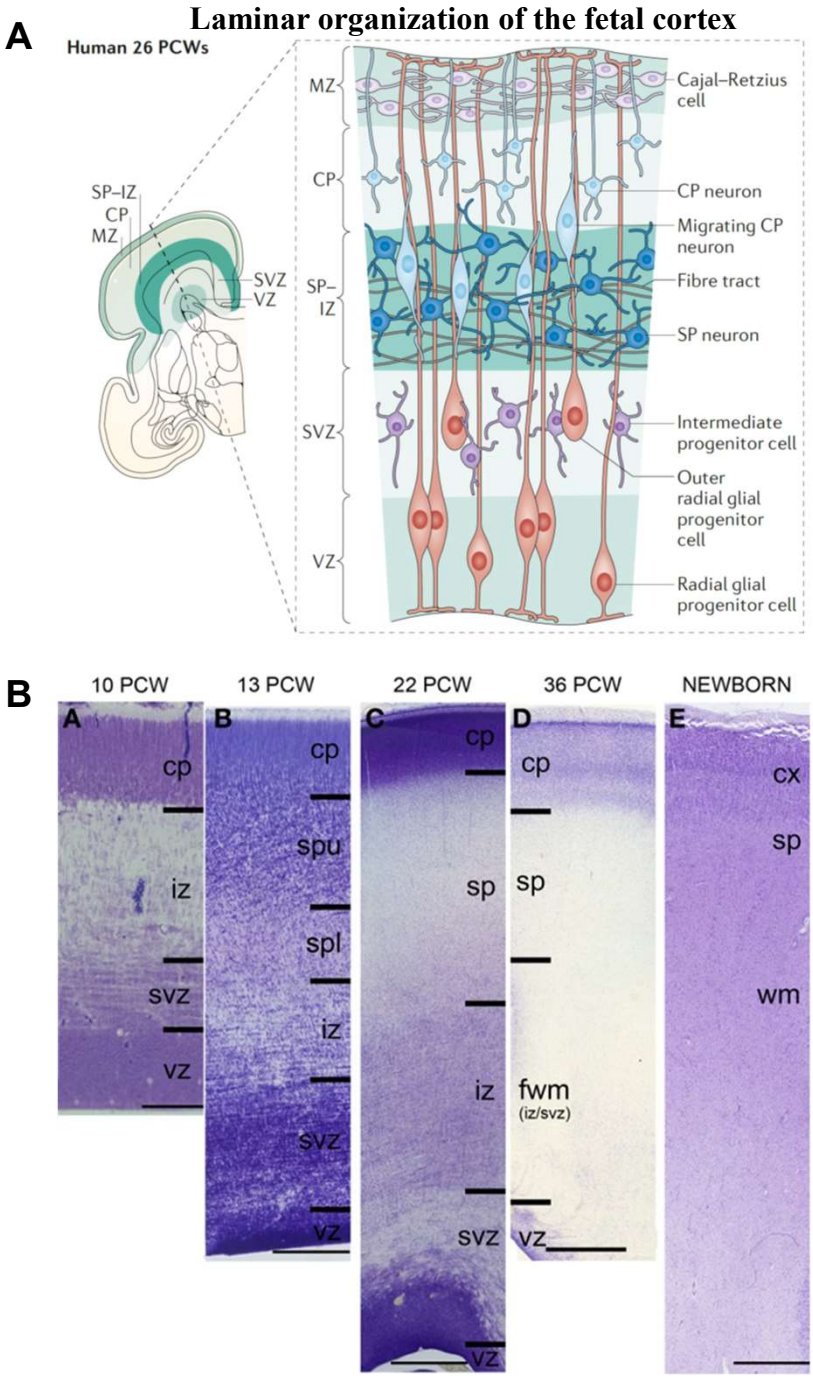

Figure 1.2: Laminar organization of the human developing cortex.
(**A**) Schematic representation of the human cerebral cortex at 26 PCW from a coronal section (left) showing the the layers of the developing cortex and indicating the correspondent cells that populate them. The intermediate zone (IZ) also contain the tangential axons innervating and departing from the cortex and separating the germinal compartments below from the post-mitotic compartments above. (**B**) The laminar organization of the cortex schematized in (A) is revealed by Nissl staining of human fetal telencephalon from 10 PCW to term. The dynamic transformation of the cortical transient layer parallels the process of neurogenesis. Scale bars in (A) = 100 µm (subpanel A), 250 µm (subpanel B), 1 mm (subpanels C–E).
Adapted from Hoerder-Suabedissen and Molnár, 2015 (A) and Judaš et al., 2013 (B).

Figure 1.3

Evolutionary expansion of OSVZ, subplate, and cortical layers 2/3 in human

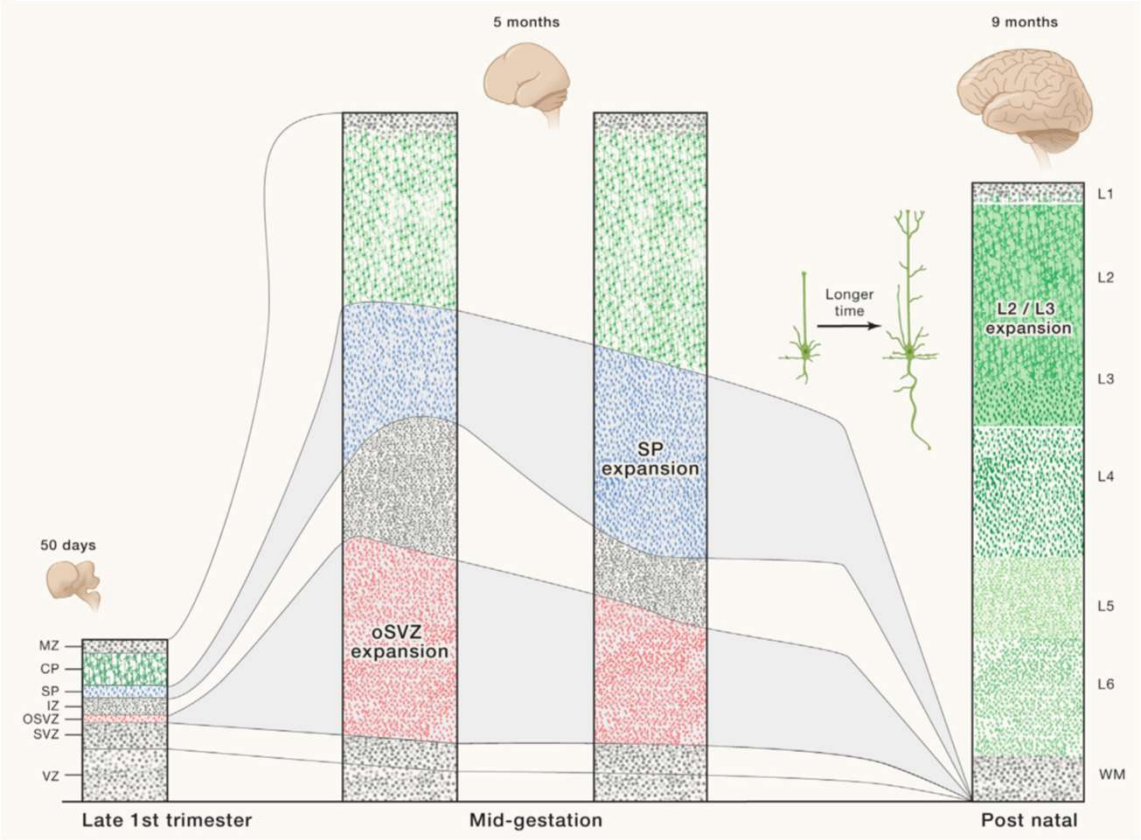

Figure 1.3: Schematic illustration of the unique features emerged during evolution in the human developing cortex.
The human developing cortex shows three major evolutionary features: the enlargement and specialization of the outer subventricular zone (oSVZ) as well as of the subplate (SP), both occurring at mid-gestation in concomitance with the most substantial innervation from the thalamocortical projecting axons (not shown) separating these two enlarged compartment by forming the intermediate zone (IZ). Finally, the human cortex show a peculiar expansion of the upper cortical layers 2 and 3 postnatally. Importantly, the generation of their neurons, also called supragranular, relies on the progenitors of the OSVZ.

Adapted from Kelley and Pasca (2021).

1.1.2 The evolution of the germinal compartments and the subventricular zone (SVZ)

Around 5-6 PCW in human, a distinct proliferative cell layer becomes evident between the highly proliferative ventricular zone (VZ) and the non-proliferative intermediate zone (IZ), which has been referred to as subventricular zone (SVZ) (Bystron *et al.* 2008). This compartment continues to expand in width and cellular complexity until the last third of gestation **(Figure 1.3).** The subventricular zone (SVZ) in humans is notably larger, more compartmentalised and has a longer developmental period compared to other studied species (Rakic *et al.* 1968; Bystron *et al.* 2008). Interestingly, while the ventricular zone (VZ) predominantly generates cortical projection neurons, the cortical subventricular zone (SVZ) contributes a more diverse array of cells, including the interneuron population (Letinic *et al.* 2002; Jakovcevski *et al.* 2011; Radonjic *et al.* 2014; Radonjic *et al.* 2014; Delgado *et al.* 2022), as well as oligodendrocytes (Jakovcevski *et al.* 2005; Ortega *et al.* 2013) and astrocytes (deAzevedo *et al.* 2003; Howard *et al.* 2008) .

Throughout development, the histological organization of the SVZ undergoes significant changes in the human fetal brain (Rakic 1972; Smart *et al.* 2002; Zecevic *et al.* 2006). At 7 PCW, the SVZ primarily consists of radially oriented cells that are a continuation of the radially arranged VZ cells, with a looser organization of the cells near the IZ. By 9 to 10 PCW, the expanding SVZ can be divided into **inner (ISVZ) and outer (OSVZ) subzones**, separated by a cell-poor region of the inner fibre layer (Bayatti *et al.* 2008) (**Figure 1.4**). This subdivision of the SVZ was first reported in monkeys (Smart *et al.* 2002). Starting from 12-13 PCW, well-defined fibre bundles traverse tangentially through the SVZ, distinctly separating the two SVZ regions (Zecevic *et al.* 2005; Molnar *et al.* 2012; Ortega *et al.* 2018). The outer subventricular zone (OSVZ) plays a crucial role in expanding the pool of progenitor cells and generating new progenitor subtypes during evolution, thus contributing to the enlargement and increased complexity of the primate cortex (Smart *et al.* 2002; Zecevic *et al.* 2005; Bayatti *et al.* 2008; Jakovcevski *et al.* 2011; Lui *et al.* 2011; Geschwind *et al.* 2013; Malik *et al.* 2013; Dehay *et al.* 2015).

Figure 1.4

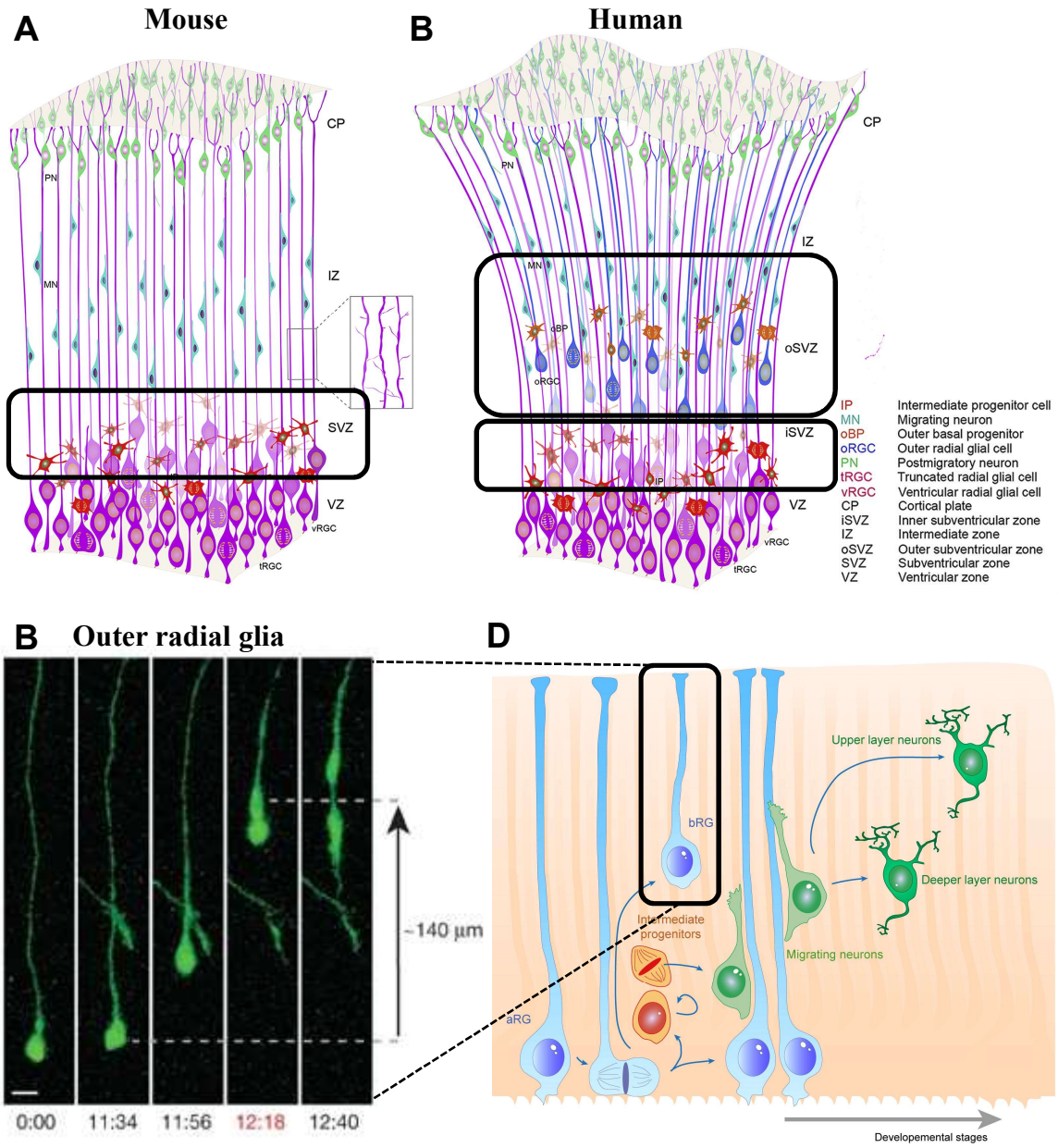

Figure 1.4: Evolution of the outer subventricular zone (OSVZ) and emergence of the outer radial glial cells (oRGC) as a specialized progenitor population in the human developing cortex.
(**A-B**) Schematic illustration of the developing mouse (A) and human (B) cortex highlighting the compartimentalization of the SVZ in primate, underlying tangential expansion of the human cortex and cortical folding. (**C**) oRGC is detected by adenoGFP-labelling (green) in a 13 PCW human cortical slice and show the presence of the basal process, along with the lack of the apical one. Time-lapse imaging (22 minute intervals between frames) reveals that oRGC undergo 'mitotic somal translocation' (MST) directly before cell division. Scale bar, 15 µm. (**D**) Schematic illustration of the radial glial cell (RG) populations (blue) in the human developing cortex. Apical radial glia (aRG) extend an apical process reaching the ventricular surface, and a basal process reaching the pial surface. Basal radial glia (bRG) (blue), on the other hand, only extend a basal process, and their soma is located away from the ventricle within the OSVZ. The basal process of both aRGC and bRGC serves as a scaffold for neuronal radial migration. aRGC and bRGC generate cortical neurons destined to the deep layers and upper layers, respectively
Adapted and modified from Cansingal et al., 2022 (A-B); Hansen et al., 2010 (C) and Ferent et al., 2020 (D) .

While the ISVZ resembles the SVZ found in rodents, the OSVZ contains RGC that lost their connection to the apical surface but maintain basal processes directed towards the pial surface, which have been consequently called basal RCG (bRGC) or **outer RGC (oRGC)** for their location in the OSVZ (Hansen *et al.* 2010) (**Figure 1.4 C-D**). These progenitors have a specific molecular profile, characterized by the expression of transcription factors like HOPX (Pollen *et al.* 2015) and play a role in generating intermediate progenitor cells, neurons and glial cells (Noctor *et al.* 2004; Hansen *et al.* 2010; Lui *et al.* 2011; Nowakowski *et al.* 2016). Furthermore, while vRGC undergo interkinetic nuclear migration (Toda *et al.*) during proliferation, oRGC have a unique behaviour known as mitotic somal translocation (MST), in which their cell body move dorsally before cytokinesis (Hansen *et al.* 2010; Ostrem *et al.* 2017) (**Figure 1.4 C**).

Recent studies have uncovered human- and primate-specific genes (Florio *et al.* 2015; Ju *et al.* 2016; Wang *et al.* 2016), as well as non-coding genetic elements (Boyd et al. 2015; Reilly et al. 2015), which regulate the generation, proliferation, and cell cycle of basal precursors. Specific genes related to extracellular matrix components, growth factors, and receptors are also highly enriched in the human cortical OSVZ compared to the rodent SVZ, and they promote neural precursor cell proliferation and neurogenesis (Kuburovic et al. ; Rash et al. 2013; Lui et al. 2014; Boyd et al. 2015).

Besides a cellular component, the OSVZ also contains tangentially and radially oriented cell processes, constituted by a mixture of RGC basal processes extending toward the pial surface, migrating cells, as well as axons, as observed in both monkey and human forebrain (Ortega *et al.* 2018). Three main fibre systems run tangentially in this overlapping region between the IZ and OSVZ: thalamocortical (TC), corticothalamic (CT), and corticocortical (CC) (i.e., callosal) projections (Smart *et al.* 2002; Molnar *et al.* 2012). Both radial and tangential fibres are important substrate for cell migration within the cortex. On the one hand, **tangentially oriented axons** aid the migration of interneurons and oligodendrocyte progenitors within the cortex (Parnavelas 2000; Marin *et al.* 2001). On the other hand, **radially oriented RGC processes** provide a scaffold through the cortex that guide the radial migration of newly born neurons to their final location in the cortical plate. During mid-gestation in human (between 17 and 24 PCW), this scaffold becomes

discontinuous, as ventricular RGC lose contact with the pial surface and only retain their ventricular attachment, giving origin to an additional subtype of progenitors with a specific molecular profile that has been labelled as "**truncated RGC**" (tRGC) (Nowakowski *et al.* 2016) (**Figure 1.5**). Interestingly, this dynamic transformation of the RGC scaffold marks the switch to upper layer corticogenesis in human, and is concomitant with an increase of OSVZ proliferative rates at the expenses of the VZ (Lukaszewicz *et al.* 2005; Martinez-Cerdeno *et al.* 2012; Nowakowski *et al.* 2016). Altogether, these observations suggest that the radial expansion of supragranular layers is driven by neurogenic divisions of oRG cells, while simultaneous tangential expansion of these layers is induced by self-renewing divisions of oRG. The disproportional tangential growth of the upper cortical layers also has a significant role in cortical folding, therefore linking oRGC to this phenomenon in gyrencephalic brains (Richman *et al.* 1975; Rakic 1988; Haydar *et al.* 1999; Chenn *et al.* 2002; Kriegstein *et al.* 2006; Reillo *et al.* 2011; Nowakowski *et al.* 2016). At the end of neurogenesis, the SVZ gradually diminishes in size but persists in a rudimentary form in the adult human brain, known as the subependymal zone (Sanai *et al.* 2011).

Figure 1.5

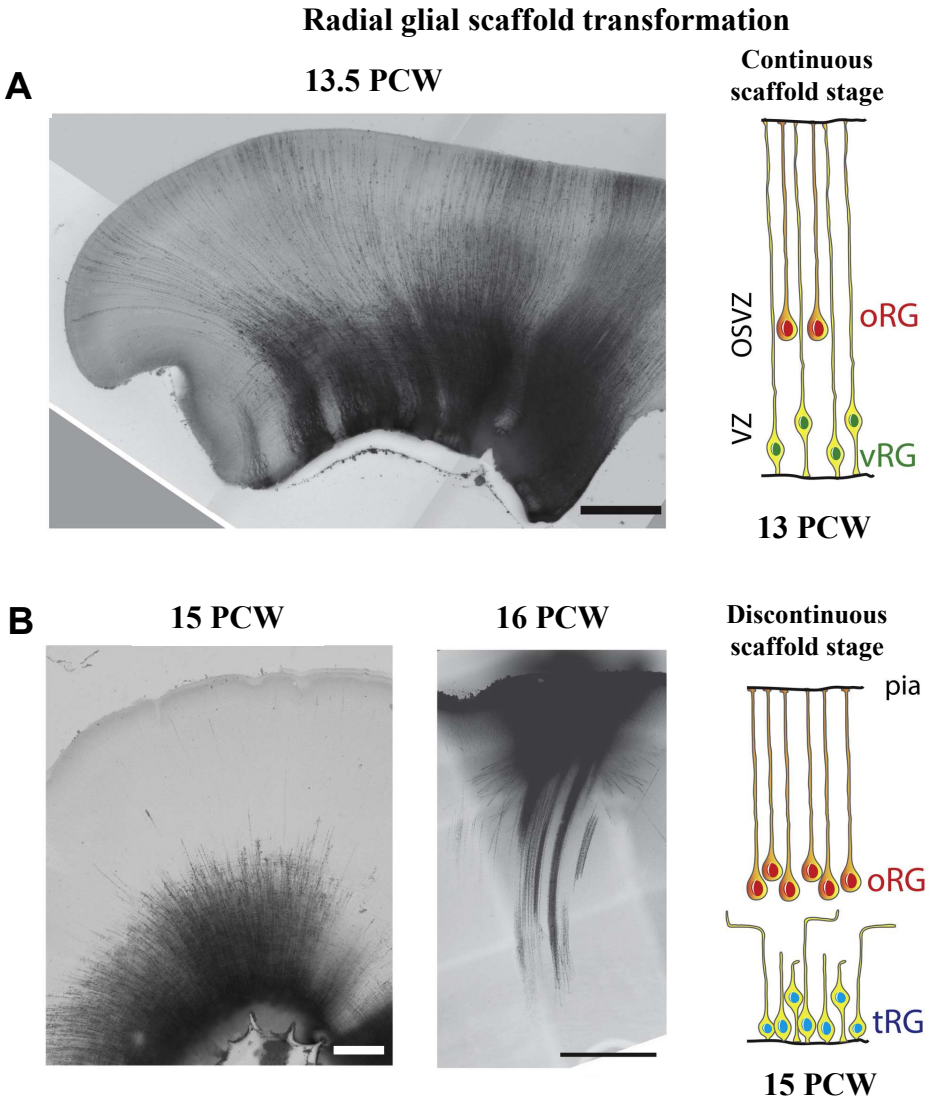

Figure 1.5: Morphological transformation of the radial glial scaffold during human cortical development and truncated radial glial cells (tRG) emergence at the time of deep-to-upper layer neurogenic switch in the human fetal brain.
(**A**) The scaffold created by the basal processes of the radial glial cells (vRG) spans the entire radial extension of the human cortex before 14.5 PCW, as revealed by DiI placement in the ventricular side at earlier stages. Outer radial glia (oRG) reaches to outer subventricular zone (OSVZ). (**B**) Afterwards, the processes appeared "truncated" and DiI signal does not reach the pial surface when placed in the ventricular side (representative image of a 15 PCW brain) and vice versa do not reach the ventricular zone when placed in the pial surface (representative image of a 16 PCW brain). The two stages are schematized on the left side of the images, respectively.
Adapted and modified from Nowakowski et al., 2016.

Extrinsic factors shaping the SVZ

The extended duration of cortical development in humans provides a greater window of opportunity for environmental factors to influence both the quantity of progenitor cells and the overall structure of the forebrain. For instance, *in vitro* functional studies that longer exposure of human RGC to key morphogens can crucially shape the output of corticogenesis (Radonjic *et al.* 2016; Lu *et al.* 2000), hence sustained exposure to these molecules can subsequently influence the neuronal output derived from these progenitors (Vaccarino *et al.* 1999; Alvarez-Medina *et al.* 2009; Munji *et al.* 2011; Rash *et al.* 2013; Watanabe *et al.* 2015). Besides classic morphogens, many cytokines are abundantly produced by neurons and glial cells in the human SVZ at mid-gestation (Rezaie *et al.* 2003; Filipovic *et al.* 2008), that can also influence cell proliferation, survival, migration, and synaptogenesis (Gutierrez-Fernandez *et al.* 2014).

Apart from endogenously-produced molecules, extrinsic molecular factors can also affect the physiology of the SVZ progenitors. For instance, Lukaszewicz and colleagues showed that cortical progenitors in the superficial part of OSVZ, where the thalamic axons are located, have a shorter S-phase than their counterparts in the deep portion of the OSVZ (Lukaszewicz *et al.* 2005), indicating that the thalamocortical projections might influence the cell cycle parameters of progenitor cells in their surroundings (Dehay *et al.* 2007). Finally, as the RGC populating the germinal compartments extend their basal processes through the entire radial extension of the cortex, another mechanism of extrinsic influence to these cells is via direct contact between their processes and the axons that run in the IZ, including TCA (Gerstmann *et al.* 2015). A summary of the cellular interactions coexisting in the human developing cortex is provided in **Figure 1.6** (Molnar *et al.* 2020).

A longer neurogenic window, alongside the more complex relationship between thalamic axons and the germinal compartments in the human cortex, might allow for a more pronounced and powerful influence of cortical neurogenesis by any of these extrinsic modulators in our species (Dehay *et al.* 2007; Molnar *et al.* 2012; Bandiera *et al.* 2022).

Figure 1.6

Mechanisms of cellular interactions in the developing cortex

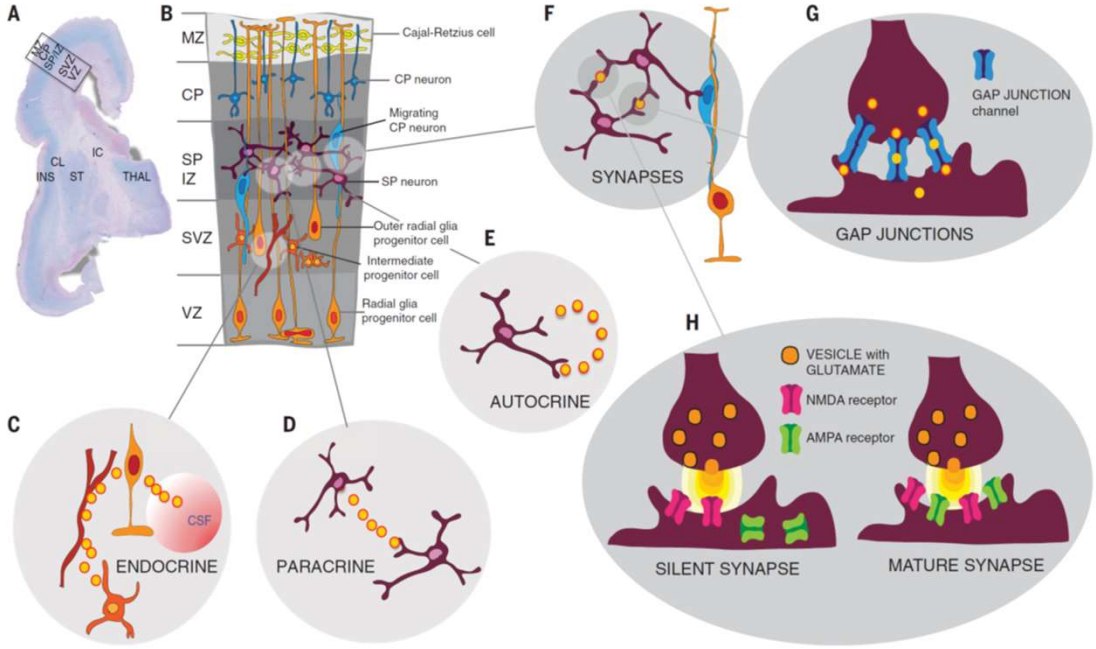

Figure 1.6: Different mechanisms of cellular interactions in the human developing cortex.
(**A**) Coronal section of the human brain at 16 PCW stained by periodic acid Shiff (PAS)-Alcian blue highlighting the subplate (SP) and intermediate zone (IZ) in blue, and germinal zones (ventricular zone, VZ; subventricular zone, SVZ) in pink. Also present the cortical marginal zone, MZ; cortical plate, CP; as well as the claustrum (CL); insula (INS); striatum (ST); thalamus (THAL), and the internal capsule (IC) for anatomical reference. (**B**) Schematics representation of the developing cortical layers at this stage in a cross section. (**C-H**) Mechanisms of cellular interactions co-occurring within the developing cortex. Dividing radial glial progenitors in VZ are in contact with cerebrospinal fluid and receive endocrine signals, some through blood vessels. Immature neurons interact through paracrine (D) and autocrine (E) mechanisms or couple into local networks through electrical (G) and chemical (H) synapses (F).
Adapted from Molnár et al., 2020.

Clinical relevance of the human SVZ

Given the crucial role played by the SVZ in generating cortico-cortical projecting upper layer neurons, and the co-existence of proliferation, migration, and differentiation of different cell types within this compartment, both intrinsic (genetic mutations) and extrinsic (*in utero* insults) alterations can have severe neurological consequences (Zecevic *et al.* 2005).

The resulting various developmental disorders include polymicrogyria, megalocephaly, periventricular heterotopia, pachygyria, and lissencephaly, often leading to intellectual impairment or epilepsy (Ortega *et al.* 2018). Moreover, hypoxia-induced insults might also affect the human SVZ, causing significant disruptions in cortical circuitry impacting cognitive and behavioural function later in life (Back *et al.* 2001; Cannon *et al.* 2002; Ortega *et al.* 2017). Recent studies showed that this cortical layer, and especially the oRGC populating it, might be especially vulnerable to hypoxic insults (Daviaud *et al.* 2019). Consistently, perinatal hypoxic insults can severely reduce brain size and cerebral cortex thickness (Malik *et al.* 2013; Ortega *et al.* 2017). Furthermore, in human subpopulations of cortical interneurons originate from the SVZ (Radonjic *et al.* 2014; Ortega *et al.* 2017), and their dysregulation contribute to complex psychiatric disorders like schizophrenia (Akbarian *et al.* 1995; Lewis *et al.* 2012), bipolar disorder (Knable 1999), and autism spectrum disorder (Geschwind *et al.* 2007). Understanding the pathogenesis of human-specific developmental brain disorders is essential for devising effective therapeutic interventions (Arshad *et al.* 2016).

1.1.3 The subplate zone

The subplate is a transient developmental compartment of the mammalian cortex lying between the cortical plate and the intermediate zone, or the future white matter. This layer is especially prominent in primates and humans (Kostovic *et al.* 1990; Molnar *et al.* 2006; Judas *et al.* 2013; Kerschensteiner 2014; Hoerder-Suabedissen *et al.* 2015; Duque *et al.* 2016). The subplate contains a heterogeneous population of neurons, which are amongst the earliest generated in the cortex (Kostovic *et al.* 2015). Around 7-8 PCW, subplate neurons already exhibit some initial synaptic activity (Molliver *et al.* 1973; Marin-Padilla 2014; Kostovic *et al.* 2015). Besides post-mitotic subplate neurons and migrating neurons, the subplate also contains glial cells and growing axonal projection, as well as an abundant extracellular matrix (Kostovic *et al.* 1990; Hoerder-Suabedissen *et al.* 2015). The subplate serves as a crucial site for neuronal differentiation and migration, as well as synapse formation especially during mid-fetal stages of brain development (Bayatti *et al.* 2008; Moore *et al.* 2011; Kostovic *et al.* 2015; Ohtaka-Maruyama *et al.* 2018; Ozair *et al.* 2018). Consistently, SP neurons show extensive dendritic arborization and widespread axonal projections (Mrzljak *et al.* 1992; Kanold *et al.* 2010).

Thanks to recent advancement in visualization techniques, we recently got insights on this enigmatic cortical compartment in the human brain, otherwise relatively inaccessible due to its transient and prenatal developmental nature. The human subplate constitute 35% of the entire cerebral wall by 16 PCW (Wang *et al.* 2010) and reaches its maximum thickness between 26-32 PCW, when it appears about four times thicker than the cortical plate (Mrzljak *et al.* 1992; Judas *et al.* 2013; Vasung *et al.* 2016), and it is most prominent in the frontal and parietal association areas (Kostovic *et al.* 2002; Duque *et al.* 2016) (**Figure 1.7**). In contrast to rodents, that subplate neurons continue to be generated until late development in primates (Smart *et al.* 2002; Lukaszewicz *et al.* 2005; Molnar *et al.* 2006; Wang *et al.* 2010). Specifically, a substantial number of neurons positive for the T-box brain gene 1 (Tbr1) are consistently added to the human subplate between 14 to 25 PCW, thus contributing to the expansion of this compartment observed simultaneously with the growth of the cortical plate (Meyer 2007). Subplate neurons express also nuclear receptor 4A2

(NR4A2; also known as nuclear receptor related 1 protein, Nurr1), corticothalamic projecting neuron marker TLE4, and deep layer neuronal marker B cell leukemia/lymphoma 11B (Bcl11b; also called CTIP2, COUP-TF-interacting protein 2, CTIP2) during human mid-gestational stages (Ozair *et al.* 2018) (**Figure 1.8**).

Figure 1.7

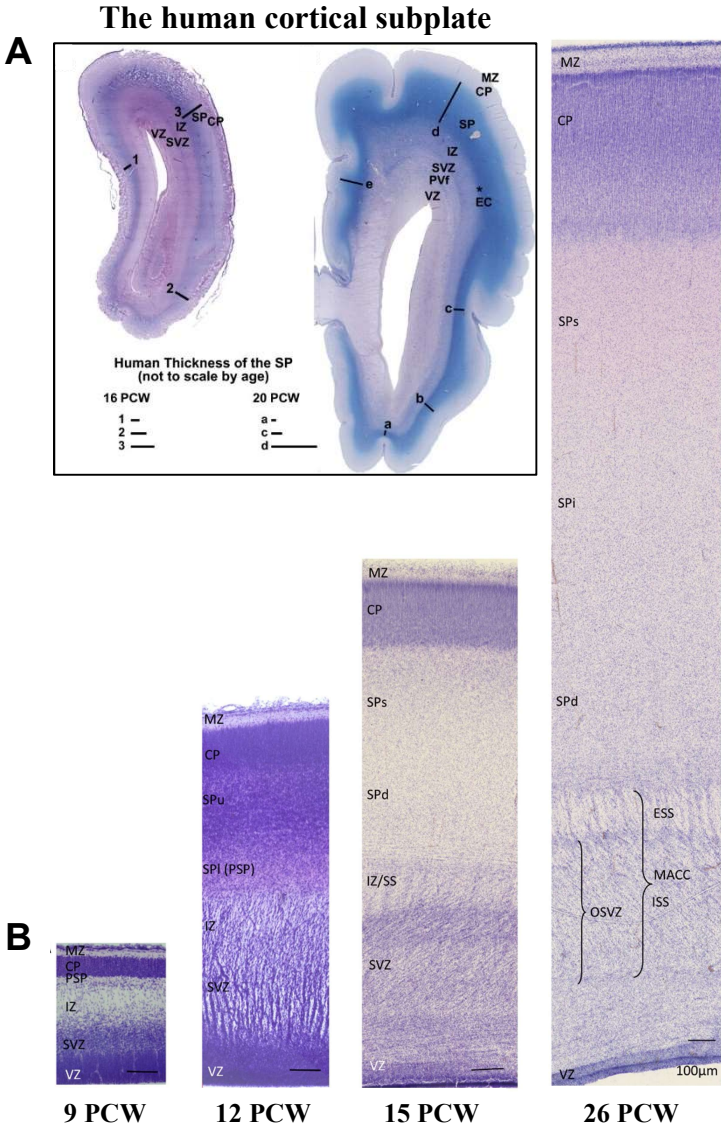

Figure 1.7: The developmental changes of human fetal subplate at four selected stages.
(**A**) Periodic acid–Schiff (PAS)-Alcian staining of human brain coronal sections at 16 and 20 PCW, revealing the subplate (SP) labelled by Alcian blue due to its high content in extracellular matrix. The SP substantially grow at mid-gestation, becoming the most prominent cortical layer by 20 PCW. (**B**) Nissl staining of the human cortex at 9, 12, 15, and 26 PCW. The initial presubplate (PSP) forms the lower subplate (SPl) at 12 PCW, and by 15 PCW is already 4 times thicker than the cortical plate (CP) and show sublamination into superficial subplate (SPs) and deep subplate (SPd). The extraordinary expansion of the SP peaks at 26 PCW when superficial SP (SPs), intermediate subplate (SPi) and deep subplate (SPd) can be distinguished.
Adapted and modified from Duque et al., 2016 (A) and Kostovic, 2020 (B).

Figure 1.8

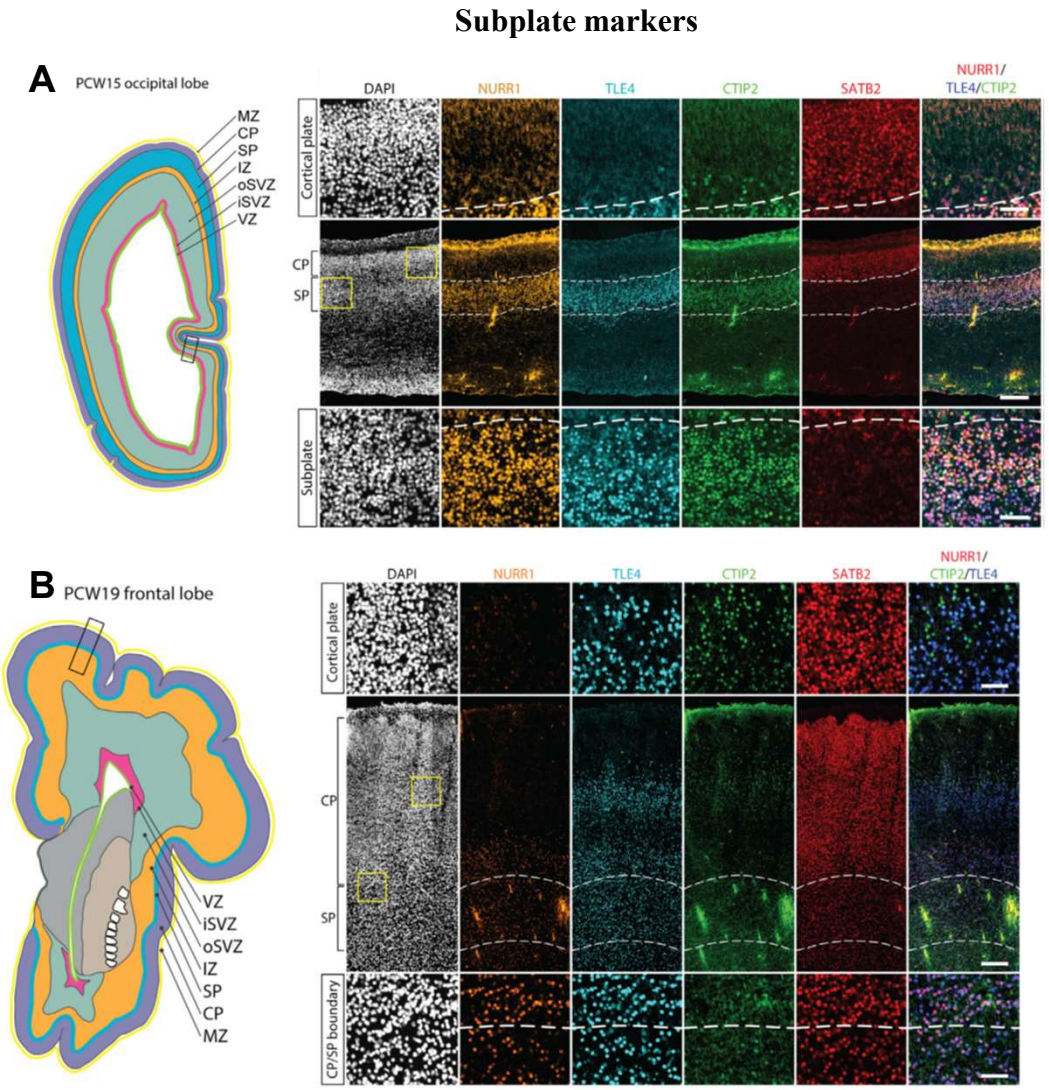

Figure 1.8: Molecular markers of the human subplate at mid-gestation.
Left panels are schematic representations of the coronal brain sections showing the laminar organization of the cerebral walls at PCW15 **(A)** and PCW19 **(B)** developmental stages. Subplate neurons express the specific marker NR4A2 (Nurr1), corticothalamic projecting neuron marker TLE4, and deep layers' marker Bcl11c (CTIP2), but are negative for upper layers' marker SATB2 at both 15 and 19 PCW. Scale bars = 50 mm (top and bottom images) and 200 mm (central images).
Adapted and modified from Ozair et al., 2018.

The "waiting period" and early transient circuits established within the subplate

The subplate receives the afferent projections arriving from subcortical region, that "wait" in this compartment for a period before reaching their target neurons in the cortical plate (Ghosh *et al.* 1993; Catalano *et al.* 1998; Hanganu *et al.* 2002; Anton-Bolanos *et al.* 2018) (discussed later, and in **Figure 1.15**). These include axons from the brain stem (12 PCW) (Nobin *et al.* 1973; Kostovic *et al.* 2015), followed by the thalamocortical axons (12-14 PCW) (Krsnik *et al.* 2017), and later the projections from the basal forebrain, other cortical areas, as well as callosal axons (Takahashi *et al.* 2012; Kostovic *et al.* 2014; Krsnik *et al.* 2017). The massive arrival of axonal fibres in the compartment at mid-gestation leads to the physical dispersion of subplate neurons (Duque *et al.* 2016). SPN also provide molecular guidance cues that direct the correct pathfinding of these axons within the cortex (Shatz *et al.* 1990; Ghosh *et al.* 1993). Most afferents innervating the subplate between 18 and 23 PCW come from the thalamus and the basal forebrain (Vasung *et al.* 2017), and the subplate is in fact critically involved in the early circuit formation with thalamocortical and basal forebrain afferent (Kostovic *et al.* 1990; Allendoerfer *et al.* 1994; Hoerder-Suabedissen *et al.* 2015; Alzu'bi *et al.* 2019).

The subplate participates in both spontaneous (Kanold *et al.* 2010) and evoked activity of the developing cortex (Allendoerfer *et al.* 1994; Molnar *et al.* 2020). Importantly, subplate spontaneous oscillations are crucial for the proper tuning and maturation of the early cortical network activity (Kanold *et al.* 2010; Luhmann *et al.* 2016; Molnar *et al.* 2020), hence SPN are considered as "amplifying hub neurons" (Kanold *et al.* 2010). The synchronized firing of subplate neurons facilitates the establishment of functional connectivity between different cortical regions (Molnar *et al.* 2020). Besides functional activity, the subplate can also shape cortical neurogenesis and circuit formation by secreting neuroactive molecules in the extracellular space, such as neuroserpin (Kondo *et al.* 2015; Adorjan *et al.* 2019).

The waiting period of thalamocortical axons within the human subplate lasts for months before they start innervating the cortical plate from 23-24 PCW onwards (Kostovic *et al.* 2007; Judas *et al.* 2013; Kostovic *et al.* 2015; Krsnik *et al.* 2017). When the afferent start moving away from this area, the subplate begins to decrease in thickness, and the subplate neuronal population is gradually reduced (Kostovic *et al.* 1990; Judas *et al.* 2013; Kostovic *et al.* 2014). The mechanism by which the subplate dissolves is not fully understood, however it has been proposed that part of the neurons populating this compartment undergo programmed cell death (Price *et al.* 1997; Arias *et al.* 2002), a phenomenon also described for primate, carnivore and human brains (Kostovic *et al.* 1980; Luskin *et al.* 1985; 1985; Meyer *et al.* 1992). SP neurons that survive will constitute the interstitial white matter neurons in the adult brain (Kostovic *et al.* 1980; 1990; Meyer *et al.* 1992; Judas *et al.* 2010; Kostovic *et al.* 2011; Judas *et al.* 2013; Kostovic *et al.* 2014), or populate cortical layer 6b (Reep 2000; Marx *et al.* 2017). The dissolution of the subplate is also driven by the reduction in ECM components after 35 PCW in human (Kostovic *et al.* 1990; Hoerder-Suabedissen *et al.* 2015). SP dissolution is faster under the sulci than it is under gyri (Perkins *et al.* 2008), possibly correlating with gyrification of the cortex (Kostovic *et al.* 1990).

The crucial importance of this transient compartment is exemplified by animal studies whereby experimental disruption of this layer lead to deficits in area-specific features of the cortex, such as ocular dominance columns in the visual cortex and the barrels in the somatosensory cortex of rodents (Kanold *et al.* 2003; Tolner *et al.* 2012). Interestingly, associative cortices receiving a greater subcortical innervation of this transient layer also have a thicker SP (Duque *et al.* 2016).

Clinical relevance of the subplate

Given its crucial involvement in circuit formation, as well as in the gyrification of the human cortex, it is not surprising that the subplate has been associated with human-specific neurodevelopmental conditions affecting both aspects, such as autism and schizophrenia (Palaniyappan *et al.* 2011; Wallace *et al.* 2013; Budday *et al.* 2014; Hoerder-Suabedissen *et al.* 2015; Kostovic *et al.* 2019). Consistently, studies have reported an excessive number of interstitial white matter cells in patients with schizophrenia (Eastwood and Harrison, 2005) (**Figure 1.9**). Finally, subplate neurons are selectively vulnerable to hypoxia-ischemic insults (McQuillen *et al.* 2003; McQuillen *et al.* 2005; Sheikh *et al.* 2019), that can lead to alteration of their connectivity and subsequent functional impairments later in development (Failor *et al.* 2010). Overall, evidence point to a crucial role played by the subplate in the establishment of the early cortical circuitry, as well as in the evolution of the human cortex and aetiology of human-specific neurodevelopmental conditions.

Figure 1.9

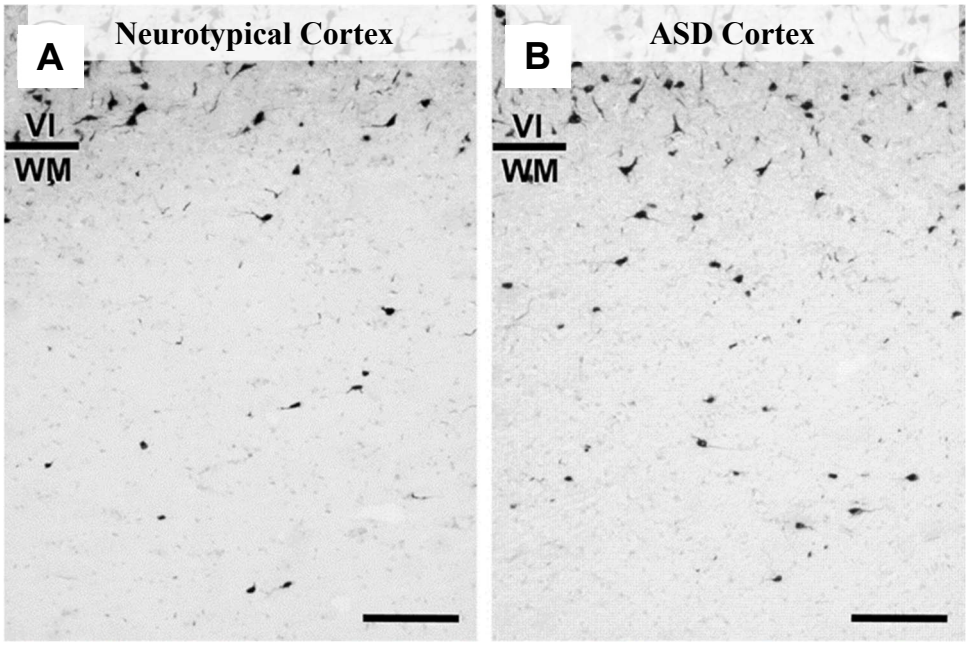

Figure 1.9: Increased density of subplate neurons in the neocortex of patients with autism spectrum disorders (ASD). On average, there are 44.7% more neurons, stained by NeuN, in the cortical subplate region of patients with ASD (**B**) than in similar area of the cortex of neurotypical subjects (**A**). The boundary between layer 6 and the white matter (WM), where the subplate was located during development, is indicated at the side of each image. Scale bar = 100 µm. From Avino and Hutsler (2021)

1.1.4 Intrinsic and extrinsic mechanisms shaping cortical development and formation of the cortical maps

Some fundamental features of the cerebral cortex, such as the presence of six layers and the relative size and density of cells in each layer, are common among most cortical subdivisions. However, variations exist in the relative thickness, cellular composition of each layer, and the primary source of afferent and efferent axonal connectivity across different cortical areas. Understanding the developmental underpinnings responsible for the emergence of shared and unique features in diverse cortical areas has been a subject of extensive research over the past several decades.

In the late 20th century, two contrasting hypotheses were articulated. One proposed that cortical areas are predetermined as a **"protomap"** by mechanisms intrinsic to the cortex itself and the progenitors that form this region (Rakic 1988). These area-specific neurons then migrate during prenatal development, assembling into “ontogenic columns” derived from radial units to form the mature cortical area map. The second hypothesis suggested that cortical progenitor cells are initially uniform and "naive" to their eventual areal positioning, forming a **"protocortex"** (O'Leary 1989) (**Figure 1.10**). The parcellation of functional cortical subdivisions is then driven by the arrival of area-specific thalamic input, either postnatally in rodents or prenatally in primates. Several evidences have been gathered in support of both theories, supporting the idea that the developmental patterning of the neocortex represents the result of an interplay between intrinsic genetically encoded mechanisms and extrinsic factors (O'Leary *et al.* 2002; Clowry *et al.* 2018; Cadwell *et al.* 2019).

Figure 1.10

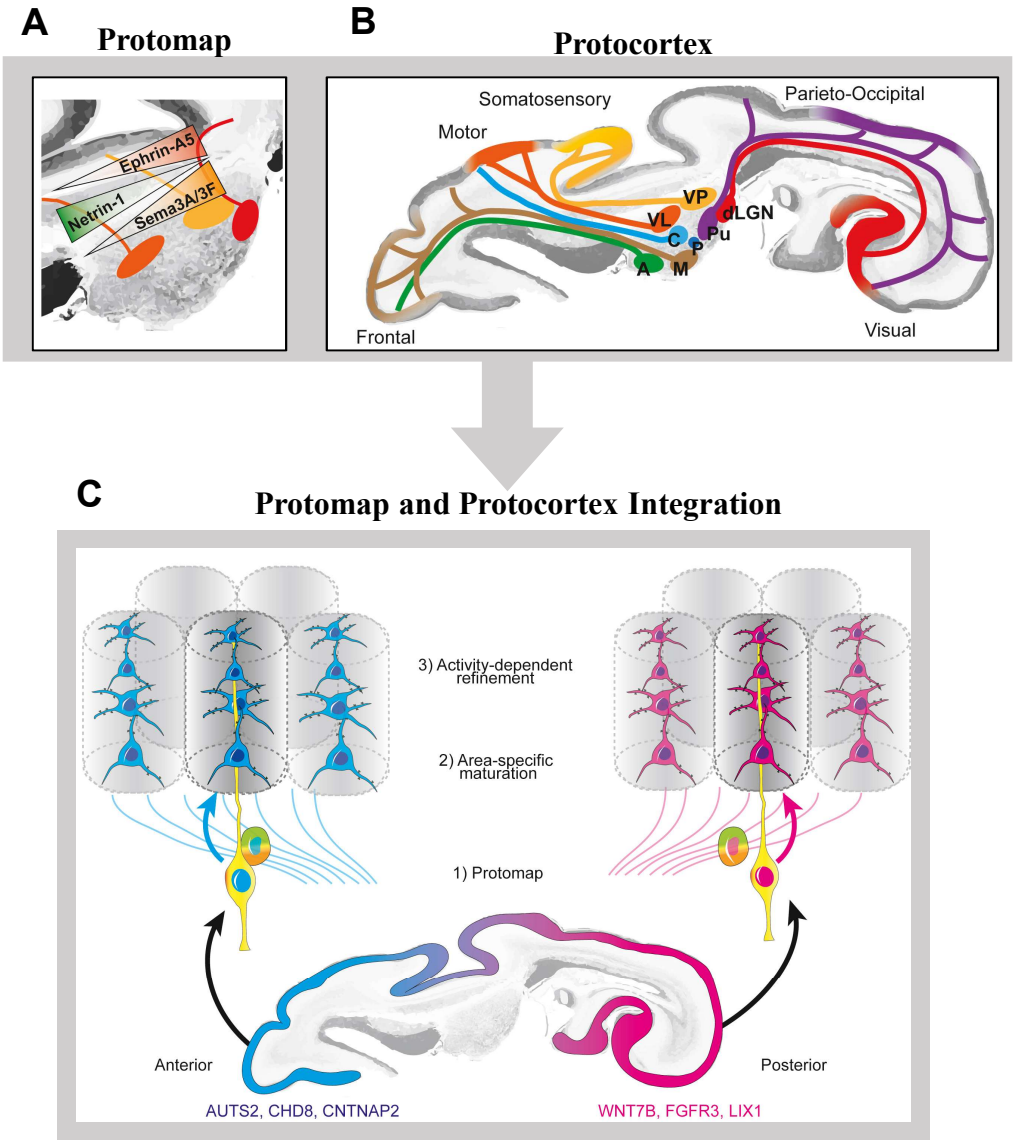

Figure 1.10: Integration of the protomap and protocortex hypotheses as a new model of cortical arealization (proposed by Cadwell et al, 2019).
The two opposing view on the mechanisms of cortical arealization, the protomap and protocortex, are reconciled into a new model of "serial homology and refinement" proposed by Cadwell and colleagues (2019). According to this model, intrinsic and extrinsic factors both contribute to the acquisition of areal identity by the developing human cortex. The former establish an initial "protomap" by endogenous expression of morphogens and transcription factors (**A**). Then, the thalamocortical projections that innervate the cortex in an area- and modality-specific manner early on during human development, provide extrinsic cues that modulate their size, maturation, and connectivity patterns (**B**). This leads to an activity-dependent refinement of these regions and the sharpening of areal boundaries in the cortex thanks to the effective integration of intrinsic and extrinsic mechanisms (**C**).
Adapted and modified from Cadwell et al., 2019.

In support of the **first hypothesis**, early studies showed that that neurogenesis, neuronal migration, and area-specific early gene expression differences can proceed without any thalamocortical input or even without any connectivity between cortex and subcortical structures (Miyashita-Lin *et al.* 1999). The initial phases of cortical arealization are influenced by **morphogens** that establish the anterior-posterior and mediolateral axes within the germinal zone of the prospective cortex (Grove et al. 1998; Fukuchi-Shimogori et al. 2001; Hebert et al. 2002; Cholfin et al. 2007; 2008; Assimacopoulos et al. 2012; Caronia-Brown et al. 2014). These morphogens influence the expression of several **transcription factors** within the ventricular zone of the early cortical primordium before thalamic afferents arrive (Suzuki *et al.* 1997; Rubenstein *et al.* 1999; Bishop *et al.* 2000; Mallamaci *et al.* 2000; Zhou *et al.* 2001; Armentano *et al.* 2007; Rakic *et al.* 2009). Consistently, mutant mice lacking thalamocortical projections still display normal cortical region-specific gene expression (Nakagawa *et al.* 1999; Rubenstein *et al.* 1999).

Nevertheless, after the 6-layer cytoarchitecture and early regionalization of the neocortex are established by intrinsic mechanisms, other area-defining cortical features that emerge later in development, such as neuronal connections and distribution of the cortical columns, are influenced by **extrinsic cues** provided during critical periods of development (Hensch 2004; Li *et al.* 2013). The major source of extrinsic patterning shaping the neurogenic programme is provided by the **thalamocortical afferents** (Jones 1985; Mountcastle 1997), that are crucial for the establishment of the architecture and distributions of cortical neurons and the acquisition of specific areal identity of cortical regions (Polleux *et al.* 2001).

Thalamocortical innervation can provide extrinsic modulation to the protomaps via different mechanisms, including secreted molecular factors (Sato *et al.* 2022), as well as by conveying spontaneous activity before sensorial stimulation (Moreno-Juan *et al.* 2017) and even sensorial information before any sensorial perception, which can further instruct the acquisition of areal identity by neocortex in an activity-dependent manner (Akerman *et al.* 2002). In support of this, studies showed that the characteristic barrels of rodent somatosensory cortex do not form in mice where thalamocortical projections do not innervate the cortex or peripheral sensory input are

experimentally disrupted in neonatal mice (Van der Loos *et al.* 1973; Jensen *et al.* 1987). If the receptor-mediated signal transduction is altered, recipient cortical layer 4 neurons do not assume the correct position to form the characteristic barrel pattern (Erzurumlu *et al.* 2012) (**Figure 1.11**). Genetic ablation of specific thalamic nuclei in transgenic mice further demonstrates the requirement of thalamic input to establish genetic and functional distinctions between primary sensory cortex and adjacent higher-order sensory cortex (Chou *et al.* 2013; Pouchelon *et al.* 2014). Similarly, in primates, depletion of the thalamic afferents results in a consistent reduction of the primary visual cortex in both early-enucleated monkey and anophtalmic patients (Dehay *et al.* 1989; Rakic 1991; Dehay *et al.* 1996) (**Figure 1.12**). In both cases the cytoarchitecture is preserved, however a substantial imbalance in the upper-to-lower layer neuronal number observed. Furthermore, bilateral enucleation in developmental stages causes the primary visual cortical areas to become smaller and exhibit responses to different sensory modalities (Dehay *et al.* 1989; Rakic *et al.* 1991; Kahn *et al.* 2002).. This phenomenon can be attributed to calcium waves propagating through thalamic nuclei associated with distinct sensory modalities (Moreno-Juan *et al.* 2017). These profound morphological and functional effects indicate that the borders between cortical areas are not fixed and support the hypothesis of a crucial role of TCA in imposing specific areal identity characteristics to the immature cortex in the primate (Rakic 1991; Dehay *et al.* 1996).

In summary, the development of the mature cortical area map involves a complex interplay between intrinsic and extrinsic factors. Early establishment of the cortical blueprint relies on intrinsic mechanisms, and subsequently, thalamic innervation refines the areal boundaries and contributes to the distinct genetic, cytoarchitectural, and functional characteristics that define cortical subdivisions.

Figure 1.11

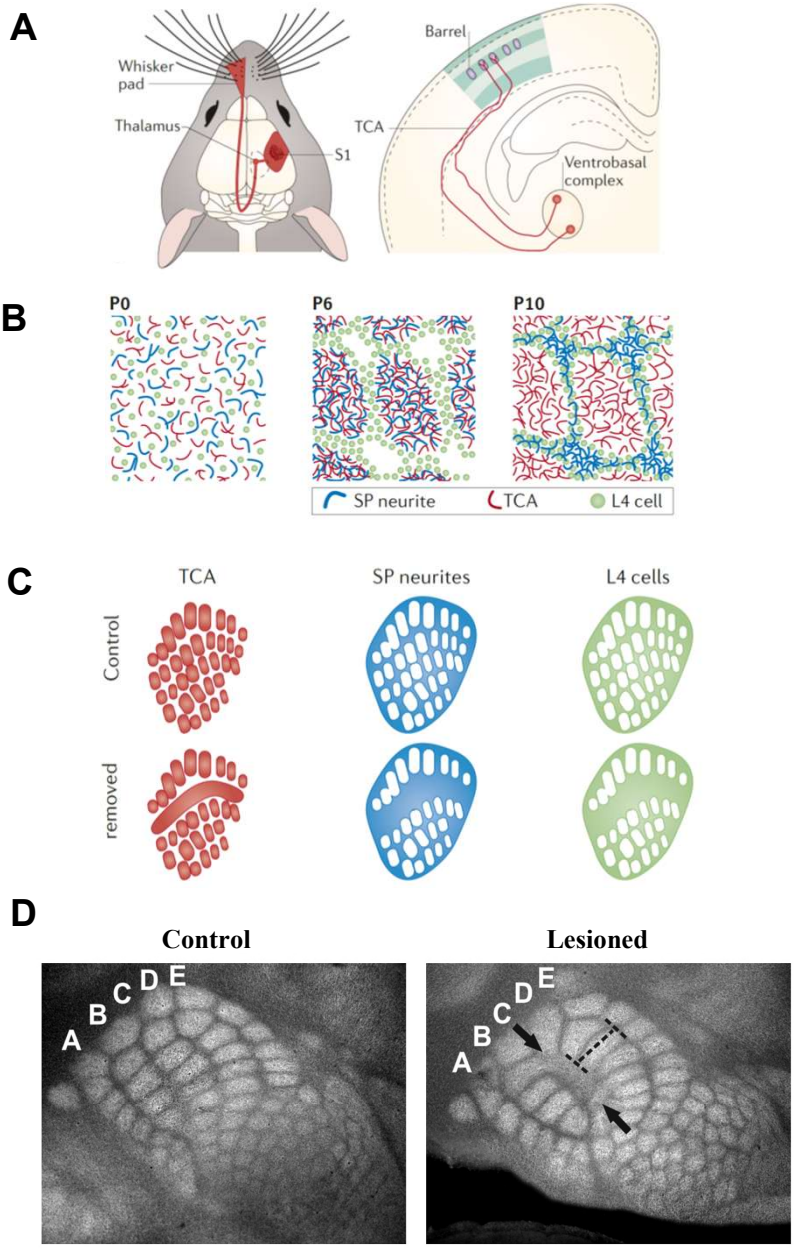

Figure 1.11: Whisker removal and impaired thalamocortical axon innervation to the rodent somatosensory cortex impairs the formation of the typical "barrels".
(**A**) Schematic illustration showing the normal pathway through which sensorial inputs are conveyed via the thalamic ventrobasal (VB) complex to the primary somatosensory cortex (S1) in a topographic manner. (**B**) Thalamic axons interacts with subplate (SP) neurons and instruct the acquisition of the typical cytoarchitecture observed in the S1 barrels, which directly relate to each whisker pad. (**C**) Whisker removal during the time of S1 cortical plasticity prevent thalamocortical afferents (TCA) to reach the correspondent prospective barrels. Hence, SP neurites or recipient cortical layer 4 neurons fail to organized in barrel-shaped structures, disrupting the normal cytoarchitecture of S1. (**D**) Shows an example of this phenomenon: on the left picture is depicted a normal S1 barrel cortex, while on the right is the result of early lesion to the whisker pad row C with subsequent malformation of the barrel row C.
Adapted from Hoerder-Suabedissen and Molnár, 2015 (A-C) and modified from Eroglu et al., 2009 (D).

Figure 1.12

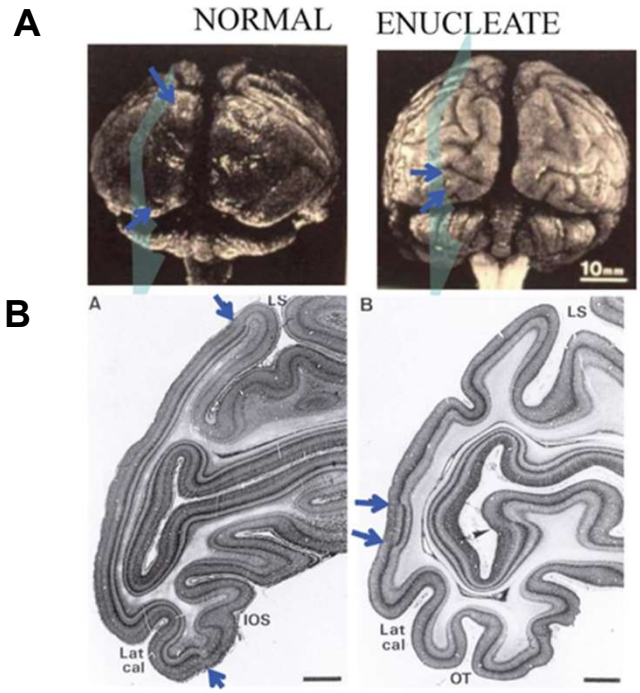

Figure 1.12: Early sensory lesions can have profound effect on the gross morphological appearance (folding) of the primate brain and demonstrate that the borders between cortical areas are not fixed. (**A**)The upper panels demonstrate the posterior view of the cerebrum of a normal 3 years-old macaque monkey (left) and and age-matched animal that underwent bilateral enucleation at E60 (right) (Rakic 1988). The development of sulci and gyri is seen in the normally smooth lateral surface of the occipital lobe. (**B**) The lower panels represent Nissl-stained histological sections from experiments of Dehay and colleagues (1996). The extent of the primary visual cortex can be determined from the extent of the Stria Gennari that corresponds to the thick layer 4 within primary visual cortex (segments between the blue arrows in the normal occipital lobe). The extent of the primary visual cortex is drastically reduced in the enucleated animal (blue arrows in the lower left panel).
Modified from Rakic, 1988 (A) and from Dehay et al., 1996 (B).

1.2 DEVELOPMENT OF THE THALAMOCORTICAL SYSTEM

The major source of extrinsic modulation to the area-specific development of the cerebral cortex is provided by the early thalamocortical afferents (O'Leary 1989). However, the details of the cellular and molecular mechanisms are not known, especially in the human brain.

1.2.1 Main events involved in the early development of the thalamocortical connection

The basic pattern of thalamocortical development is similar in all mammals, and are summarized in **Figure 1.13** from extended literature in rodent models (Hanashima *et al.* 2006). Upon departing from the thalamus, TCA travers the prethalamus, and exit the diencephalon by crossing the diencephalic-telencephalic boundary (DTB). Then, they extend along the primitive internal capsule, and cross the pallial-subpallial boundary (PSPB) dividing the ventral and dorsal telencephalon, to approach the immature cortex (Hanashima *et al.* 2006) (**Figure 1.13**). Here, they extend transversally forming side branches in the intermediate zone (IZ), and finally accumulate within the subplate zone and interact with its early-born neuronal population (Molnar *et al.* 2020). Pioneer axons from thalamic reticular nucleus, and perireticular nucleus, and tangentially migrating neurons in the internal capsule, the so-called corridor cells (Hanashima *et al.* 2006; Lopez-Bendito *et al.* 2006; Bandiera *et al.* 2022) provide an early scaffold to guide the thalamocortical afferent outgrowth through this trajectory, and facilitate their entry into the telencephalon (De Carlos *et al.* 1992; Metin *et al.* 1996; Molnár 1998; Molnar *et al.* 1999; Tuttle *et al.* 1999). Similarly, their topographic organization is maintained by several factors, such as molecular gradients established at the level of the ventral telencephalon (**Figure 1.13**).

In mouse, the corticothalamic projecting neurons, which are generated between E11-E13 in mouse, are already present at the time TCA reach the cortex around E15.5 (Miyashita-Lin *et al.* 1999; Auladell *et al.* 2000; Lopez-Bendito *et al.* 2003; Gezelius *et al.* 2017; Anton-Bolanos *et al.* 2018). These neurons sent corticothalamic axons (CTA) in the direction of the thalamus. The two reciprocal fibre systems meet at the PSPB, and, after a "handshake" near the internal capsule (Molnár 1998; Molnar *et al.* 1998), guide each other over it along the remaining part of their reciprocal

trajectories (Molnar *et al.* 1991; 1995). Importantly, CTA are essential to guide the TCA at this level (Lopez-Bendito *et al.* 2003; Chen *et al.* 2012; Molnar *et al.* 2012; Doyle *et al.* 2021) (**Figure 1.13**).

Figure 1.13

Main events in the development of the thalamocortical system

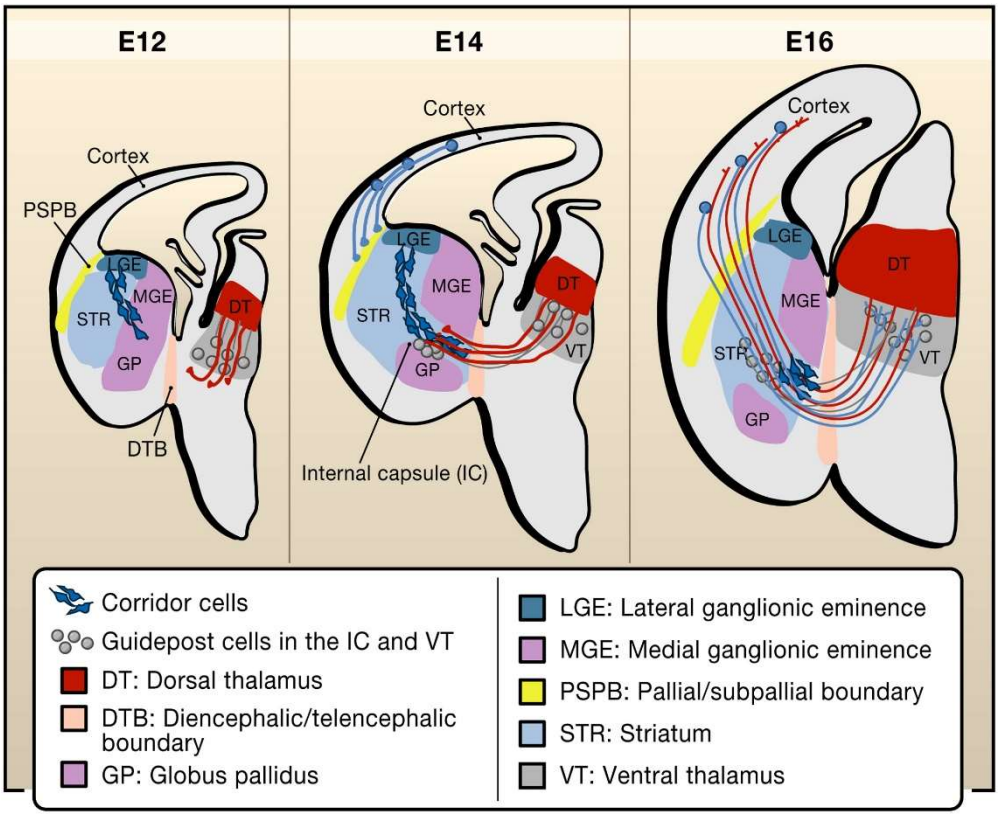

Figure 1.13: Overview of the multiple factors involved in the development of early thalamocortical connectivity.
The main events occurring during the development of thalamocortical connections can be divided into three stages in mouse. At E12-14, the ventral thalamus (i.e. prethalamus) and internal capsule contain guidepost cells (gray) that already developed projections to the dorsal thalamus (Braisted et al. 2000) and guide the thalamic projections towards the internal capsule through the diencephalic and telencephalic boundary (DTB). Corridor cells (dark blue) originate from the lateral ganglionic eminence (LGE) at embryonic day 12 (E12) and migrate tangentially toward the diencephalon, where they form a permissive "corridor" for the thalamic projections (red) to navigate through the internal capsule. Perireticular cells also influence the entrance of TCA into the subpallium, whereas corridor cells orient the internal pathfinding of TCA inside the MGE. Subsequently the early corticothalamic projections guide the thalamic projections through the pallial-subpallial boundary (PSPB) as originally proposed in the handshake hypothesis by Molnár et al. (1995).
Adopted from Hanashima et al., 2006.

Although classic studied using acetylcholinesterase (AChE) histochemistry (Kostovic *et al.* 1984) suggested that these events follow a similar timing in **human** (Krsnik *et al.* 2017; Zunic Isasegi *et al.* 2018), a recent study that used other specific markers for human TCA revealed that these projections approach the PSPB at an earlier stage of development as compared to what observed in rodents (i.e., 7.5 PCW) (Alzu'bi *et al.* 2019) (**Figure 1.14**). Considering that the cortical projecting neurons of layer 6 are produced in approximately 20 days starting from 7 PCW (Workman *et al.* 2013), it is unlikely that these axons reach the PSPB before the TCA at substantial level to guide them past this boundary, as is the case in rodents (Alzu'bi *et al.* 2019). This is also supported by a slightly asynchronous development of the thalamic and cortical neurons in primates. Differently from rodents, where they are generated at the same time (Shi *et al.* 2017), in the macaque brain the thalamic neurogenesis (E30-E45) (Spadory *et al.* 2022) precedes cortical neurogenesis (E45-E102, visual cortex) (Rakic 1974).

These observations highlight that in primate different relationship between TCA and CTA are established, and their "handshake" may occur at an earlier time point in primates, or in a different anatomical location, rather than at the PSPB (Alzu'bi *et al.* 2019).

Figure 1.14

Timeline of mouse and human earliest TCA

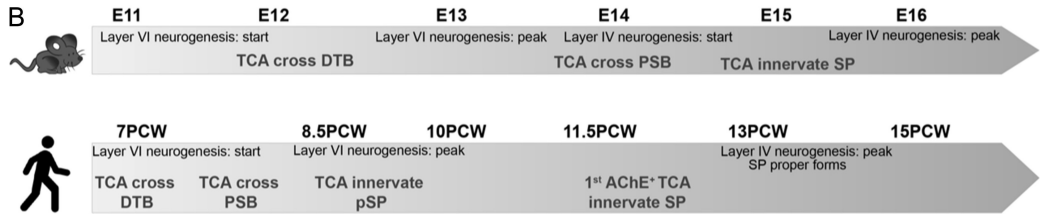

Figure 1.14: Comparison of timelines of development of TCA and neocortex in mouse and human
In mouse, layer 4 neurogenesis precedes the entry of thalamocortical afferents (TCA) into the cortex by three days. In human, thalamic fibres cross from the DTB to the PSB in 4-5 days compared with 2 days in mouse and invade the presubplate almost as soon as it is formed. This is contrast to previous studies which employed AChE histochemistry and suggested TCA join the subplate as it undergoes expansion at around 13 PCW.
Adapted and modified from Alzu'bi et al, 2019.

1.2.2 Dynamic functional interaction of eearly thalamic axons and the cortex

The first interaction between the pSP and the TCA occurs from the time of thalamocortical projections arrive to the cortex and the earliest thalamocortical synapses are forming (Kostovic *et al.* 1990; Bayatti *et al.* 2008; Harkin *et al.* 2017). Therefore, the first functional interaction between these axons and the cortex is in form of **spontaneous activity conveyed by thalamic neurons** throught the pSP to the CP (Moreno-Juan *et al.* 2017). Thalamocortical projections form functional synapses in subplate from the time of their arrival as demonstrated in thalamocortical slices (Higashi *et al.* 2002; Molnar *et al.* 2003). By conveying spontaneous activity from the thalamus to the cortex, early TCA aid their functional tuning and connection (Minlebaev *et al.* 2011; Moore *et al.* 2011). This could also influence the expression of genes governing cortical arealisation (Moreno-Juan *et al.* 2017). Given the earlier arrival of TCA in the human cortex (Alzu'bi *et al.* 2019) (**Figure 1.14**) and the extended human gestation time, this phenomenon might occur before and last longer in our species, thus possibly explaining the greater complexity of cortical arealisation achieved in human and monkey brains (Buckner *et al.* 2013; Mundinano *et al.* 2015; Clowry *et al.* 2018; Krubitzer *et al.* 2018).

The subplate, in turn, coordinates the entry of thalamic axons into the cortical plate (Ghosh *et al.* 1990; Allendoerfer *et al.* 1994; Kanold *et al.* 2010) (**Figure 1.15 A**). The transient circuitry established between SP neurons and TCA functions as a “bridge” guiding the proper and precise wiring between thalamic axons and layer 4 cortical neurons. The temporary circuits established between subplate neurons, thalamic afferents, and layer 4 neurons are now widely acknowledged as a critical mechanism for early circuit development (Kanold *et al.* 2010; Molnar *et al.* 2020). Furthermore, both spontaneous and synaptic activity established first within the subplate can regulate the production and secretion of growth factors, neurotransmitter, and the maintenance of gap junctions (Katz *et al.* 1996). Interestingly, the longer "waiting period" in primates and humans (Kostovic *et al.* 1990), increases the importance of these transient early connections in primates and human.

Starting from 22-24 PCW, spontaneous activity transients **shift from subplate to cortical plate activity** (Vanhatalo *et al.* 2005; Vanhatalo *et al.* 2006) (**Figure 1.15 B**). Since the shift between subplate and cortical plate activity occurs gradually, during the third trimester the thalamocortical afferents are involved in two co-existing cortical circuitries: a transient one with the subplate, and the nascent circuit connecting them with their permanent target in cortical plate (Takahashi *et al.* 2012; Judas *et al.* 2013; Kostovic *et al.* 2015; Krsnik *et al.* 2017) (**Figure 1.15 A**). The latter circuit represents the initial stage of the circuitry later maintained in the adult brain. Interestingly, the duration of the coexistence of the transient thalamo-subplate and permanent thalamo-cortical plate circuitries varies across cortical areas, with longer times observed in phylogenetically younger regions, such as the human associative prefrontal cortex, indicating a potentially extended time of refinement of cortical circuits in these areas (Anderson *et al.* 2014; Kostovic *et al.* 2014; Kostovic *et al.* 2014).

Figure 1.15

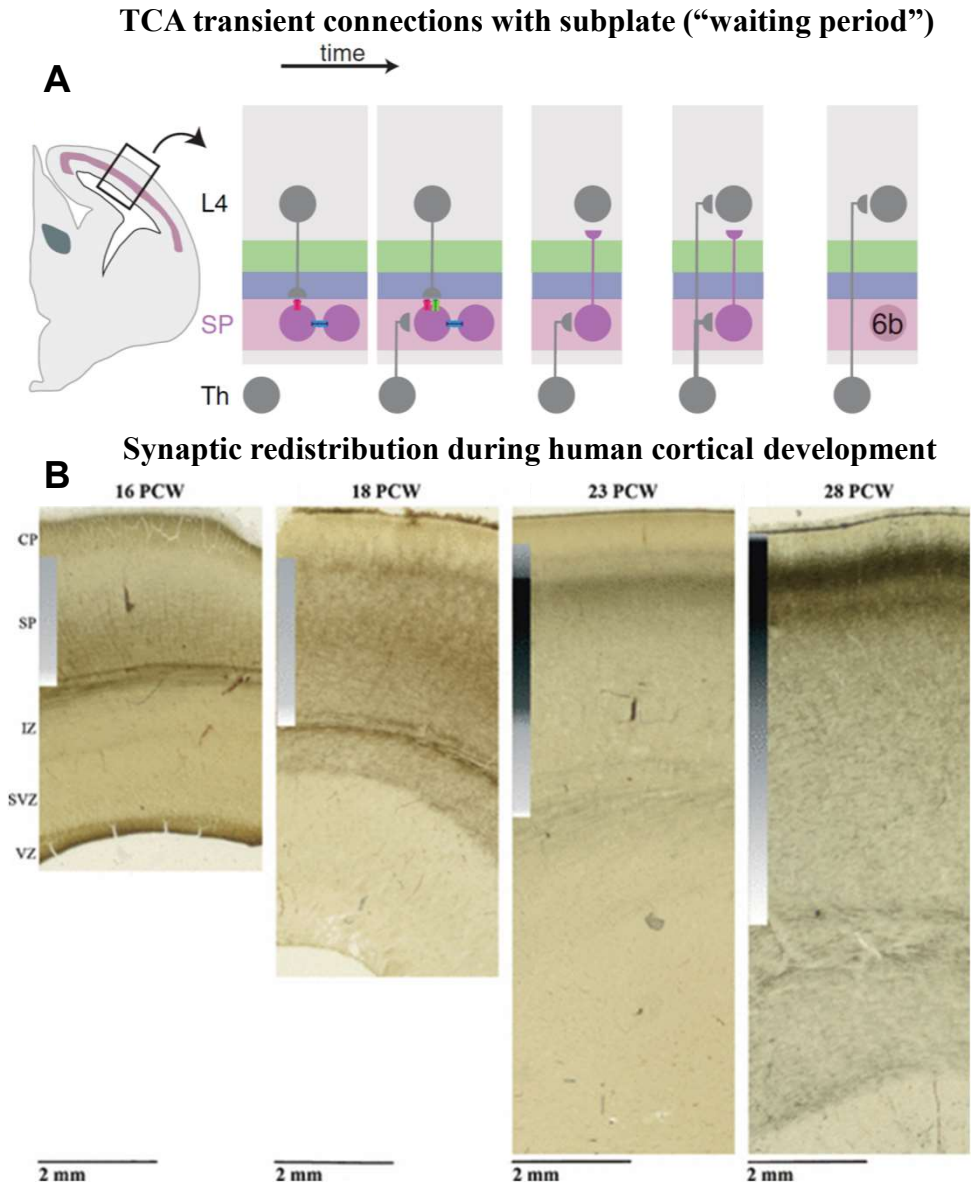

Figure 1.15: Synaptic redistribution to the cortical plate after the "waiting period" of thalamocortical axons withing the subplate in the human fetal cortex.
(**A**) Schematic representation of the dynamic interaction between the thalamic axons and the human developing cortex. Thalamocortical projections first establish synaptic connection with the mature subplate neurons, that act as a mediator for the formation of the permanent connection between these axons and their target cortical cells of layer 4. The two circuits co-exist for a transient period.
(B) Shows the same process by using acetylcholinesterase (AChE) immunohistochemistry to detect the thalamocortical projections (dark staining) and indicating the synaptic distribution in the inlets for each age analysed. Grey intensity is proportional to the number of synapses across the layers. Early thalamocortical fibres are observed in the subplate between 16 PCW and 18 PCW, they reach the upper subplate by 23 PCW and finally innervate the cortical plate at 28 PCW. Synaptic connections are present only in the SP until 24 PCW.
Adapted from Molnar et al., 2020 (A) and Kostovic et al., (B).

1.2.3 Interaction of thalamocortical axons and the cortical subventricular zone in primates

The interaction between thalamic axons and cortical progenitors has been explored in rodents. Gerstmann and colleagues showed that, thalamic axons directly contact the basal processes of RGC in the developing mouse cortex through ephrin A5 ligand interaction with its receptor EphA4, expressed in the RGC membrane (Gerstmann *et al.* 2015). This in turn regulate the division of RGC and the ultimate production of intermediate progenitor cells (IPC). Additionally, in mouse neuroactive molecules like VGF (non-acronymic) are specifically secreted from thalamic axonal terminals in the prospective cortical areas they innervate (Sato *et al.* 2012), and modulate their progenitors pool by paracrine mechanisms (Monko *et al.* 2022). However, studies in animal models did not address these phenomena in non-sensorial cortices, nor did they investigate specific progenitors of the OSVZ. The proximity between the TCA and the germinal zones is especially apparent in carnivores (Shatz *et al.* 1981) and primates, and in the human brain thalamic axons and OSVZ cells co-exist in an overlapping region referred to as multilaminar axonal-cell compartment (MACC) (Zunic Isasegi *et al.* 2018). Given the evolutionary changes in germinal compartments, their progenitor populations, and the distinct innervation patterns provided by early thalamocortical axons, it is plausible to hypothesize that the impact of thalamic axons on cortical development could be more substantial in larger and evolved brains. The drastic changes in cell numbers and brain folding after early enucleation in gyrencephalic species (macaque and ferret) further supports this hypothesis (Rakic 1988; Reillo *et al.* 2011) (**Figure 1.16**). Thalamic axons influence the physical scaffold created by the progenitors of the OSVZ and affect the formation of cortical folds in the gyrencephalic ferret (Reillo *et al.* 2011). On the other hand, in the primate brain, the reduction of thalamic axons after enucleation directly affects the mitotic rate of OSVZ progenitor cells, and the formation of proper areal boundary between adjacent V1 and V2 cortices (Smart *et al.* 2002). Interestingly, observation, mitotic rates of human progenitor cells in the OSVZ specifically correlate with tangential expansion of the cortical areas and subsequent folding of the cortex (Reillo *et al.* 2011) (**Figure 1.17**), providing a strong evidence of the potential involvement of thalamic axons in mediating this phenomenon.

Figure 1.16

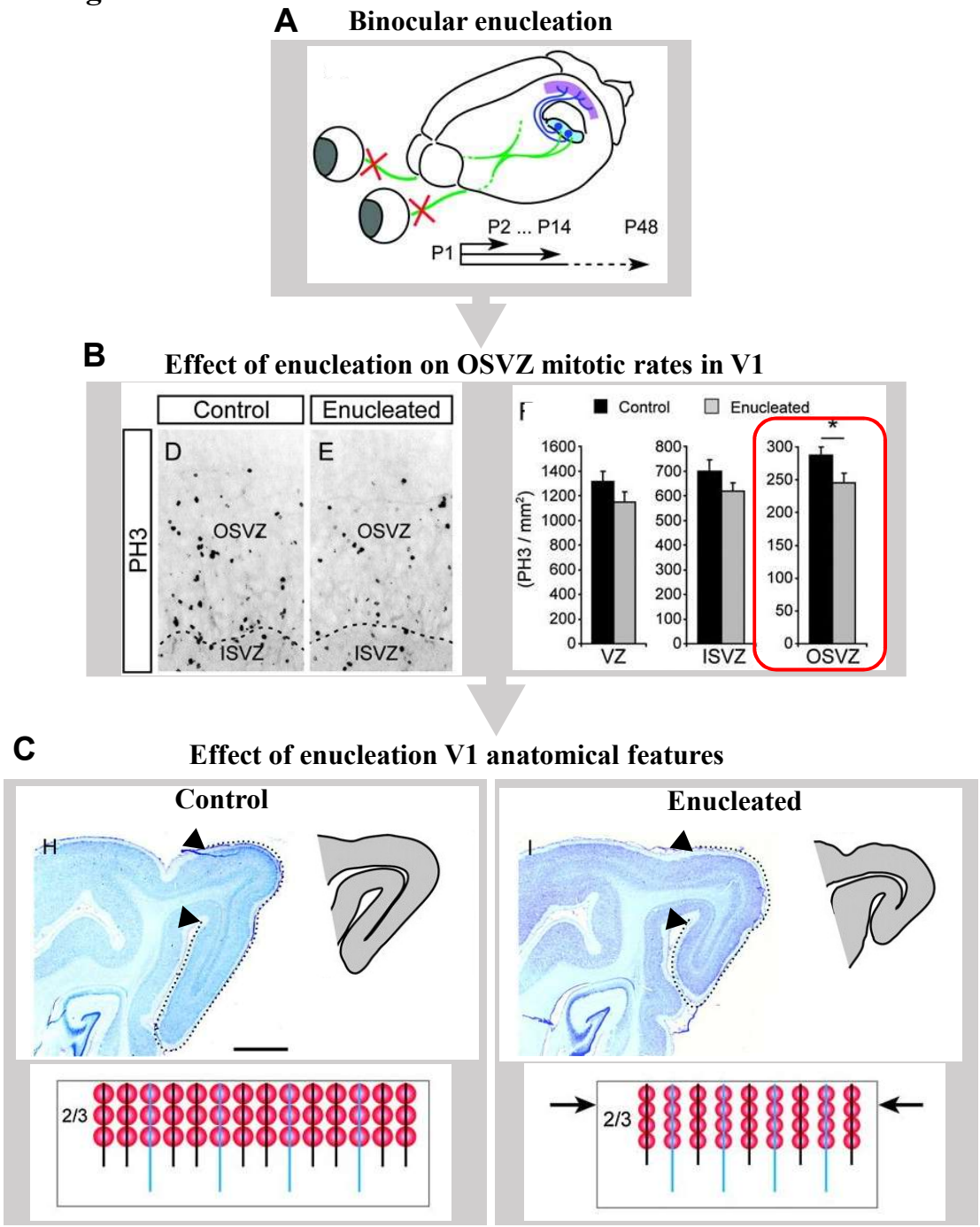

Figure 1.16: Effects of binocular enucleation on OSVZ proliferation and cortical expansion in ferret primary visual cortex.

(**A**) Schematic of the experimental design. Binocular enucleation at P1 results in degeneration of retinal axons (green) projecting to the LGN (blue), which itself projects to the primary visual cortex (purple). Animals were analyzed at various postnatal ages. (**B**) Immunohistochemical analysis of proliferation rates by mitotic marker phospho-histone 3 (PH3) in the prospective V1 cortex (area A17) of control and enucleated ferrets at P2 reveals a specific reduction of mitotic figures within the OSVZ. **(C)** The alteration at the level of the OSVZ observed in the enucleated animals leads to a significant anatomical rearrangement of the primary visual cortex, as shown by Nissl staining of sagittal section at the level of the occipital pole performed postnatally (P48). Dotted line and arrowheads show the borders of area A17, and highlight the reduced tangential expansion of the cortex at this level upon enucleation. The schematics at the bottom summarize the underlying mechanisms: even though the radial units form properly, their tangential expansion is impaired, suggesting that the OSVZ progenitors are necessary for the proper migration of neurons and ultimately the tangential expansion of cortical areas observed in gyrencephalic brains. *P < 0.05, t-test. Scale bar= 2mm.

Adopted and modified from Reilllo et al., 2011.

Figure 1.17

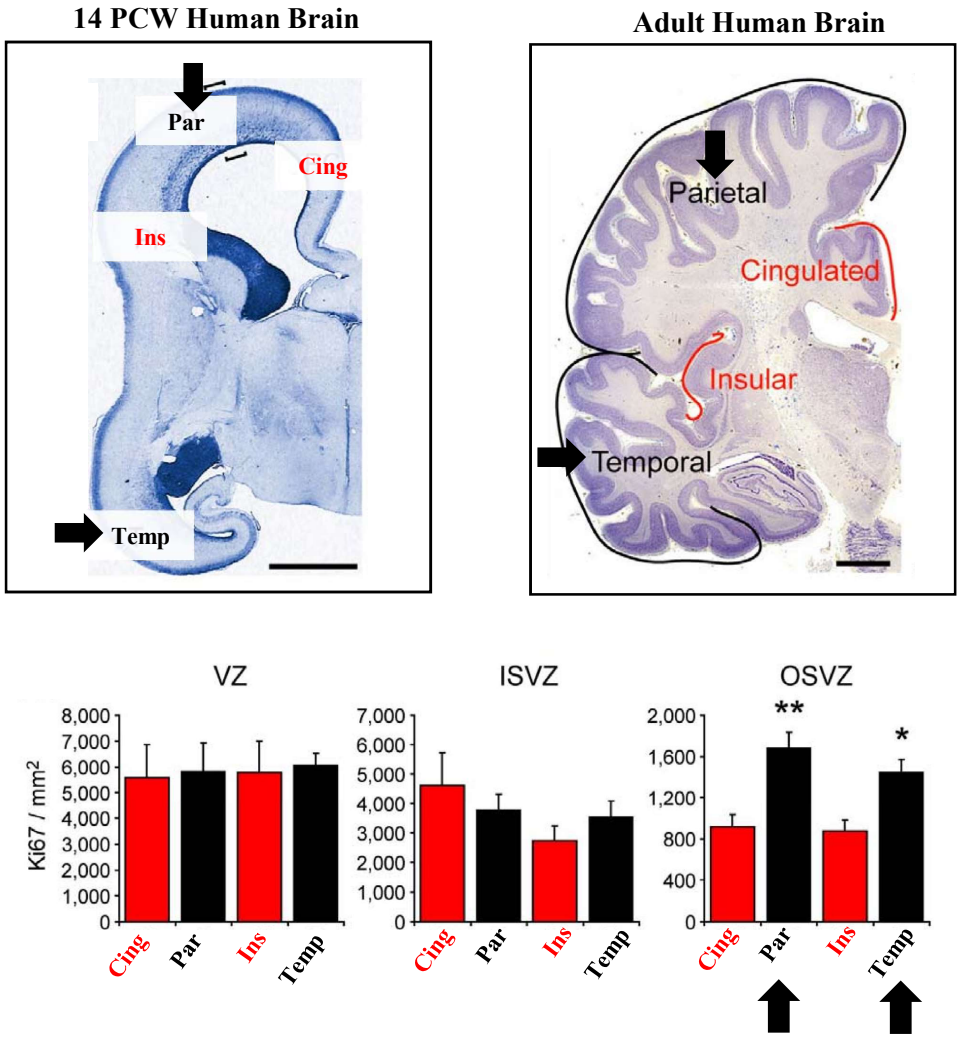

Figure 1.17: Tangential expansion of cortical areas in the human brain depends on mitotic rates within the OSVZ specifically during cortical development.
(**A**) Nissl staining of a 14 PCW (left) and an adult (right) human brain coronal sections, showing the relatively greater expansion of specific cortical areas (i.e., parietal and temporal) as compared to others (i.e., cingulated and insular). (B) Measuring proliferation rates in the germinal compartments of the human fetal brain by detection of Ki67-positive cells reveals a significantly higher number of mitoses within the parietal and temporal cortices which is restricted to the OSVZ, with no relevant differences in the other cortical areas, nor in the inner proliferative compartments (i.e., the ISVZ and the VZ). This suggest a specific role of the OSVZ in the tangential expansion and folding of cortical areas in the human brain.
Adopted and modified from Reilllo et al., 2011 (Supplementary Materials).

1.2.4 Relevance of early thalamic axons in human cortical evolution and pathologies

As previously mentioned, studies in animal models have mostly focused in the specification of primary sensory cortices, where the thalamus primarily drives the development and maturation of layer 4 neurons. In other systems, such as the prefrontal cortex (PFC), the earliest projections from the thalamic mediodorsal nucleus (MD) interact and drive maturation of layer 3 rather than layer 4 (Leonard 1969; Krettek *et al.* 1977), thus potentially influencing the developmental programmes in a different manner. Upper layer neurons (layer 2/3) are generated from OSVZ neurogenesis (Zecevic *et al.* 2011; Malik *et al.* 2013), have larger soma and greater number of dendritic spines in human (Elston *et al.* 2005), and they are crucially involved in higher brain functions in humans (Rakic 2009) (**Figure 1.3**). As the development and maturation of the PFC is prolonged as compared to other brain areas, an even finer and more complex modulation of corticogenesis by the thalamic axons might take place, underlying the mechanisms of human PFC evolution and expansion. On the other hand, these same characteristics also renders the PFC more susceptible to dysregulation and insults, as evidenced in neurodevelopmental conditions that notoriously impact the prefrontal associative circuits and synaptic maturation of cortical neurons of this area, such as autism and schizophrenia (Wible *et al.* 2001; Salgado-Pineda *et al.* 2007; Selemon *et al.* 2015; Ouhaz *et al.* 2018).

The clinical relevance of early TCA in these conditions may have been underestimated due to the predominant focus on sensory systems in rodent studies. Understanding the role of TCA in the early development of the human cortices is crucial, as it holds potential implications for both unique human brain function, as well as specific neuropsychiatric disorders. Evidence already showed structural and functional alteration of associative thalamic nuclei in patients with psychotic disorders before the onset of the symptoms (Andreasen 1997; Ferrarelli *et al.* 2011; Woodward *et al.* 2012; Anticevic *et al.* 2014; Dorph-Petersen *et al.* 2017; Ramsay 2019; Steullet 2020). Similarly, a reduction of MD activity during early developmental stages might cause a decrease in synaptic density in the PFC of schizophrenic patients (Zipursky *et al.* 1992; Schlaepfer *et al.* 1994; Minzenberg *et al.* 2012). These observations strongly suggest a role of altered or abnormal thalamic connections to the prefrontal cortex in the aetiology of these conditions.

1.3 VGF AS A THALAMIC MODULATOR OF CORTICAL DEVELOPMENT

Previous literature suggests VGF as a candidate thalamic factor that might account for the simultaneous interaction with both progenitor cells (Monko *et al.* 2022) and post-mitotic cortical neurons (Sato *et al.* 2012), and the data presented in this Thesis will further corroborate these observation in human (Bandiera 2022).

1.3.1 VGF: expression, transport, and functional effects

The neurosecretory protein VGF (non-acronymic), also known as secretogranin VII, is a member of the extended granin family of neuropeptides (Helle 2004; Bartolomucci *et al.* 2011). These proteins are all involved in the regulated secretory pathway delivering peptides, hormones, neurotransmitters, and growth factors in a controlled fashion. Human VGF is encoded by a simple-structured gene in chromosome 7q22, containing two intronic regions and one exon coding for the full-length protein (615 amino acids) (Salton 1991; Canu *et al.* 1997). VGF is a well conserved molecule, sharing 84.33% homology with the full-sized murine VGF (617 amino acids) (Levi *et al.* 2004) (**Figure 1.18 A**). VGF was first identified as a nerve growth factor (NGF)-inducible gene (Levi *et al.* 1985). Later, it was recognized that the expression of VGF is also promoted by other neurotrophins, especially brain-derived neurotrophic factor (BDNF), and neurotrophin 3 (NT3) (Salton 1991; Salton *et al.* 1991; Hawley *et al.* 1992; Bonni *et al.* 1995; Ferri *et al.* 1996; Alder *et al.* 2003).

VGF protein is produced in the endoplasmic reticulum, and it is routed to the secretory pathway by its signal peptide ($VGF_{1–22}$) (Garcia *et al.* 2005), where it is inserted in large dense core vesicles (LDCV) (Possenti *et al.* 1989; Trani *et al.* 2002; Merighi 2018). LDCV also contain enzymes such as members of the prohormone convertase (PC) family that process the precursor protein, thus generating a plethora of biologically active VGF peptides upon maturation of the vesicles (Trani *et al.* 1995; Seidah *et al.* 1999; Bartolomucci *et al.* 2011) (**Figure 1.18 B**). This occurs while the granules are being transported in the cell body and dendrites, and axonal terminals (Levi *et al.* 2004). Secretion of the granules containing VGF occurs in an activity-dependent manner by depolarization

of the neurons (Possenti *et al.* 1989; Salton *et al.* 1991). Once in the extracellular space, both VGF and its derived peptides engage receptors on the cell body, setting off a cascade of intracellular action potentials. This in turn prompts a rapid synthesis of VGF mRNA, effectively replenishing the levels of intracellular VGF protein (Levi *et al.* 2004; Severini *et al.* 2008; Fargali *et al.* 2014; Leal *et al.* 2017; Quinn *et al.* 2021).

VGF-derived peptides

As previously mentioned, VGF is processed into at least **12 neuroactive peptides** (Ferri *et al.* 1996; Salton *et al.* 2000; Quinn *et al.* 2021) (**Figure 1.18 A**), which are well conserved across species (Bartolomucci *et al.* 2011). These can be broadly classified as N-terminal endocrine and C-terminal neuroactive peptides. Interesting, in the adult human brain, C-terminal VGF-peptides were detected more extensively than the N-terminal ones (Cocco *et al.* 2010). Amongst the latters, some noteworthy examples are particularly relevant in the context of neurodevelopment, such as **TLPQ-62** (human $VGF_{554-615}$) that can act in an autocrine, endocrine, or paracrine fashion and promotes neurogenesis and synapse formation and maturation via calcium-mediated modulation of gene expression (Thakker-Varia *et al.* 2014; Lin *et al.* 2015; Behnke *et al.* 2017). **AQEE-30** has also been shown to trigger a positive feedback loop, leading to augmented BDNF and VGF transcription and synaptic plasticity (Hunsberger *et al.* 2007).

Figure 1.18

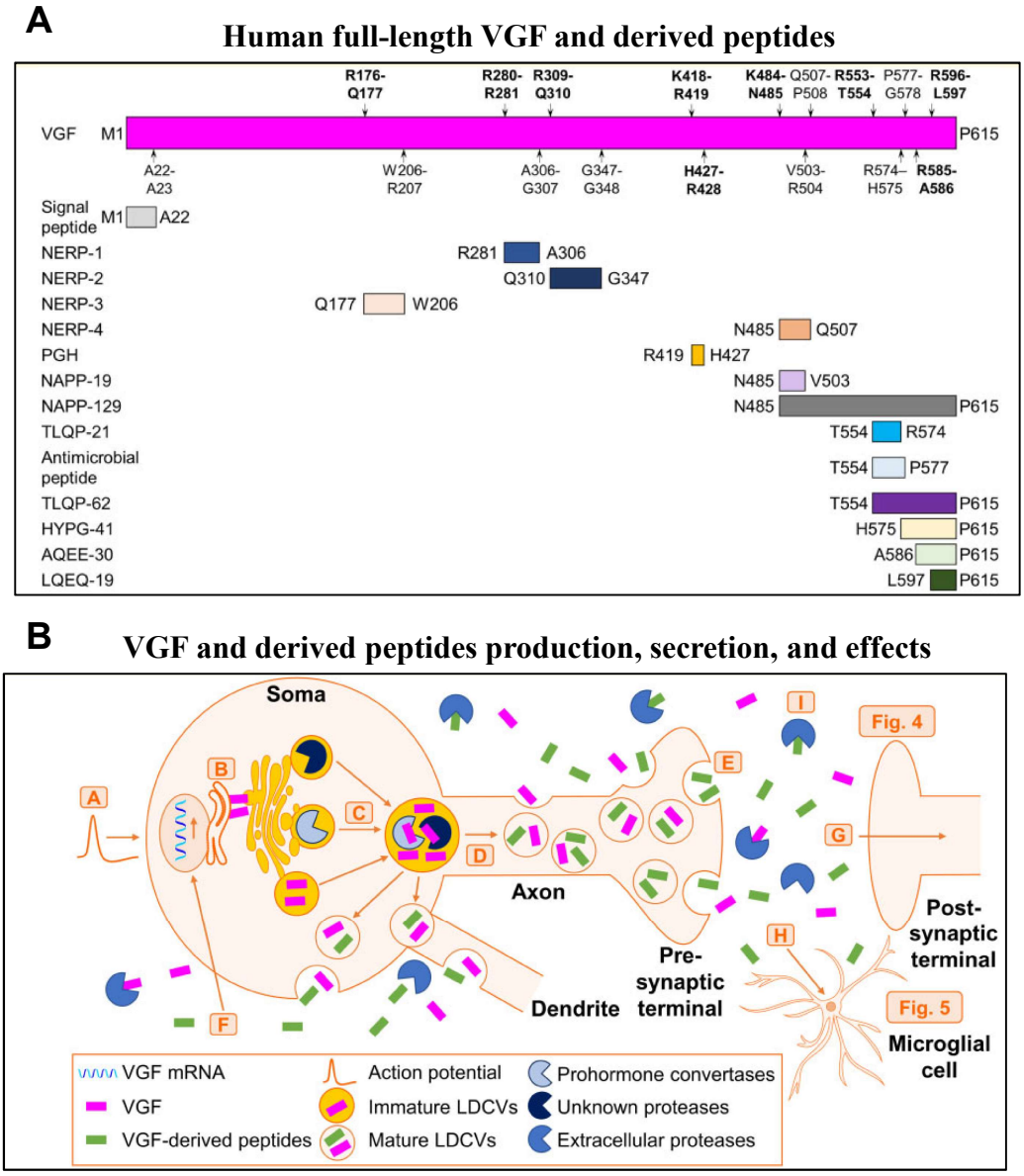

Figure 1.18: Human full-length VGF (615 amino acids) and derived peptides.
(**A**) Schematic representation of human VGF 1-615 showing the known sites of proteolytic processing, indicating the N- and C-terminal amino acid of each derived peptide. In bold are indicated the putative cleavage sites for prohormone convertases (PC), whereas the other cleavage sites are created by unknown proteases. (**B**) Schematic illustration of VGF regulated processing, secretion, and the resulting effects on microglia and neurons. VGF mRNA expression is induced by neuronal activity, neurotrophins (i.e. NGF, BDNF, NT3), as well as other factors. BFG is produced in the endoplasmic reticulum (ER) and included in large dense core vesicles (LDCV). Upon maturation of the secretory granules, VGF is processed into neuroactive peptides by intracellular enzymes, as well as extracellular proteases upon secretion. VGF is released in an activity-dependent manner, and it activates receptors in microglia and post-synaptic neurons (paracrine) as well as within the same cell secreting it (autocrine).
Adapted from Quinn et al., 2021.

VGF receptors and roles in neurophysiology

The specific receptors that full-length VGF binds have not been identified. Conversely, information has been gathered regarding some of its peptides. Specifically, TLQP-62 can activate neuronal N-methyl-D-aspartate glutamate receptor (NMDAR) and metabotropic glutamate receptor 5 (mGluR5) (Thakker-Varia *et al.* 2007), as well as BDNF/NT-3 growth factors receptor Tropomyosin kinase B (TrkB) (Thakker-Varia *et al.* 2007; Lin *et al.* 2015). Via activation of these receptors, TLQP-62 increases glutamatergic and BDNF signalling resulting in enhanced hippocampal neurogenesis, synaptogenesis and memory formation (Fred *et al.* 2019; Jiang *et al.* 2019). The ability TLQP-62 of increasing neural precursors division observed in the hippocampus (Thakker-Varia *et al.* 2014) will be extremely relevant in the context of my Thesis, as I hypothesise that VGF and its peptides might have a similar effect on cortical progenitors.

Three main receptors have been identified also for TLQP-21: microglial complement 3a receptor 1 (C3aR1) (Hannedouche *et al.* 2013; Cero *et al.* 2014; El Gaamouch *et al.* 2020), globular head of complement component 1q receptor (gC1qR) (Chen *et al.* 2013), and heat shock protein family A member 8 (HSPA8) (Akhter *et al.* 2017). Specifically, activation of C3aR1 by TLQP-21 promotes microglia chemotaxis and phagocytic activity in mouse (Elmadany *et al.* 2020), and to lower extent in human (Li *et al.* 2023). TLPQ-21 has also promotes neuronal survival via activation of HSPA8 (Severini *et al.* 2008; Akhter *et al.* 2017).

VGF in human neuropathologies

In line with their physiological role, VGF and VGF-derived peptides have been consistently identified as dysregulated in neurodegenerative and neurodevelopmental diseases in human. For instance, VGF has been identified as a key driver of Alzheimer's Disease (AD) in a causal, objective, and data-driven manner (Beckmann *et al.* 2020), alongside proteomic studies (Bai *et al.* 2020; Pedrero-Prieto *et al.* 2020; Quinn *et al.* 2023). Altered levels of VGF-derived peptides have been also reported in other neurodegenerative conditions (Ruetschi *et al.* 2005; Noda *et al.* 2015; Noda *et al.* 2020; Rajkumar *et al.* 2020), supporting the observation of a crucial role of VGF and derived peptides in the neuronal generation and survival in physiological contexts.

Altered levels of VGF and VGF-derived peptides have been reported in neurodevelopmental conditions (Bartolomucci *et al.* 2011). VGF-immunoreactive hypothalamic neurons are reduced in *post mortem* brains of ***schizophrenic*** patients as compared to controls (Busse *et al.* 2012), and a specific VGF-derived peptide, APPG-40 ($VGF_{23–62}$), has been identified as a promising and specific CSF biomarker for first-onset drug-naive schizophrenia (Huang *et al.* 2006; Huang *et al.* 2007). VGF mRNA levels appeared significantly reduced also in the hippocampus and the dorsolateral prefrontal cortex of patients with ***bipolar disorder*** (BD) (Thakker-Varia *et al.* 2010). In line with these findings, VGF-mutant mouse models show ***depression***-like phenotypes (Thakker-Varia *et al.* 2007; Bozdagi *et al.* 2008; Jiang *et al.* 2019; Mizoguchi *et al.* 2019). Nevertheless, the specific mechanisms the specific mechanisms behind VGF dysregulation in these conditions to be elucidated.

Consistently, VGF and its peptides have been proposed as novel therapeutic agents, due to their emerging neuroprotective effects as well as anti-depressive properties (Hunsberger *et al.* 2007; Noda *et al.* 2015; Li *et al.* 2017; Akhter *et al.* 2018; Beckmann *et al.* 2020; El Gaamouch *et al.* 2020; Elmadany *et al.* 2020).

1.3.2 VGF expression pattern and role in the thalamocortical system

In the post-natal and adult human brain, VGF expression can be detected in both GABAergic and glutamatergic neurons throughout the cortex, the latter being located in the deep layers (Quinn *et al.* 2021). At regional level, the human hypothalamus is the region with the greatest VGF expression levels (Quinn *et al.* 2021). Within the cerebral cortex, VGF expression is high in the medial frontal gyrus, inferior frontal gyrus, inferior temporal gyrus, postcentral gyrus, and throughout the associative areas of the parietal and temporal cortices and the angular gyrus (Quinn *et al.* 2021), Unfortunately, mRNA analysis cannot provide any information regarding the regional and cellular distribution of VGF-peptides, that share the same transcript as the full-length protein.

Despite the information available on VGF expression pattern in the adult brain, much less is known about this molecule during development. Evidence shows that VGF expression is developmentally regulated, and therefore the findings obtained from adult stages cannot be readily extrapolated to developmental periods. Early studies using *in situ* hybridization, Western Blot and immunohistochemical analysis in the visual system of rats from prenatal developmental (E11) to adulthood (Lombardo *et al.* 1995). mRNA and protein showed a peak of expression in the visual thalamic dorsolateral geniculate nucleus (dLGN) between E16-18, respectively, to the first two post-natal weeks, a specific time window that coincides with the critical period in the rat visual cortex. Notably, a concomitant robust and transient VGF-positive signal was detected at protein level within the subplate at E18, indicating that the thalamic axons arrived in the cortex and transported the protein to their terminals. At the end of the critical period, the levels of VGF started decreasing and remained low in the adult rat brain. This pivotal study suggested for the first time a potential involvement of VGF of synaptogenesis and/or synaptic stabilization in the developing thalamocortical connections in the rodent visual system. However, at the time the function of the protein was not elucidated, nor was tested in this specific work.

Later, Sato and colleagues identified VGF as a promising candidate molecule mediating thalamic extrinsic modulation of the maturation of primary sensorial cortices in mouse (Sato *et al.* 2012) (**Figure 1.19**). Besides confirming VGF specific expression pattern in the sensorial thalamus (i.e.

ventrobasal (VB) and dorsolateral geniculate (dLG) nuclei) of the mouse during the establishment of thalamocortical connections (E18-P14), they employed an *in vitro* approach to test the functional effects of this factor. Specifically, they showed that VGF was able to induce maturation of stellate neurons of cortical layer 4 by promoting their dendritic arborization in a cell-specific manner (Sato *et al.* 2012) (**Figure 1.20 B**). The same group recently confirmed these results *in vivo* for VGF and showed that this paracrine mechanism is involved in the thalamic extrinsic modulation of the development of the somatosensory cortex in mouse (Sato *et al.* 2022) (**Figures 1.20 B**). An independent group tested the effects of thalamic VGF at earlier stages of cortical development at embryonic stages in mouse (Monko *et al.* 2022) (**Figure 1.20 A**). By analysing the effect of thalamus specific Vgf conditional knockout (cKO) they revealed that this factor was crucial for the generation of layer 4 neurons, which occurs at E14 in the mouse cortex. However, as the total number of both RGC and IPC was not altered, the authors concluded that VGF did not affect the progenitor population dynamics, but was rather involved in their fate commitment toward RORβ-expressing lineage of thalamocortical recipient cells destined to form cortical layer 4 (Monko *et al.* 2022). Overall, these studies suggested that thalamic VGF is involved in the acquisition of cortical areal features in the primary sensorial systems in rodents via promotion of cortical layer 4 neuron generation and functional maturation (Sato *et al.* 2012; Monko *et al.* 2022; Sato *et al.* 2022).

Nevertheless, none of these observations have been confirmed in the human developing brain. Furthermore, these studies showed a restricted and specific role of VGF in the development of primary sensorial cortices. Finally, the specific effects of thalamic VGF on either cortical subplate neurons or outer RGC were assessed. Considering that these cell populations are the most exposed to paracrine molecules secrete by thalamic axons in the human brain, as described in the previous sections of the Chapter, it would be important to establish the potential effects of VGF in these cortical cells in the human developing brain.

Figure 1.20

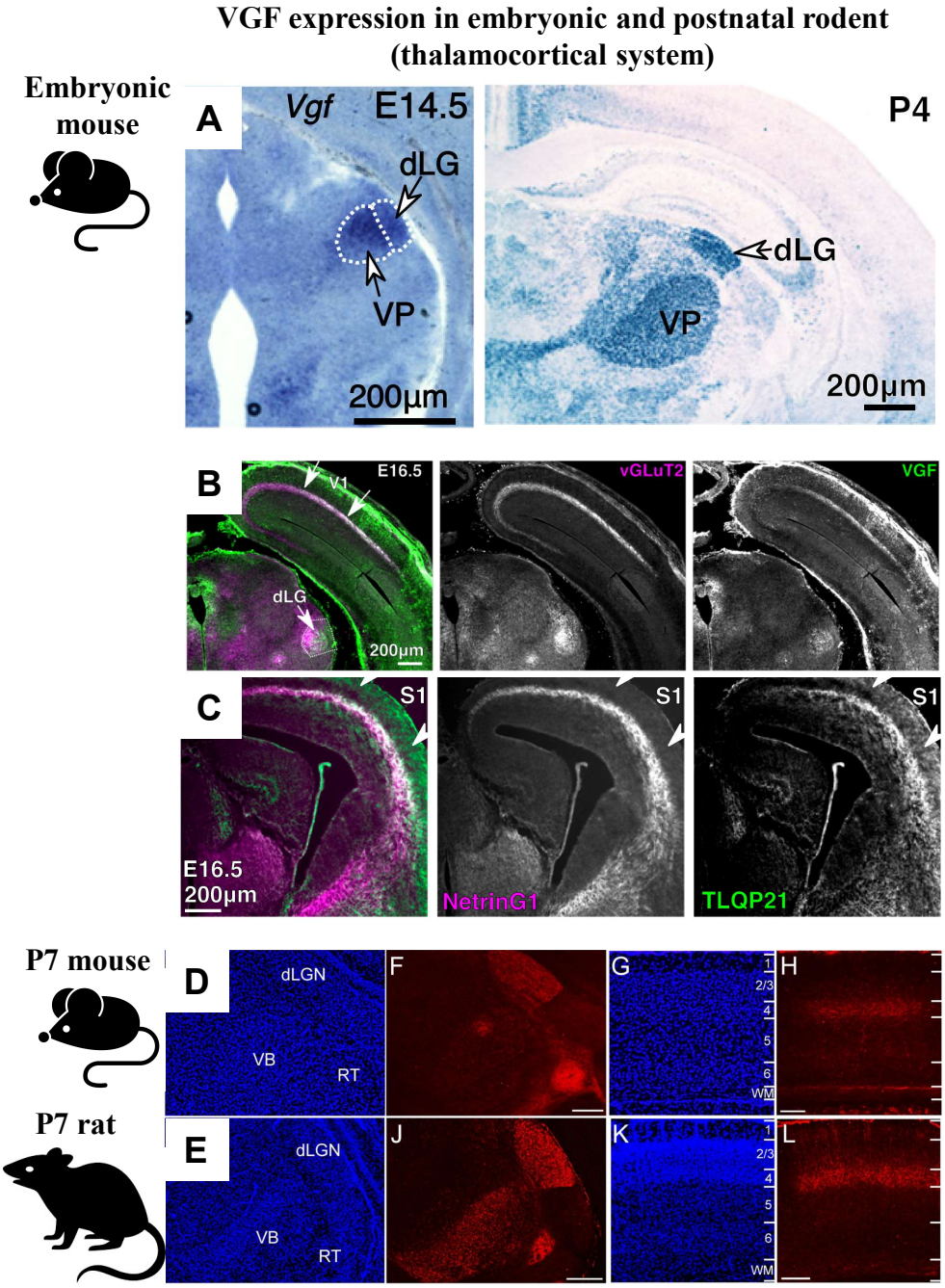

Figure 1.19: VGF is specifically expressed by sensory thalamic nuclei in the prenatal and postnatal rodent brain, and it is detected in layer 4 for primary sensory cortices where it is transported and secreted by thalamocortical afferents (TCA).
(**A**) *In situ* hybridazion for VGF mRNA in E14.5 and P4 mouse brain show specific expression in the sensorial thalamic nuclei (dorsolateral geniculate,dLG and ventrobasal, VB). (**B, C**) Immunofluorescence staining show both VGF and VGF-derived TLQP-21 peptide in the E16.5 somatosensory cortex (S1) where it is transported by TCA stained specifically by vGlut2 (B) and NetrinG1 (C). (**D, E**) A similar VGF protein protein distribution was detected in the postnatal mouse (D) and rat (E) brain (red). VGF is detected specifically in layer 4 of S1. DAPI counterstaining is used to reveal thalamic nuclei and cortical layers. Scale bar = 500 µm (thalamus) and 200 µm (cortex).
Adopted and modified from Monko et al., 2022 (A-C) and Sato et al., 2012 (D-E).

Figure 1.20

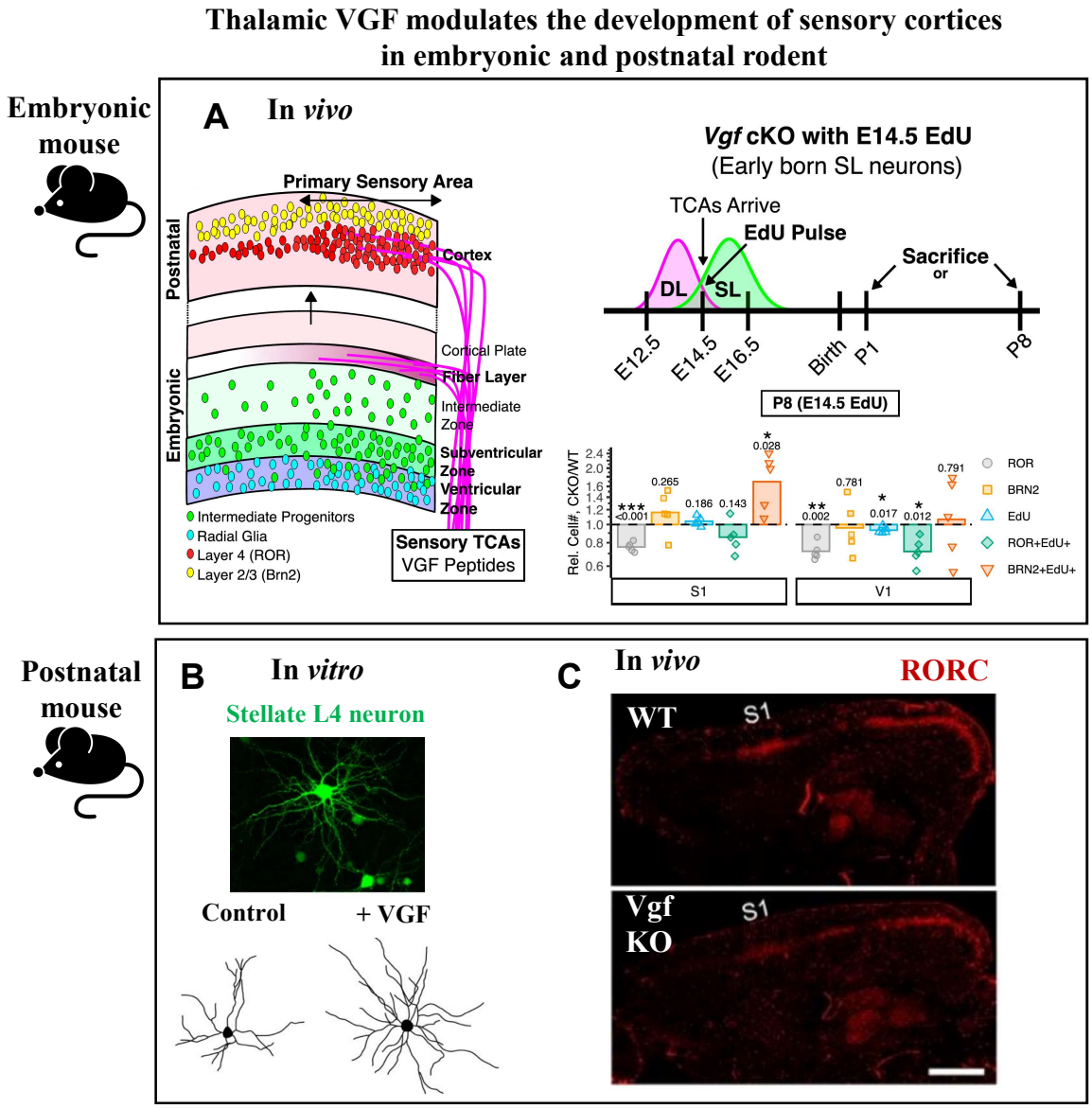

Figure 1.20: Thalamic VGF mediates the extrinsic modulation of sensorial cortices in rodents by affecting their progenitor cells prenatally and layer 4 neuron maturation postnatally.
(**A**) Schematics of the hypothesis tested by Monko and colleagues where thalamic VGF is transported by the early TCA in the embryonic prospective sensorial cortices in mouse and it modulates their areal identity early during development. TCA arrive at the time of switch between deeper and upper layer neurogenesis, and by secreting VGF they modulate progenitor cell fate commitment toward generation of layer 4 neurons (ROR-positive) and against upper layer neurogenesis (Brn2-positive cells). This is selectively impaired by knock-out of VGF at embryonic stages (left). (**B**) Exogenous application of VGF promote layer 4 stellate neuron dendritic arborization and growth in a cell-specific manner in organotypic cortical slices from P1 mouse brain. (**C**) Sagittal sections of P7 wild-type (upper) and VGF-KO (lower) primary somatosensory cortex (S1) srained by layer 4 neuronal marker RORC show a significant reduction of the thalamocortical recipient layer in the mutant mice, confirming the role of thalamic VGF in the proper acquisition of this characteristic feature of sensorial cortices in rodents. Scale bar = 1mm.
Adopted and modified from Monko et al., 2022 (A), Sato et al., 2012 (B), and Sato et al., 2022 (C).

1.3.3 VGF processing enzymes

The full array of enzymes capable of processing VGF into peptides remains incompletely characterized. Most evidence suggest that **pro-hormone convertases** (PC, also referred to as proprotein convertases and PCSK) are involved in its cleavage (Ferri *et al.* 1996; Trani *et al.* 2002; Levi *et al.* 2004; Garcia *et al.* 2005; Pan *et al.* 2005; Bartolomucci *et al.* 2006; Pan *et al.* 2006; Mishiro-Sato *et al.* 2010). Interestingly, these proteases are also responsible for processing BDNF (Rouille *et al.* 1995; Bathina *et al.* 2015). However, the role of the pro-hormone convertases on human VGF processing is largely unexplored. Other proteases have also been predicted to cleave VGF (Wegrzyn *et al.* 2010), including calpains, metalloproteases, and cathepsins. However, to date only calpain 1 and cathepsin S have been tested experimentally on human VGF (Quinn *et al.* 2023). In the context of this Thesis, calpain and cathepsins will be further analysed as promising predicted VGF cleaving enzymes.

Calpains, a calcium-dependent cysteine protease superfamily, engage in diverse physiological processes, spanning embryogenesis, differentiation, apoptosis, cytoskeletal remodelling, and neuronal modulation (Liu *et al.* 2019). Their roles extend to synaptic plasticity, neuronal activity, and cerebellar development (Leclerc *et al.* 2012; Baudry *et al.* 2015; Wang *et al.* 2016). Notably, calpain-triggered calcium signalling exhibits neuroprotective effects (Wang *et al.* 2013; Baudry *et al.* 2016), whereas overactivation has opposite effects (Li *et al.* 2017). Classic calpains, including human calpain 1 and 2 (CAPN1 and CAPN2, or μ- and m-calpain), form heterodimers with unique large subunits and common small subunits (Sorimachi *et al.* 2011), and are extensively studied (Li *et al.* 2017). Human calpains show notable homology across species (Velez *et al.* 2020).

Cathepsins are mainly found in acidic endo/lysosomal compartments, and fulfil diverse functions (Yadati *et al.* 2020). Thy are classified according to their active site's amino acid into metallo, serine, threonine, aspartic, and cysteine proteases. Cathepsin B (CTSB), a cysteine protease, has roles in both neurophysiological and neuropathological processes, including activity-dependent neurite and spine outgrowth (Goo *et al.* 2017; Padamsey *et al.* 2017; Tran et al., 2018; Jiang *et al.* 2020), and promotion of synaptic plasticity (Tran *et al.* 2021). Cathepsin D (CTSD), an aspartic

protease, is highly expressed in the brain (Patel *et al.* 2018), and is significantly increased in the brain of patients with autism (Sheikh *et al.* 2010). Interestingly, the "calpain–cathepsin hypothesis" suggests a coordinated dysregulation of calpain 1 and cathepsin B, implicating them in neurodegeneration in Alzheimer's disease and related dementia (ADRD) (Yamashima 2016; Knopp *et al.* 2021). This further support the evidence of a crucial role played by these families of enzymes in neuronal physiology, survival, and eventually pathological state.

In conclusion, neurosecretory protein VGF has been identified as a crucial factor in several physiological and pathological processes associated with neural development. In particular, evidence suggest that in the human brain its role in thalamocortical system might go beyond what observed in animal models, and further investigation on its expression pattern, molecular pathways, enzymatic processing, and cell-specific effects should be done in human brain development.

RATIONALE AND AIMS OF THE STUDY

The extent of the extrinsic modulation exerted by area-specific thalamocortical projections on the regionalisation of the developing cortex might be especially relevant in primate, especially in human cerebral cortex, where: (1) TCA involvement might go beyond the specification of sensory vs non-sensory areas, which has been the focus in rodent studies; (2) Gestational period and cortical neurogenesis are more protracted, possibly leading to a more extensive modulation of intrinsic programmes by TCA; (3) transient cortical layers involved are massively expanded, and might be associated with human higher cognitive abilities as well as human neurodevelopmental disorder (i.e. schizophrenia, autism).

In support of this hypothesis, the two cortical transient compartments directly adjacent to the early arriving thalamocortical axons within the human brain, namely the subplate and the outer subventricular zone (SP and OSVZ), undergo significant expansion in concomitance with the arrival of these axons at mid-gestation. This, coupled with their distinctive specialization, correlates with the acquisition of critical cortical features of the human cerebral cortex, including the tangential expansion of the cortical plate, subsequent folding, and the later disproportionate growth of the supragranular layers (layers 2/3) involved in cortico-cortical connections. Compelling evidence also arises from pathological conditions, indicating that disruptions in neurodevelopment can stem from dysregulation in both the subplate and the OSVZ, as well as defects in the appropriate establishment of thalamocortical connectivity.

Various potential mechanisms through which thalamic axons can exert substantial influence on the cortical cell populating the subplate and the OSVZ have been identified. Amongst these, the activity-dependent secretion of paracrine factor VGF into the extracellular space by TCA has been identified as a promising mechanism to investigate in the context of thalamocortical system development (Sato *et al.* 2012; Monko *et al.* 2022; Sato *et al.* 2022). In rodent, it serves as a pivotal mediator for thalamic extrinsic modulation of the development of the primary sensory cortices at

embryonic and post-natal stages. However, the expression pattern of VGF and its role in the development of the thalamocortical system have yet to be explored in humans, where evidences suggest its influence potentially extends beyond the sensory systems. This aligns perfectly with the differences in the developmental patterns characterizing the development of the human cerebral cortex described so far.

With this in mind, I sought to investigate the dynamic interactions between the early thalamocortical projections and the developing human cortex. Specifically, I set out to identify the earliest cortical compartments involved in these events, as well as their cellular population targeted by the early TCA. Furthermore, I tried to explore the potential molecular mechanisms through which the interaction with these cortical cell population might occur, focusing on the secreted paracrine molecule VGF. I assessed its expression pattern and protein distribution in the human fetal brain, and I started explored the potential molecular processes occurring upon its secretion in the developing cortex. My main hypotheses are:

1. Thalamic axons interact with both post-mitotic and germinal cortical compartments in the human brain
2. Thalamic VGF mediates the interaction between thalamic axons and these different cortical cell populations, possibly by means of distinct neuroactive peptides
3. The conserved VGF molecule has undergone a repurposing over evolution to serve its pivotal role in cortical development of evolved associative areas in the human brain

CHAPTER 2

Material and Methods

2.1 HUMAN BRAIN SAMPLES

2.1.1 Human fetal brain specimens

Human fetal tissue from terminated pregnancies was provided by the joint MRC/Wellcome Trust-funded Human Developmental Biology Resource (HDBR), University of Newcastle according to the material transfer agreement issued with the Molnár Laboratory, Department of Physiology, Anatomy and Genetics, University of Oxford (NU-008095). The samples received from the HDBR and used for this study are listed in **Table 2.1**. All tissue was collected with appropriate maternal consent and approval from the Newcastle and North Tyneside NHS Health Authority Joint Ethics Committee. The brains were dissected and some of them was immersion fixed in 4% paraformaldehyde (PFA in 0.1 M PBS) for at least 24 hours with minimal *post mortem* delay. These samples were then stored in 0.1 M PBS with 0.05% Sodium Azide at 4°C to avoid bacterial contamination. One of the hemispheres from three brains (one 13 PCW; two 20 PCW) were processed as above, but the second hemispheres, were immediately frozen upon sample collection without fixation, and have been shipped in dry ice and appropriately stored at -80°C upon arrival in the laboratory (**Figure 2.1**). All specimens were shipped according under a Material Transfer Agreement (MTA H-20068526) between the University of Newcastle and the University of Oxford, and processed for all further analysis to Department of Physiology, Anatomy and Genetics at Oxford. The donated samples have been screened for gross brain abnormalities, or common genetic defects and has been found to be suitable for our investigations. Sex and ethnicity of the donated specimen has not been disclosed to us as it was not considered relevant for the purpose of the study.

In this study, only one brain sample was not provided by the HDBR, but derived from a collection of formalin-fixed paraffin-embedded (FFPE) tissues that has been described and used in previous studies (Meyer *et al.* 2000) and was kindly donated to the laboratory of Professor Zoltán Molnár by Professor Gundela Meyer, Universidad de La Laguna, Department of Anatomy, Pathological Anatomy and Histology. Briefly, the sample was fixed in Bouin's fixative, embedded in paraffin and cut into series of 10 μm thick coronal sections. As specified in the published work, all samples from the collection derived from spontaneous or medically induced abortions in accordance with Spanish legislation, and supervised by the Ethical Committee of the University Hospital La Laguna. The specific sample used in this study is included in **Table 2.1**

Table 4.1. Human brain specimens used in the study

Sample ID	Age (PCW)	Brain Hemisphere(s)	Type of fixation
HDBR 16045	**7**	Whole brain	4% PFA
HDBR 15927	**13**	Whole brain	4% PFA (Left h.) Unfixed-frozen (Right h.)
HDBR 15489	**16**	Left hemisphere	4% PFA
HDBR 14958	**17**	Left hemisphere	4% PFA
HDBR 15983	**20**	Whole brain	4% PFA (Left h.) Unfixed-frozen (Right h.)
HDBR 15984	**20**	Whole brain	4% PFA (Right h.) Unfixed-frozen (Left h.)
Case #13 **(Meyer's collection)**	**10**	**Slide #A134** **Slide #C171**	FFPE

Figure 2.1

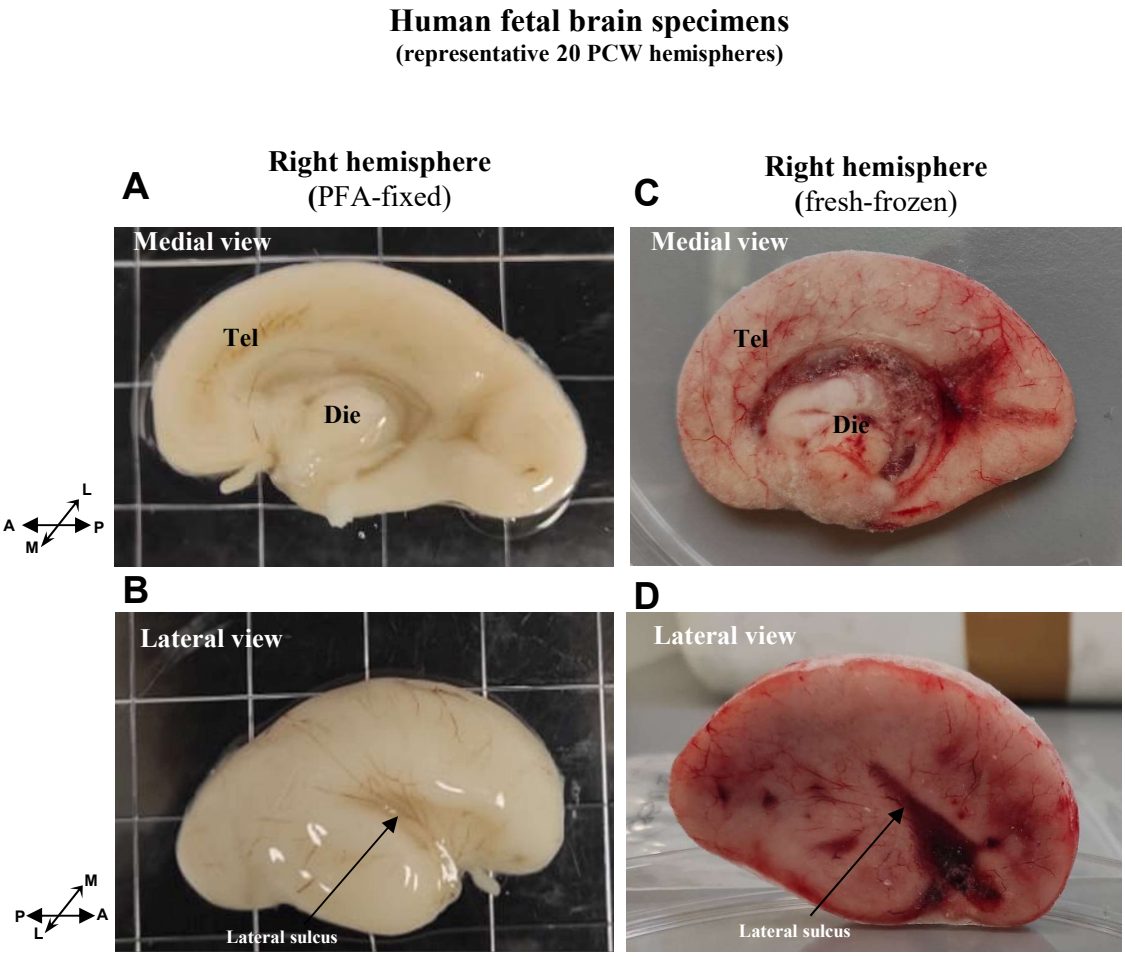

Figure 2.1: Representative images of two 20 post-conception weeks (PCW) human brain right hemispheres used in the study.
(**A, B**) PFA-fixed and (**C, D**) fresh-frozen human right brain hemispheres collected from two 20 PCW fetuses and provided by the HDBR for this study. Medial view (A, C) highlights the telencephalon, diencephalon, and the two sulci visible from this aspect: the parieto-occipital sulcus and the calcarine sulcus. Lateral view (B, D) shows the lateral sulcus (also known as Sylvian fissure) used as anatomical landmark for manual dissection of the specimens.

2.1.2 Human Tissue Storage

Both human unfixed and defrosted and PFA-fixed brains were cut into coronal 0.5-1cm- thick sections manually by using a long surgical blade before further microdissection or histological sectioning. The serial coronal blocks/slabs were numbered in anteroposterior order starting from the most frontal to the most dorsal (**Figure 2.2 A, B**). Fixed tissue was kept at 4°C in 0.1X PBS 0.05% Sodium Azide before being sectioned by vibrating microtome (VT1000S, Leica System), with the exception of the medial blocks containing either the thalamus and/or the internal capsule. These blocks were used for carbocyanine dye tracing by placing DiI crystals immediately after cutting the blocks and kept at room temperature (see carbocyanine dye tracing method). The human fresh frozen brain samples were immediately microdissected as described below, to minimize thaw-freezing periods, and stored at -80°C.

2.1.3 Brain tissue sectioning

The 4% **PFA-fixed samples** that were used for DiI-tracing and immunohistochemical staining were embedded in 3% low gelling temperature Agarose (SIGMA) and cut with a vibrating microtome (VT1000S, Leica System) with speed 8-9 and frequency 9 at 70-200 µm-thick transversal sections. All the slices were collected in 6- or 12-well plates and stored in 0.1X PBS 0.05% Sodium Azide (SIGMA) at 4°C until further processing.

Human **fresh frozen samples** used for molecular biology studies were transported to Oxford on dry ice and then stored at -80°C freezer. For further dissections the frozen brains were removed from -80°C and placed on ice until they thaw. Then these brains were manually microdissected with surgical tools into regionally-defined pieces roughly 1-2 mm in diameter, following main anatomical landmarks (**Figure 2.2 C**). All microdissections were performed by the same persons (Professor Zoltán Molnár with my assistance) for consistency. Tissue was collected into clean RNAse-free 1.7-2.0 ml tubes and some samples were immediately processed (i.e. RNA and protein extraction). Other tissue samples were stored at -80°C until further processing.

Figure 2.2

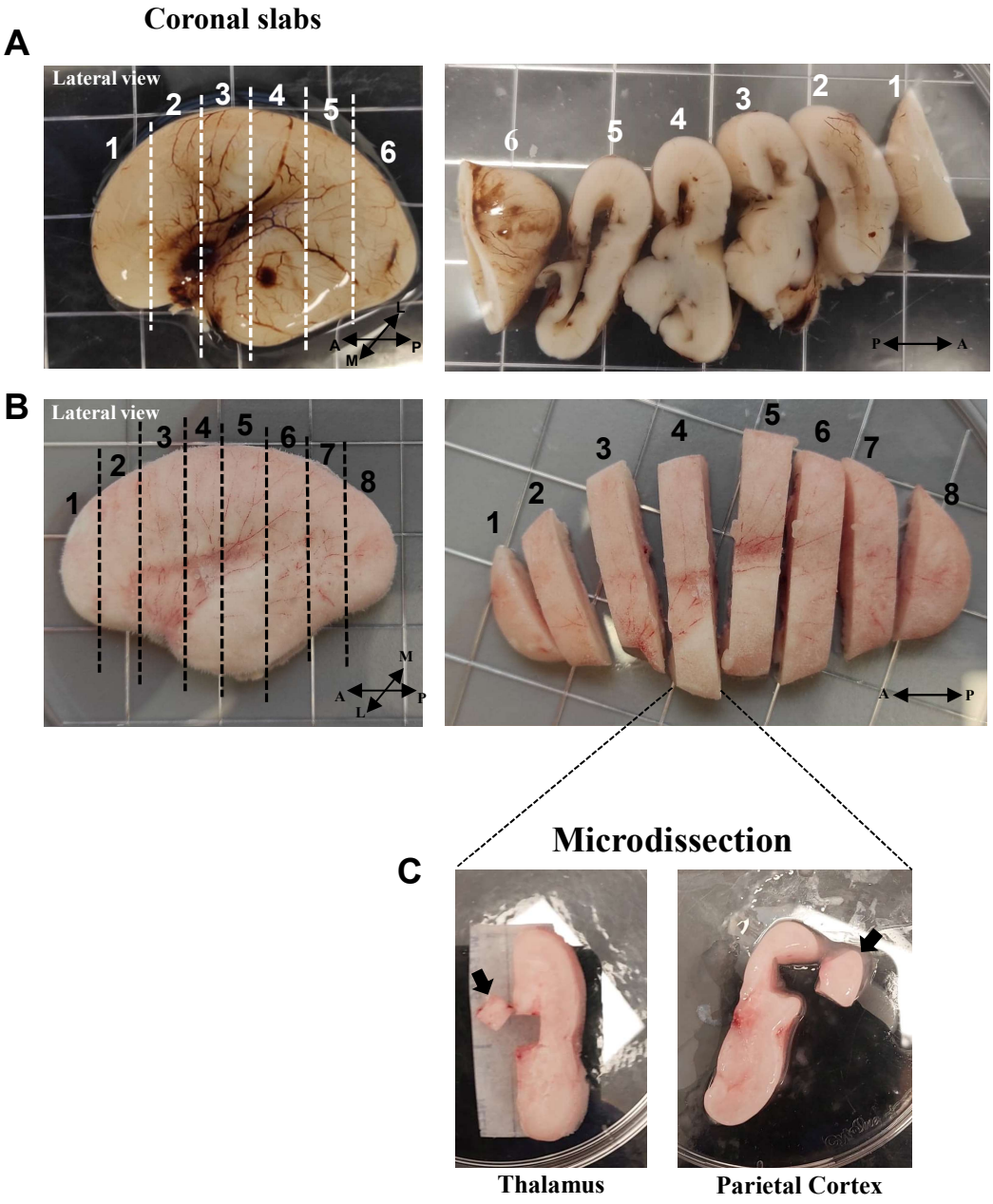

Figure 2.2: Representative images of two 20 post-conception weeks (PCW) human brain right hemispheres used in the study.
(**A, B**) Lateral view of a PFA-fixed (A) and fresh-frozen (B) left hemisphere of two 20 PCW human brains and the coronal slabs obtained in the antero-posterior axis. The correspondent right hemisphere of both sampels is shown in Figure 2.1. (**C**) Representative image showing the manual microdissection of specific brain regions, the thalamus on the left and the parietal cortex on the right, from the fresh-frozen samples (slab #4 shown) and used for molecular biological analyses at regional level in this study. Microdissections were performed following the anatomical landmarks visible in the samples and by consulting atlases of the prenatal human brain.

2.2 HISTOLOGICAL TECHNIQUES

2.2.1 Carbocyanine dye (DiI) axonal tracing

Neuroanatomical tracing of the thalamocortical axons was conducted on 7 PCW (N=1), 13 PCW (N=1), 17 PCW (N=1) human 4%PFA-fixed brains by the placement of lipid soluble carbocyanine dye in form of crystals (DiI, 1'-dioctadecyl-3,3,3'3'-tetramethylindocarbocyanine perchlorate, Molecular Probes, Eugene, OR). Due to its lipid solubility, the dye is incorporated within the phospholipidic membrane of the cells located in the vicinity of the site of crystal placement and passively diffuse along membranes of both unfixed and fixed tissue (Godement *et al.* 1987; Molnár *et al.* 2006). To trace the thalamocortical axons, crystals placements were targeted to the putative dorsal thalamus and to the internal capsule. Specific details about each sample will be provided in Chapter 3, and the site of crystal placement is schematized for each slab in **Figures 3.6, 3.12, and 3.18** for the 7, 13, and 17 PCW brains, respectively. The targeted anatomical structures were identified by the use of a brightfield surgical microscope. I placed several crystals for each site by using stainless tungsten needles under a surgical microscope.

2.2.2 Immunohistological staining

2.2.2.1 Immunofluorescence staining (IF)

70- to 200- µm-thick free-floating sections were selected for immunofluorescence staining to reveal immunoreactivity for various cellular and molecular markers. Antigen retrieval was performed by incubating the section in 10mM Sodium Citrate in 0.1M Phosphate buffered saline (PBS) (SIGMA) at 65°C for 20 minutes. Sections were then blocked in 20% normal donkey or goat serum (Sigma-Adrich) 0.3% Triton X-100 (Sigma) (blocking solution) for at least 6 hours at room temperature. Primary antibodies were diluted in blocking solution (**Table 2.2**) and applied for 48 hours at 4°C. Sections were washed for 1 hour with 0.1 M PBS and then incubated in secondary antibodies solution (**Table 2.2**). An additional hour of washing in 0.1 M PBS was performed to

remove excess of antibody, followed by incubation in DAPI 1:1000 in 0.1M PBS for 30 minutes at room temperature for nuclear counterstaining. Sections were mounted on glass coverslips with FluorSave reagent (MerkMillipore) and sealed with nail polish to avoid drying.

Some relevant sections from the DiI-labelled brains were selected for co-immunostaining for selected cellular markers, to reveal the interaction between the DiI labelled thalamic axons and cortical cell populations. These slices were stained with the same protocol as described above, with the exception that the detergent Triton-X100 was not added to any solutions used due to the technical incompatibility of the use of this detergent with the lipid soluble carbocyanine dye.

The protocol was tested in a preliminary set of staining experiments on 100-150 μm-thick sections, including some free-floating 50 μm-thick sections of mouse brain (P14) and ferret brain (P36) for comparison during the optimization. Negative controls for the staining procedure where the primary antibody incubation was omitted were also included during the optimization of the protocol and evaluation of the antibody specificity (not shown).

Immunofluorescence staining protocol on human **organotypic cortical slides** (see Chapter 6, **Figure 6.3**) was done according to the protocol just described for *post mortem* brain tissue, except that concentration of Triton-X100 in all solutions was increased to 0.5%, as appropriate for the greater thickness of the slices (280 μm).

Immunofluorescence staining protocol on **iPSC-derived cortical cultures** (see Chapter 6, **Figure 6.2**) was performed according to standard protocols by Laura Pearson under supervision of Dr. Becky Carlyle.

2.2.2.2 Immunohistochemistry (IHC)

For immunohistochemical analysis, 4% PFA-fixed human brain slices were mounted onto SuperfrostPlus slides (ThermoScientific) and let firmly attach to the glass at room temperature for 1-3 hours, according to the thickness of the slice. Before proceeding with the immunostaining protocol the slices were then rinsed twice with 0.1M PBS. The Washing Solution was prepared by adding 0,3% v/v Triton X-100 (Sigma) in 1X PBS.

For IHC of the FFPE-section, the protocol was adjusted according to the protocol described by (Meyer *et al.* 2000). The sections was deparaffinized in serial immersion in xylene, cleared with pure ethanol, and rehydrated in serial descending ethanol dilutions, rinsed in TBS, and put in a humid chamber for subsequent staining steps. Washing solution used in the following protocol for permeabilization, washing and antibody dilutions was prepared by adding 0,1% v/v Triton X-100 (Sigma) in 1X TBS pH 7.4.

All tissue sections were then incubated in 0,3% H_2O_2 for 15 min at room temperature to inactivate the endogenous peroxidase activity, permeabilized with washing solution, and blocked with 20% (PFA-fixed tissue) or 3 % (FFPE tissue) normal donkey or goat serum (Sigma-Aldrich) in washing solution. Additional avidin and biotin blocking steps were performed by applying the ready-to-use solutions (Vector Laboratories) directly onto the slides for 15 minutes each. Slides were then incubated with the primary antibody (**Table 2.2**) appropriately diluted in a solution of blocking solution and incubated at 4°C overnight. Slides were put in humid chamber and covered with parafilm to avoid evaporation and drying of the solution on the slides' surface. The following day, tissues were washed three times with washing solution and incubated with the species-appropriate biotinylated secondary antibody (**Table 2.2)** diluted 1:500 (PFA-fixed tissue) or 1:100 (FFPE tissue) in blocking solution for 3 hours at room temperature, in a humid chamber and covered by parafilm. After rinsing in PBS 1X, sections were incubated with the Avidin–Biotin peroxidase complex (Vector Laboratories) 1 hour at room temperature, and staining was visualized with 3,3'-diaminobenzidine (DAB) with metal enhancer (Sigma) (FFPE tissue) or without metal enhancer (Vector Laboratories) (PFA-fixed tissue). The reaction was monitored under dissecting microscope

and blocked at the point of reaching the desired staining by washing the sections with distilled water. Tissues were counterstained with hematoxylin (Sigma-Aldrich) (7 seconds immersion) to detect cellular nuclei and washed under running water to remove the excess staining. Finally, sections were dehydrated with ascending ethanol series, cleared with xylene (Merck), and mounted with a synthetic DePeX xylen-based mounting medium (Serva, VWR).

Table 2.2. List of primary and secondary antibodies used for immunohistology in the study

Primary Antibodies (Target)	**Host Species**	**Supplier**	**Code/Cat.N.**	**Working Dilution**
HOPX	Rabbit	Bioscience Ltd	HPA030180	1/100
TBR1	Rabbit	Abcam	ab31940	1/100
KI67	Rabbit	Abcam	ab833	1/100
VGF	Rabbit	Invitrogen	PA5-84900	1/100
GAP43	Rabbit	Abcam	ab7462	1/100
GFAP	Rabbit	DAKO	Z0334	1/500
ROBO1	Rabbit	Abcam	ab7279	1/100
NURR1	Goat	R&D	AF2156	1/200
MAP2	Chicken	Abcam	ab92434	1/200
βIII Tubulin	Mouse	Abcam	ab78078	1/500
Secondary Antibodies (Target)				
Rabbit IgG Alexafluor647	Donkey	Invitrogen	A-31573	1/500
Mouse IgG Alexafluor488	Donkey	Invitrogen	A21202	1/500
Chicken IgG Alexafluor488	Donkey	Thermo Fisher	A78948	1/500
Mouse IgG Alexafluor568	Donkey	Invitrogen	A31571	1/500
Goat IgG Alexafluor488	Donkey	Thermo Fisher	A11055	1/500
Goat IgG Alexafluor568	Donkey	Thermo Fisher	A11057	1/500
Rabbit IgG Biotinylated	Donkey	Abcam	ab97109	1/200
Rabbit IgG Biotinylated	Goat	Abcam	ab7089	1/200

2.2.3 Cresyl Violet (Nissl) staining

Cresyl Violet (Nissl) staining was used to identify the cellular structures and their cytoarchitectural organization in both PFA-fixed brain sections. The brain slices were mounted onto Superfrost Plus slides (ThermoScientific) and let attach to the slides overnight at 4ºC, as described in the previous sections on IHC. Sections were incubated for 10 minutes at 37ºC in 0.1% Cresyl Violet Acetate solution (Sigma), appropriately filtered before use. Sections were then differentiated in 95% ethanol with the addition of 1% v/v glacial acetic acid (Sigma) for 2-10 minutes. The time of differentiation was decided for each indivual sample by inspecting the ongoing process at close intervals. The sections were finally dehydrated in 100% ethanol, cleared in xylen, and mounted with DePeX mounting medium as previously described for the IHC protocol.

2.2.4 Imaging

2.2.4.1 Epifluorescence Microscopy

To analyse the DiI-labelled sections, I used an epifluorescence microscope (DMR; Leica, Germany). 5x and 10x objectives were used for taking the images reported in this work. All samples used for axonal tracing with carbocyanine dye were imaged soon after sectioning since in about 7-10 days the displaced carbocyanine dyes can label additional tissue on the cut surface therefore decreasing the accuracy and specificity of the signals detected. As I did not intend to perform quantitative analyses of the DiI signal detected and documented, I adjusted the parameters to be optimal for each individual image. Nevertheless, the majority of the parameters were kept constant within the same set of imaging sessions. All images were manually processed by using ImageJ software.

2.2.4.2 Confocal Microscopy

A laser-scanning confocal microscope (Zeiss LSM710) was used for further analysis of DiI-labelled fibres and for detection of specific cellular markers (see **Table 2.2**). Imaging parameters independently according to each tracing and immunoreactivity, sample thickness and general conditions. However, most of the parameters have been kept as constant and consistent as possible across different samples and imaging session to avoid misinterpretation of the detected signal. Where not specified otherwise, I used an optical zoom of 1x with all the objectives. Low-power tiled scan were taken with a 5x/0.16 NA dry objective to visualize the specific anatomical structures involved. The images were taken with 10x/0.45 NA, 20x/0.8 NA dry-based and 40x/1.3 NA, 63x/1.4 NA oil-based objectives. Contrast and brightness of each individual image were adjusted as a whole by using ImageJ software.

2.2.4.3 Neurolucida

Brightfield images and scans of samples stained by immunohistochemistry were acquired with an Olympus BX53 microscope with motorized stage and Neurolucida Software (v2021.1.1 64-bit, Microbrightfield). The images were taken with 1.6x/0.05NA, 10x/0.30 NA, and 20x/0.5 NA dry-based objectives.

2.2.4.4 Image acquisition and from HDBR Digital Image Hub

Human brain samples younger than 13 PCW are most difficult to obtain. To analyse these developmental stages, I benefitted from the archived material available through the HDBR Atlas, Digital Image Hub (https://www.hdbr.org/) (in **Figure 2.3** a representation of the interactive interface). Images of 6-8 µm-thick paraffine-embedded sections of human brain (**Table 2.3**) were acquired according to the instruction provided by the HDBR (https://hdbr.org/uploads/default/factsheets/Viewing_HDBR_slides_in_the_DIH.pdf). 3D models of the cutting planes were kindly provided by Janet Kerwin (Newcastle University) and were inserted in the correspondent images for anatomical reference (see **Figures 3.1-3.5**).

The human brain samples selected for this work are listed below and are available online for consultation in the HDBR Digital Image Hub.

Table 2.3. List of human brain sections selected and analysed from thr HDBR Digital Hub

Sample ID	Age	Selected Slide	Staining Imaged
HDBR 1032	6.5 PCW (CS19)	#077	CalR; SCGN
HDBR 12204	8 PCW (CS23)	#47	CalR; SCGN
HDBR 13341	10 PCW	#186	CalR; SCGN
HDBR 12968	12 PCW	#19	CalR; SCGN

Figure 2.3

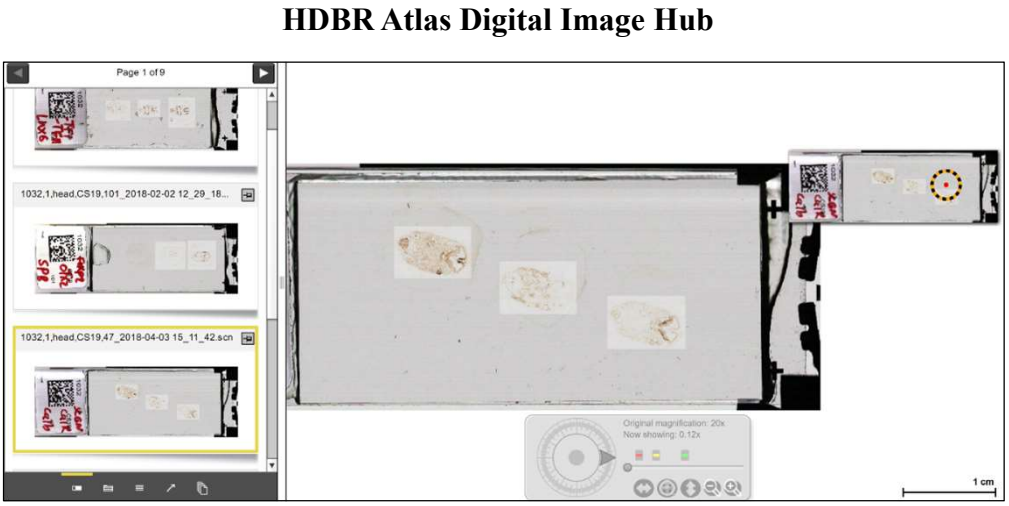

Figure 2.3: HDBR Atlas Digital Image Hub interface.
Representative image showing the interface of the HDBR Digital Image Hub used for image acquisition of immunostained sections for time-course evaluation of the earliest thalamo-cortical interactions. At the centre of the screen, a zoomed image of a slide appears once the operator select it from the full list of available slides (on the left) appears at the centre of the screen. The slide can be navigated by using the interactive tool at the bottom, which allows the operator to zoom in and modify the orientation of the slide as in a real microscope setting.

2.2.5 Anatomical annotation of the brain sections

The brain sections used for histology and immunohistochemical staining were manually annotated with the assistance of various resources. The annotation of the embryonic (Carniage stage 19) and the early fetal (8 PCW) human brains was made by matching these transvers sections with the anatomical references found in "The virtual Human Embryo" resource (https://www.ehd.org/virtual-human-embryo/) and by selecting the slides form the correspondent developmental stage for age-matched comparison. For anatomical annotation of all the fetal brain samples, the atlas 'The Human Brain During the Second Trimester (Atlas of Human Central Nervous System Development)' by Bayer and Altman (Bayer *et al.* 2005), served as a frequent reference. Additionally, reference atlases of the 15 and 21 PCW human brain from the Brainspan website (https://www.brainspan.org/static/atlas) were consulted. To accurately select the appropriate slice, I cross-referenced Nissl and Acetylcholinesterase staining on the website with my samples, aiding in the precise identification of the cortical compartments, as well as the anatomical location of thalamic axons and thalamic nuclei (**Figure 2.4**). More detailed information on the precise location and relative boundaries of the cortical layers at different stages of human brain development was gathered from other publications that analysed comparable fetal samples (Huang 2010; Miller *et al.* 2014; Vasung *et al.* 2016; Zunic Isasegi *et al.* 2018; Alzu'bi *et al.* 2019; Kostovic *et al.* 2019), as shown in **Figure 2.5**. In these studies, different stages of development were annotated by comparison of magnetic resonance imaging, cresyl violet (Nissl) and Acetylcholinesterase (AChE) stainings to detect neuronal and axonal organization at different stages of human cortical development.

Figure 2.4

Anatomical annotation of the human fetal brain from the Brainspan atlas

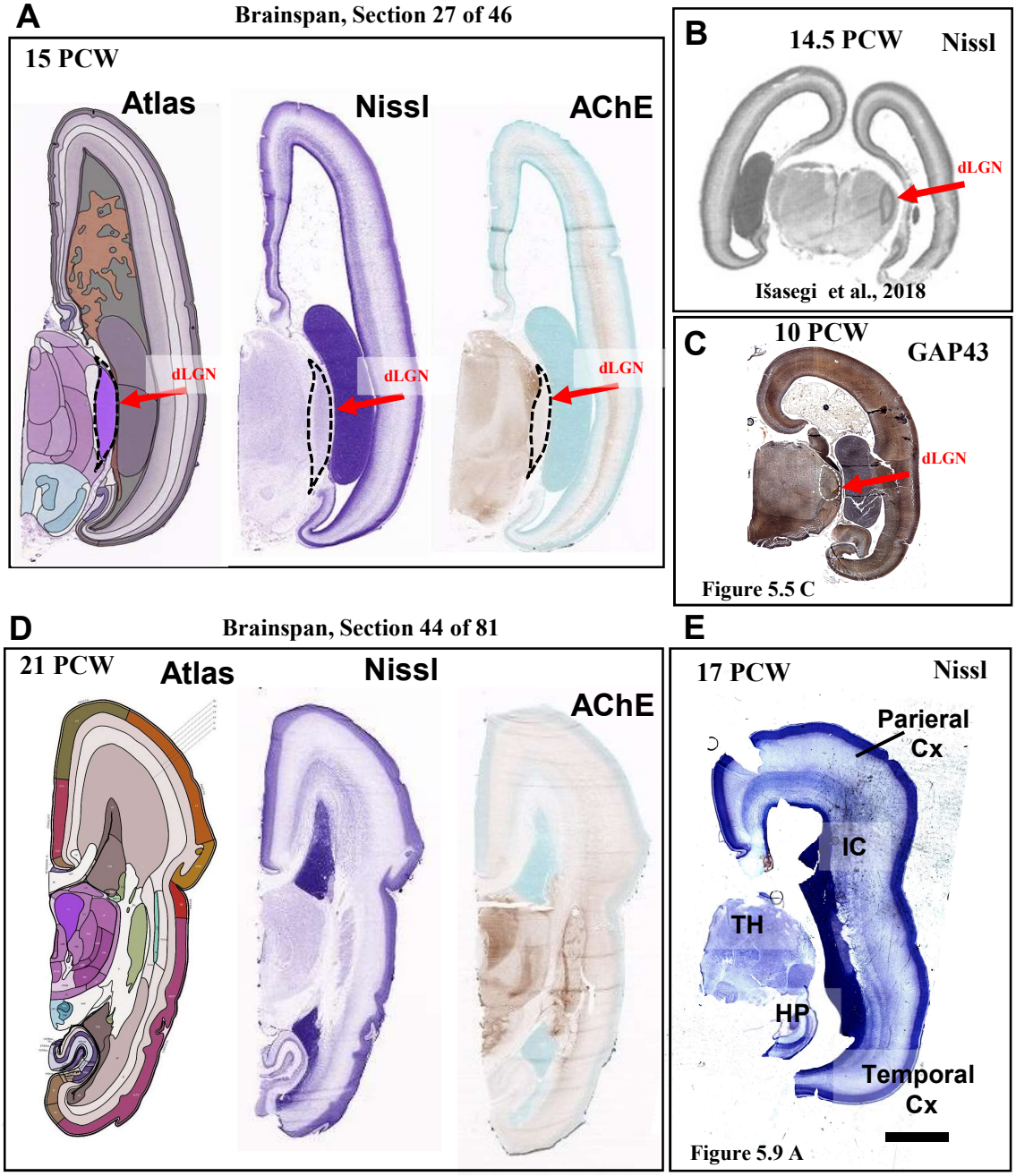

Figure 2.4: Representative illustration of the anatomical reference atlas used for the annotation of the major brain structures of the human fetal brain.

(**A**) Representative example of the comparison made across Brainspan Atlas, Nissl and AChE stained serial sections of the 15 PCW human brain with other available publications (**B**) to pinpoint the location of the prospective dorsolateral geniculate nucleus (dLGN) in the 10 PCW human brain shown in Figure 5.5 in this work (**C**). (**D**) Similar example of the comparison made across Brainspan Atlas, Nissl and AChE stained serial sections of the 21 PCW human brain for the annotation of the 17 PCW sample shown in Figure 5.9 (**E**).

Panels A and D are taken from Brainspan.org. Panel B is adapted from Išasegi et al., 2018.

Figure 2.5

Anatomical annotation of the human fetal cortical layers from previous studies

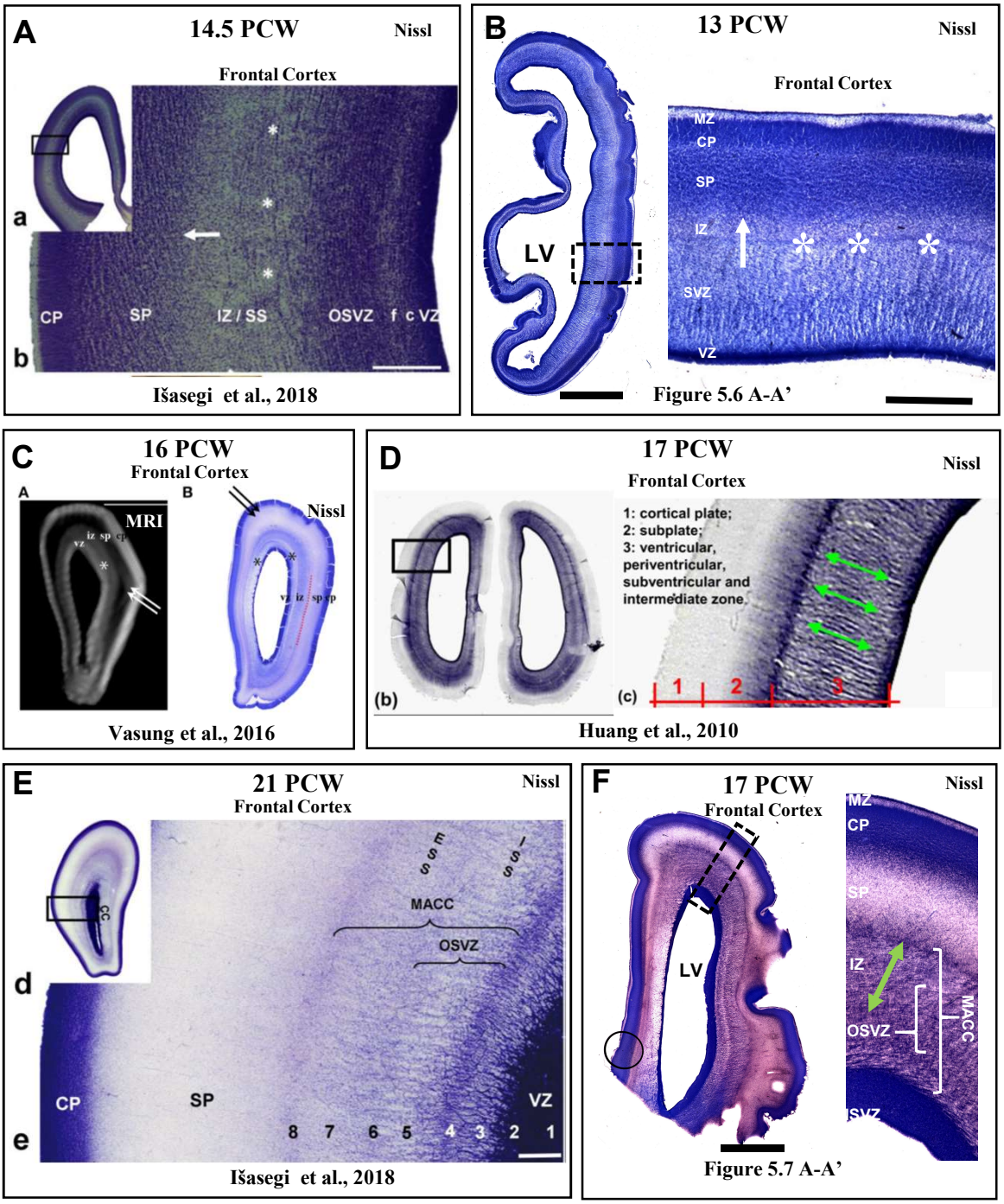

Figure 2.5: Representative illustration of the anatomical annotation of the cortical compartments in the developing frontal cortex by comparison with previous studies on the human fetal brain.

(**A**) Representative Nissl stained coronal section of the human frontal cortex at 14.5 PCW highlighting the border between the intermediate zone (IZ) and the subplate (SP) (arrow) and the major bundles of tangential fibres (asterix). Both landmarks have been used for the annotation of a similar frontal cortical section from the 13 PCW human brain shown in Figure 5.6 in this work (**B**). (**C**) T1-weighted magnetic resonance imaging (MRI) and Nissl stained sections of the 16 PCW human frontal cortex confirming the anatomical location of the transient subplate (arrows) and the tangential path of the axonal fibres (red dotted curved line). (**D**) The remaining ventricular sector contains the germinal compartments where a green double-head arrow highlights the the radial structures prominent at this level of the human fetal cortex. The anatomical landmarks from Panels C and D are reported in panel **F**, illustrating a coronal section of the 17 PCW frontal cortex from Figure 5.7 of this thesis. (**E**) A more detailed annotation of the overlapping region between OSVZ and IZ in the human cortex, labelled as "multilaminar axonal-cellular compartment" (MACC) and also reported in panel F.

Adopted from Išasegi et al., 2018 (Panels A, E); Vasung et al., 2016 (Panel C); Huang et al., 2010 (Panel D).

2.2.6 Semi-quantitative analysis of DiI-positive axonal signal (17 PCW cortex)

Five epifluorescence microscopic images were selected from the 17 PCW human brain slab, where DiI crystals were placed in the internal capsule. All the selected images depicted the same cortical area from serial coronal sections, where both the subplate (SP) and outer subventricular zone (OSVZ) were clearly visible. To ensure consistent analysis, all images were converted to 8-bit format, and adjustments to contrast and brightness were made to accentuate the DiI-positive signal in both cortical compartments uniformly. In each image, three regions of interest (ROIs) were manually delineated for both SP and OSVZ, avoiding any intense or oversaturated signals from the intermediate zone (IZ) to minimize outlier data. ROIs were systematically numbered from 1 to 3 in a distal-to-close fashion relative to the site of DiI placement—ROI 1 being the farthest and ROI 3 the closest. Special attention was given to maintaining consistent and equivalent delineation for each level in both SP and OSVZ (i.e. SP ROI 1 mirrored the distance to the DiI placement site as OSVZ ROI 1). Mean intensity of the signal was calculated for each ROI and normalized for the correspondent ROI area. The normalized values measured for each image were averaged by ROI and cortical layer. Statistical analysis was performed by basic R language using One-Way ANOVA test with a significance threshold set at 0.05 for each analysis. Bar graphs illustrating the normalized mean values and standard deviations for the three ROIs were separately plotted for the SP and OSVZ by using ggplot2 package with R. A ratio between the value measured at the OSVZ and SP levels for each individual ROI was calculated, and similarly illustrated in a separate bar graph. The same statistical approach was applied to this analysis.

2.3 MOLECULAR BIOLOGY TECHNIQUES

2.3.1 RNA extraction

The protocol was carried out in RNAse free conditions. The dissections was performed on a cleaned surface thoroughly wiped with RNAse-Zap (Sigma) to avoid RNAse contamination. All tools, such as pipettes and pipette tip boxes, were wiped with RNAse-Zap. Clean lab coats and surgical masks were worn at all times, to avoid RNA/DNA contamination. Filtered tips and RNAse-free tubes were used for the entire protocol. Samples were kept on ice , unless specific incubation temperature was required (specified). All micro-centrifugation steps in the following protocol were carried out at 12000 x *g* at 4°C.

Total RNA content was extracted from microdissected tissue of 13 PCW (N=1) and 20 PCW (N=2) human fresh-frozen brains. The brain tissue used for each region was roughly 1-2 mm in diameter. The brain tissue samples were defrosted from -80ºC storage temperature on ice. Each piece of tissue was transferred into 2ml CK14 soft Precellys homogenising tubes (Stretton Scientific) with 1.4mm ceramic (zirconium oxide) beads designed for soft tissue homogenization and resuspended in 1ml TRIzol solution (Invitrogen). Tissue samples were subjected to homogenization at 5500 rpm for 30 seconds twice, and transferred to new clean RNAse-free tubes before proceeding with RNA extraction protocol. Chloroform (Sigma-Aldrich) was added at 1:5 v/v ratio to each sample, and mixed thoroughly. Samples were spun for 15 minutes, and the resulting aqueous phase (approximately half of the initial volume) was transferred into new tubes. An equal amount of 95% ethanol was added to each sample, according to the individual sample volume. The final sample volume was transferred into RNA purification columns (Monarch) fitted with a collection tube and spun for 1 minute, and the flow-through was discarded. 500 µl of Wash Buffer (Monarch) were applied to each column, followed by 1minute spinning to allow the buffer to pass through the membrane and wash the RNA bound to it.

A first *in-column* treatment with DNAse I (AMBION) was carried out by adding 60 µl of DNAse I mix prepared as datasheet suggestions directly to each column. All samples were incubated for 30

minutes at 37° C. After the treatment, the RNA samples were cleaned up by using the Clean Up kit (Monarch) according to the datasheet. Briefly, RNA Priming Buffer was added to each column, followed by 1 minute of centrifugation. Similarly, Wash Buffer was added to the column, followed by a step of centrifugation for 1 minute. Finally, RNA was eluted with 100 µl Nuclease-Free water and collected into a new clean RNAse-free tube. A second *in-tube* treatment with DNAse I (AMBION) was carried out by adding 60 µl of DNAse I mix to each RNA elute, and incubating for an additional 30 minutes at 37° C. This optional step was included in the protocol to remove any DNA contamination from the RNA, as suggested by the Troubleshooting section of Monarch RNA extraction kit, and was optimized for the human brain tissue used in preliminary tests. Following the second treatment with DNAse I, all RNA samples were cleaned up as described previously and finally eluted with 100 µl Nuclease-Free water and collected into a new clean RNAse-free tube.

All samples were mixed by pipetting and quantified at Nanodrop by measuring the absorbance at 260 nm. The ratio of absorbance at 260 nm and 280 nm was used to assess the purity RNA: a ratio equal or greater than 2.0 was considered as indicative of RNA sample clean from protein contamination. Similarly, the ratio of absorbance at 260 nm and 230 nm was used to assess for eventual contamination from salts and/or reagents: ratios equal or greater than 2.0 were accepted. In case either of these conditions were not met, samples were subjected to further clean-up steps as described, and quantified again.

To avoid sample degradation, RNA was immediately retrotranscribed into cDNA as described in the next section, as cDNA is more stable over time. RNA extracts that were not retrotranscribed were stored at -20ºC.

2.3.2 Quantitative polymerase chain reaction (qPCR)

Reverse Transcription

RNA isolated from the snap-frozen human brain tissue was reverse transcribed and subjected to qPCR as described below. cDNA was generated from 1 µg of total RNA using a LunaScript RT SuperMix Kit (New England BioLabs).

Primer Design

Sequence for each gene of interest was retrieved from the National Center for Biotechnology Information (NCBI) (https://www.ncbi.nlm.nih.gov/). Primer sets complementary to each sequence were designed by using Primer-BLAST software (NCBI). PCR product size was set between 70 and 200 nucleotides as recommended by the Luna(R) Universal qPCR Master Mix datasheet. Where possible, exon-spanning primer sets were used to control for possible genomic DNA contamination.

Specificity of each primer was checked by blasting the sequence to the reference gene by using BLAST (NCBI), and prior testing was performed to determine the specificity of all the primer sets.

qPCR

cDNA was subsequently diluted to 1/30 ratio in Nuclease Free-Water before performing qPCR.

qPCR was subsequently performed using Luna(R) Universal qPCR Master Mix (M3003, New England BioLabs) and QuantStudio™ 5 Real-Time PCR System (Thermo Fischer Scientific). Luna(R) Universal qPCR Master Mix (2X), 0.25 µM forward and reverse primers, 2 µL of the diluted cDNA and nuclease-free H_2O were mixed. The primer sequences are shown in **Table 2.4**. qPCR followed by melt curve analysis was performed for 40 cycles with 15 seconds of denaturation at 95°C and annealing and extension at 60°C for 30 seconds. Some no-RT and at least one no-template controls were added to each experiment performed. TBP was used as a housekeeping gene to determine relative gene expression using the -ΔCt method.

Table 2.4. Sequence of the primer pairs used for qPCR

Gene	Accession No.	Primer Sequence	Product Size
human VGF	NM_003378.4	5′-CAGGCGCGTATGCCCGACAG-3′ (forward) 5′-CTTGGACAGGGGTGCCAATGCCTCG-3′ (reverse)	108 b.p.
human BDNF	NM_170735.6	5'-CAATAAGGACGCAGACTTGTACA-3' (forward) 5'-GGACATGTTTGCAGCATCTAG-3' (reverse)	121 b.p.
human TBP	CR456776.1	5'-TGACCCAGCATCACTGTTTCTT-3' (forward) 5'-CAAGCCCTGAGCGTAAGGTG-3' (reverse)	198 b.p.
human CAPN1	BC008751.2	5’- CTTCCTGGTTGGGCCCTG (forward) 5’- GTACACCGGCGTGATGATCT (reverse)	114 b.p.
human CAPN2	NM_001748.5	5’- CTCAACCAGGACTACGAGGC-3’ (forward) 5’- GCAGATCTCCGTGGGGC-3’ (reverse)	165 b.p.
human CAPN5	NM_004055.5	5’- CTCGGCCGGTGTTCCC-3’ (forward) 5’- CCGGCGTGCCCTTATAGTAG-3’ (reverse)	179 b.p.
human CAPN7	NM_014296.3	5’- TGTTTTATTACAAGGAAGCTGCACA-3’ (forward) 5’- CAGCACTCTTTGACTGAACTGC-3’ (reverse)	141 b.p.
human CTSB	BC095408.1	5’- GCGCTGGGTGGATCTAGGA-3’ (forward) 5’- GTTGACCAGCTCATCCGACA-3’ (reverse)	128 b.p.
human CTSD	BC016320.2	5’- TTCATCGGCCGCTACTACAC-3’ (forward) 5’- CTGCTCTGGGACTCTCCTCT-3’ (reverse)	127 b.p.
human PCSK1/3	NM_000439.5	5’- AGAATTGGGACTTCATGTCTGTTC-3’ (forward) 5’- TGCTCTGGCTGAGAAGAGGTC -3’ (reverse)	154 b.p.

Notes:

- Primer sequences for human VGF are modified based on the mouse sequences in the following study (Mizoguchi *et al.* 2018).
- Primer sequences for human BDNF are modified based on the mouse sequences in the following paper (Berton *et al.* 2006).
- Primer sequences for human TBP are modified based on the following publications: (Gillentine *et al.* 2017) (forward primer); (Augustyniak *et al.* 2023) (reverse primer).
- Primer sequences for human PCSK1/3 are taken from validation assay ID# qHsaCIP0031391 (BioRad).

2.3.3 Protein extraction

2.3.3.1 Protein extraction from fresh-frozen brain tissue for Western Blot analysis

Proteins were extracted from microdissected tissue of 13 PCW (N=1) and 20 PCW (N=2) human fresh-frozen brains. The brain tissue used for each region was roughly 1-2 mm in diameter (**Figure 2.2 C**). The brain tissue samples were defrosted gently from -80ºC storage temperature on ice. Each piece of tissue was transferred into 2ml CK14 soft Precellys homogenising tubes (Stretton Scientific) with 1.4mm ceramic (zirconium oxide) beads designed for soft tissue homogenization, resuspended in 1ml freshly-prepared 1X Ripa Buffer (Abcam) with the addition of Complete Inhibitor Cocktail (Sima-Aldrich). Total protein content was extracted by homogenizing at 5500 rpm for 30 seconds twice, followed by mechanical disruption by sonication. Ultrasonic frequencies were applied for 30 sec twice by using an Ultrasonic Liquid Processor XL-2000 (Misonix). The samples were then spun at 12.000 x *g* 10 min and the protein-containing supernatant was transferred in a new 1.5 ml eppendorf tube. Protein extracts that were not immediately prepared for Western Blot analysis were in a -20°C freezer. Protein quantification was performed using a Bicinchoninic Acid (BCA) Protein Assay Kit (Thermo Fisher). To avoid protein degradation and repeated thawing of the protein extracts, samples were immediately prepared for SDS-PAGE as described.

The total amount of protein content was then prepared for Western Blot analysis by mixing it with Western-Ready™ Protein Sample Loading Buffer (5X) (Biolegend) 10% v/v sodium dodecyl sulfate (SDS) (Life Technologies). The appropriate lysis buffer used for protein extraction (RIPA Buffer or High-TRIS Lysis Buffer) was used to reach the final desired volume, as previously calculated. Samples were then heated at 95°C for 5 min, spun, and stored at -20°C until the day SDS-PAGE was carried out. Final volumes were calculated prior to sample preparation to obtain a final concentration of protein extracts compatible with the limit of 15 µL volume of the gel's wells.

.

2.3.3.2 Protein extraction from PFA-fixed brain tissue for Western Blot analysis

Proteins were also extracted from microdissected tissue of the 17 PCW (N=1) human 4% PFA-fixed brain previously used for DiI-axonal tracing. The following brain regions were manually microdissected with the help of surgical tools, and are shown in more details along with the results from their analysis in Chapter 5 (**Figure 5.5**):

- Parietal cortex (prospective somatosensory cortex), ventral aspect
- Parietal cortex (prospective somatosensory cortex), dorsal aspect
- Thalamus

The brain tissue was transferred into 2ml CK14 soft Precellys homogenising tubes (Stretton Scientific) with 1.4 mm ceramic (zirconium oxide) beads designed for soft tissue homogenization, resuspended in 1ml freshly-prepared High-TRIS Lysis Buffer previously optimized for protein extraction from fixed tissue (Thacker *et al.* 2021) and tested on the human fetal tissue prior to use. The extraction buffer was prepared as follows: 500mM TRIZMA-Base (Sigma-Aldrich), 100mM Sodium Chloride (Sigma-Aldrich), 2% w/v Sodium Dodecyl Sulfate (Sigma-Aldrich), 1% v/v Triton X-100 (Sigma-Aldrich), 1% IGEPAL (Thermo Fisher Scientific), with the addition of Complete Inhibitor Cocktail (Sigma-Aldrich). pH was finally adjusted to 7.4 with hydrogen chloride. Total protein content was extracted by homogenizing followed by mechanical disruption by sonication, as previously described for fresh-frozen brain tissue. Following tissue disruption, samples were incubated at 90ºC for 90 minutes, as suggested by the protocol described in (Thacker *et al.* 2021). Tissue was vortexed for 30 seconds twice at regular intervals of 30 minutes during the period of incubation. The samples were then spun at 12.000 x *g* 10 min and the protein-containing supernatant was transferred in a new 1.5 ml Eppendorf tube. Protein extracts that were not immediately prepared for Western Blot analysis were in a -20°C freezer. Protein quantification was performed using a Bicinchoninic Acid (BCA) Protein Assay Kit (Thermo Fisher). Protein extracts were prepared for SDS-PAGE as described for frozen tissue in Section 2.3.3.1. As protein yield was significantly lower, the total volumes were adjusted accordingly and prepared at a final concentration of 0.6 µg/µL. Samples were finally heated at 95°C for 5 min, and stored at -20°C until further use.

2.3.3.3 Protein extraction from fresh-frozen brain tissue for Mass Spectrometry

Proteins were extracted from microdissected tissue of a 20 PCW (N=1, sample ID HDBR15984) human fresh-frozen brain. Two sections were manually microdissected from slab #6 (correspondent to medial and lateral portion of posterior temporal lobe (see **Figure 2.2 B**).

The brain tissue samples were defrosted gently from -80ºC storage temperature on ice. Each piece of tissue was transferred into 2ml CK14 soft Precellys homogenising tubes (Stretton Scientific) with 1.4 mm ceramic (zirconium oxide) beads designed for soft tissue homogenization, resuspended in 1ml freshly-prepared 8M Urea Buffer with the addition of 4M ammonium bicarbonate, and Complete Inhibitor Cocktail. Total protein content was extracted by homogenizing at 5500 rpm for 30 seconds twice.The samples were then spun at 12.000 x *g* 10 min and the protein-containing supernatant was transferred in a new 1.5 ml Eppendorf tube. Protein quantification was performed using a Bicinchoninic Acid (BCA) Protein Assay Kit (Thermo Fisher). Sample volumes equivalent to 50 µg total protein were sent to the Mass Spectrometry Research Facility (Chemistry Research Laboratory, University of Oxford, https://massspec.chem.ox.ac.uk/proteomics) for Liquid Chromatography Tandem Mass Spectrometry (LC-MS/MS) analysis (**Figure 2.6**).

Figure 2.6 **Proteomic analysis - pipeline**

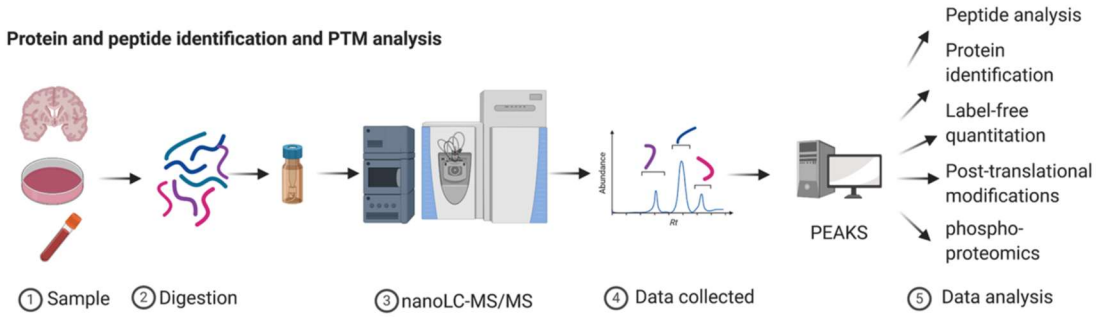

Figure 2.6: Pipeline of proteomic analysis. Representative snapshot taken from the website of the Mass Spectrometry Facility (https://massspec.chem.ox.ac.uk/proteomics) and illustrating the pipeline of the experimental work performed for proteomic analysis.

2.3.4 SDS-PAGE and Western Blot Analysis

Protein extracted from fixed or fresh frozen samples (**Sections 2.3.3.1 and 2.3.3.2**, respectively), or provided by Dr. Faye McLeod from organotypic cortical slices (stored at -80°C) were brought to room temperature and mixed by pipetting to ensure homogeneity of the protein content, before taking the amount needed for Western Blot. An equal homogenate amount was loaded on each gel (15 µg of protein from fresh-frozen brain tissue extraction; 7 µg of protein from PFA-fixed brain tissue extraction). Proteins were separated by Sodium dodecyl-sulfate polyacrylamide gel electrophoresis (SDS-PAGE) in a 4–20% Mini-PROTEAN® TGX™ Precast Protein Gels (BioRad) using Tris/Glycine/SDS 1X Running Buffer (BioRad). Electrophoresis was carried on for about 1.5-2 hours at a constant voltage of 100V. Proteins were then transferred onto iBlot® Gel Transfer Stacks Nitrocellulose membranes (Invitrogen) using an iBlot® Dry Blotting System (Invitrogen). The pre-designed programme #3 was selected, by following the datasheet of the instrument. Briefly, 20 V current was applied for 5 minutes (optimized transfer time for BDNF protein) or 7 minutes (optimized transfer time for VGF and CAPN1 proteins). Transfer parameters were selected according to the datasheet of the iBlot® Gel Transfer Device (pre-designed programme P3) and the transfer time was optimized according to each protein's molecular weight. Specifically, an electric current of 20V was applied for 5 minutes (transfer of BDNF protein) and 7 minutes (transfer of VGF and CAPN1 proteins). Membranes were washed 3 times in TBS-T solution (Tris-buffered saline with 0.1% Tween-20, pH 7,4) before proceeding with immunoblot analysis. Membranes were blocked 1 hour at room temperature with a 5% w/v solution of dried skimmed milk powder (SIGMA) in TBS-T (blocking solution) and then incubated with primary antibodies overnight at 4°C (**Table 2.5**) diluted in blocking solution to the appropriate concentration. After 3 washes of 10 min with TBS-T, membranes were incubated at room temperature with the species-appropriate horseradish peroxidise (HRP)-conjugated secondary antibodies (**Table 2.5)** appropriately diluted in blocking solution. Immunoreactivity was revealed with Clarity Western ECL Substrate (BioRad) and detected using a Bio-Rad ChemiDoc XRS+ system with Image Lab 6.0 software (Bio-Rad). Densitometric

measurements were analysed using Fiji (http://fiji.sc/Fiji) and each protein band was normalised to the correspondent loading control (GADPH or β-actin housekeeping gene).

Plots of the relative measurements were done using ggplot2 package in R.

Table 2.5. List of primary and secondary antibodies used for Western Blot analysis in the study

Primary Antibody (Target)	**Host Species**	**Supplier**	**Code/Cat.N.**	**Working Dilution**
VGF	Rabbit	Sima-Aldrich	ABN652	1/1000
BDNF	Rabbit	Abcam	ab108319	1/1000
GADPH	Mouse	Cell Signalling Technology	97166	1/2000
Beta-Actin	Rabbit	Abcam	ab8227	1/10000
Calpain 1	Rabbit	Proteintech	10538-I-AP	1/5000
Secondary Antibody HRP-conjugated				
Rabbit IgG	Goat	Abcam	ab97051	1/2000
Mouse IgG	Goat	Cell Signalling Technology	7076P2	1/2500

For each antibody is listed the molecular target, the species where it was raised, supplier name and specific code or catalogue number, and the working diution used for Western Blot protocol.

2.3.5 Enzyme-linked immunosorbent assay (ELISA)

Media from a 13 PCW (N=12 slices), 14 PCW (N=1 slice), and 17 PCW (N=2 slices) was tested to assess for the levels of VGF secreted by the human organotypic cortical slice into the culture medium were quantified using the Human VGF Nerve Growth Factor Inducible (VGF) ELISA kit (Abbexa abx25837).

Cortical slices from the 14 and 17 PCW brains were tested separately, as they were cultured into 6-well plates and the amount of individual medium that was retrieved from each well was sufficient for running the test in triplicates as defined below. The media from the 13 PCW cortical slices were cultured in smaller 12-well plates, therefore the media from 3 slices was pulled together into one experimental group before testing it by ELISA. The slices were pulled according to the experimental treatment they would have received after media change. Specifically, the medium was collected on the day of medium change over the culture protocol (after 4 days from the last media change) to ensure that any secreted molecule from the brain slice was present at the highest concentration that could be detected in culture. The medium was not further diluted for the ELISA test, and it was applied directly on the appropriate well of the 96-well plate provided by the kit. All the reagents and solutions needed for the analysis were prepared according to the datasheet of the kit. The pre-coated 96-well microplates was brought to room temperature, and 100 µl of standard and samples as triplicate were loaded into the wells and incubated for 1 hour at 37ºC. All liquid was discarded and 100 µl of Detection Reagent A was added to each well without prior washing. The plate was incubated for an additional hour at 37ºC, followed by 3 washes with 100 µl of Wash Buffer. 100 µl of Detection Reagent B was added to each well and the plate was incubated for 30 minutes at 37ºC, followed by additional 5 washes. Finally, 90 µl of TMB substrate was added to each well and incubated for 20 minutes at 37ºC covered from light sources. Afterwards, 50 µl of Stop Solution was added to each well and optical densities were measure at 490 nm by using a microplate reader, with wavelength correction at 570 nm. Two sets of standards were included: one diluted in Standard Diluent provided with the kit, and one diluted in culture medium. Medium components can interfere with the absorbance parameters, and lead to misinterpretation of the readings from the samples

tested. After evaluating the standard curves obtained, the standard dilutions prepared with culture medium was considered more appropriate for the analysis and therefore used for the analysis. An eight point-standard curve was generated using known concentrations of recombinant human VGF (500 pg/ml, serial dilution 1:2). Data analysis was performed by interpolating unknown concentrations with the recombinant human VGF standard curve after non-linear regression fit on log-transformed data (as described in the GraphPad Prism manual).

2. 4 BIOINFORMATICS

2.4.1 Bioinformatic analysis of Brainspan's datasets

Transcriptomic data on the human prenatal brain have been retrieved from the "**Developmental Transcriptome**" section of Brainspan (brainspan.org), which comprises of RNA-seq data collected across 13 developmental stages in 8-16 brain structures. Details about the donors, and the procedure for data acquisition are available in the section "Documentation" of the website.

For this study, I performed a first differential search by using the "*Differential Search*" tool. The search was performed with the two thalamic regions available (i.e. dorsal thalamus, DTH; mediodorsal nucleus of the thalamus, MD) as main target structure, and all the remaining neural tube structure available as a contrast structure. All prenatal (8-38 PCW) and perinatal (0-5 months) ages were selected for the search. The first 2,000 entries with their respective p-values and fold-change values were downloaded and analysed by using R programming language in R Studio.

The expression of VGF gene was also explored by a simple "*Gene Search*", without performing a differential search. The expression values of VGF in Dorsal Thalamus were plotted in form of log2 RPKM (reads per kilobase per million). Expression levels of a canonical cortical and one thalamic marker (i.e. SATB2 and GBX2, respectively) have been plotted together for comparison and ease of visualisation. All graphs have been generated using ggplot2 package of R.

The expression values of VGF in all thalamus and respective neocortical areas were plotted in a heatmap for visualization, in form of relative Fragments Per Kilobase of transcript per Million mapped reads (FPKM) values (0-6) with Morpheus software (https://software.broadinstitute.org/morpheus/).

The following brain regions have been selected as "thalamic" (TH):

- Dorsal thalamus, DTH
- Mediodorsal nucleus of the thalamus, MD

The following brain regions have been selected as “neocortical” (NCX):

- Dorsolateral prefrontal cortex, DFC
- Ventrolateral prefrontal cortex, VFC
- Anterior (rostral) cingulate (medial prefrontal) cortex, MFC
- Orbital frontal cortex, OFC
- Primary motor cortex, M1C
- Primary motor-sensory cortex (samples), M1C-S1C
- Parietal neocortex, PCx
- Primary somatosensory cortex (area S1, areas 3, 1, 2), S1C
- Posteroventral (inferior) parietal cortex, IPC
- Primary auditory cortex (core), A1C
- Temporal neocortex, TCx
- Posterior (caudal) superior temporal cortex (area 22c), STC
- Inferolateral temporal cortex (area TEv, area 20), ITC
- Occipital neocortex, Ocx
- Primary visual cortex (striate cortex, area V1/17), V1C

Microarray data available in the “**LMD Microarray**” section of Brainspan were also analysed, for integrating a more detailed spatial information on the expression pattern of genes of interest. This dataset comprises high-resolution neuroanatomical transcriptional profiles of ~300 distinct structures spanning the entire brain for four mid-gestational prenatal specimens (15 PCW; 16 PCW N=1; 21 PCW N=2). Details about the donors, and the procedure for data acquisition are also available in the section “Documentation” of the website. Expression levels of genes of interest are visualized in form of z-scores showing low-to-high presence of the specific transcript in schematic representations of coronal brain slices. These schematics are generated in the website, and shown in this work as snapshot taken from the webpage. Annotation of the brain regions was performed manually according to the “Reference Atlas” of Brainspan.

2.4.2 Bioinformatic analysis of single-cell RNA sequencing datasets

Raw read files selected for the single-cell transcriptomic analysis of the thalamus and cortical areas described in this work have been generated by the group of Professor Arnold Kriegstein (USCF) and deposited in the Nemoarchive data repository (link at: https://data.nemoarchive.org/biccn/grant/u01_devhu/kriegstein/transcriptome/scell/10x_v2/human/processed/counts/). All the files analysed were selected from sample "GW18" only (correspondent to 16 PCW). Read files deposited are already aligned to the GRCh38 human genome sequence (Genome Reference Consortium, 2011).

Data collection methods are available along with the files in the data repository.

The following datasets have been selected and downloaded for further analysis:

- GW18_thalamus (16 PCW thalamus)
- GW18_PFC (16 PCW prefrontal cortex)
- GW18_motor (16 PCW primary motor cortex)
- GW18_somato (16 PCW primary somatosensory cortex)
- GW18_V1 (16 PCW primary visual cortex)

All datasets were analyzed using R programming language in R Studio version 2021.09.1.

Cells with a gene count < 300, and genes that were detected in less than N=3 cells were removed from the dataset. Mitochondrial DNA content higher than 10% was used as a threshold to further filter out cells that were considered of poor quality from the dataset (i.e. dying cells). Cells that passed quality control criteria were included in the next steps of the analysis, which was performed using Seurat (Satija *et al.* 2015; Butler *et al.* 2018; Stuart *et al.* 2019; Hao *et al.* 2021). Data were first normalized by a scale of 10^6, and the first 2,000 variables were identified with the FindVariableFeatures tool in Seurat (method 'vst') and selected for Principal Component Analysis (PCA). To estimate the dimensionality of each datasets, and subsequently decide how many principal components to retain in the downstream analysis, Elbow Plots and Jackstraw Plots were generated for each dataset, using the ElbowPlot, JackstrawScore, and JackStrawPlot functions of

Seurat. Each Elbow Plot contains an intercept in the x-axis (dashed red line) showing the "elbow" separating the PCs that were considered relevant (on the right) and therefore retained, and the ones that were removed from further analysis (on the left) from each dataset (**Figure 2.7**). Specifically, the following numbers of PCs were retained from the datasets:

- 16 PCW_thalamus: 8 PCs
- 16 PCW_PFC (prefrontal cortex): 12 PCs
- 16 PCW_M1 (motor cortex): 8 PCs
- 16 PCW_S1 (somatosensory cortex): 10 PCs
- 16 PCW_V1 (visual cortex): 12 PCs

K-nearest neighbour (KNN) graph was created using the FindNeighbors function in Seurat with *k*-parameter set to 5. Clustering of the cells according to their transcriptomic signature similarity was performed with the Louvain method, with a resolution parameter set to 0.5 for all datasets. To visualize the data, non-linear dimensionality reduction was performed by both Uniform Manifold Approximation and Projection (UMAP) and t-distributed stochastic neighbour embedding (t-SNE).

Differential expression between clusters was calculated using the function FindAllMarkers in Seurat. Significantly differentially expressed genes were defined as ≥ 2-fold change and a Benjamini–Hochberg corrected p-value <0.25. Feature plots and Violin plots of marker genes were generated using the FeaturePlot and VlnPlot functions of Seurat.

Figure 2.7

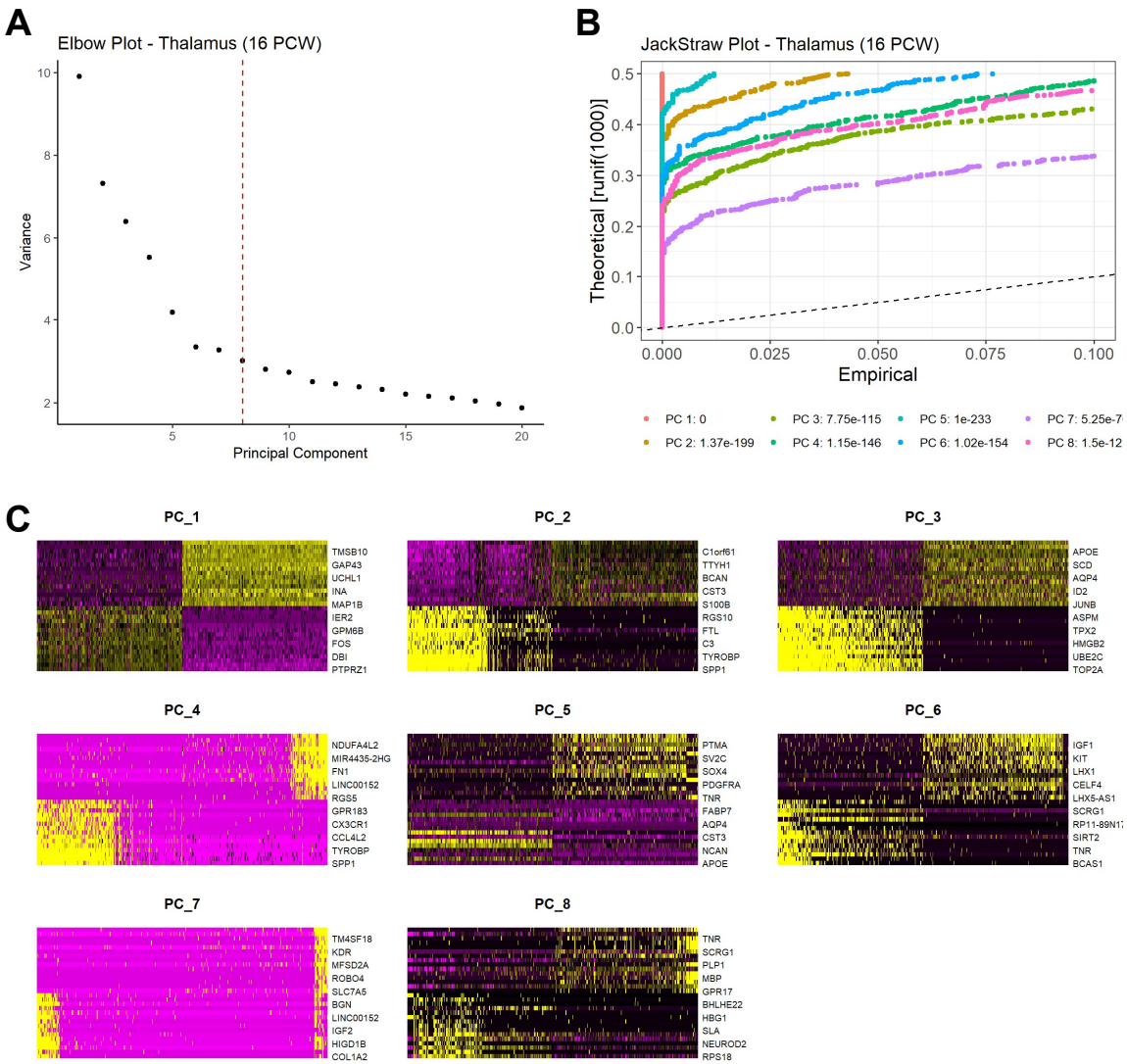

Figure 2.7: Representative steps of the pipeline used for single cell transcriptomics analysis of the 16 PCW human thalamus

(**A**) Elbow Plot showing the explained variation (y-axis) by each Principal Component (PC) (x-axis) after PC analysis (PCA). A dashed red line shows the cut-off arbitrarily chosen in the specific dataset for further downstream analysis. (**B**) The Jackstraw Plots provide a simple visualization of the statistical test (JackStrawScore) performed in each of the principal component retained, and representing their significance as a p-values. The dashed black interpolating line represents the normal distribution (null hypothesis of the statistical test). The closer the p-values of the PCs are found to this interpolating line, the less significant they are in explaining the variability of the dataset. (**C**) Heatmaps of the 10 most differentially expressed genes (DEGs) for each retained PC. All panels were generated on R Studio with Seurat pipeline for scRNAseq analysis.

2.4.3 Bioinformatic prediction of VGF-processing enzymes using Proteasix

A comprehensive list of peptides derived from the proteolytic cleavage of human VGF was extracted from the study by (Quinn *et al.* 2021) (see Chapter 1, **Figure 1.18 A**), and used as input in the Proteasix peptide-centric prediction tool (http://proteasix.cs.man.ac.uk/). This tool allows for the automatic reconstruction of N- and C- terminal cleavage sites and identification of observed and predicted proteases involved in the proteolysis of these cleavage sites in human, mouse, and rat, based on MEROPS specificity matrices (https://www.ebi.ac.uk/merops/). The MEROPS database is a resource for peptidases and peptidase inhibitors. At the time when this search was performed, the last released version of MEROPS was 12.4.

The following information on the peptides was used to build a table (**Table 2.6**), according to the guideline for user input from the Proteasix website:

- *Peptide identifier*: a unique name for each peptide on the list (labels of VGF peptides from Quinn *et al.,* 2021 were maintained)
- *Parent protein*: UniProt accession (AC) of the protein subjected to proteolytic cleavage (i.e. human VGF UniProt AC = O15240)
- *Start amino acid (AA)*: a number that indicates the Start amino acid position in the Parent protein sequence (from **Figure 1.18 A**, Quinn *et al*., 2021)
- *Stop amino acid (AA)*: a number that indicates the Stop amino acid position in the Parent protein sequence (from **Figure 1.18 A**, Quinn *et al*., 2021)

The output of such search by Proteasix Knowledge Base is a list of predicted proteases based on two prediction modes:

(i) *Observed*: matching against cleavage site associations collected from the literature to find proteases;

(ii) (ii) *Predicted*: calculating the probability of cleavage by a protease based on MEROPS (www.ebi.ac.uk/merops/) specificity matrices.

The output file from Proteasix was manually checked, and only proteases with a listed entry for Homo sapiens (column #6) were further retained.The resulting list was then manually adjusted into an excel file containing 3 columns, which was used as a "New Network" for Cytoscape version 3.9.1(https://cytoscape.org/). Specifically, the following information was extracted: (i) Peptide ID, (ii) Protease [Human only], Cleavage site, from

This information was used to build a network for vizualizing the results by using Cytoscape.

Table 2.6. Input list of human VGF peptides for protease prediction by Proteasix

Peptide ID	Parent Protein ID	Start AA	Stop AA
Signal Peptide	O15240	1	22
NERP-1	O15240	281	306
NERP-2	O15240	310	347
NERP-3	O15240	117	206
NERP-4	O15240	485	507
PGH	O15240	419	427
NAPP-19	O15240	485	503
NAPP-129	O15240	485	615
TLPQ-21	O15240	554	574
Antimicrobial Peptide	O15240	554	577
TLPQ-62	O15240	554	615
HYPG	O15240	575	615
AQEE-30	O15240	586	615
LQEQ	O15240	597	615

Input list of human VGF peptides with correspondent start and stop amino acids used as input of the search performed in Proteasix and derived from Quinn *et al.,* 2021.

2.5 *IN VITRO* TECHNIQUES

2.5.1 *In vitro* culture of human iPSC-derived cortical neurons

Human cortical neurons were derived from genetically engineered induced pluripotent stem cell (iPSC) containing a doxycycline-inducible neurogenin 2 (NGN2) transgene inserted into the AAVS1 "safe-harbor". The i3N iPSC have isogenic, integrated, and inducible NGN2 expression and neurons derived from them have been named i3Neurons. The two-step protocol used for deriving i3Neurons has been previously described (Wang *et al.* 2017; Maguire *et al.* 2019; Boecker *et al.* 2020; Boecker *et al.* 2021), includes (i) iPSC proliferation and (ii) pre-differentiation. The protocol, schematized in **Figure 2.8**, has been shown to yield large amounts of i3Neurons with minimal well-to-well variability. i3Neurons obtained from this protocol have also been extensively characterized in these studies. Importantly, upon treatment with doxycycline, NGN2 iPSC rapidly exit the cell cycle and become entirely post-mitotic within three day (Day 0). At this stage, cells express classic markers for neural progenitor cells (Pax6, Sox2, and Nestin; observation from the laboratory); however, they are not mitotically active anymore. Within a week from sub-plating, they exhibited neuron-like morphology and they finally mature within 3-4 weeks in the absence of glia (Wang *et al.* 2017). All i3Neurons express vesicular glutamate transporter 1 (VGlut1), a marker of glutamaergic neurons. *In vitro* protocols involving iPSC-derived cultures were carried out in the laboratory of Professor Richard Wade Martins (DPAG, University of Oxford) by Dr. Becky Carlyle and Laura Pearson.

Figure 2.8

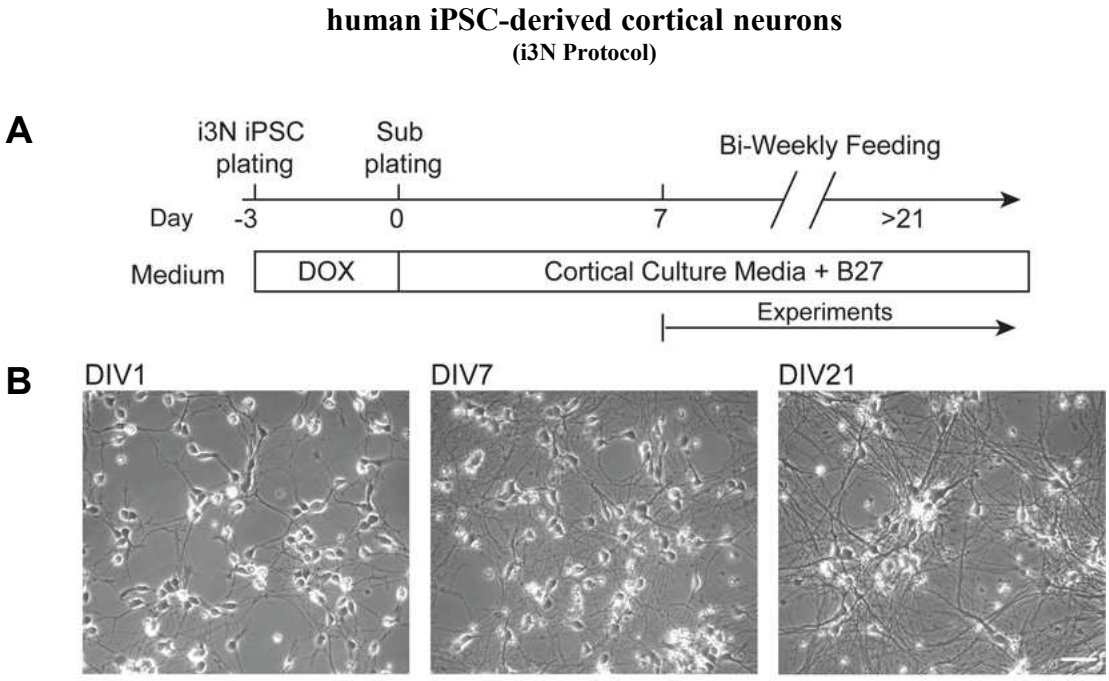

Figure 2.8: Schematic of the protocol used for differentiation of i^{3}Neurons from doxycycline(DOX)-inducible NGN2 induced pluripotent stem cells (iPSC). (B) Representative bright-field microscope images of the cells at different timepoints of the differentiation protocol. Scale bar =50 μm.
Adapted from Boeker et al. 2020.

2.5.2 *In vitro* culture of human cortical organotypic slices

Human fetal brain tissue was obtained from the joint MRC/Wellcome Trust funded HDBR (https://www.hdbr.org/Project 200428) at the University of Newcastle. All tissue was collected with appropriate maternal consent according to the ethical approval granted from the Newcastle and North Tyneside NHS Health Authority Joint Ethics Committee (REC reference: 18/NE/0290). Cultures were prepared from unfixed foetal brains (N=1 from 13 PCW; N=1 from 14 PCW; N=2 from 17 PCW). Slices were sectioned using a 5100mz Vibratome (Camden Instruments) (280 µm), and then transferred to 6-transwell plates containing BrainPhys (5790; Stemcell Technologies) culture media supplemented with 1 x N2, 1 x B27, 40ng/ml Brain-derived Neutrophic Factor (BDNF), 20ng/ml Glia-derived Neurotrophic Factor (GDNF), 30ng/ml Wnt7a, 200 nM ascorbic acid, 1 mM dibutyryl cyclic AMP and 1 µg/ml laminin. Culture media, which was changed every 4 days. The plates were maintained at 37°C, 5% CO2 in ambient O2 and 90% humidity.

Sample collection, cutting, and maintenance was entirely performed by Dr. Faye McLeod in Newcastle in dedicated facility of the Biosciences Institute, Medical School (University of Newcastle). The experimental procedure described in this work were carried out under Dr. McLeod supervision in the same facilities. Further details of the protocol used for human cortical slices are available in the supplementary material of the study by Dr. McLeod (McLeod *et al.* 2023).

2.5.3 *In vitro* application of recombinant human VGF

Human recombinant VGF protein (Abbexa) was resuspended in sterile distilled water with the addition of 0.1% bovine serum albumin (BSA), at a final concentration of 200 ng/µL and stored into stock aliquots at -20ºC until used. The amount of stock protein resuspension was calculated according to the amount of fresh media added on the day of media change for each sample, and added directly into the culture media of both organotypic brain slices and i3Neurons.

Dosage for the treatments were chosen following the protocols used for similar experiments carried out in rodent organotypic slices (Sato *et al.* 2012), as followed:

- Low dose VGF = 12 ng/mL
- Medium dose VGF = 120 ng/mL
- High dose VGF = 1200 ng/mL

Untreated controls were replaced media without addition of VGF.

Recombinant VGF was applied for 4.5 days *in vitro*. Neuronal cultures and cortical slices were then fixed in 4% PFA before staining (see Chapter 6, **Sections 6.1.1 and 6.1.2.1**), or analysed for calcium-imaging on the last day of treatment (see Chapter 6, **Section 6.1.2.2**).

Content of the Thesis

My thesis is organized into four experimental chapters, including a concluding comprehensive discussion at the end of each. In **Chapter 3**, I analyse the dynamics of the earliest thalamocortical projections in the human prenatal brain by immunohistochemical and carbocyanine-based axonal tracing analyses. I show that thalamocortical afferents (TCA) reach the immature cerebral cortex very early during human brain development, maintain close anatomical relationship with the germinal compartments, and by mid-gestation they start projecting not only toward the subplate as in other mammals, but also into the outer subventricular zone (OSVZ). By co-immunostaining, I further show that both Tbr1-positive subplate neurons and HOPX-positive outer radial glial cells (oRGC) are contacted by these early thalamocortical axons, which in turn might exert an influence via paracrine mechanisms. A promising candidate mediator of this action is neurosecretory protein VGF (Sato *et al.* 2012; Monko *et al.* 2022; Sato *et al.* 2022). In **Chapter 4** I present my hypothesis on the evolutionary adaptation of this factor in the development of human thalamocortical system. According to this hypothesis, VGF was repurposed over evolution from its role in the functional maturation of primary sensory cortices, to sustain the development of evolved associative areas in the human brain. To validate this proposition, I analyse the area-specific expression pattern of VGF mRNA in the human fetal brain by using available transcriptomic datasets (microarrays, bulk RNA-seq, single-cell RNA-seq). I showed that VGF is preferentially expressed by the thalamus as compared to the cortex. The identity of VGF-expressing thalamic cells is unveiled as mature projecting excitatory neurons. These findings are further corroborated by my qPCR analysis conducted on *post mortem* human fetal brain tissue.

In **Chapter 5**, I explore VGF protein distribution throughout the thalamus and cortical areas of the human fetal brain (13-20 PCW) by Western Blot and immunohistochemical analyses, and show that VGF protein can be detected not only in the thalamus, but also throughout the cortical areas where it is transported via thalamic axons. Within the cortex, VGF is not confined to the intermediate zone (IZ) where thalamic axons extend tangentially, but it is also diffusely detectable within post-mitotic compartments and the germinal zones. In line with my hypothesis, the frontal cortex, where MD axons

project, exhibits a particularly abundant amount of VGF protein. A preliminary proteomic analysis further confirms the presence of VGF protein in the human fetal cortex, although at significantly lower levels than in the adult, suggesting a developmental regulation of endogenous VGF expression in the human cortex. Finally, I start addressing the mechanisms involved upon VGF secretion from thalamic axons in the fetal cortex in **Chapter 6**. I employ two complementary *in vitro* approaches to assess the functional effects of full-sized VGF in human progenitor cells in 2D iPSC-derived cell cultures and a human 3D organotypic cortical slice culture. My findings suggest that while full-sized protein does not affect progenitor mitotic rates, it does increase the spontaneous calcium activity in the SPN as early as 13 PCW. Since VGF can undergo proteolytic processing and produce different neuroactive peptides that cannot be easily detected by conventional molecular analysis, I apply an indirect approach to investigate this aspect. I used a bioinformatic approach to predict the potential proteases that might cleave VGF. After selecting some interesting candidates, I assessed their expression profiling in the human fetal brain by using similar approaches employed for VGF profiling at mRNA level (Chapter 4), and at protein level for one selected case (Calpain 1).

In the general discussion **Chapter 7**, I link up the findings of my experimental chapters, highlight limitation of the study, and outline the potential avenues for future explorations. My experimental observations pave the way for further investigations into VGF peptide distribution, release and function and eventually get some insights into the specific molecular mechanisms involved in the modulation of human cortical progenitors of the OSVZ and neurons of the SP by early thalamic axons. These interactions could contribute to the developmental processes that shape the cortex to differentiate into circuits that perform their region-specific computational functions.

CHAPTER 3

Tracing of the earliest thalamocortical axons in the human fetal brain

INTRODUCTION

The environmental influences for most sensory input reach the cerebral cortex through the thalamocortical projections. The role of extrinsic modulation exerted by early thalamic axons in the arealization of the human cerebral cortex during fetal development remains poorly characterized. On the one hand, rodent studies often lack validation in the primate brain, in particular for associative and prefrontal areas which might not exist in rodent, thus limiting our insight and assumption to the specification of sensory vs non-sensory (i.e. motor) areas. On the other hand, the impact of thalamic axons on the developmental process of the human cortex is of crucial importance. In our species, cortical neurogenesis is significantly prolonged, and the transient compartments near the ingrowing and accumulating thalamic axons, such as the subplate zone and the outer subventricular zone, are particularly expanded.

In this Chapter, my objective was to investigate the spatiotemporal dynamics of the earliest interactions between thalamic axons and the developing neocortex in humans. I focused on assessing the earliest timepoints and the specific compartments that thalamic axons reach, aiming to gain an overall understanding of these initial interactions. To this aim, I firstly performed a time-course analysis of the thalamic axonal invasion of the prospective cortex to determine the earliest timepoint where these interactions are established during human brain development. To do so, I conducted immunohistochemistry analysis of one embryonic (carniage stage 19) and three early fetal human brains (8, 10, and 12 PCW) stained for the early marker of human thalamocortical axons (Mountcastle) secretogranin (SCGN), and corticothalamic axons (CTA) calretinin (CalR) (Alzu'bi

et al. 2019). My observations were in line with recent literature showing that thalamocortical axons successfully cross the diencephalic-telencephalic boundary (DTB) and pallial-subpallial boundary (PSPB) earlier than the reciprocal corticothalamic axons, and reached the cortex by 8 PCW in human (Alzu'bi *et al.* 2019).

Then, I explored the earliest cortical target(s) of thalamic axons by performing a carbocyanine dye-based axonal tracing experiment to characterize the cortical target(s) of TCA in human *post mortem* fixed brain. Specifically, I analysed one embryonic (Carniage Stage 21, CS 21) and two mid-gestation (13 and17 post conception weeks, PCW) human brains, and I investigated the cortical regions reached by DiI-labelled thalamic axons that were traced directly from the dorsal thalamus by epifluorescence and confocal microscopy. I observed innervation of cortical areas by thalamocortical axons (Mountcastle) by 13 PCW with this method and the immunohistochemical analysis indicates that this might even start earlier. The DiI labelled thalamocortica axons exhibited a close anatomical relationship with the germinal compartments. Interestingly, by 17 PCW, TCA not only innervated the subplate, which is a well-known target for thalamic axons in various mammalian species, but they also innervated the outer subventricular zone (OSVZ). This cortical layer represents the largest compartment of the germinal zones in the human brain at this age. This phenomenon, previously observed only in monkeys (Macaca mulatta) with similar tracing methods (Carney *et al.* 2004; Carney *et al.* 2007). No such interaction has been described in other species, suggesting that it may be a transient and species-specific event. It potentially enables extrinsic cues from the thalamus to exert a more precise and refined modulation of cortical development in the complex human brain.

Overall, the data presented in this Chapter provide insights into the early and complex dynamics of the thalamocortical axon interactions with the developing human cortex. These findings suggest the presence of a novel mechanism for the extrinsic modulation of human cortical development through the modulation of outer subventricular zone (OSVZ) progenitors.

3.1 Time-course analysis of the earliest thalamic innervation of the human fetal cortex by immunohistochemistry (embryonic and early fetal periods)

Recent immunohistochemical analysis have shown that thalamic axons start interacting with the developing cortex at exceptionally early stages in humans (Alzu'bi *et al.* 2019). Therefore, I first aimed to confirm this observation by examining available data. I also wanted to confirm these findings with direct carbocyanine dye tracing from dorsal thalamus, since the immunohistochemical labelling does not reveal the precise origin or the destination of these projections. However, during these initial stages, the human brain is small, making it challenging to perform DiI placement experiments, especially with the limited availability of samples at these timepoints. Therefore, relying solely on DiI-based axon tracing would have been inappropriate. To overcome this limitation, I utilized the open-source collection of brightfield images in the open-source Atlas provided by the Human Developmental Biology Resource (HDBR). This database includes a series of immunohistochemistry images of human brain sections, which span from embryonic to fetal stages. This approach allowed me to include the earliest timepoint, around 7 PCW, where thalamic axons were observed reaching the immature telencephalon in humans (Zunic Isasegi *et al.* 2018; Alzu'bi *et al.* 2019). By combining this image analysis with DiI-tracing experiments, I could achieve a more comprehensive characterization of these earliest thalamocortical interactions across a broader range of developmental ages. Specifically, I selected serial slides stained for the secretogogin (SCGN), a calcium-binding protein specifically expressed by projecting thalamic neurons at early stages of development (Alzu'bi *et al.* 2019). SCGN can be detected both in the cell body and axon of these neurons thus allowing for a reliable tracing of the earliest TCA (Alzu'bi *et al.* 2019). I also evaluate in parallel the dynamics of the reciprocal corticothalamic axon (CTA) extending from cortical projecting neurons expressing calretinin (CalR) (Alzu'bi *et al.* 2019) to the thalamic region by selecting serial sections from the same samples. I specifically focused on the earliest stages of fetal development when thalamocortical connections reaching the cortex have been reported (Meyer *et al.* 2000; Krsnik *et al.* 2017; Alzu'bi *et al.* 2019). One embryonic human brain (CS 19, corresponding to 6.5 PCW) and three fetal brains (8, 10, and 12 PCW) were included in this analysis.

A representative snapshot of the full-sized sections is illustrated in **Figure 3.1**. Serial sections were stained for both CalR (**Figure 3.1 A, C, E, G**) and SCGN (**Figure 3.1 B, D, F, H**). All tissue sections were 4μm-thick paraffine embedded (see Methods Chapter 2 Section 2.2.4.4).

SCGN-positive thalamocortical projecting neurons were detected at **6.5 PCW** in the diencephalic region (**Figure 3.2 B**). These neurons already extended their axons past the telencephalic-diencephalic boundary (**DTB**) and are found close to the pallial-subpallial boundary (**PSPB**) (**Figure 3.2 D**). Since I found the anatomical landmarks ambiguous I decided to extend my analysis to region-specific markers that define them at molecular level. Even though the pioneer TCA were already extended to the telencephalon, no expression of SCGN was detected in the cortical territory at this early timepoint (**Figure 3.2 F**). **CalR**-positive pioneer neurons were detected within a discrete region of the ganglionic eminences at the PSPB (**Figure 3.2 A, C**). Some of these neurons were labelled extending along the trajectories of the lateral cortical stream (Gonzalez-Gomez *et al.* 2014). No CalR-positive signal was detected at the level of the immature cortex (**Figure 3.2 E**), suggesting that the corticothalamic projecting neurons have yet to be generated and/or express calretinin at substantial level at this time.

SCGN-positive pioneering axons successfully crossed the PSPB and extended toward their final target in the cortex as early as **8 PCW** (**Figure 3.3 B, D**). Here, they extended tangentially to the cortical surface within the intermediate zone (IZ), between cortical plate (CP) and germinal zone (ventricular zone, VZ) (**Figure 3.3 F**). CalR-positive corticofugal axons were now visible in the cortex close to their origin(Meyer *et al.* 2000) (**Figure 3.3 A, E**) and in the internal capsule, where they extend adjacent to the thalamocortical afferents. The CalR-positive signal was not detected at the level of the DTB at this stage (**Figure 3.3 A, C**).

By **10 PCW**, the corticofugal axons have reached the diencephalic region, as previously reported by Alzu'bi and colleagues (Alzu'bi *et al.* 2019). However, it is important to note that the CalR-positive signal detected at the level of the thalamus represents also an intrinsic expression of this marker by thalamic neurons. The CalR-immunoreactivity signal significantly increased in intensity

especially at the level of the cortex by this time (**Figure 3.4 A, C, E**). The corticofugal axons extend within the IZ close to the SCGN-immunoreactive thalamocortical axons, which reached the cortex by 10 PCW (**Figure 3.4 E, F**). Notably, the thalamocortical afferents were located deeper within the IZ, and they appeared closer to the germinal zones on the ventricular side, while the corticothalamic efferents ran more superficially to these fibers (Zunic Isasegi *et al.* 2018).

By **12 PCW**, both SCGN-positive thalamocortical afferents and CalR-positive corticothalamic efferents were observed in the intermediate zone of the cortex. These axons extended near to each other as they travelled within the internal capsule towards their respective targets. (**Figure 3.5**). As previously reported (Alzu'bi *et al.* 2019), the immunoreactivity for CalR in the cortical IZ was weaker, while its intensity increased in the axonal fibers projecting to the thalamus via the internal capsule (**Figure 3.5 C, E**). On the other hand, SCGN-positive signal remained strong, and visible at the level of the thalamus (**Figure 3.5 B**), the PSPB and internal capsule (**Figure 3.5 D, F**), as well as in the cortical IZ (**Figure 3.5 H**). At this stage, the pattern of distribution of CalR and SCGN within the cortex was less sharply defined, as compared to the 10 PCW brain (**Figure 3.5 G, H**).

Overall, this time-course analysis of the earliest interaction between thalamic afferents and the developing human cortex were in line with the observations by Alzu'bi and colleagues (Alzu'bi *et al.* 2019) and suggested a very early arrival of TCA into the developing cerebral cortex in the human brain.

Figure 3.1

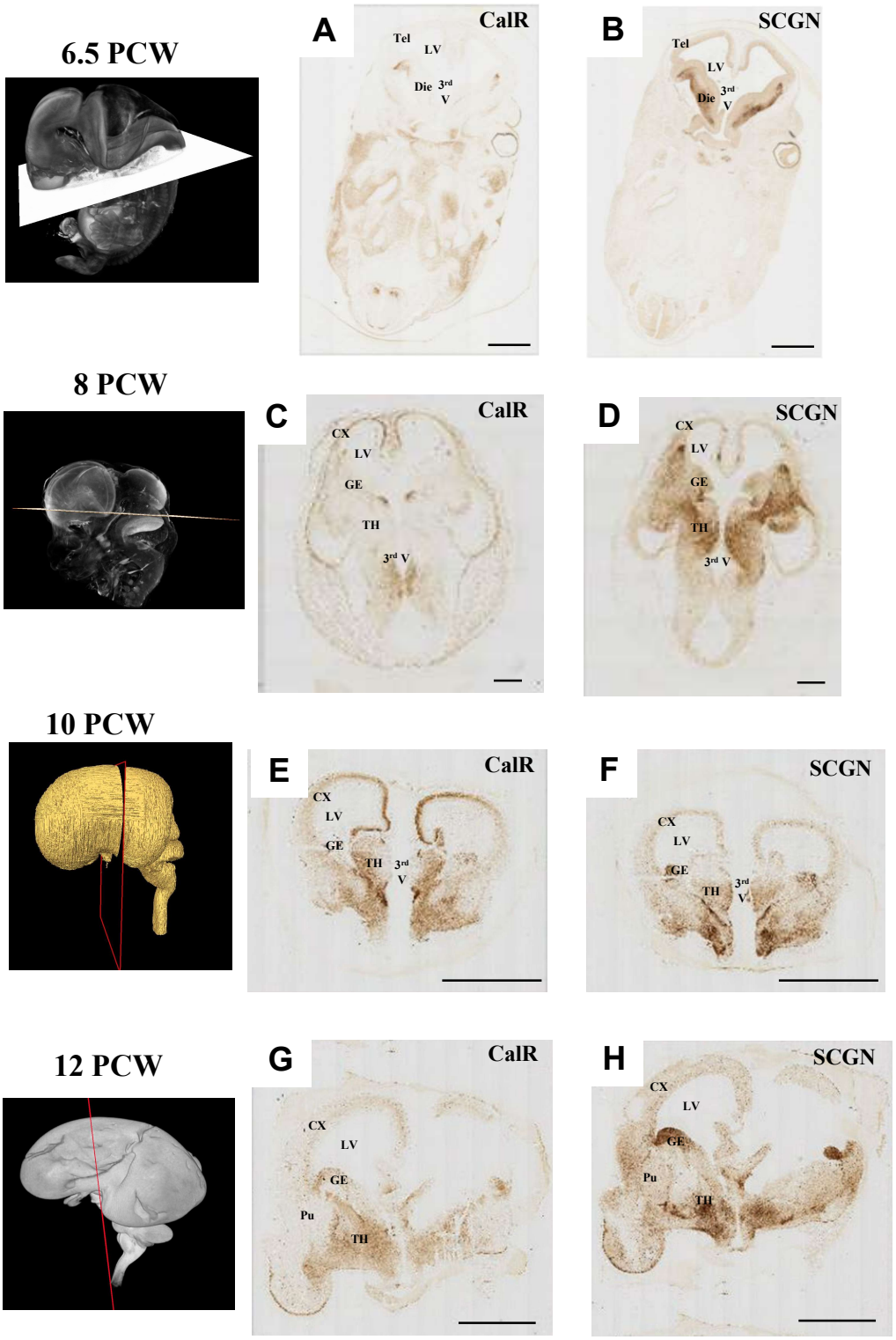

Figure 3.1: Representative snapshots of the whole-head section of the four human samples analysed by immunohistochemistry for Secretagogin (SCGN) and Calretinin (CalR) to reveal the earliest thalamocortical and corticothalamic axons, respectively. The plane of each section is indicated on the 3D model for each prenatal stage on the left side. The following samples were analysed: one embryonic brain from Carniage Stage 19 (ca. 6.5 PCW) (A, B); three fetal brain samples from 8 PCW (C, D), 10 PCW (E, F), and 12 PCW (G, H). Scale bars = 1 mm (A-D); 5 mm (E-H).

Figure 3.2

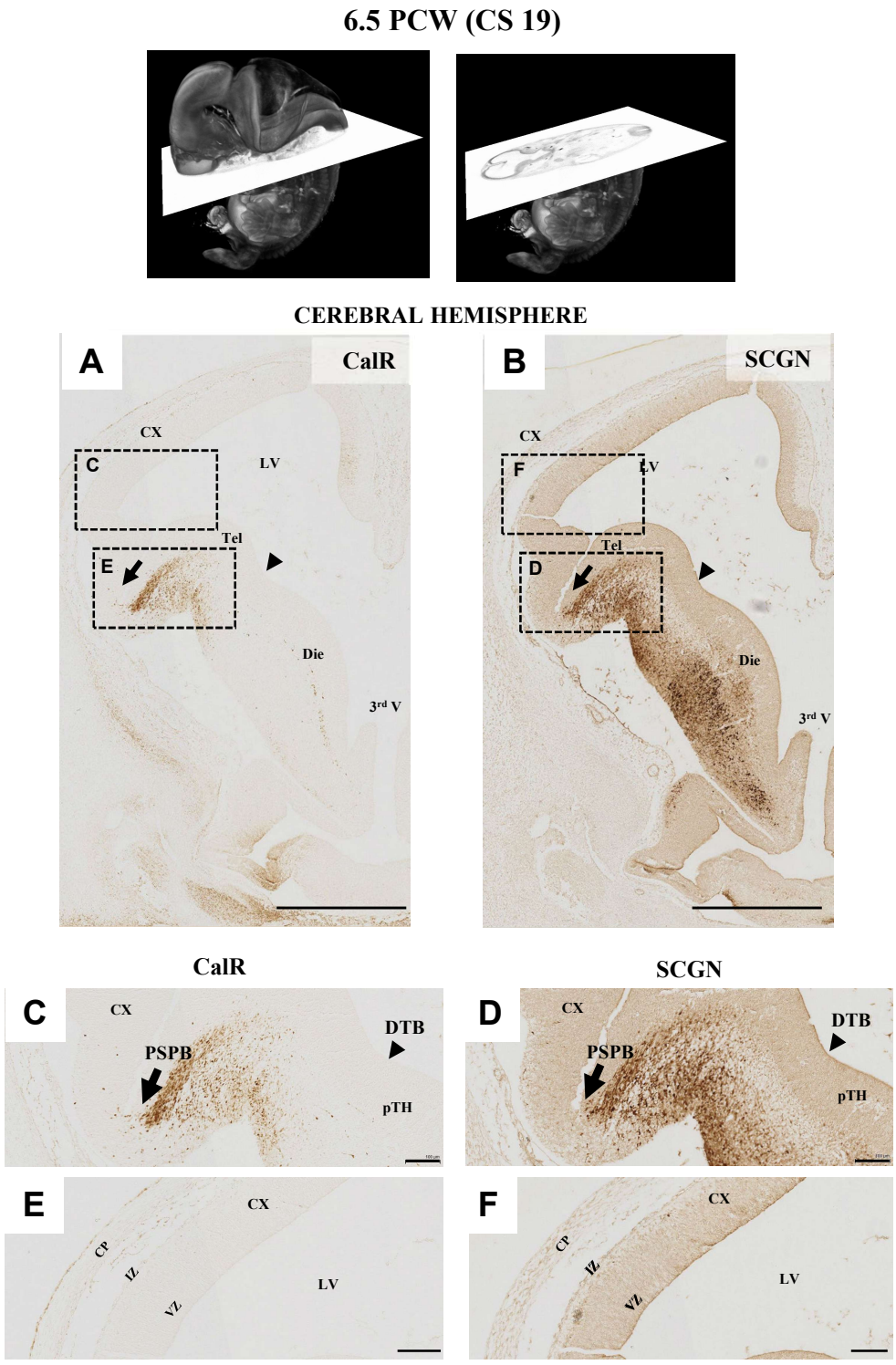

Figure 3.2: Secretagogin (SCGN)-positive thalamocortical axons and Calretinin (CalR)-positive corticothalamic axons in transversal sections of 6.5 PCW (CS 19) human brain. The plane of section (transversal) is indicated on the 3D model of the 6.5 PCW human brain on the top. (**A**) CalR-positive neurons at this stage are pioneer migrating neurons of the ventral migratory stream near the PSPB (arrow) (**C**). No corticofugal neurons are detected with this marker at 7 PCW in the primordial cortex (**E**) nor projecting past the DTB (arrowhead) (**C**). (**B**) SCGN immunoreactivity revealed thalamic projections originating from the diencephalon. The signal is positively detected at both the DTB (arrow) and the PSPB (arrowhead) (**D**). No signal is yet detected at cortical level at this stage (**F**). Scale bars = 1 mm (A, B); 100 µm (C-F).

Figure 3.3

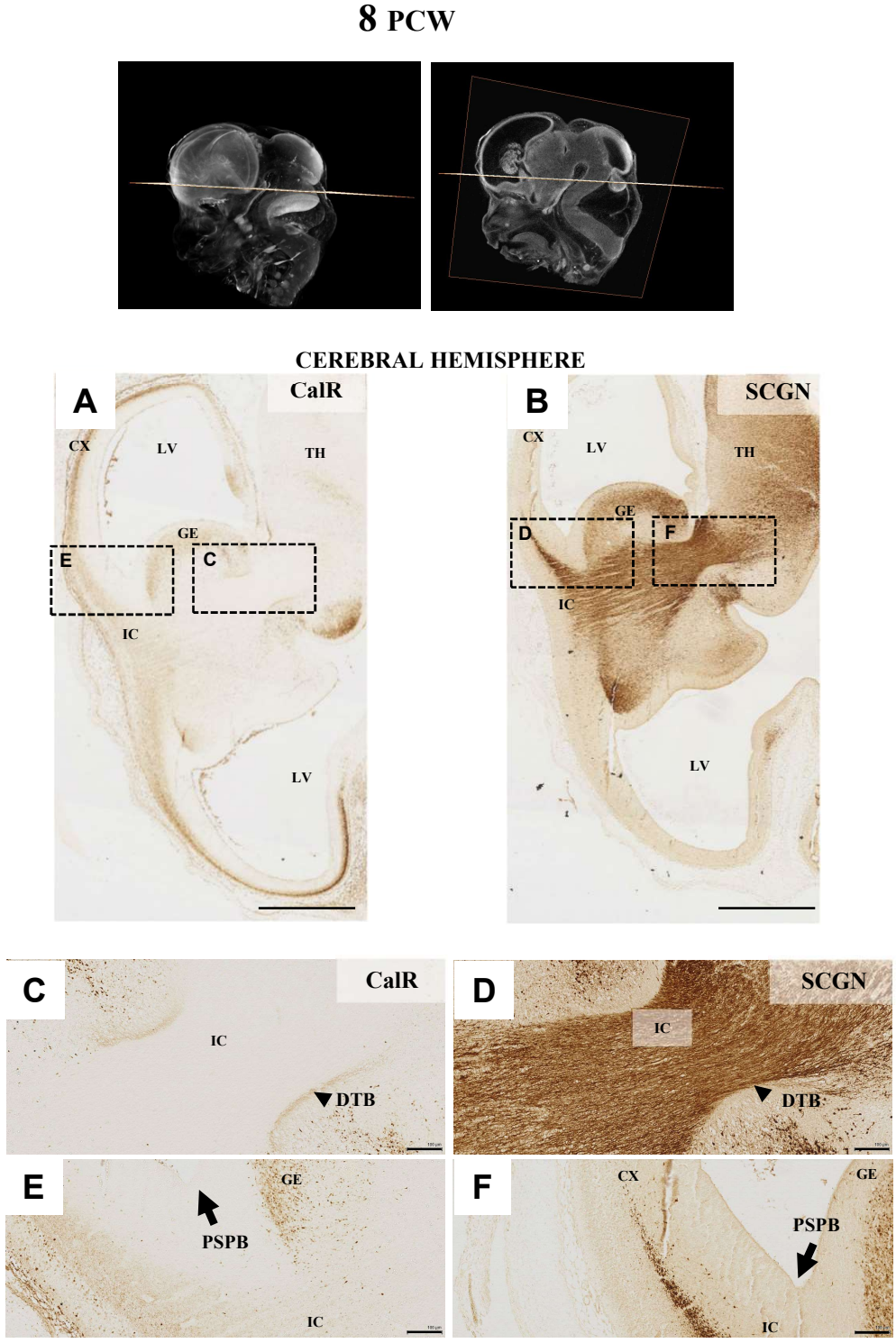

Figure 3.3: Secretagogin (SCGN)-positive thalamocortical axons and Calretinin (CalR)-positive corticothalamic axons in horizontal sections of 8 PCW human brain. The plane of section (horizontal) is indicated on the 3D model of the 8 PCW human brain on the top. **(A)** CalR-positive neurons at this stage are positively detected in the cortex and project their axons in the internal capsule crossing the PSPB (arrow) (E) but not yet the DTB (arrowhead) (C). Conversely, SCGN-positive axons from thalamocortical projecting neurons are detected at both boundaries (D, F), and already reached the cortical territories by this age. Scale bars = 1 mm (A, B); 100 µm (C-F).

Figure 3.4

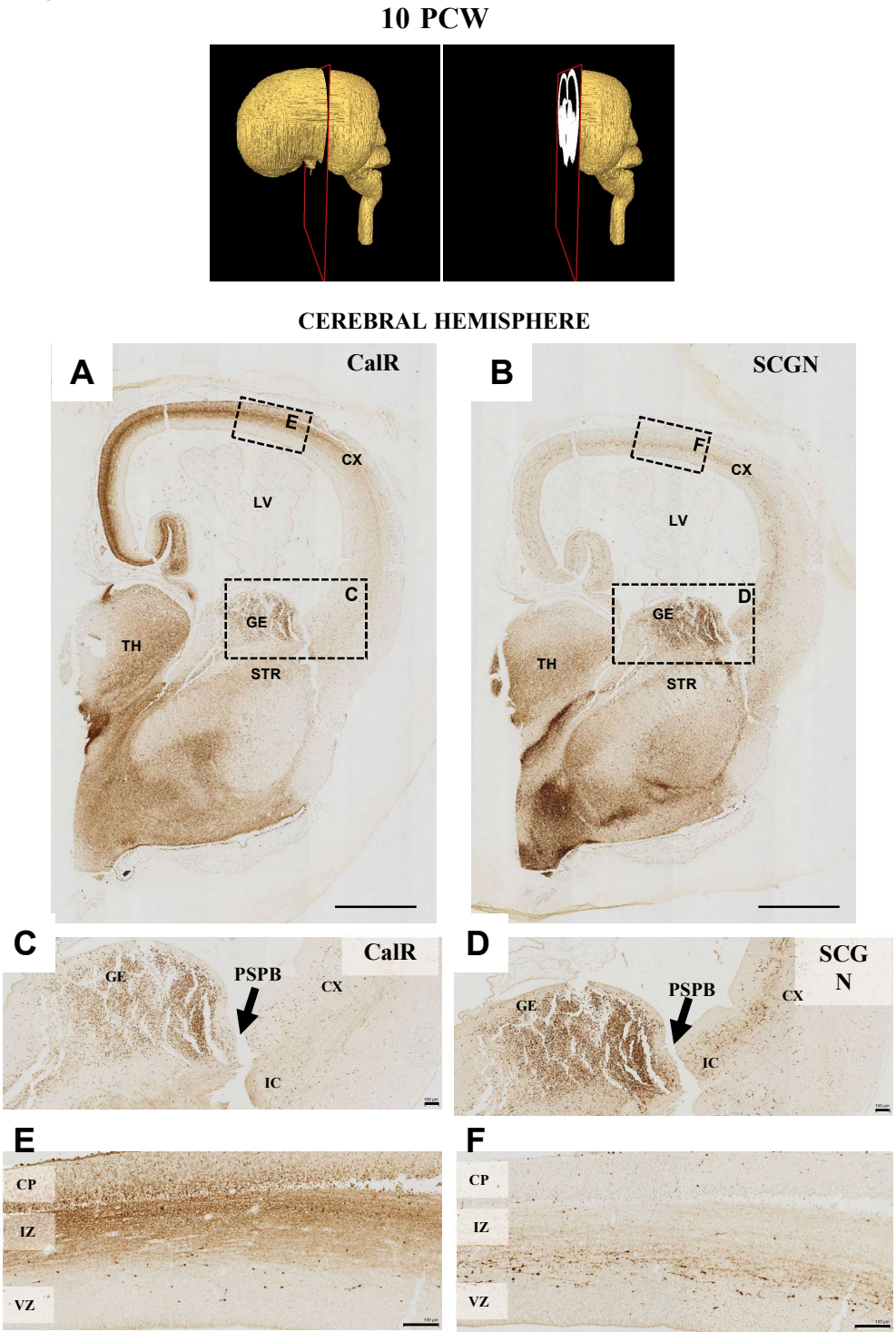

Figure 3.4: Secretagogin (SCGN)-positive thalamocortical axons and Calretinin (CalR)-positive corticothalamic axons in coronal sections of 10 PCW human brain. The plane of section (coronal) is indicated on the 3D model of the 10 PCW human brain on the top. (**A**) CalR-positive signal is strongly detected in the cortex (**E**), through the internal capsule (**C**) and throughout the thalamus. CalR-positive signal is also strongly detected in the lateral ganglionic eminance (**A, C**). (**B**) SCGN-positive signal is detected in the thalamus, especially in its medial aspect, as well as in the internal capsule after crossing the PSPB (arrow) (**D**). SCGN-positive signal is also found the cortical IZ ventrally to the CalR-positive axons (**D**). Scale bars = 1 mm (A-D); 100 µm (E-H).

Figure 3.5

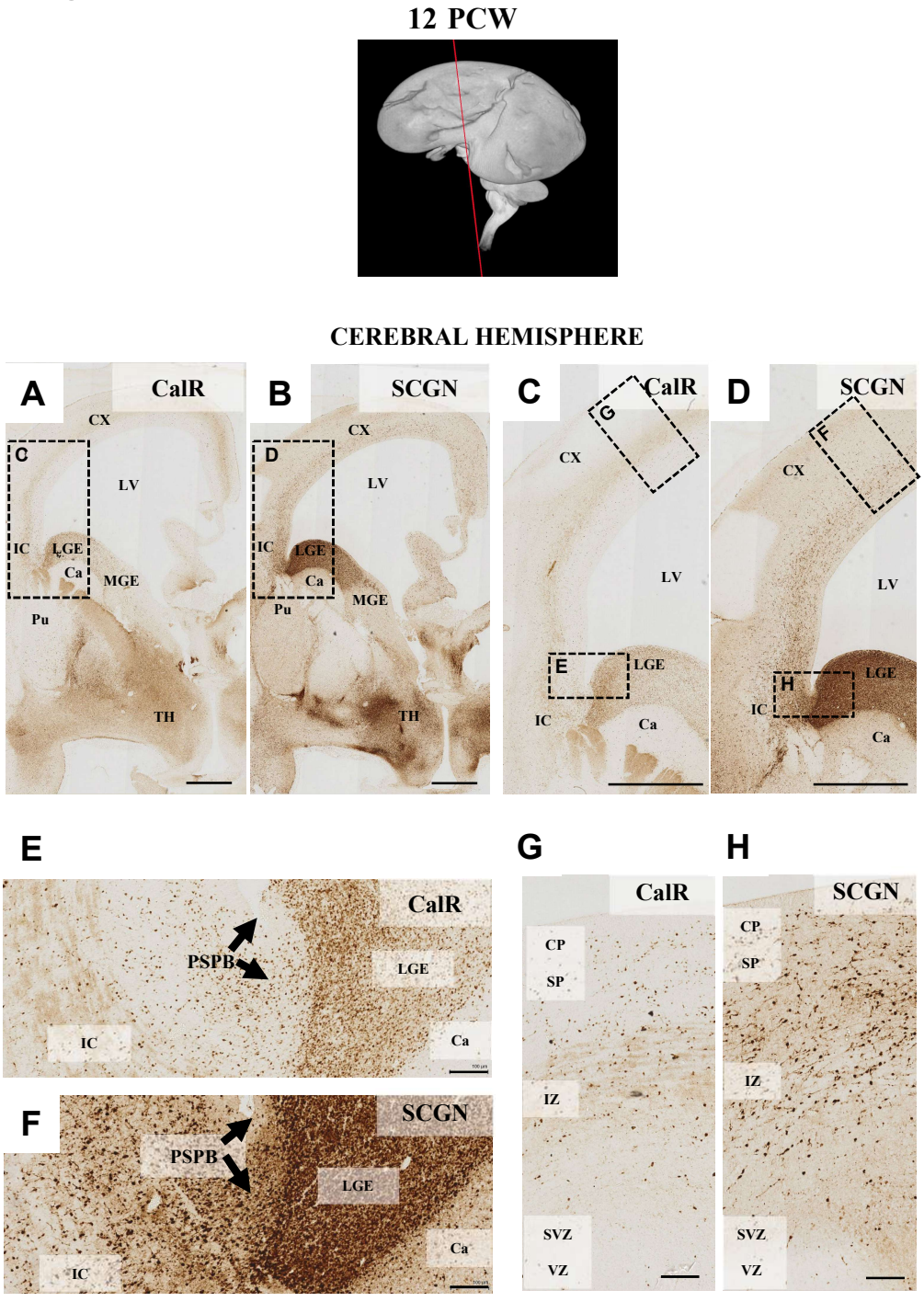

Figure 3.5: Secretagogin (SCGN)-positive thalamocortical axons and Calretinin (CalR)-positive corticothalamic axons in coronal sections of 12 PCW human brain. The plane of section (coronal) is indicated on the 3D model of the 12 PCW human brain on the top. (**A**) CalR-positive signal is detected in the cortical IZ (**C, G**), through the internal capsule (**C, E**) and throughout the thalamus. CalR-positive signal is also strongly detected in the lateral ganglionic eminance (**C, E**). (**B**) At 12 PCW, SCGN-positive signal is observed not only in the thalamus, internal capsule (**D, F**), but is also distributed in the cortical IZ ventrally to the CalR-positive axons (**D, H**). Scale bars = 1 mm (A-D); 100 µm (E-H).

3.2 Carbocyanine dye-tracing of thalamic axons in the human fetal brain

3.2.1 7 post-conception week (PCW) (Carniage Stage 21)

The earliest stage of development used for axonal tracing with carbocyanine dye (DiI) was Carniage Stage 21 (CS21), correspondent to 7 PCW. For consistency of the nomenclature, in this section the age is indicated as post conception weeks rather than Carniage Stage. Notably, this sample represents an intermediate stage of development between the first two samples analysed by immunohistochemistry in Section 3.1 (i.e., 6.5 and 8 PCW, see **Figures 3.1 A-D; 3.2; 3.3**).

Figure 3.6 A depicts the sample, as a whole head before being processed for the experiment. The brain was cut at the level of the boundary between the diencephalic ("Die") and rhombencephalic ("Rhomb") vesicles in order to expose the posterior surface of the prospective thalamus. **Figure 3.6 B** shows the location of the DiI crystal placement into the dorsal aspect of the diencephalon. DiI crystals were placed bilaterally (not shown). After a few weeks of incubation of the sample at room temperature to allow for diffusion of the lipophilic tracer along cell membranes, the brain was embedded into agarose and sectioned at 100 μm in the coronal plane. As shown by the schematics of the slices (**Figure 3.6 C**), the plane of sectioning is not perfectly coronal and therefore the two hemispheres sampled in each slice do not represent the exact same level of the antero-posterior axis. The anatomical annotation reflects the actual structures present in each slice.

Dorsal thalamic DiI placements broadly labelled the diencephalic region in the 7 PCW brain. The site of injection was consistently visible in all the sections analysed along the antero-posterior axis. Thalamic progenitor cells that were labelled at the level of the crystal placement site could be observed projecting from their cell bodies near the site of DiI placement to the ventricular side (**Figures 3.7 A-D**).

From the dorsal thalamus, DiI-labelled axons were observed **crossing the DTB** (**Figures 3.9 A, B; 3.11 A, B, E-J**). Immunofluorescence staining for Roundabout Guidance Receptor 1 (ROBO1), a classic marker of thalamocortical axons (Marcos-Mondejar *et al.* 2012; Alzu'bi *et al.* 2019), was used to confirm the region delineated as diencephalic boundary. ROBO1-immunopositive signal in Slice D is shown in **Figure 3.11 B, D, F** overlapping extensively with the DiI-positive fibres in **Figure 3.11 A, C, E.** Despites the results from the immunohistochemistry analysis presented in **Section 3.1** and recent literature suggesting otherwise (Alzu'bi *et al.* 2019), the tracing of thalamocortical axons by DiI revealed only a small bundle of axons **crossing the PSPB** at this early stage. This was observed only in a coronal section very close to the site of crystal placement (Slice D, shown in **Figure 3.11 G-J**). This event was not observed in more anterior sections, as shown in **Figure 3.9 A-C** (Slice B).

In fact, in the latter section the DiI-positive signal was instead detected in a restricted sector near the PSPB (**Figure 3.9 D**). However, this signal did not appear to originate from axonal processes, but rather from **somata of cells**. Importantly, this pattern of labelling was consistently observed in other sections of the brain (**Figure 3.10 C**). These cells in the vicinity of the internal capsule and PSPB resembled the distribution pattern of the ventrolateral migrating stream. Their processes followed the trajectories of the radial glia of the region. Unfortunately, due to technical limitations, co-staining could not be performed on this sample to confirm their exact identity. However, a strong signal was observed throughout the pial surface of the telencephalon, which appeared to be in continuity with the signal detected at lateral subpallial level (**Figures 3.8 and 3.9**). A closer examination of this signal revealed its highly restricted presence in the pial surface and marginal zone, with no labelling observed at other levels of the developing cortex (**Figure 3.9 C-F**). Moreover, the horizontal orientation of the DiI-positive processes resembled the characteristic alignment of cells within the marginal zone, suggesting these might be *bona fide* Cajal-Retzius Cells (CRC) of the MZ. The continuity of the signal from the subpallium to the MZ suggest these might be tangentially migrating Cajal-Retzius cells populating the cortical MZ at very early stages. The mode of labelling is puzzling and possible contamination through pial labelling should be also considered.

Figure 3.6 7 PCW - DII AXON TRACING

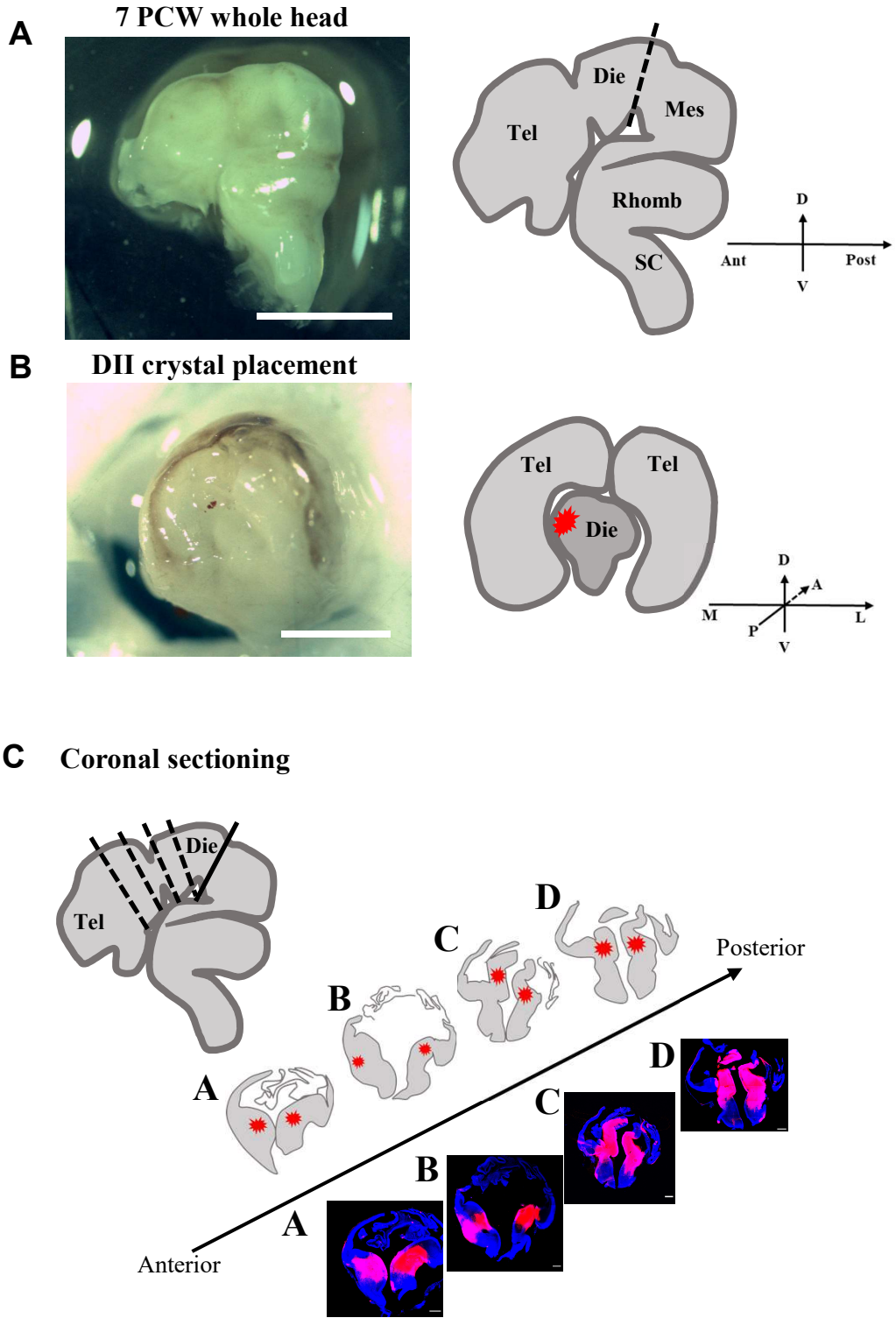

Figure 3.6: Summary of the thalamocortical axon tracing by carbocyanine dye (DiI) in the 7 PCW human brain. **(A)** A lateral view of a 7 PCW human brain (anterior to the left) showing the main subdivisionsof the neural tube in the antero-posterior axis: telencephalon ("Tel"), diencephalon ("Die"), mesencephalon ("Mes"), rhombencephalon ("Rhomb"), and the spinal cord ("SC"). (B) The posterior aspect of the diencephalon was exposed to place DiI crystals in the dorsal prospective thalamus (red sign). (C) Representative images and schematics of the coronal sections analysed in Figures 3.7-3.11, organized in the antero-posterior axis. Scale bars = 1 cm.

Figure 3.7

Thalamus and "migrating" cells

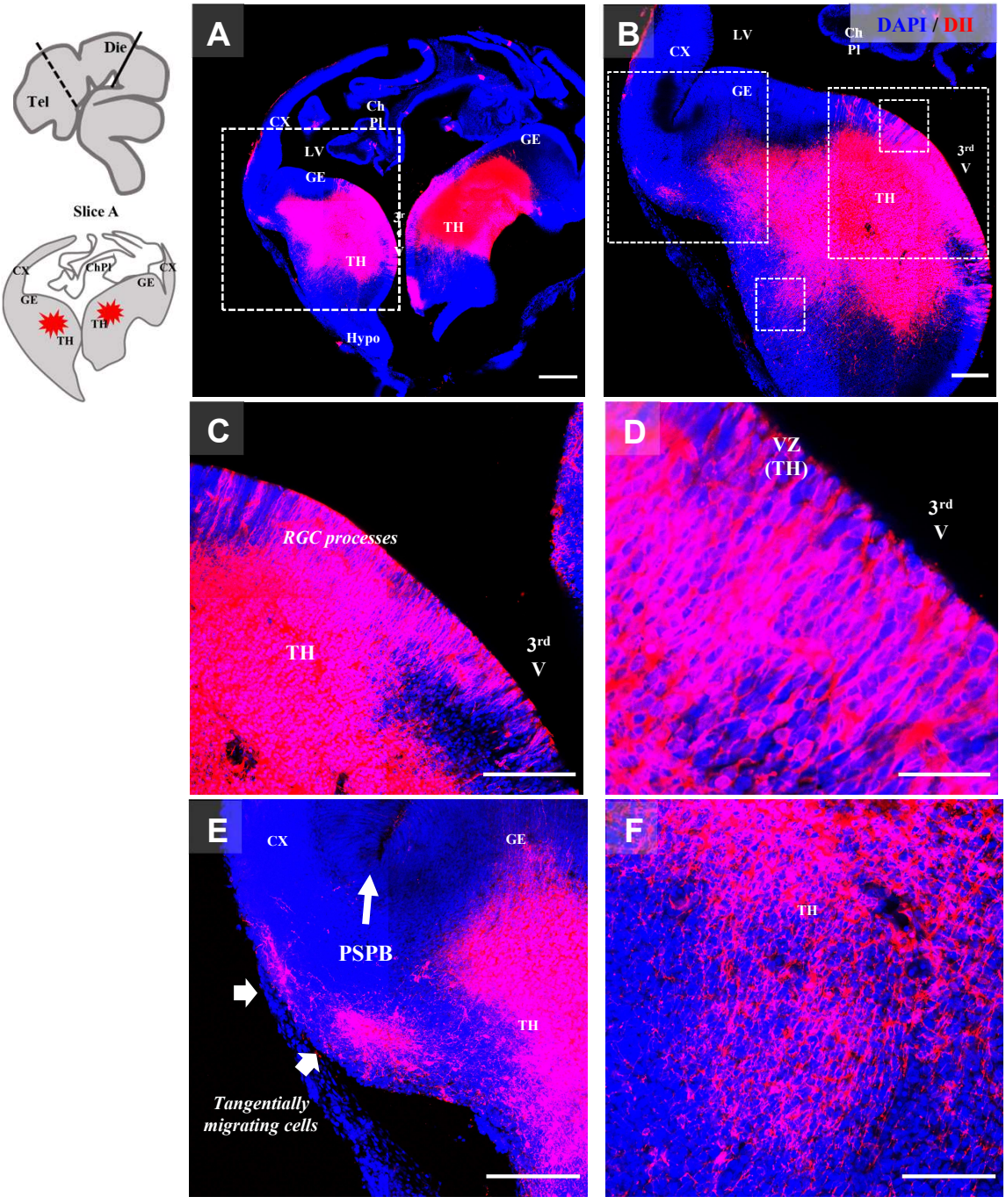

Figure 3.7: DiI crystal placement in the dorsal diencephalon reveals thalamic progenitor cell processes, as well as "migrating" cells located at the boundary between pallium and subpallium in the 7 PCW human brain (Slice A). The plane of cutting and structure of the section is indicated on the top. (**A**) Confocal scanning of the whole section the main anatomical structures in Slice A. (**B**) Confocal scanning of the area analysed in C-F. (**C, D**) Confocal images of the diencephalic region showing the radial glial processes labelled by DiI in the area and extending to the ventricular side. (**E, F**) Confocal image of the region near the pallial-subpallial boundary (PSPB) (arrow) showing DiI-positive cells oriented transversally and apparently *en route* to the cortex (thick arrows). Scale bars = 500 µm (A-C); 100 µm (D-F).

Figure 3.8

Cortex: Marginal Zone

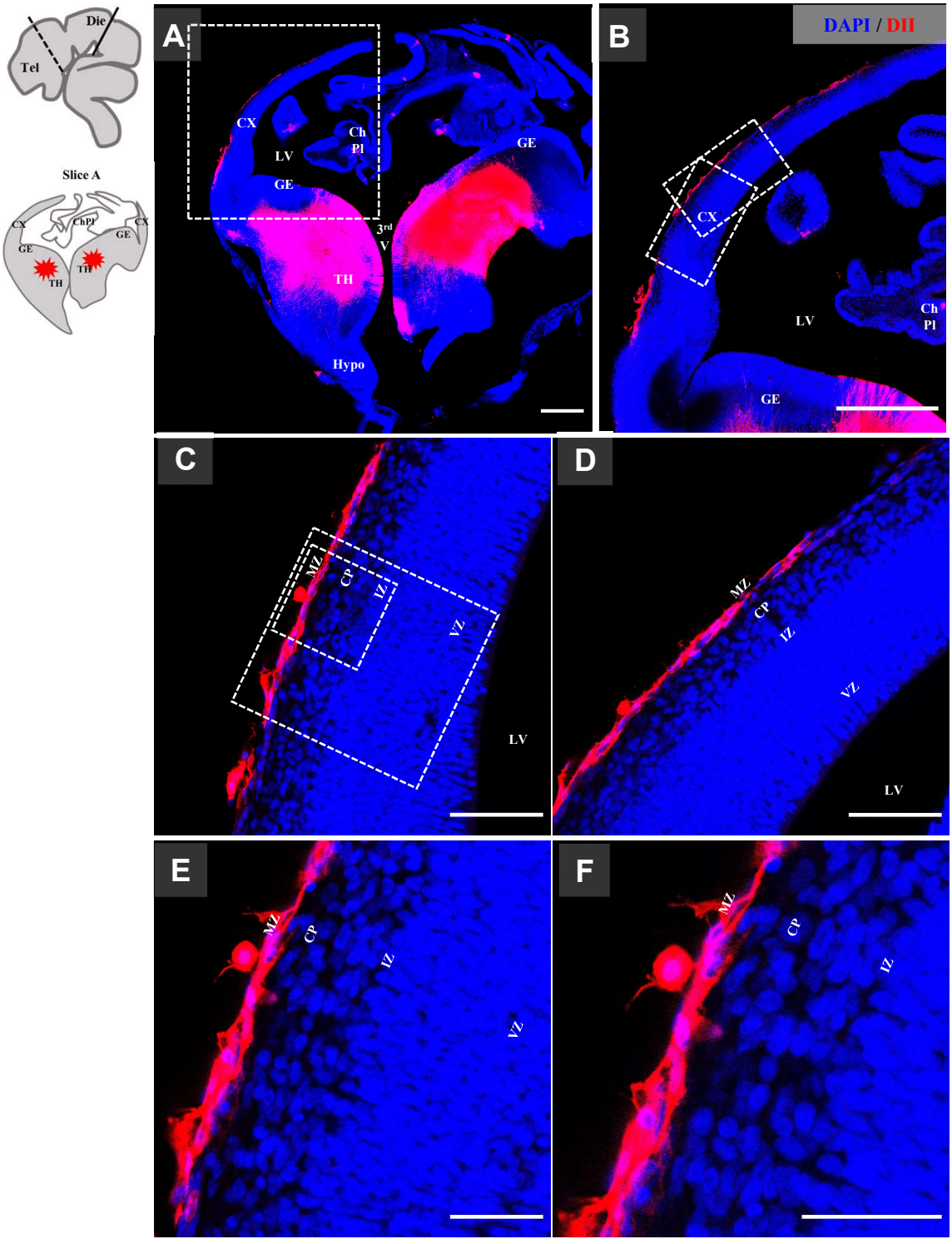

Figure 3.8: DiI crystal placement in the dorsal diencephalon reveals a signal at the level of the marginal zone in the cortex in the 7 PCW human brain (Slice A). The plane of cutting and structure of the section is indicated on the top. (**A**) Confocal laser scanning reconstruction of the whole section the main anatomical structures in Slice A. (**B**) Confocal laser scanning reconstruction of the area analysed in C-F. (**C, D**) Confocal images of the cortex showing the DiI-positive signal detected in the marginal zone (MZ) (**E, F**) and resembling Cajal-Retzius cell populating the area. Scale bars = 500 µm (A, B); 100 µm (C, D); 50 µm (E, F).

Figure 3.9

Cortex: MZ and "migrating" cells

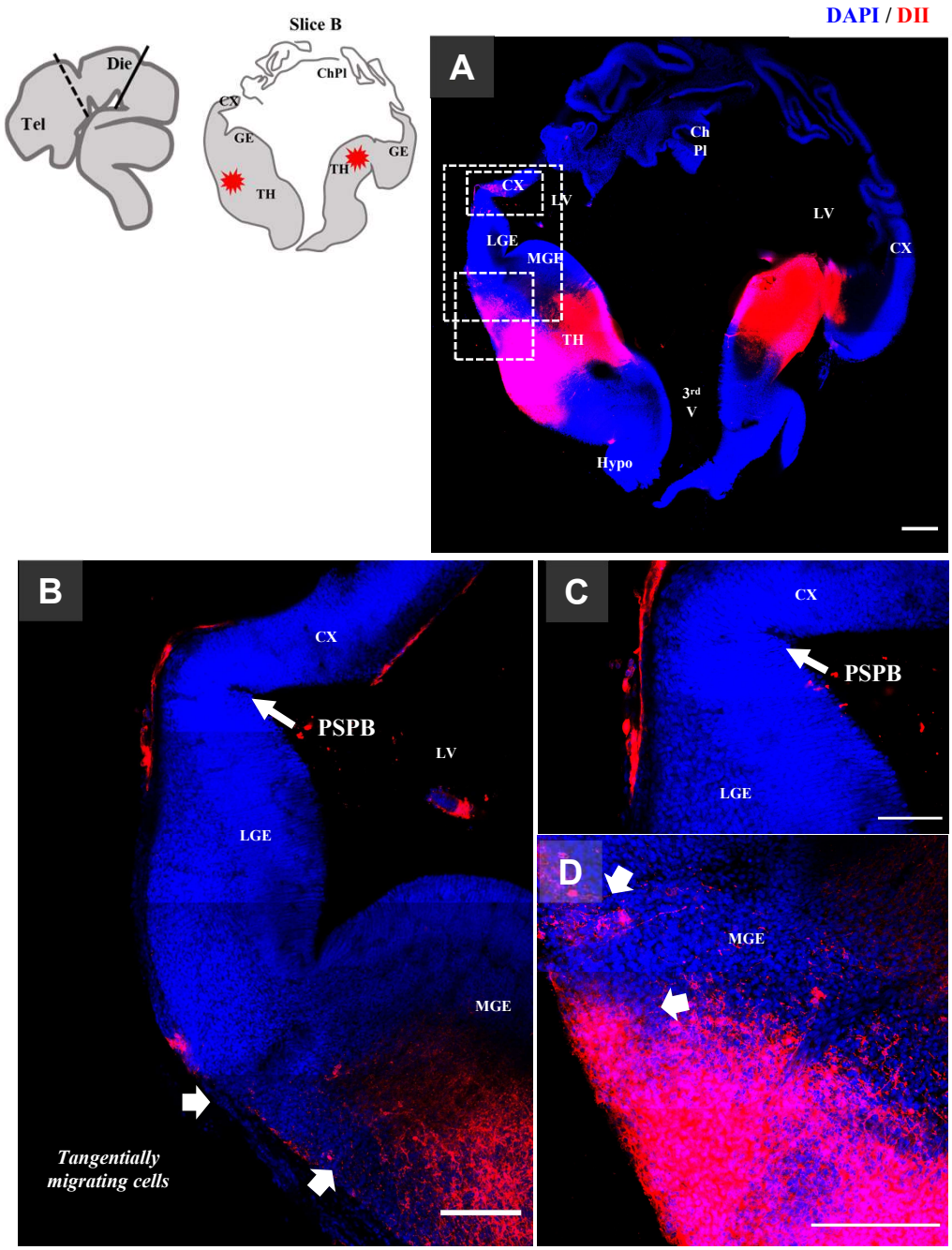

Figure 3.9: DiI crystal placement in the dorsal diencephalon reveals labelling at the level of the marginal zone in the cortex, in anatomical continuity with the cells in the lateral aspect of the ganglionic eminences (GE) in the 7 PCW human brain (Slice B). The plane of cutting and structure of the section is indicated on the top. (**A**) Confocal scanning of the whole section the main anatomical structures in Slice B. (**B**) Confocal scanning of the area showing the lateral and medial ganglionic eminences (LGE and MGE) and the pallial-subpallial boundary (PSPB) (arrow) (zoomed in **C**) showing the apparent continuity of the DiI-positive signal detected in these regions with the one in the cortical marginal zone (MZ) (zoomed in **D**) (thick arrows). Scale bars = 500 µm (A, B); 100 µm (C, D).

Figure 3.10

Ventral Thalamus and Ganglionic Eminences

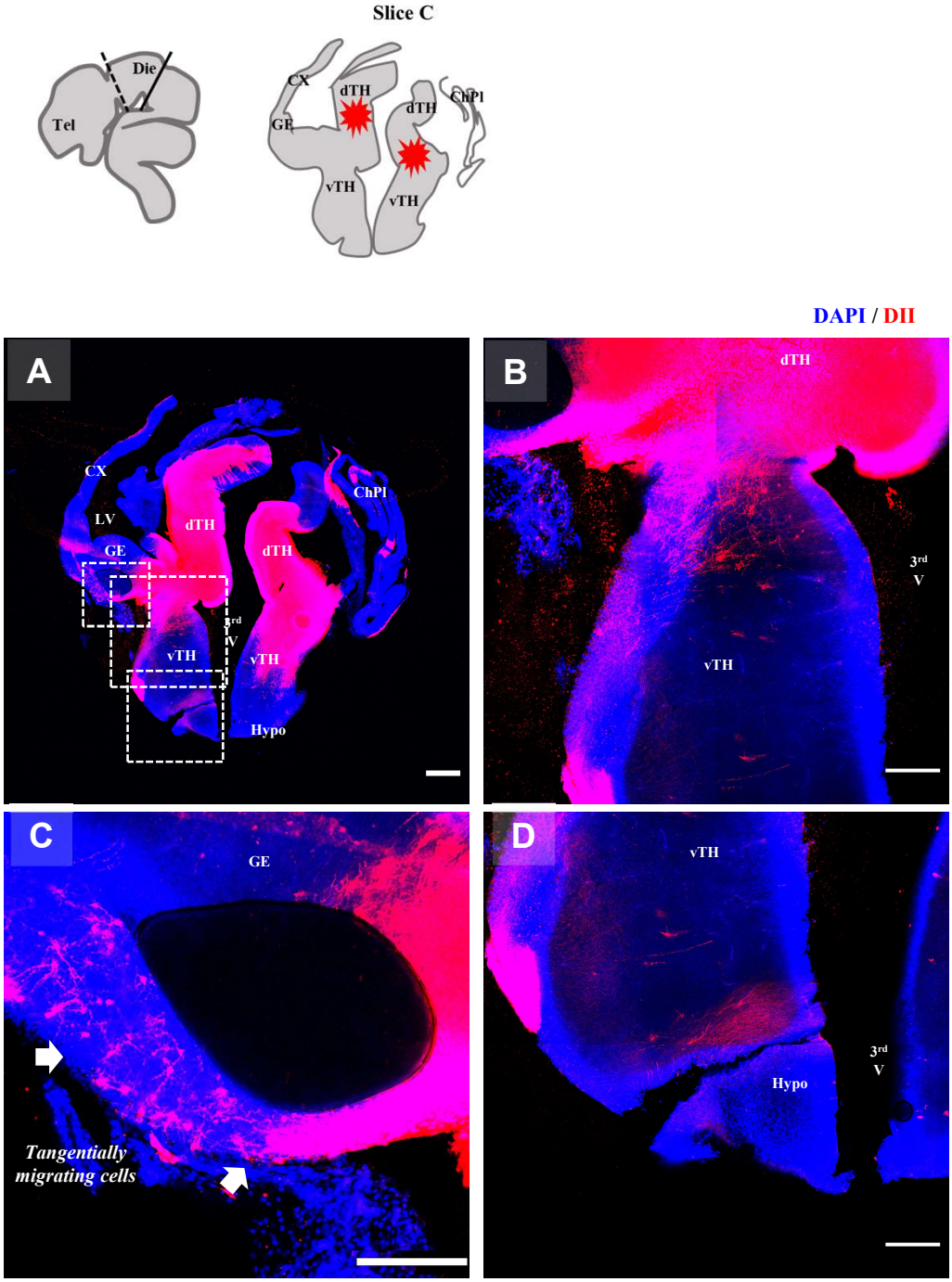

Figure 3.10: DiI crystal placement in the dorsal diencephalon reveals some fibre and cell body labelling in the ventral thalamus, and a positive signal at the level of the lateral aspect of the ganglionic eminences (GE) in the 7 PCW human brain (Slice C). The plane of cutting and structure of the section is indicated on the top. (**A**) Confocal laser scanning microscopic reconstruction of the whole section the main anatomical structures in Slice C. (**B**) Confocal image of the diencephalic region close to the DiI placement site in its dorsal aspect (dorsal thalamus, dTH) and showing partial labelling of the ventral thalamus (vTH) (zoomed in **D**). Scale bars = 500 µm (A, B); 200 µm (C, D).

Figure 3.11

Diencephalic-Telencephalic Boundary & Pallial-Subpallial Boundary

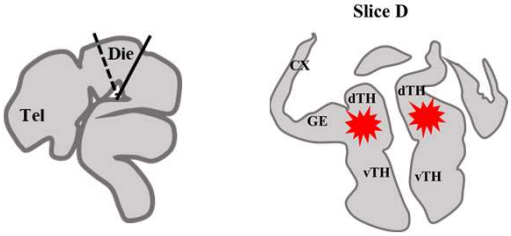

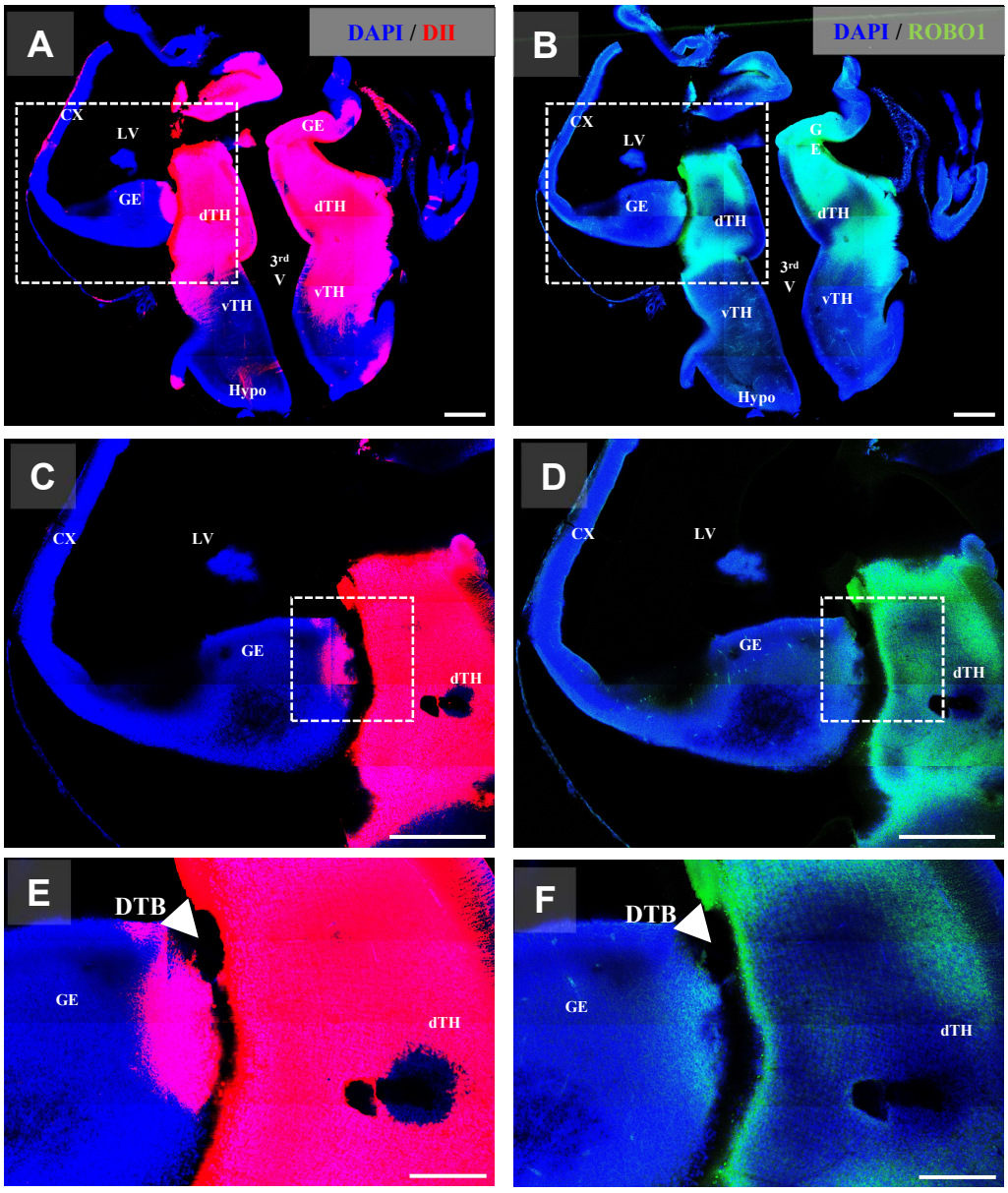

Figure 3.11

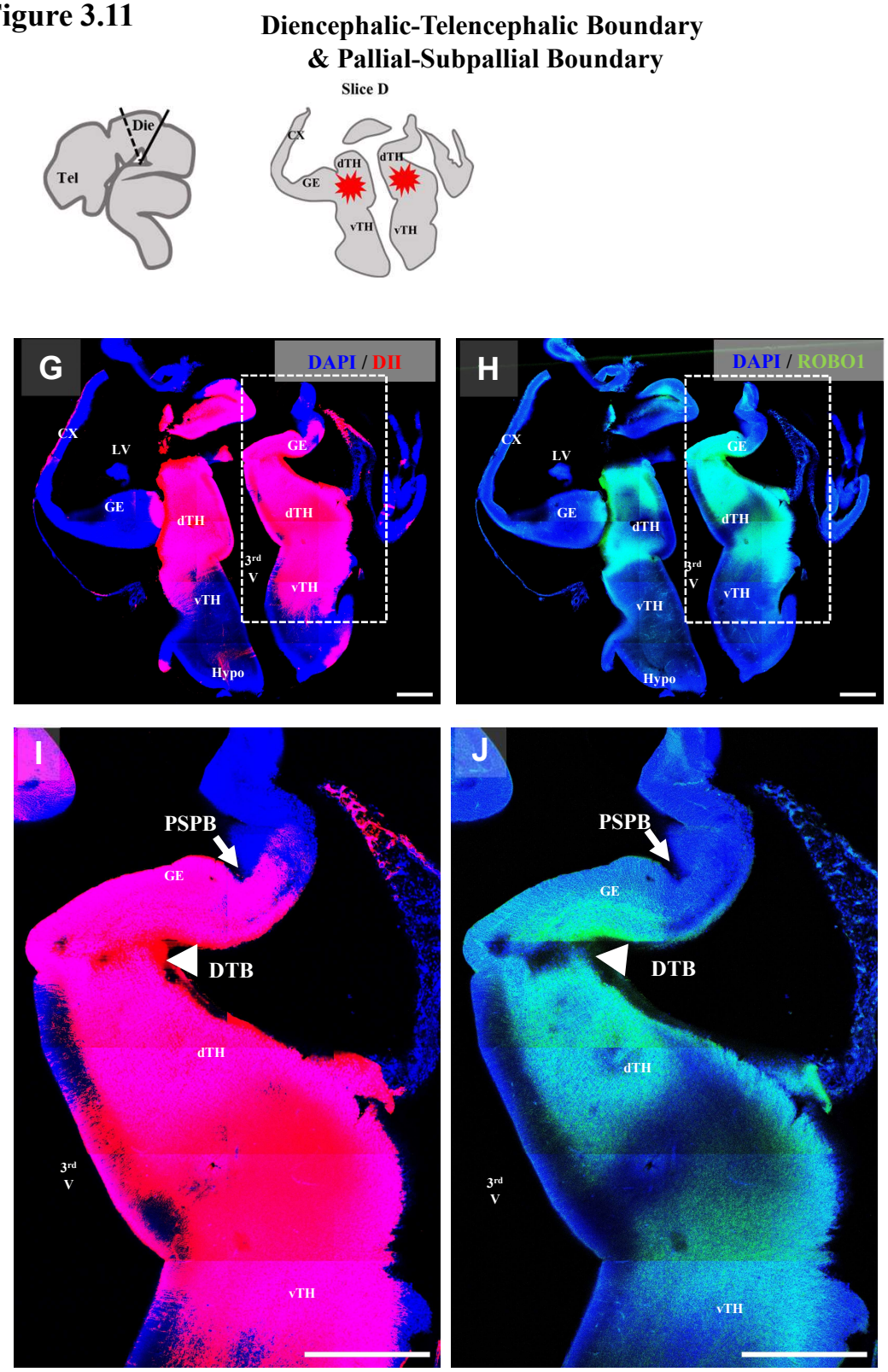

Figure 3.11: DiI crystal placement in the dorsal diencephalon reveals strong labelling of the area, with some axons crossing the diencephalic-telencephalic boundary (DTB) and only a few projections extending past the pallial-subpallial boundary (PSPB) in the 7 PCW human brain (Slice D). The plane of cutting and structure of the section is indicated on the top. Confocal scanning of the whole section showing DiI-positive signal (A, G) co-localizing with the thalamic marker ROBO1 (B, H) in slice D. Scale bars = 500 µm (A-D, G-J); 200 µm (E, F).

3.2.2 13 post-conception week (PCW)

I placed DiI crystal at the level of the internal capsule connecting the thalamus with the developing cortex of two coronal slabs from a 13 PCW human brain (**Figure 3.12**), in both anterior and posterior aspect of slab #2 (**Figure 3.12 B**), and on the posterior aspect of slab #3 (**Figure 3.12 C**). Although the thalamus was present in the latter slab, the diencephalic region was physically detached from the telencephalic vesicle (**Figure 3.12 C**), therefore TCA axonal tracing was not possible by crystal placement at the level of the thalamus due to the disruption of tissue continuity.

Labelled fibres were observed extending from the site of crystal placement in the internal capsule tangentially towards the cortex ("*Tangential axons*" in **Figures 3.14 B; 3.15 C, D, G, H; 3.16**). By this age, the thalamocortical projections could be detected extending from the site of crystal placement in the internal capsule tangentially towards the telencephalon, and successfully reaching the prospective cortex (**Figure 3.16 C-D'; 3.17**). Here these axons continued their tangential trajectory within the intermediate zone (IZ), splitting the germinal compartments below (ventricular and subventricular zone, VZ and SVZ) from the post-mitotic ones above (subplate, SP; cortical plate, CP; marginal zone, MZ) (**Figures 3.17**). No axons were observed extending toward the overlying subplate yet, although this was expected at this stage of development. However, this might be due to a technical issue and the efficacy of the DiI tracing.

One of the most intriguing findings was the remarkably close **association between the thalamocortical axons and the germinal compartments**, particularly the SVZ. This observation supported the previous work of Isasegi, who identified an overlapping region where the thalamic axons and SVZ coexist in the developing human cortex through histological analysis by Cresyl Violet (Nissl) and AChE staining (Zunic Isasegi *et al.* 2018). Right from the beginning of their trajectory in the internal capsule, the thalamic axons were in a region that overlapped with the SVZ (**Figures 3.14 B; 3.16 B**). As they reached the cortex, their close anatomical association with the SVZ persisted (**Figures 3.16 D'; 3.17**). In this small-sized brain with a likewise thin cortex, it was challenging to clearly distinguish the inner and outer portions of the SVZ. No clear inner fibre layer (IFL) splitting the two apart was visible at this stage. Therefore, the annotations in the figures taken

from the 13 PCW human brain shows the SVZ as a single layer. These two compartments start acquiring their characteristics and distinguishable cell organization from 12 PCW in human (Bayatti *et al.* 2008), therefore I was looking at a very initial stage of this histological event. However, it was clear that the DiI-labelled axons extended in closer proximity to the outer subventricular zone (OSVZ), and in fact no DiI-positive signal was detected at any level of the ventricular zone (VZ). Similar observations were made in the 17 PCW brain described in the following paragraph.

Radial glial cells (RGC) located near the site of crystal placement exhibited back-labelling, and both their processes extending toward the pial surface (**Figures 3.14**), as well as in their soma residing within the outer SVZ (**Figure 3.13**) were positive for DiI signal. This finding suggested two scenarios. These cells directly uptook the dye at the site of crystal placement via their basal processes, which was physically located close enough to the DiI crystals, as suggested by **Figure 3.15**. Alternatively, the basal processes established physical connections with the axons extending tangentially within the internal capsule, thereby enabling transneuronal labelling of these cortical progenitor cells (**Figures 3.14 A, B; 3.16 A, B**). Notably, no back-labelled somata of RGC were detected in the inner portion of the SVZ, or the VZ (**Figure 3.13**), despite the basal processes of ventricular RGC (vRGC) population also extend to the pial surface. If the dye had been taken up by RGC solely due to the physical proximity of their basal processes to the crystal placement site, as suggested by the first explanation, both ISVZ/VZ and OSVZ radial glial cells should have exhibited DiI labelling in their soma, which was not observed. Transneuronal labelling of oRGC was further supported by the detection of DiI-positive signal within a group of cell bodies located in the nearby SVZ, but not in direct contact with the site of DiI placement (**Figure 3.13**).

Overall, these observations suggested a possible physical interaction between axons of the internal capsule and basal processes of the RGC, with subsequent transneuronal labelling of outer RGC (oRGC). This interaction appeared to be restricted to the OSVZ, with no similar phenomenon observed in the inner germinal compartments, and thus suggesting a specific type of direct interaction between oRGC and TCA.

Figure 3.12

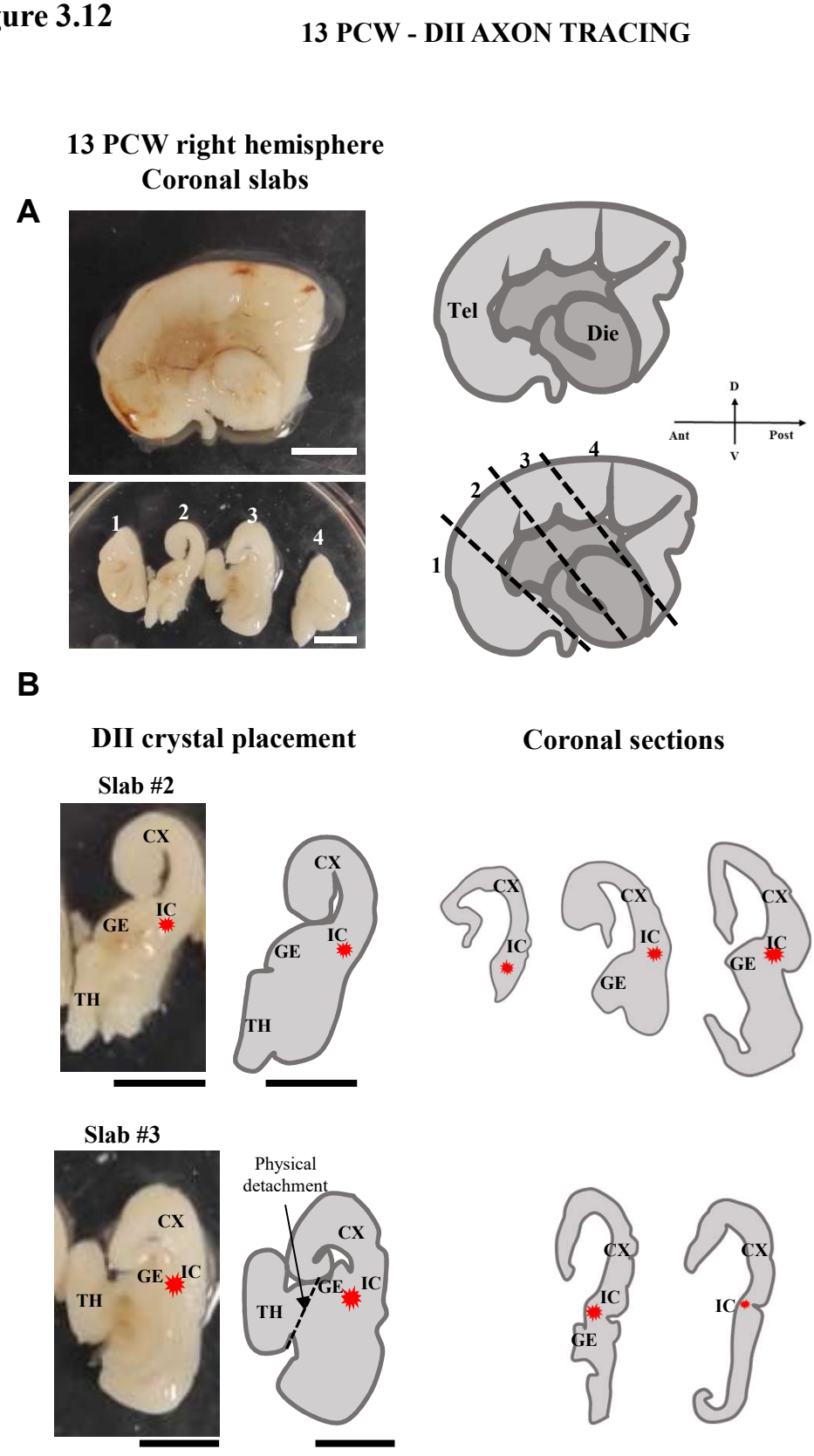

Figure 3.12: Summary of the thalamocortical axon tracing by carbocyanine dye (DiI) in the 13 PCW human brain. (A) Medial view of the right hemisphere of a 13 PCW human brain showing the telencephalon ("Tel") and diencephalon ("Die"), and the four coronal slabs obtained in the antero-posterior axis. (**B**) Schematics of the DiI crystal placement sites in the internal capsule of slab #2 and slab #3, and relative coronal sections analysed from both samples in Figures 3.13-3.17. Scale bars = 1 cm.

Figure 3.13

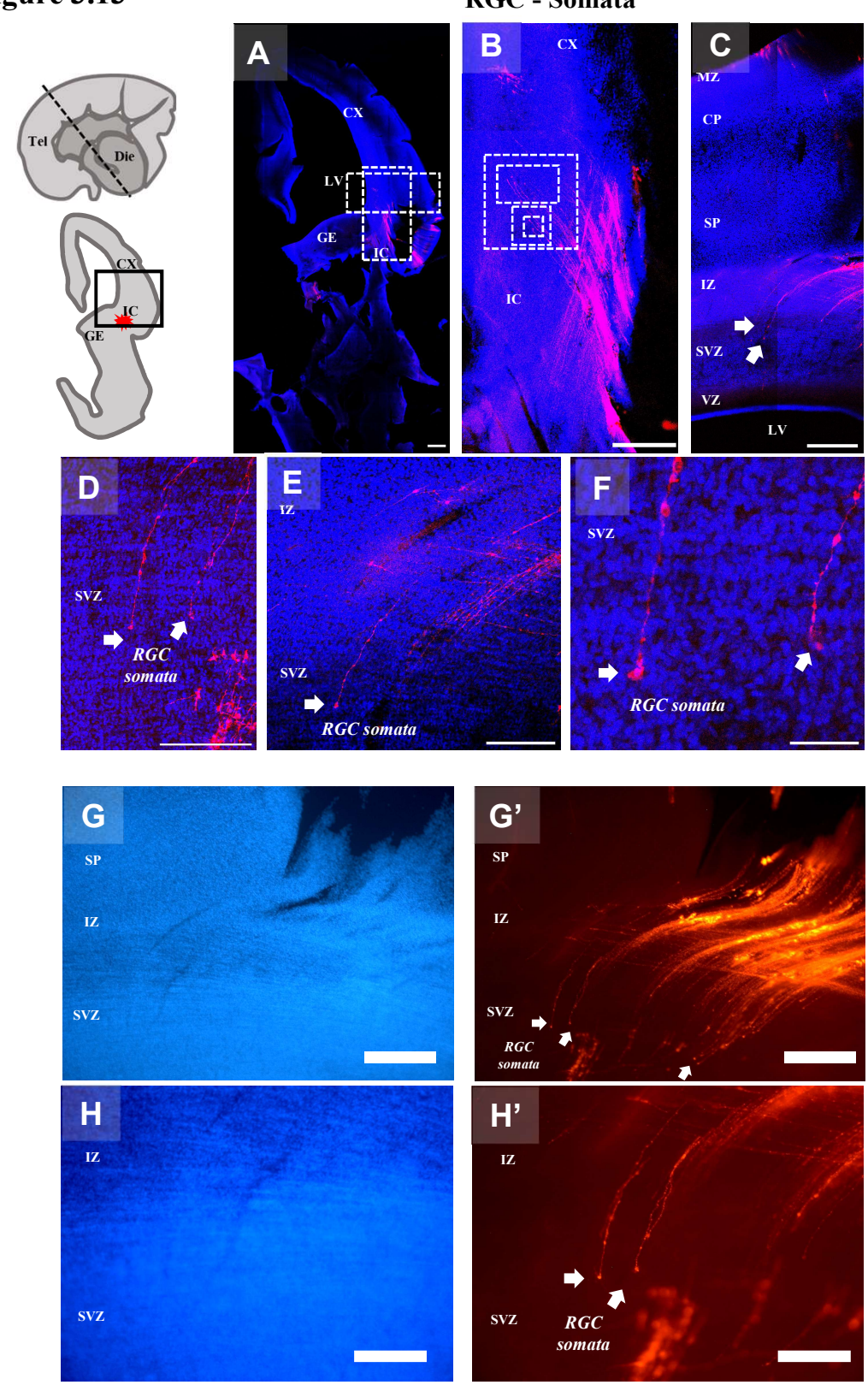

Figure 3.13: DiI crystal placement in the internal capsule reveals labelling of the radial glial cells in the subventricular zone (SVZ) in the 13 PCW human brain. The plane of section (coronal) is indicated on the 3D model of the 13 PCW human brain. Confocal (**A-F**) and epifluorescence (**G-H'**) images showing the radial glial cells (RGC) bodies labelled by DiI and located within the SVZ near the site of crystal placement. Scale bars = 1 mm (A); 500 µm (B, C, G-H'); 200 µm (D, E); 50 µm (F).

Figure 3.14 **RGC – Basal Processes**

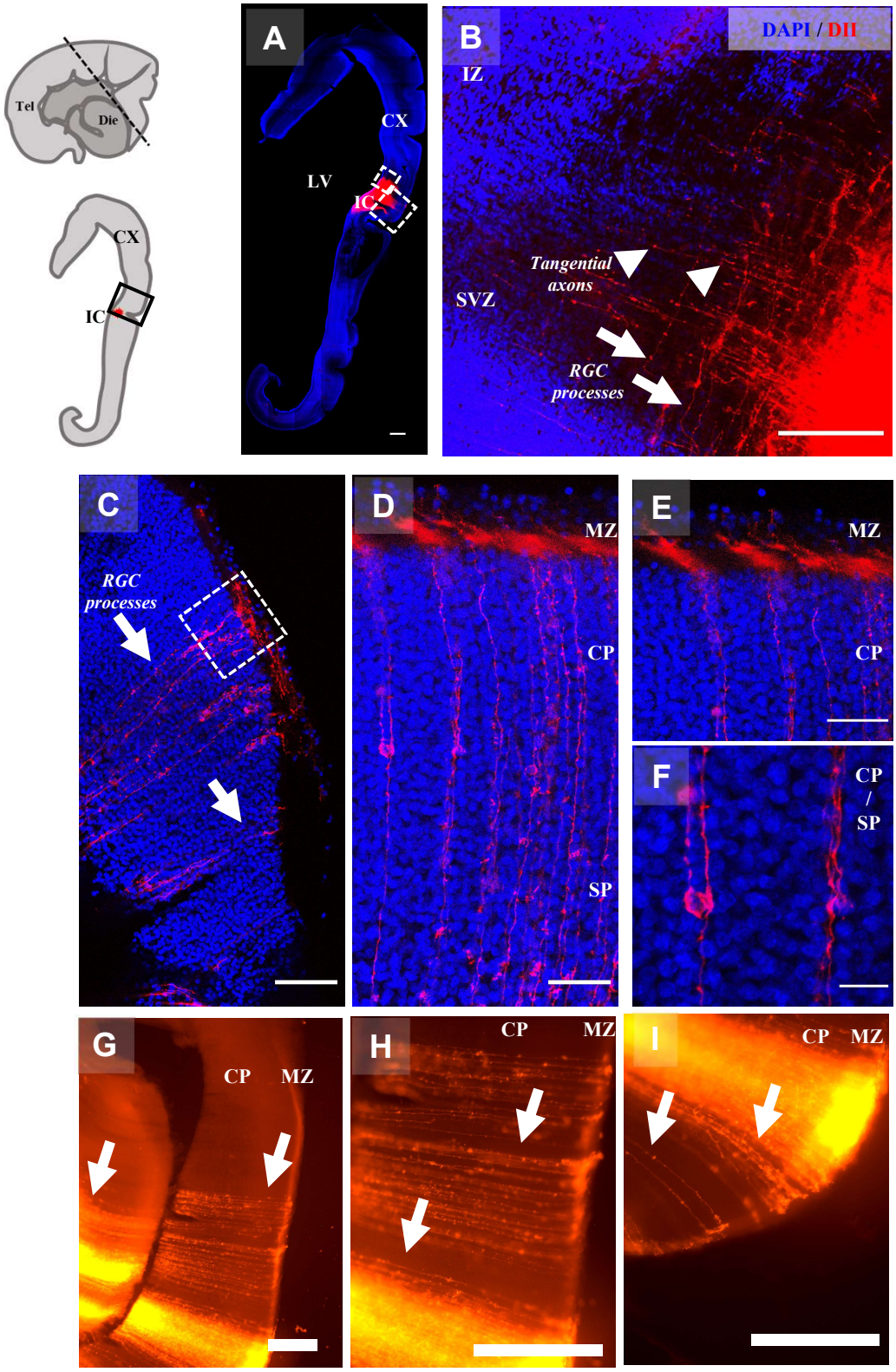

Figure 3.14: DiI crystal placement in the internal capsule reveals radial glial cells in the subventricular zone (SVZ) in the 13 PCW human brain. The plane of section (coronal) is indicated on the 3D model of the 13 PCW human brain. Confocal (**A-F**) and epifluorescence (**G-I**) images showing the radial glial cells (RGC) processes (arrows) oriented radially to the axons departing tangentially in internal capsule and labelled by DiI (arrowheads). These processes are labelled throughout their extension to the pial surface (C-I). Scale bars = 1 mm (A); 500 µm (G-I); 200 µm (B); 100 µm (C); 50 µm (D-F).

Figure 3.15

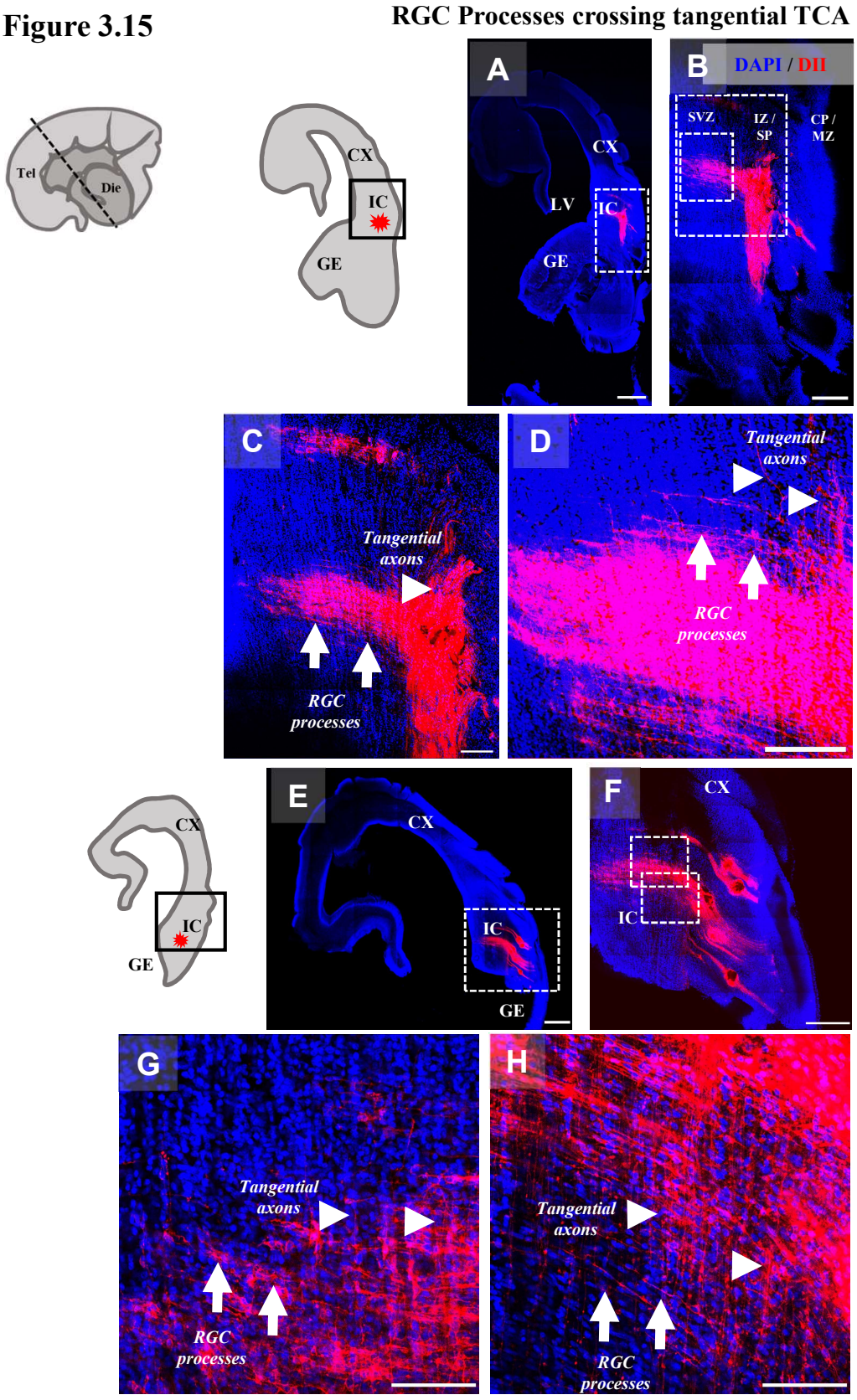

Figure 3.15: DiI crystal placement in the internal capsule reveals radial glial cell (RGC) processes oriented radially and the axons of the internal capsule oriented tangentially from the site of DiI placement in the 13 PCW human brain. The two adjacent sections analysed in the image are schematized on the left side. The radial glial cells (RGC) processes (arrows) oriented radially to the axons departing tangentially in internal capsule and labelled by DiI (arrowheads) in two coronal sections from slab #2 (**A-D** and **E-H**, respectively). Scale bars = 1 mm (A, E); 500 µm (B, F); 200 µm (G, H).

Figure 3.16

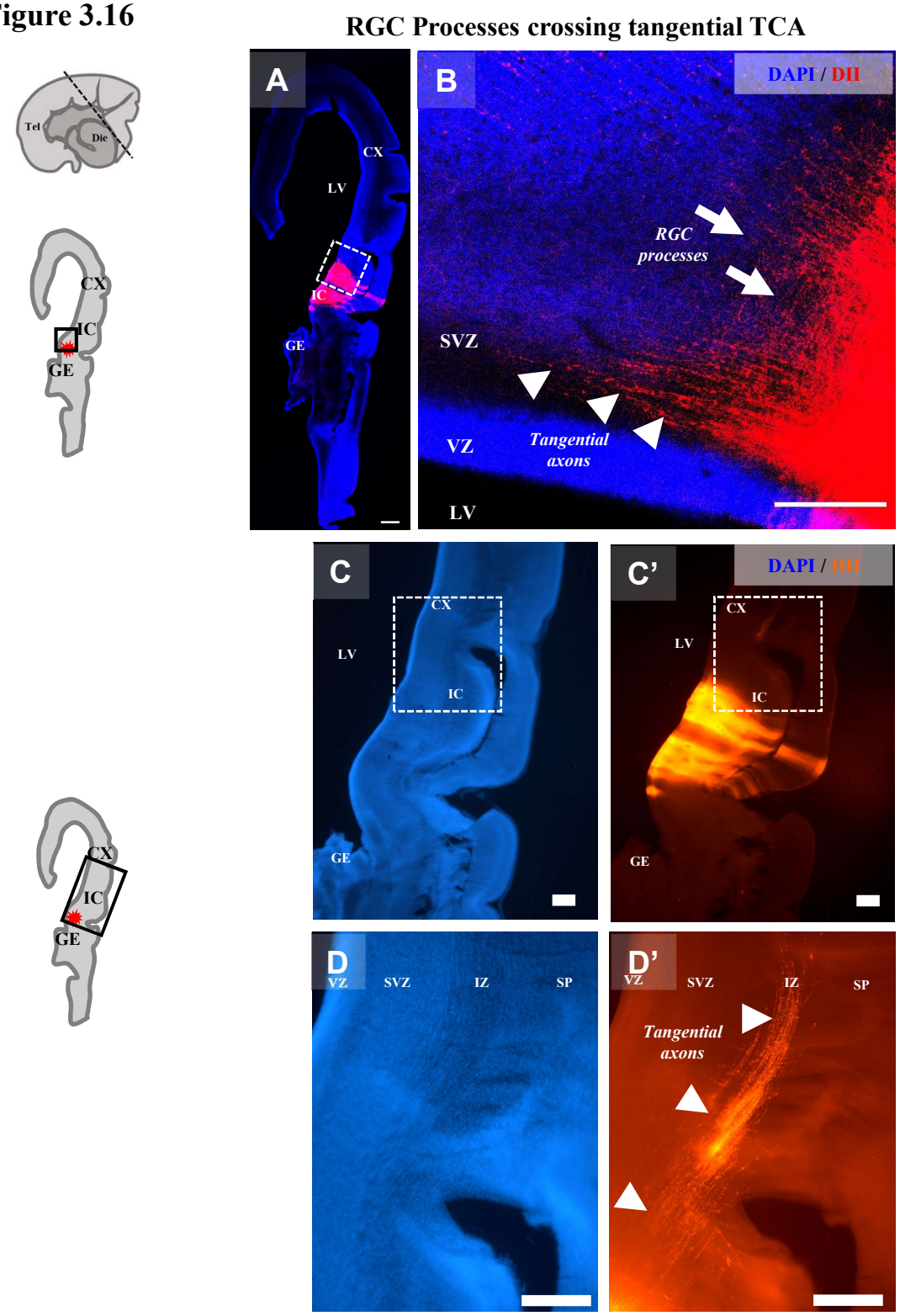

Figure 3.16: DiI crystal placement in the internal capsule reveals the axons of the internal capsule departing from the site of crystal placement and extending tangentially to innervate the cortical intermediate zone (IZ) in the 13 PCW human brain. The two adjacent sections analysed in the image are schematized on the left side. (**A, B**) Confocal scanning showing the initial segment of the DiI-labelled axons departing from the internal capsule and extending toward the cortex. (**B**) Highlights the radially oriented radial glial cells (RGC) processes (arrows) crossing the path of these axons (arrowheads) and closely associated to the subventricular zone (SVZ). (**C-D'**) Epifluorescence images showing the length of extension of the DiI-labelled axons within the cortical intermediate zone (IZ). Scale bars = 1 mm (A); 500 µm (C-D'); 200 µm (B).

Figure 3.17

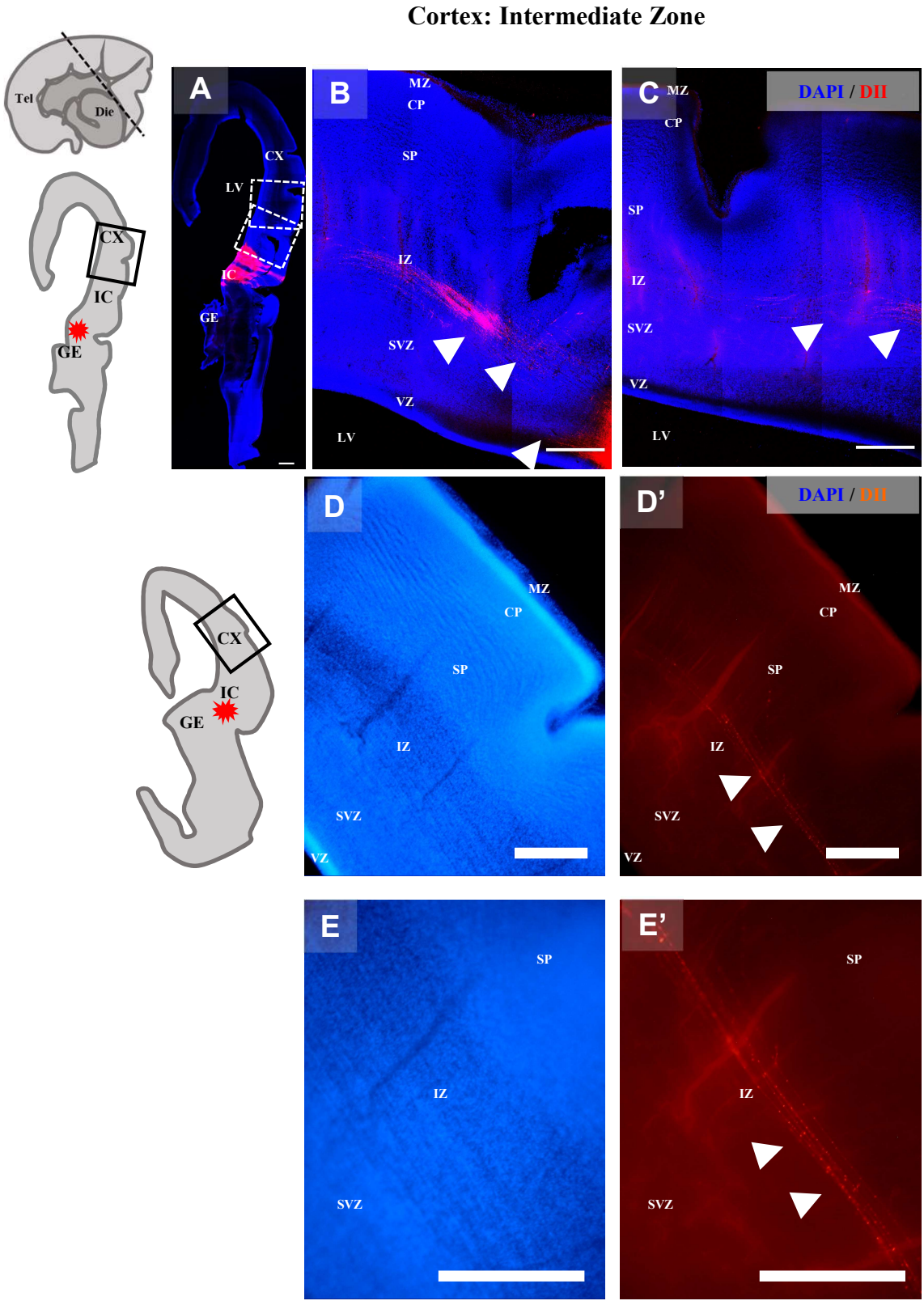

Figure 3.17: DiI crystal placement in the internal capsule reveals that the thalamic axons reached the cortical intermediate zone (IZ) in the 13 PCW human brain. The two adjacent sections analysed in the image are schematized on the left side. (**A-C**) Confocal scanning and (**D-E'**) epifluorescence images showing the DiI-labelled axons that reached the cortex and extending in the intermediate zone (IZ) for long distances from the site of crystal placement. Scale bars = 1 mm (A); 500 µm (B-E').

3.2.3 17 post-conception week (PCW)

I performed an axonal tracing analysis by placing crystals of DiI in the internal capsule (slab #5) and the dorsal thalamus (slab #6) of a 17 PCW human fetal brain (**Figure 3.18 A**). At this age, the TCA already reached the prospective cerebral cortex, allowing me to analyse the more advanced innervation pattern at this level. Several DiI crystals were placed at either location (**Figure 3.18 B**). As the hemisphere was big in size, the slabs were incubated for about 9 months at room temperature to allow for sufficient diffusion of the dye over a long distance. I performed an extensive imaging analysis of the samples by using both epifluorescence and confocal microscopy. Specifically, I analysed the trajectory of thalamic axons from the site of crystal placement throughout their path to the cortex. I also conducted an analysis of the cell population contacted and/or interacting with the DiI-labelled thalamic axons. In both cases the axonal tracing revealed that TCA successfully reached the dorsal, lateral, and ventral aspects of the neocortex. While the intermediate target structures of TCA were analysed in both slabs, cortical targets of TCA were studied on slab #5 (anterior), and are presented in this Chapter. Unfortunately, the preservation of the cortical region in slab #6 was not optimal after slicing with the vibrotome, thus not allowing for a detailed analysis at this level. However, important intermediate stations encountered by TCA were revealed by crystal placement in the dorsal, including the reticular nucleus of the thalamus, perireticular cells, and subpallium, and are worth to be reported. These results are reported in **Supplementary Figures S1-5**.

Figure 3.18

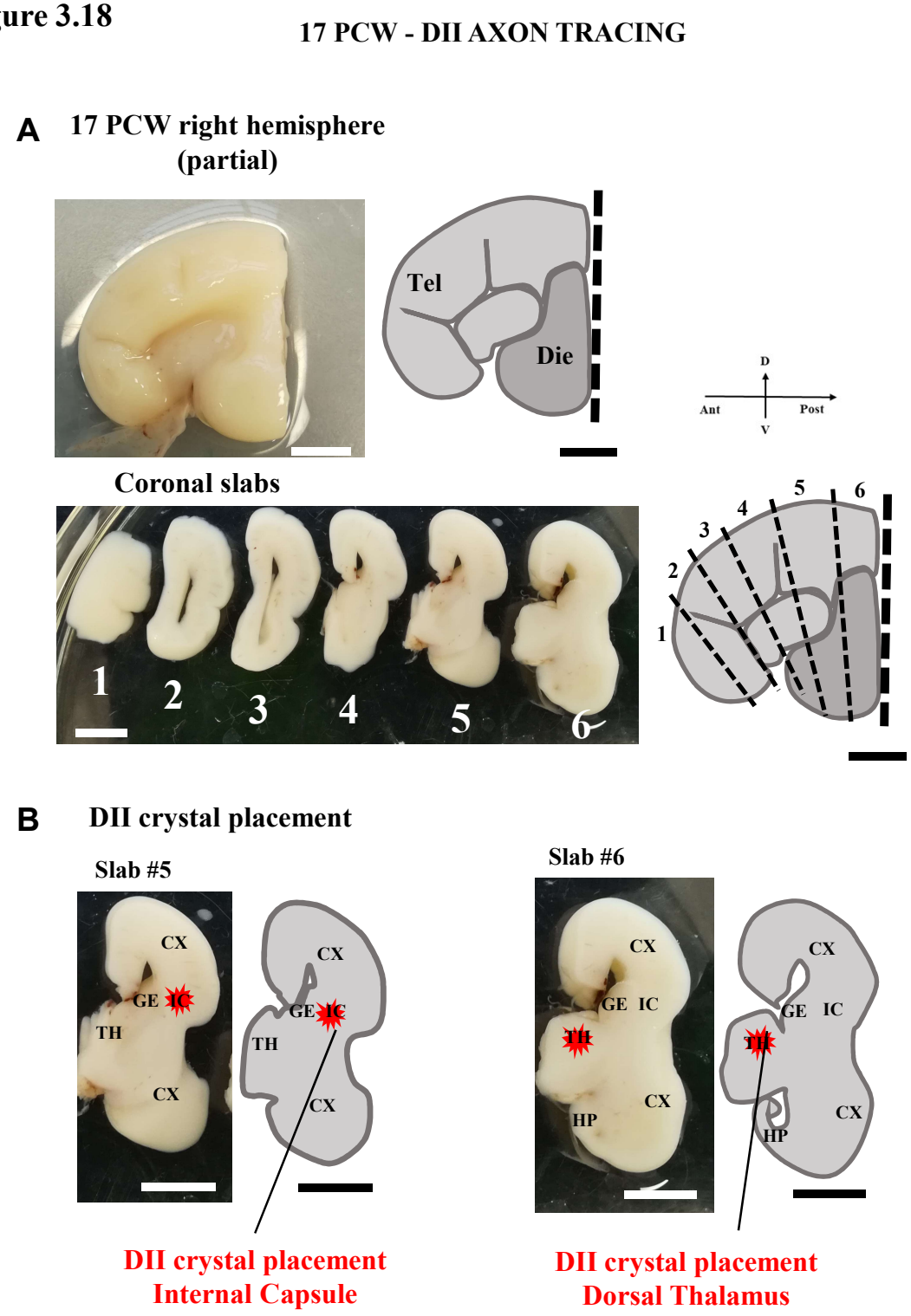

Figure 3.18: Summary of the thalamocortical axon tracing by carbocyanine dye (DiI) in the 17 PCW human brain. (A) Lateral view of the partial right hemisphere of a 17 PCW human brain showing the telencephalon ("Tel") and diencephalon ("Die"), and the six coronal slabs obtained in the antero-posterior axis. (**B**) Schematics of the site of placement of DiI crystals in the internal capsule of slab #5 and in the dorsal thalamus of slab #6 analysed in this work. Scale bars = 1 cm.

Figure 3.19

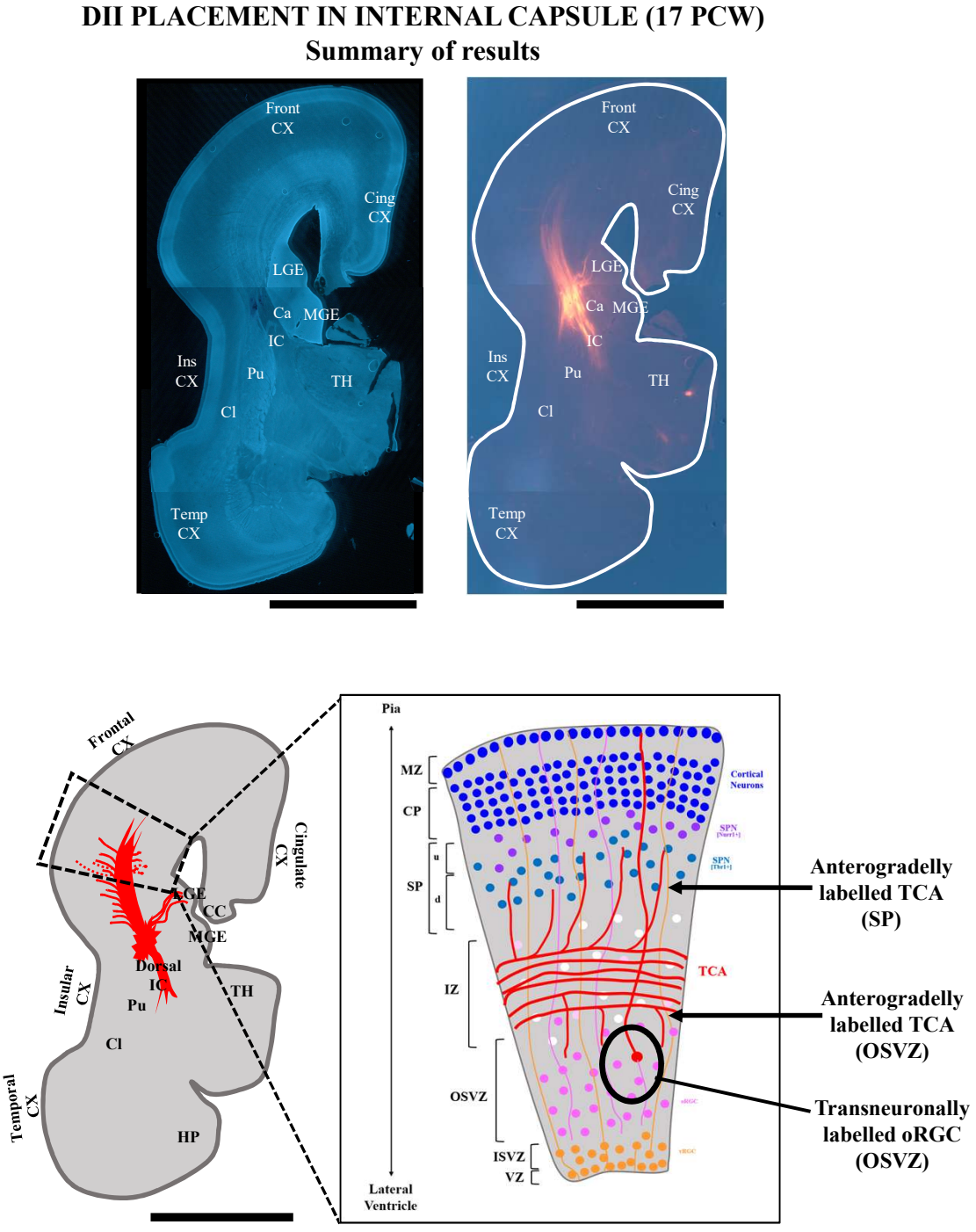

Figure 3.19: Summary of the results from axon tracing by DiI crystal placement in the internal capsule of the 17 PCW human brain (slab #5). (**A**) DAPI nuclear staining reveals the main anatomical structures in the coronal sections analysed. (**B**) DiI-positive signal detected in the coronal sections and schematized in detail in (C). (**C**) Schematic representation of the coronal sections from slab #5, indicating the site of DiI crystal placement in the dorsal aspect of the internal capsule. The pattern of labelling obtained at cortical level is highlighted on the right schematic cross section on the right and indicating anterogradely labelled axons departing from the intermediate zone (IZ) and reaching the deep subplate (dSP), and the outer subventricular zone (OSVZ). A few cases of transneuronally labelled outer radial glial cells (oRGC) in the latter compartment were also observed. Scale bars = 1 cm

TCA trajectory from the internal capsule to the cortex

In slab #5, several crystals of DiI were placed in the initial segment of the internal capsule, just laterally to the medial and lateral ganglionic eminence (**Figure 3.18 B**). This area was correspondent to the site where DiI was placed in the 13 PCW brain (see **Section 3.2.2**), thus allowing for a direct comparison between the two developmental stages. DAPI nuclear staining was used to visualize the cytoarchitecture of the structures present at this specific level of the brain (**Figure 3.19 A**). A schematic representation of the main findings is shown in **Figure 3.19 B**.

The DiI placement site within the internal capsule contains thalamocortical afferent axons and also the corticofugal axons, which by this age successfully reached the thalamus. It is worth mentioning that the anterograde diffusion of DiI is more effective than the retrograde diffusion (Molnár *et al.* 2006). Therefore, when DiI is placed in the thalamus, it initially reveals the processes departing from that area before the retrograde labelling through the terminals will become obvious in fixed *post mortem* tissue. Conversely, when crystals are placed in the internal capsule, they can equally reveal axons traveling in both directions - towards the cortex (thalamocortical axons) and towards the thalamus (corticofugal axons). Anterograde labelling of CTA from the site of crystal placement would reveal the section of these axons approaching and entering the thalamus, more than the segment departing from the deep cortical plate and subplate where the axons originate. Consistently, at cortical level I did not observe many cases of back-labelled neuronal cell bodies in the deep CP / SP that at this stage project their axons to the thalamus. Furthermore, back-labelling of thalamic projecting neurons and anterograde labelling of corticothalamic axons reaching the thalamus was not as successful as the labelling of the segment reaching the cortex. In fact, the DiI-positive signal at the level of the thalamus was not as extensive or strong in comparison. Nevertheless, to discern as much as possible from the two reciprocal projections, most of the analysis in this slab was made at cortical level, thus preferentially focusing on the TCA rather than the CTA.

Nearby the site of DiI crystal placement within the internal capsule, I detected fibers crossing their path just laterally of the ganglionic eminences (**Figures 3.20 A-D'**). Upon closer examination

at higher magnification, it became apparent that some of these processes originated from cell bodies located near the lateral ganglionic eminence (LGE) and extended their axons toward the internal capsule, forming a "bridge" between the two structures (**Figure 3.20 E-H''**). These processes appeared to be continuous with the bundle of fibres crossing paths with the axons of the internal capsule and extending ventrally, suggesting that they might represent the axonal projections originating from neurons located near the LGE. Alternatively, they might represent basal progenitor located in the very initial section of the cortical SVZ, close to the ganglionic eminences. In this case, the DiI-labelled fibers would consist of their basal processes, which up-took the dye directly from the site of crystal placement just adjacent to their initial segment, and were labelled throughout their extension toward the pial surface of the lateral cortex. However, immunostaining was not performed for specific markers, and therefore I could not discern the specific identity of these cells. Surprisingly, DiI placement at the level of the internal capsule did not result in a similar labelling pattern in the MGE as the one described in the previous section.

Proceeding beyond the area proximal to the site of DiI placement, I detected diffusion of the dye over long distances and revealing the innervation of the adjacent lateral cortex (insular cortex) and dorsal cortex (putative frontal cortex). Upon reaching the cortical areas, DiI-labelled axons were found in the intermediate zone (IZ), which by this age was substantially thicker as compared to the 13 PCW brain (see **Figures 3.15 and 3.16).** As previously mentioned, the identity of the fibres observed within the intermediate zone (IZ) could represent either anterogradely-labelled thalamic fibres innervating the cortex or back-labelled cortical fibres extending from projecting neurons. However, due to the limitations of the technique used, it was not possible to distinguish between these two types of fibres within the IZ. As also noted previously, the dye is more effectively transported anterogradely than retrogradely where cell bodies take more time to get sufficient amount of dye to be visible. Therefore, the proportion of fibres originating from corticofugal axons was expected to be smaller than the ones belonging to the thalamocortical axons reaching the area. Importantly, no significant presence of DiI-labelled cell nuclei was detected in the post-mitotic compartments (subplate and cortical plate), nor did the fibres extend to the upper subplate or lower

cortical plate where corticofugal axons are known to originate from deep layer neurons. Based on these observations, it was reasonable to assume that most fibres labelled by DiI originate from the thalamus and other regions, rather than originating from the cortex itself.

As expected, I observed numerous fibres branching from the IZ and invading the deeper portion of the subplate (**Figures 3.21 E, F, G, I and 3.22 A-B', thick arrows**). Surprisingly, a proportion of DiI-labelled fibres invaded the upper portion of the OSVZ in a comparable manner (**Figures 3.21 E, F, H, J and 3.22 A, A', C, C', thin arrows**). This phenomenon has been previously reported only in the foetal monkey (Carney *et al.* 2004). Therefore, I specifically focused my analysis on these two cortical regions, which are both fully mature and highly expanded at 17 PCW (Duque *et al.* 2016). In fact, the subplate represents the largest post-mitotic compartment of the human cortex during mid-gestation. Likewise, the OSVZ represents the most expanded germinal layer at this stage. Notably, in a few cases the radially-oriented fibres labelled by DiI belong to cell bodies located in the interface between the IZ and the OSVZ (**Figure 3.23, arrowhead**). These cell bodies did not resemble typical radial glial cells (RGC), as their processes were relatively short and restricted to the area around the cell body. Instead, they might represent **intermediate precursor cells** (**IPC**), which coexist with basal RGC in the OSVZ but were not specifically analysed in this study due to unsuccessful staining for their marker EOMES (Tbr2). IPCs can also establish physical contacts with thalamocortical axons similarly to RGC (Gerstmann *et al.* 2015), which could potentially explain the transneuronal labelling of these progenitors in this case. Alternatively, these cell bodies could be differentiating **post-mitotic neurons** in the process of radial migration toward the subplate (SP) or cortical plate (CP) and might have been transneuronally labelled at the level of the IZ. Unfortunately, their morphology did not provide a clear indication to favour one scenario over the other.

Figure 3.20

DiI placement in IC and progenitors of the GE

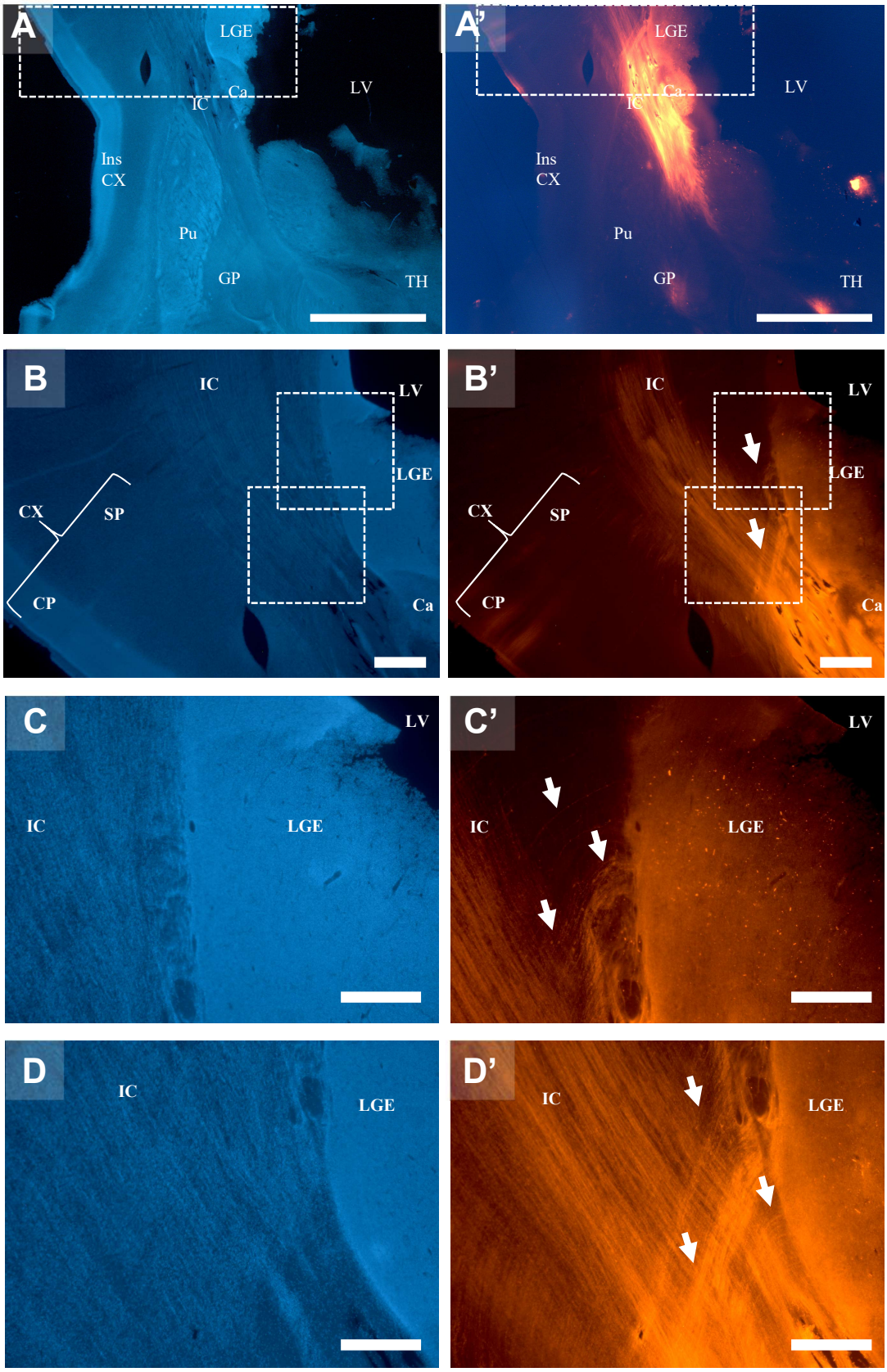

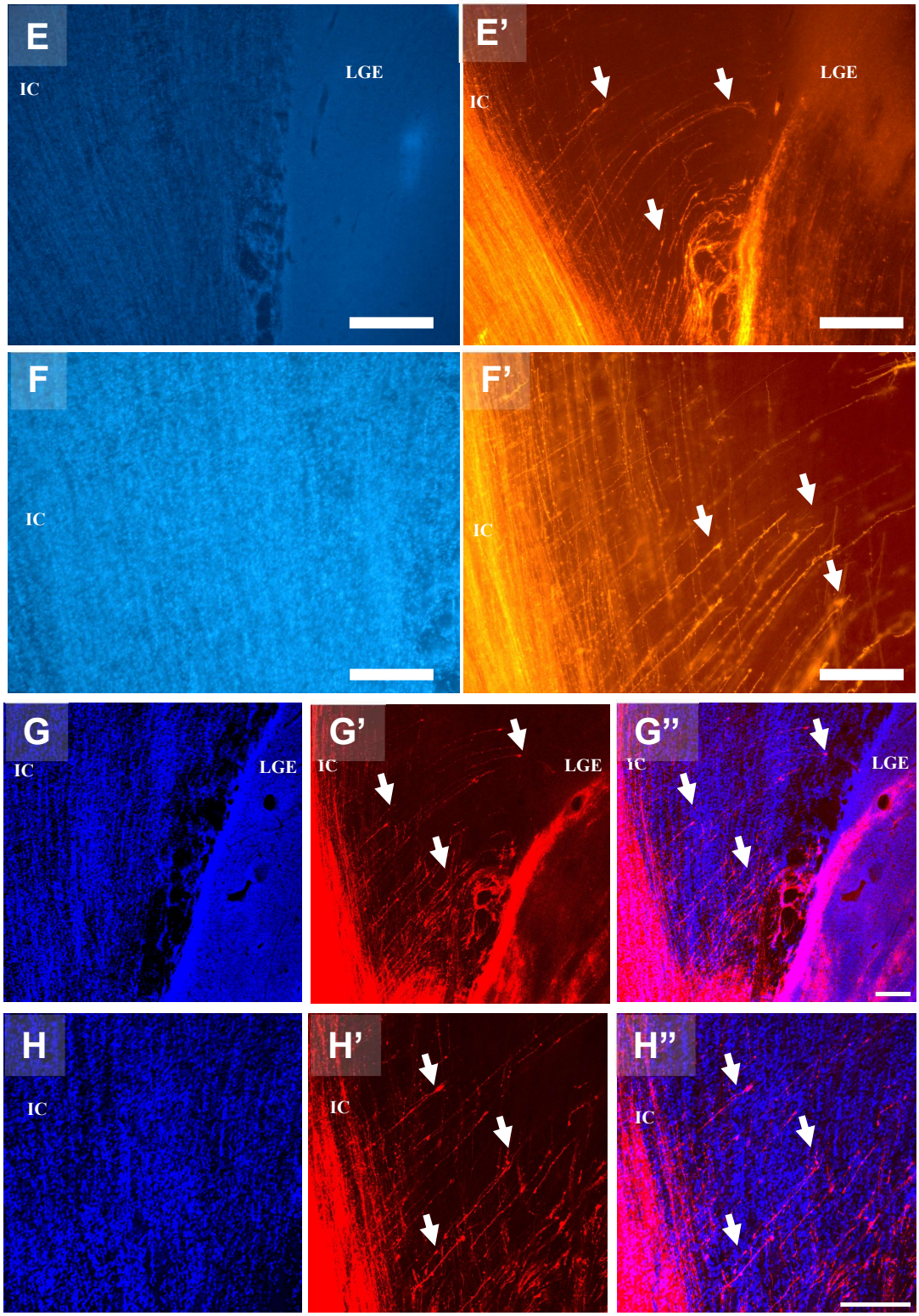

Figure 3.20: DiI crystal placement in the internal capsule labels the axons extending tangentially toward the cortex, along with progenitor cells in the vicinity and extending their process toward the lateral cortex in the 17 PCW human brain. The two adjacent sections analysed in the image are schematized on the left side. (**A, A'**) Epifluorescence image of the coronal section showing the main anatomical structures (A) and the site of DiI placement in the internal capsule (A'). (**B-F'**) Epifluorescence and (**G-G''**) confocal images depicting the area near the site of crystal placement and highlighting the radial glial cells (RGC) bodies and basal processes crossing the trajectory of the internal capsule (arrows). Scale bars = 5 mm (A, A'); 1 mm (B, B'); 500 µm (C-F'); 100 µm (G-H'').

Figure 3.21

Tangential trajectory of TCA within the IZ

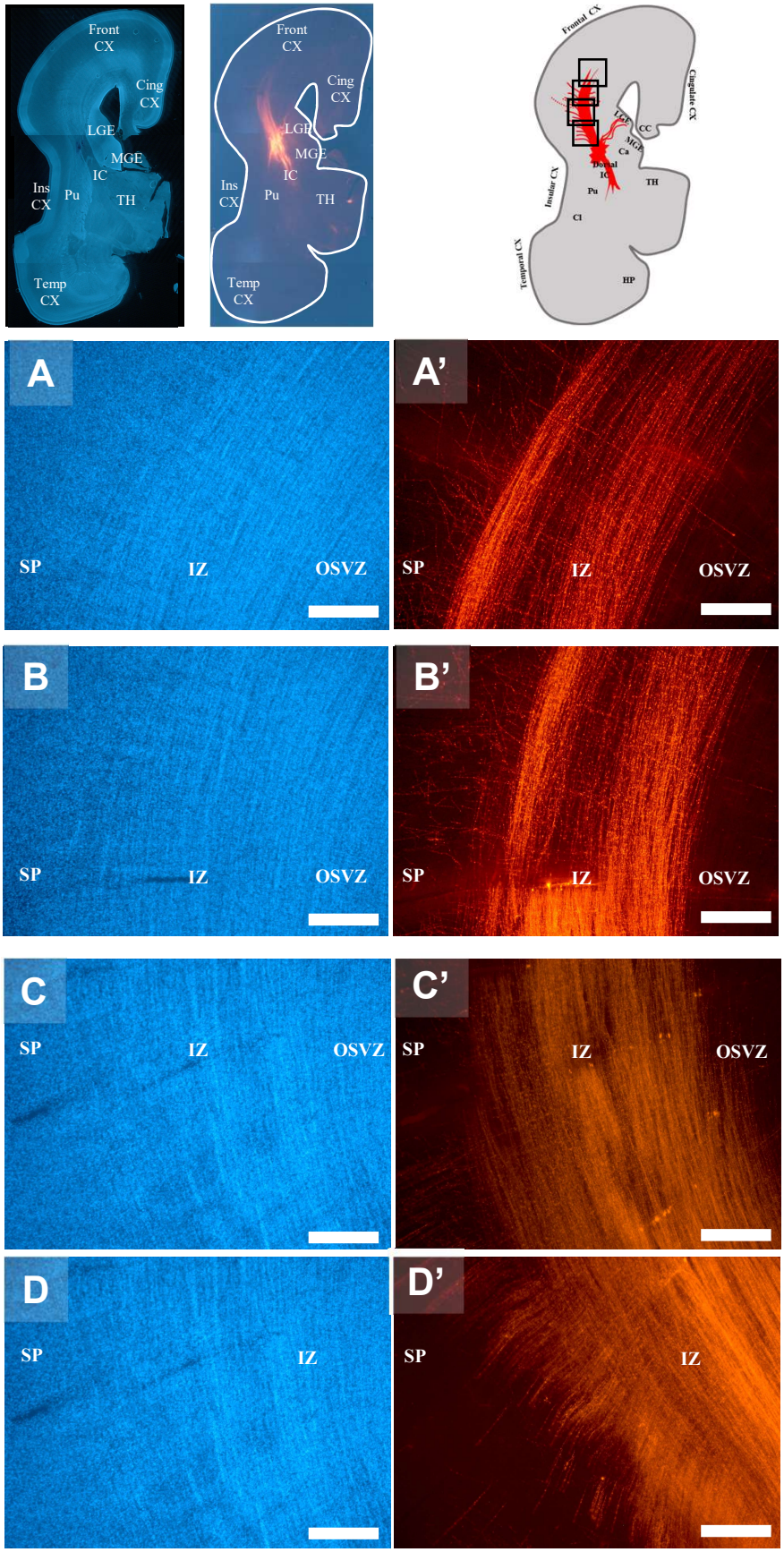

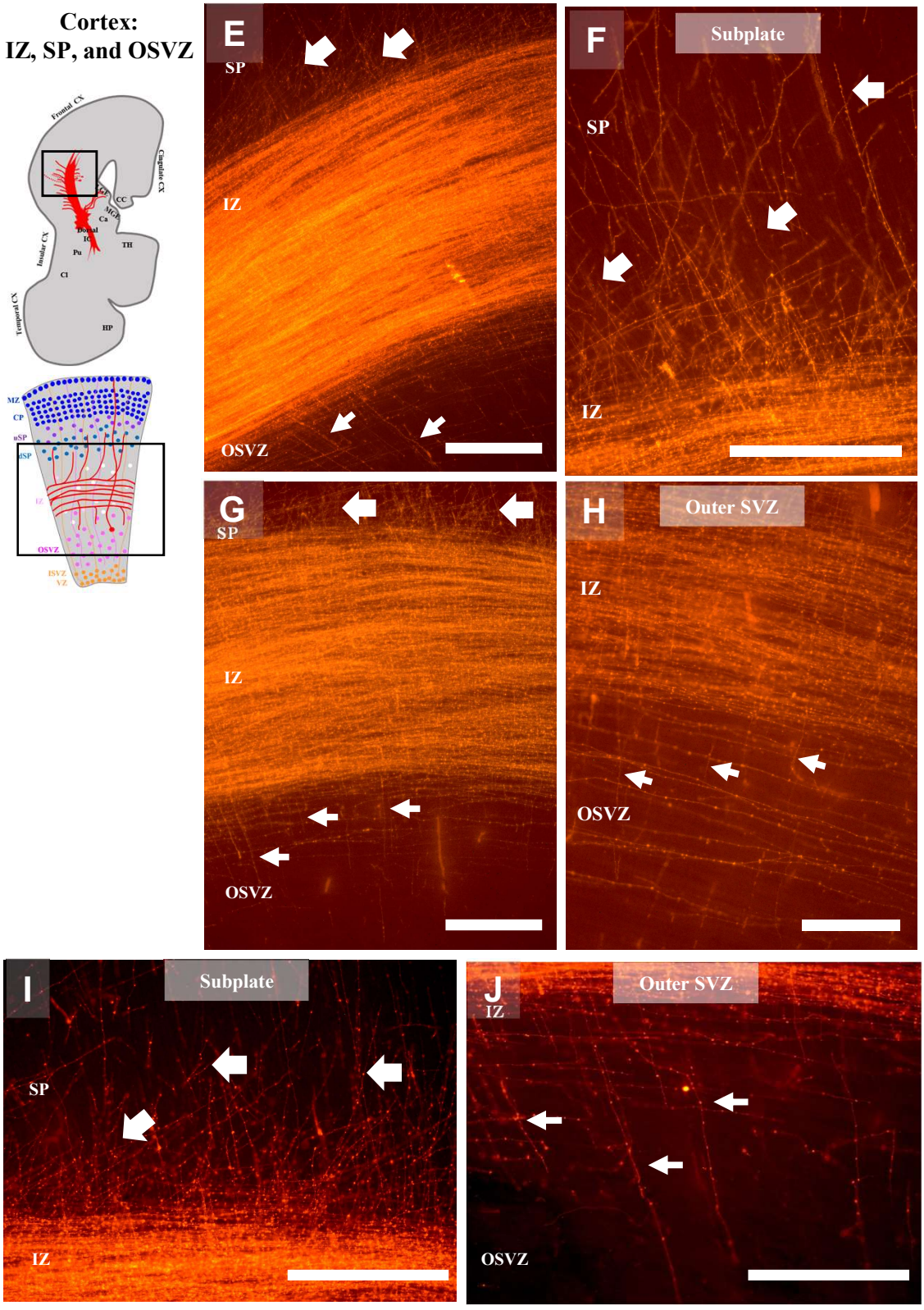

Figure 3.21: The axons labelled by DiI crystal placement in the internal capsule are visible for a long distance within the cortical intermediate zone (IZ) of the 17 PCW human brain, where they reach the subplate (SP) and the outer subventricular zone (OSVZ). Representative low power images and schematics of the coronal section are presented on the top for reference. Epifluorescence image of the trajectory of the DiI-labelled axons within the intermediate zone (IZ) of the lateral (**C-D'**) and dorsal (**A-B'**) cortex, corresponding to the prospective insular and frontal cortices, respectively. (**E-H**) The DiI-labelled axons depart from their tangential trajectory in the IZ to reach the subplate (thick arrows) and the OSVZ (thin arrows), as highlighted in the zoomed-in images of the subplate (**F, I**) and OSVZ (**G, J**). Scale bars = 500 µm.

Figure 3.22

Cortex:
IZ, SP, and OSVZ

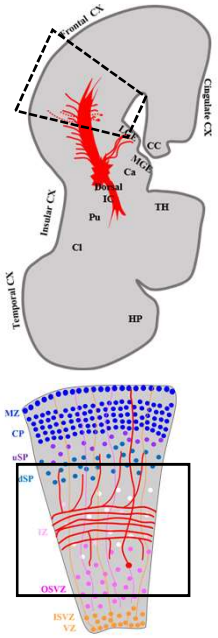

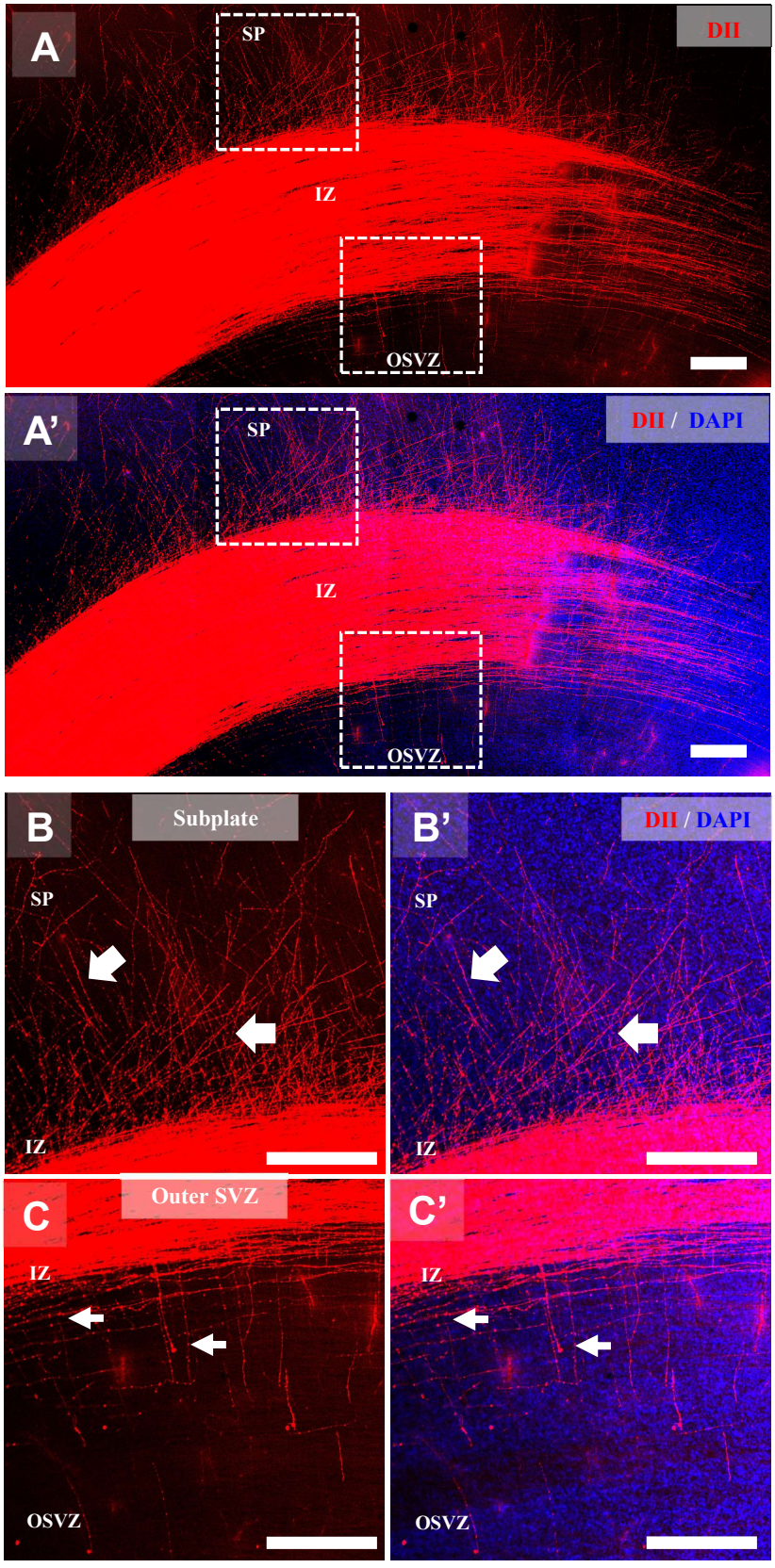

Figure 3.22: DiI-labelled axons extend tangentially in the cortical intermediate zone (IZ) of the 17 PCW human brain, and project toward the subplate (SP) and the outer subventricular zone (OSVZ). (A, A') Confocal scans of the cortical region where DiI-labelled axons are detected within the intermediate zone (IZ) of the prospective frontal cortex. The DiI-labelled axons depart from their tangential trajectory in the IZ to reach the subplate (thick arrows) and the OSVZ (thin arrows). Confocal images highlight these fibres radially projecting into the subplate (**B, B'**) and OSVZ (**C, C'**). Scale bars = 500 µm.

Figure 3.23

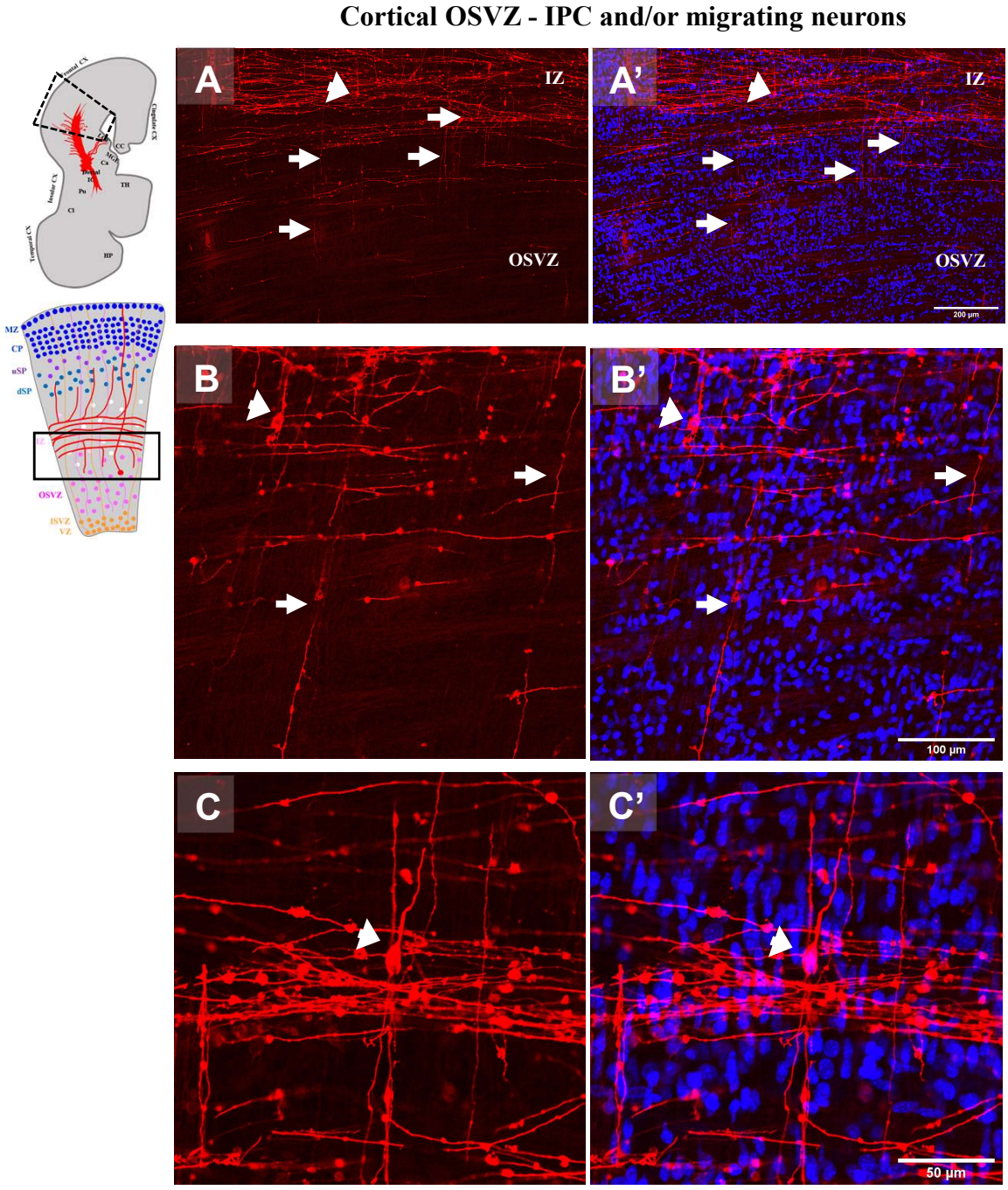

Figure 3.23: DiI crystal placement in the internal capsule reveals radially oriented fibres extending between the intermediate zone (IZ) and the outer subventricular zone (OSVZ), as well as few transneuronally labelled cells at the boundary between these compartments in the 17 PCW human brain. (A, B') Confocal scans of the region between the IZ and the OSVZ highlighting several radially oriented DiI-labelled fibres (arrows) and one cell body (arrowhead). The latter is depicted at higher magnification in (C, C'), and does not resemble the morphology of a radial glial cell (RGC), hence likely representing a radially migrating neuron. Scale bars = 200 µm (A, A'); 100 µm (B, B'); 50 µm (C, C').

TCA innervate the subplate zone

The cortical compartment where most DiI-labelled fibres were observed was the subplate (**Figures 3.21 and 3.22, thick arrows**). To address whether DiI-labelled fibres were establishing any contact with SP neurons, I stained some brain slices for Nuclear Receptor Subfamily 4 Group A Member 2 (NR4A2, also referred to as Nurr1), a specific marker for subplate neurons (SPN) (Wang *et al.* 2010). Differently from other known markers for SPN such as CTGF or Complexin-3, this molecular marker should be already expressed by 17 PCW (Wang *et al.* 2010). However, I only detected **Nurr1-positive signal in the upper portion of the SP (uSP)**, which was not reached by the DiI-labelled axons (**Figure 3.24**). This is in line with previous reports in the human developing cortex (Wang *et al.* 2010).

Therefore, I used T-box brain transcription factor 1 (Tbr1) as a marker for newly generated neurons (Bulfone *et al.* 1995; Hevner *et al.* 2001) which is also expressed in the human fetal SPN at this age (Bayatti *et al.* 2008). DiI-labelled fibres were detected in close proximity to Tbr1+ neurons in the deeper portion of the SP (**Figures 3.25**). Despite Tbr1 being a marker for subplate neurons at this age, it is also expressed by deep layer neurons of the cortical plate. The annotation of the Tbr1-positive cells as subplate neurons was therefore made according to their anatomical location within a clearly distinguishable subplate layer by DAPI staining, and by proximity with the intermediate zone. Surprisingly, I did not observe many cases of Tbr1-positive neuronal bodies back labelled by DII, and most DiI-labelled fibres were observed at extremely close contact with the nuclei of these neurons instead (**Figure 3.25 B-E'''**). This physical proximity between TCA and SPN might suggest both cases of transient synaptic contact being made, as well as potential paracrine influence exerted by thalamic axons via secretion of molecules in the extracellular space. Both cases might occur during human brain development.

Figure 3.24

Cortical Subplate (upper)

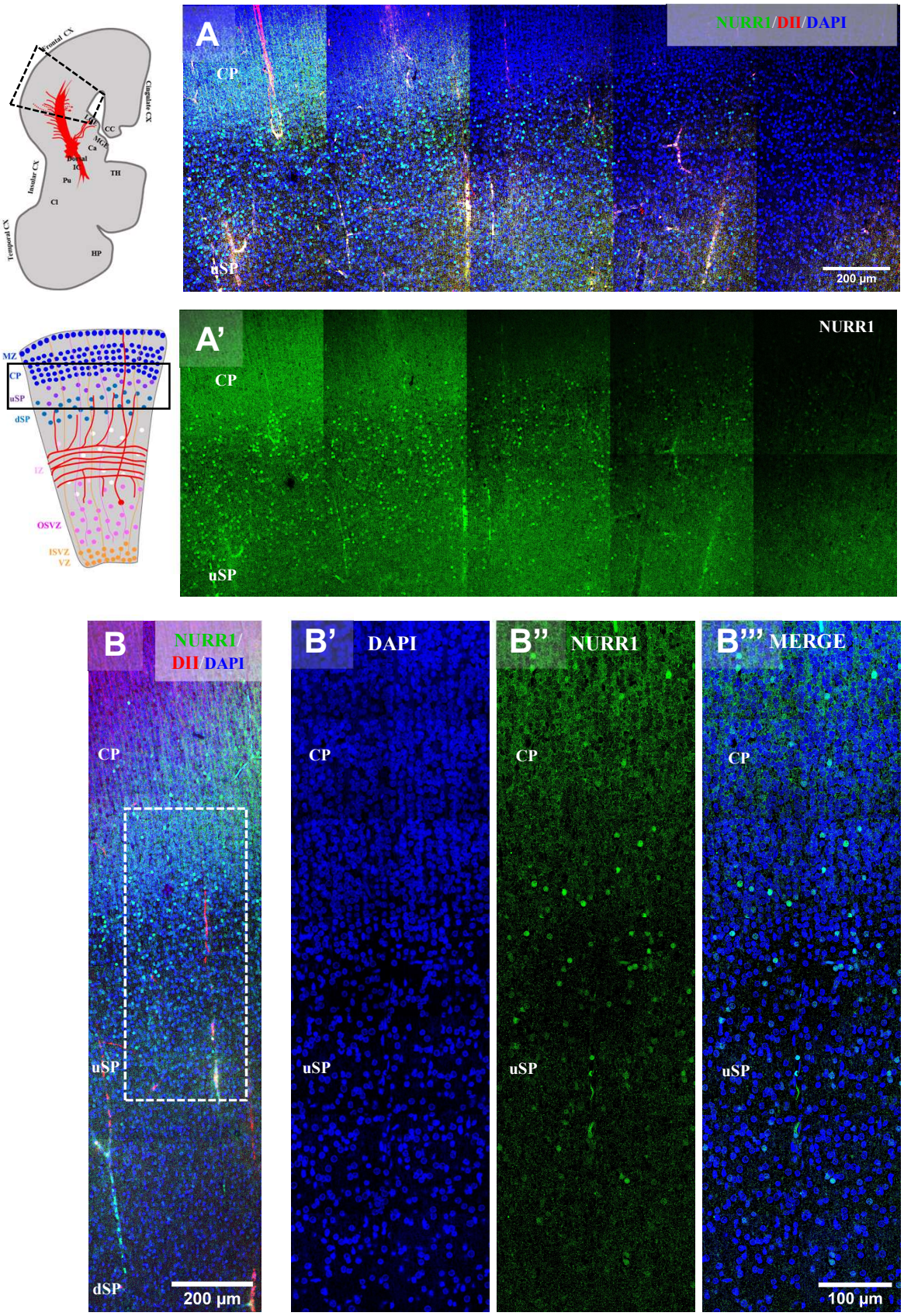

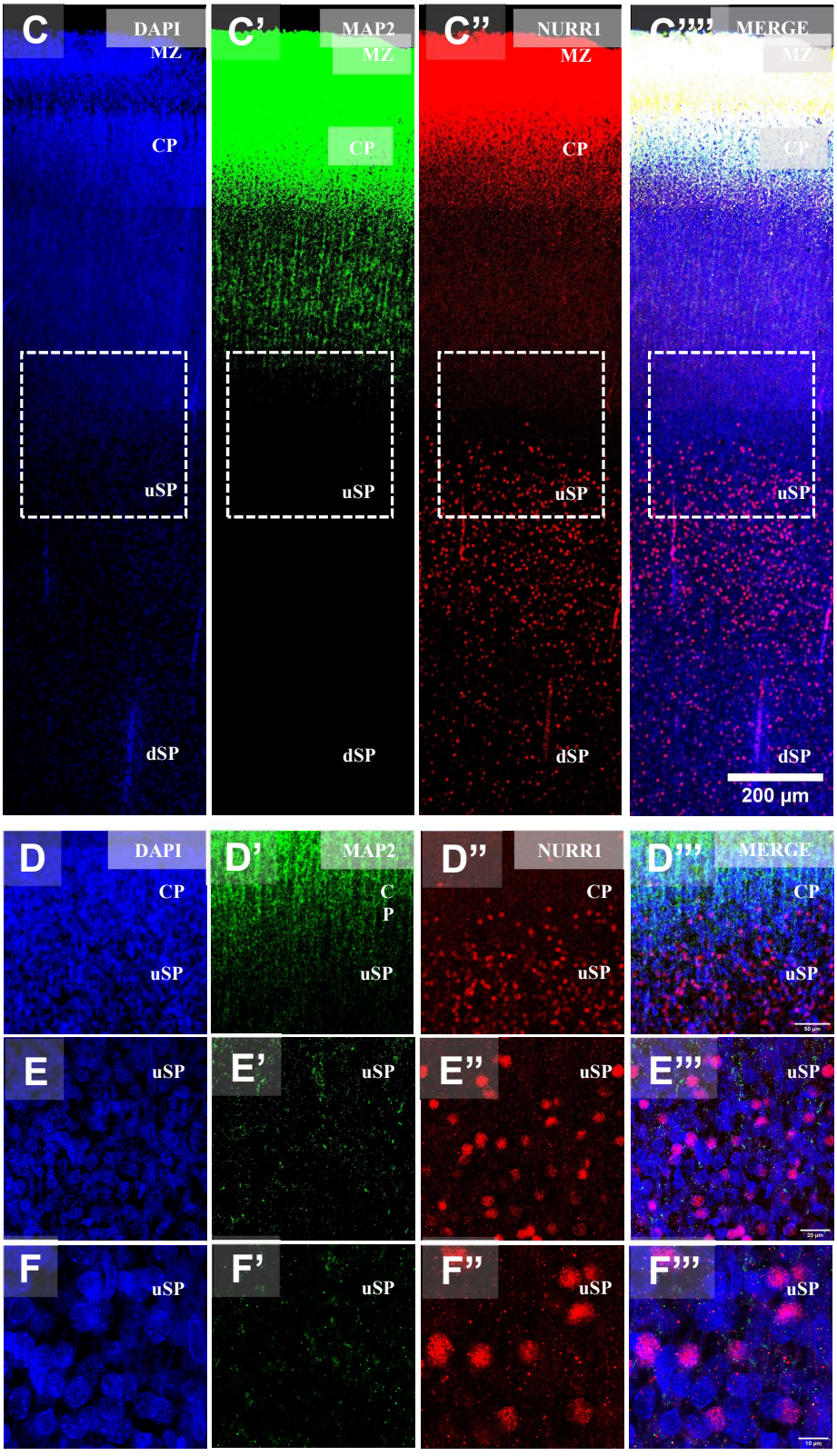

Figure 3.24: Thalamic axons labelled from DiI crystal placement in the internal capsule do not reach the upper portion of the subplate (uSP) where Nurr1-positive subplate neurons are located the 17 PCW human brain. (A, A') Confocal scanning of the boundary between cortical plate (CP) and upper subplate (uSP) where Nurr1-positive subplate neurons are detected (green). (**B**) DiI-positive axons (red) are not found in the Nurr1-positive area (B'-B'''). (**C, C'''**) Confocal scanning of the 17 PCW cortex co-immunostained for subplate neuron marker Nurr1 (red) and cortical plate neuronal marker MAP2 (green) to reveal the boundary between the two layers (**D-E'''**) snapshots at increasing magnification of the region highlighted in C-C''' (dashed box). Scale bars = 200 µm (A, A', B, C-C'''); 100 µm (B', B'''); 50 µm (D-D'''); 20 µm (E-E'''); 10 µm(F-F''').

Figure 3.25

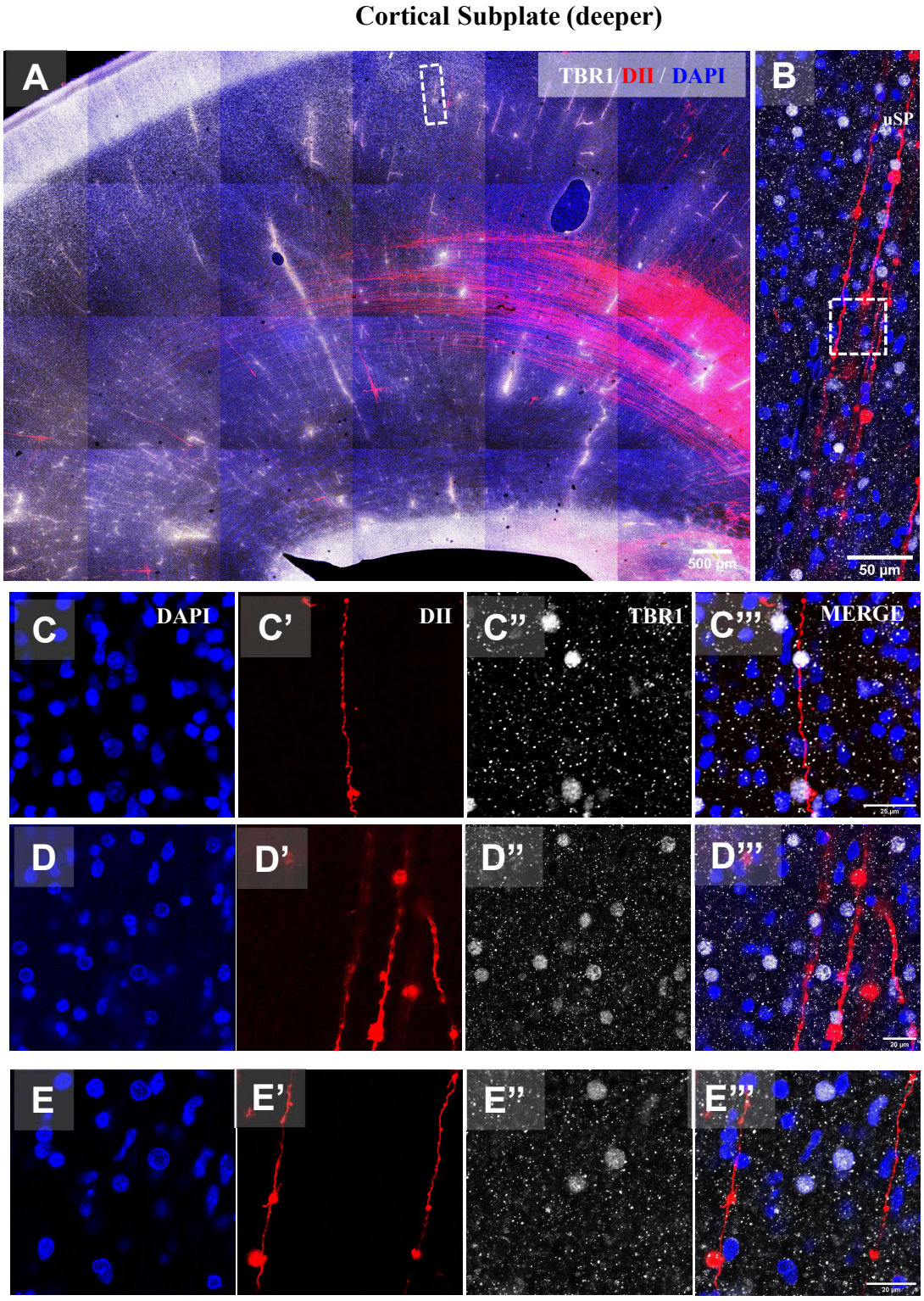

Figure 3.25: Thalamic axons labelled from DiI crystal placement sites in the internal capsule innervate the deeper portion of the subplate (dSP) where they project closely to Tbr1-positive subplate neurons in the 17 PCW human brain. (A) Confocal scanning of the whole cortical area (frontal) analysed for DiI-positive signal (red) and subplate neuronal marker Tbr1 (white) in the Figure. (B) High magnification confocal scanning of the area indicated in A (dashed box) and revealing radially oriented DiI-positive axons extending in close proximity with the post-mitotic neurons of the deep subplate (dSP), revealed by nuclear marker Tbr1 (white). These are depicted at high magnification in (C-E'''). Scale bars = 500 µm (A); 50 µm (B); 25 µm (C-C'''); 20 (D-F''').

TCA interact with the OSVZ progenitors

The second cortical region targeted by DiI-positive fibres was the upper portion of the OSVZ (**Figures 3.21 and 3.22, thin arrows**). This phenomenon was consistently detected in the coronal sections cut for the imaging analysis. In these sections, numerous radially-oriented fibers were observed crossing the intermediate zone (**Figures 3.22 C, C'; 3.23 A-B'; 3.20**). Their orientation and morphology resembled that of radial glial cell (RGC) apical processes (**Figure 3.26**), which extend from the RGC cell bodies either in the VZ/ISVZ (**Figure 3.26 B-B'**) or in the OSVZ up to the pial surface, as shown by staining for RGC specific marker Glial Fibrillary Acidic Protein (GFAP). The apical processes of RGC traverse both the IZ (**Figure 3.26 A-A''**) and the SP (**Figure 3.26 C-C''**) where they can physically interact with DiI-positive TCA, potentially leading to transneuronal labelling of these cells.

However, due to the cutting and slicing of the sample, many of these fibres were severed at the surfaces of the sections, making it difficult to determine their origin and destination. Additionally, the intense signal in the IZ made it difficult to track the trajectory of individual fibers within this region. Only in one exceptional case was this phenomenon visualized, and reported in representative **Figure 3.27**. Although specific staining for RGC markers was not performed in this specific case, it seemed evident that the DiI-labelled fiber in this instance was extending from a cell body located in the OSVZ and spanning from there up to the subplate, crossing the entire width of the IZ, and unequivocally belonging to a basal RGC.

To gain more insight into the relationship between the DiI-labelled fibres and the cell populations in the OSVZ, I performed staining using HOP Homeobox (HOPX), a marker specific to outer radial glial cells (oRGCs) (Pollen *et al.* 2015) (**Figure 3.28**).

DiI-labelled fibres might represent either transneuronally labelled oRGC that incorporated the DiI through their apical process, or anterogradely labelled thalamic axons invading the germinal zones. Interestingly, I observed examples for both circumstances **(Figures 3.29 – 3.30)**. In the **first case**, the extremity of the DiI-labelled fibres within the OSVZ seemed to co-localize with the nuclear

DAPI staining, and HOPX-positive signal (**Figure 3.29**). This suggested a potential transneuronal labelling, which might be indicative of direct physical interaction between oRGC and TCA as previously hypothesised **(Figures 3.28 and 3.29)**. It is worth to note that the neither the HOPX-positive signal, nor the DiI-labelled tip of the fibre shown in **Figure 3.29** perfectly co-localize with the nucleus of the cell. However, as the transcription factor HOPX can be detected at both nuclear and cytosolic level, and the shape of HOPX-positive signal is specifically matching the one of the DiI-labelled fibre, it is reasonable to assume that the majority of the dye was revealing the soma of the cell, where HOPX is also detected.

The **second scenario** represented most of the cases observed in the sample, where the tip of the DiI-labelled fibre invading the OSVZ did not co-localize with the nuclear staining DAPI, nor with HOPX-positive signal **(Figures 3.30)**. This observation, along with the characteristic morphology, suggested that this might represent a growth cone decorating the extremity of a thalamic axon. Collateral of thalamic axons protruding within the OSVZ have never been observed in rodents by similar experiments, and the only case where this phenomenon has been reported is the fetal monkey (Carney 2004). This suggest a novel mechanism of interaction between early TCA and cortical progenitors in the primate brain.

TCA have been reported to have a mitogenic effect on cortical progenitors in mouse (Dehay *et al.* 2001). To explore the possibility that this phenomenon might occur in human, where they establish an especially tight interaction, I further evaluated whether the progenitors observed near the TCA were proliferating cells by staining for the mitotic marker Ki67. Interestingly, I observed numerous dividing cells especially within the IZ and at the border with the OSVZ (**Figures 3.31)**, in line with previous observation in the fetal monkey (Carney *et al.* 2004). However, whether the TCA actively modulate the mitotic rate of the neurogenic pool remains to be determined.

Figure 3.26

RGC basal processes and radial scaffold

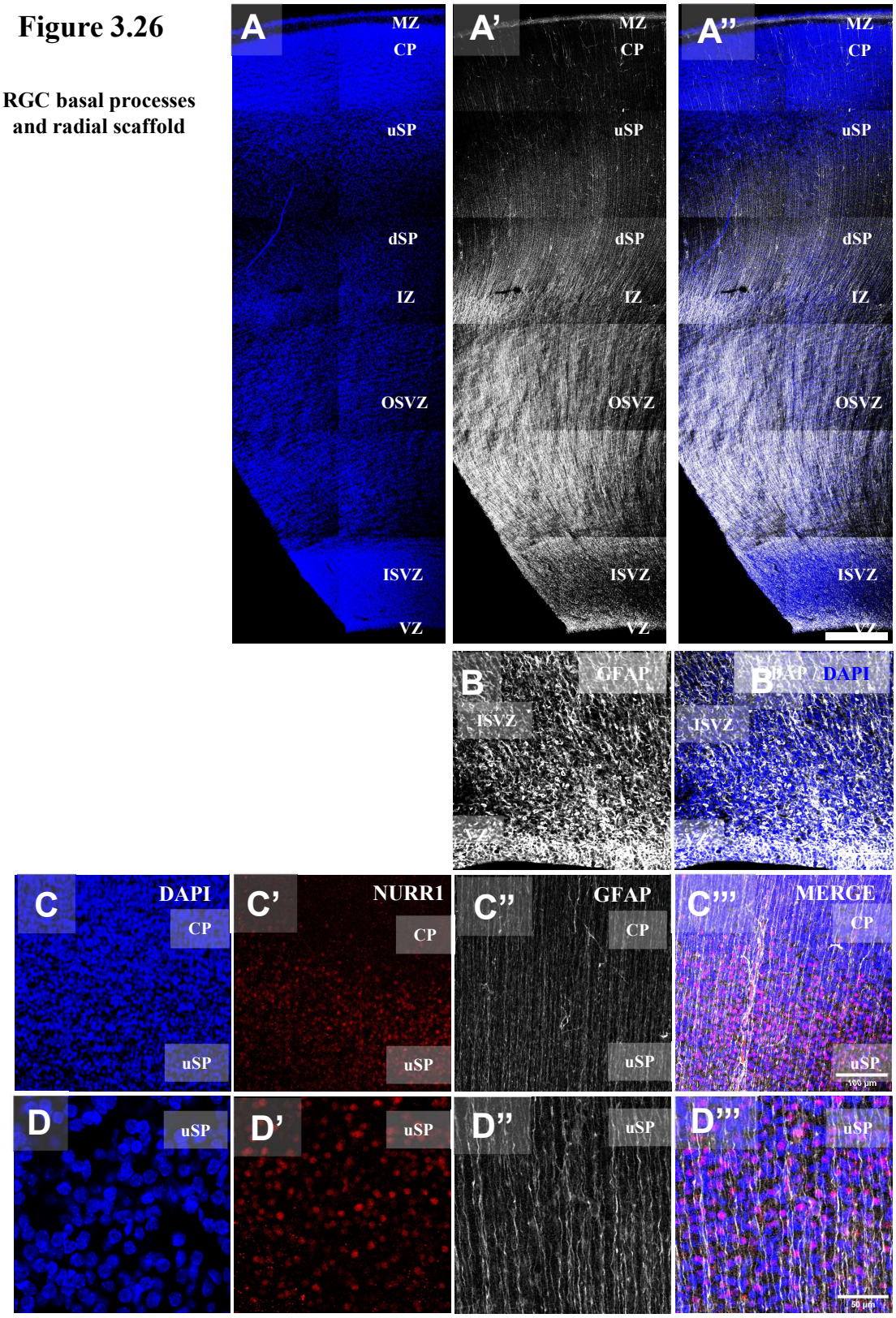

Figure 3.26: Glial fibrillary acidic protein (GFAP)-immunoreactive radial glial cells (RGC) extend their basal processes from the germinal zones, through the intermediate zone, crossing the Nurr1-positive subplate zone to reach the pial surface in the 17 PCW human brain. (A) Confocal scanning of the entire cortical depth of the 17 PCW human brain stain for RGC specific marker GFAP (white). GFAP-positive signal can be observed from the ventricular side (highlighted in B, B'), throughout the extension of the RGC basal processes surpassing the subplate neurons stained by Nurr1 in the upper subplate (uSP) (red, in **C-D'''**) to reach the marginal zone (MZ). Scale bars = 500 µm (A-A''); 100 µm (B-C'''); 50 µm (D-D''')

Figure 3.27

Cortical OSVZ – transneurnally labelled oRGC

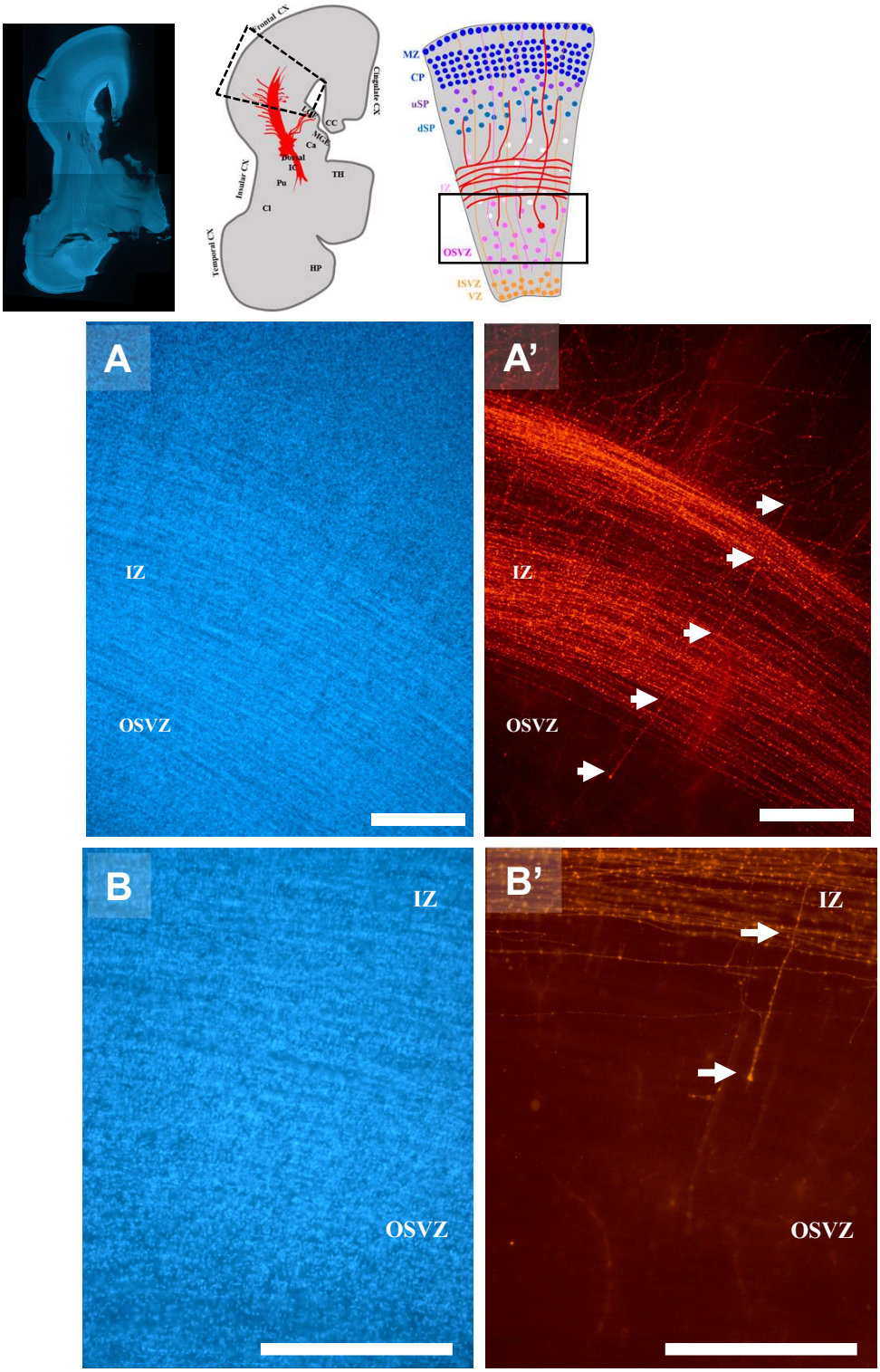

Figure 3.27: DiI crystal placement in the internal capsule reveals outer radial glial cells (oRGC) of the outer subventricular zone (OSVZ), suggesting transneuronal labelling through possible physical interaction between these progenitors and the thalamic axons in the 17 PCW human brain. (A, A') Epifluorescence imaging of a oRGC labelled by DiI throughout its basal process extending across the intermediate zone (IZ) (arrows). The soma of this progenitor is in the OSVZ, as highlighted in the zoomed-in image (B, B'). Scale bars = 500 µm.

Figure 3.28

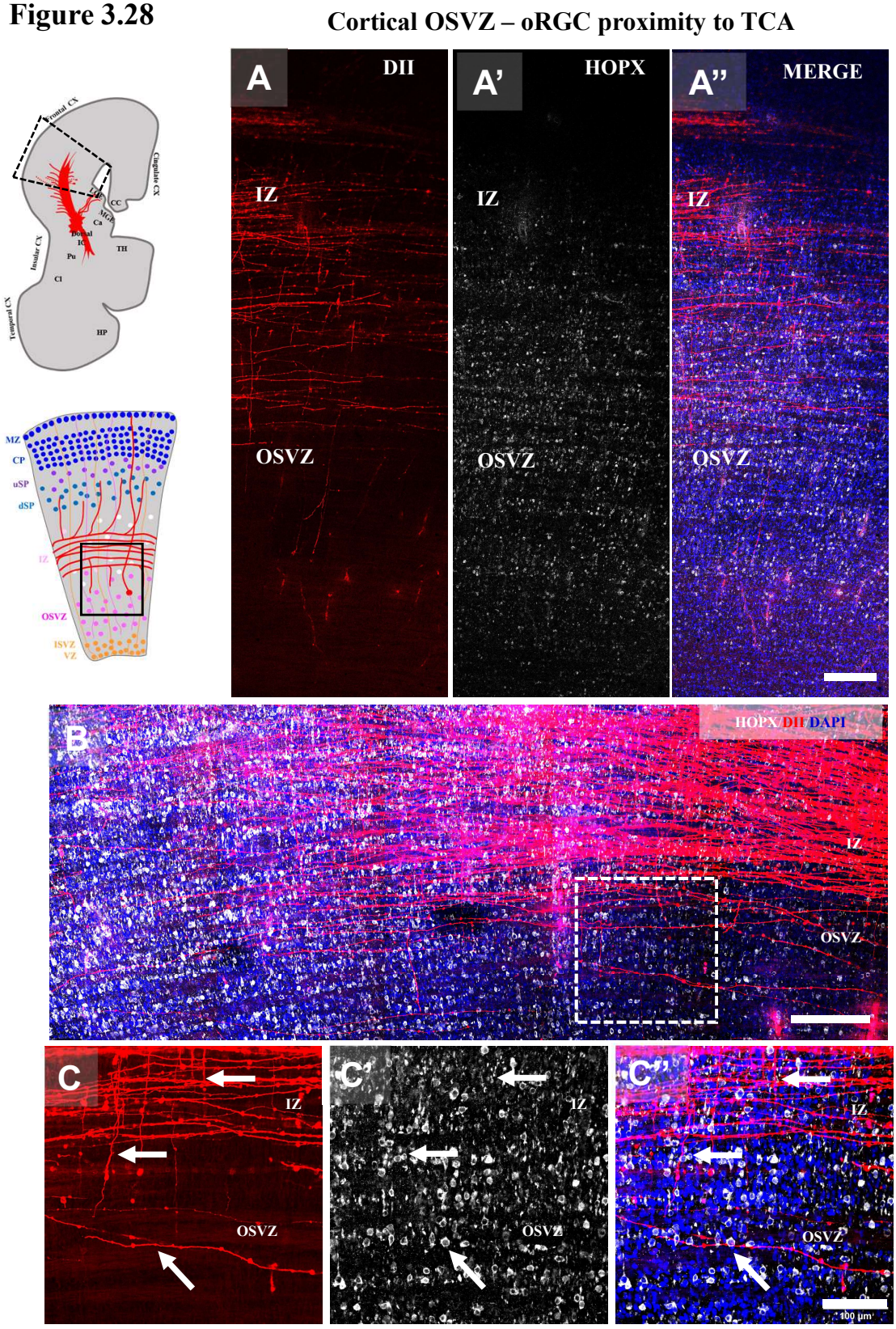

Figure 3.28: DiI-labelled fibers are detected in close proximity with the HOPX-positive outer radial glial cells (oRGC) in the OSVZ in the 17 PCW human cortex. (**A-B**) Tiled scans of DiI labelled fibres (red) within a region of the OSVZ that contain HOPX immunoreactive cells (white). (**C-C''**) show a snapshot at the boundary between IZ and OSVZ, highlighted in C (dashed box) and depicting the close relationship between DiI-labelled fibres and the cell nuclei of the basal RGC in this region (arrows). Scale bars = 200 µm (A-B); 100 µm (C-C''')

Figure 3.29

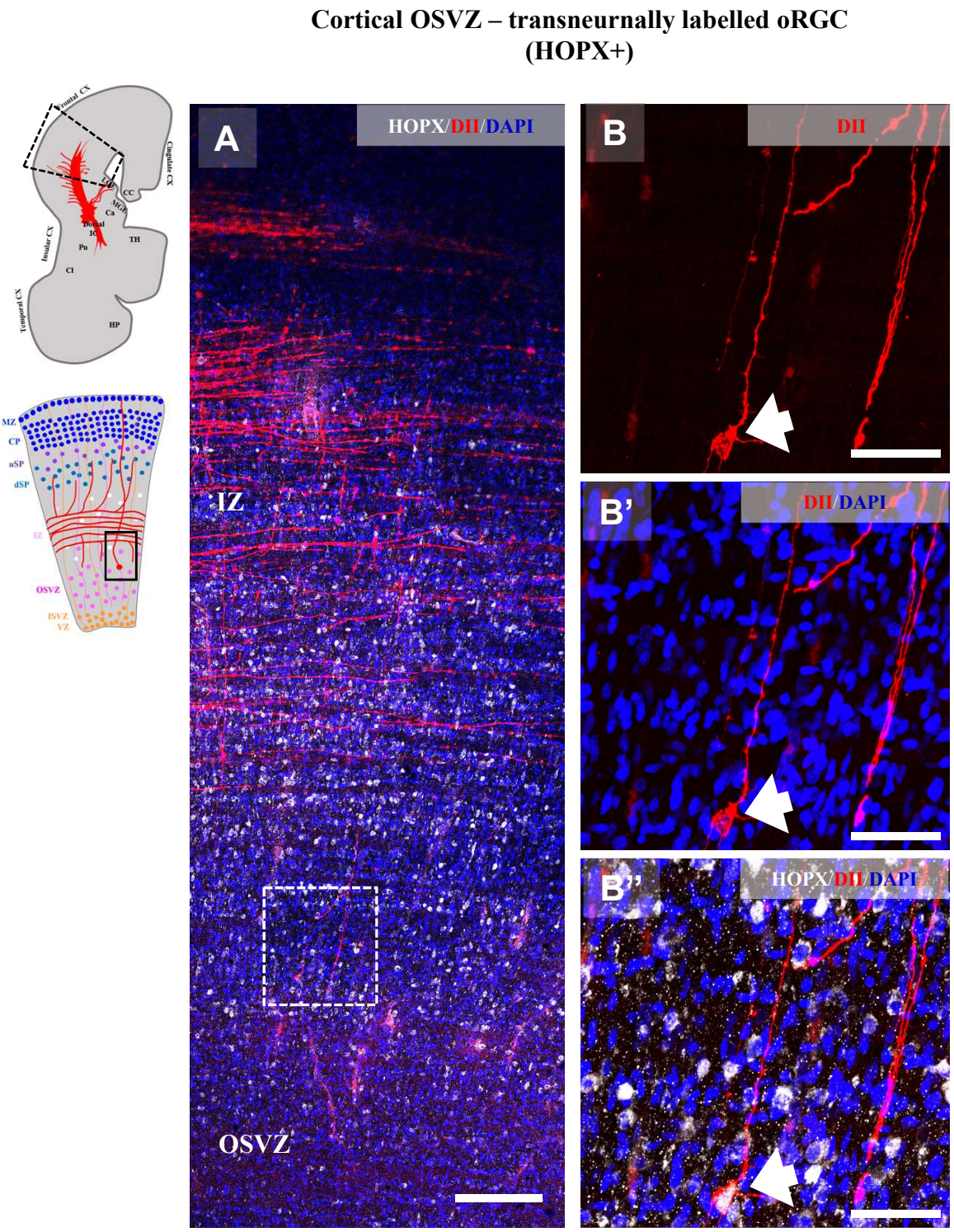

Figure 3.29: Representative examples of a HOPX-positive outer radial glial cells (oRGC) that were labelled from the DiI labelled thalamic projections in the OSVZ in the 17 PCW human cortex. (**A**) Tiled scans of the region where B-B''' were taken. (**B-B'''**) Maximum intensity projection image of the tip of a radially oriented fibre labelled by DiI and protruding from the IZ to the OSVZ, which shows co-localization with oRGC marker HOPX (white) and partial co-localization with nuclear DAPI. Scale bars = 200 µm (A); 100 µm (B-B''').

Figure 3.30

Cortical OSVZ – TCA projects toward oRGC (HOPX+)

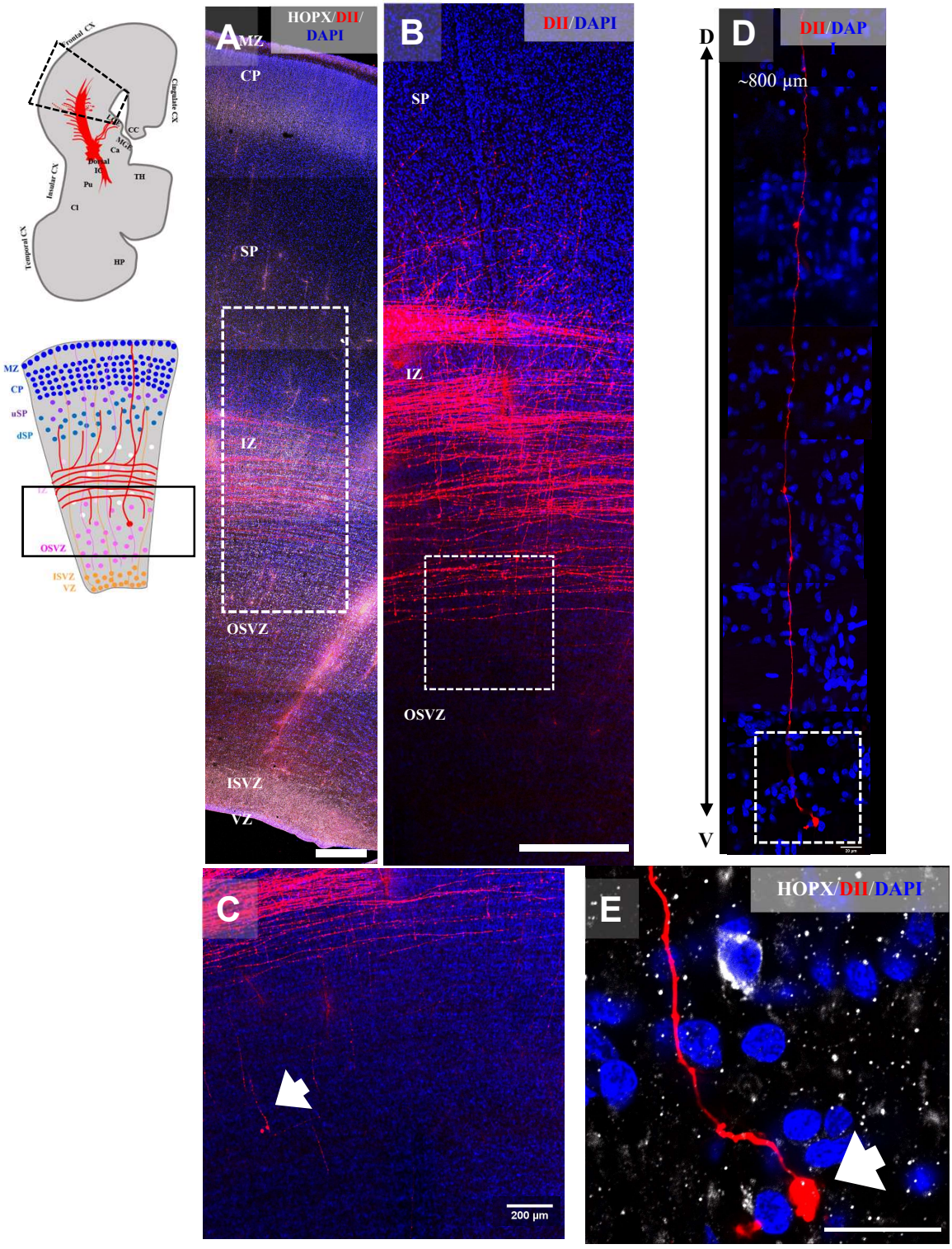

Figure 3.30: Representative case of a DiI-labelled axonal terminal projecting to the outer subventricular zone (OSVZ) and ending in a growth cone-shaped tip close to the nucleus of a HOPX-positive outer radial glial cells (oRGC) in the 17 PCW cortex. Tiled scans (**A, B**) and low power snapshot (**C**) of the area where D, E were taken (**D**) Snitched z-stacks tracking the entire length of a radially-oriented DiI-positive fibre from its starting point (arbitrary) in the IZ to its endpoint in the OSVZ. The tip of the fibre, shows a growth cone-like morphology and it is close to the HOPX-positive nucleus of a oRGC, but not co-localizing with this signal, suggesting the case of an anterogradely labelled axonal projection. Scale bars = 500 µm (A, B); 200 µm (C); 20 µm (C, D).

Figure 3.31 **Cortical OSVZ – mitotic progenitors and TCA**

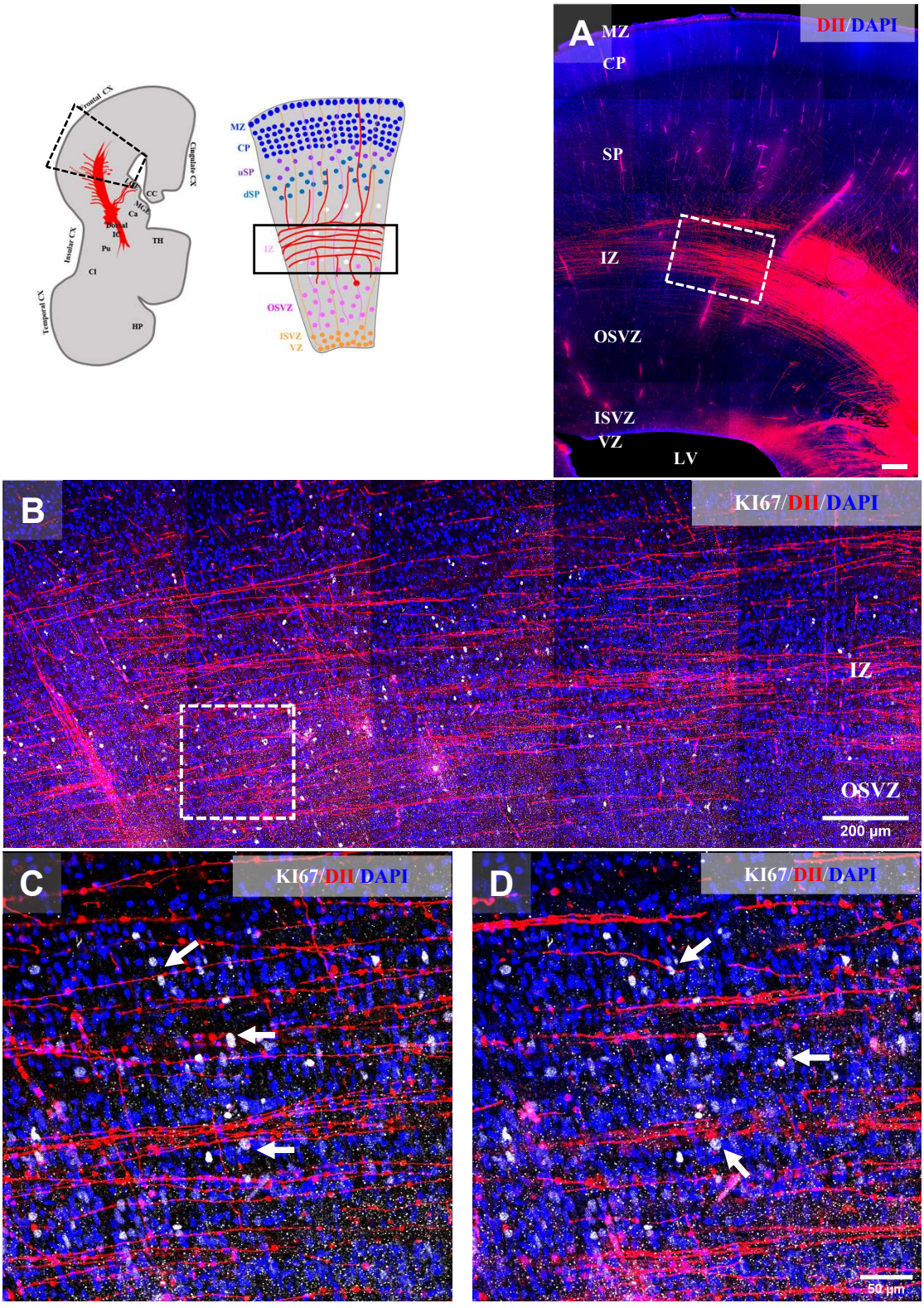

Figure 3.31: DiI-labelled fibres are detected in an overlapping region where proliferating Ki67-positive progenitor cells are in the intermediate zone (IZ) and outer subventricular zone (OSVZ) in the 17 PCW human cortex. (**A**) Tiled scans of the whole cortical region imaged in panels B-D were taken. (**B**) Tiled scan showing the overlap between DiI labelled fibres (red) and Ki67-positive mitotic cells (white) in the IZ and upper portion of the OSVZ. (**C, D**) Ki67-positive nuclei are found in close proximity with the tangential axonal projection labelled by DiI (arrows). Scale bars = 500 µm (A); 200 µm (B); 50 µm (C, D).

Semi-quantitative analysis of DiI-labelled axons in the SP and OSVZ

To conclude the characterization of the cortical innervation pattern analyzed in this chapter, I conducted a semi-quantitative analysis of the signal intensity of the labelled fibres from thalamus detected at various levels of the cortex for both the subplate (SP) and the outer subventricular zone (OSVZ). I considered inappropriate to directly compare the amount of collaterals stained by DiI in the SP and OSVZ, as these two sets of fibres may represent distinct and independent phenomena. The innervation to the SP is a well-characterized transient step toward achieving proper innervation of the cortical plate later in development. In contrast, the collaterals observed in the OSVZ represent a mixture of transneuronally-labelled RGC basal processes and anterogradely labelled subcortical axons, as suggested by **Figures 3.29 and 3.30**, respectively. However, considerations could be made regarding their respective amounts relative to the distance along the intermediate zone (IZ). Cortical areas proximal to the origin of the axons (i.e., the thalamus) might or might not receive more extensive innervation earlier than distal cortical regions. With this in mind, I arbitrarily selected three regions of interest (ROIs) along the tangential path of these axons within the SP and OSVZ, labelled as 1 (most distal), 2 (medial), and 3 (most proximal) according to their relative distance from the thalamus and the site of DiI placement in the proximal segment of the dorsal internal capsule (IC). As mentioned earlier, an accurate tracing of individual axon collaterals was not possible in this study; therefore, I measured the mean intensity signal from the DiI labelling across these ROIs (**Figure 3.32**).

The strongest signal intensity was noted closer to the DiI placement site (ROI 3) in both the SP (**Figure 3.32 B-B'**) and OSVZ (**Figure 3.32 C-C'**), gradually decreasing with augmenting distance from it (ROI 1). However, neither of these trends appear statistically significant when comparing the mean values for each region of interest (ROI). Consequently, the observed differences between them cannot be deemed substantial enough to preclude the possibility of random chance as a plausible explanation for the observed trend.

Figure 3.32

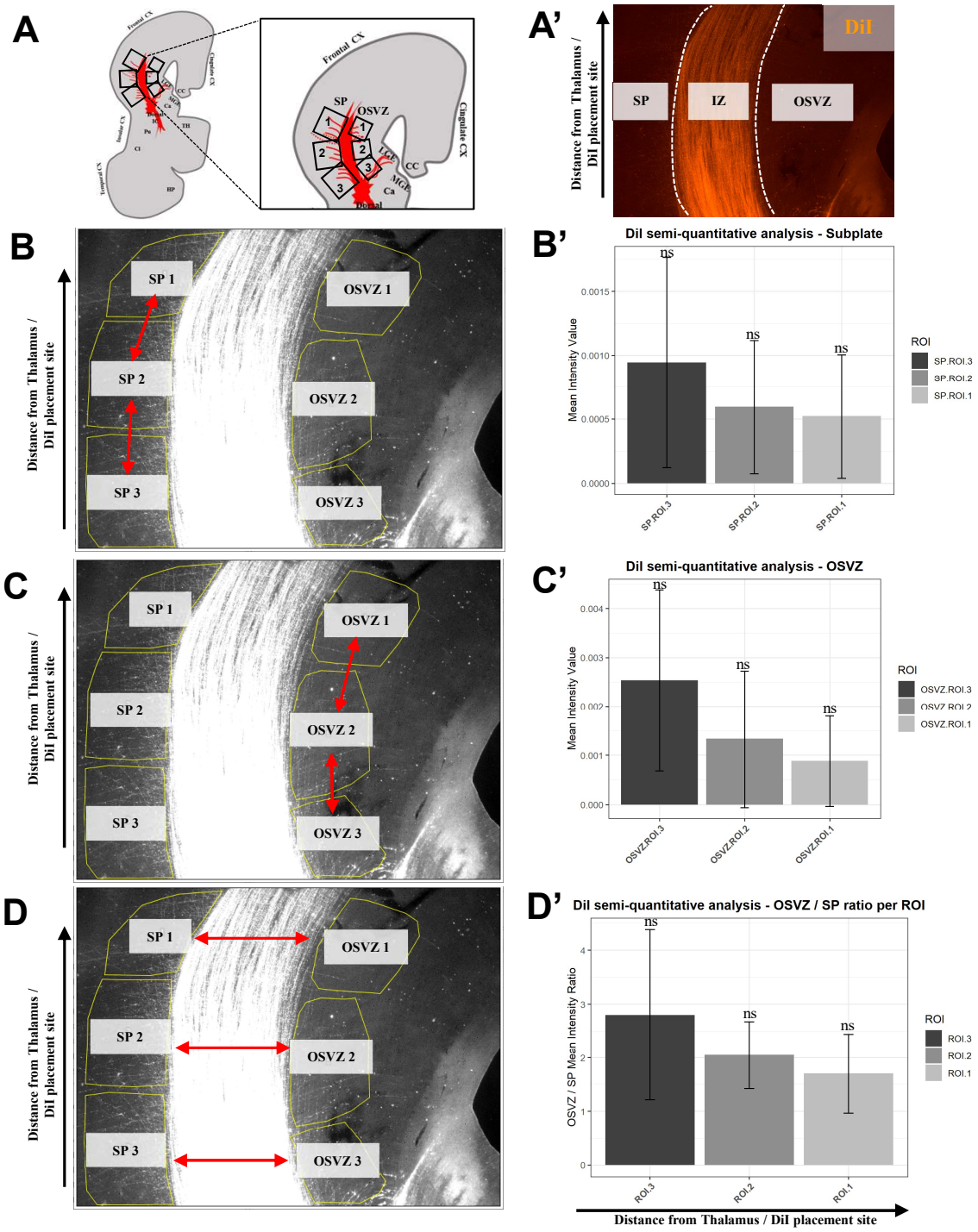

Figure 3.32: Semi-quantitative analysis of DiI-positive signal in the cortical subplate (SP) and outer subventricular zone (OSVZ) of the 17 PCW human brain. (**A-A'**) Schematics of the brain region analysed and representative epifluorescence imaging of DiI-positive signal detected at cortical level and showing the anatomical boundaries used to select the ROIs for quantification of the signal intensity in the SP and OSVZ. (**B-B'**) Quantification of the mean signal intensity in the three ROIs within the SP. (**C-C'**) Quantification of the mean signal intensity in the three ROIs within the OSVZ. (**D-D'**) Quantification of the ratio between mean signal intensity in the two cortical compartments, OSVZ and SP, across the three ROIs. Error bars refers to average of the values measured for each image analysed (N= 5). One-way ANOVA test. Statistical significance is set at p-value <0.05.

CONCLUSIONS

In this chapter, I investigated the spatiotemporal dynamics of the earliest interactions between thalamic axons and the developing neocortex in humans. The data presented support the idea that thalamic axons not only have interactions with the postmitotic cells in subplate, but they are also in contact with the proliferative zone. The contact could be established by direct innervation of the SVZ by TCA, or through physical interactions along the trajectory of the oRG's basal process, most probably within the intermediate zone. By closely interacting with the progenitors of the OSVZ, the early TCA are in a position to exert a major influence on the cortical neurogenic programme in the human brain.

First, I analysed the earliest timepoints of human brain development when the interaction between TCA and the cortex is established (between CS19 and 12 PCW). By using known immunohistochemical markers for thalamocortical and corticothalamic axons at these early stages, I showed that the first axon tract to cross the boundary between the telencephalic and diencephalic boundary on their way to their target is the TCA, in line with previous literature (Bystron *et al.* 2008; Alzu'bi *et al.* 2019). Labelled thalamic axons were observed past the pallial-subpallial boundary by 8 PCW, and they reached the cortex where they travel within the cortical intermediate zone.

By using a direct axon tracing technique, I analysed the development of TCA in human *post mortem* fixed brain (between CS21 and 17 PCW). DiI-based axon tracing allowed me to describe the intermediate structures interacting with the TCA on their way to the cortex, as well as analysing in detail the cortical targets by epifluorescence and confocal microscopy.

I showed that as early as 13 PCW, thalamic axons have already reached to the telencephalon where they extend transversally within the intermediate zone (IZ). By 17 PCW, TCA extensively innervate the overlying subplate, in line with previous literature which recognizes this compartment as the first cortical target of thalamic axons. Upon reaching the SP, TCA establish their first transient contacts with the mature neurons populating this region (Kostovic *et al.* 1980; Shatz *et al.* 1986; Kostovic *et al.* 1990; Kanold *et al.* 2010). Interestingly, I also observed some DiI-labelled fibres

innervating the outer SVZ (OSVZ) below. This transient proliferative compartment that extended considerably in larger rodent and primate brains (Smart *et al.* 2002; Garcia-Moreno *et al.* 2012; Dehay *et al.* 2015) is associated with the evolution of larger cerebral cortex and at this stage accounts for most of the germinal zones in the human cortex.

Overall, the analysis presented in this Chapter revealed an early innervation of the prospective neocortex by the thalamic axons in the human brain. The pattern of innervation observed at cortical level further suggest that in our species the thalamic axons might not only interact with the post-mitotic transient subplate neurons, but also with the proliferative population of progenitors of the OSVZ.

DISCUSSION

Time-course analysis of the earliest thalamocortical interactions by immunohistochemistry

A preliminary time-course analysis by immunohistochemistry for TCA marker SCGN revealed that the thalamic afferents reach the developing cortex at early stages of development (around **8 PCW**, one of the earliest stages analysed). This put the thalamic afferents in an optimal time window to exert a major control on human corticogenesis. In fact, the neurogenic programme is at its earliest stages, and most cortical neurons are yet to be generated at this point. Moreover, the asynchrony between thalamocortical and corticothalamic axonal projection, as revealed by comparing SCGN-positive TCA with CalR-positive CTA, was in line with other studies (Deck *et al.* 2013; Alzu'bi *et al.* 2019) and suggested that TCA might be necessary for the correct pathfinding of cortical axons to the thalamus (Deck *et al.* 2013).

Axonal tracing of thalamocortical axons by carbocyanine dye (7-17 PCW)

The interpretation of the results from DiI-based axon tracing should consider the intrinsic limitations of the technique, particularly when applied to small and delicate samples like the embryonic human brain. It is technically difficult to place the crystal in a specific and restricted brain region, which introduces some ambiguity in the interpretation of the resulting labelling pattern in some instances. Furthermore, sectioning the brain sections using a vibrotome after dye incubation can lead to distortion of the anatomical structures or damage of the sections. In larger samples, the loss of a single section may have minimal impact, but in small brains, losing a section can significantly affect the overall analysis, especially if the phenomenon of interest is spatially restricted. Additionally, carbocyanine dyes, including DiI, rely on passive transport along lipophilic membranes, and their diffusion is not 100% efficient. If the phenomenon being investigated is rare, it may become undetectable using this technique alone. Complementing DiI-based axon tracing with parallel immunohistochemical analysis, especially during the embryonic stages of gestation, as was done in this work, provided a more comprehensive understanding of the observed phenomena. and helped overcome some of the challenges associated with the interpretation of the results.

- **7 PCW:**

DiI tracing of TCA at embryonic stage CS21 (7 PCW) resulted in slightly different observations than the ones presented for the immunohistochemical analysis of similar stages of development (compare **Sections 3.1 and 3.2.1**). While SCGN-immunoreactivity revealed pioneer thalamic axons crossing the PSPB as early as 8 PCW, carbocyanine dye tracing from dorsal aspect of diencephalon in the 7 PCW did not. This discrepancy might be attributed to the fact that the TCA cross the PSPB between 7 and 8 PCW, or to the different technical approach used to reveal these events. The only exception to this observation (**Figure 3.11 G-J**) does not allow to draw strong conclusions, as the large crystal placements in this small-sized sample, alongside the physical distortion of the structures in the section might mislead the interpretation. The delineation of the boundary itself was challenging, and it would require a more precise annotation by co-staining for specific regional markers.

DiI-positive signal was consistently detected at the level of the cortical **marginal zone (MZ)** and pial surface across the sections analysed from this brain. Similarly, DiI-positive signal was detected within a restricted region of the brain, in the lateral aspect of the PSPB. The latter appeared to stain tangentially oriented, possibly migrating cells, rather than axonal projection from thalamocortical network. This suggested two scenarios. According to the specific location of these cells, those could be corridor cells of the internal capsule (Lopez-Bendito *et al.* 2006), which are responsible for the guidance of TCA into PSPB and entrance into the cortical region. The cells could have obtained the labelling through close interactions with the thalamocortical projections in the fixed tissue. Alternatively, those might be Cajal-Retzius cells migrating tangentially from the ventral pallium (Garcia-Moreno *et al.* 2018), establishing contacts with labelled axons. Continuity between cortical MZ signal and DiI-labeled cells near PSPB supports the latter hypothesis (**Figure 3.7 E**), recapitulating observations in developing mice (Tamamaki *et al.* 1997; Lopez-Bendito *et al.* 2006). Finally, this signal might also derive from a technical artefact, as the the surface of the telencephalon could have been contaminated accidentally by the lipophilic dye during the incubation, as it was the most exposed portion of the brain at the time of crystal placement.

- **13 PCW:**

As discussed regarding the 7 PCW brain, DiI diffusion efficacy affects labelling. In the 13 PCW brain, sparse cortex labelling resulted mainly from limited dye diffusion rather than the small number of axons in the cortex *per se*. Less and smaller crystals were placed in the internal capsule of the 13 PCW brain as compared to the 17 PCW, according to previous optimizations (Molnar *et al.* 1998; Molnar *et al.* 1999), with the aim to reduce aspecific labelling in the small brain. This is important to consider when comparing results of the DiI tracing in the two samples (see **Section 3.2.3**).

The most relevant observation made in this sample was the tight relationship existing between the early thalamocortical axons and the germinal zones of the cortex, and especially with the outer portion of the subventricular zone (OSVZ). The OSVZ was first described by Smart and colleagues (Smart *et al.* 2002) typically emerges as a distinct layer around 12 PCW, coinciding with the production of the first *bona fide* outer radial glial cells (Hansen et al., 2010; Cadwell 2019). The proximity of the axons to these dynamic proliferative compartments holds significant relevance, especially as it occurs at the initial stages of the formation of this critical layer in the human cortex.

The segment of the "tangential axons" might represent the beginning of the extension of the "inner fiber layer" (IFL), that typically divide the ISVZ and the OSVZ (Smart *et al.* 2002; Molnar *et al.* 2012; Saito *et al.* 2019). Its corticopetal or corticofugal origin is still under debate. Unfortunately, carbocyanine dyes can also be transported both anterogradely and retrogradely in fixed *post mortem* tissue, revealing the presence of exiting corticofugal axons alongside the incoming thalamocortical axons. Considering that retrograde labelling in the sample was not efficient, as shown by virtually no back labelled neurons at cortical level, these "tangential axons" most likely belong to thalamocortical projecting neurons, thus indicating a subcortical origin of the IFL (Molnar *et al.* 2012; Dehay *et al.* 2015).

- **DII 17 PCW:**

Finally, the carbocyanine dye-based axonal tracing of a **17 PCW** human fetal brain revealed that the thalamic axons invaded two largely expanded transient layers of the developing cortex: the mature subplate (SP) and the proliferative outer subventricular zone (OSVZ). The OSVZ is similarly invaded by TCA around mid-gestation only in the primate brain (i.e. Macaca mulatta) (Carney *et al.* 2004). The massive expansion of both subplate and OSVZ during mid-gestation, in concomitance with TCA innervation of these layers, is considered a hallmark of human cortical evolution, suggesting a crucial involvement of thalamic modulation in the evolution of human cortex.

- ***DiI-labelled fibres in the cortical subplate zone***

At this age, the innervation of the **subplate zone** by TCA was expected. The subplate is in fact well-recognized to be an important transient station of incoming TCA (Kostovic *et al.* 1990; Kanold *et al.* 2010). Upon arrival in the cortex, thalamic axons accumulate and "wait" within this compartment for long time ("waiting period") before reaching their ultimate target in the CP above, as discussed in the introduction on this cortical compartment (Chapter 1, Section 1.1.3) (Ghosh *et al.* 1993; Catalano *et al.* 1998; Hanganu *et al.* 2002; Anton-Bolanos *et al.* 2018). As suggested by the Tbr1-immunostaining (**Figure 3.25**), thalamic fibres extend close to the postmitotic neurons of this region, thus allowing for both synaptic connections and paracrine interactions between these neurons and the TCA to be established. However, synaptic connections were not further explored in this study as immunostaining for synaptic elements (i.e. SNAP 25) was not successful (data not shown), due to the relative thickness of the tissue and the technical incompatibility of carbocyanine dye tracing with permeabilization methods (i.e. Triton-X100). It is also important to note that Tbr1 does not only reveal subplate neurons, but also stain for newly generated post-mitotic neurons destined to the deep CP and radially migrating toward the pial surface (Hevner *et al.* 2001). Therefore, complementary approaches should be used in the future to evaluate for this functional interaction.

Subplate neurons also constitute some of the earliest neurons projecting their axons to the thalamus (McConnell *et al.* 1994; Grant *et al.* 2012; Hoerder-Suabedissen *et al.* 2015), and were expected to be back-labelled by placement of the dye in either the thalamus or the internal capsule at this age. However, this was not the case, contrasting the expectations as well as observations in rodents, where the corticothalamic projections can be back-labelled much earlier (Shatz *et al.* 1981; Clasca *et al.* 1995; Molnar *et al.* 1999). Surprisingly, the presence of cell bodies labelled by DiI and DAPI was observed exclusively in the OSVZ and IZ, rather than in the post-mitotic compartments. In some instances, these might represent differentiating neurons that had already extended their axons within the IZ while migrating towards the CP (**Figure 3.23 C, C'**).

- ***DiI-labelled fibres in the cortical outer subventricular zone***

Thalamic input might also influence the **proliferative compartment** (Dehay *et al.* 2001; Lukaszewicz *et al.* 2005; Gerstmann *et al.* 2015), especially in the primate brain. My results show that 17 PCW human brain, not only the DiI-labelled TCA kept their anatomical proximity with the outer portion of the SVZ, but they actively also projected some collaterals within this compartment (**Figures 3.21 and 3.22**). To confirm the nature of these collateral projections invading the OSVZ, I assessed whether the tip of these fibres co-localized with nuclear DAPI staining.

Interestingly, several cases observed in the sections did not appear to stain for nuclei or neuronal bodies, thus confirming the hypothesis of these fibres being axonal projections with growth cones rather than back-labelled cells of the OSVZ. Although I was unable to specifically immunostaining these terminals with growth cone markers, such as actin, I showed that these DiI labelled fibres projecting within the OSVZ for several μm were DAPI-negative, thus not representing back-labelled or transneuronally labelled cells. Most importantly, the growth-cone shaped tips were found at very close distances from HOPX-positive oRGC (**Figure 3.30**), supporting the hypothesis off a possible paracrine interaction occurring between TCA collaterals and these progenitors.

Nonetheless, case of transneuronally labelled oRGC were also observed, in smaller proportion (**Figures 3.27 and 3.29**). Tracking the entire length of the basal process of an individual RGC proved

to be challenging, as these processes are long and most likely severed during sectioning. Furthermore, once the basal process crossed the IZ, where the DiI-positive signal was intense, it became technically impossible to continue tracing the individual fibre. However, in rare cases, such as the one depicted in **Figure 3.27**, I had high confidence in identifying the DiI-labelled cell as an oRGC based on the distinct morphology of the basal process and the location of the cell body within the OSVZ. This observation suggested a potential direct physical interaction that might occur between TCA and oRGC basal processes at the level of the IZ, where they cross their path.

In addition to HOPX-positive oRGC, there are other intermediate precursor cells (IPC) present in the OSVZ, and these progenitor cells can also be influenced by molecules secreted by TCA invading the compartment. However, it is unlikely that these cells would be transneuronally labelled via their processes, that do not extend as far as the basal processes of RGC. Occasionally, cells resembling IPC, with short processes and lying at the boundary between OSVZ and IZ, were labelled by DiI (Figure 3.23 C-C'). Alternatively, these cases represented radially migrating neurons, or a technical epiphenomenon due to long time of incubation of the sample for the tracing study.

Finally, I observed numerous Ki67+ dividing cells especially at the border between the IZ and the OSVZ (**Figure 3.31**), in line with previous observation in primate (Carney *et al.* 2004). This set the anatomical basis for a potential mitogenic effect by TCA on the dividing progenitors, a phenomenon previously reported in animal studies (Dehay *et al.* 2001; Lukaszewicz *et al.* 2005). However, additional time-points of analysis and the employment of a more functional model would be necessary to determine whether TCA actively modulate the mitotic rate of neural progenitors.

- ***Semi-quantitave evaluation of DiI-labelled fibres in the cortical SP and OSVZ***

The results from the semi-quantitative analysis of the DiI-labelled fibres detected in the 17 PCW cortical SP and OSVZ and presented in **Figure 3.32** can be explained in two separate ways:

(i) a biological explanation, suggesting that regions anatomically closer to the thalamus and the proximal segment of the internal capsule (IC) receive innervation earlier, resulting in a higher density of DiI-positive fibres. This is consistent with the observed comparable results in both the outer subventricular zone (OSVZ) and subplate (SP). In line with this explanation, the ratio between the values measured in the outer subventricular zone (OSVZ) and subplate (SP) remains constant along the tangential path of the axons. This consistency suggests that two distinct phenomena—innervation of cortical neurons and transient projections to cortical progenitors—exhibit similar patterns, attributed to a shared factor, such as anatomical proximity/distance of the brain region analysed and the site of origin of the axons traced.

(ii) A technical explanation, suggesting that the reduction in the signal intensity detected along the tangential path of the axons is proportional to the distance from the site of DiI placement rather than the specific origin of the axons *per se*. Thus, a lower number of labelled fibers detected at distal locations (i.e. ROI 1) is due to a lower amount of DiI molecules successfully reaching those points compared to more proximal axons (i.e. ROI 3), that will be labelled more intensely by consequence. This explanation is supported by the almost complete absence of DiI-positive signal at more dorsal locations of the cortex, even though they receive thalamic innervation at this stage of development.

Neither biological nor technical explanation can be definitively favoured, though a combination of both may offer the most plausible interpretation for the observed trend in both cortical layers.

Innervation of the subplate is not a transient phenomenon over distance from the thalamus, but rather transient in the sense that thalamic axons eventually leave subplate and move to innervate the overlaying cortical plate (CP). At increasing distances from the thalamus, the cumulative number of collaterals within the SP (**Figure 3.32 B'**) would increase until reaching a state of homogeneity where all cortical areas are innervated before further network refinement occurs. In contrast, the active

projections of collaterals into the OSVZ are a transient phenomenon *per se*. It is plausible that instead of accumulating uniformly before disappearing, these collaterals are temporarily extended in a close-to-distant "wave" pattern, where the closest regions are innervated and retracted first, simultaneous with the innervation of more distal locations from the thalamus. However, the trend observed in **Figure 3.32 C'** might support both scenarios, as it might be indicative of a similar pattern of innervation of the SP – which it closely mirrors-, or else representing a snapshot of a transient innervation that would invert trend over time if observed for longer time. A more comprehensive characterization of this phenomenon and its transient nature would require a similar analysis at slightly earlier and/or later timepoints.

Overall, my observations confirmed what reported in the non-human primate brain at similar gestation stages, suggesting that a tighter extrinsic control by thalamic axons over cortical development might be in place in more evolved primate brains, and involving not only the TBR1-positive neurons of the subplate, but also HOPX-positive progenitor cells of the OSVZ. Considering the close anatomical proximity of both cell population with the early TCA innervating the cortex, it is likely that both receive paracrine influence from these axons. Therefore, in the following Chapter, I focus my attention on selecting a promising paracrine molecule that might account for this effect in both cortical cell population.

CHAPTER 4

Expression of VGF by thalamocortical projecting neurons in the human fetal brain

INTRODUCTION

In order to narrow the focus of my study to molecular mechanisms that mediate the thalamocortical interactions during development, I conducted an extensive literature review to identify potential secreted molecules produced in the thalamus that could be involved in regulating cortical development. Among the candidates, VGF (neurosecretory protein), a 615 amino acid neurotrophin, emerged as a promising factor. VGF is expressed in the developing and adult mammalian brains (van den Pol *et al.* 1994; Snyder *et al.* 1997; Snyder *et al.* 1998). Notably, VGF has been recently implicated in thalamus-mediated specification of prospective primary sensorial cortices in the developing mouse brain (Sato *et al.* 2012; Monko *et al.* 2022; Sato *et al.* 2022).

Importantly, in addition to its potentially similar role in prenatal human brain development, VGF may have undergone evolutionary shifts in its functions in our species. This is supported by evidence implicating VGF in various human brain conditions, including neurodegenerative and neurodevelopmental disorders that are not exclusively related to the sensory cortices (Thakker-Varia *et al.* 2010; Busse *et al.* 2012; Quinn *et al.* 2021). These findings suggest that VGF might play a role in the development of associative cortices beyond sensory areas. Consistently, VGF has emerged as a promising candidate biomarker for the diagnosis of these disorders and holds potential as a therapeutic agent for a wide range of human brain conditions (Quinn *et al.* 2021; Alqarni *et al.* 2022).

To explore this hypothesis, I established a set of criteria that must be validated in order to ascertain whether this secreted molecule, VGF, is indeed responsible for the extrinsic regulation of cortical development and specification in human. Specifically:

1. VGF has to be *selectively*, or at least *preferentially*, expressed *in the thalamus* as compared to the cortical areas (Chapter 4)
2. VGF expression has to be *sustained throughout* the timeframe of *cortical neurogenesis* and specification (Chapter 4).
3. VGF *protein* needs to be *actively transported* from the region of production (i.e. Thalamus) *to the cortical areas* where it is secreted in a functionally active form of full-length protein or neuropeptides (Chapter 5)
4. VGF has to have a *functional effect* upon secretion in the transient SP and OSVZ (Chapter 6).

In this Chapter, I addressed the first two criteria. To this aim, I evaluated VGF gene expression in the thalamus and various key cortical areas of the human prenatal brain by surveying available transcriptomic datasets and finally validating the findings by qPCR in the human fetal brain tissue.

The data presented in this Chapter demonstrate that VGF expression is primarily restricted to the thalamus throughout gestation, with the only exception of a transient upregulation of VGF expression in the cortex that is observed during mid-gestation (19-24 PCW). This may be attributed to the extensive secretion of other neurotrophins into the extracellular space by developing thalamic axons that are innervating the cortex during this developmental stage. Moreover, through single-cell transcriptomic analysis, I show that thalamic VGF is selectively expressed in mature excitatory neurons that project to the cortex.

4.1 VGF regional expression profiling in the human developing brain shows a high, sustained, and preferential thalamic expression of VGF

4.1.1 VGF is differentially expressed in the human prenatal thalamus vs all brain regions (RNAseq data)

To evaluate whether VGF expression is specific or preferential to the thalamus throughout prenatal stages of development, I used the Brainspan resource (brainspan.org) to explore the transcriptomic profile of the developing human thalamus. I first performed an **exploratory differential search** selecting the thalamus (i.e. both dorsal thalamus [DTH] and mediodorsal nucleus of the thalamus [MD]) as a main target structure, with all the remaining regions of the neural tube sampled as a contrast structure. All the prenatal (8-38 PCW) and peri-natal ages (0-5 months) were included into the search. The output of this search is a list of all genes investigated in the RNAseq experiment, with their specific expression values as RPKM for each region and each developmental timepoint selected. The fold-change of expression level between the target structure (i.e. thalamus) and the contrast structure (i.e. neural tube) is calculated and provided along with the p-value expressing the statistical significance of the difference in expression between the two.

As I was interested only in the most highly expressed genes in the thalamus, I downloaded only the data for the first 2,000 DEGs with a positive fold-change value, and I considered as significant only the DEGs with a p-value <0.01. These genes are plotted in a Volcano plot (**Figure 4.1**) according to the log2 fold-change (y-axis) and the correspondent negative log10 of the p-value (x-axis). The significance cut-off as a dashed line intercepting the x-axis at negative log10 of 0.01, and significant genes are shown in red, whereas non-significant ones are in black. Labels show the gene name of the top 10 most significant DEGs in the gene list, among which is the well-known thalamic markers such as TCF7L2 (Murray *et al.* 2007).

VGF appeared as one of the most DEGs in the thalamus, with a fold-change of **3.386** and a p-value of **0.00645**.

Figure 4.1

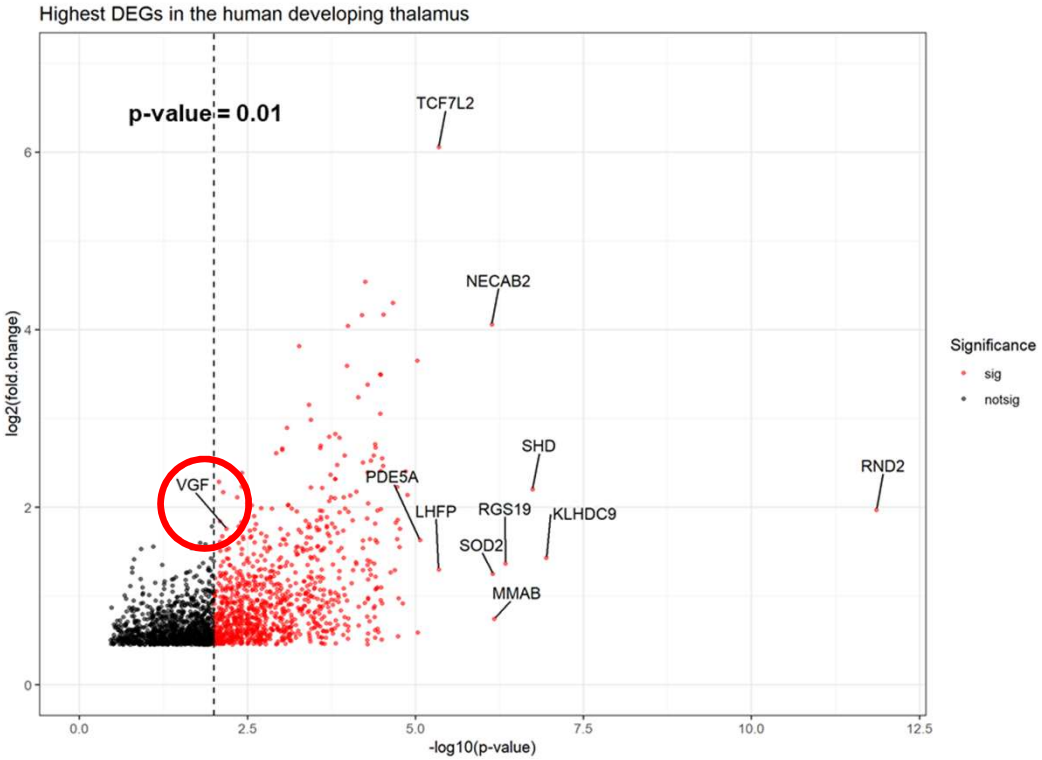

Figure 4.1: Volcano plot showing the first 2000 DEGs in the thalamus as compared to the rest of the neural tube. X-axis shows the negative log10 of their p-values, and y-axis the log2 of their fold-change. A dashed vertical line shows the cut-off of significance considered (p-value <0.01), with significant genes plot in red and non-significant ones in black. Labels are assigned to the top 10 most significant DEGs, and the gene of interest (VGF) in the plot. VGF is highlighted by a red circle.

4.1.2 VGF is highly expressed in the human prenatal thalamus (RNAseq data)

To confirm the strong expression of VGF in the thalamus, VGF expression levels were analysed **without performing a differential analysis**. This in fact might lead to an underestimation of the expression levels of a gene within a structure, as they are expressed in terms of fold changes and/or p-values as parameters of a direct comparison, rather than absolute expression level values. For instance, the thalamus will be expressing at high level other sets of genes, such as classic thalamic marker genes like TCF7L2 (Murray *et al.* 2007; Nagalski *et al.* 2016). Similarly, other genes might be expressed throughout many if not all thalamic cell populations, making their overall expression values greater than genes, such as VGF, with a potentially restricted expression in one population of cells (i.e., mature glutamatergic neurons) but still restricted and specific of the thalamus.

For this reason, I evaluated VGF expression in the thalamus as expressed by log2 RPKM values, which give an idea of the absolute expression of the gene rather than a relative up- or down-regulation of such gene in the region of interest. In order to include a broad range of RPKM values that can be considered as "absolute low" and "absolute high", I plotted VGF expression levels along with Special AT-rich sequence-binding protein 2 (SATB2), a classical cortical marker that should be expressed at very low levels in the thalamus (Huang *et al.* 2013; Toma *et al.* 2014; Cera *et al.* 2019), and Gastrulation Brain Homeobox 2 (GBX2), which on the contrary is considered as a classical thalamic marker during development and shows high absolute expression levels (Chatterjee *et al.* 2012; Nagalski *et al.* 2016) (**Figure 4.2**).

As shown in the graph, the expression levels of VGF in the thalamus can be considered high in absolute terms, and comparable to recognized thalamis marker GBX2.

Figure 4.2

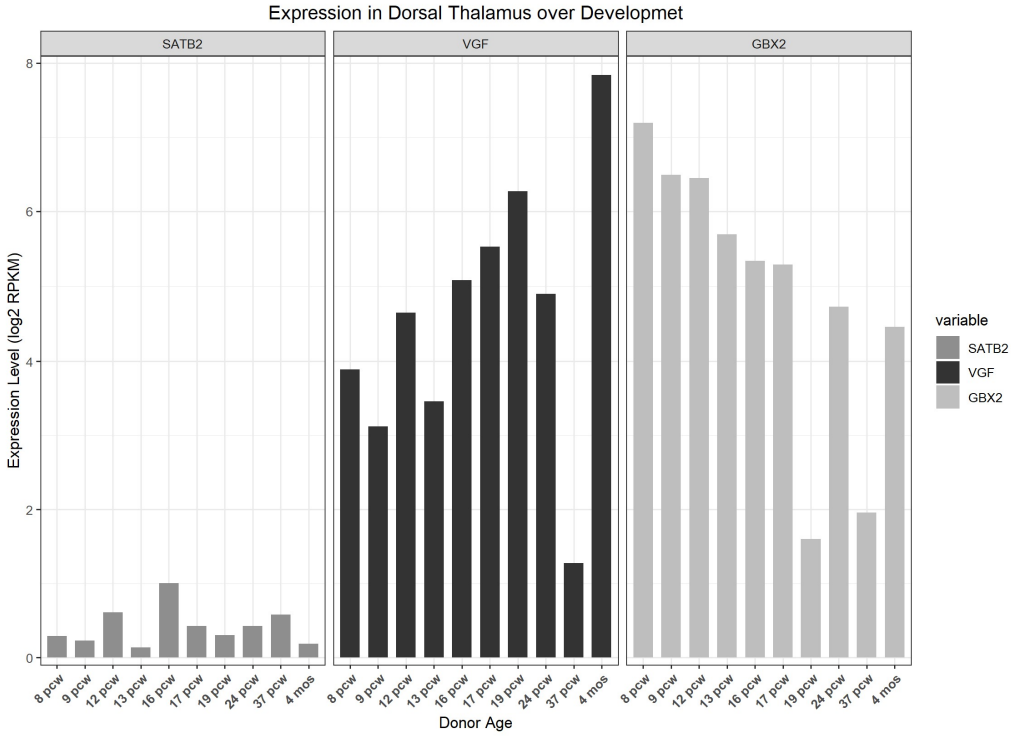

Figure 4.2: Histogram showing the level of expression of VGF in the dorsal thalamus throughout gestation and peri-natal stages. The expression levels are represented as log2 of the RPKM values (y-axis), and each developmental time-point sampled is represented by an individual bar in the x-axis. VGF expression levels are plotted along with SATB2 (cortical marker) and GBX2 (thalamic marker) for comparison.

4.1.3 VGF is differentially expressed in the human prenatal thalamus vs all neocortical areas (RNAseq data)

Furthermore, I analysed the data available in the developmental transcriptome tool of Brainspan (brainspan.org), which comprises of **RNA-seq data** collected across 13 developmental stages in 8-16 brain structures. I selected all thalamic regions sampled, namely dorsal thalamus (DTH) and mediodorsal nucleus (MD), along with all primary cortical areas collected in the same specimens, and all prenatal ages available in the dataset (8-38 PCW). The timepoints are clustered into 6 developmental stages, and I maintained these time ranges in the plot of the data for consistency and simplicity. I compared the data in form of RPKM values ranging between 0-6 (with maximum value of the range set arbitrarily according to the maximum value of RPKM across timepoints) with Morpheus software (https://software.broadinstitute.org/morpheus/). Data are plotted in form of separate heatmaps for each developmental stage (**Figure 4.3**).

The graph clearly illustrates the high expression of VGF in the surveyed thalamic regions throughout human gestation, including the neurogenic window. In contrast, VGF levels are significantly reduced in all primary cortical areas.

An interesting exception to this pattern can be observed between 19 and 24 PCW, during which VGF expression appears transiently upregulated in the cortex. The endogenous cortical upregulation of VGF expression appears to be initially confined to motor areas (i.e. M1C) and later spreading throughout the neocortex. This resolves within few weeks before birth.

Figure 4.3

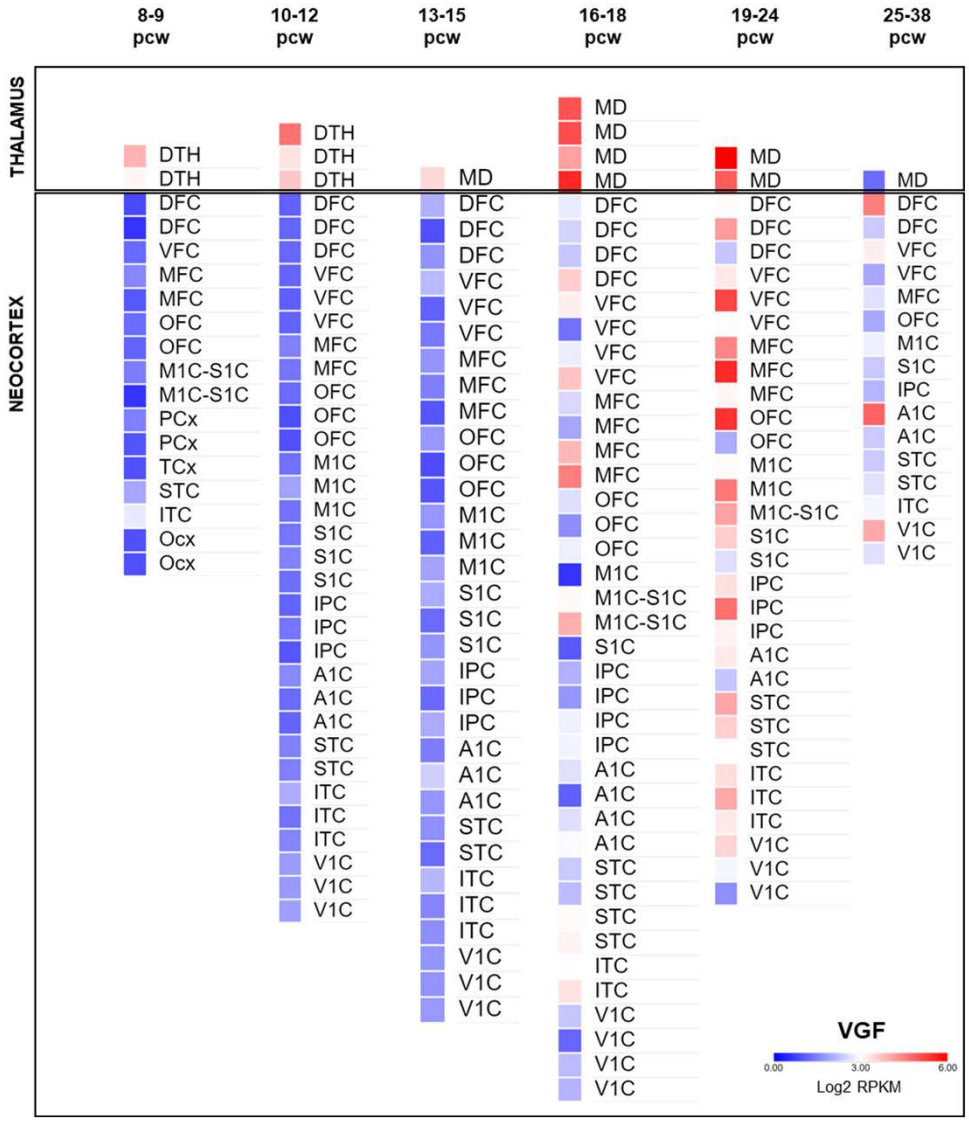

Figure 4.3: Heatmap of VGF expression levels in the prenatal human thalamus and neocortex. Values are reported as Log2 RPKM between 0 (low, in blue) and 6 (high, in red). Gestation ages are clustered into 6 time windows, in line with the Brainspan website filter criteria. Each squared-dot of the plot represents an individual brain region sampled from a specific donor within the time window, therefore some areas show repeated values as they come from different donors and have not been averaged together.

4.1.4 VGF is differentially expressed in the human prenatal thalamus vs all brain regions and neocortical areas (Exon Array data)

Finally, I analysed the transcriptomic dataset of the human brain available in the "Human Brain Transcriptome" website (hbatlas.org) (Kang *et al.* 2011). These data consist of exon arrays obtained with Affymetrix GeneChip Human Exon 1.0 ST Array platform, from transient prenatal structures and 16 brain regions, including hippocampus (Keller *et al.*), amygdala (AMY), striatum (STR), cerebellar cortex (CBC), and most relevant for this study, the mediodorsal nucleus of the thalamus (MD) and 11 neocortical areas (NCX). The brain samples have been collected from healthy donors ranging in age from 4 PCW (period 1) to 60 year + (period 15) (Kang *et al.* 2011).

Figure 4.4 A (Expression in Brain Regions): As shown in graph A, VGF expression levels are relatively lower at all prenatal ages (periods 1-7) throughout the brain, especially at early stages of gestation before 16 PCW (log2 levels between 5-6, as compared to the adult brain with all levels >6.. VGF expression levels steadily increase after birth, peaking during the first year of life, with the exception of the cerebellar cortex where VGF expression appears to decrease instead.

The mediodorsal nucleus of the thalamus (MD, represented by the green line) stands out as an exceptional case, with relatively higher levels of VGF expression compared to other brain regions even before birth. The expression levels in the MD gradually increase and reach a peak rate of almost 8 by the period of 19-24 PCW (period 6). This further supports the observations from the Brainspan LMD microarrays (**Table 4.1; Figures 4.5, 4.6**).

Figure 4.4 B (Expression in Neocortical Areas): When evaluating the 11 neocortical areas separately, VGF expression appeared to have a relatively homogeneous and similar pattern of expression. Its levels are relatively lower at prenatal ages, and tend to increase around perinatal and early post-natal developmental stages. The increase in the expression before birth, continuing in the early post-natal life suggests that the averaged value plotted as "NCX" in **Figure 4.4 A** is the result of a generalized and widespread upregulation of VGF expression throughout the neocortex areas, rather than due to a localized peak that ultimately modify the average value when considering the areas altogether.

Figure 4.4

A **VGF Expression Levels (Brain Regions)**

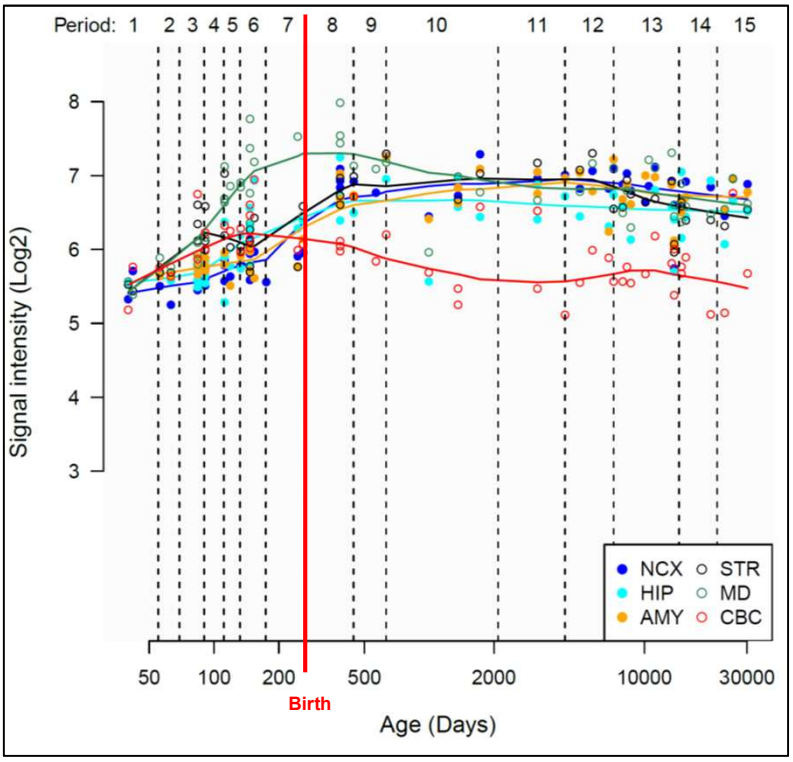

B **VGF Expression Levels (Neocortical Areas)**

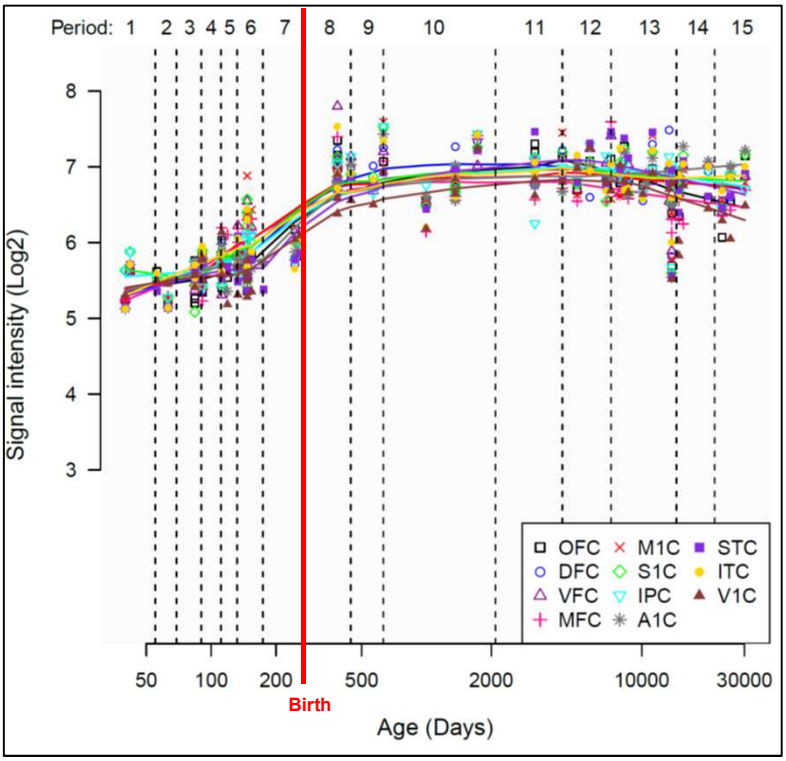

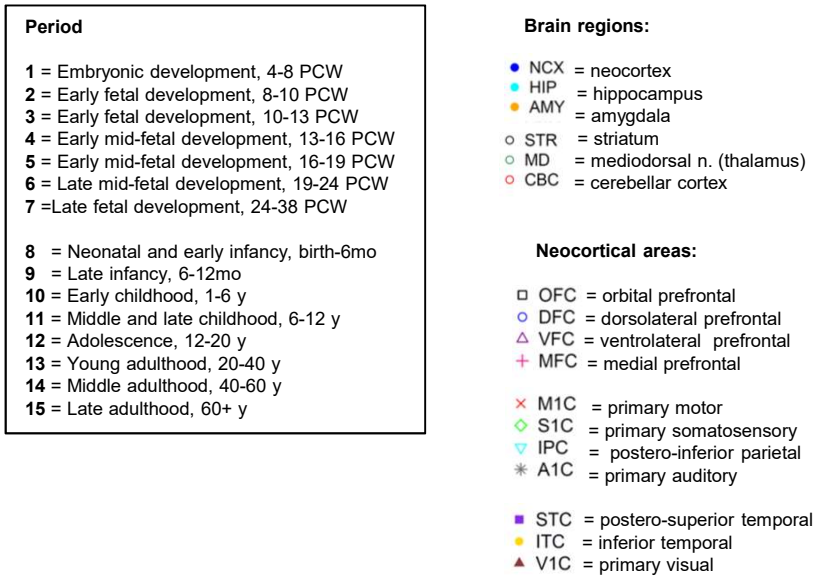

Figure 4.4: Line chart graphs of VGF expression levels in the human brain regions (A) and neocortical areas (B) from embryonic development to adulthood. Expression levels are represented by log2 signal intensity (y-axis), and ages are expressed in day (x-axis). A red line highlights birth, dividing prenatal and postnatal periods. Data from Kuang et al., 2011, and downloaded from hbatlas.org.

4.2 VGF sub-regional expression profiling in the human developing thalamus and neocortex reveals a different expression pattern than in the rodent developing brain

In order to gain more detailed insights into the spatial distribution of the VGF transcript at sub-regional level, I used the Microarrays data obtained from laser micro-dissected tissue accessible on the Brainspan website. While the microarray data may have lower reliability and only a limited number of developmental timepoints are available in this dataset, these data offers higher spatial resolution. By combining them data with the previously analysed datasets, it can aid in the interpretation and understanding of the VGF expression patterns.

The following tables (**Tables 4.1-4.4**) summarise the data collected from one 15 PCW (donor ID H376.IIIA.02) and one 21 PCW (donor ID H376.IV.02) brain sample, and selecting one of the two VGF probes (A_24_P129326). Expression values are reported as z-scores of the RPKM levels.

Specifically, **Table 4.1** shows the data collected from the thalamic region, that was further micro-dissected into the major ***thalamic nuclei***. Data are shown for the associative mediodorsal nucleus (MD), and the sensorial ventral posterior lateral nucleus (VPL, somatosensory), ventral posterior medial nucleus (VPM, somatosensory), and dorsolateral geniculate nucleus (dLGN, visual).

Differently from what observed in the rodent brain (Sato *et al.* 2012), VGF expression within the thalamus is not restricted to the sensorial nuclei. In fact, not only a strong expression of VGF is observed in the associative mediodorsal nucleus of the thalamus, but its z-score levels (1.14568 and 2.31687, at 15 and 21 PCW respectively) are higher as compared to the both visual dLGN (0.651165 and 1.60991, at 15 and 21 PCW respectively) and the somatosensory ventral posterior group, including VPL (1.59747, 21 PCW) and VPM (2.11771, 21 PCW).

The MD directly projects to the PFC (Funahashi 2013), therefore suggesting that thalamic VGF may play a role in the development of associative cortices, and not being limited to the specification of sensory areas as is the case in rodents. This could be attributed to the evolutionary repurposing of

a conserved molecule to support the development of more crucial and expanded regions in the human brain such as the prefrontal cortex.

Tables 4.2-4.4 show the data collected from different ***cortical layers***. Transient developmental layers micro-dissected are: ventricular zone (VZ), subventricular zone (SVZ), intermediate zone (IZ), and subplate (SP). All these transient compartments have been sampled once per donor, hence there is no information provided on eventual areal difference in expression level of any gene, including VGF. Data on those layers are reported in **Table 4.2**.

In contrast, the post-mitotic compartments, specifically the cortical plate (CP) and marginal zone (MZ), were sampled individually from various cortical areas. I focused on four main cortical areas: prefrontal cortex, somatosensory cortex, motor cortex, and visual cortex. These specific neocortical regions were chosen for both the microarray analysis and the subsequent single-cell analysis described in Section 4.3 of this Chapter. VGF expression levels in the CP and MZ of these four areas are reported separately in **Table 4.3 and 4.4**, respectively.

VGF expression appeared extremely low in almost all the cortical layers analysed, at both developmental ages. A few exceptions can be noted. VGF is upregulated in the CP of the dorsolater prefrontal cortex (dlPFC) at 15 PCW (z-score 1.152363), and in primary somatosensory cortex (S1) at 21 PCW (z-score 1.16537) (**Table 4.3**). Another exception to the low cortical expression of VGF is the IZ of the 15 PCW brain (z-score 1.14349) (**Table 4.2**).

A representative schematic illustration summarizing the z-scores levels reported in the **Tables 4.1-4.4** is shown in **Figures 4.5 and 4.6**. As well summarized in these illustrations, VGF expression appears mainly restricted to the thalamic regions at both 15 and 21 PCW. In fact, the cortical areas are generally scarce in this transcript, with only a few exceptions to this scenario as previously discussed.

Table 4.1. Expression values of VGF in laser micro-dissected (LMD) thalamic nuclei in 15 and 21 PCW human brain.

Thalamic nucleus	z-score of VGF expression [15 PCW]	z-score of VGF expression [21 PCW]
Mediodorsal (MD)	1.14568	2.31687
Ventral Posterior Laterar (VPL)	No data	1.59747
Ventral Posterior Medial (VPM)	No data	2.11771
Dorsolateral Geniculate (dLGN)	0.651165	1.60991

Expression values of VGF as z-score values in one associative thalamic nucleus (mediodorsal nucleus, MD) and three sensorial thalamic nuclei (ventral posterior lateral, VPL, and ventral posterior medial, VPM, both somatosensory; dorsolateral geniculate nucleus, dLGN, visual). Data from Brainspan LMD microarrays, donor ID H376.IIIA.02 (15 PCW), H376.IV.02 (21 PCW); VGF probe ID A_24_P129326.

Table 4.2. Expression values of VGF in laser micro-dissected (LMD) cortical transient developmental compartments in 15 and 21 PCW human brain.

Cortical transient layers	z-score of VGF expression [15 PCW]	z-score of expression level [21 PCW]
Ventricular Zone (VZ)	-0.772908	-0.179405
Subventricular Zone (SVZ)	-0.231731	0.145789
Intermediate Zone (IZ)	1.14349	0.173288
Subplate (SP)	-0.0829123	0.00607445

Expression values of VGF as z-score values in transient cortical ventricular zone (VZ), subventricular zone (SVZ), intermediate zone (IZ), and subplate (SP). Data from Brainspan LMD microarrays, donor ID H376.IIIA.02 (15 PCW), H376.IV.02 (21 PCW); VGF probe ID A_24_P129326.

Table 4.3. Expression values of VGF in laser micro-dissected (LMD) cortical plate in four major cortical areas of 15 and 21 PCW human brain.

Cortical Plate (CP) – Cortical Areas	z-score of VGF expression [15 PCW]	z-score of VGF expression [21 PCW]
Dorsolateral Prefrontal Cortex (dlPFC)	1.152363	-1.44426
Primary Somatosensory Cortex (S1)	-1.20024	1.16537
Primary Motor Cortex (M1)	0.345075	-0.928527
Primary Visual Cortex (V1)	1.2398	-0.441096

Expression values of VGF as z-score values in the cortical plate (CP) of dorsolateral prefrontal cortex (dlPFC), primary somatosensory cortex (S1), primary motor cortex (M1), and primary visual cortex (V1). Data from Brainspan LMD microarrays, donor ID H376.IIIA.02 (15 PCW), H376.IV.02 (21 PCW); VGF probe ID A_24_P129326.

Table 4.4. Expression values of VGF in laser micro-dissected (LMD) marginal in four major cortical areas of 21 PCW human brain (15 PCW data not available).

Marginal Zone (MZ) – Cortical Areas	z-score of VGF expression [15 PCW]	z-score of expression level
Dorsolateral Prefrontal Cortex (dlPFC)	No data	-1.30098
Primary Somatosensory Cortex (S1)	No data	0.199877
Primary Motor Cortex (M1)	No data	0.00446981
Primary Visual Cortex (V1)	No data	0.666602

Expression values of VGF as z-score and Log2 RPKM in the marginal zone (MZ) of dorsolateral prefrontal cortex (dlPFC), primary somatosensory cortex (S1), primary motor cortex (M1), and primary visual cortex (V1). Data from Brainspan LMD microarrays, donor ID H376.IIIA.02 (15 PCW), H376.IV.02 (21 PCW); VGF probe ID A_24_P129326.

Figure 4.5

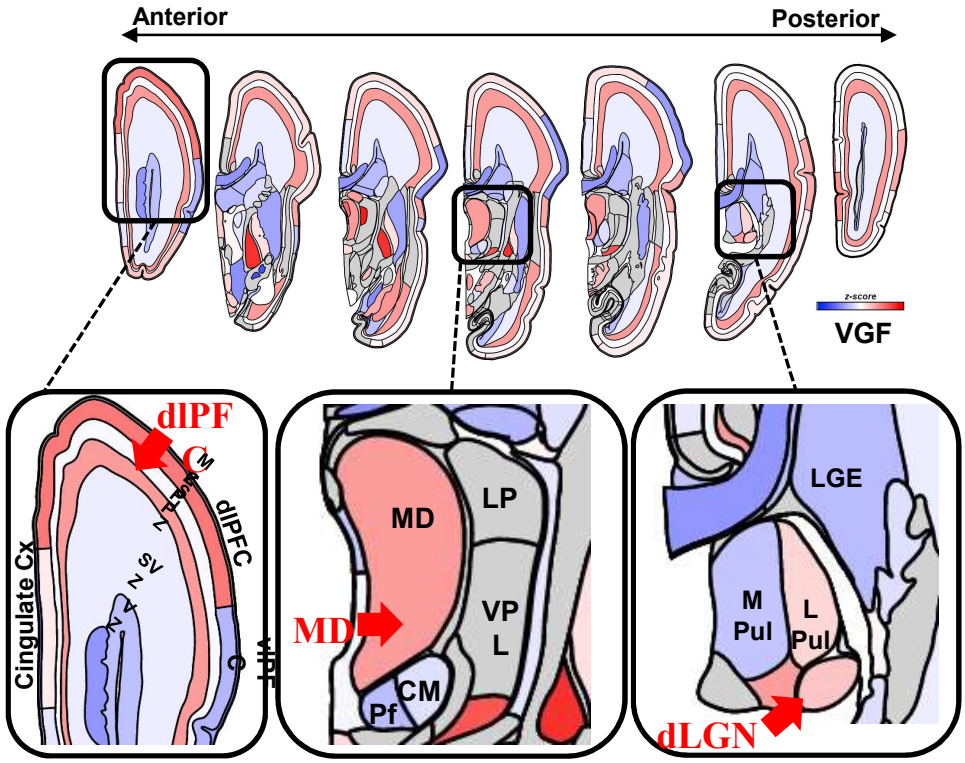

Figure 4.5: Schematic representation of **15 PCW brain sample** depicting the expression level of VGF in coronal sections as z-scores (blue is low expression, red is high expression). Highlighted in the box insert on the bottom right are some of the data from Table 2-3 (cortical transient layers and cortical plate of the dorsolateral prefrontal cortex, dlPFC) highlighting the upregulation of VGF in the intermediate zone (IZ) where cortico-projecting axons are located, and the post-mitotic cortical plate (CP) of this specific cortical region, which represents an exception from the relatively low expression levels of VGF in the same compartments of the other cortical areas analysed (Table 3). The insert in the centre shows the strong expression of VGF in the associative mediodorsal nucleus of the thalamus (MD) directly projecting to the dlPFC, which is in contrast with data from mouse (Sato et al., 2012) where VGF is selectively expressed by sensorial thalamic nuclei during development. The insert on the left shows the relatively high expression levels of VGF in the visual dorsolateral geniculate nucleus (dLGN), that on the other hand is in line with data from rodent (Sato et al., 2012). Data from Brainspan LMD microarrays, donor ID H376.IIIA.02 (15 PCW); VGF probe ID A_24_P129326.

Figure 4.6

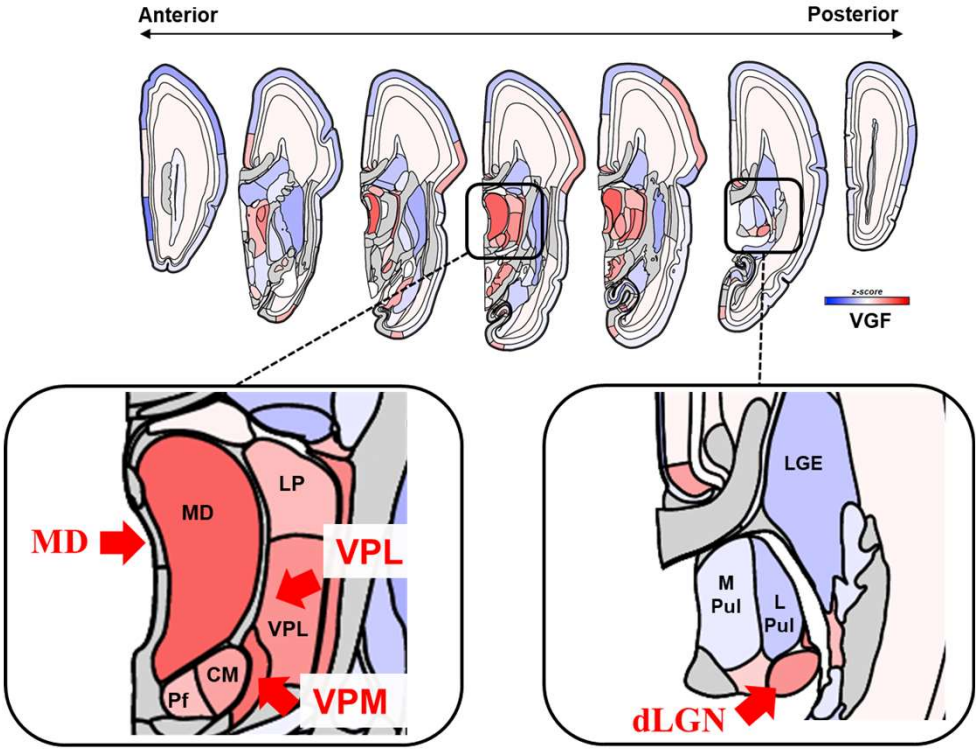

Figure 4.6: Schematic representation of **21 PCW brain sample** depicting the expression level of VGF in coronal sections as z-scores (blue is low expression, red is high expression). Highlighted in the box inserts on the bottom are the four thalamic nuclei analysed (Table 1) and illustrating that the expression levels of VGF are not confined to the sensorial nuclei (i.e. somatosensory VPL and VPM; visual dLGN) but are rather high in the associative MD projecting to the prefrontal cortex. Data from Brainspan LMD microarrays, donor ID H376.IV.02 (21 PCW), VGF probe ID A_24_P129326.

4.3 VGF single-cell expression profiling in the human thalamus identifies specific expression of VGF by mature excitatory thalamocortical projecting neurons

The bulk RNA-seq dataset used in this study provided valuable information on the regional distribution of VGF expression throughout various stages of human brain development. However, it did not allow for the identification of **specific thalamic cell type(s)** responsible for the expression of this molecule.

To address this, I used a single cell transcriptomic approach. I selected a dataset obtained by Kriegstein and collaborators in UCSF. The data were collected from human fetal brains where specific regions were microdissected and subsequently subjected to RNA sequencing using the 10X Chromium technology. The raw output data from the sequencing experiments were accessible for download in the Neuroscience Multi-omic archive (nemoarchive.org). To analyse these data, I employed the Seurat pipeline (Hao *et al.* 2021) in the R Studio environment.

This allowed for the identification and characterization of individual cell types within the thalamus, enabling a more detailed investigation of VGF expression patterns at the cellular level.

Specifically, I selected the thalamus (TH), along with the four main cortical areas previously analysed in the bulk RNA-seq dataset for comparison (see **Section 4.2**). These include two sensorial areas, the prospective primary somatosensory (S1) and visual (V1) cortices, and two non-sensorial areas, the prospective primary motor cortex (M1) and the prefrontal cortex (PFC).

My analysis confirmed that VGF expression is expressed by the human thalamus during mid-gestation (**Figure 4.7**), but it is virtually absent in all the four cortices analysed (**Figures 4.9-4.12**).

More specifically, VGF is expressed by a specific group of thalamic cells that cluster together and separately (cluster 2). Differential expression of genes in cluster 2 compared to all the other clusters was calculated using the function FindAllMarkers in Seurat. As shown by **Figure 4.8**, cluster 2 classic marker genes were used to manually annotate all datasets.

By performing a differential expression analysis between cluster 2 and all the other clusters of the dataset with the function FindAllMarkers of Seurat, I showed that the transcriptomic profile of these cells is specifically enriched for classic markers of excitatory thalamocortical projecting neurons, such as SLC17A6 (also known as VGLUT2), TCF7L2, NGN1, NTNG1, GAP43, ACHE, and CALB2 (**Figure 4.8**). Based on the analysis of the gene markers, I annotated the cell identity of cluster 2 as "excitatory thalamocortical projecting neurons".

Furthermore, the output of this analysis provided more detailed information on the expression of VGF by cluster 2 cells: VGF is expressed by 53.3% of cluster 2 cells, as compared to all the other clusters where only 6.1% of cells are positive for VGF expression (with an average log2 fold-change of 1.382). These data can be visualized in the Dot Plot (**Figure 4.8 B**).

Figure 4.7

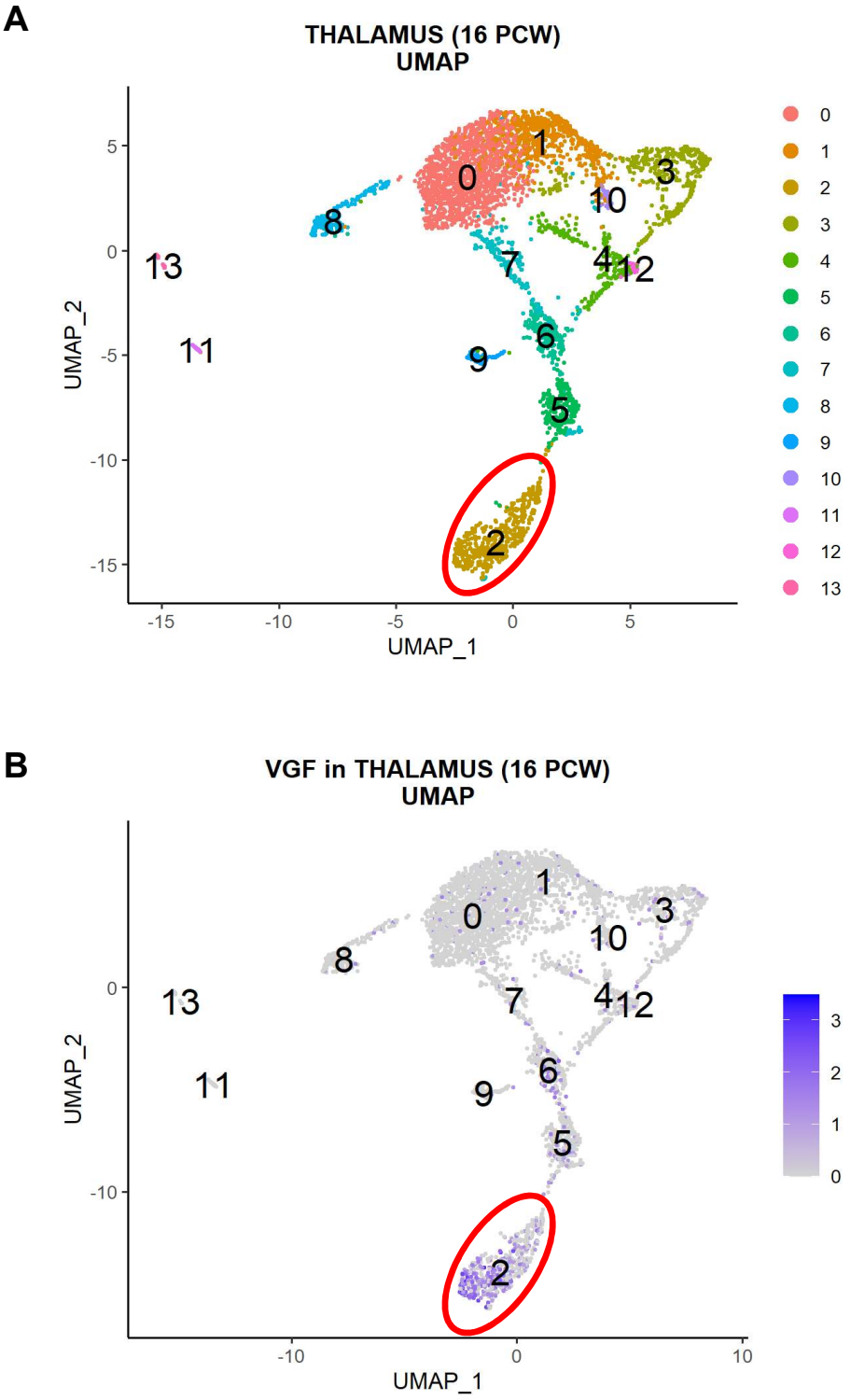

Figure 4.7: UMAP representation of the 16 PCW Thalamus dataset. Scatterplot of 4,076 cells after Principal Components Analysis (PCA) and Uniform Manifold Approximation and Projection (UMAP), coloured by cluster (N=14) (**A**), and VGF expression (**B**). Highlighted in red cluster 2, annotated as excitatory thalamocortical neurons (see Figure 4.8 for the annotation) and expressing VGF at the highest percentage in the 16 PCW human thalamus.

Figure 4.8

A

Scatter Plots

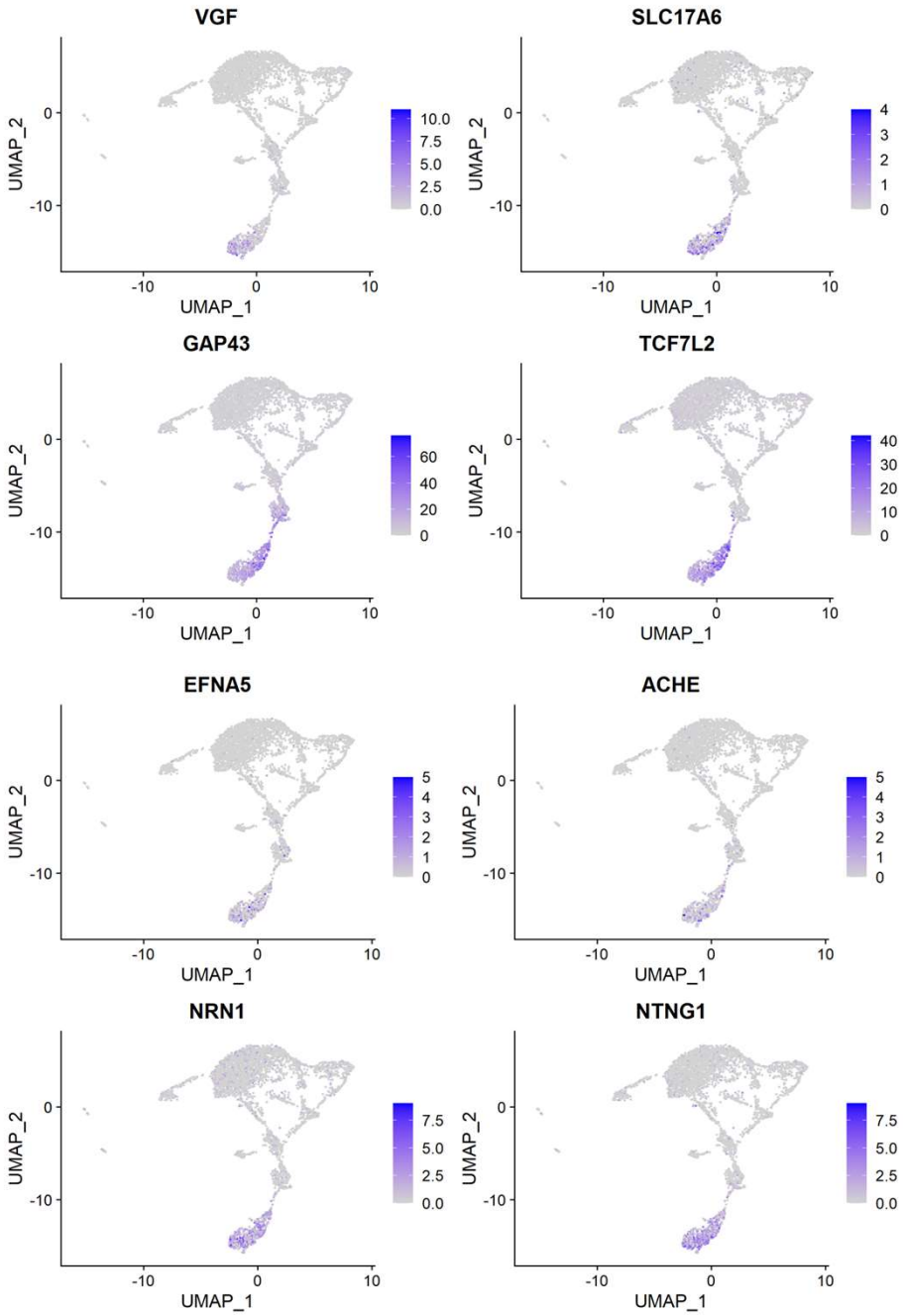

Figure 4.8

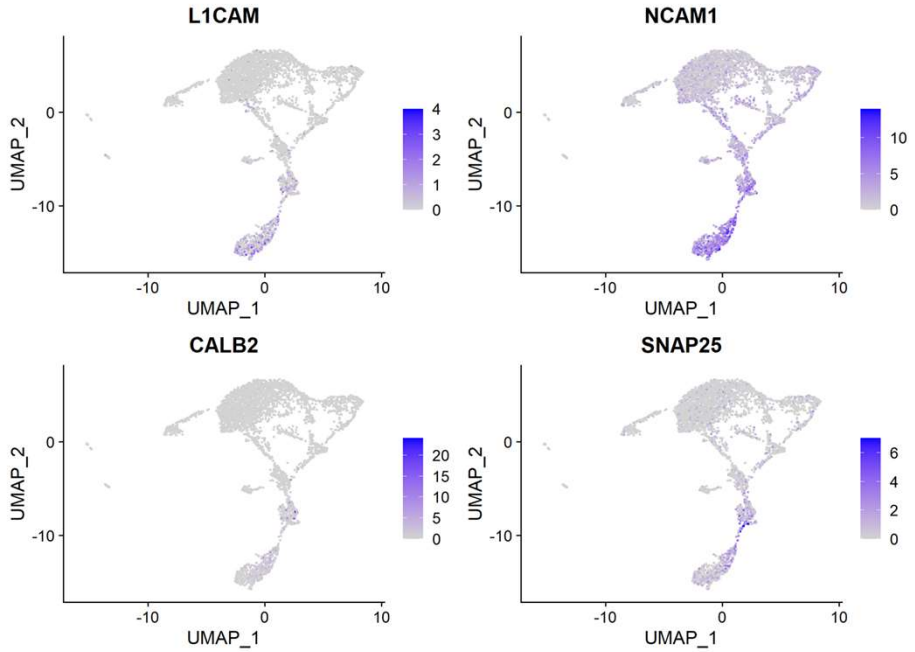
L1CAM
NCAM1
CALB2
SNAP25
UMAP_1
UMAP_2

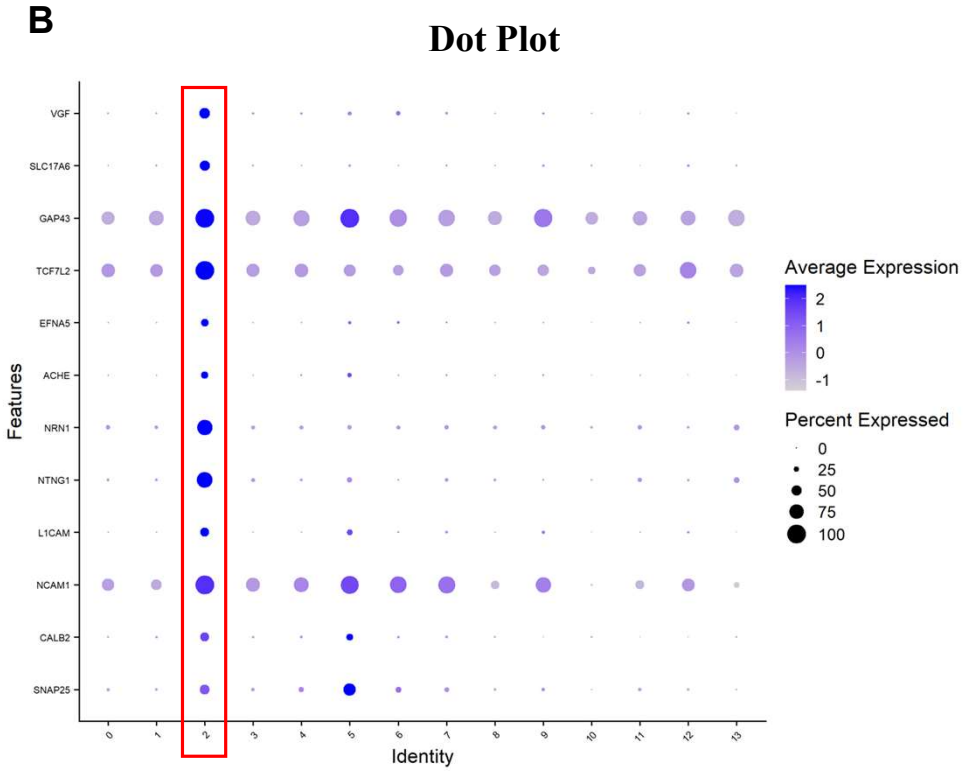
B
Dot Plot
VGF
SLC17A6
GAP43
TCF7L2
EFNA5
ACHE
NRN1
NTNG1
L1CAM
NCAM1
CALB2
SNAP25
Features
Identity
Average Expression
Percent Expressed

Figure 4.8

C

Violin Plots

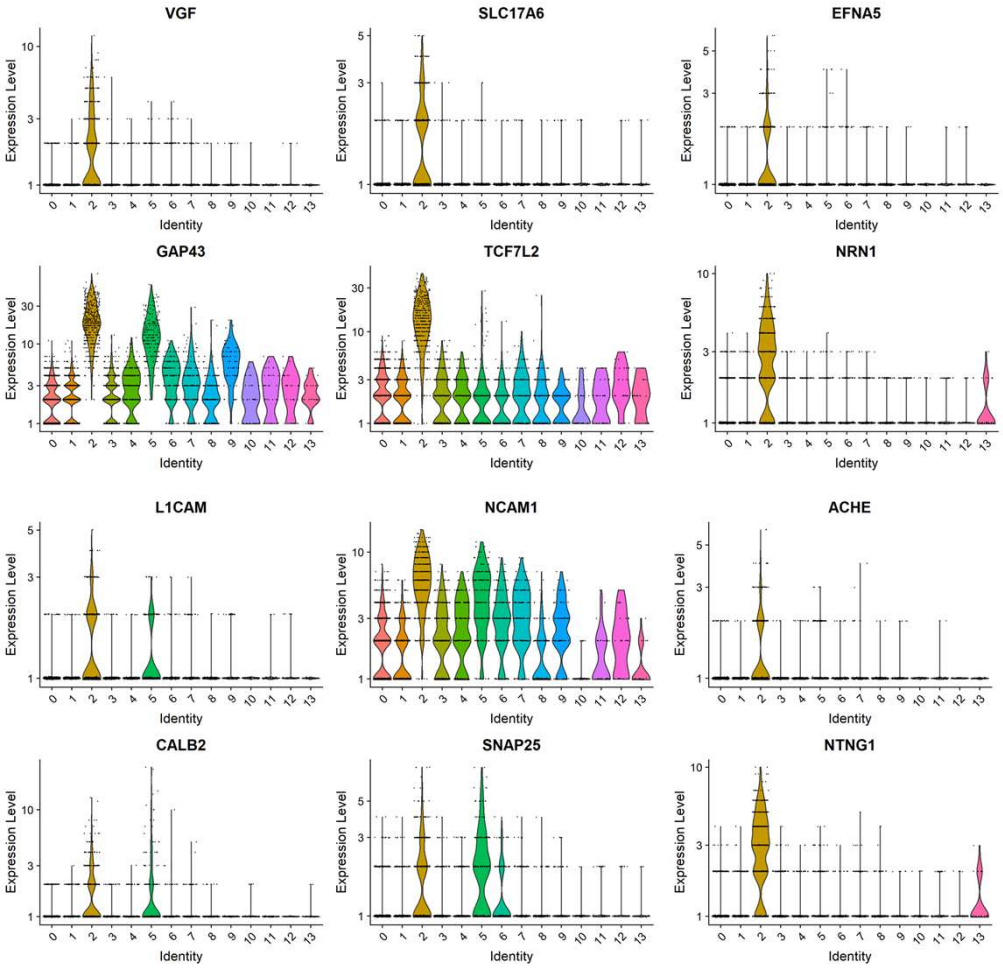

Figure 4.8: Different representation of the expression of gene markers used for the annotation of cluster 2 of the 16 PCW thalamus dataset as excitatory thalamocortical projecting neuron identity. (A): Scatter Plots where data are represented in the UMAP space. A gradient of violet is used to show expression, from lowest levels (light) to highest ones (dark). **(B):** Dot Plots of the same data. The average expression level of each genes by individual cell clusters is represented by gradient of violet, with low expression in light violet and high expression in dark violet. The size of each dot in the plot is proportional to the percentage of cells within each cluster that are positive for the expression of each marker gene. **(C)** Violin Plots with the cluster identity in the x-axis, and the expression levels of each marker in the y-axis. The colours are relative to the cluster identity (as Figure 4.7 A).

Figure 4.9

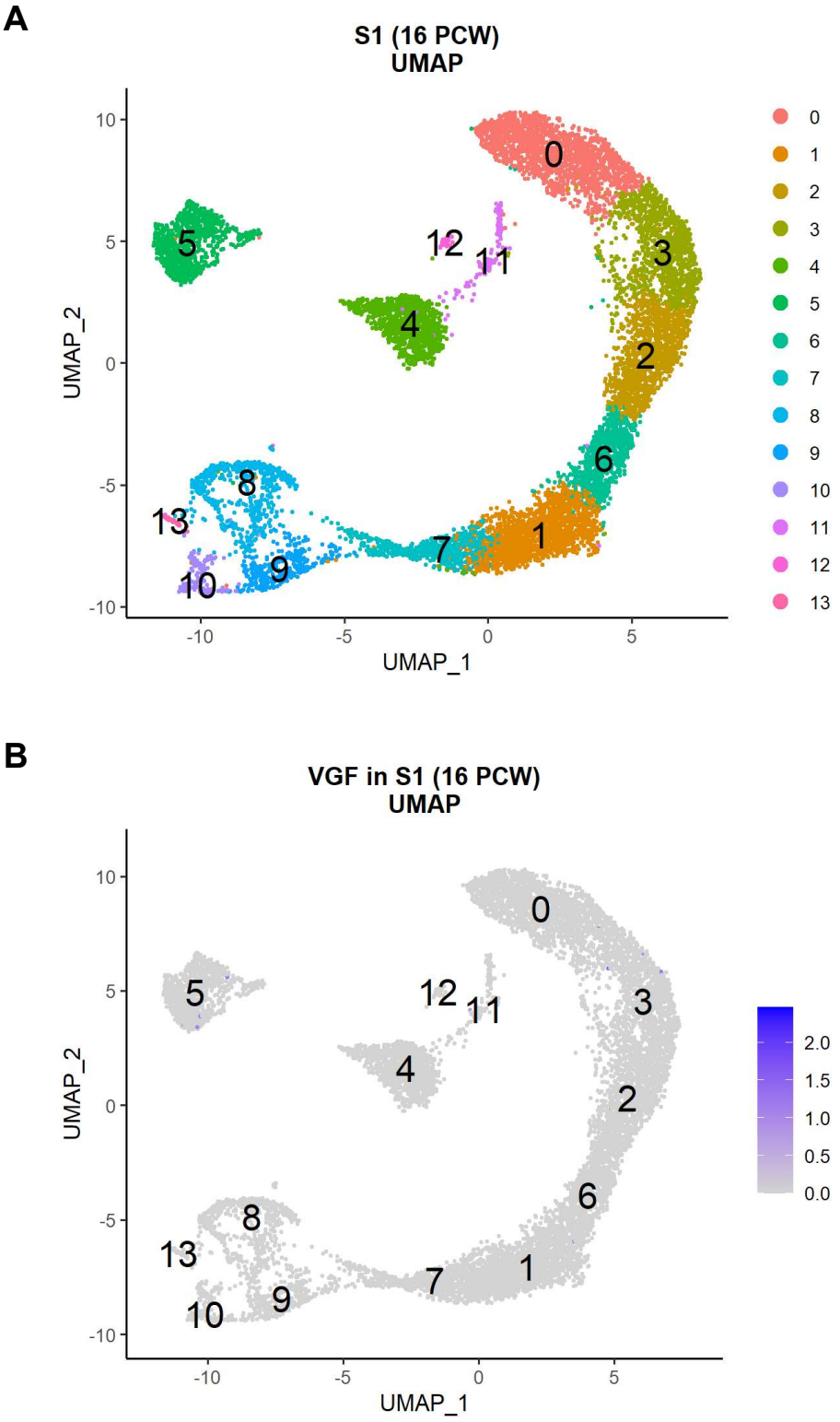

Figure 4.9: UMAP representation of the 16 PCW Somatosensory Cortex dataset. Scatterplot of 10,915 cells after Principal Components Analysis (PCA) and Uniform Manifold Approximation and Projection (UMAP), colored by cluster (N=14) (**A**), and VGF expression (**B**).

Figure 4.10

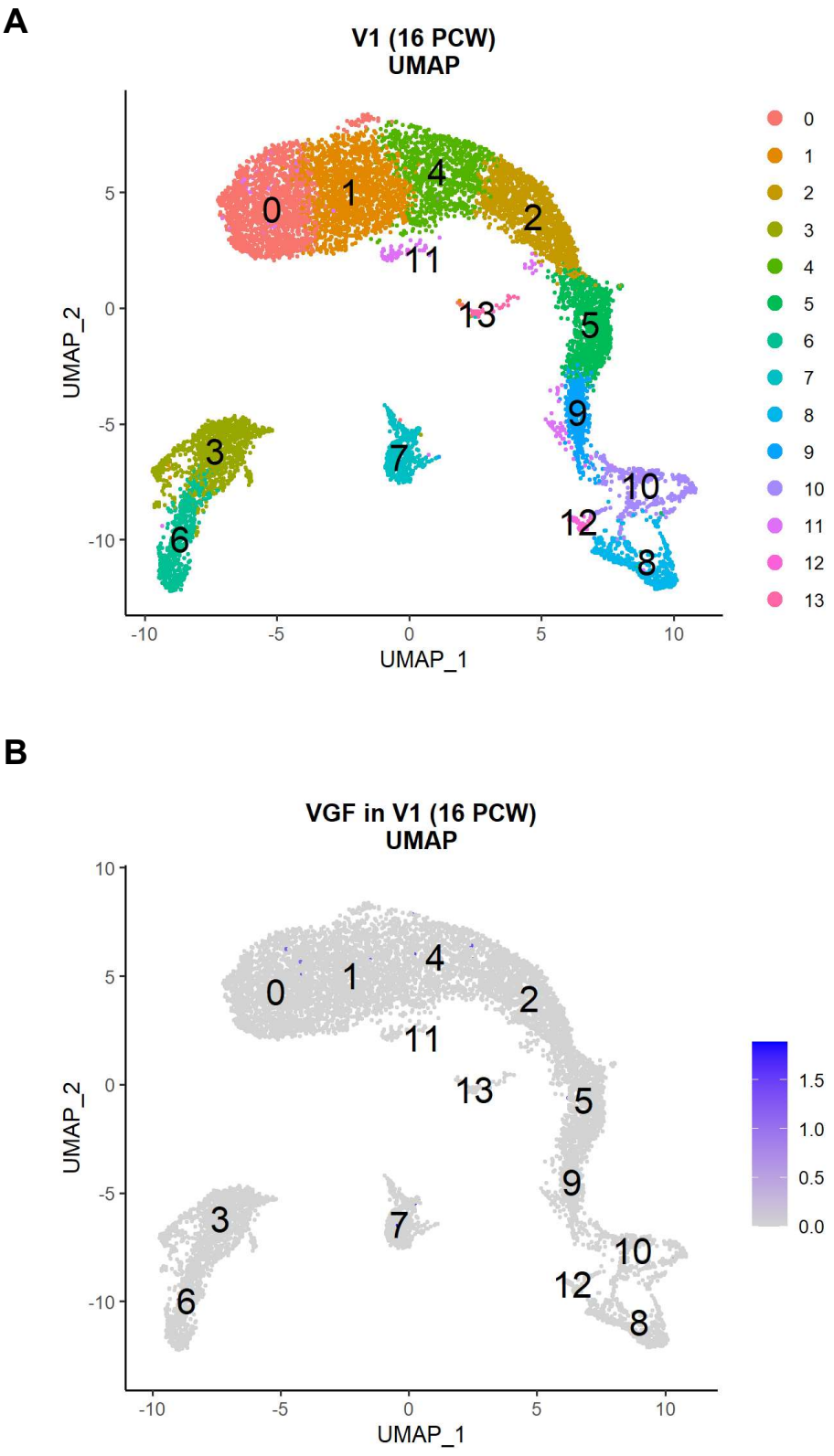

Figure 4.10: UMAP representation of the 16 PCW Visual Cortex dataset. Scatterplot of 10,541 cells after Principal Components Analysis (PCA) and Uniform Manifold Approximation and Projection (UMAP), colored by cluster (N=14) (**A**), and VGF expression (**B**).

Figure 4.11

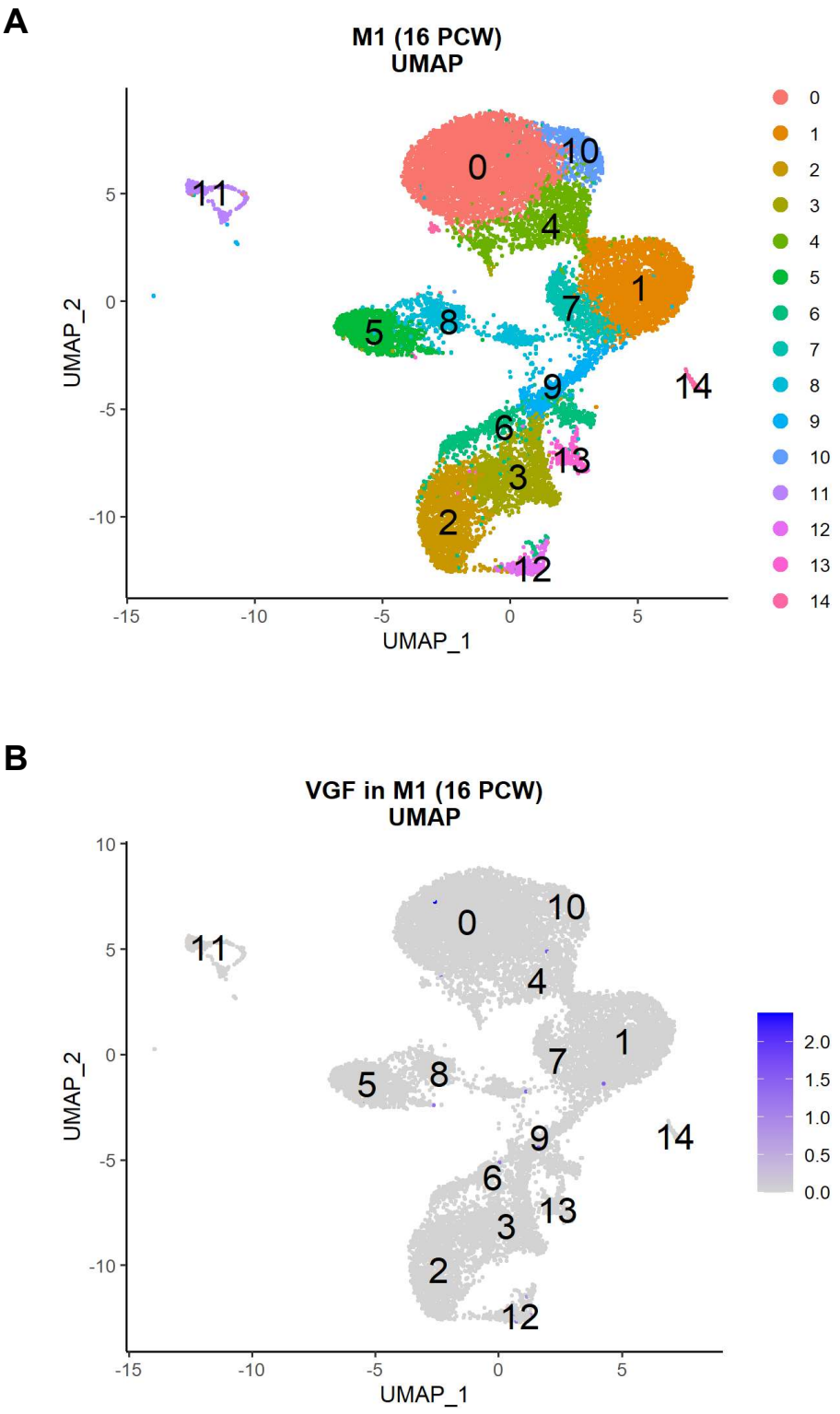

Figure 4.11: UMAP representation of the 16 PCW Motor dataset. Scatterplot of 16,883 cells after Principal Components Analysis (PCA) and Uniform Manifold Approximation and Projection (UMAP), colored by cluster (N=15) (**A**), and VGF expression (**B**).

Figure 4.12

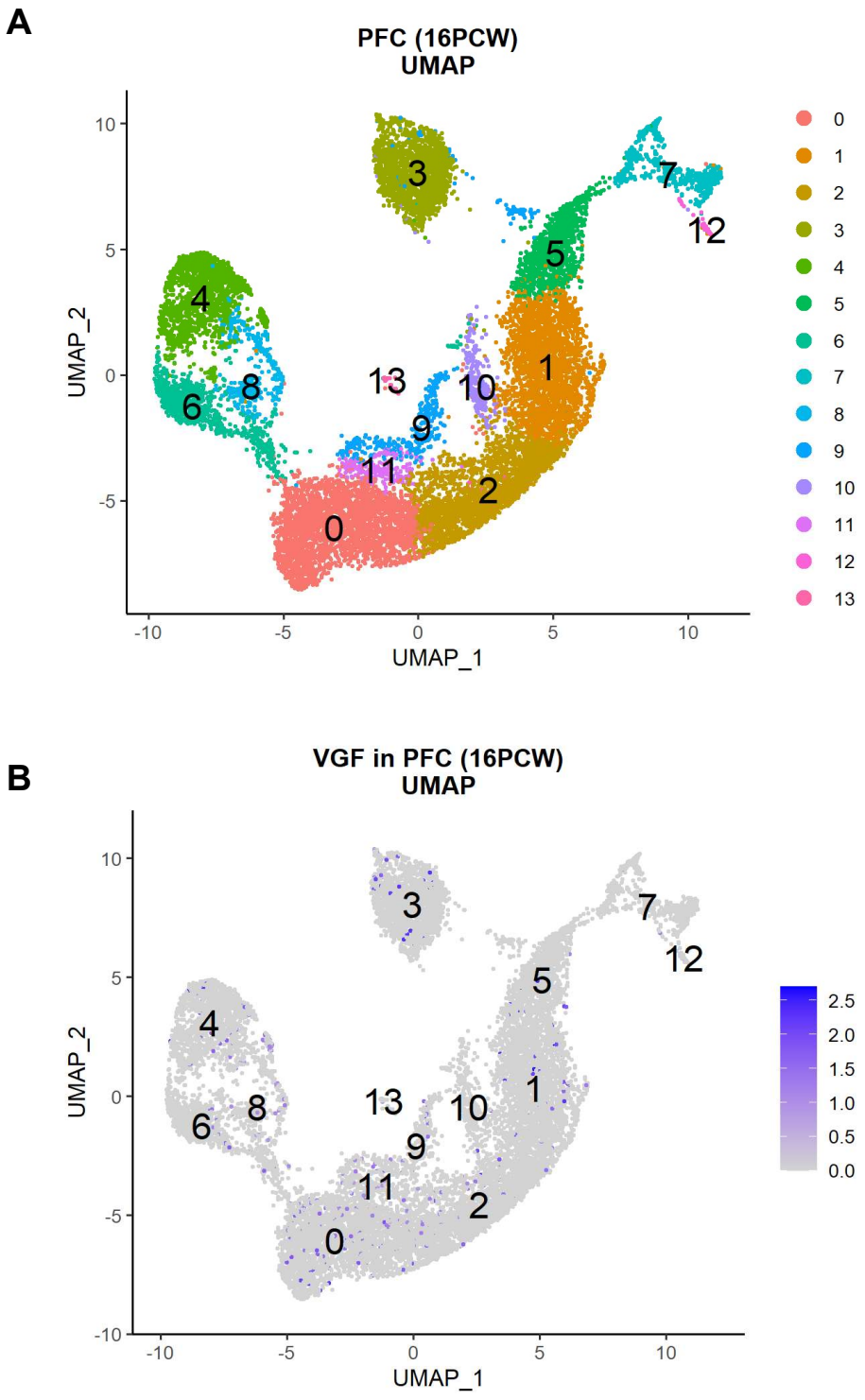

Figure 4.12: UMAP representation of the 16 PCW Prefrontal Cortex dataset. Scatterplot of 15,060 cells after Principal Components Analysis (PCA) and Uniform Manifold Approximation and Projection (UMAP), colored by cluster (N=14) (**A**), and VGF expression (**B**).

4.4 Validation of the expression pattern of VGF by qPCR analysis

Finally, to confirm the predictions based on the analysis of VGF expression patterns in the transcriptomic datasets, I performed a quantitative PCR (qPCR) validation on microdissected brain region of one 13 PCW and two 20 PCW human fresh-frozen brains. The main areas of interest (i.e. the thalamus, and main neocortical areas) are plotted in **Figures 4.15 and 4.16**. Microdissections of these areas from each brain were performed according to the overall preservation of each sample, and the ease of identification of the boundary of those areas. For this reason, microdissection differs across samples, and although the qPCR analysis was performed within the same plate with the same experimental conditions, the results are plotted separately for each brain. At **13 PCW**, VGF expression (**Figure 4.15 A**) is higher in the thalamus as compared to the neocortical regions. A significant exception to this pattern is represented by the insular cortex, where the expression appears higher than in other neocortices. In this regard, it is important to note that the brain region labelled as "insular cortex" eventually contains also the claustrum, as the two areas are virtually impossible to distinguish and microdissect separately with naked eyes. At **20 PCW**, VGF levels remain significantly more expressed in the thalamus as compared to the neocortex, in both individuals (20 PCW #1 and #2) (**Figure 4.15 A, B**). Levels of VGF expression are relatively stable, and do not appear to change significantly in the neocortical areas from 13 PCW. Notably, VGF increases of more than 10-fold in the thalamus between 13 PCW (0.019) and 20 PCW brains (0.211 and 0.623). Vice versa, neocortical values of VGF do not change significantly from 13 to 20 PCW, with all values < 0.025 in the areas analysed.

Overall, the qPCR data overall confirmed the observations made in the transcriptomic analysis, and show a restricted expression of VGF in the thalamic region, with an extremely low level of the mRNA in any of the cortical areas investigated. VGF expression levels are generally higher in the 20 PCW brains, suggesting an increase in the production of this molecule throughout the brain over development, in line with the transient endogenous upregulation observed in the neocortical regions of the Brainspan samples (**Figure 4.3**).

Figure 4.13

A

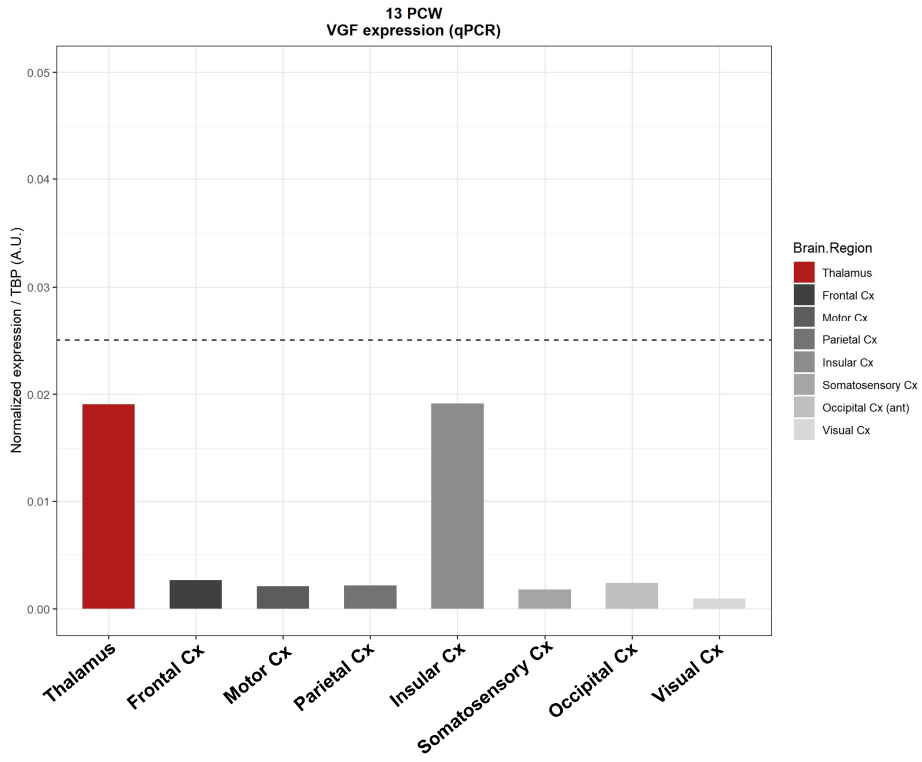

B

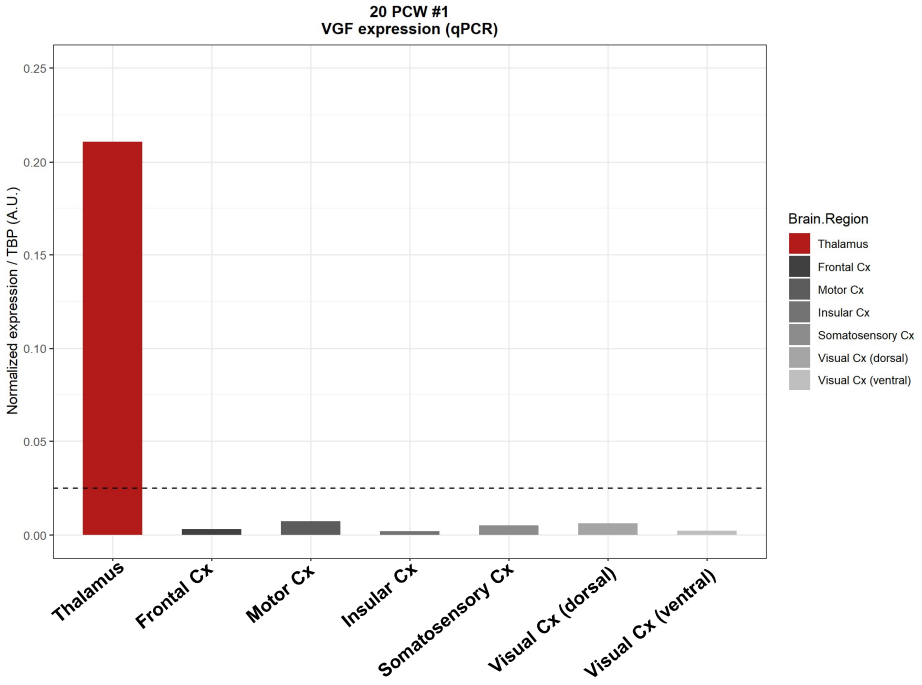

Figure 4.13

C

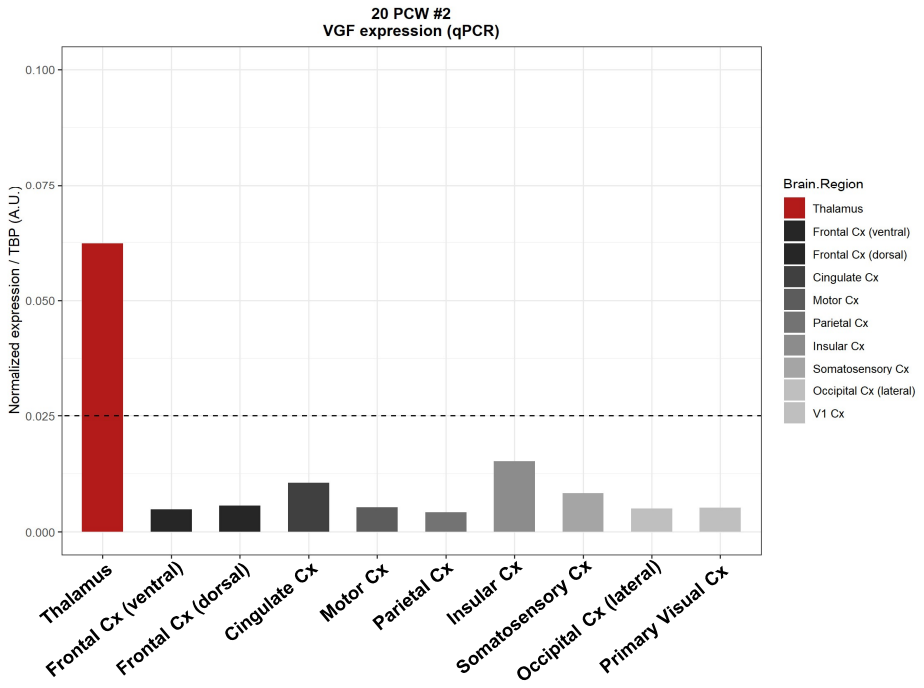

Figure 4.13: Quantification of VGF expression levels in the 13 PCW (A) and 20 PCW (B, C) human thalamus and neocortical areas evaluated with qPCR. Gene expression values are normalized relative to the housekeeping gene TBP. Values are absolute arbitrary units (A.U.) calculated with the ΔCt method. Statistics does not apply due to the small sample size.

CONCLUSIONS

Taken together, transcriptomic analysis of the human developing brain at both bulk and single cell level showed that VGF expression is sustained throughout cortical neurogenesis and it is restricted to the thalamus, where VGF is specifically expressed by the mature excitatory neurons projecting to the cortex at mid-gestation.

Unfortunately, microdissection of frozen brain samples does not allow for a detailed analysis of the VGF expression at anatomical level. In order to get further insights on the regional pattern of expression, such as layer-specificity in the cortex, nuclear-specificity in the thalamus, *in situ* hybridization techniques should be employed in the future to corroborate the findings presented in this section.

DISCUSSION

Considerations on the expression profile of VGF in the thalamus and neocortical areas of the human developing brain

VGF expression is consistently strong and specific to the thalamic region across all datasets analysed. This fulfils the first two criteria for the consideration of VGF as a candidate extrinsic factor modulating human cortical development, as presented at the beginning of this Chapter.

Strikingly, the expression pattern of VGF in the human prenatal brain does not precisely mirror the one described in the developing rodent brain (Sato *et al.* 2012; Sato *et al.* 2022). In fact, elevated VGF expression is detected at the level of the associative mediodorsal nucleus (MD), rather than solely in the sensorial thalamic nuclei. Not only, but VGF appears even more strongly expressed in the first than in the latter (**Table 4.1**, **Figures 4.5 and 4.6**). As the MD directly projects to the prefrontal cortex (Funahashi 2013), this finding supports the hypothesis of a different role played by VGF in the specification of the human cortical areas as compared to the rodent brain, where VGF specifically influences the development of primary sensorial areas of the cortex. This phenomenon could be attributed to the evolutionary adaptation of a conserved molecule, wherein its function has been redirected to facilitate the development of vital and expanded regions in the human brain, including the prefrontal cortex. Furthermore, this observation aligns with the existing evidence from the literature, which indicates that dysregulation of VGF is implicated in various neuropsychiatric and neurodevelopmental disorders that primarily affect the prefrontal cortex and its specialized functions in humans.

However, it is important to note that the experimental techniques used to investigate VGF spatial expression patterns in mice and humans differ significantly. In this study, the analysis involved laser microdissection (LMD) microarrays on human brain tissue, while previous studies in mice have utilized in situ hybridization (ISH), which should be also perform on human fetal brain tissue to corroborate these findings.

There are a few notable exceptions to the general pattern of low VGF expression levels in the cortex and its restricted expression in the thalamus. As highlighted by the RNAseq data (**Figure 4.3**), VGF expression is endogenously upregulated at cortical level between 19 and 24 PCW. This phenomenon could potentially be attributed to the concurrent increase in innervation of cortical areas by both thalamic and non-thalamic axons (Vasung *et al.* 2010; Krsnik *et al.* 2017; Zunic Isasegi *et al.* 2018; Alzu'bi *et al.* 2019). These axons not only release various neurotrophins into the extracellular space but also establish synaptic connections with cortical neurons during this developmental stage (Kostovic *et al.* 2007). It is well known that neurotrophins such as BDNF, NGF, and even VGF itself, as well as synaptic activity, can strongly induce the upregulation of VGF expression (Hawley *et al.* 1992; Alder *et al.* 2003; Lewis *et al.* 2015). The cortical upregulation of VGF is transient in nature, as the levels of VGF in the cortex return to their original baseline within a few weeks. Interestingly, VGF levels starts increasing around birth and this trend continues at post-natal stages in all neocortical areas (Figure 4.4 B). This is in line with previous literature showing substantial expression of this factor in the adult human cortex (Carlyle *et al.* 2017; Yu *et al.* 2023).

At sub-regional level, the LMD microarray data similarly show exceptions to the generally low expression levels of VGF in the cortical areas. Namely, the dorsolateral prefrontal cortex (dlPFC) at 15 PCW and the somatosensory cortex (S1) at 21 PCW show already sign of VGF endogenous upregulation at the level of the cortical plate (**Table 4.3**). However, these exceptional values remain equal or lower than all thalamic nuclei reported in **Table 4.1**, especially the correspondent thalamic nuclei innervating those areas directly, namely the MD and the VPM/VPL, respectively.

A different case is represented by the intermediate zone (IZ), where VGF is primarily detected within the cortex (**Figures 4.5 and 4.6**). The IZ mainly serves as a pathway for axonal projections to and from the cortex, and contains only a small number of cell bodies. Therefore, it is likely that the majority of transcripts, including VGF, found in this region are actively transported through axonal transport rather than being locally produced by cortical cells.

It is important to note that the LMD microarray data presented in **Section 4.2**, although interesting and complementary to the RNA-seq data (Section 4.1), might present technical limitations leading to either underestimation or overestimation of the expression of any candidate genes. In fact, different probes used to produce the microarray data have different specificity, sensitivity, and the overall results are not as consistent and reliable as the data produced by different approaches. Specifically, VGF expression has been evaluated with two different probes, labelled as A_24_ P129326 and CUST_6379_PI416261804, that gave two sets of results in each sample analysed.

Finally, the techniques used for quantifying the transcript in these datasets (**Figures 4.4** exon arrays) and then validating it in the human tissue (**Figures 4.13**), are substantially different, and direct comparisons between them may not be entirely valid. Moreover, inter-individual variability is clearly present, as evident from the distinct expression patterns observed in the two 20 PCW brain samples (**Panels B and C** of **Figures 4.13**). This limitation is unavoidable in human studies as further discussed in Chapter 7, and should be always considered when interpreting and comparing experimental results.

Considerations on the single cell transcriptomics

Since VGF is a growth factor that can be also locally secreted to support the development of thalamic neurons (autocrine function), as the thalamus itself is undergoing development, it was important to ascertain that VGF was specifically expressed by those neurons able to transport it to the cortex (paracrine function). Surprisingly, thalamic GABAergic interneurons did not express VGF at this stage of development (not shown), despite evidence suggesting otherwise in rodents (Selten *et al.* 2023) and the adult human brain (Quinn *et al.* 2021). However, this does not rule out the possibility of VGF production by interneurons later in thalamic development.

Another important consideration is that the cluster of cells identified as "cluster 2" labelled as “excitatory thalamocortical projecting neurons" consists of potentially different *subtypes* of excitatory neurons (**Figure 4.8**). A higher resolution parameter in the clustering process would be required to distinguish these subtypes, but for the purpose of this analysis, a broader classification of excitatory neurons was considered appropriate. Future re-analysis can be conducted to further characterize these subtypes based on their emerging transcriptomic profiles. Similarly, it would be of interest to analyse the *lineage progression* of these VGF-expressing neurons, either by analysing later timepoints of development available in the data repository, or by using trajectory prediction methods such as RNA Velocity (La Manno *et al.* 2018). In fact, this dataset only provides a snapshot of a dynamic process and sequence of events, such as brain development.

Amongst the cortical datasets, the prefrontal cortex (PFC) is the only neocortical region showing detectable levels of VGF mRNA (**Figure 4.12**), despites they remain relatively lower than in the thalamus. In contrast to the thalamus, where VGF expression is confined to a specific cell cluster (**Figure 4.7**), in the PFC this appears to be more scattered across various cell clusters, suggesting the possibility of an early upregulation of endogenous cortical VGF in this area. This phenomenon might be explained by an earlier innervation of PFC by thalamic axons, that secrete neurotrophic factors and establish synaptic connections, ultimately triggering the upregulation of VGF expression. This, along with the extended time of development and maturation of the PFC (Merve Cikili 2018; Chini *et al.* 2021) can allow VGF itself to exert a prolonged influence on the development of the human prefrontal cortex. This finding further supports the hypothesis of an evolutionary repurpose of VGF in favour of supporting the development of the expanded PFC in the human brain, as mentioned earlier in this discussion.

CHAPTER 5

Thalamocortical projecting neurons produce and transport VGF protein to the developing human cortex

INTRODUCTION

In the previous Chapter, I established a set of criteria that I aim to evaluate to validate VGF as a thalamic factor responsible for the extrinsic regulation of cortical development and specification in human (see Introduction Chapter 4). After assessing the expression pattern of VGF at mRNA level in the human developing brain (Chapter 4), and confirming its specific expression in thalamocortical projecting neurons (criteria 1 and 2), the next step was to validate the presence of VGF at the protein level (criterium 3). Specifically, I had to demonstrate that VGF protein is actively transported from the region of production, the thalamus, to the cortical areas where it is secreted in a functionally active form of full-length protein or neuropeptides. VGF secretion in the cortical areas would be induced by the synaptic activity established between thalamic and early-born cortical neurons.

While evidences have been gathered in the developing mouse brain indicating that VGF protein is produced and transported to immature neocortical areas where is ultimately released (Sato *et al.* 2012; Monko *et al.* 2022; Sato *et al.* 2022), there is currently a lack of data regarding this aspect in the human brain. Furthermore, the data collected on the expression pattern of VGF mRNA in the previous chapter suggest that VGF may have additional functions in the human brain, indicating that it might not solely operate based on conserved mechanisms.

In fact, based on the expression pattern of VGF, I hypothesize that VGF may not only participate in the communication between sensory thalamic nuclei and primary sensory cortices, as observed in rodent models, but also play a role in the maturation of prefrontal associative areas. If VGF is indeed

transported from the thalamic mediodorsal nucleus (MD) to the prefrontal cortex (PFC), I anticipate detecting its presence at the protein level in these regions.

To assess my hypothesis and investigate the protein distribution of VGF in the fetal human brain, I used a variety of methods to detect VGF at protein level. First, I perform Western Blot analysis on the protein extracts from the same 13 and 20 PCW fresh-frozen brains where VGF mRNA expression pattern was analysed by qPCR in Chapter 4. This analysis confirmed that the protein product of VGF expression observed in the thalamus can be found throughout the neocortex where it is transported.

To obtain additional spatial information regarding the distribution of VGF protein in the human thalamus and neocortex, I conducted immunohistochemical analysis using available fixed brain samples (see **Table 2.1**). VGF is specifically detected at the level of the intermediate zone (IZ) of the developing cortex, where thalamic axons run transversally between the germinal zones and the overlying subplate. Interestingly, immunohistochemistry data confirm the observations made in the transcriptomic datasets regarding the thalamic expression pattern of VGF, which is not restricted to the sensorial nuclei but rather detected at the level of the associative mediodorsal nucleus (MD) in the human developing brain.

Finally, I employed Mass Spectrometry analysis to confirm the presence of VGF in the 20 PCW neocortex at proteomic level. Interestingly, the detected levels of VGF were significantly lower compared to what is typically observed in the adult human cortex using the same technique. This finding supports the hypothesis that VGF is primarily transported to the neocortex at this stage rather than being locally produced by cortical cells.

5.1 Evaluation of VGF at Western Blot analysis in the human fetal cortex

To explore the axonal transport of VGF from thalamocortical projecting neurons to target cortical areas with generally low endogenous expression, I conducted an analysis of VGF protein distribution using Western Blot on microdissected regions of fresh frozen human brain samples at 13 PCW (N=1) and 20 PCW (N=2). As demonstrated in the previous Chapter, neocortical areas exhibit minimal endogenous expression of the VGF molecule. Consequently, any detection of VGF by Western Blot in these regions should be attributed to its exogenous transport from the thalamus, which, conversely, expresses VGF at high levels.

5.1.1 Distribution of VGF protein across brain regions (thalamus and neocortex)

First of all, I quantified the levels of VGF in the three brain samples separately, and focusing on the distribution of the protein across different brain regions of the same individual. In fact, the three samples have been analysed in three separate experiments, therefore a direct comparison between them is not entirely accurate. However, it is possible to accurately quantify VGF protein across brain regions microdissected from the same sample. These results are presented in **Figures 5.1-5.3**.

Full-length VGF (~75 kDa)

Full-length VGF protein was detected as a Western Blot band separated around 75 kDa in all samples analysed (**Figures 5.1 A; 5.2 A; 5.3 A**).

At **13 PCW** VGF is relatively equally distributed in the cortical areas, with no substantial differences across them (**Figure 5.1 B**). The greater amount of VGF at the level of the insular cortex can be easily explained by an especially high endogenous production of this protein within this cortex at this developmental stage, as observed by qPCR analysis (see **Figure 4.13 A**). It is therefore unlikely that more of VGF protein is transported from the thalamus to the insular gyrus, as compared

to other cortical areas. Interestingly, the thalamus itself appears to retain the lowest amount of VGF protein, despites being the major contributor for its expression at mRNA level (see **Figure 4.13 A**).

At **20 PCW** the scenario appears to be more homogeneous (**Figures 5.2 B and 5.3 B**).

In one of the two sample (**20 PCW #1**), VGF protein is distributed according to an antero-posterior decreasing gradient, with highest levels detected in the frontal lobe and the lowest in the occipital visual areas (**Figure 5.2 B**). Interestingly, the endogenous expression of VGF mRNA is extremely low in all the neocortical samples (see **Figure 4.13 B**), suggesting that the neurotrophin is actively transported to this area in an antero-posterior decreasing fashion. However, this observation is not recapitulated in the other brain from the same age (**Figure 5.3 B**), and therefore it cannot be interpreted as a general rule. Finally, the thalamus appears to have relatively low level of VGF protein, similarly to what described for the 13 PCW brain.

In the second 20 PCW brain (**20 PCW #2**), full-length VGF shows a different pattern of distribution (**Figure 5.3 B**). Frontal, motor, and parietal cortex show lower level of VGF than both of the two thalamic regions analysed (i.e. antero-medial thalamus, labelled as "Thalamus" for consistency with the other two donors; and Posterior Thalamus). The visual cortex has a slightly higher amount of full-length VGF than the thalamic areas, differently from what described for the other 20 PCW sample. Interestingly, the insular cortex shows the highest levels of VGF in this brain, similarly to the scenario seen in the younger sample. This is in contrast with the mRNA data from this brain, where the endogenous expression of VGF is very low (see **Figure 4.13 C**). The visual cortex appears to be the least enriched neocortical area for VGF mRNA in this sample. Surprisingly, the somatosensory cortex also has relatively higher levels of VGF as compared to the other neocortical areas, though not reaching the levels quantified in the insular cortex. This is in contrast with mRNA levels in this area as quantified by qPCR in this sample (see **Figure 4.13 C**), which are extremely low.

These findings suggest that VGF is transported abundantly to the primary sensorial cortices (i.e. S1 and V1), although this pattern is observed in only one of the two 20 PCW brains and may not be universally applicable. Similar to the other samples, VGF was detected at lower levels in the thalamus compared to most cortical areas, despite the thalamus showing higher mRNA expression

of this neurotrophin (see **Figure 4.13 C**). This observation can be more easily generalized for the human fetal brain between 13 and 20 PCW, as it is noticed in all samples analysed.

VGF as sum of its proteoforms

In addition to the full-length VGF, which was detected at approximately 75 kDa, three other intermediate proteoforms of VGF were detected in the membrane between 50 and 20 kDa in molecular weight (**Panel A** in **Figures 5.1-5.3**). These have not been specifically characterized, in this work nor in the literature. For this reason, I arbitrarily labelled them as "mid_1" (~50 kDa), "mid_2" (~25 kDa), and "lowest" (~20 kDa) bands respectively. VGF full size in this analysis is labelled as "Highest band", for consistency with the arbitrary names given to the proteoforms. The quantification of the **total amount of VGF**, considered as the sum of its proteoforms, appears to follow the same patterns as previously described for the full-length-only form in all three brains analysed. The quantification of total VGF, alongside the relative contribution of each proteoform to the sum (as **relative percentages**), are shown in Panel C and D of **Figures 5.1-5.3**, respectively.

Overall, these Western Blot analyses show that, *differently from the mRNA* (Chapter 4), VGF protein is detected at considerate levels in all the cortical areas sampled, suggesting that VGF is indeed transported to the cortical areas through the thalamic projections.

Figure 5.1

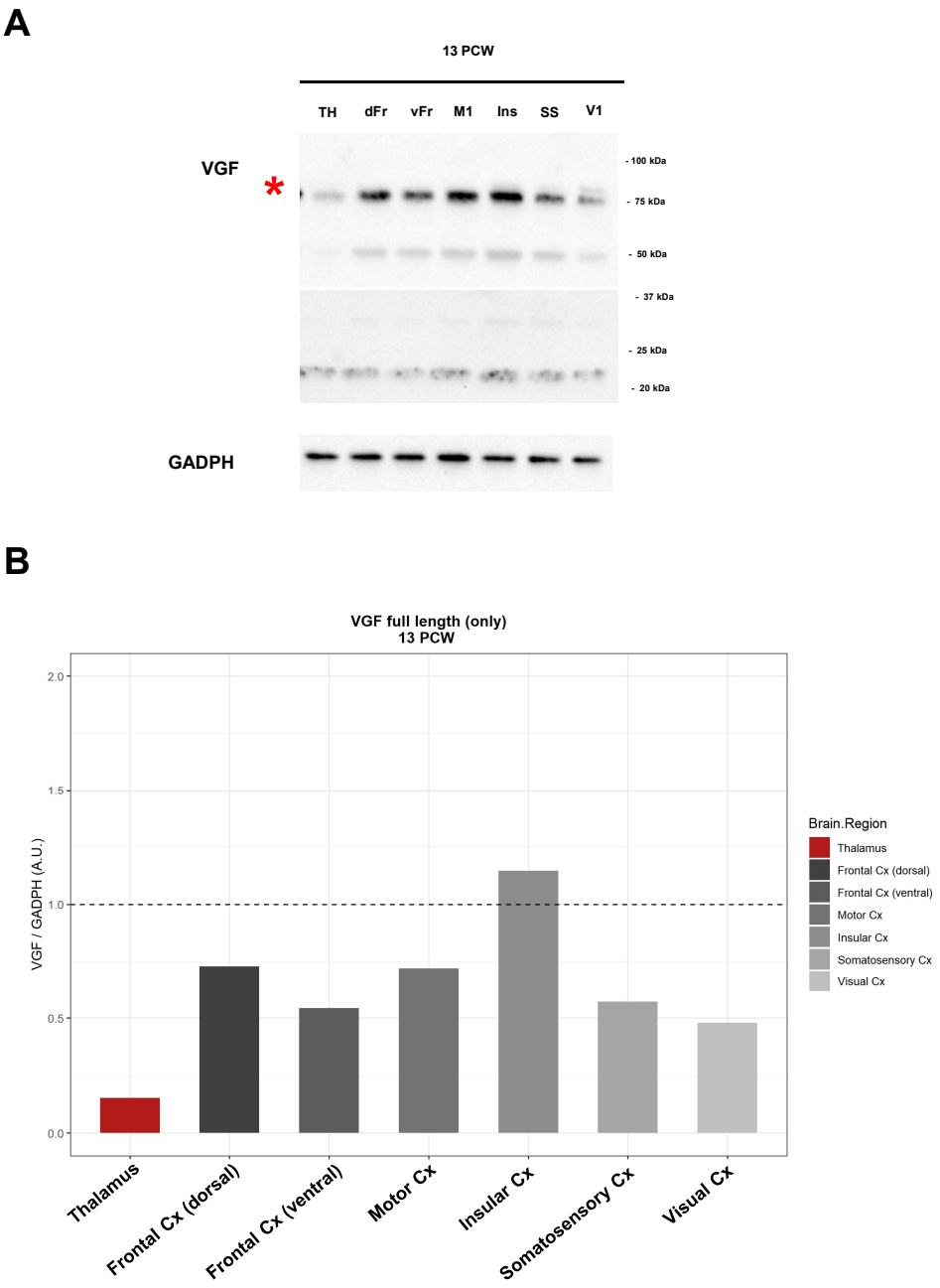
A
13 PCW
TH
dFr
vFr
M1
Ins
SS
V1
VGF
*
- 100 kDa
- 75 kDa
- 50 kDa
- 37 kDa
- 25 kDa
- 20 kDa
GADPH
B
VGF full length (only)
13 PCW
VGF / GADPH (A.U.)
2.0
1.5
1.0
0.5
0.0
Thalamus
Frontal Cx (dorsal)
Frontal Cx (ventral)
Motor Cx
Insular Cx
Somatosensory Cx
Visual Cx
Brain.Region
Thalamus
Frontal Cx (dorsal)
Frontal Cx (ventral)
Motor Cx
Insular Cx
Somatosensory Cx
Visual Cx

Figure 5.1

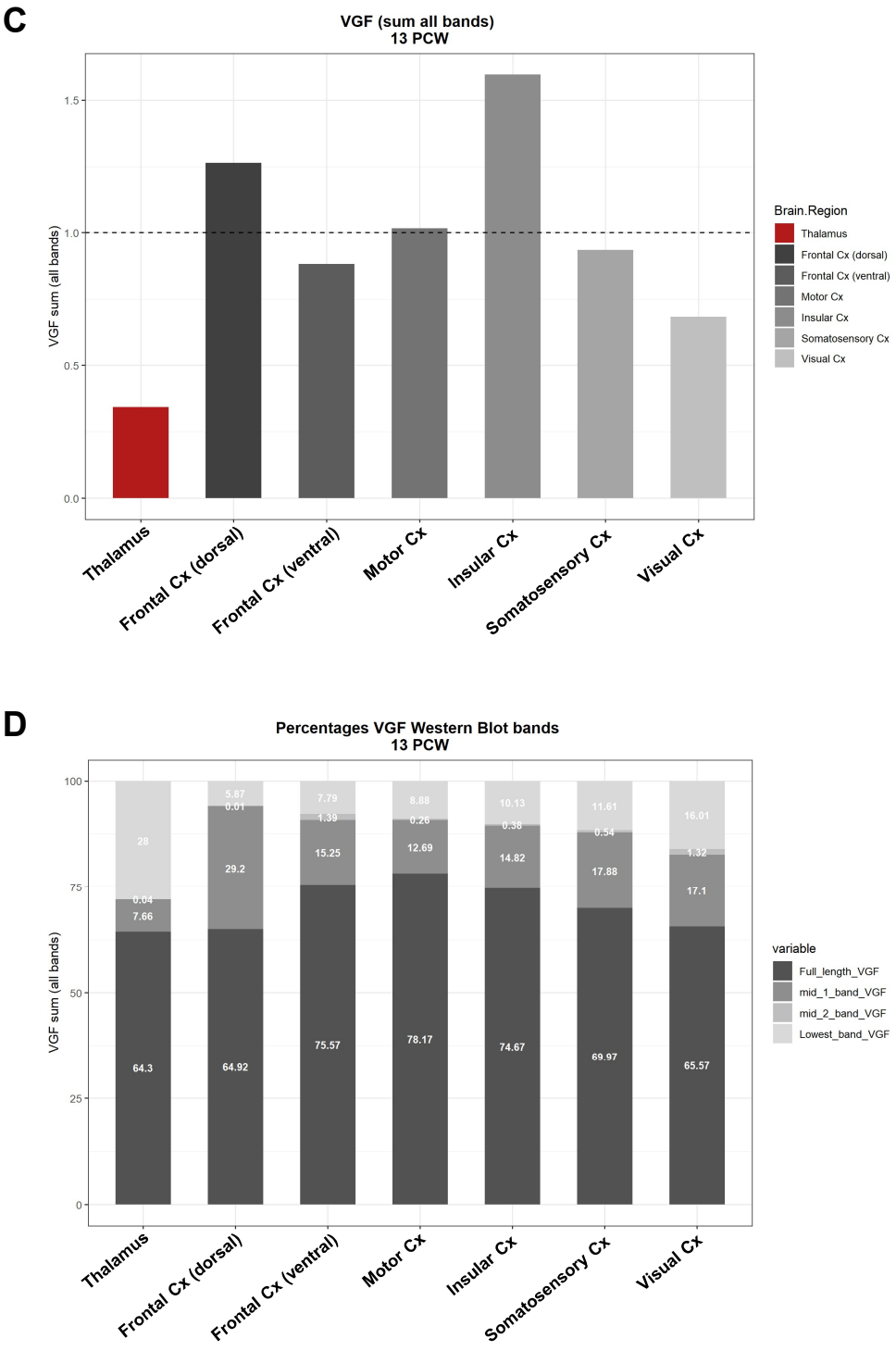

Figure 5.1: VGF protein quantification in the 13 PCW human brain. (**A**). Representative image of the blot for VGF quantified in B. GADPH was detected at 37 kDa and used for normalization and loading control. (**B**) VGF densitometric measurement performed by including only the full size VGF, detected as a single band at 75 kDa. A dashed line intercepts the y-axis at 1 for comparison. Colour coded by brain region. (**C**) VGF densitometric measurement performed by including all the 4 proteoforms detected by Western Blotting. A dashed line intercepts the y-axis at 1 for comparison. Color-coded by brain regions. (**D**) Relative percentage of each proteoform of VGF in the total amount of protein quantified in A. Color-coded by VGF Western Blot band (i.e. proteoform).

Figure 5.2

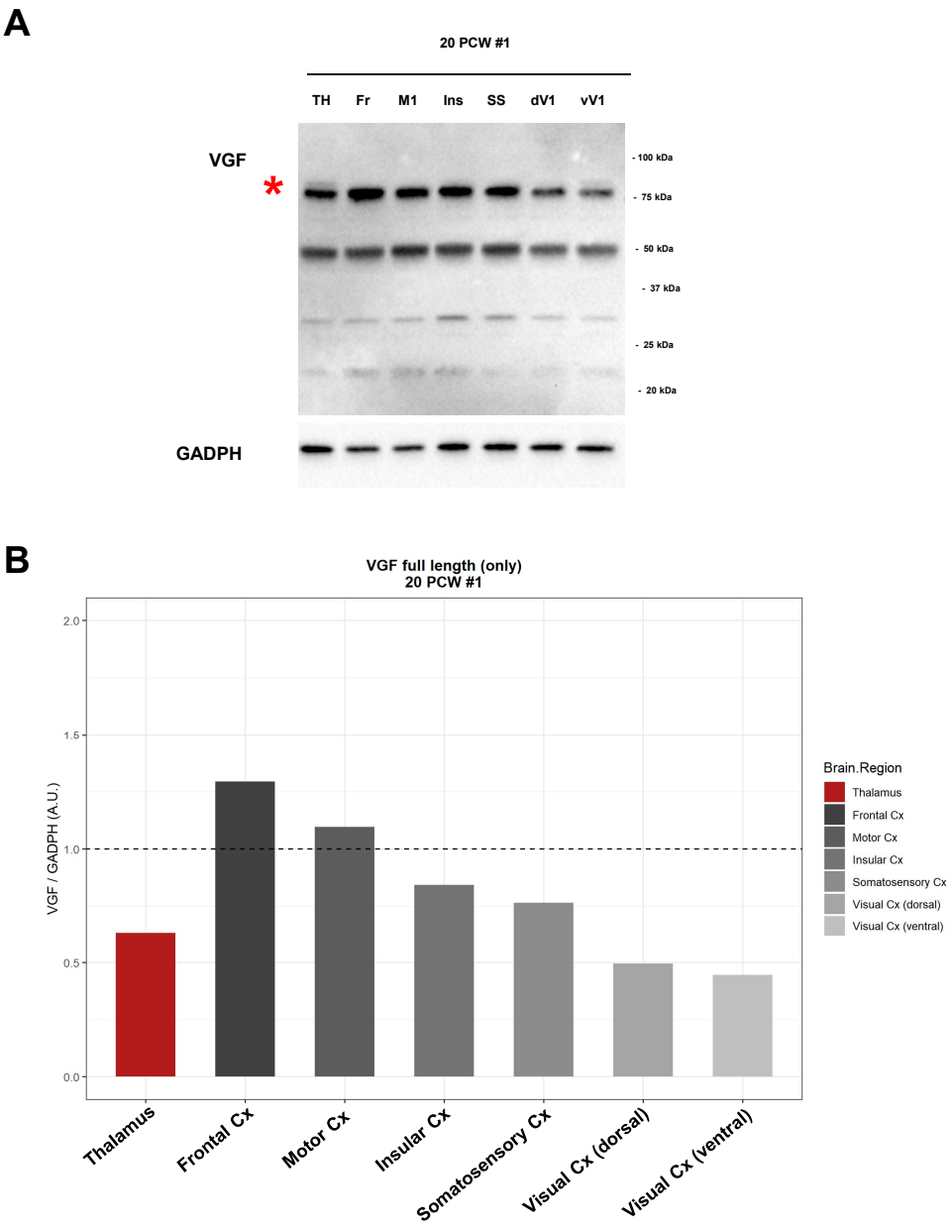
A
20 PCW #1
TH
Fr
M1
Ins
SS
dV1
vV1
VGF
*
- 100 kDa
- 75 kDa
- 50 kDa
- 37 kDa
- 25 kDa
- 20 kDa
GADPH
B
VGF full length (only)
20 PCW #1
VGF / GADPH (A.U.)
2.0
1.5
1.0
0.5
0.0
Thalamus
Frontal Cx
Motor Cx
Insular Cx
Somatosensory Cx
Visual Cx (dorsal)
Visual Cx (ventral)
Brain.Region
Thalamus
Frontal Cx
Motor Cx
Insular Cx
Somatosensory Cx
Visual Cx (dorsal)
Visual Cx (ventral)

Figure 5.2

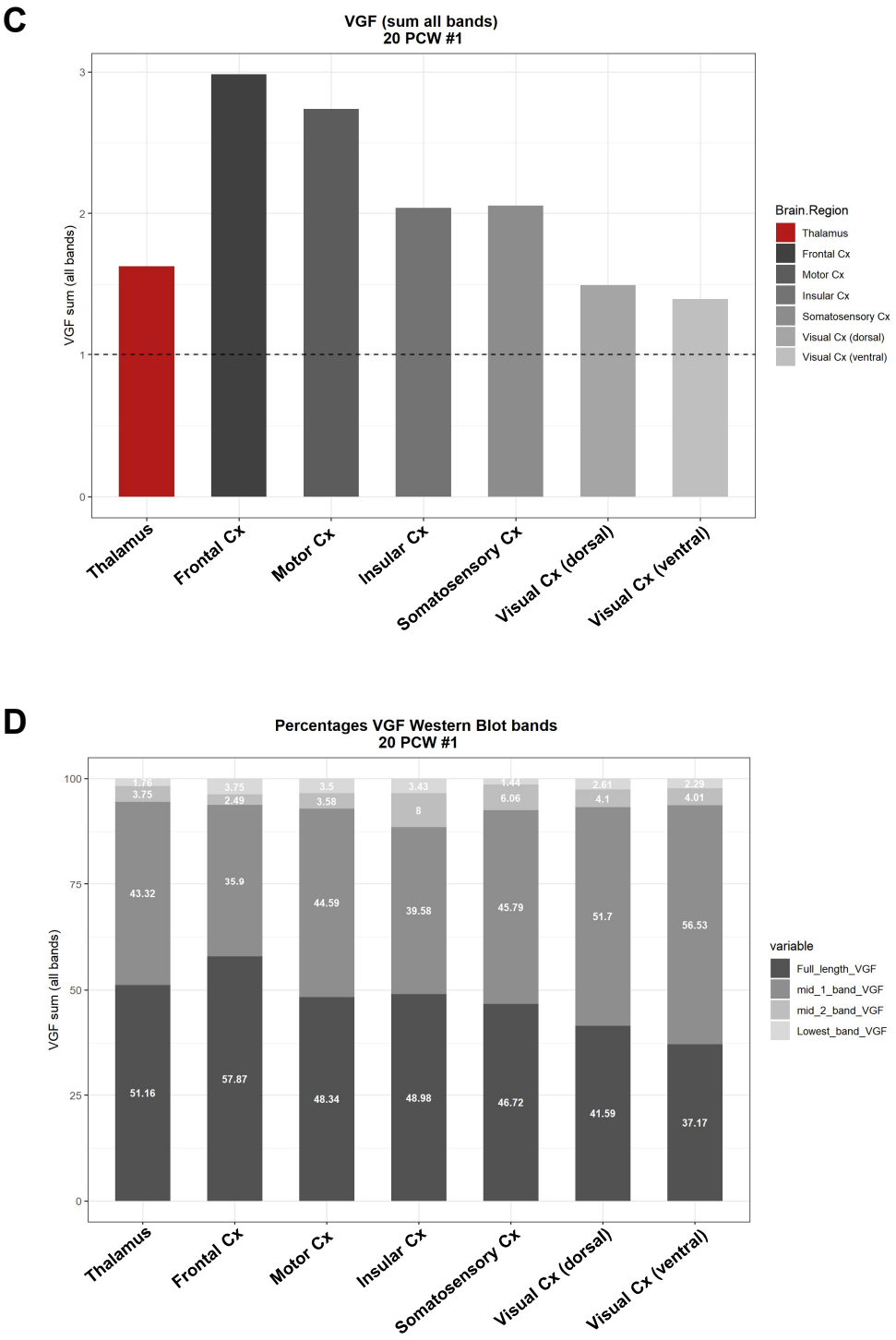

Figure 5.2: **VGF protein quantification in the 20 PCW human brain (#1 donor).** (**A**). Representative image of the blot for VGF quantified in B. GADPH was detected at 37 kDa and used for normalization and loading control. (**B**) VGF densitometric measurement performed by including only the full size VGF, detected as a single band at 75 kDa. A dashed line intercepts the y-axis at 1 for comparison. Colour coded by brain region. (**C**) VGF densitometric measurement performed by including all the 4 proteoforms detected by Western Blotting. A dashed line intercepts the y-axis at 1 for comparison. Color-coded by brain regions. (**D**) Relative percentage of each proteoform of VGF in the total amount of protein quantified in A. Color-coded by VGF Western Blot band (i.e. proteoform).

Figure 5.3

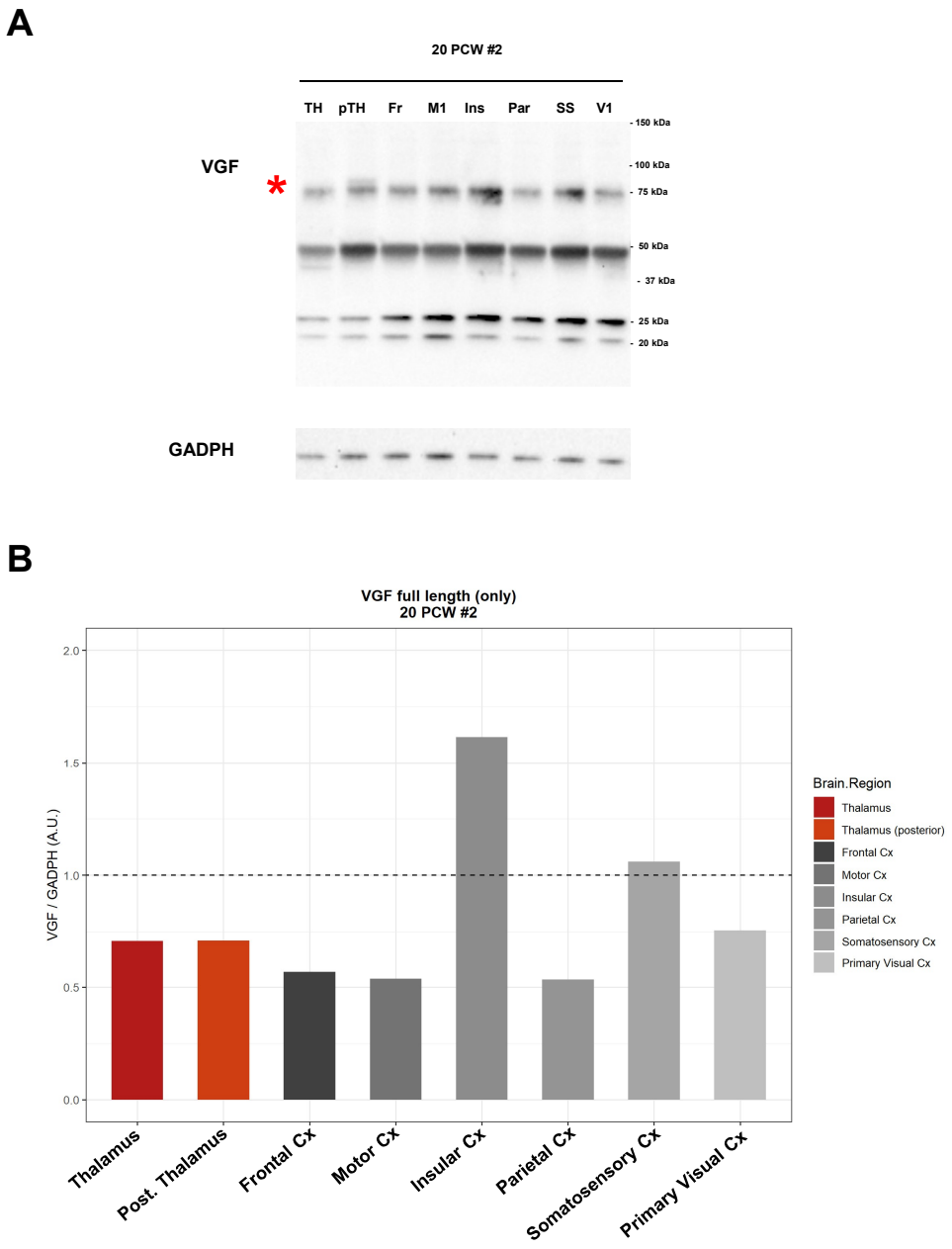
A
20 PCW #2
TH
pTH
Fr
M1
Ins
Par
SS
V1
150 kDa
100 kDa
75 kDa
50 kDa
37 kDa
25 kDa
20 kDa
VGF
*
GADPH
B
VGF full length (only)
20 PCW #2
VGF / GADPH (A.U.)
2.0
1.5
1.0
0.5
0.0
Thalamus
Post. Thalamus
Frontal Cx
Motor Cx
Insular Cx
Parietal Cx
Somatosensory Cx
Primary Visual Cx
Brain.Region
Thalamus
Thalamus (posterior)
Frontal Cx
Motor Cx
Insular Cx
Parietal Cx
Somatosensory Cx
Primary Visual Cx

Figure 5.3

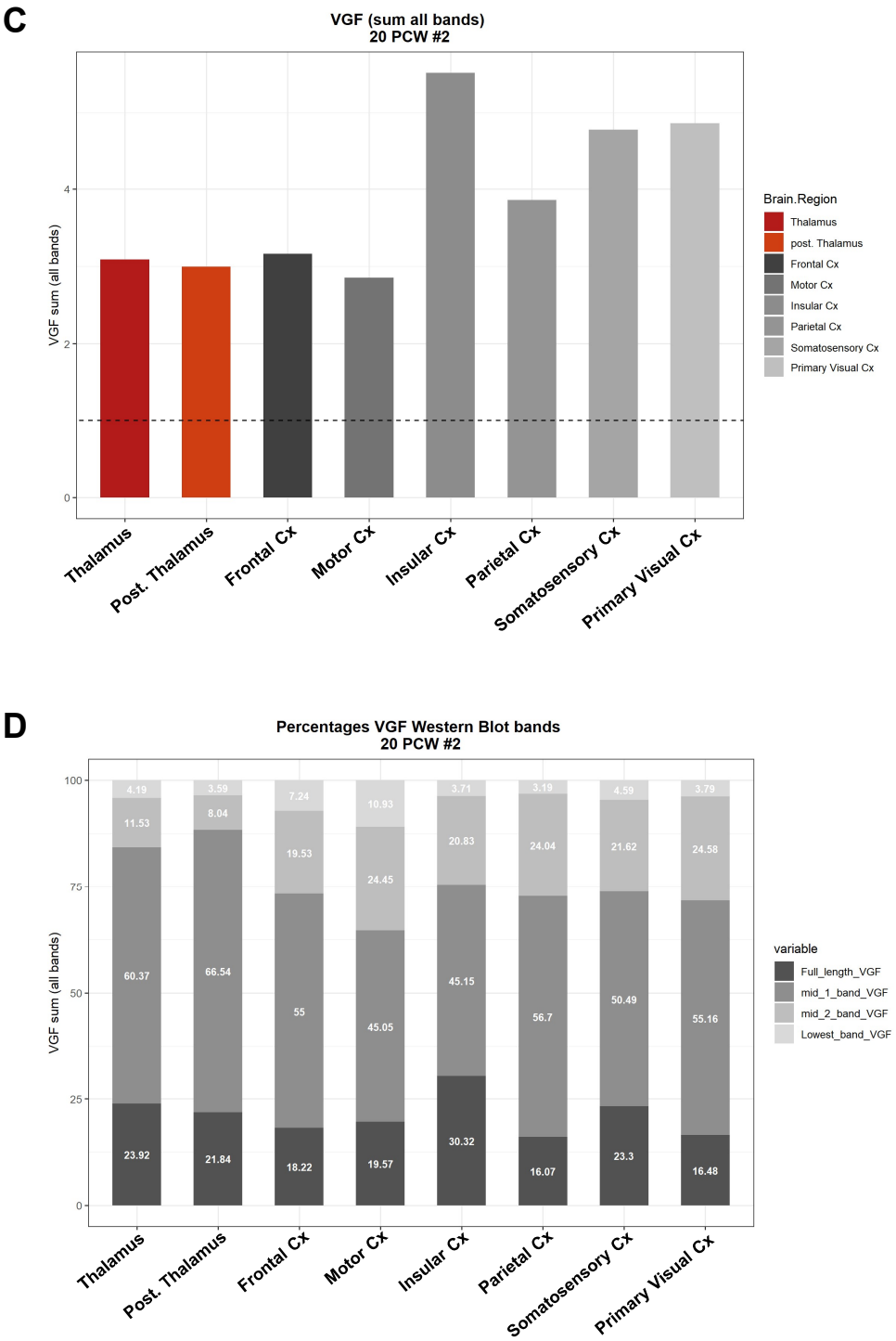

Figure 5.3: **VGF protein quantification in the 20 PCW human brain (#2 donor).** (**A**). Representative image of the blot for VGF quantified in B. GADPH was detected at 37 kDa and used for normalization and loading control. (**B**) VGF densitometric measurement performed by including only the full size VGF, detected as a single band at 75 kDa. A dashed line intercepts the y-axis at 1 for comparison. Colour coded by brain region. (**C**) VGF densitometric measurement performed by including all the 4 proteoforms detected by Western Blotting. A dashed line intercepts the y-axis at 1 for comparison. Color-coded by brain regions. (**D**) Relative percentage of each proteoform of VGF in the total amount of protein quantified in A. Color-coded by VGF Western Blot band (i.e. proteoform).

5.1.2 VGF protein is detected in PFA-fixed human brain tissue (17 PCW)

Finally, Western Blot analysis has been performed also in fixed brain tissue previously used for DiI axonal tracing (see **Chapter 3 Section 3.2**), by using an optimized protocol for protein extraction in fixed tissues (detailed protocol in **Chapter 2 Section 2.3.3.2**). Although this analysis cannot be conduct in parallel with qPCR due to inferior quality of mRNA retrieved in fixed tissues, it allowed to link the observations made by immunohistochemistry and Western Blot analysis on the distribution of VGF protein in the human fetal brain. For this reason, I used a serial section immediately adjacent to the ones stained with Nissl and VGF in the 17 PCW brain sample also used for DiI tracing.

Importantly, fixed tissue allowed me to manually dissect the regions of interest with slightly more accuracy due to the sample being less soft and fragile at room temperature. A small section of the ventral and dorsal aspects of the prospective somatosensory cortex (vS1 and dS1, respectively), along with the thalamic region (TH) and a small portion of the midbrain (MB) have been dissected and used for total protein extraction (**Figure 5.4 A**).

Interestingly, Western Blot analysis reveals that VGF protein is indeed present not only in the thalamus, but also at the level of the cortex where it is detected in the thalamic axons innervating the region in a serial section of the same sample by immunohistochemistry (**Figure 5.4 B**).

Figure 5.4

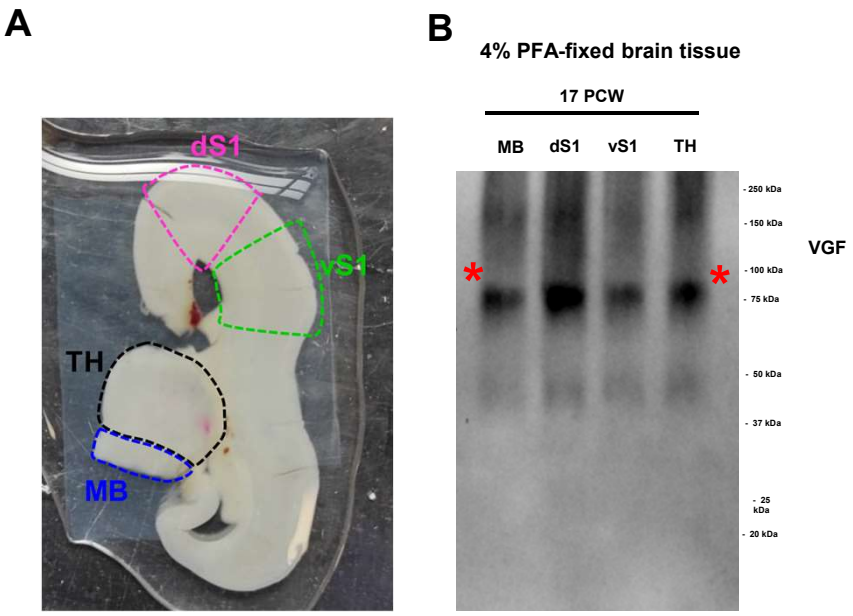

Figure 5.4: **VGF protein is detected by Western Blot analysis in the fixed human brain tissue (17 PCW).** (**A**) Representative picture of the 17 PCW coronal section showing the region microdissected for the analysis. (**B**) Representative image of the blot for VGF. Regions analysed: ventral and dorsal putative somatosensory cortex (vS1 and dS1, respectively); dorsal thalamus (TH); a small portion of the midbrain (MB). Normalization and quantification were not performed.

5.2 Immunohistochemical evaluation of VGF protein distribution in the human fetal brain

To further evaluate VGF protein distribution in the human fetal brain, I performed immunohistochemical staining on selected coronal sections from 10 PCW (N=1), 16 PCW (N=1), and 17 PCW (N=1) brain samples. The younger sample was included in a collection of formalin-fixed paraffin-embedded (FFPE) human brain samples (4 µm in thickness), whereas all the other sections were cut from 4% paraformaldehyde (PFA)-fixed brains (all ~100 µm in thickness).

This analysis did not only support the molecular analysis described before in this Chapter, but it also allowed for a more precise examination of the distribution of VGF immunoreactivity with an enhanced spatial resolution. Unlike the protein extracts used for Western Blot analysis, which were obtained from entire brain regions and did not preserve spatial details, immunohistochemistry provided a more comprehensive understanding of the sub-regional distribution of VGF protein. This included insights into the distribution within specific nuclei of the thalamus, as well as different layers of the neocortex.

10 PCW human brain (medial coronal plane)

I selected sections from the medial-to-posterior coronal plane of the **10 PCW** brain sample (**Figure 5.5**). Two coronal planes are shown in the panel: one medial at the level of the boundary between frontal and parietal lobe including the medial thalamus (**Figure 5.5 A, B**), and one slightly posterior where the ganglionic eminence converge, and posterior nuclei of the thalamus start developing (**Figure 5.5 C, D**). GAP-43 immunohistochemistry was performed in immediately adjacent slices to reveal the anatomical structures, and especially the axonal pathways from the thalamus to the immature parietal cortex (**Figure 5.5 A, C**).

In the first slice, VGF is not present at any level of the thalamus, but it is confined to the small portion of the midbrain located dorsally (**Figure 5.5 B**). Beyond the thalamus, a faint VGF-positive signal is detected at the level of the internal capsule and the intermediate zone of the cortical area sampled in this section.

In the second slice, VGF is observed as a pale immunoreactive signal at the level of the thalamus where the prospective dorsolateral geniculate nucleus (dLGN) will start forming (**Figure 5.5 D,** dashed white line). At this early age, however, it was not possible to properly discern this nucleus, and a precise annotation of the dLGN was not possible besides comparing GAP43-immunoreactivity (**Figure 5.5 C**) with the Brainspan Reference Atlas (not shown). Detection of VGF protein in the thalamic sensorial nuclei of the human brain at this stage is consistent with previous findings in animal studies (Sato et al., 2012).

In this posterior section of the 10 PCW brain, I observed a similar cortical distribution of VGF immunoreactivity as the one described for the medial section (**Figure 5.5 D**). The signal is faint but sharply delineated, primarily localized to the intermediate zone that separates the germinal (proliferative) and post-mitotic compartments of the prospective parietal cortex.

Figure 5.5

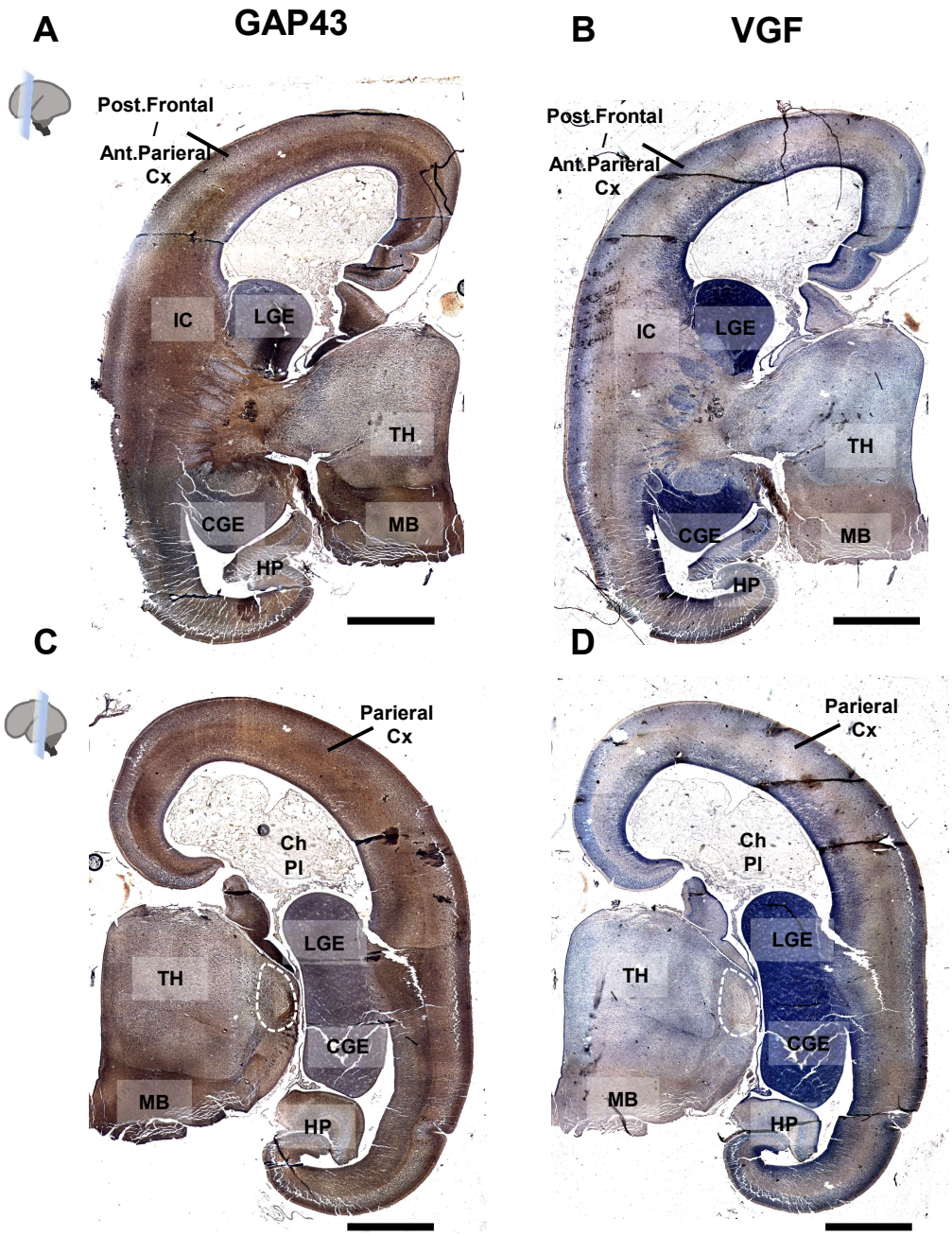

Figure 5.5: **Immunohistochemistry of axonal marker GAP43 and VGF in human 10 PCW coronal brain slices.** All slices are from the same brain, with sections in A-B being slightly more anterior than sections in C-D (see representantive schematics of the coronal plane on the top left side of A-C). (**A-C**) GAP43 signal is used to demarcate anatomical boundaries. (**B-D**) VGF is detected at low levels throughout both brain regions, with a faint signal restricted to the prospective dorsolateral geniculate nucleus of the thalamus (highlighted with dashed line in C-D). VGF is also detected in the intermediate zone of both fronto-parietal cortex dorsally, and the temporal cortex ventrally. VGF is also detected in the developing midbrain (MB) (not discussed). Scale bars = 2 mm.

13-17 PCW human frontal cortex (anterior coronal plane)

Two similar sections from the **frontal cortex** were analysed in the **13 and 17 PCW** brains, and they are directly compared to each other in **Figures 5.6** and **5.7**. At this level, the VGF-positive band is overlapping with the germinal compartments, spanning the entirety of the SVZ (13 PCW) / OSVZ (17 PCW), and ending at the level of the ISVZ/VZ (**Figures 5.6 A', B'** and **5.7 A', B'**).

At **13 PCW**, there is no obvious demarcation between outer and inner portion of the subventricular zone (SVZ), and the intermediate zone (IZ) largely overlaps with the SVZ. The overlapping region exhibited strong immunoreactivity for VGF. In contrast, the ventricular zone (VZ) appeared visually dark due to haematoxylin revealing the high cellular density revealed by haematoxylin.

By **17 PCW**, the OSVZ appears as a separate layer from the ISVZ as highlighted by the different cytoarchitectural organization at Nissl staining (**Figure 5.7 A, A'**). Similarly, to what described for the 13 PCW frontal cortex, VGF-immunoreactive region is sharply defined and limited to the IZ and -in this case- the OSVZ (**Figure 5.7 B, B'**). The cortical plate is completely depleted from VGF, while the marginal zone has some of the neurotrophin. However, it is not possible to determine whether the latter signal is due to an "edge effect," which commonly occurs in immunohistochemical staining. Interestingly, VGF-positive signal is distributed in a radially oriented pattern, resembling the "palisade" formed by the radial glial processes spanning this region and projecting toward the cortical plate.

Figure 5.6

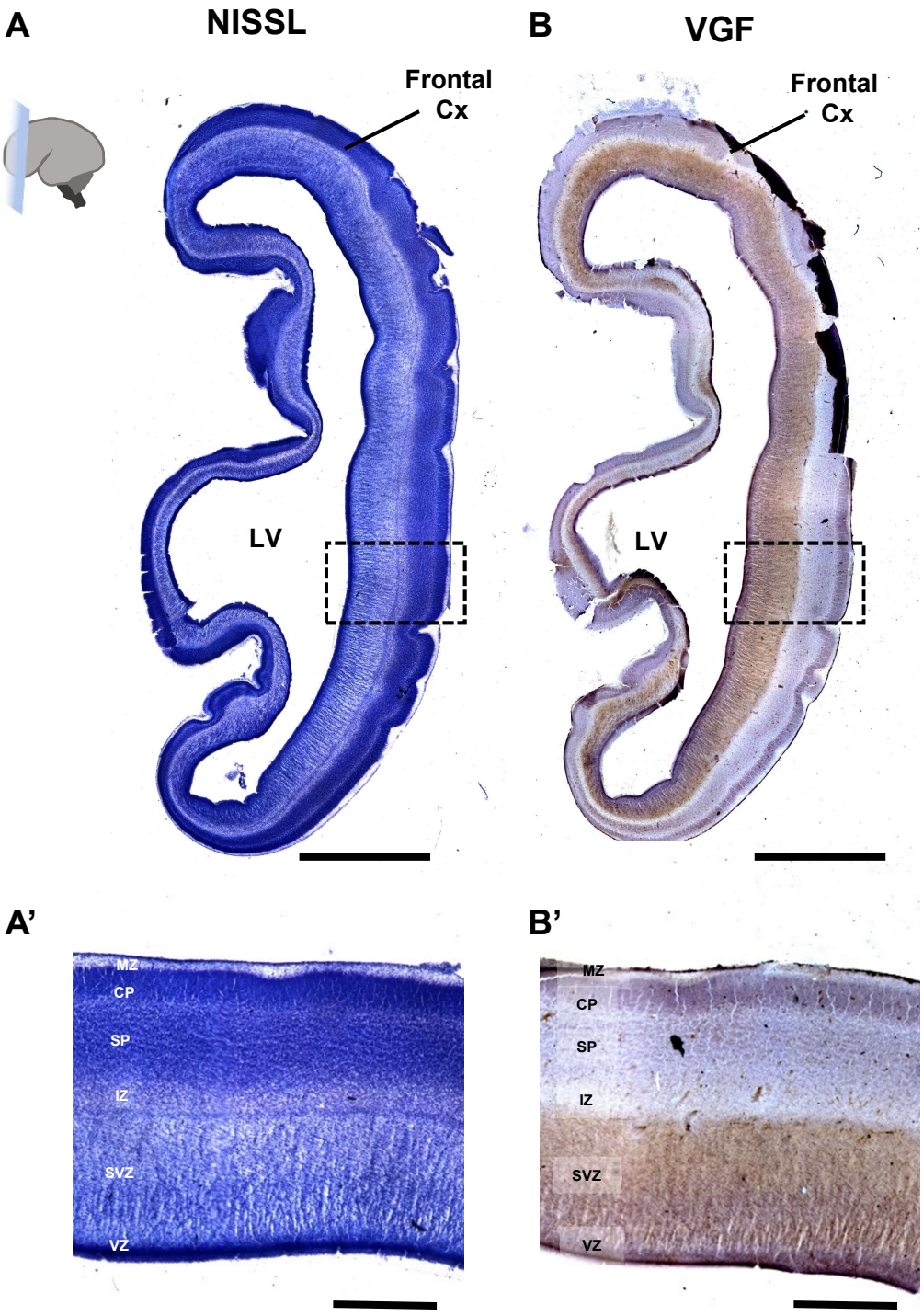

Figure 5.6 : **Immunohistochemistry of VGF in human 13 PCW coronal slice of the frontal cortex.** (**A**) Nissl staining on serial section is used to highlight the cytoarchitecture. (**B**) VGF immunoreactive region is sharply delineated at the level of the intermediate zone and appears particularly strong throughout the subventricular zone. (**A'-B'**) show a zoom-in of the area indicated by a dashed box in A-B. Scale bars = 5 mm (A, B) and 1 mm (A', B').

Figure 5.7

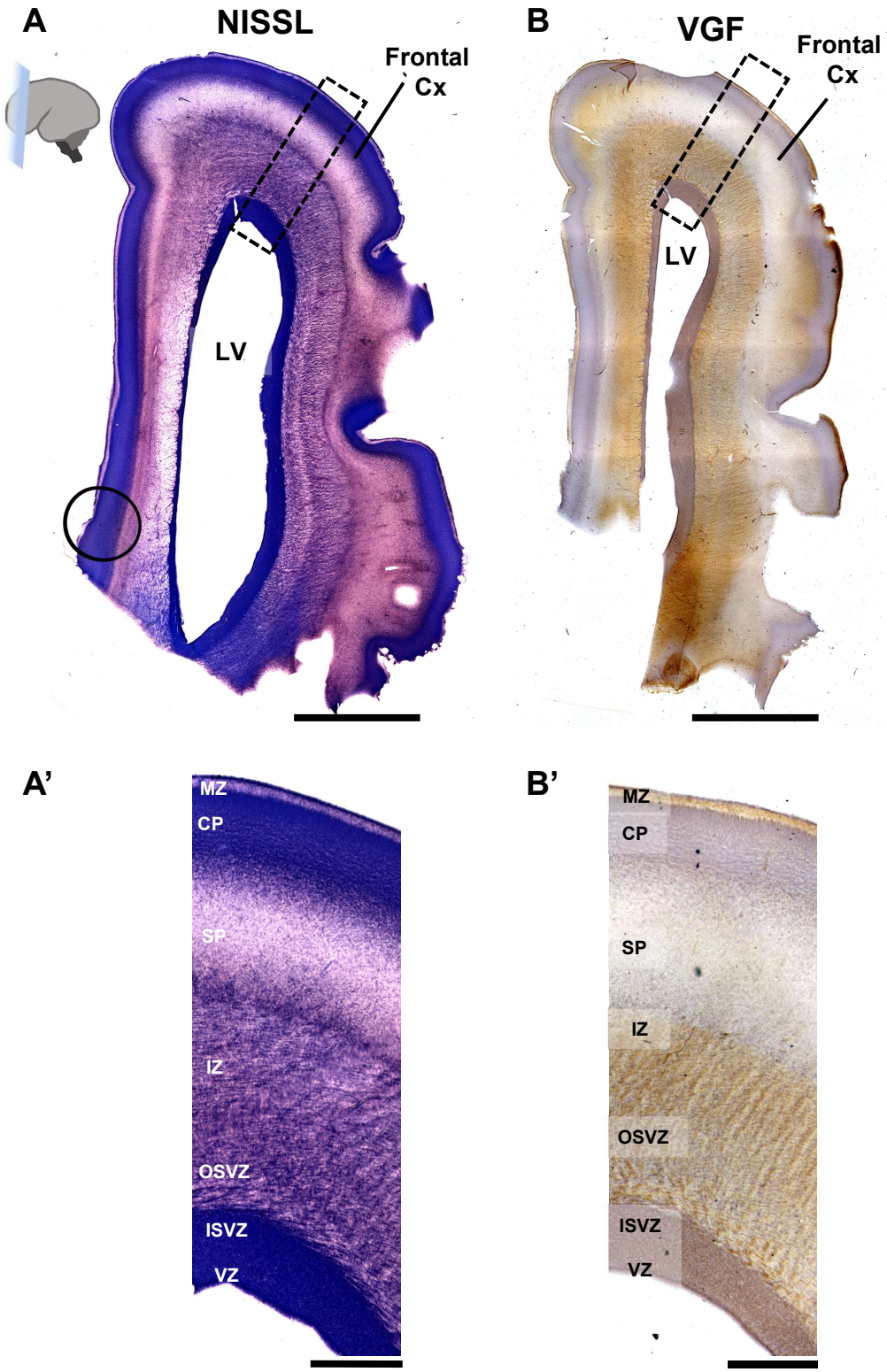

Figure 5.7: Immunohistochemistry of VGF in human 17 PCW coronal slice of the frontal cortex. (**A**) Nissl staining on serial section is used to highlight the cytoarchitecture. (**B**) As in the 13 PCW frontal cortex, VGF immunoreactivity is sharply delineated at the level of the intermediate zone. VGF immunoreactivity is also strongly detected at the level of the outer subventricular zone (OSVZ), which by this age is distinguishable as a separate layer to the inner SVZ (ISVZ). (**A'-B'**) show a zoom-in of the area indicated by a dashed box in A-B. Scale bars = 5 mm (A, B) and 1 mm (A', B').

16-17 PCW human brain (medial coronal plane)

Proceeding to a more medial plane**,** where cortical and thalamic regions can be sampled together in a coronal section of the brain, I selected a few slices from a **16** and **17 PCW** brain, respectively (**Figures 5.8 A, B** and **5.9**). Specifically, the brain slices from the 17 PCW sample stained by IHC and described in this section represent serial sections directly adjacent to the ones used for axonal tracing with carbocyanine dye (Chapter 3), as well as the protein extraction for Western Blot analysis in fixed brain tissue presented earlier in this Chapter (**Section 5.1.3** and representative **Figure 5.4**).

At **16 PCW** (**Figure 5.8 B**), VGF immunoreactivity appears stronger and more widespread at the level of the prospective parietal cortex as compared to a similar region of the 10 PCW (see **Figure 5.5**). The cortical IZ and the internal capsule are in a continuum, and both appear to be VGF-immunoreactive, suggesting that the protein is transported within the axons laying in these structures. Conversely, other regions present in the section have no immunoreactivity for VGF. Finally, at the level of the cortex VGF spreads out to the subplate and cortical plate at this age.

The thalamus imaged in the first section showed a widespread immunoreactivity for VGF (**Figures 5.8 B**). However, it was not possible to define and annotate any specific nucleus at this level, even by Nissl staining (**Figures 5.8 A**). Therefore, I performed VGF immunostaining and correspondent Nissl coloration in serially adjacent sections of the thalamus, slightly posterior to these just described. These thalamic sections are shown in **Figure 5.8 C, D**. In these slides, the thalamus was more prominent, thus allowing for delineation of some anatomical structures. Although pinpointing specific thalamic nuclei is relatively difficult, it is possible to distinguish the area where the anterior nuclei are located from the ventral group, labelled as anterior and ventral nuclei (AN and VN) respectively in Figure **5.8 C, D**. Interestingly, VGF immunoreactivity is mainly distributed in the medial portion of the thalamus, spanning the anterior nuclei but leaving the region of the ventral nuclei relatively immuno-negative (**Figure 5.8 D**).

In a slightly more posterior coronal plane of the **17 PCW brain**, the distribution of VGF becomes more widespread throughout the cortical layers (IZ, SP, OSVZ) (**Figure 5.9 B, B'**). The diffuse nature of the VGF signal in the SP and OSVZ suggests that it is secreted within these layers, whereas within the IZ, where the thalamic axons that transport VGF are located, the immunoreactivity appears to be more anatomically restricted. VGF immunoreactivity is observed not only in the prospective parietal cortex but also in the temporal cortex, which is present in this particular section.

In the **thalamus**, the intensity of VGF signal becomes substantially stronger. In this sample, it was easier to identify and annotate some of the thalamic nuclei, as shown in **Figure 5.9** by both Nissl and VGF immunostaining. While VGF is detected throughout the entire thalamic section, the signal appeared particularly strong not only in the dorsal lateral geniculate nucleus (dLGN), but also in the associative mediodorsal nucleus (MD). This observation was confirmed by immunofluorescence staining of the thalamic area in a serial section from the same sample (**Figure 5.10**). This finding aligned with the elevated level of VGF immunoreactivity detected in the frontal cortex at this age (**Figure 5.7 B, B'**), which receives direct innervation from thalamic neurons originating from the MD.

Figure 5.8

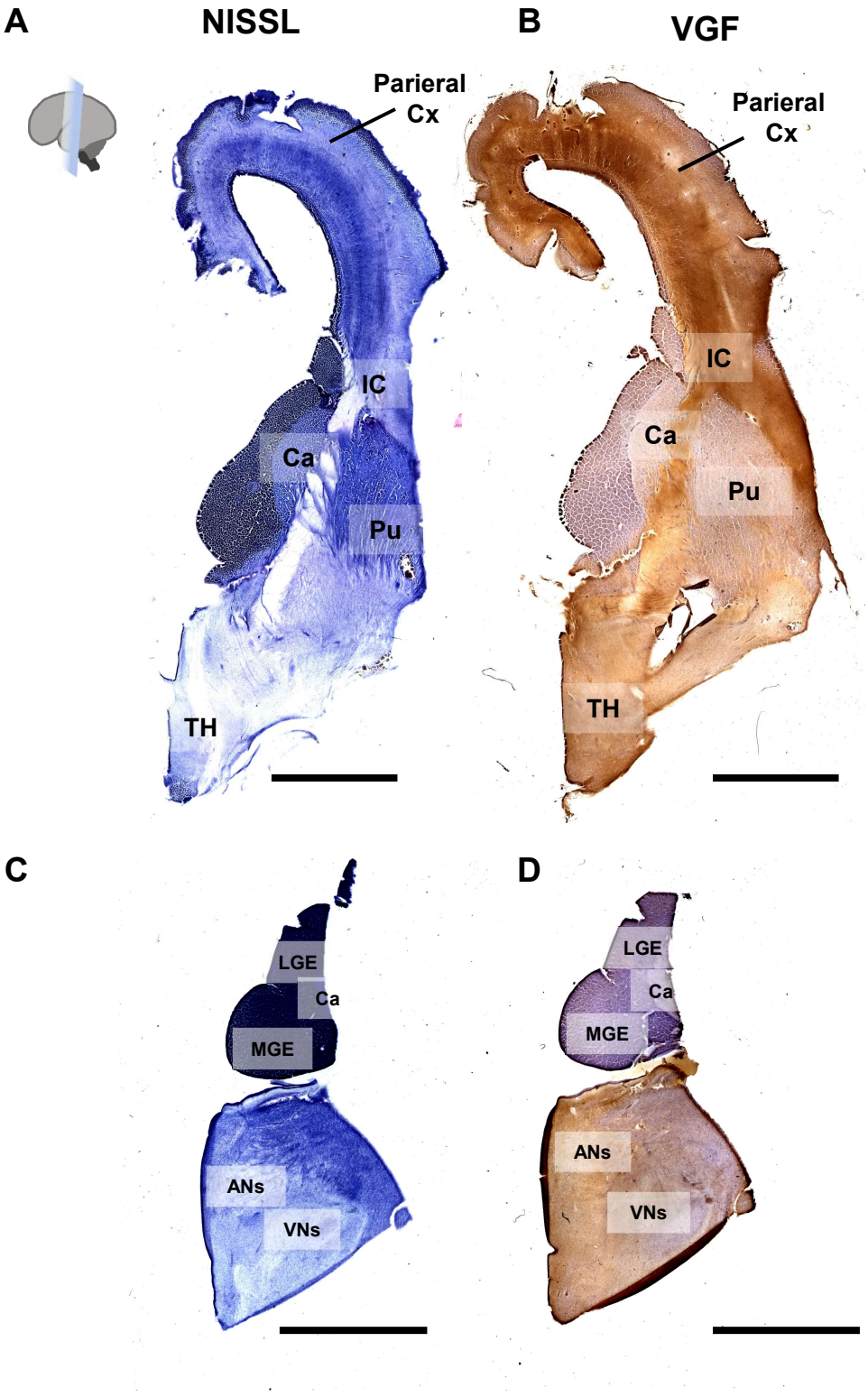

Figure 5.8: **Immunohistochemistry of VGF in human 16 PCW coronal brain sections.** (**A**) Nissl staining on serial section is used to highlight the cytoarchitecture. (**B**) shows a section containing both the parietal cortex and the thalamic region stained for VGF. (**C, D**) show a section with only the ganglionic eminences and the thalamic region. (**C**) The Nissl-stained slices shows a demarcation between anterior and ventral nuclei (ANs and VNs, respectively) of the thalamus, but a more detailed annotation is not possible in this section. (**D**) VGF is detected in the thalamic region, especially in the medial aspect. Scale bars = 5 mm.

Figure 5.9

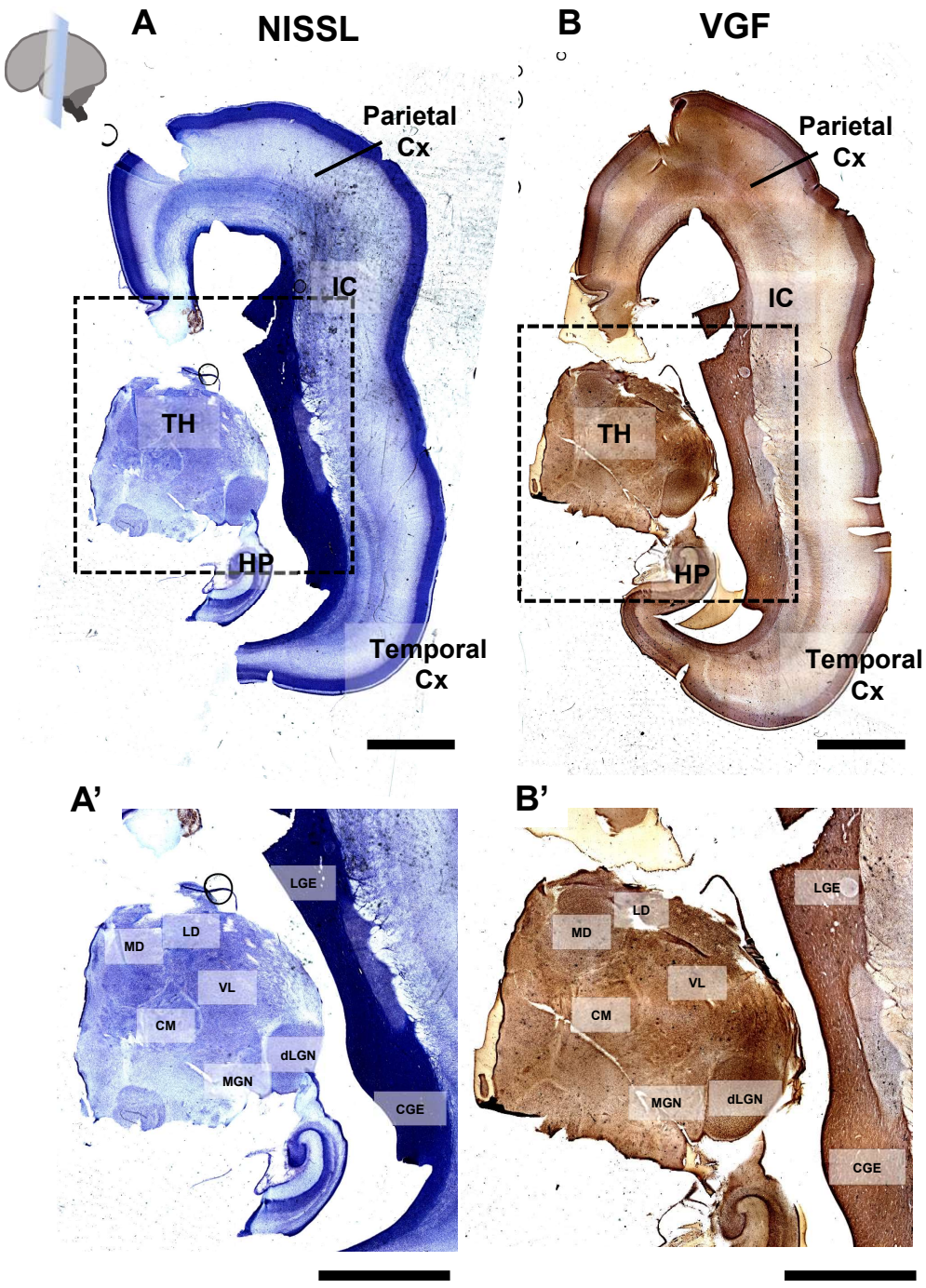

Figure 5.9: **Immunohistochemistry of VGF in human 17 PCW coronal brain sections.** (A) Nissl staining on serial section is used to highlight the cytoarchitecture. (**B**) shows a section containing both the parietal cortex and the thalamic region stained for VGF. (**A', B'**) show a zoomed image of the thalamic region indicated with a dashed line in A and B. Some of the thalamic nuclei can be annotated in B: lateral dorsal (LD), mediodorsal (MD), ventrolateral (VL), central medial (CM), dorsolateral geniculate nucleus (dLGN), medial geniculate nucleus (MGN). VGF immunoreactivity is detected in the thalamic region (B'), and its signal is particularly strong at the level of the visual dLGN and the associative MD. Scale bars = 5 mm.

Figure 5.10

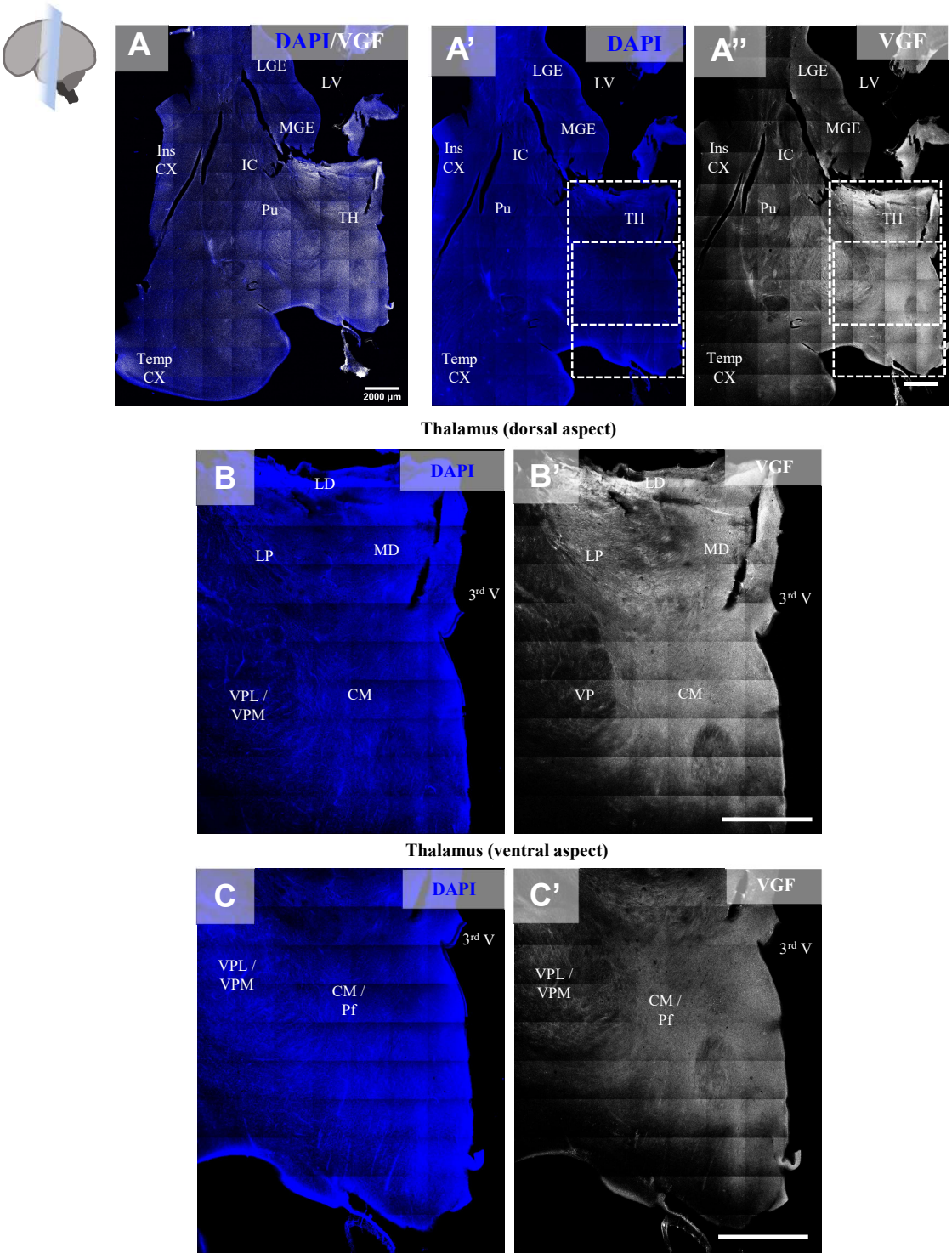

Figure 5.10: **Immunofluorescence staining for VGF in human 17 PCW coronal brain sections.** (**A-A''**) Confocal tiled scans of the 17 PCW coronal brain section where the main structures are revealed by DAPI nuclear staining (blue, A') and VGF signal is revealed in white (A''). Dashed-line boxes show the location where panels B-C' were taken.

(**B**) VGF immunoreactivity is detected in the dorsal thalamic region (**B'**), and it is particularly elevated in the associative mediodorsal nucleus (MD). (**C**) The ventral aspect of the thalamus also shows VGF-positive signal (**C'**), although less intense. Scale bars = 2 mm.

Overall, the data collected by immunohistochemistry confirmed the observation from the Western Blot analysis presented earlier, and corroborate the hypothesis that VGF is predominantly expressed by the thalamus during human brain development. The molecule is detected in the axons of thalamocortical projecting neurons within the internal capsule and intermediate zone of the developing neocortical areas. Interestingly, VGF is transported and eventually secreted in the germinal compartments of the frontal cortex at both 13 and 17 PCW. In more posterior sections, such as the parietal and temporal cortex, VGF is detected in the post-mitotic subplate, cortical plate, and marginal zones. Notably, thalamic expression of VGF begins in sensorial nuclei early during development, similar to what has been observed in rodent brains (Sato *et al.* 2012; Monko *et al.* 2022; Sato *et al.* 2022). However, by 17 PCW, VGF expression becomes prominently expressed in the associative MD of the thalamus. These findings highlight the dynamic expression pattern of VGF during human brain development and suggest a potential role for VGF in the communication between the thalamus and frontal cortex during early human brain development, that has not been previously reported in the rodent brain.

5.3 VGF detection in the human fetal cortex by Mass Spectrometry analysis

Unfortunately, neither western blot analysis nor immunohistochemistry are suitable techniques for detecting VGF-derived small peptides. In fact, on one hand antibodies against peptide sequences are also going to target the same sequence in the full length VGF protein; on the other hand, the extremely small size of the peptides makes it almost impossible to discern for their presence in classical protein separation by SDS-PAGE. For this reason, I performed a proteomic analysis of the human 20 PCW cortex by Mass Spectrometry analysis. The aim of this experiment was to further confirm the presence of VGF polyprotein in this sample (as previously shown in this Chapter by WB) and give an indication of which VGF-derived peptides are present and can be selected for further studies (i.e., functional validation).

To this aim, total protein content was extracted in Urea Buffer from the medial and lateral portion of the posterior temporal lobe of a 20 PCW (N=1) human fresh-frozen brain. The donor was previously labelled as "20 PCW #1" in this work. The protein extract was run separately for the two portions of the brain area collected, namely medial and lateral. However, these were considered as technical replicates rather than biological ones. Samples were analysed by Liquid Chromatography Tandem Mass Spectrometry (LC-MS/MS) by the Mass Spectrometry Research Facility (Chemistry Research Laboratory, University of Oxford).

Specifically, two runs of LC-MS/MS were performed for each sample. The first shorter run (2 hours long) was mainly used to assess the experimental approach and the validity of the dataset obtained. However, a second 3 hours-long experimental was additionally run to detect VGF by proteomics.

5.3.1 Evaluation of the quality and reliability of the proteomic dataset (Gene Ontology Enrichment Analysis)

The first trial was performed by a 2 hour-long LC run, with the main scope to assess the quality of the dataset obtained, and the general suitability of the sample to this experimental approach. Besides the technical parameters checked by the personnel in the facility, I evaluated the quality of the proteomic dataset obtained by performing **Gene Ontology Enrichment Analysis.**

Table Supplementary S1 shows the total number of terms for all the categories included that are significantly over-represented in the human fetal cortical dataset (p-value <0.001), while a Manhattan Plot shows these results for the three primary categories: Biological Process (BP), Cellular Compartments (CC), and Molecular Function (MF) (**Figure 5.11**). A more comprehensive overview is presented in **Figure 5.12**, which displays the top 15 most enriched terms for each category plotted based on their adjusted p-values.

Just by looking at the categories "TISSUES" it appears immediately clear that the sample analysed is from the human central nervous system (i.e. enriched terms including "Central nervous system", "Nervous system", "Brain", and "Head"). Similarly, for the category "DISEASES" the most over-represented terms are related to CNS pathologies, especially neurodegenerative diseases, as expected from the analysis of a cortical sample. Numerous terms also enriched in the dataset further indicate the fetal nature of the sample tested (i.e. "Nervous System Development", "Developmental disorders of mental health", "Specific Developmental Disorders") The most interesting over-represented terms in the context of this study are Brain-derived neurotrophic factor (BDNF) signalling pathway (WikiPathways), "Axon guidance" and "Vesicle-mediated transport" (Reactome Pathways). The overall outcome of this GO enrichment analysis is in line with the expected results from a proteomic survey of a human cortical sample, therefore I considered the datasets obtained by LC-MS/MS as solid and reliable for the purpose of the study.

Figure 5.11

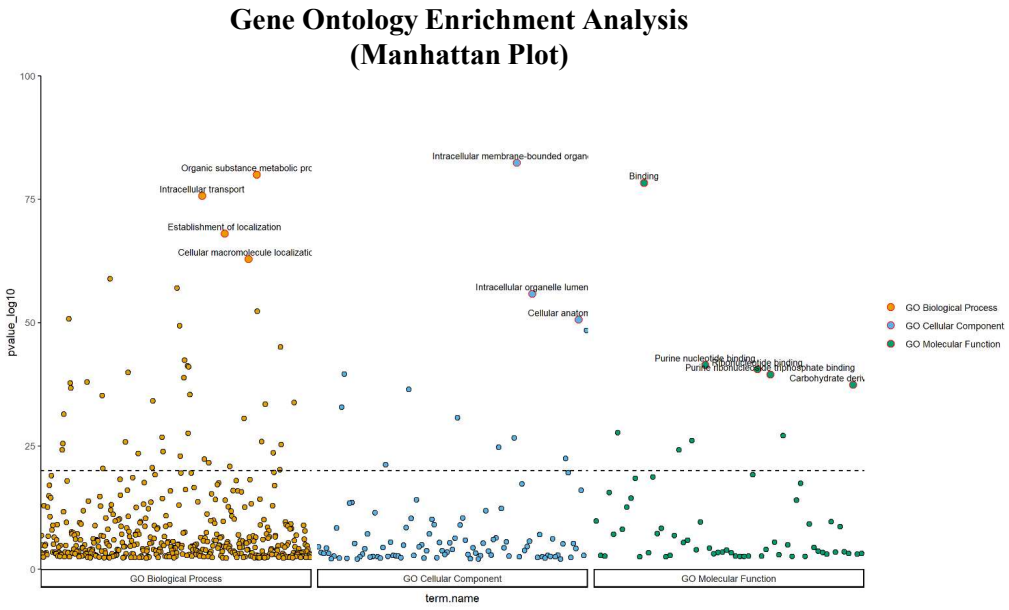

Figure 5.11: Manhattan plot showing Gene Ontology (GO) enrichment analysis of the proteomic survey in the human 20 PCW neocortex. The X-axis are the G.O. functional terms coloured by category. Each coloured dot represents a GO term. The most enriched terms in each category are labelled. The Y-axis are the adjusted -log10 p-values. Figure shows enrichment in the 20 PCW human brain dataset as compared to the human genome reference dataset. MF: Molecular Function; BP: Biological process; CC: Cellular component.

Figure 5.12

Gene Ontology Enrichment Analysis
(Top 15 Terms)

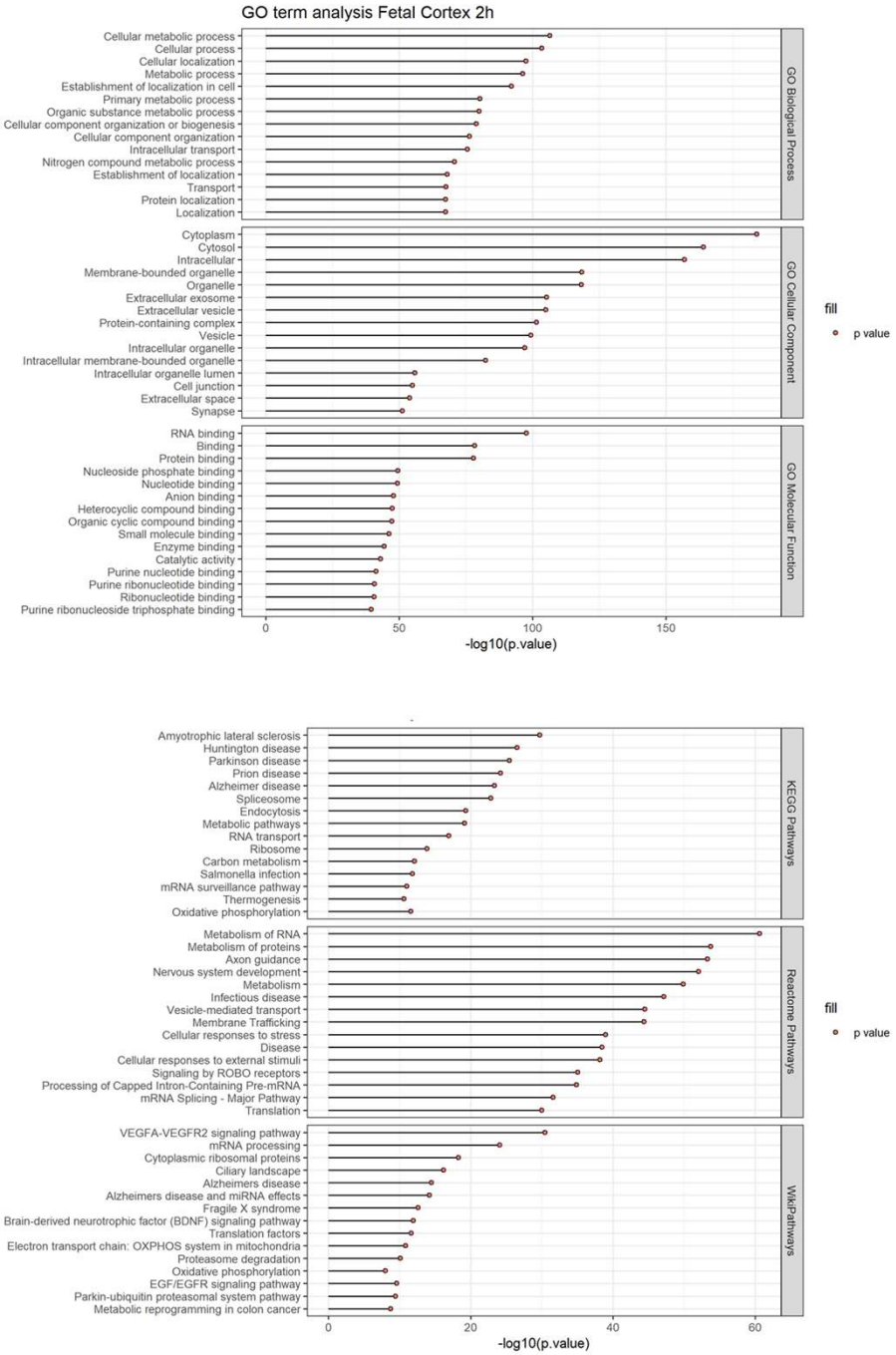

Figure 5.12

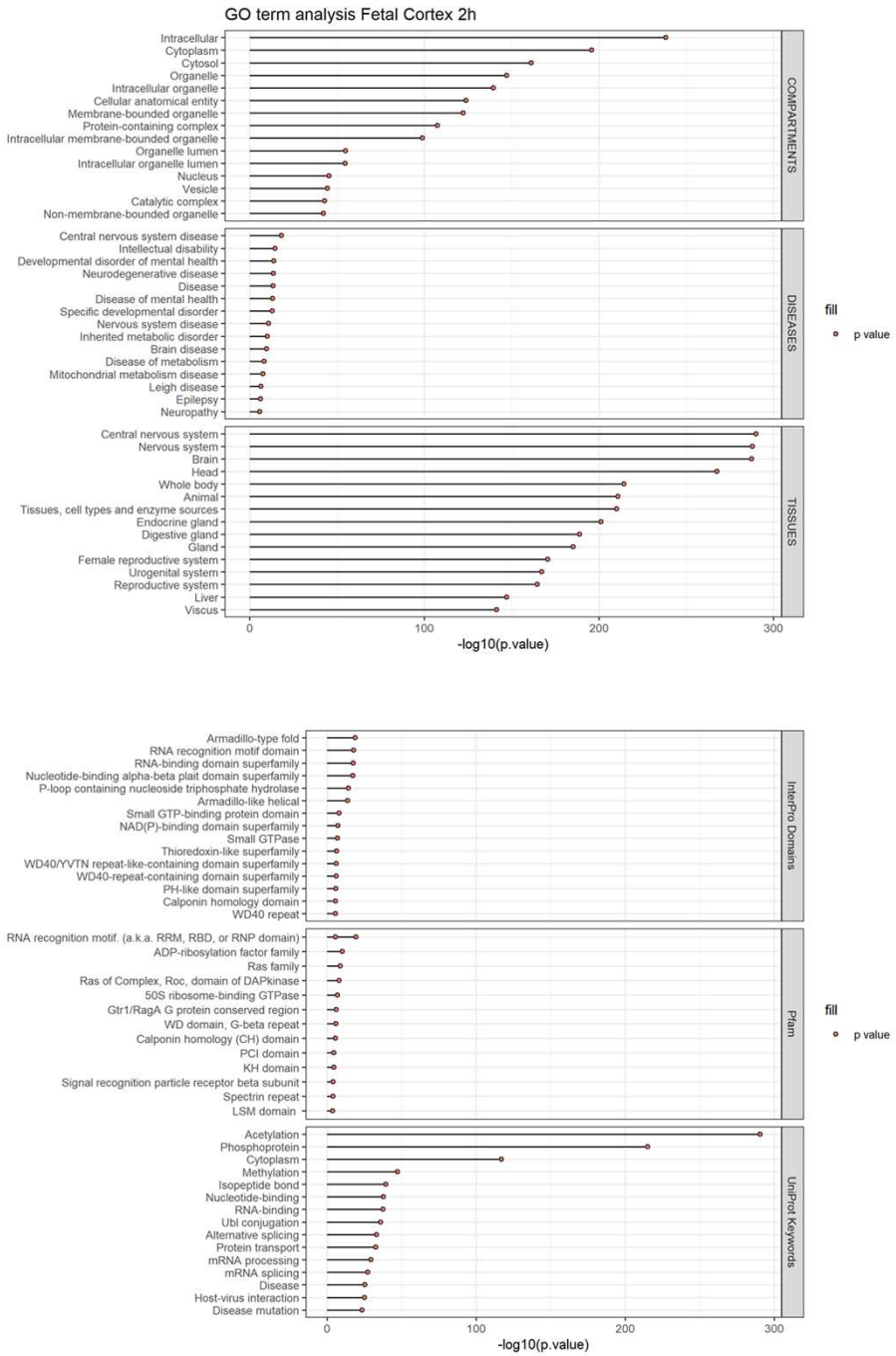

Figure 5.12: Representative plot of the 15-most over-represented terms for each category analysed by Gene Ontology Enrichment analysis. Term names for each category are listed in the y-axis according to their enrichment, according to the negative log10 of the adjusted p-value plotted in the x-axis.

5.3.1 Detection of VGF in the proteomic dataset of the human fetal cortex

Surprisingly, VGF was not detected in the first 2 hours-long liquid chromatography separation. The protein was only detected after separating the protein content in a 3-hour run of liquid chromatography. Furthermore, VGF was positively identified only in one of the two technical replicates included, although this is not reported as the donor was only one and no averaging was performed. Strikingly, VGF was identified by means of only one unique peptide mapping onto its amino acid sequence. This result is in contrast with previously published proteomic data on VGF in the adult human cortex. To compare the fetal and adult human cortex, I analysed the data from a similar experimental approach (single run of individual brain protein extract in LC-MS/MS) performed in cortical samples of adult healthy donors by Carlyle and collaborators (Carlyle *et al.* 2017). I selected only the cortical (Prefrontal Cortex, PFC; Primary Visual Cortex (V1C)) and thalamic (mediodorsal nucleus of the thalamus, MD) regions analysed in the adult brain, and reported the average number of unique peptides detected for VGF protein sequence. The adult thalamus was included even though I had no proteomic data on the fetal thalamus to compare with it (**Table 5.1)**. This confront highlighted two main points: VGF protein distribution is different in fetal and adult brains, and cortical VGF is abundant in the adult and in fact comparable to the thalamus.

The relatively low detection of VGF protein in the human fetal cortex suggests that this molecule does not derived from an extensive endogenous transcription at cortical level, but it is rather transported to it.

Taken together, these findings indicate that while VGF is detected in the human fetal cortex at 20 PCW, its presence is comparatively less abundant than in the mature adult cortex. These results suggest that VGF is primarily delivered to the fetal neocortex through extracortical regions, such as the thalamus, via axonal transport. However, in the adult brain, cortical cells themselves are responsible for the endogenous production of this factor, thus explaining the higher amount of it.

Table 5.1: **VGF detection by proteomic survey of the human fetal and adult brain.**

Brain Region (Fetal Human Brain)	**# Individual sampled**	**VGF peptides counts (average)**
Posterior Temporal Cortex (medial and lateral)	**1**	**1**
Brain Region (Adult Human Brain)	**# Individual sampled**	**VGF peptides counts (average)**
Dorsolateral Prefrontal Cortex (**DFC**)	11	12.3
Primary Visual Cortex (**V1C**)	10	7.0
Mediodorsal Thalamic Nucleus (**MD**)	10	10.6

(data on the adult brain from Carlyle et al., 2017)

CONCLUSIONS

The data presented in this Chapter demonstrate that VGF, despite being produced by projecting neurons of the thalamus (see Chapter 4), is detected at protein level throughout the human developing neocortex. A similar pattern of distribution can be described for VGF-interacting protein BDNF.

By using a variety of complementary techniques, I showed that VGF protein is present not only within the thalamic axons that actively transport this factor outside the region where it is transcribed, but is also present in most of the immature cortical areas of the human brain where it is transported and secreted. Notably, VGF protein is especially detected within the germinal compartments at both 13 and 17 PCW by immunohistochemistry. This finding further supports the hypothesis of a close interaction between thalamic axons and the cortical progenitor cells previously discuss in Chapter 3. Furthermore, it provides a possible mechanistic explanation of the extrinsic modulation exerted by the thalamus to the development of the human cortex by means of a direct tuning of cortical precursors via the paracrine molecule VGF.

Additionally, I showed that VGF production within the thalamus is not limited to the sensorial nuclei, as observed in the developing mouse brain (Sato *et al.* 2012; Monko *et al.* 2022; Sato *et al.* 2022). Instead, it is rather strong in the associative mediodorsal nucleus (MD), which has direct afferent projections to the prefrontal cortex. Consistent with this finding, the levels of VGF detected in the prefrontal cortex are particularly elevated. These observations suggest a potential role for VGF in the development and functional connectivity of the human prefrontal cortex, thus supporting the hypothesis of an evolutionary deployment of this factor from its original role in specifying the sensorial cortices to facilitating the development of more evolved regions of the human brain, such as the prefrontal cortex.

Finally, a proteomics survey of the 20 PCW human neocortex revealed that VGF protein, though detectable, are not as abundant as in the adult human cortex. This further confirms that VGF is developmentally regulated, and even though is known to be endogenously expressed by the cortical neurons in the adult human brain, at prenatal ages this factor is most likely only transported from other regions (such as the thalamus) to the immature neocortical areas.

DISCUSSION

Considerations on the Western Blot Analysis for VGF protein

- ***Technical and general considerations***

In the first analysis, I used Western Blot to detect protein levels in the same brain samples analysed at mRNA level by qPCR. VGF was detected as four different bands, the heaviest of which corresponding to the full-size protein. The other forms of VGF detected were considered as intermediate product of cleavage of this protein by proteases, similarly to what previously detected in other works in human brain samples (Busse *et al.* 2012; Quinn *et al.* 2023).

I chose to analyse the different forms of VGF separately for several reasons. Firstly, the only characterized form was the full-size VGF (75 kDa). The bands detected at lower molecular weights (ranging from 50 to 20 kDa) did not correspond to the characterized VGF peptides, that are typically smaller than 20 kDa, but rather represented intermediate form of VGF cleavage. On the other hand, however, it would have been inappropriate to quantify solely the full-size form of VGF. It is highly probable that VGF undergoes extensive processing, especially at the peak of neurogenesis (around 20 PCW) as its peptides are likely the primary functional forms of the protein. This is further discussed in the next Chapter in **Section 6.2** and relative discussion. Therefore, it was important to quantify and consider the overall representation of VGF during this critical period of cortical development, including its various forms. The significance of this dual quantification is exemplified by the case of the 20 PCW sample, especially sample #2. As shown in **Figure 5.3 D**, the full-length VGF form was not the most abundant proteoform detected in any of the brain areas considered. By focusing solely on the full-length form, I would have missed important data regarding the total amount of VGF detected and the overall maturation state of VGF (i.e., the proportion already depleted through enzymatic processing).

Furthermore, it is important to note that the **antibody used** in this study targeted a specific region of the C-terminus of the VGF protein. It was expected to yield multiple bands, as previously mentioned. While the authors of the 2011 study (Busse *et al.* 2012) claimed that N-terminus

antibodies might provide greater specificity for detecting the full length of the protein, my focus was primarily on the peptides generated from the C-terminus of VGF. This choice was driven by the fact that these C-terminus peptides have been more extensively linked to neuroactive functions, in contrast to the neuroendocrine roles associated with the N-terminus peptides (Lewis et al., 2015). Since the Western blot membranes (**Panel A** in **Figures 5.1-5.3**) revealed proteoforms that were detected using a C-terminal epitope of the VGF sequence, this indicates that these proteoforms retained the epitope and can be considered as intermediate forms in the cleavage process that ultimately generates the specific peptides. Therefore, in the context of this study, they were included in the quantification and plotted as both the total VGF signal and as relative percentages (**Panel C, D** in **Figures 5.1-5.3** and **Panels B-D** in **Supplementary Figure S9**) to capture the relevant information.

Another important consideration must be made regarding the inter-individual variability observed, particularly when comparing the two samples from the same age (20 PCW sample #1 and #2) with each other (**Figures 5.2 and 5.3**). In fact, this may be attributed to technical variability rather than biological variability. The brains were microdissected separately and using different methods, with the sample labelled as 20 PCW #2 being utilized for other experimental analyses. This technical variability could account for at least a portion of the observed differences between the two brains. Due to these factors, it was deemed inappropriate to directly compare the two samples. However, the 13 PCW and 20 PCW #1 brains underwent a more similar microdissection process, making them suitable for a direct age comparison, as outlined in Section 5.2.

- ***Considerations on biological relevant results of VGF protein distribution***

As shown in **Panel B** of **Figures 5.1-5.3**, lower levels of full-length VGF were detected in the thalamus as compared to the neocortical areas. This could be due to a more intense **enzymatic processing of VGF within the thalamus** leading to a decrease in its pro-protein form. Alternatively, it can be explained by a significant deployment of this molecule from the soma of thalamic cells to axonal terminals, where it is actively transported to thalamic cortical targets and more abundantly

detected. The latter explanation appears more plausible, particularly considering that a similar pattern is also observed when considering the sum of all intermediate VGF proteoforms, rather than just the full-length precursor (**Panel C** in **Figures 5.1-5.3**). This suggests that VGF primarily functions as a paracrine molecule rather than an autocrine factor involved in thalamic development. This is consistent with the characteristics of secretogranins, which are produced in the endoplasmic reticulum to be inserted in secretory vesicles that are carried to distal targets via axonal transport (Bartolomucci *et al.* 2011).

Interestingly, the same observation can be done for the neocortical areas, where VGF generally follows the **same pattern** when considering either the full-size protein, or the sum of its proteoforms (**Panels B, D** in **Figures 5.1-5.3**). The notable difference between these two quantifications was the relative proportion of intermediate forms detected, as illustrated in Panel D of Figures 5.1-5.3. Differences in electrophoresis runs and signal acquisition affect quantification, make direct comparison between different gels technically incorrect. To address this, I utilized a "common normalizing sample" which was loaded in two gels and calculated a ratio to compare VGF levels between ages. The normalized data across ages (one 13 PCW and one 20 PCW brain) are presented in **Supplementary Figure S9**, and generally validate these observations. In fact, the different proportion of intermediate VGF forms becomes even more evident in this direct comparison between the two age groups (see **Supplementary Figure S9 B, D**), indicating that if VGF does undergo more extensive processing during development, this process is likely consistent across brain regions of the same age. However, as the analysis lack statistical evaluation, this observation is limited to the description of the general trend depicted in all the graphs presented.

Altogether, the data presented in this Chapter regarding the uncharacterized intermediate forms of human VGF protein might be interesting to re-analyse in future studies that aim to focus specifically on the characterization of the enzymatic processing of VGF by known and newly-identified VGF proteases. This aspect is further explored and discussed in the following Chapter.

Considerations on the immunohistochemistry Analysis for VGF protein

To further confirm that VGF protein is transported from the thalamus to the cortex, and gaining further insights on sub-regional spatial distribution of the protein within the cortex – lacking in Western Blot analyses - I used immunohistochemistry and showed that VGF is specifically detected in the axons traveling through the intermediate zone (IZ) at cortical level (**Figures 5.7-5.11**).

Notably, while the medial thalamus does not appear to produce VGF in the earliest developmental stage analysed (10 PCW) (**Figure 5.5 B**), the axons originating from the more posterior portion of the thalamus, where VGF is detected (**Figure 5.5 D**), could travel in a ventro-lateral direction to form the IC and subsequently reach the cortical areas located in the medial coronal plane sampled in **Figure 5.5 A, B**. This would explain the observed presence of VGF in the IC/IZ, considering that this protein is not endogenously expressed in the cortex at this age (see Chapter 4).

An intriguing aspect that emerged from the immunohistochemical analysis is the remarkable abundance of VGF protein detected in the frontal cortex at both 13 and 17 PCW (**Figures 5.6 and 5.7**). Notably, in the frontal cortex, the VGF-positive signal exhibited pronounced intensity within the germinal compartments, specifically the subventricular zone (SVZ) at 13 PCW (**Figure 5.6 B'**) and its subsequent sub-compartment, the outer subventricular zone (OSVZ), at 17 PCW (**Figure 5.7 B'**). Conversely, at the level of the parietal and temporal cortices sampled in more posterior sections (**Figures 5.8 and 5.9**), VGF is also detected in the post-mitotic subplate, cortical plate, and marginal zones. Furthermore, the peculiar pattern organized into radially-oriented "palisades" in the frontal areas suggests that the signal is either detected within axonal collaterals of the thalamic afferents invading the germinal compartments, a human-specific phenomenon previously described in Chapter 3 Section 3.2, or originates from secreted VGF accumulating at the level of the radial processes of the oRGC populating the compartment. In either cases, the results from this analysis suggests an especially strong influence played by thalamic VGF in the germinal compartments of the frontal areas, as compared to previously reported parietal and temporal cortices.

Additionally, immunohistochemistry allowed for the confirmation of VGF protein production at the **thalamic level**, thereby validating the transcriptomic data. Strikingly, the start of the thalamic

VGF expression is in sensorial nuclei, similarly as observed in rodent brain (Sato *et al.* 2012; Monko *et al.* 2022; Sato *et al.* 2022), however it appears highly present in the **associative MD** nucleus by 17 PCW, in line with the mRNA data collected from the LMD microarrays (see **Figure 4.5 and 4.6**), and contrasting previous literature in the developing mouse brain (Sato *et al.* 2012; Sato *et al.* 2022). Both observations support the hypothesis, already proposed and discussed in the previous chapter, of a potential role for VGF in the development and functional connectivity of the human prefrontal cortex, whereby VGF might have undergone an evolutionary repurposing to sustain the development and maturation of associative prefrontal areas in human.

Interestingly, strong VGF-immunoreactivity was detected at the level of the two ganglionic eminences (lateral and medial, LGE and MGE respectively) in this section of the 17 PCW brain **(Figure 5.8**). This was not detected at earlier stages (**Figure 5.5**), where the ganglionic eminences appear strongly counterstained with haematoxylin but were negative for GAP43 and VGF. The expression of VGF in the GEs appears to be transient and potentially not endogenous, as no evidence of endogenous VGF expression by GEs was found in the literature or available datasets (USCS Cell Browser, not shown). It is important to note that the thalamus projects not only to the cortex but also to various other brain structures, including the GEs. Consequently, any paracrine molecule transported and secreted at the cortical level might simultaneously affect these structures. GEs are recognized transient targets of both thalamocortical axons (TCA) and corticothalamic axons (CTA) en route to their final destination (Metin *et al.* 1996). Therefore, it is possible that the first bundle of axons can release VGF not only in the cortex, as observed in this study, but also at the level of this intermediate structure they reach. While this occurrence may not impact my working hypothesis, it highlights those fibres seemingly originating in the dorsal thalamus pause when reaching the GE, acting as a potential cellular guidepost, as demonstrated by (Ulfig 2000). The GEs, on the other hand, do not project directly to the cortex. Thus, even if VGF expression was endogenous, despites the evidence suggesting otherwise, it is unlikely that VGF produced at this level is transported to the cortex to act as a paracrine GE-derived factor. While it would be interesting to explore the potential role of VGF in the development of these structures beyond the scope of this thesis, it is unlikely that

VGF acts as a paracrine molecule transported from GEs all the way to the cortex. Consequently, the presence of VGF at the level of the GEs is not considered a direct contradiction to my working hypothesis.

Alternatively, the observed expression patterns of VGF in GEs could potentially be attributed to artefacts resulting from the staining technique and the thickness of the stained slices. GEs often present as cell-dense regions where immunoreactive background signals tend to concentrate, a phenomenon even evident in a 10-µm thin slice counterstained by haematoxylin (**Figure 5.5)**. The samples depicted in **Figures 5.6-5.10** were cut at 100 µm thickness, making it difficult to avoid such background interference, particularly when utilizing a DAB-based immunohistochemistry reaction.

Considerations on the proteomic dataset

A final comment is necessary regarding the proteomic dataset analysed in **Section 5.3**. To perform Gene Ontology Enrichment analysis, all the proteins present in the dataset were compared to the complete human genome as a background dataset to evaluate relative enrichment. My analysis did not involve comparing experimental (e.g., treated/diseased) samples to control (e.g., untreated/healthy) samples, but rather focused on exploring the protein content of the neocortical fetal sample as an initial step to identify interesting and relatively abundant proteins of interest. Therefore, it was considered appropriate to use the entire human genome as the background gene set for enrichment analysis. The GO Enrichment analysis was only used to evaluate the overall quality of the dataset, rather than identifying relevant and/or enriched pathways present in the sample. For the latter, it would be more appropriate to use the healthy adult human brain as a background reference. This is because when comparing fetal cortical tissue to the entire human genome, the comparison may lead to an overestimation of naturally enriched pathways in the developing brain, such as synaptic functions, cell signalling, neurotransmission, originating from a general enrichment of such terms in the brain, rather than a biologically-relevant enrichment of these terms in the sample under consideration.

CHAPTER 6

VGF functional effects and peptidases prediction

INTRODUCTION

To investigate the potential role of VGF, and its neuroactive peptides, I employed two different experimental approaches that I describe in detail in this Chapter.

On the first part, I present a pilot functional study, where recombinant human VGF protein was applied to two different *in vitro* models of human cortical neurogenesis. For the first model, I used a 2D iPSC-derived cortical cell culture, and for the second a 3D organotypic cortical slice culture obtained from 13 PCW human fetal brains. First, I evaluate the effects of different doses of recombinant VGF on the proliferative rates of human cortical precursor cells in the 2D cultures. However, no significant effect was observed. Afterwards, I employed organotypic cortical cultures to assess whether VGF influences the spontaneous activity of subplate neurons, which are a known early target of thalamic axons as described in Chapter 3. Before using this *in vitro* model, I had to assess whether it was suitable for the purpose of my study. To do so, I evaluated the presence, distribution, and secretion of VGF protein in the slices in culture. I confirmed that VGF distribution resembles the pattern observed in the human fetal brain described in the previous Chapter 5. Significantly, the secretion of this molecule in the culture media is minimal, as assessed by ELISA test, and thus it can be disregarded as a potential cause of any observed effects resulting from recombinant VGF treatment. Finally, I treated a few samples from a 13 PCW human brain (frontal lobe) with a high dose of recombinant VGF for 4.5 days, and I measured the spontaneous activity of subplate neurons by used calcium imaging. The preliminary results suggest that VGF can increase the spontaneous activity of subplate neurons, as both the size and frequency of spontaneous calcium waves generated in those neurons appear significantly greater upon treatment of the slices with the

recombinant protein (collaboration with Dr. Gavin Clowry and Dr. Faye McLeod, Faculty of Medical Sciences, Newcastle University).

On the second part of the Chapter, I attempted to predict the proteases that might be responsible for the cleavage of VGF into functionally active peptides. Many physiological functions attributed to VGF have been associated to its neuroactive peptides rather than the full-size protein. To this aim, I used a bioinformatic approach for predicting the enzymes that can cut VGF according to its amino acid sequence, and I then investigated the expression pattern of some selected proteases from the output prediction by transcriptomic analysis and experimental validation in the human tissue. My analysis indicates that the expression pattern of VGF proteases differs and might be indicative of different VGF peptides produced. This might underly the variety of effects that VGF is responsible for, as well as its ability to modulate the physiology of different cell population in a paracrine manner.

6.1 Functional validation of VGF in *in vitro* models

To validate VGF as a thalamic modulator of human cortical development, I aimed to test the potential effect(s) of VGF on the two main cortical cell populations identified as targets of the earliest thalamocortical afferents reaching the cortex in human, namely subplate post-mitotic neurons and OSVZ mitotic progenitors.

As functional manipulation is not possible in fixed post-mortem human brains, I employed two distinct and complementary approaches to model human cortical development:

1. 2D *in vitro* cultures of human iPSC-derived cortical cells
2. 3D *in vitro* cultures of human organotypic cortical slices

In both scenarios, thalamic VGF can be replaced by the recombinant human protein, which can be applied to treat both *in vitro* systems to evaluate potential effects (**Figure 6.1**). Furthermore, this approach enables the investigation of cell-specific effects of VGF in the two population of cortical cells under study. On the one hand, iPSC-derived cell cultures can be treated at various selected times of the differentiation protocol, when cells mostly resemble either the precursors (day 0 – day 3 *in vitro*) or the post-mitotic state (day 4 onwards) (**Figure 6.1 A**). This allows for modelling the effects of VGF on OSVZ progenitors or subplate neurons, although the iPSC-derived cell cultures cannot fully replicate the characteristics of neither of these specific cell populations. On the other hand, a similar approach can be employed to treat organotypic cortical slices derived from human mid-gestation brains (**Figure 6.1 B**). This system provides a more physiological and realistic representation of human cortical development, and it includes *bona fide* subplate neurons and OSVZ progenitors simultaneously. However, this approach requires infrastructure in place to obtain and process suitable human donor specimen.

In the following paragraphs, I will describe the results obtained by VGF treatment of cortical progenitors in the iPSC-derived cultures, and of subplate neurons in the organotypic slices.

Figure 6.1

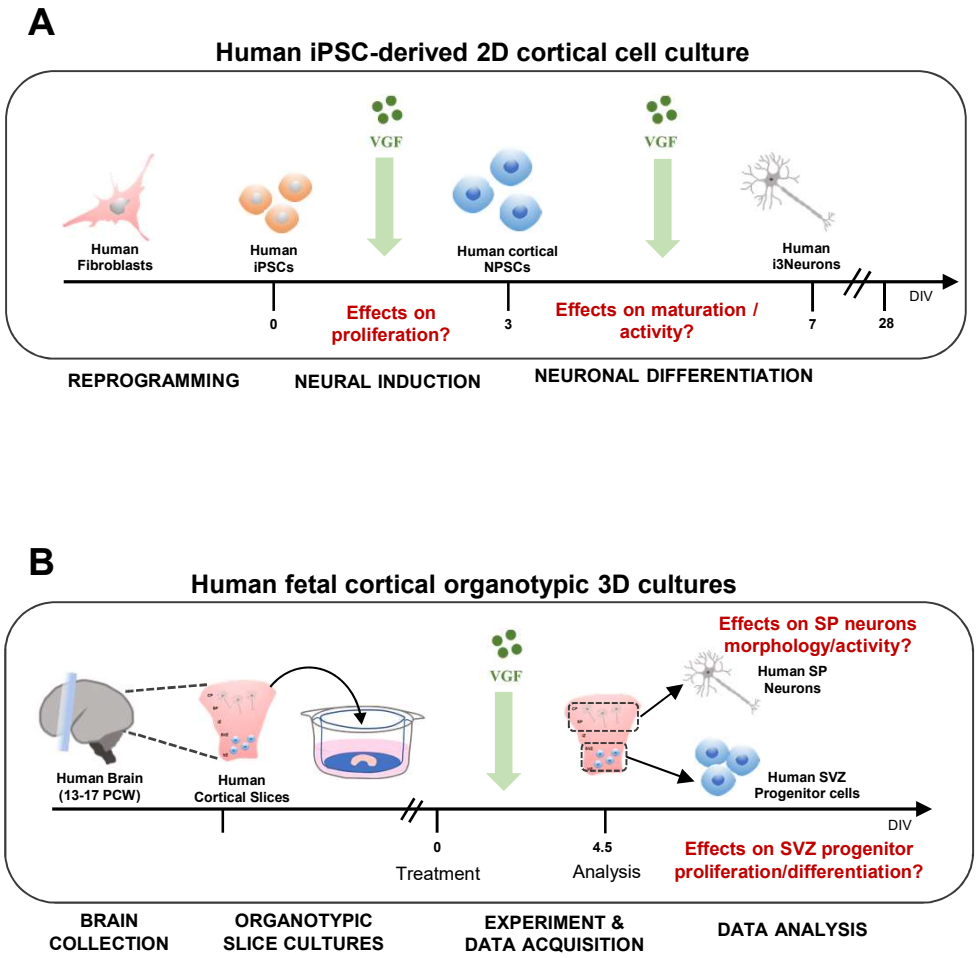

Figure 6.1: Schematic representation of the approach for the validation of VGF functional effect(s) in in vitro models of the human developing cortex. (**A**) Experimental design employing 2D cultures of human iPSC-derived cortical progenitors (day 0-3) and neurons (from day 4). Application of recombinant VGF at different timepoint of the protocol can provide an indication of any effects at the level of either cell populations. (**B**) Experimental design employing 3D cultures of human organotypic cortical slices obtained from mid-gestation brain samples. Application of recombinant VGF onto these cultures can simultaneously provide an indication of any effects at the level of *bona fide* SP neurons and OSVZ progenitors.

6.1.1 Effects of VGF application in iPSC-derived cortical cells *in vitro*

Firstly, I attempted a preliminary functional validation of VGF in a 2D human iPSC-derived cortical cell cultures. Although neither subplate neurons nor OSVZ progenitors are clearly and specifically distinguishable in these cultures, this model might be complementary to the organotypic cultures. In fact, cortical induction and differentiation of iPSC-derived neural progenitors can be considered as a simplistic model of human cortical neurogenesis. Furthermore, 2D iPSC-derived cell cultures allowed me to partly encompass the technical limitations imposed by organotypic cortical slices, such as the restricted availability of the samples, homogeneity of cortical slice samples, and overall replicability of the experiments.

Specifically, I tested three different doses of VGF: a high dose (1,200 ng/ml), a medium dose (120 ng/ml), and a low dose (12 ng/ml). Untreated control was included in the experiments. The dosage was chosen by checking previous studies using a similar approach, and more specifically to be consistent with recombinant VGF treatment of mouse organotypic slices described by Sato and collaborators (Sato *et al*, 2012). This approach would have allowed me to assess a dose-dependency of any effects observed by treating these cultures with recombinant VGF, and eventually set the minimum amount of extrinsic VGF required to obtain it. All the experiments described in this section have been done in collaboration with Dr. Becky Carlyle (DPAG, Oxford) and Laura Pearson (Visiting undergraduate student from the University of Manchester).

VGF was administered throughout the entire process of neural induction, spanning from day 0 to day 3 (**Figure 6.2 A**). During this critical timeframe, reprogrammed pluripotent stem cells undergo neural fate acquisition while retaining their proliferative capacity. Subsequently, cell division ceases, rendering them no longer "precursor cells" in the traditional sense, and thus assessing mitotic rates becomes irrelevant beyond day 3 in this protocol. The initial cell density at day 0 was determined by classic counting cellular nuclei upon plating the iPSCs to initiate the induction protocol. Following 3 days of VGF treatment, DAPI nuclear counts were conducted using Harmony high-content imaging and analysis software. The difference in cell numbers between day 3 and day 0 can be attributed to mitotic divisions that occurred within this time window, and thus representing an indication of the

proliferative rates during the cells' "progenitor state" in the *in vitro* system. The experiment was performed in replicates (N=3 wells for each experimental condition). Cells were plated at a density of 10,000 cells/well in a half-area 96-well plate. However, the results presented were obtained from only one pilot experiment, that was conducted as an exploratory screening of potential effects of VGF on cortical precursors.

I performed a comparative analysis of the mitotic rates between human induced neural progenitor cells (NPCs) treated with VGF and those left untreated. Additionally, different doses of VGF treatment were compared against each other. All comparisons were subjected to the One-Way ANOVA test, with a significance threshold set at $p < 0.05$. The results, as depicted in the plot presented in **Figure 6.2 B,** indicate that there were no significant changes in the proliferative rates of NPCs when treated with VGF, regardless of the dosage administered. Representative fluorescence images were captured from randomly selected regions within the wells for each condition, and no discernible differences were observed, further supporting the obtained results (**Figure 6.2 C**).

Figure 6.2

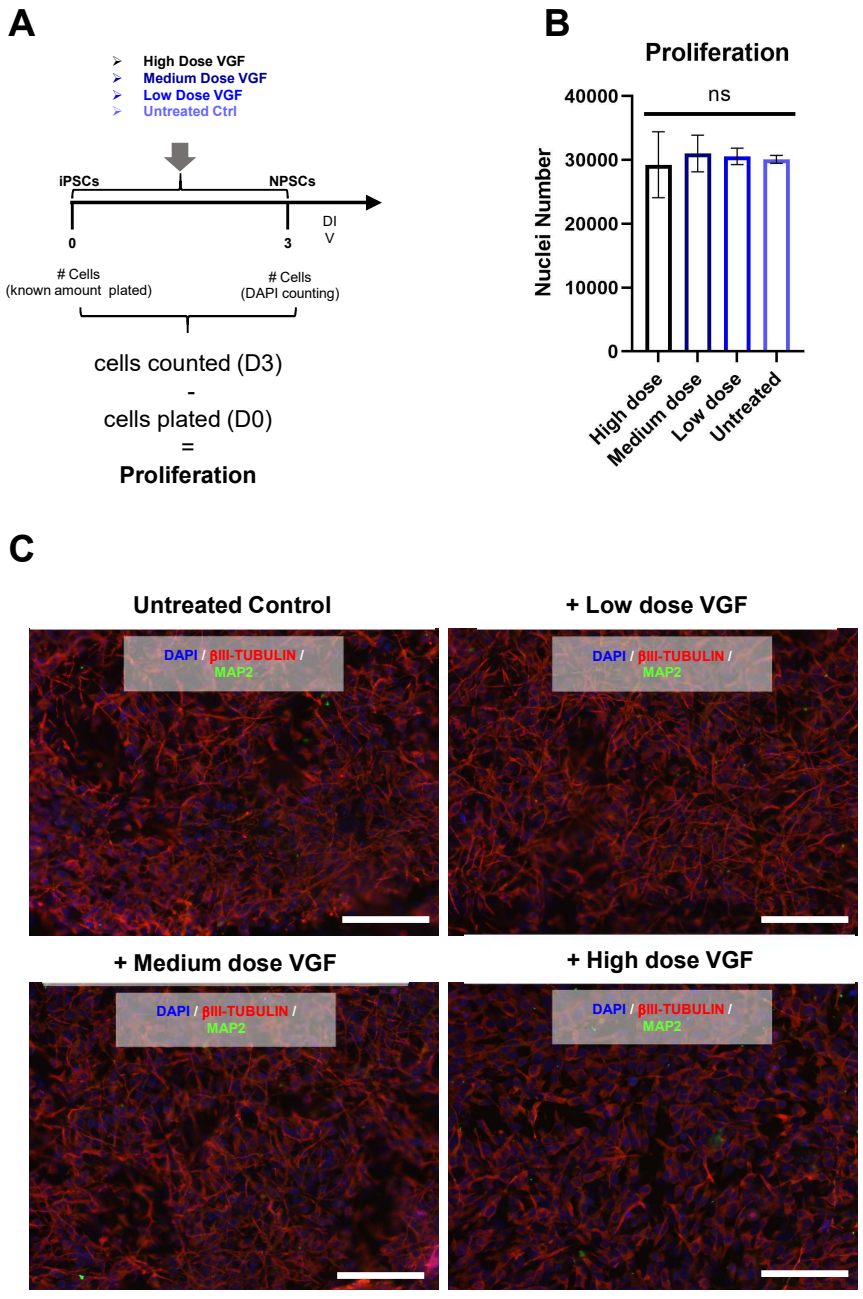

Figure 6.2: Effects of VGF treatment in iPSC-derived human cortical progenitors in vitro. (**A**) Schematics of the experimental design. (**B**) Results of the analysis of mitotic rate in the induced-NPC show no significant difference among experimental conditions. One-Way ANOVA test, p-value <0.05. (**C**) Representative fluorescence images of the iPSC-derived NPC at day 3 of induction protocol and stained for neuronal markers MAP2 and βIII-tubulin, and counterstained by DAPI. No obvious differences are observed in the density of DAPI-positive nuclei in the four experimental conditions analysed. Scale bar= 100 µm.

6.1.1 Effects of VGF application in cortical organotypic slices from human fetal brain

Organotypic cortical cultures were obtained by human mid-gestational fetal brain (13-17 PCW). This protocol has been optimized by Dr. Faye McLeod in Newcastle University, who collaborated with me for all the experiments described in this section. The protocol for obtaining and maintaining human fetal cortical slices *in vitro* has been described in detail in previous publications (McLeod *et al.* 2023). Importantly, this *in vitro* system can model human cortical development in a reliable and physiological manner, as the slices maintain the complex cytoarchitecture of the human neocortex, the specific cell populations present within each cortical layer, and their biological activity over several weeks in culture (McLeod *et al.* 2023). Importantly, these organotypic slices contain the cortical cell populations targeted by the early thalamocortical axons, namely the subplate neurons and the OSVZ progenitors. For this reason, I considered appropriate to employ this system as a physiological functional model of the human developing cortex in this study to assess the effect(s) of exogeneous VGF.

The experimental design I choose to adopt to test VGF activity on cortical cells is the application of the recombinant human protein in the culture medium for a brief time (4.5 days *in vitro*).

6.1.2.1 Preliminary evaluation of the model

Before performing any experimental analysis, I had to evaluate whether the organotypic cortical slices were indeed a suitable model for the research questions I aimed to investigate. Even though they have been well characterized and previously tested (McLeod *et al.* 2023), endogenous expression and secretion of VGF was not examined, making it crucial to assess these aspects within this context prior to treating the slices with the recombinant protein. To this purpose, I carried out similar analyses previously performed in the *post-mortem* human tissue, to compare the *in vitro* system with the human fetal brain. Specifically, I used immunofluorescence staining for VGF to assess whether the protein distribution in the cortical slices *in vitro* resembles the pattern observed

in the *post-mortem* cortical slices (described in Chapter 5). Similarly, I used Western Blot analysis to quantify VGF in the cortical slices over time in culture (up to 4 weeks *in vitro*), to compare it with VGF protein levels previously analysed by the same technique in *post-mortem* tissue. In addition, I used ELISA test to evaluate the endogenous secretion of VGF in the culture media, to assess a baseline before proceeding with the exogenous application of this growth factor *in vitro*.

Immunofluorescence staining

First, I performed immunohistochemical evaluation of VGF protein in organotypic cortical slices obtained from 14 and 17 PCW human frontal cortex fixed for staining straight upon brain collection (0 days in culture). I compare the results with the data collected in the *post-mortem* fixed tissue at similar ages, described in Chapter 5. In line with my previous results, VGF is detected at the level of the cortical intermediate zone (IZ) at both developmental ages (**Figure 6.3**).

At 14 PCW (**Figure 6.3 A**), the signal overlaps with the germinal zones, extending throughout the entire subventricular zone (SVZ). This observation closely aligns with the findings described in the fixed frontal cortex at 13 PCW (see **Figure 5.8**).

At 17 PCW, VGF is clearly observed in the axons departing from the transversal path and innervating the OSVZ below at 17 PCW (**Figure 6.3 C**). A comparable "palisade" pattern was observed in the frontal cortex at 17 PCW (see **Figure 5.9**), thereby confirming the authenticity of this evidence. This further confirms not only the expression pattern of VGF, but also the innervation of the germinal compartments at 17 PCW in human.

Figure 6.3

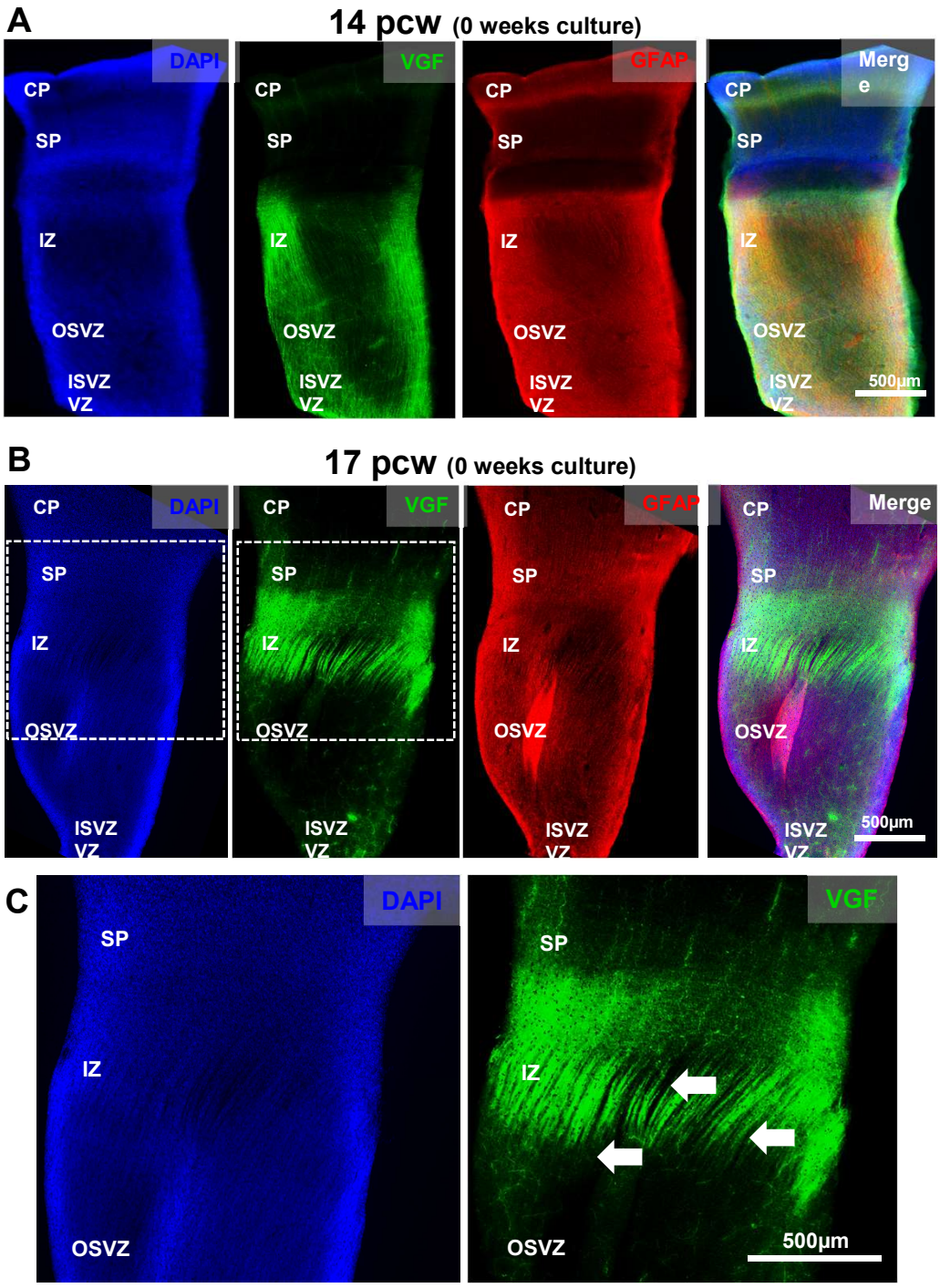

Figure 6.3: **Immunofluorescence images of VGF (green) and radial glial cell marker GFAP (red) in human organotypic cortical slices from a 14 and 17 PCW human brains that were fixed immediately after collection and sectioning.** (**A**) VGF protein is detected throughout the intermediate zone where thalamic axon terminals are still present after severing to obtain the cortical slices. The signal is also detected throughout the progenitor compartments (SVZ and VZ) at this age. GFAP (red) highlights RGC population and their radially-oriented processes spanning the entirety of cortical depth. (**B**) At 17 PCW, VGF protein distribution is more restricted and is detected in the IZ and the OSVZ. The latter compartment is easily identified by this age. (**C**) Zoomed-in of the area delimited by a dashed box in (B) and highlighting the peculiar radial organization of VGF-positive fibres (white arrows). All slices are counterstained by nuclear DAPI (blue). Both cortical slices have been fixed for staining on the day of brain collection (0 weeks in culture). Scale bars = 500 µm.

Western Blot Analysis

As previously described in Chapter 4 and 5, VGF is not endogenously expressed by cortical cells in substantial amount, and the protein detected in the cortical region is thus transported to it through axonal terminals from other brain regions, such as the thalamus via the thalamocortical afferents. However, during the initial acquisition and cultivation of organotypic slices, the thalamic axons that reach the cortical territory are severed, resulting in the absence of additional exogenous growth factors during the *in vitro* culture period. To assess for the presence of VGF protein over time in culture, I analysed total protein content from slices obtained from a 17 PCW brain and cultured for a month. Specifically, extractions were made after 2, 3 and 4 weeks, starting from the day the brain was first dissected (week 0). Data have been averaged by time-point (errors are not calculated due to the small sample size of N=2). The results of the densiometric quantification of VGF is presented in **Figure 6.4**. For simplicity, I focused on the total protein as measured by summing together the 4 proteoforms detected in the blot (**Figures 6.4 A-B**). Relative contribution to this sum is shown as absolute values in **Figure 6.4 C**, and relative percentages in **Figure 6.4 D**.

Interestingly, the amount of VGF protein detected at the beginning of the culturing protocol did not appear to drastically change over time in culture, as shown by the representative blot (**Figure 6.4 A**) and the correspondent densiometric quantification of the signal (**Figure 6.4 B-D**). Each WB band has been labelled according to the names used in Chapter 5 (**Section 5.1**) for consistency. Notably, the relative percentage of full-size VGF is low, and the most represented form of the protein at this time-point seems to be the "mid_1" intermediate form (**Figure 6.4 D**). This resembles more closely the results obtained in the 20 PCW brain samples analysed in Chapter 5, rather than the younger brain from the 13 PCW donor, thus supporting the hypothesis that VGF is subject to a more extensive enzymatic cleavage over time of development and the progression of cortical neurogenesis.

As the thalamic regions are resected from the cortex before culturing, the thalamic axons do not receive any new VGF-loaded vesicle from the neuronal soma located in the thalamus. Instead, they retain their original content, and potentially new locally translated VGF, within their terminals in the cortex over a month in culture. VGF reservoirs are not depleted, as synaptic activity is substantially

reduced in the cortical slices due to the removal of their synaptic partners during culture procedure. The small amount of VGF subject to release in the media might also be endogenously restored by cortical cells due to BDNF (Brain Derived Neurotrophic Factor) being added in the culture media (see Material and Methods, Chapter 2).

Figure 6.4

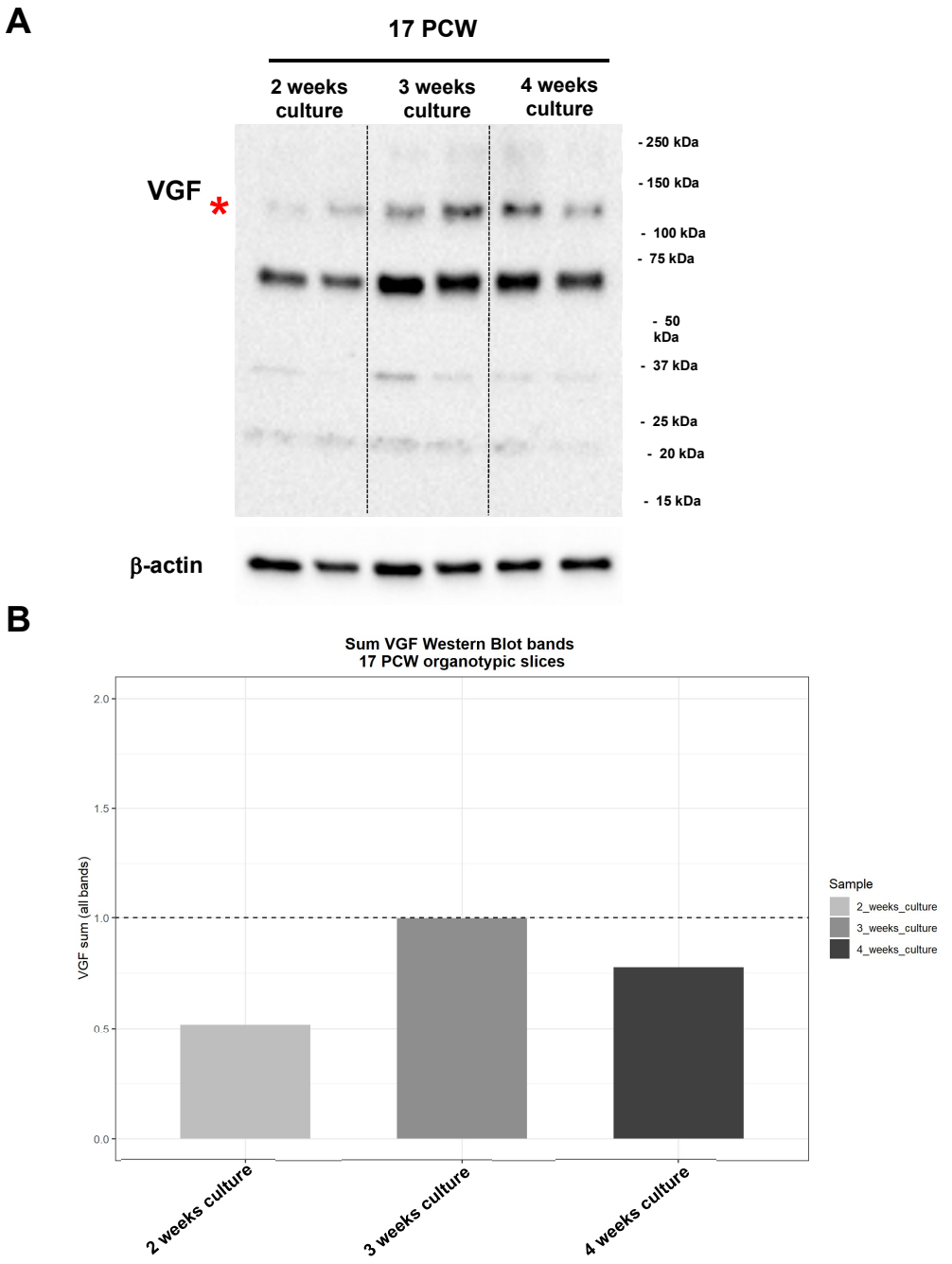

Figure 6.4

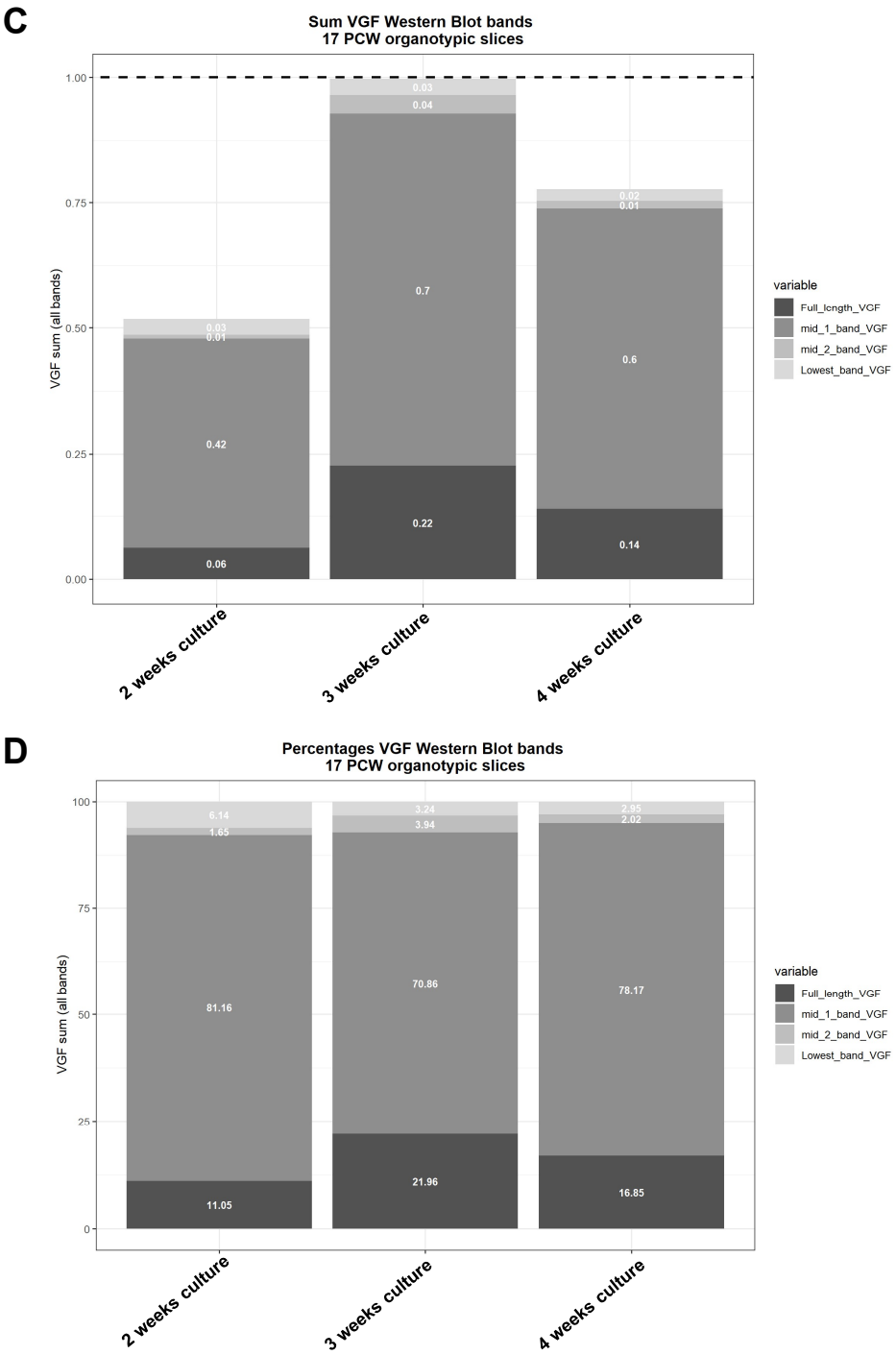

Figure 6.4: VGF protein quantification in organotypic cortical slices from a 17 PCW human brain over 4 weeks in culture (Western Blot analysis). (**A**) Representative image of the blot for VGF. β-actin was detected at 42 kDa and used for normalization and loading control. (**B**) Representative VGF densitometric measurement performed by including all the 4 proteoforms detected by Western Blotting. A dashed line intercepts the y-axis at 1 for comparison across timepoints, as well as with densitomeric measurements of VGF protein in the *post-mortem* human brain samples (see Figures 5.1-5.4). Color-coded by timepoint of the culture protocol analysed. (**C**) Relative contribution of each proteoform of VGF to the sum as absolute values. (**D**) Relative percentage of each proteoform of VGF in the total amount of protein quantified in A. (B, D) Color-coded by VGF Western Blot band (i.e. proteoform). N=2 slices for each group.

ELISA

Finally, I assessed the endogenous secretion of VGF in the conditioned culture medium by ELISA test after various periods of culturing. In fact, since the protein is clearly present in the resected axonal terminals, as demonstrated by immunofluorescence and Western Blot analyses in the previous sections, it was crucial to quantify the level of secreted VGF in the culture medium of these slices prior to administering exogenous recombinant protein. The most suitable method for detecting antigens in supernatants is standard sandwich ELISA.

Being aware of the endogenous content of VGF in the media was important for both selecting a proper dose to add for experimental treatment of the slices, as well as properly interpreting the results observed. Furthermore, as just mentioned above, BDNF is added in the culture medium. By consequence, even though the VGF protein content quantified by Western Blot (**Figure 6.3**) was in line with previous observations in the *post-mortem* brain samples analysed in Chapter 5 (see **Figures 5.1-5.5**), it is possible that over time in culture VGF starts being upregulated endogenously in the cortical cells themselves that receive BDNF continuously in their media. This induced overproduction of VGF might lead to additional secretion of VGF in the media as well.

ELISA test was performed on the day when media was changed (occurring every 4 days), thus enabling the concentration of any secreted protein in the tested medium. This ensured that the highest detectable amount of the cultures' secreted VGF was measured.

Efforts were made to obtain similar size of cortical slices, which were cultured separately in 12-well plate. All samples used in this experiment were collected from the same frontal area of the cortex. Each slice was considered as an individual sample in this experiment. I measured secreted VGF in slices from 13 PCW (N=4), 14 PCW (N=1), and 17 PCW (N=2) human fetal brains.

As demonstrated in **Figure 6.5**, the baseline levels of VGF in the medium are consistently low in all samples tested, and do not exhibit significant variations across different ages. All slices secrete a modest amount of VGF considering the volume of media used for each well (300 µl per well), with the protein being detected at levels below 20 pg/ml in all samples. Importantly, some of the 13 PCW

cortical slices tested in this assay were later used for the experimental treatment with recombinant VGF and tested for functional effects. The dose used for their treatment was considered as “high” by comparison to the endogenous protein present in the media as assessed here by ELISA.

Figure 6.5

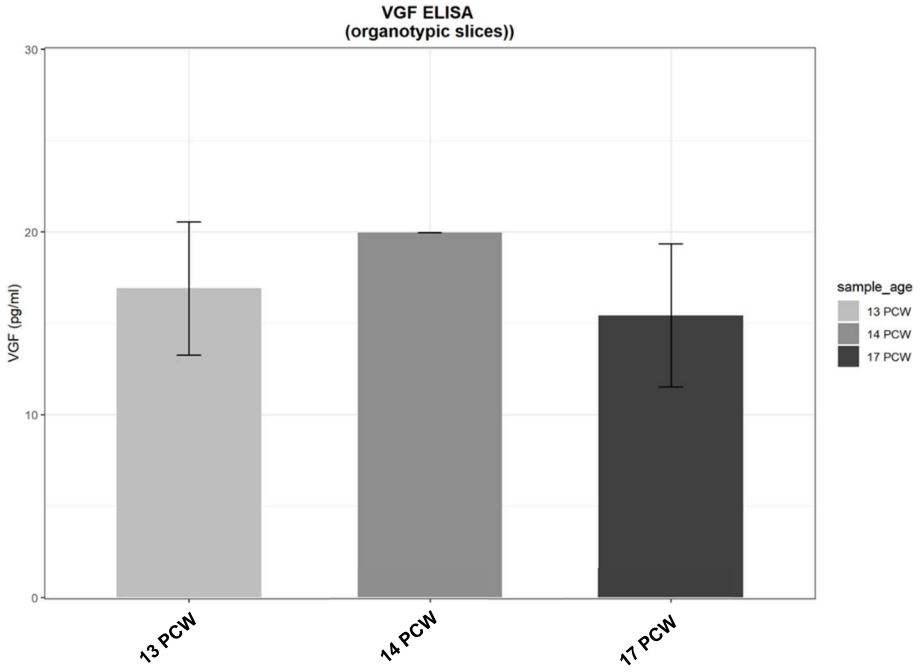

Figure 6.5: Endogenous secretion of VGF by human organotypic slices in the *culture* medium tested by ELISA. Slices were grouped by donor age, shown in x-axis. VGF detected by ELISA test is expressed in pg/ml medium tested. Error bars refers to average of the values measured for individual slices (13 PCW N=4; 14 PCW N=1; 17 PCW N=2).

6.1.2.2 Effects of exogenous application of VGF in organotypic cortical slices

I applied a high dose of recombinant human VGF (1200 ng/ml) to the medium of two slices obtained from the frontal cortex of a 13 PCW human brain. The treatment was performed for 4.5 days in culture, followed by calcium imaging to assess for spontaneous activity of subplate neurons. To visualize calcium events, the slices were transfected with AAV9-hsyn-GCaMP6f applied for 2 weeks *in vitro*. Untreated control slices were only transfected with the genetically encoded calcium sensor, but no recombinant VGF was applied to the medium at any point. For each slice, 6-7 recording were taken for the quantification of both size and frequency of the spontaneous calcium activity shown in **Figure 6.6**. Specifically, calcium events are considered as an indication of spontaneous activity in these neurons (Hanganu *et al.* 2008; Singh *et al.* 2019; Molnar *et al.* 2020). No exogenous stimulation was provided to the culture.

When treated with recombinant VGF, subplate neurons showed a significant increase in the frequency of calcium events, and a similar trend as regarding for their size (**Figure 6.6 C, D**). However, lower doses of VGF were not tested, and the small sample size (N=2 slices for treatment group) do not allow a strong and conclusive interpretation of these results. Nevertheless, these first data overall suggest that VGF can modulate the functional properties of human subplate neurons as early as 13 PCW. Additional experiments are needed to infer the strength of these observations. Specifically, I would need to perform at least one other test in this *in vitro* model, by treating older samples (16-18 PCW) with the recombinant protein. In fact, at this stage of development both subplate and OSVZ are more expanded and mature, making the analysis more feasible. Moreover, the neurons of the subplate show a much higher spontaneous activity at baseline, which would increase the reliability and power of any observation made at calcium imaging. Unfortunately, I was not able to evaluate the effect of VGF in the progenitor cells as neither BrdU staining, nor classic immunohistochemical marker analysis for proliferation were successful. Therefore, by repeating this experiment, I aim to reanalyse the potential effect of VGF exogenous treatment on the progenitor cells as well.

Figure 6.6

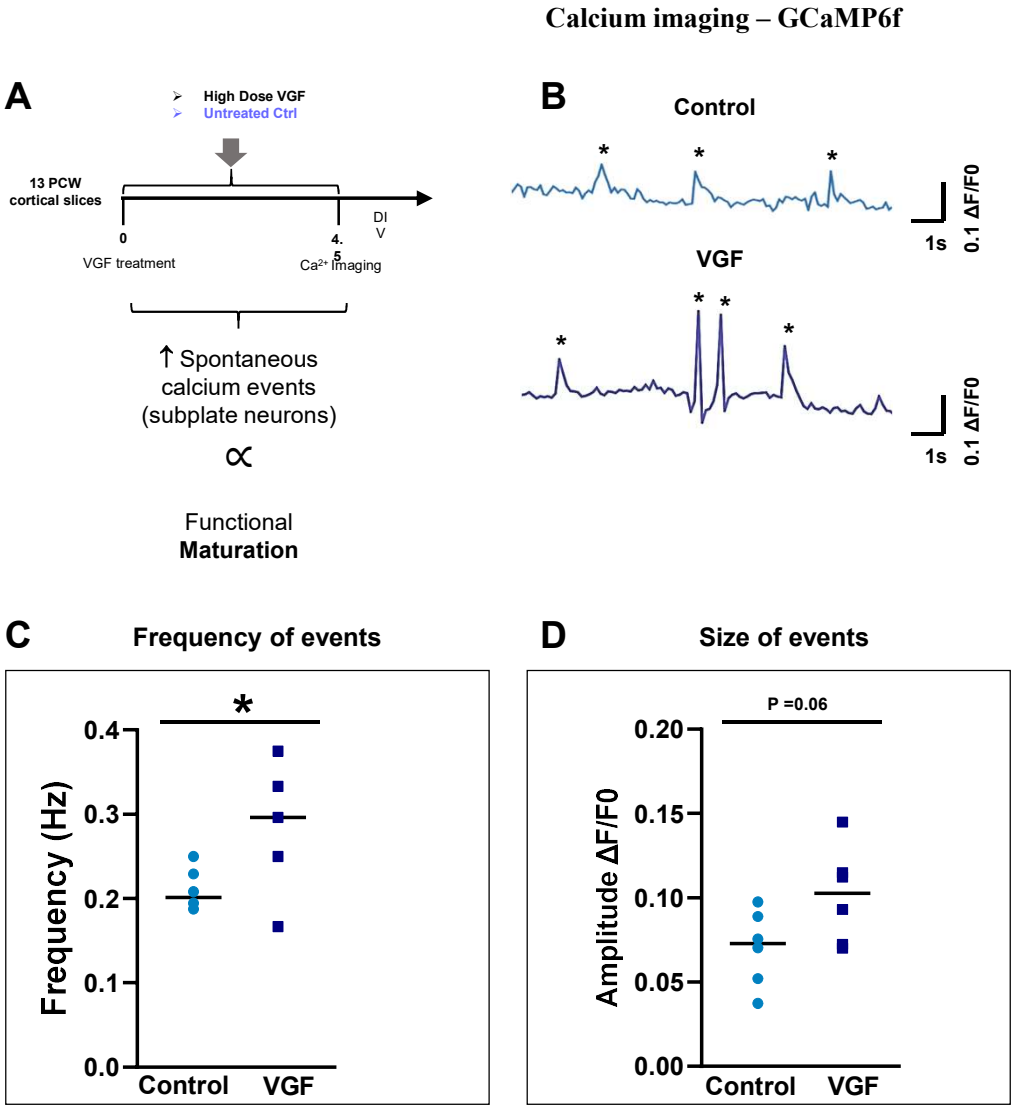

Figure 6.6: Spontaneous activity of subplate neurons recorded by calcium imaging in the 13 PCW human cortical slices upon treatment with VGF. (**A**) Schematics of the experimental design. (**B**) Representative traces showing peaks of activity detected during the experimental recording in treated and untreated slices. (**C-D**) Analysis of the frequency (**C**) and size (**D**) of the calcium events recorded during the experiment in VGF-treated and untreated control slices. N= 2 slices/treatment group, 6-7 image regions; 13 PCW tissue sample, frontal cortex treated with recombinant VGF (1200ng/ml) for 4.5 days. Imaging conducted at 3 weeks in vitro. AAV9-hsyn-GCaMP6f applied for 2 weeks in vitro. Statistical significance is set at p-value <0.05.

6.2 PREDICTION AND EXPRESSION PROFILING OF VGF ENZYMES

The presence or absence of an observed effect in the functional validation experiments may be attributed to the role of VGF peptides rather than the full-size VGF protein itself. This introduces potential bias when treating *in vitro* models, as the absence or scarcity of necessary proteases in these models can hinder their interaction with VGF. Additionally, the extensive processing of VGF within transporting vesicles inside the cells that produce and transport the full-size molecule (i.e., thalamic projecting neurons) further complicates the accessibility of VGF to these proteases. As noted before, thalamic neurons are separated from the cortical sample used for the cultures. If an observed effect is present, it can be attributed to either the sufficient presence of full-size VGF or the coincidental presence of the appropriate enzymes in the *in vitro* system for its processing. Conversely, the absence of an observed effect can be similarly explained by the inadequate processing of the protein into its functional peptide or peptides form, which is responsible for producing such effects.

With this consideration in mind, I attempted to bridge this knowledge gap and enhance the understanding of the underlying mechanisms behind the screened effects by investigating VGF peptides. Unfortunately, direct testing of recombinant peptides was not feasible due to limited access. Moreover, the detection of small VGF peptides presents significant challenges. In fact, specific expression profiling at mRNA level is not possible as they are encoded by the same VGF gene. At protein level, the identical amino acid sequence with portion of the full-size VGF renders them epitopes of VGF itself and therefore not distinguishable. Moreover, their small size (all < 5 kDa) is beyond the accuracy limits of classic SDS-PAGE and Western Blot detection. Technically, conducting a comprehensive study solely on these peptides is highly demanding. Therefore, I employed a slightly indirect approach by directing my attention towards the investigation of both known and newly identified VGF peptidases.

6.2.1 Bioinformatic prediction of VGF proteases by Proteasix

The best characterized proteases responsible for VGF processing into peptides are pro-protein convertase subtilisin/kexin type 1 (PCSK1) and type 2 (PCSK2) (Trani *et al.* 2002; Zhang *et al.* 2010). However, recent studies suggest that other proteases can also cut VGF based on its amino acid sequence (Quinn *et al.* 2023). To gain a broader understanding of the peptidases involved in the processing of VGF into functional neuropeptides, extending beyond PCSKs, I employed a bioinformatic approach.

Specifically, I used **Proteasix** (http://proteasix.cs.man.ac.uk/), a web-based tool that focuses on peptides and enables the reconstruction of N- and C-terminal cleavage sites using the amino acid sequence of input peptides via the "peptide-centric prediction tool". (see detailed methods in **Chapter 2 Section 2.4.3**) Briefly, I used as inputs for this prediction the human VGF peptides labelled as in (Quinn *et al.* 2021), alongside their start and stop amino acids also provided in the publication, and the human VGF UniProt accession (AC). I selected both "Observed" and "Predicted" modalities for the search, to obtain both known and predicted enzymes listed in the output results. Following a manual inspection of the list and the removal of terms exclusively related to rodent species (resulting in the removal of a single enzyme), the refined list was utilized as input for Cytoscape. The resulting plot in **Figure 6.7** provides a graphical representation of the comprehensive landscape of VGF peptides and correspondent peptidases as identified by Proteasix prediction method.

Interestingly, among the list of potential peptidases cleaving VGF into peptides, I found some enzymes with well recognised important functions in the context of brain development, and more specifically cortical neurogenesis. For instance, several members of the family of **matrix metalloproteases** (MMPs) are represented, as well as **kallikrein** (KLK) family of serine proteases which have been associated with neuroinflammation and neurodegeneration (Ethell *et al.* 2007; Scarisbrick *et al.* 2008; Small *et al.* 2016). Members of the families of **cathepsins** (CTSs) are also present, and have been associated with physiological processes of neurodevelopment and synaptic plasticity (Moon *et al.* 2016; Tohda *et al.* 2017) as well as neuropathological conditions (Vitner *et*

al. 2010; Subramanian *et al.* 2019). Notably, previous independent predictions have indicated the potential involvement of both cathepsins and metalloproteases in the cleavage of VGF (Wegrzyn *et al.* 2010), although this has never been validated experimentally. Furthermore, the two best characterized members of **calpain family**, Calpain 1 and 2 (also known as μ- and m-calpain, respectively) appear multiple times in association with different VGF peptides. Interestingly, both enzymes have crucial roles in neurodevelopmental processes (Li *et al.* 2009; Baudry *et al.* 2016; Duquette *et al.* 2020; Wang *et al.* 2020).

All the data obtained by this prediction are limited to the curated data deposited and available in the database used at the time when the search was performed (March 2023).

Figure 6.7

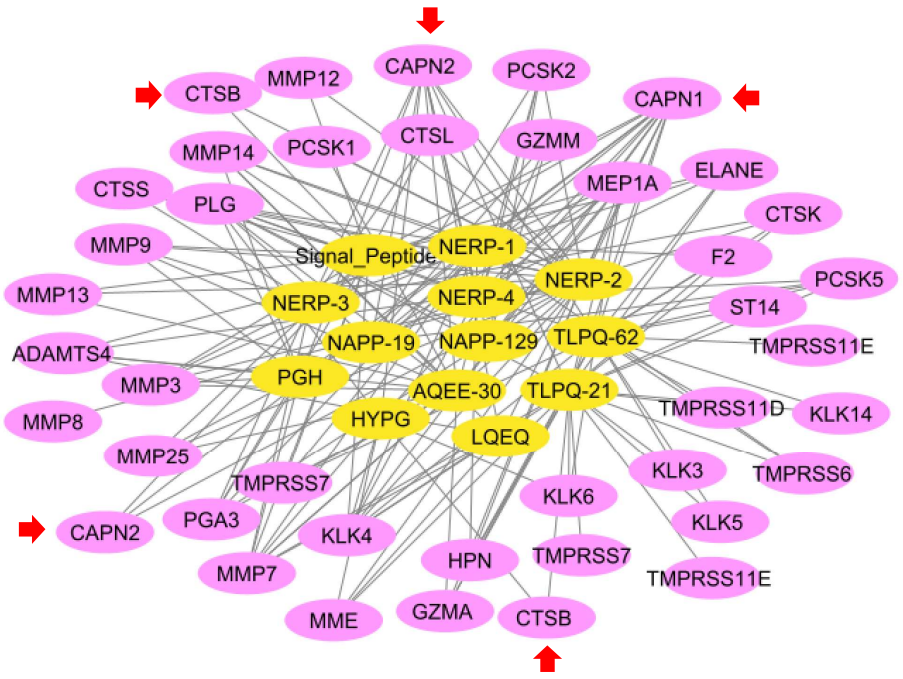

Figure 6.7: Landscape of predicted proteases cleaving human VGF into neuropeptides.
Network showing human VGF-derived peptides (from Quinn et al.) Each peptide is represented by a yellow node, while the enzymes are depicted as pink nodes. Edges represent a specific cleavage sequence that link a single peptide with the predicted (or observed) peptidase that might recognise it. Hence, multiple cleavage sequences are associated to each node. Red arrows highlight enzymes that belong to the calpain and cathepsin families discussed in the Chapter. The network was created with Cytoscape by using the list of VGF peptides and predicted proteases combination obtained by PROTEASIX as a circular layout.

6.2.2 Selection of predicted proteases to validate based on proteomic dataset

While the proteomics analysis did not provide conclusive evidence regarding the presence of VGF peptides in the developing human cortex, the dataset generated by LC-MS/MS offered valuable insights into the existence of VGF proteolytic enzymes. I decided to focus on calpains and cathepsins from the output list generated by Proteasix prediction, according to previous hypotheses and observations (Wegrzyn *et al.* 2010; Quinn *et al.* 2023). I cross-searched for their presence in the proteomics dataset acquired from the 20 PCW neocortex. I specifically selected the generic family names for calpains "CAPN" and cathepsins "CTS" without specifying individual gene names (such as “CAPN1” or “CTSB”). In fact, both families of peptidases contain numerous members, many of which are included in the prediction list. In this way, I subset those members that are highly likely to be abundant at the protein level in the cortex, where VGF is secreted. This approach would also facilitate the subsequent validation of their protein content after a preliminary assessment of their expression profile at the mRNA level, at least to some extent.

From this search, I successfully obtained a list of all members of both peptidase families that exhibited enrichment in the fetal cortical tissue at proteomic level. Along with these newly predicted enzymes, I also searched for the two characterized peptidases cleaving VGF, namely PCSK1 and PCSK2. Results of the proteomic analysis of these peptidases are summarized in **Table 6.1**. It is important to note that this search excluded any enzyme that might be specifically enriched in the thalamus, where VGF is produced and stored. VGF. Furthermore, since proteomics analysis focused on a single cortical area, the resulting list of enriched calpains and cathepsins may be biased if there are significant regional differences in the distribution of these enzymes across cortical areas.

Strikingly, newly identified proteases, belonging to the calpain and cathepsin families, were found to be abundant in the developing human cortex. Both unique large subunits of Calpain 1 (CAPN1) and Calpain 2 (CAPN2), along with the common small subunit that participates to the formation of their functional heterodimeric form (CAPNS1) were detected in the 20 PCW neocortex (**Table 6.1**). Interestingly, non-classical calpains, namely Calpain 5 (CAPN5) and Calpain 7

(CAPN7), were also detected in the dataset. These less characterized members of the Calpain family might also play pivotal roles in the nervous system (Singh *et al.* 2014) (**Table 6.1**).

Surprisingly, neither PCSK1 nor PCSK2, the most characterized VGF enzymes, were detected in the 2h-long run of MS. Only the latter enzyme was observed in the longer liquid chromatography separation (3h) by means of 1 unique peptide in half of the tissue analysed, similarly to VGF (Chapter 5, see Table 5.1 for comparison) (**Table 6.1**). Even more remarkably, Pro-protein convertase inhibitor (PCSK1N) is indeed detected in the sample in both proteomics datasets (not shown) further suggesting a potential low level of activity for the already scarce PCSK enzymes. cathepsins. These enzymes have the potential to recognize specific cleavage sites within the amino acid sequence of VGF, leading to the generation of different neuroactive peptides.

Table 6.1: Detection of predicted VGF-cleaving calpain and cathepsin proteases by proteomics in the 20 PCW human neocortex.

ENZYME (Gene Name)	# Average unique peptides	LC-MS/MS dataset used
CAPNS1	4.5	2h
CAPN1	10.5	2h
CAPN2	3	2h
CAPN5	1	2h
CAPN7	1	2h
CTSB	1	2h
CTSD	9	2h
PCSK2	0.5	3h

Each protease and/or protease subunit is labelled by gene name. For each protein, the number of unique peptides used for its identification are indicated as average between the two technical replicates run in the 2- or 3-hour long LC-MS/MS described in Chapter 5.

These data suggest that when thalamic VGF is secreted into the extracellular space in the human fetal cortex, it may not undergo processing into neuroactive peptides by pro-protein convertases as proposed in previous literature (Ferri *et al.* 1996; Trani *et al.* 2002; Pan *et al.* 2005; Bartolomucci *et al.* 2006; Pan *et al.* 2006; Mishiro-Sato *et al.* 2010; Zhang *et al.* 2010). However, it is plausible that VGF encounters elevated levels of other proteases within the cortical ECM, such as calpains.

6.2.3 Expression profiling of the selected VGF proteases

To explore this aspect, I started investigating the expression patterns of both previously known and newly predicted VGF peptidases that were selected from the proteomic dataset. By using a similar approach to the one described in Chapter 4 for VGF, I employed available transcriptomic datasets to comprehensively investigate the expression patterns of these enzymes in the human fetal brain. The focus was specifically on the thalamus and neocortical regions. By using different and complementary datasets, I was able to explore the expression profiles of VGF enzymes at various levels, including regional differences, neocortical area variances, layer specificity, and even some insights into cell specificity at the single-cell level within the neocortex. Specifically, in this section I will provide an overview on the findings from the following transcriptomic datasets: (a) Brainspan LMD-Microarray from Brainspan; (b) Exon-array analysis from Human Brain Transcriptome (HBT, hbatlas.org); (c) Single-cell RNA-seq dataset from Nowakowski et al., 2017 (Nowakowski *et al.* 2017)(USCS Cell Browser).

Furthermore, these observations were validated in the human fetal brain tissue available in the laboratory, to confirm and strengthen the results obtained from the transcriptomic dataset by qPCR expression profiling at mRNA level, and Western Blot analysis of protein distribution (only for calpain 1, CAPN1).

a. LMD microarrays (15-21 PCW)

Classic Calpains (CAPN1, CAPN2)

Calpain 1 (CAPN1) at 15 PCW (**Figure 6.8 A**) is downregulated in the germinal compartments, the ventricular zone (VZ), and subventricular zone (SVZ), while it appears upregulated in the post-mitotic layers, the subplate (SP) and cortical plate (CP). At 21 PCW (**Figure 6.8 A'**), its expression decreases in the SP and remains sustained only within the CP.

Interestingly, **Calpain 2** (CAPN2) follows a complementary pattern of expression, with high expression in the germinal zones and a general downregulation in the post-mitotic compartments (**Figure 6.8 B**). This pattern is not altered at later stages (**Figure 6.8 B'**).

Non-classic Calpains (CAPN5, CAPN7)

Calpain 5 (CAPN5) at 15 PCW (**Figure 6.8 C**) is ubiquitously expressed throughout cortical layers, except for the VZ. At 21 PCW (**Figure 6.8 C'**) this expression pattern is not altered substantially. Furthermore, the brain region represented in the schematics in all panels of Figure 6.7 includes two different cortical areas, namely the motor cortex dorsally (frontal lobe) and the somatosensory cortex ventrally (parietal lobe). The expression of CAPN5 in the CP – the only cortical layer which has been sampled from different cortical areas in this dataset – follows an opposite pattern. At 15 PCW CAPN5 is elevated in the CP of the first area and downregulated in the latter. At 21 PCW, the pattern is reversed.

Calpain 7 (CAPN7) has a low expression throughout the cortical layers, except for the SP at 15 PCW (**Figure 6.8 D**), and the VZ at 21 PCW (**Figure 6.8 D'**).

Cathepsins (CTSB, CTSD)

Cathepsin B (CTSB) at 15 PCW (**Figure 6.8 E**) show a sharp restriction to its expression in the intermediate zone (IZ) and the SP, which at this age extensively overlap. On the other hand, the expression is downregulated in all germinal compartments. Conversely, at 21 PCW (**Figure 6.8 E'**) CTSB appears upregulated throughout the layers instead.

Cathepsin D (CTSD) is highly expressed throughout the layers at 15 PCW (**Figure 6.8 F**), especially at the level of the CP in the motor cortex. Its expression remains sustained at 21 PCW (**Figure 6.8 F'**), while it slightly decreases in the SP.

Pro-protein Convertases (PCSK1, PCSK2)

Pro-protein convertase 1 (PCSK1) shows a clear complementary pattern at 15 PCW (**Figure 6.8 G**), with upregulation in the germinal compartments, and downregulation throughout the post-mitotic ones. The pattern is like the one described for CAPN2. At 21 PCW (**Figure 6.8 G'**) the expression decreases drastically and levels out across layers.

Pro-protein convertase 2 (PCSK2) is extremely low everywhere but the SP at 15 PCW (**Figure 6.8 H**), where it appears upregulated. At 21 PCW (**Figure 6.8 H'**) the pattern remains the same, but at this stage both SP and CP are expressing it at elevated levels.

Pro-protein convertases represent another interesting example of complementarity of expression pattern between germinal and post-mitotic compartments, like the case described for classic calpains.

Figure 6.8

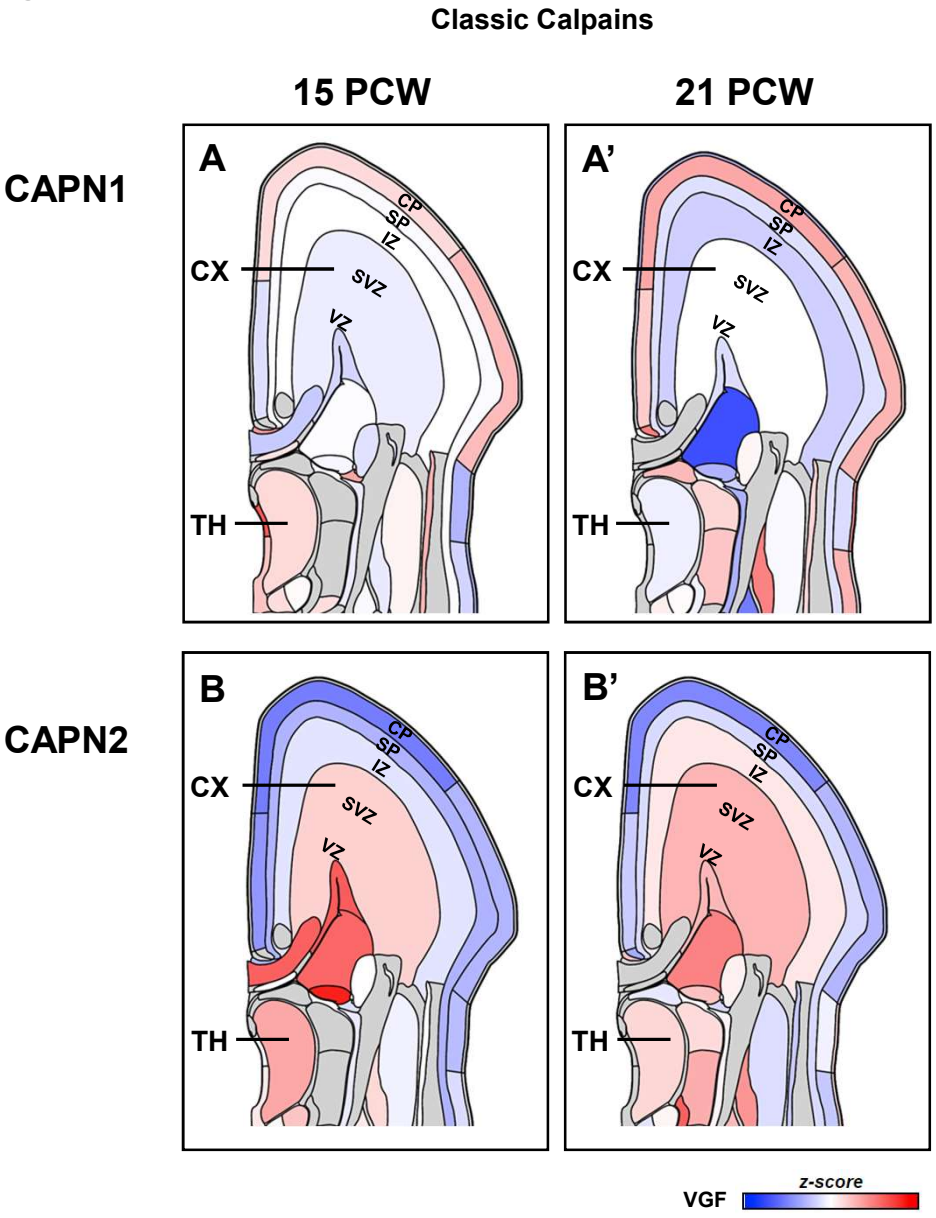
Classic Calpains
15 PCW
21 PCW
CAPN1
CAPN2
A
A'
B
B'
CP
SP
IZ
SVZ
VZ
CX
TH
VGF
z-score

Figure 6.8

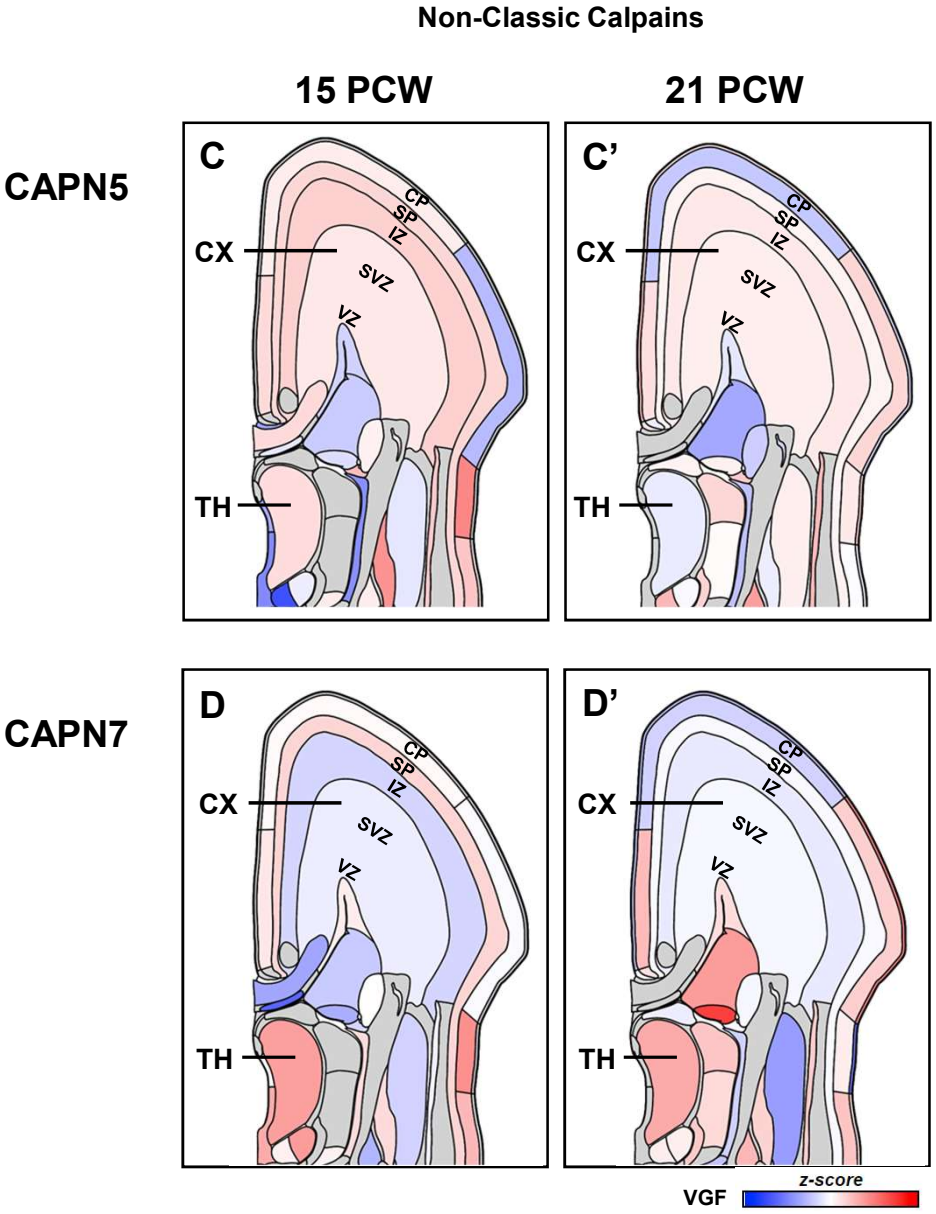
Non-Classic Calpains
15 PCW
21 PCW
CAPN5
CAPN7
C
C'
D
D'
CX
TH
CP
SP
IZ
SVZ
VZ
VGF
z-score

Figure 6.8

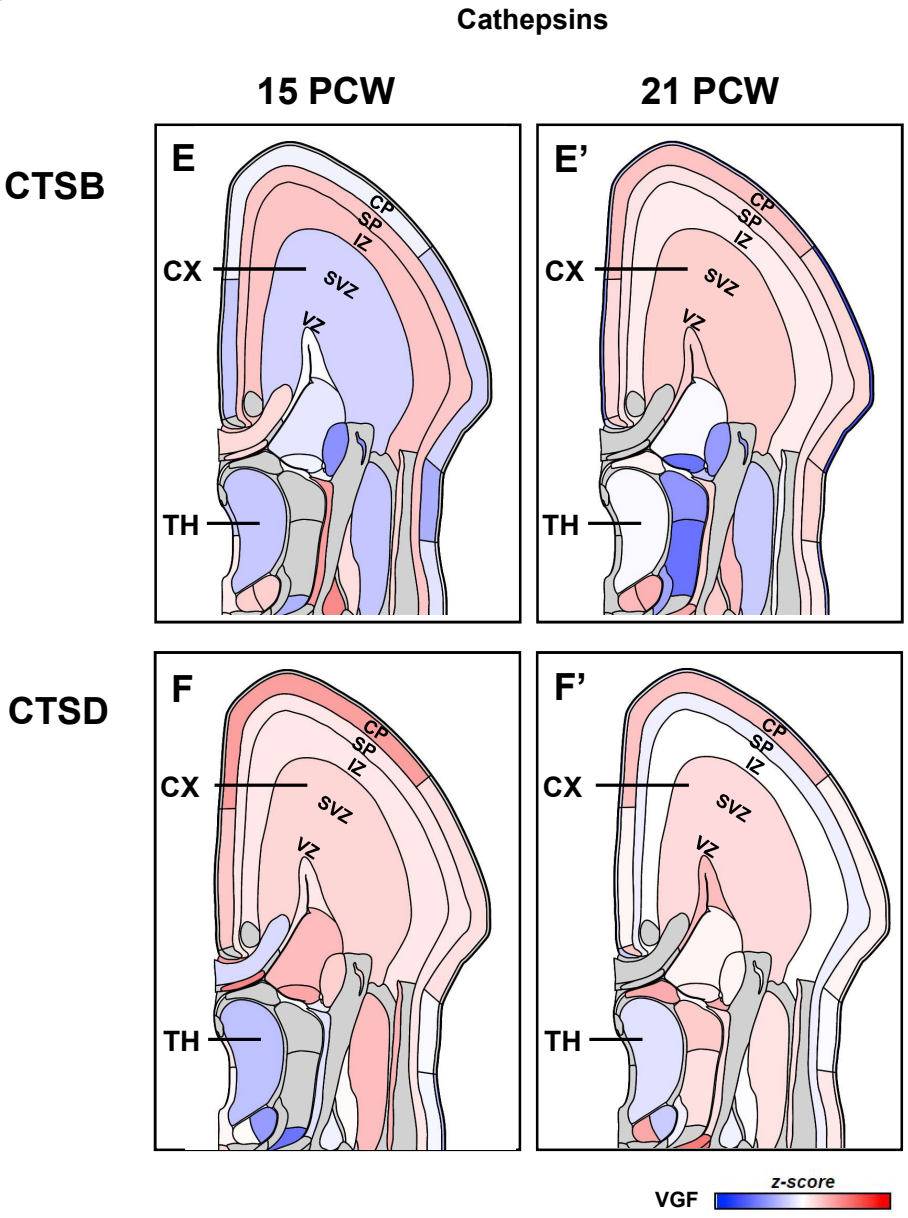
Cathepsins
15 PCW
21 PCW
CTSB
CTSD
E
E'
F
F'
CP
SP
IZ
SVZ
VZ
CX
TH
VGF
z-score

Figure 6.8

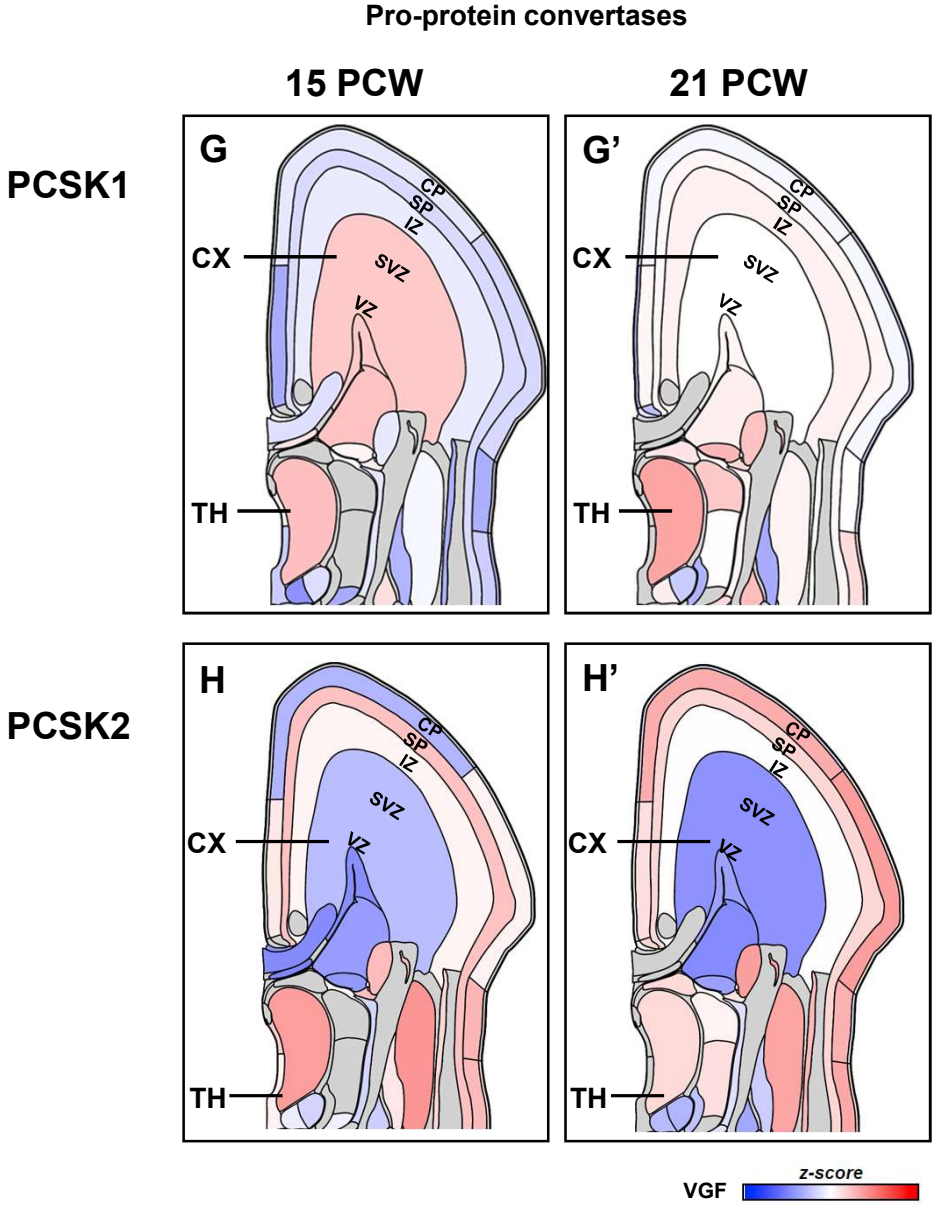

Figure 6.8: LMD-microarrays expression profiling of VGF enzymes in human 15 and 21 PCW thalamus and cortex (data from Brainspan). Schematic representation of the expression of VGF enzymes as detected by laser-microdissected (LMD) microarray in the 15 PCW (**A-H**) and 21PCW (**A'-H'**) human brain (Brainspan). Data are presented in coronal sections of the brain as z-scores of log2 intensity signal (blue is low expression, red is high expression). Data from Brainspan LMD microarrays, donor ID H376.IIIA.02 (15 PCW) and ID H376.IV.02 (21 PCW).

b. Exon-array hbatlas.org (all developmental ages)

All data are from (Kang *et al.* 2011), and have been downloaded from the Human Brain Transcriptome (HBT, hbatlas.org). Expression levels are reported as log2 transform of the signal intensity values from the exon-array, as described in the original publication.

Classic Calpains (CAPN1, CAPN2)

CAPN1 expression level is detected between 7-9 across brain regions throughout developmental stages (**Figure 6.9 A**), and it remains constant except for the mediodorsal nucleus of the thalamus (MD, green line) that shows especially elevated levels of CAPN1 at midgestation. Neocortical areas show no specific differences (**Figure 6.9 A'**).

CAPN2 starts at higher levels early on during gestation (**Figure 6.9 B**). However, its expression drastically drops at midgestational stages except for the cerebellum (red line). Like for CAPN1, no areal differences are observed across neocortical areas (**Figure 6.9 B'**).

Non-classic Calpains (CAPN5, CAPN7)

CAPN5 is initially expressed at low levels (<6-7) and sharply increases by mid-gestation (**Figure 6.9 C**). This transient upregulation resolves by birth, and CAPN5 expression returns to its original levels thereafter. Neocortical areas show no differences (**Figure 6.9 C'**).

CAPN7 expression is sustained throughout prenatal stages, with no major alteration noticeable (**Figure 6.9 D**). It drops perinatally and remains constantly lower after birth, except for the cerebellum (red line). Once again, the neocortex shows no areal differences (**Figure 6.9 D'**).

Cathepsins (CTSB, CTSD)

CTSB is initially expressed at relatively elevated levels (~8-9) and keeps increasing until birth and first stages of postnatal development (**Figure 6.9 E**). The expression levels settle after the first year of life. Neocortical areas show a tightly identical trend of expression levels (**Figure 6.9 E'**).

CTSD expression pattern appears relatively similar to CTSB (**Figure 6.9 F**). It starts high (~ 9-10) and with some slight fluctuations remains high until birth, especially in the MD (green line). The neocortex has a drop in CTSD expression levels around midgestation (blue line). However, no areal differences are observed in the latter (**Figure 6.9 F'**).

Pro-protein Convertases (PCSK1, PCSK2)

PCSK1 expression exhibits a high degree of brain region-specificity (**Figure 6.9 G**). Initially, it is detected at minimal levels (<5) in the hippocampus, and a maximum of ~7.5 in both neocortex and MD. Its expression then drops around midgestational ages in all brain regions. Only at perinatal ages PCSK1 levels increase up to its initial values, with a sharp inversion of the curve. After birth it is detected at elevated levels, with a general trend toward further upregulation. The analysis of neocortical areas did not reveal significant variations (**Figure 6.9 G'**), and interestingly, the graph depicting these areas underscores a noticeable decline in PCSK1 expression during mid-gestation.

PCSK2, differently from PCSK1, is initially expressed at slightly higher levels, with its maximum in the neocortex (blue line) amongst the brain regions analysed (**Figure 6.9 H**). During gestation, its levels increase to reach a peak at late midgestation phase. Afterwards, PCSK2 expression remains constant, except for the cerebellar cortex (red line) where it decreases. This is in line with its successful detection at proteomics levels, where PCSK1 was in fact not detected. Interestingly, PCSK2 represents a case where neocortical areas show more heterogeneity (**Figure 6.9 H'**): frontal areas, especially the orbital prefrontal (black line) and dorsolateral prefrontal cortex (dark blue line) show the lowest expression of this enzyme, followed by the ventrolateral prefrontal

cortex (in violet) and the visual cortex (in brown). Higher levels are detected in the other areas sampled, with a maximum in all the temporal lobe areas analysed.

This finding is particularly significant considering the proteomics results, which indicated a distinct detection pattern for this enzyme compared to PCSK1. It is worth noting that the sample analysed by LC-MS/MS was specifically obtained from the temporal lobe, adding further relevance to this observation.

Figure 6.9

Classic Calpains

A **CAPN1 Expression Levels (Brain Regions)**

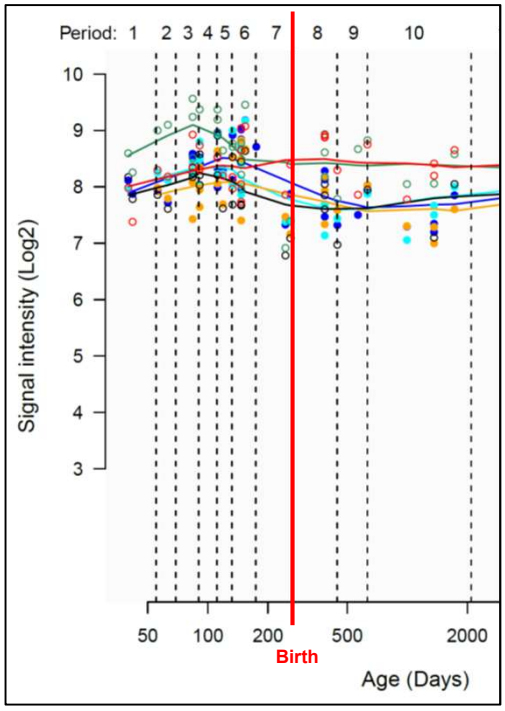

A' **CAPN1 Expression Levels (Neocortical Areas)**

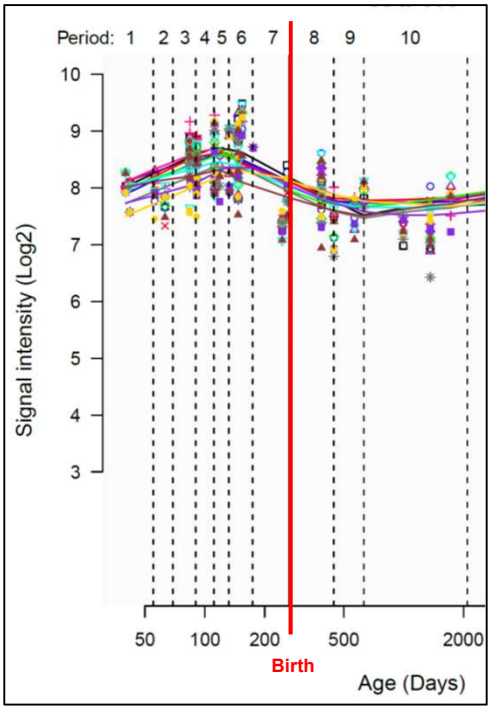

B **CAPN2 Expression Levels (Brain Regions)**

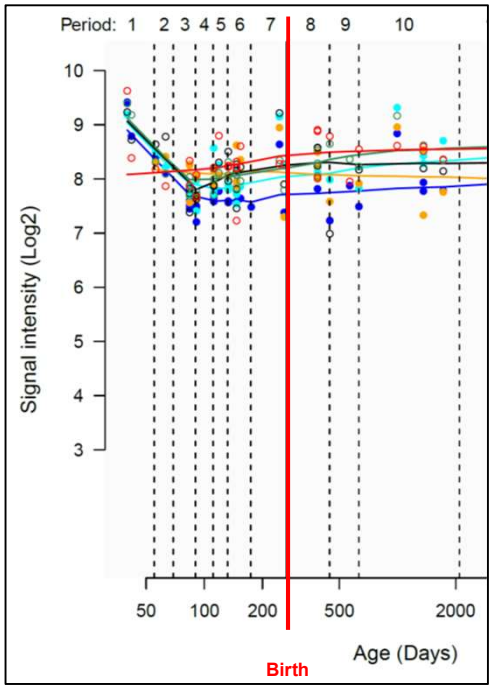

B' **CAPN2 Expression Levels (Neocortical Areas)**

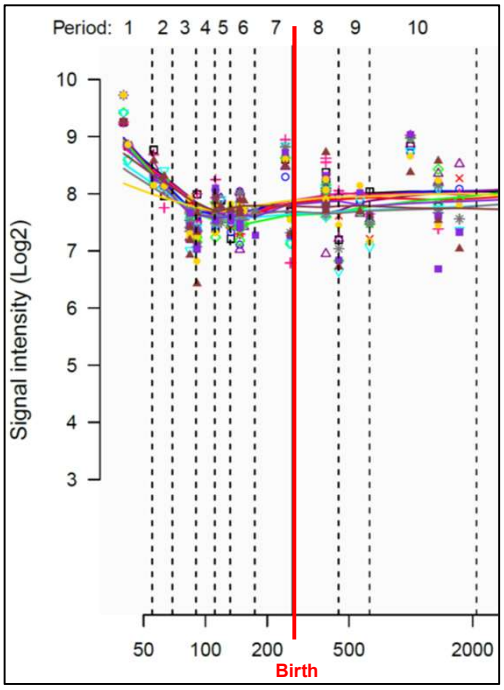

Figure 6.9

Non-Classic Calpains

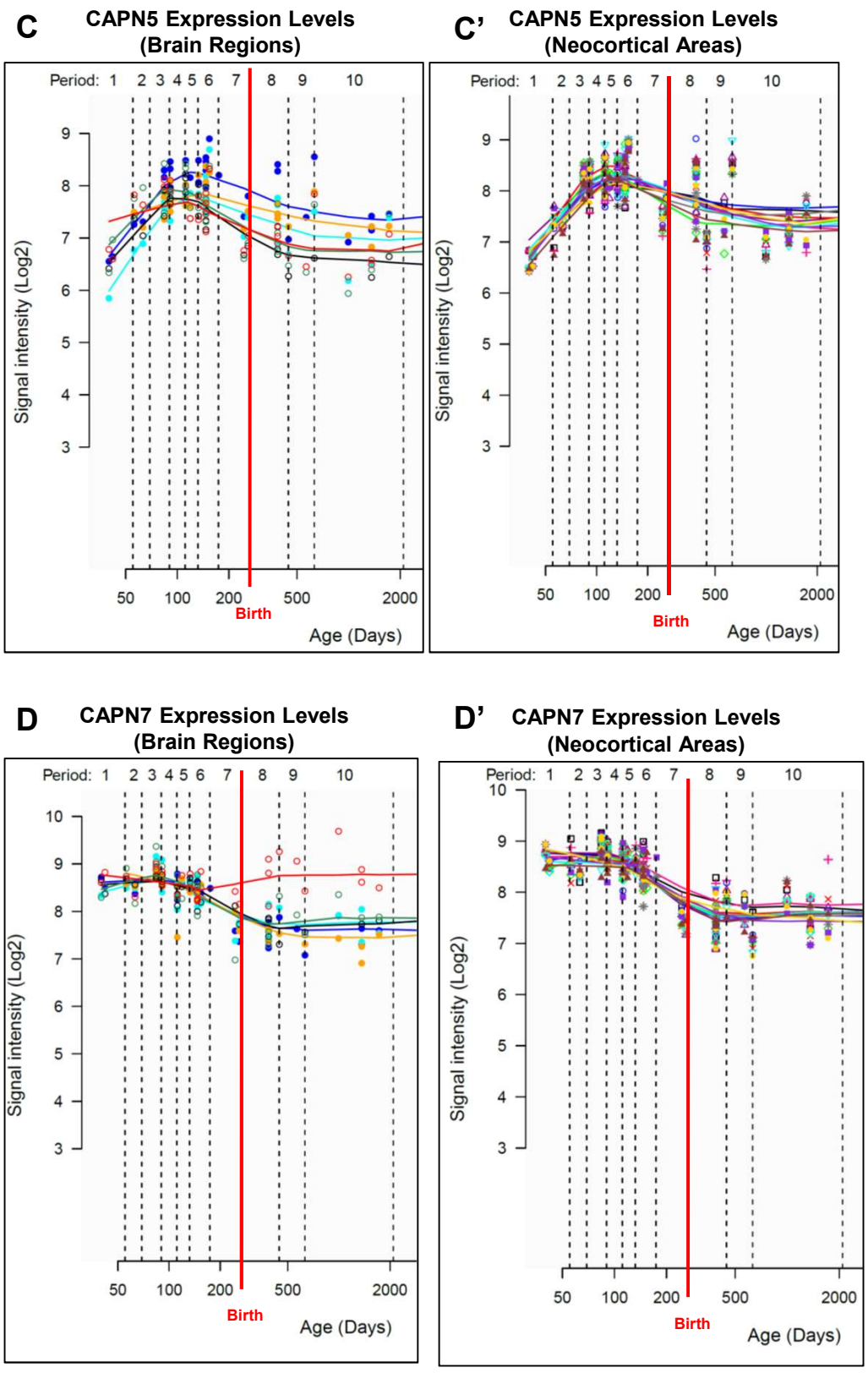

Figure 6.9

Cathepsins

E **CTSB Expression Levels (Brain Regions)**

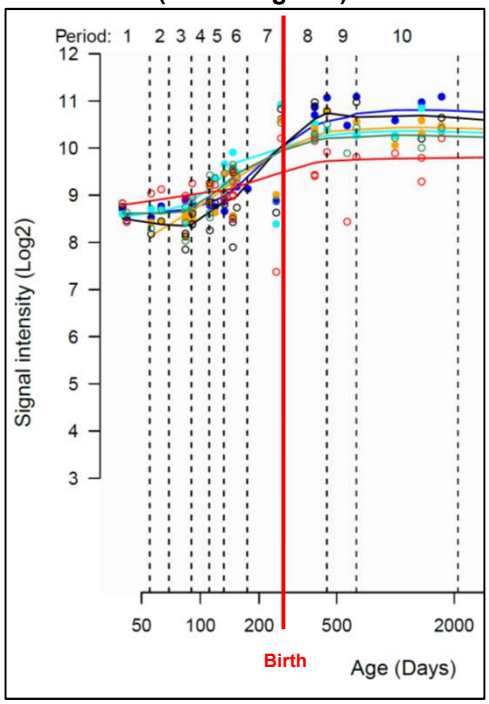

E' **CTSB Expression Levels (Neocortical Areas)**

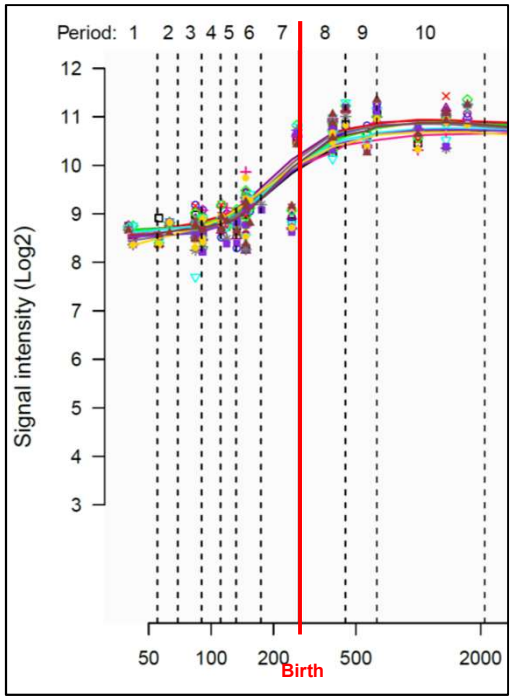

F **CTSD Expression Levels (Brain Regions)**

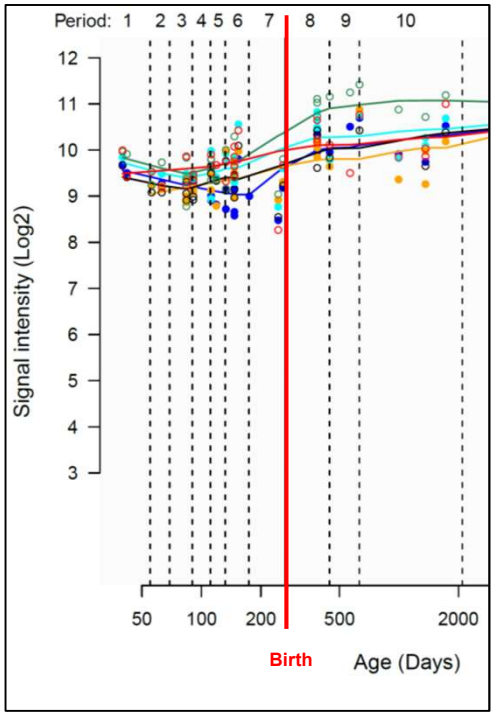

F' **CTSD Expression Levels (Neocortical Areas)**

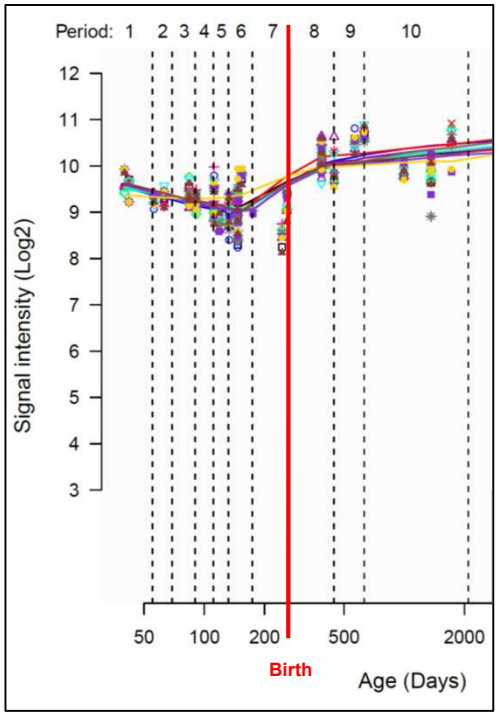

Figure 6.9

Pro-protein convertases

G **PCSK1 Expression Levels (Brain Regions)**

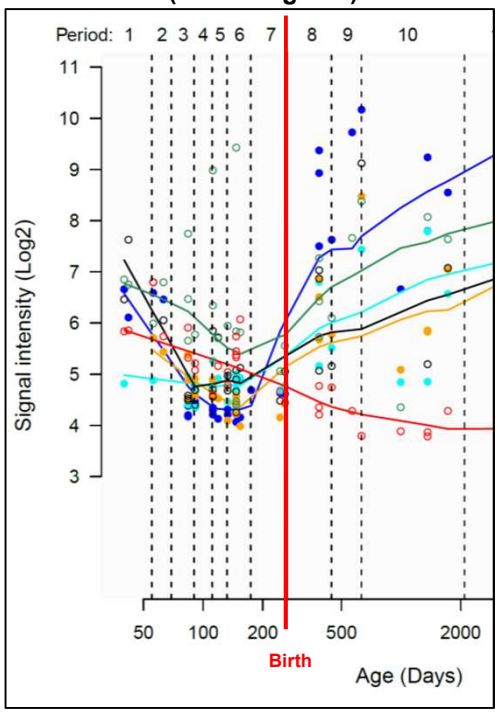

G' **PCSK1 Expression Levels (Neocortical Areas)**

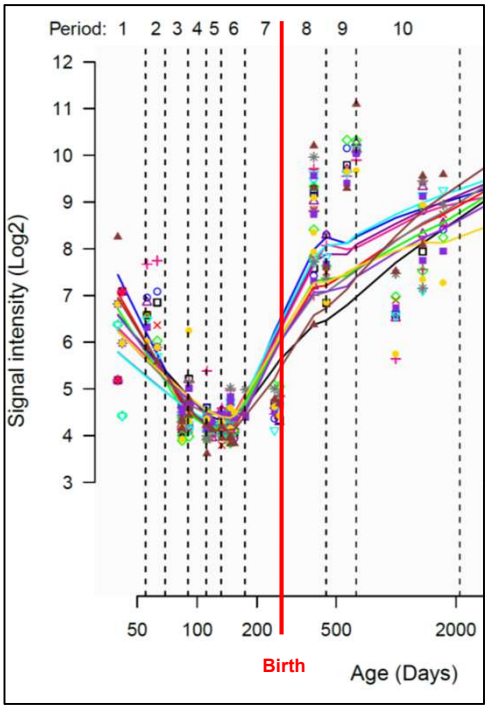

H **PCSK2 Expression Levels (Brain Regions)**

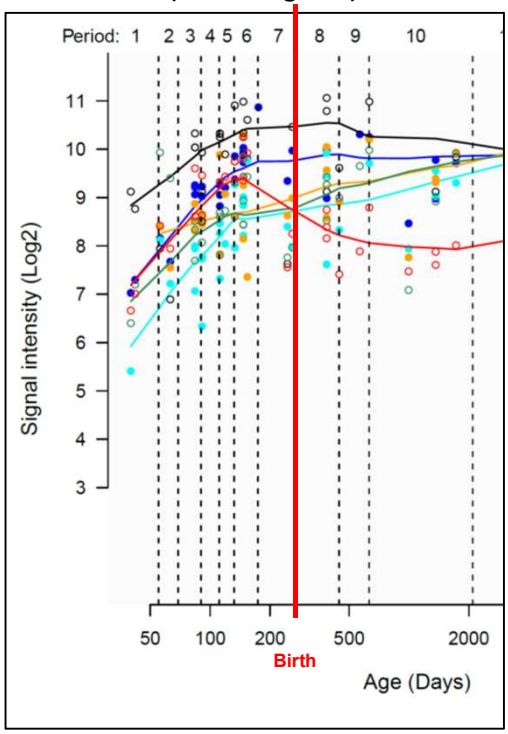

H' **PCSK2 Expression Levels (Neocortical Areas)**

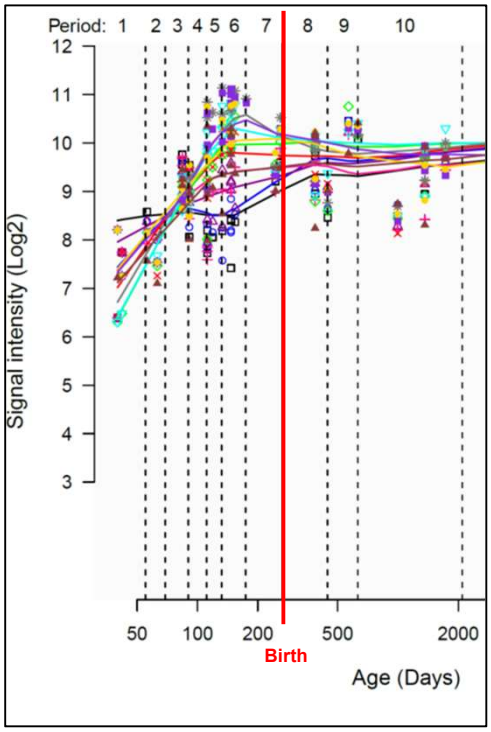

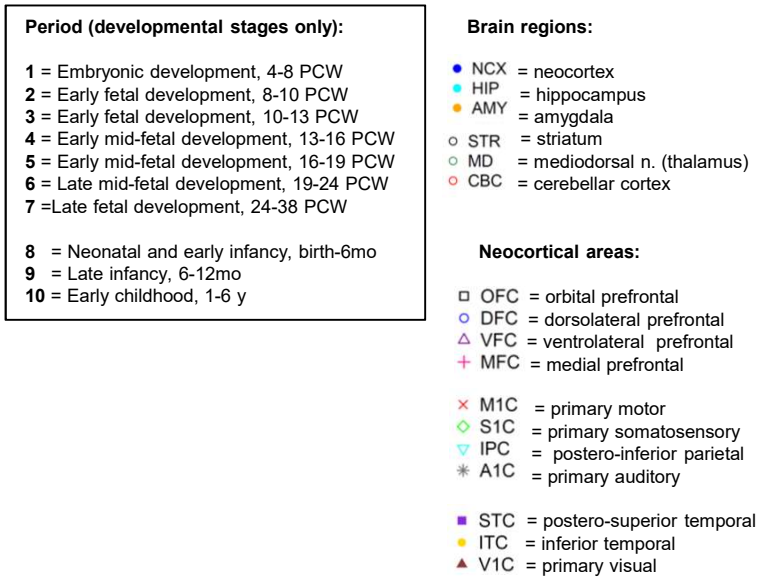

Figure 6.9: Exon-arrays transcriptomics of VGF enzymes in the human developing brain (data from HBT, hbatlas.org). Line chart graphs of VGF enzymes expression levels in the human brain regions (**A-H**) and neocortical areas (**A'-H'**) from embryonic development to early childhood. Expression levels are represented by log2 signal intensity (y-axis), and ages are expressed in day (x-axis). A red line highlights birth, dividing prenatal and postnatal periods. Data from Kuang et al., 2011, and downloaded from hbatlas.org.

c. scRNAseq dataset (USCS Cell Browser)

The data described here are from (Nowakowski *et al.* 2017) and have been downloaded directly from the USCS Cell Browser (https://cells.ucsc.edu/) (Speir *et al.* 2021). The dataset is available as "Cortex Development". Specifically, the authors performed single-cell mRNA sequencing (scRNA-seq) in primary cortical and medial ganglionic eminence (MGE) samples across stages of peak neurogenesis. Furthermore, they compared the same cell typed between prefrontal cortex (PFC) and primary visual cortex (V1) in 13 paired samples. Although these data do not include the thalamus, I preferred to use this dataset to get an insight into eventual cell-specificity in the expression of VGF enzymes under examination rather than the scRNAseq dataset used for VGF profiling in Chapter 4 (Section 4.1.3), as this dataset has been already meticulously annotated by the authors and therefore provide details on the cell cluster identity. This allowed me to explore whether specific cell populations in the developing cortex selectively express VGF enzymes. The expression profile of all the enzymes in the scRNAseq datasets analysed in Chapter 4 (both thalamus and main cortical areas in the 16 PCW brain) is plotted in **Supplementary Figures S11-S15**. Future annotation of these datasets would be insightful for completing this expression profiling of VGF enzymes.

Classic Calpains (CAPN1, CAPN2)

Expression of **CAPN1** appears scattered throughout the cell clusters, and surprisingly at low levels (**Figure 6.10 A**). This is contrast with the other results described for this enzyme.

CAPN2 transcript is more abundant (**Figure 6.10 B**). Its expression is also sparse throughout the cell types; however, it is more represented in the progenitor clusters, all defined by the shared "Radial Glial Cells (RG)" labelling.

Non-classic Calpains (CAPN5, CAPN7)

The expression of **CAPN5** is low and sporadic (**Figure 6.10 C**).

While also detected in most cell types without any specific pattern, **CAPN7** is noticeably more highly expressed (**Figure 6.10 D**).

Cathepsins (CTSB, CTSD)

CTSB expression levels appear high, except for interneurons clusters (shared "IN" label) (**Figure 6.10 E**). Especially elevated levels are detected in the microglia cell cluster.

CTSD is comparatively less expressed, with especially elevated levels detected in microglia similarly to CTSB (**Figure 6.10 F**).

Pro-protein Convertases (PCSK1, PCSK2)

PCSK1 is almost absent in the developing cortex (**Figure 6.10 G**), as previously noticed.

PCSK2 is also detected at low levels (**Figure 6.10 H**), however a very cell-specific expression can be observed in the clusters annotated as "Excitatory Neurons" of the prefrontal and visual cortex, more specifically "EN-PFC1", "EN-V1-3", and to a lesser extent in "EN-V1-1". This data is remarkably interesting, as it indicates that this enzyme is expressed in a cell-specific manner by excitatory neurons, though without areal specificity. Therefore, this observation would not be evident in other datasets that primarily focus on cortical areas rather than cell identity.

Figure 6.10

Classic Calpains

A

CAPN1

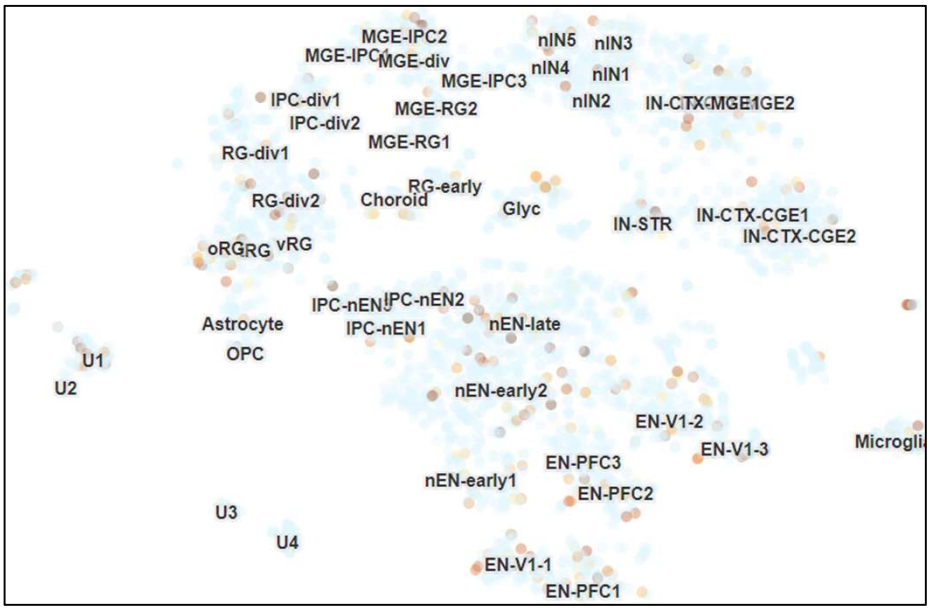

B

CAPN2

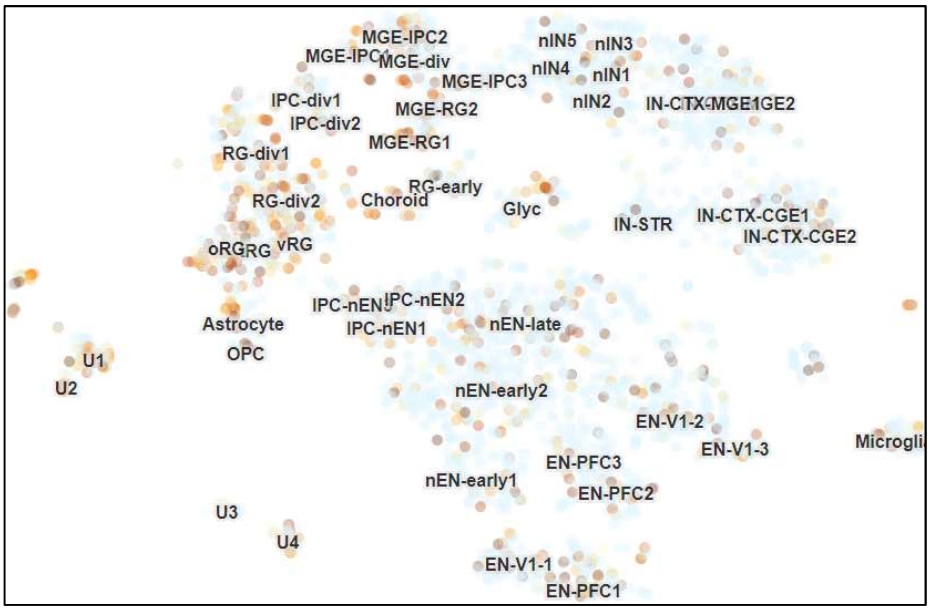

Figure 6.10

Non-Classic Calpains

C

CAPN5

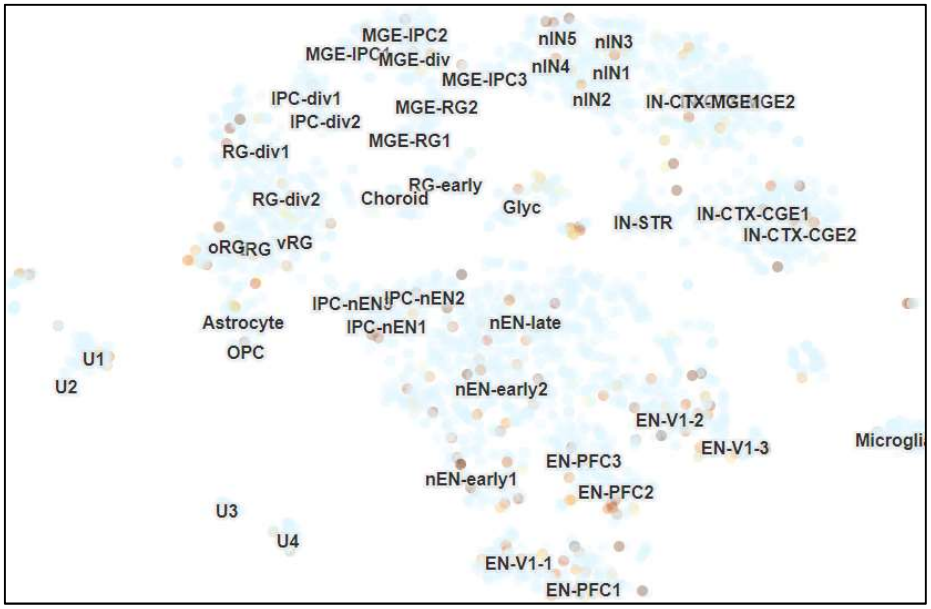

D

CAPN7

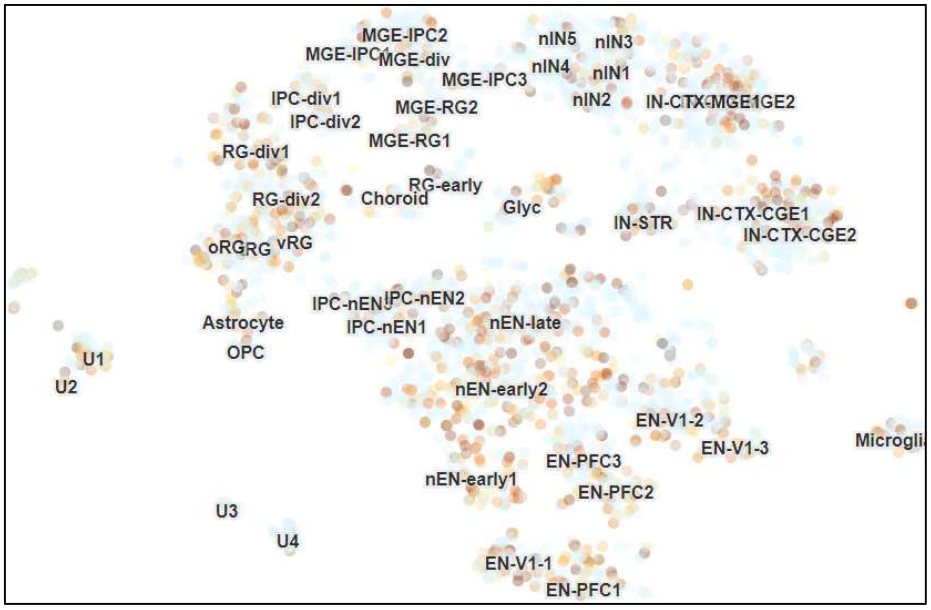

Figure 6.10

Cathepsins

E

CTSB

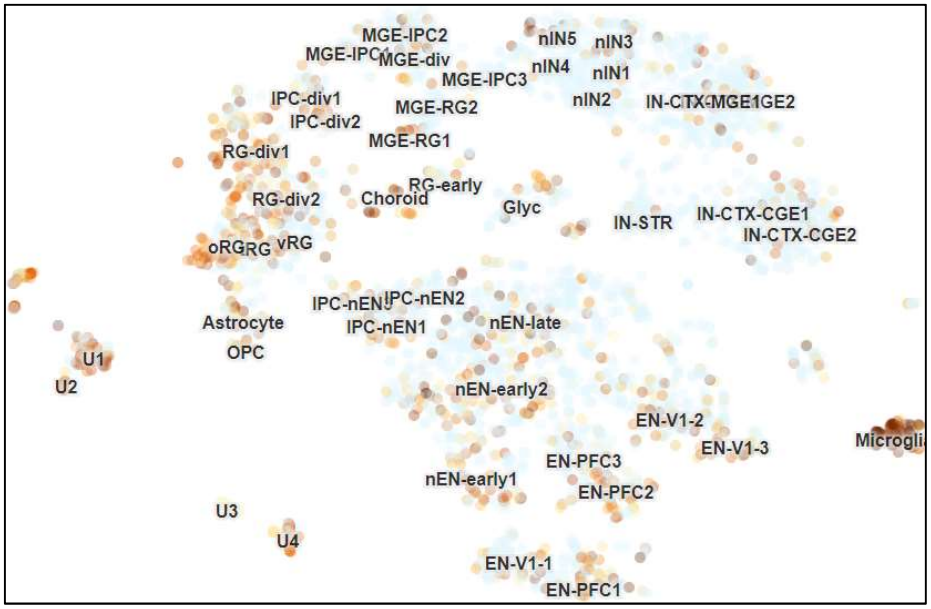

F

CTSD

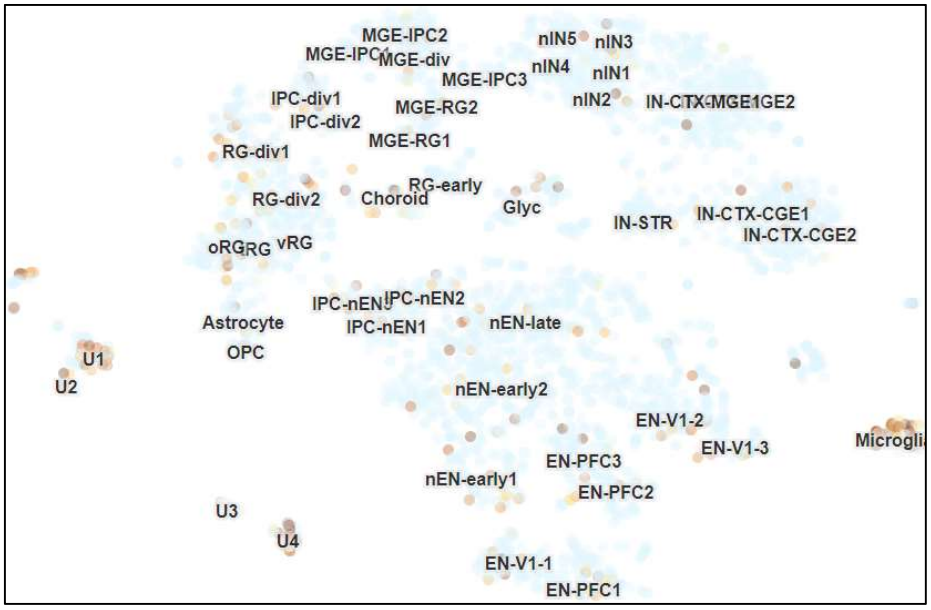

Figure 6.10

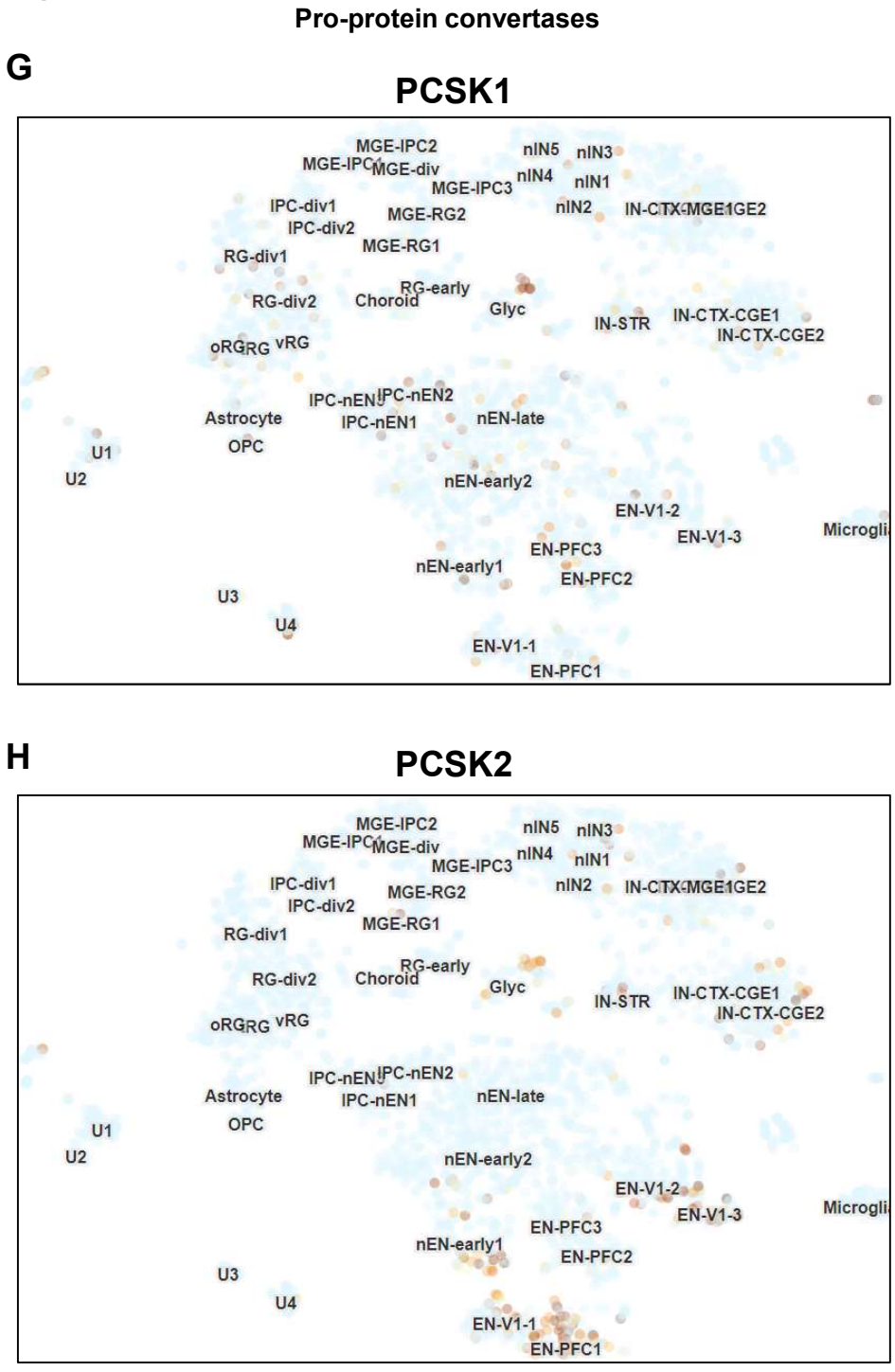

Figure 6.10: Single-cell transcriptomics of VGF enzymes in the human developing cortex (data from UCSC Cell Browser). Scatterplot of 4,261 cells after t-distributed stochastic neighbor embedding (t-SNE) on Weighted Correlation Network Analysis (WGCNA). Scatterplot of 4261 cells after principal components analysis and t-stochastic neighbor embedding (tSNE), colored by expression levels of each of the VGF enzymes analysed. Annotation of cell cluster identities was kept as in the original publication (Nowakowski et al., 2017) and is based on Weighted Correlation Network Analysis (WGCNA). Data were downloaded from the "Cortex Development" dataset in the UCSC Cell Browser (https://cells.ucsc.edu/) (Speir et al. 2021).

d. qPCR validation (13-20 PCW)

Classic Calpains (CAPN1, CAPN2)

CAPN1 expression levels are higher in all regions analysed at 20 PCW as compared to 13 PCW, especially in the thalamus and the frontal cortex (**Figure 6.11 A**). Its expression appears slightly lower only in the visual cortex.

CAPN2, on the other hand, appears less variable between the two ages (**Figure 6.11 B**). The expression only decreases in the thalamus between 13 and 20 PCW, while the opposite is observed in the the frontal neocortex.

Non-classic Calpains (CAPN5, CAPN7)

CAPN5 expression appears low in all areas analysed, as well as across ages (**Figure 6.11 C**). Frontal, somatosensory, and visual cortex has a slight increase of CAPN5 expression by 20 PCW.

CAPN7 expression is homogeneous across brain regions (**Figure 6.11 D**), with only few differences noticeable between the two ages analysed: the thalamus has a slightly higher expression levels at 20 PCW, as the insular and visual cortex. A moderate decrease is instead observed in the frontal and somatosensory cortex.

Cathepsins (CTSB, CTSD)

Both cathepsins exhibit higher expression levels compared to all the calpains in absolute terms, as can be seen thanks to the dashed line set arbitrarily at 0.5 in all graphs.

CTSB has an overall homogeneous trend of expression (**Figure 6.11 E**). From 13 to 20 PCW, its expression either remains the same, such as in the thalamus, insula, and somatosensory cortex, or else is moderately increased, like is the case for frontal, motor, parietal, and visual cortex.

CTSD is expressed at even higher levels than CTSB, but it exhibits a slightly different trend (**Figure 6.11 F**): the thalamus has exceptionally high levels of expression at 13 PCW, which are drastically decreased by 20 PCW. By this age, CTSD levels out to the expression detected in the neocortical areas. In the latter, a similar pattern is followed only by the insular cortex. The other areas do not show major differences across ages.

Pro-protein Convertases (PCSK1 only)

PCSK1 expression is extremely low as compared to all the other enzymes analysed so far (**Figure 6.11 G**), in line with the previous observation described in this section. Even more strikingly, between 13 and 20 PCW its expression levels decrease both in the thalamus and in the neocortical areas, which supports the RNAseq data from Kang and colleagues (Kang *et al.* 2011) showing a drastic drop of its expression in concomitance with midgestation.

As for PCSK2, I did not validate the expression by qPCR due to poor primer specificity.

Figure 6.11

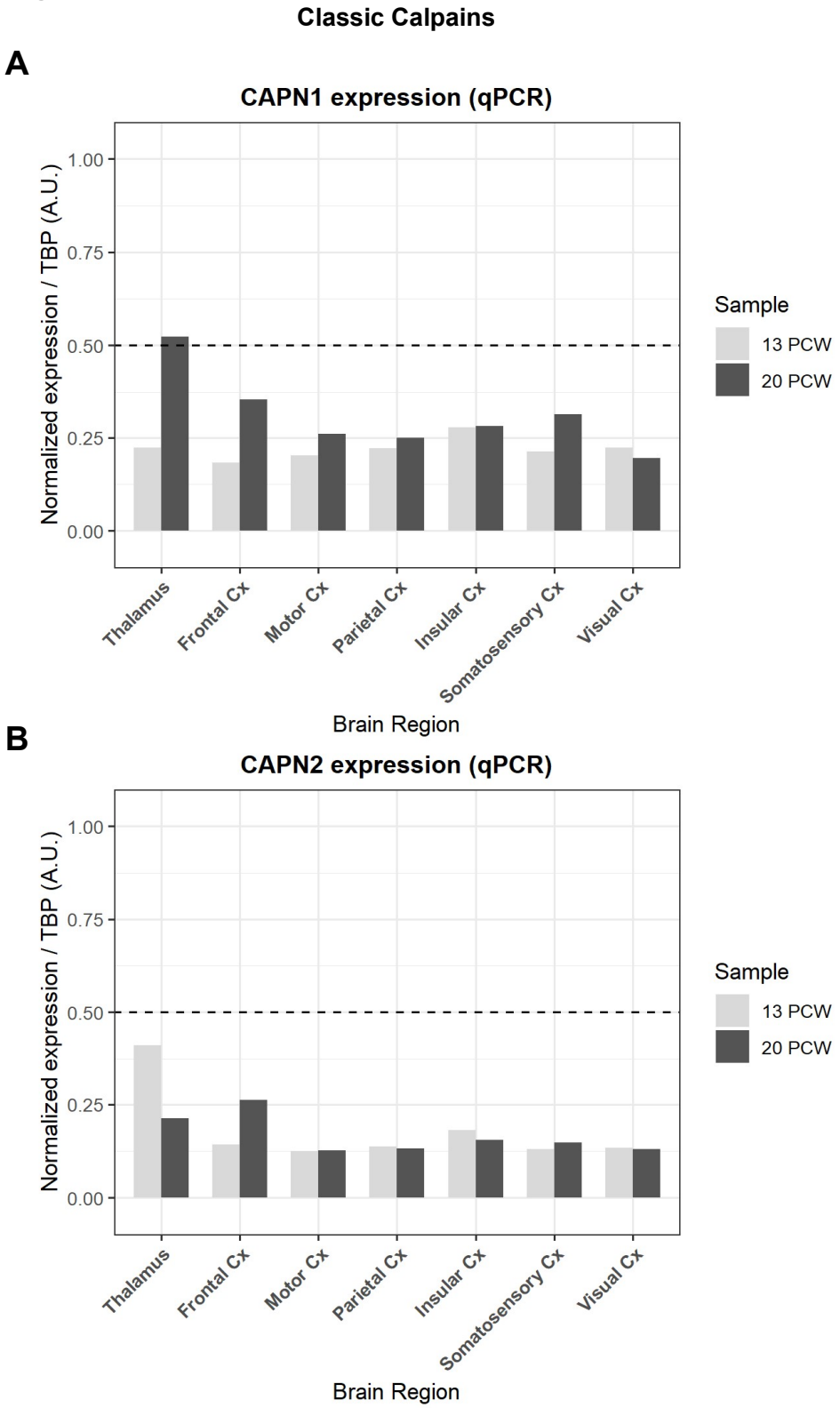
Classic Calpains
A
CAPN1 expression (qPCR)
Normalized expression / TBP (A.U.)
1.00
0.75
0.50
0.25
0.00
Thalamus
Frontal Cx
Motor Cx
Parietal Cx
Insular Cx
Somatosensory Cx
Visual Cx
Brain Region
Sample
13 PCW
20 PCW
B
CAPN2 expression (qPCR)
Normalized expression / TBP (A.U.)
1.00
0.75
0.50
0.25
0.00
Thalamus
Frontal Cx
Motor Cx
Parietal Cx
Insular Cx
Somatosensory Cx
Visual Cx
Brain Region
Sample
13 PCW
20 PCW

Figure 6.11

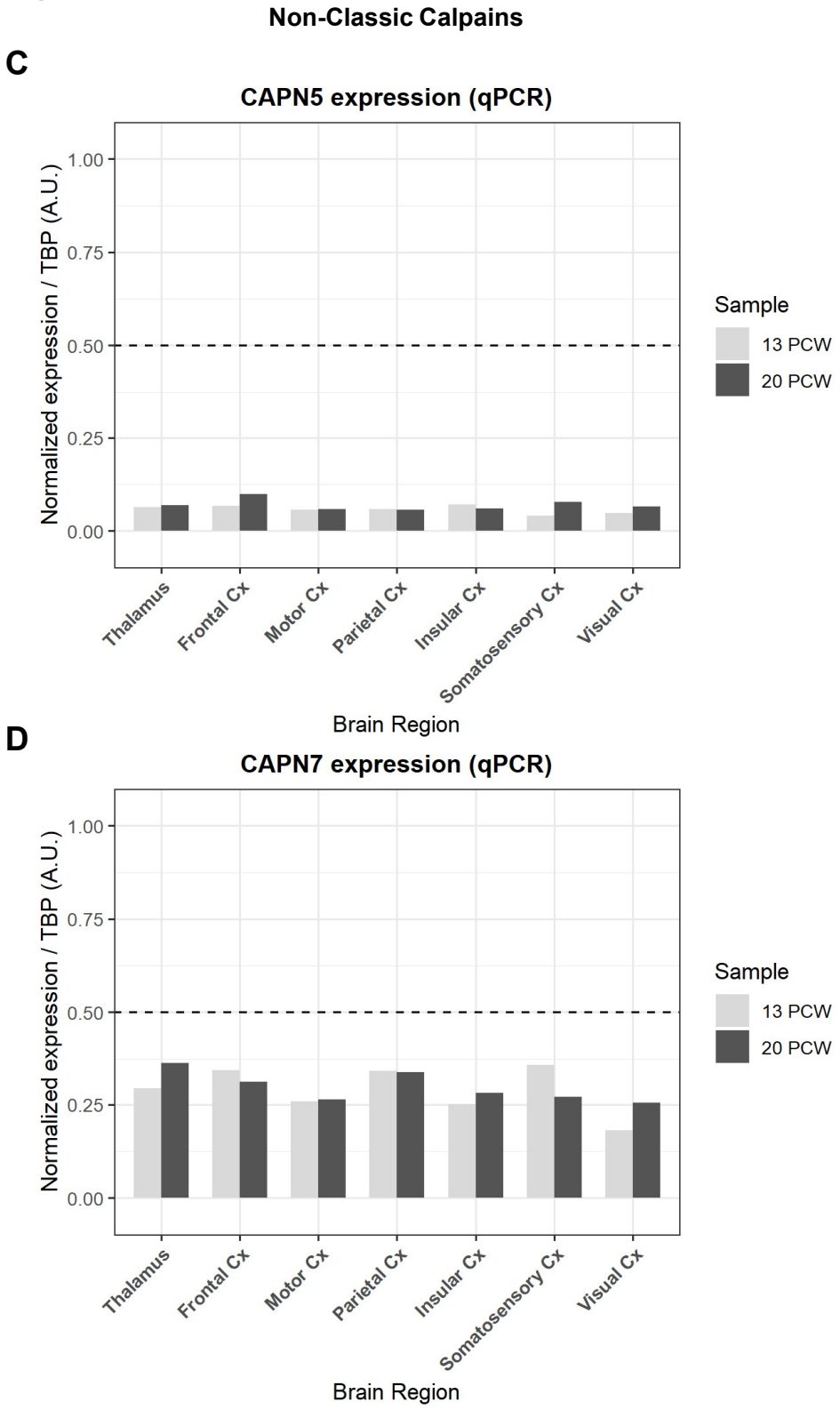
Non-Classic Calpains
C
CAPN5 expression (qPCR)
Normalized expression / TBP (A.U.)
1.00
0.75
0.50
0.25
0.00
Thalamus
Frontal Cx
Motor Cx
Parietal Cx
Insular Cx
Somatosensory Cx
Visual Cx
Brain Region
Sample
13 PCW
20 PCW
D
CAPN7 expression (qPCR)
Normalized expression / TBP (A.U.)
1.00
0.75
0.50
0.25
0.00
Thalamus
Frontal Cx
Motor Cx
Parietal Cx
Insular Cx
Somatosensory Cx
Visual Cx
Brain Region
Sample
13 PCW
20 PCW

Figure 6.11

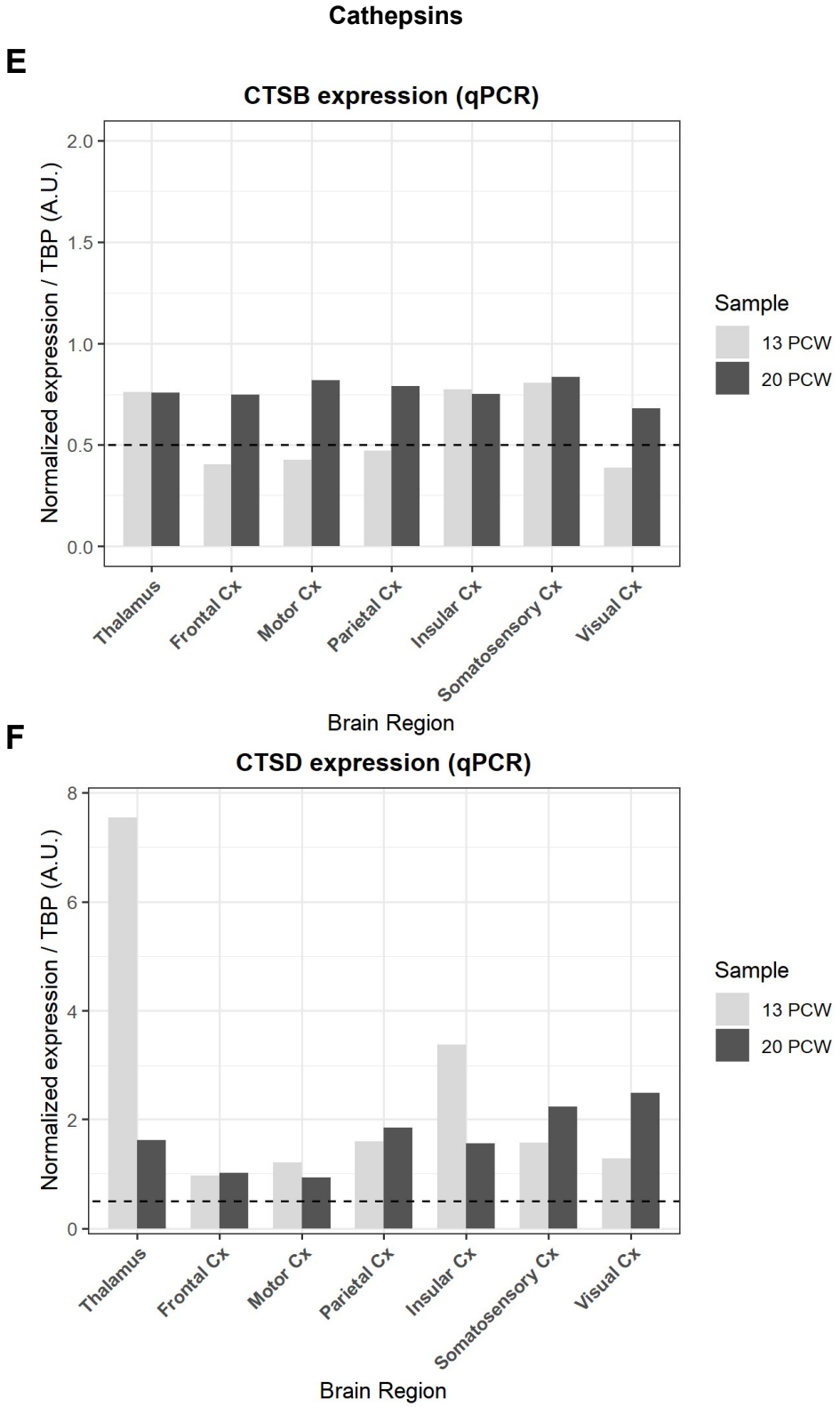
Cathepsins
E
CTSB expression (qPCR)
Normalized expression / TBP (A.U.)
2.0
1.5
1.0
0.5
0.0
Thalamus
Frontal Cx
Motor Cx
Parietal Cx
Insular Cx
Somatosensory Cx
Visual Cx
Brain Region
Sample
13 PCW
20 PCW
F
CTSD expression (qPCR)
Normalized expression / TBP (A.U.)
8
6
4
2
0
Thalamus
Frontal Cx
Motor Cx
Parietal Cx
Insular Cx
Somatosensory Cx
Visual Cx
Brain Region
Sample
13 PCW
20 PCW

Figure 6.11

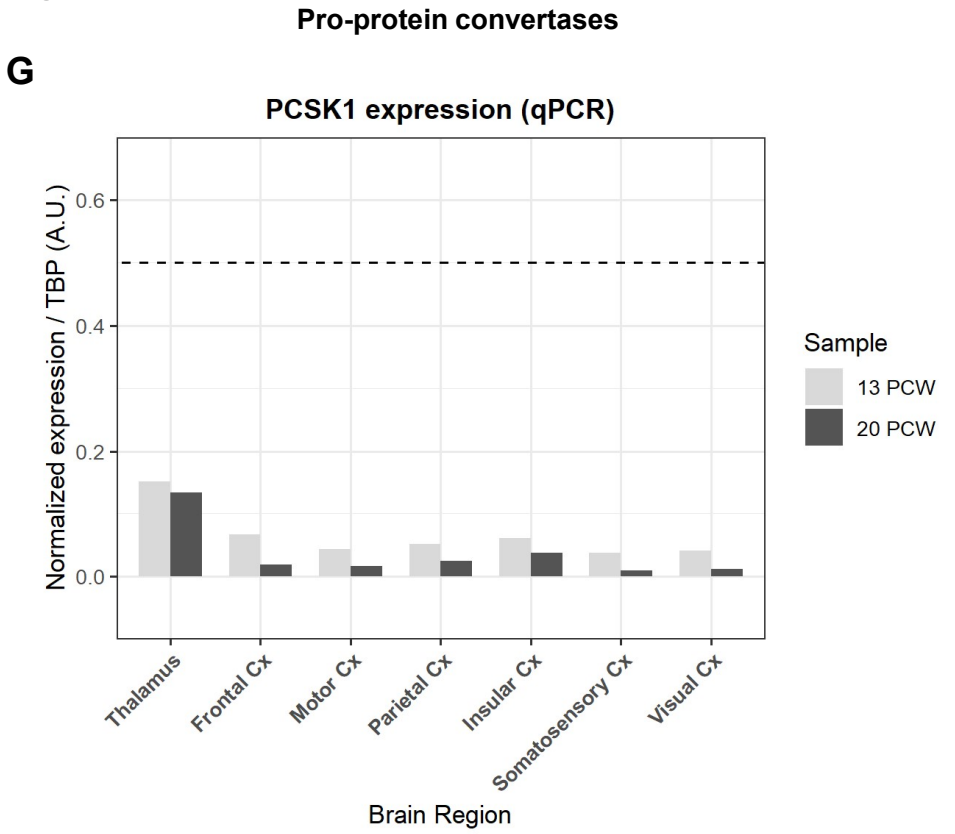

Figure 6.11: Validation of the expression pattern of VGF enzymes by qPCR (13-20 PCW). Quantification of VGF enzymes' expression levels in the 13 and 20 PCW human thalamus and neocortical areas evaluated with qPCR. Gene expression values are normalized relative to the housekeeping gene TBP. Values are absolute arbitrary units (A.U.) calculated with the ΔCt method. Statistics does not apply due to the small sample size.

e. Western Blot validation (20 PCW)

To conclude the expression profiling of VGF enzymes, I included a further validation at protein level by using Western blot analysis. I selected **CAPN1** as an interesting candidate amongst the list of novel predicted VGF enzymes discussed so far. In fact, its expression levels appear sustained during human brain development across different datasets analysed, apart from the single-cell transcriptomic dataset from Cell Browser. Importantly, CAPN1 is expressed both in the thalamus and in the neocortical areas. Therefore, its substrate full-length VGF, might encounter this enzyme not only within the vesicles in the thalamocortical neurons, where it is stored, transported to the axon terminals, and maturate, but also in the extracellular space in the cortex where it is released.

The analysis on CAPN1 protein content was performed in the same tissue extracts previously used for detection of VGF by Western Blot (see Chapter 5 Section 5.1.1) and obtained from one of the fresh-frozen brain samples available, namely donor "20 PCW #2".

Consistently with the other observations, and especially with qPCR data, CAPN1 is expressed throughout all regions, with moderately higher levels of the protein in the motor, parietal, insular and somatosensory cortices (**Figure 6.12**). As noticed in the other datasets, there is no major difference across neocortical regions, or the thalamus and the neocortex.

Figure 6.12

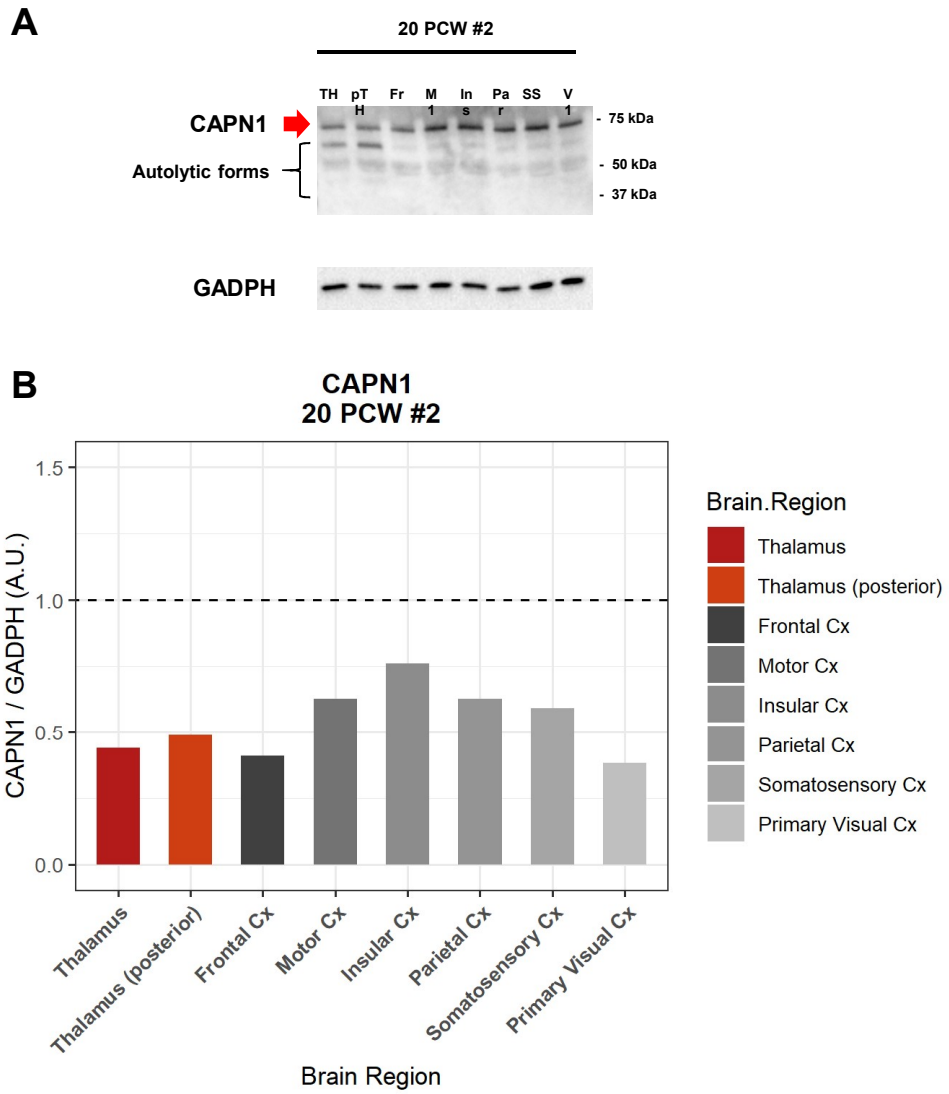

Figure 6.12: **CAPN1 protein levels in the 20 PCW human brain**. (**A**) Representative image of the blot for CAPN1 quantified in B. CAPN1 is detected as a band at 75 kDa. Lower bands are autolytic products of the enzyme and were not included in the quantification. GADPH was detected at 37 kDa and used for normalization and loading control. (**B**) CAPN1 densitometric A dashed line intercepts the y-axis at 1 for comparison. Colour coded by brain region.

Collectively, these findings demonstrate the presence of both previously characterized and newly identified proteases responsible for the enzymatic cleavage of VGF into neuroactive peptides. These enzymes can be detected at both the mRNA level (transcriptomic datasets; qPCR) and the protein level (proteomics) in the developing human cortex. Furthermore, these results indicate that VGF peptidases are not only present in the thalamic cells involved in VGF production, where they contribute to its maturation within the vesicles that store and transport this factor to axon terminals. They are also endogenously produced by human cortical cells, that can secrete these peptidases in the extracellular space, thus allowing full-size VGF to undergo additional enzymatic processing into various functional peptides upon its release in the target cortex. My analysis did not reveal strong area specificity in the expression of proteases responsible for the enzymatic cleavage of VGF into neuroactive peptides. These findings offer a potential explanation for the diverse roles that VGF may play in the modulation of neocortical development. They also shed light on the factor's ability to interact with and modulate various cell populations, including mitotic progenitors and post-mitotic neurons.

CONCLUSIONS

The data presented in this Chapter attempt to go beyond the simple expression profiling of the candidate molecular factor VGF in the human developing brain. They describe what might occur upon its release by the early thalamocortical afferents reaching the immature cortical areas.

VGF can interact with the two cortical cell populations identified as targets in Chapter 3, namely the progenitors of the OSVZ and the neurons of the SP. To test the potential effects of this molecular factor on these two cell populations by employing *in vitro* models of human cortical development, namely 2D iPSC-derived human cortical cell cultures, and 3D human organotypic cortical slices.

VGF did not alter the mitotic rates of human cortical precursor cells when applied to the first *in vitro* model. However, further characterization of the system is necessary, and it may be beneficial to modify the protocol for obtaining human cortical precursors. The current protocol employed may not adequately model this particular cell population due to the rapid phase of neural induction and subsequent exit of progenitors from the cell cycle. On the other hand, this protocol might be more appropriate to investigate the effects of VGF at later stages of differentiation when the cells are fully post-mitotic. Finally, it is important to examine the effects of VGF peptides specifically, as they may be the active components acting on cortical progenitors, rather than the full-size proprotein. Testing the peptides will provide a clearer understanding of the effects of VGF on human cortical progenitor cells.

On the other hand, this factor appeared to have a significant effect on human subplate neurons in the organotypic slices obtained from a 13 PCW human frontal cortex. The spontaneous activity of subplate neurons plays a vital role in various processes throughout cortical development (Hanganu *et al.* 2001; Singh *et al.* 2019; Molnar *et al.* 2020). As the application of VGF led to an increase in spontaneous activity specifically in the cortical subplate, my results suggest that VGF is involved in the developmental processes that depend on this activity.

Besides its action(s) as a full-size protein, VGF can also encounter specific proteases in the extracellular space, that can recognize this molecule and cleave it into neuroactive peptides.

VGF cleavage results in the formation of neuroactive peptides, which might be responsible not only for the functional effects of VGF on cortical precursors and neurons but also for the cell-specific influence on these different targets. To understand this mechanism of action, I investigated the potential proteases involved in VGF cleavage and their expression profiles in the developing human brain, particularly in the thalamus and the cortical subplate and germinal zones. This approach allowed me to indirectly explore the processing of VGF into neuroactive peptides, bypassing the limitations associated with directly studying small peptides derived from VGF. Future studies will focus on elucidating the interaction between these peptidases and human VGF, aiming to identify the specific peptidic products that are responsible for the cell-specific effects of VGF.

DISCUSSION

Consideration on the *in vitro* models used for VGF functional analysis

Early thalamocortical axons in the human brain target two different cell populations: SP neurons and OSVZ progenitors. The effects of thalamic VGF secretion on these cells may vary. To study their responsiveness to VGF, I used two *in vitro* approaches: human reprogrammed cortical cell cultures and organotypic cortical slices from human fetal brain (**Figure 6.1**). Both systems present intrinsic limitations, that should be considered. 2D cultures are a higher throughput and more standardized system and are valuable for conducting preliminary screenings of potential effects of VGF and determining optimal dosages for *in vitro* treatments. However, only limited cell populations can be consistently obtained, and neither the OSVZ nor the SP can be well modelled in 2D cell cultures. An alternative approach would be to utilize cerebral organoids, where the presence of OSVZ progenitors has recently been confirmed (Kadoshima *et al.* 2013; Lancaster *et al.* 2013; Qian *et al.* 2016). However, their identification within the organoid structure depends on *a posteriori* analysis of their expression profiles, thus limiting the range of experimental approaches that can be employed. Furthermore, there have been no reports of organoid structures that faithfully replicate the *in utero* subplate (Di Lullo *et al.* 2017; McLeod *et al.* 2023). Therefore, organoids do not present a significantly improved alternative to 2D iPSC-derived cortical cell cultures as a simplified model of human cortical development. The organotypic cortical slice model, on the other hand, is a low-throughput system and it does not allow easily for large sample sizes and biological replicates. Furthermore, inter-individual variability at both technical and biological levels are unavoidable. To mitigate limitations associated with each technique, I combined the two approaches together. All the results from in vitro experiments presented in this Chapter derive from pilot tests and need to be repeated in the future.

Considerations on the effect of VGF treatment of cell cultures

No notable change was observed in the proliferation rates of the induced progenitor cells by VGF treatment (**Figure 6.2**). This suggest that either VGF has simply no influence on mitosis of human neural progenitors, as previously observed in developing mouse cortex (Monko *et al.* 2022), or it does not as a full-sized protein but needs to be further processed into a specific peptide to have such effect. The latter interpretation aligns with observations in rodents, where adult hippocampal neurogenesis was increased by administration of TLQP-62 (Thakker-Varia *et al.* 2014). The presence or absence of the enzymes required for VGF processing in the *in vitro* system remains unknown and requires further investigation. Alternatively, as a complementary approach, using the specific peptide(s) may be necessary to observe any effect on cortical progenitor cells. On a technical level, more precise methods, such as using mitotic markers and/or BrdU birthdating, should be employed to assess more accurately cell proliferation than simple counting DAPI-stained nuclei. Finally, it might be necessary to reconsider the choice of protocol to derive induced human NPC *in* vitro, as the rapid differentiation process (See Chapter 2 Section 2.5.1) (Wang *et al.* 2017; Maguire *et al.* 2019; Boecker *et al.* 2020; Boecker *et al.* 2021) drastically limits the window for accurate manipulation and observation of effects in the progenitors. This protocol might be more advantageous for studying the effects of VGF into mature neurons, which are obtained in large amounts and within a brief time of differentiation *in vitro*.

Considerations on the preliminary characterization of the organotypic slice cultures

A preliminary characterization of the organotypic slice model was performed (**Figures 6.3-6.5**) and confirmed that the observations made regarding VGF in the *post-mortem* human fetal brain. This step was crucial before employing this system, as the slices were derived from whole brains, which preserved the intact cytoarchitecture of the cortex, but also partial segments of the axons innervating the region, including thalamic projections. The latter have been shown in this study to transport and secrete VGF in the cortex (Chapters 4 and 5), therefore if the axonal terminals were present in the cortical slices, the basal levels of VGF present in the cultures needed to be assessed. Although over

time *in vitro*, the reservoirs of VGF may be depleted by activity-dependent release, and not restored as normally would happen in the whole brain by thalamic production of new VGF-loaded vesicles, at first VGF would be released from the existing vesicles, even if in small quantities. Additionally, use of BDNF in the culture maintaining medium could potentially induce VGF upregulation in the cortical cell population (Alder *et al.* 2003; Jiang *et al.* 2019), which do not naturally express elevated levels of VGF (as discussed in Chapter 4). Therefore, basal levels of VGF should be accounted to determine the appropriate dosage for experimental treatment with the recombinant protein and eliminate these potential confounding factors.

Interestingly, the pattern of VGF protein distribution in the cortex appears remarkably identical to the post mortem brain samples analysed in Chapter 5 (**Figure 6.2**), with VGF-positive signal detected throughout the IZ, but also spread extensively into the germinal compartments at earlier stages (**Figure 6.3 A;** compare with **Figure 5.8)** and becoming more restricted and radially-organized by 17 PCW **(Figure 6.3 B, C;** compare with **Figure 5.9**). The distinct "palisade-shaped" pattern of VGF distribution was even more pronounced and well-defined in these cultures. This could be attributed to the relatively fresh state of the tissue and the short fixation time that ensured the exposure of protein epitopes for antibody binding.

Considerations on the effect of VGF treatment of the organotypic slice cultures

Spontaneous activity precedes sensory-driven stimuli, it is initially mediated by gap junctions, and establish a template for later emerging evoked activity (McVea *et al.* 2012; Ackman *et al.* 2014; Yang *et al.* 2018; Molnar *et al.* 2020). Notably, spontaneous activity can be detected at various levels: from sensorial organs, such as the retina, through thalamic cells where it originates calcium transients at mid-gestation in mice all the way to the cerebral cortex. These events are crucial in the early establishment of topography within the immature cortex where they are conveyed via thalamocortical axons, and they also regulate the projection path of these axons in a frequency-dependent manner and their collateral branching both *in vitro* and *in vivo* (Herrmann *et al.* 1994;

Uesaka *et al.* 2007; Mire *et al.* 2012; Castillo-Paterna *et al.* 2015; Moreno-Juan *et al.* 2017; Anton-Bolanos *et al.* 2018; Martini *et al.* 2018; Anton-Bolanos *et al.* 2019).

During late gestation period in rodents, synchronous spontaneous events represent the main pattern of activity within the thalamus (Moreno-Juan *et al.* 2017). These thalamic calcium waves are transferred to the cortical subplate neurons (SPN), which are functionally mature and form extensive local networks through gap junctions and chemical synapses (Dupont *et al.* 2006; Singh *et al.* 2019). These intricate connections allow thalamic spontaneous activity to be transferred to the cortex, actively participating in the establishment of cortical column units and the control of cortical area size. Stimulation of the embryonic thalamus elicits cortical responses in thalamocortical slices *in vitro*, as revealed by current source density analysis and with optical recording (Molnar *et al.* 2003; Higashi *et al.* 2005). This process has been observed during experience-independent stages of development in different animal models, including mouse, cats, ferrets, and in the prenatal primate brain (Rakic 1976; Crair *et al.* 1998; Crowley *et al.* 2000; Anton-Bolanos *et al.* 2019). Thanks to the advent of calcium-sensitive indicators, spontaneous calcium activity has been also investigated in brain slices *in vitro* by live-imaging, confirming intermittent gap-junction-mediated activation of cortical cell groups that mirror the functional patterns observed in adult cortical columns (Yuste *et al.* 1992).

Considering this critical role played by spontaneous activity in subplate (SP) neurons during the initial stages of cortical development and its significance in synchronizing thalamic and cortical functional units, it is the most pertinent functional output for assessing potential effects of thalamic VGF secretion at the cortical level. The observation that VGF application increased spontaneous activity in the cortical subplate suggests the involvement of VGF in the developmental processes that rely on this activity. This specific effect of VGF have not been previously reported in mouse (Sato *et al.* 2012; Sato *et al.* 2022), indicating this represents a newly-acquired mechanism of action of VGF in the developing human brain. However, as this has not been specifically investigated in animal model, it does not exclude the possibility that VGF might have similar effects on subplate neurons in other mammalian brains, and it encourages further investigations. This gap in literature

can be because most studies in animal models focused on later timepoint of development, potentially missing the critical period during which the effects of VGF on the transient subplate could be observed.

Some limitations of this experiment are noteworthy. Firstly, the cortical samples used in this pilot experiment were obtained from a very early stage of human brain development, specifically 13 PCW. The formation of the subplate in the frontal cortex, that is the area where these slices are taken from, represents the principal form of cortical laminar reorganization at this age (Kopić *et al.* 2023), thus possibly representing the earliest that this experiment could be performed. Consistently, neurons exhibited a low baseline activity at calcium imaging. In slices from 16-17 PCW brains, subplate neurons revealed a much stronger and more frequent spontaneous activity of these neurons, in line with the functional maturation of the transient subplate by this age (observation from unpublished data by Dr. McLeod). Furthermore, the small sample size (N=2 slices per condition tested) reduce the confidence of the results obtained. To address these limitations, I will need to repeat this experiment in a larger number of slices, and specifically including older samples. This would strengthen the statistical significance of the findings, and simultaneously enhance the technical and biological relevance of the observed signal, as more mature and spontaneously active subplate neurons would be recorded.

Consideration on the Protease Prediction, Selection, and Expression Profiling

Our understanding of the proteases responsible for VGF cleavage remains limited, despite the acknowledgment that VGF is processed into various peptides in both humans and rodents (Levi *et al.* 2004; Bresciani *et al.* 2019; Quinn *et al.* 2021). Recognized enzymes associated with VGF maturation belong to the proprotein convertase subtilisin/kexin (PCSK) family (Trani *et al.* 2002; Garcia *et al.* 2005; Zhang *et al.* 2010), though recent evidence proposes the involvement of other proteases as well (Quinn *et al.* 2023). My attempt to predict potential peptidases involved in VGF processing (**Figure 6.7**) revealed some members with recognized functions in brain development, particularly cortical neurogenesis, such as metalloprotease (MMP) family, that could be interesting

candidates for future investigations. My selection of enzymes in this study was pragmatic, aiming to limit the number of candidates for examination. The focus on the calpain and cathepsin families, among other predicted enzymes, was influenced by discussions with my collaborator Dr. Carlyle, who shared insights from her work on VGF cleavage before its publication (Quinn *et al.* 2023). Although in the output list of predicted proteases only two members of the calpain family were represented, namely CAPN1 and CAPN2, this was biased by their more extensive characterization than other calpains that led to the creation of entire databases dedicated to these enzymes (duVerle *et al.* 2010; DuVerle *et al.* 2011; duVerle *et al.* 2019). Nevertheless, since it is likely that many of the calpains share similar recognition patterns and thus process the same substrate (Sorimachi *et al.* 2012). Therefore, I manually checked which other calpains were also present in the list and I included those in my study. However, additional evidence and functional assays are required to test the hypothesis that these enzymes indeed cleave VGF. By profiling their expression, I offered an initial framework to select the specific VGF for further validation.

An interesting aspect emerged from this analysis already, that is the depletion of well-known enzymes responsible for its processing, such as PCSK1, in the developing human brain (**Figures 6.9 G-G'; 6.10 G; 6.11 G**). This finding holds implications not only for this VGF study but also for investigations into other molecules like BDNF (Rouille *et al.* 1995; Bathina *et al.* 2015), which are thought to be cleaved by the same enzyme. This observation raises intriguing points about the relevance of findings derived from the adult brain to the prenatal period. Furthermore, it demonstrates that the mere presence of molecules like VGF or BDNF in transcriptomic datasets doesn't necessarily indicate the presence of their functional forms at the gene transcription site. If these factors necessitate enzymatic processing, the absence or misplacement of that enzyme can significantly impact outcomes, and measuring its mRNA or even the full-size protein levels alone might not accurately mirror its functional activity.

The expression profiling of VGF proteases has also revealed an intriguing pattern of *layer-complementarity* among certain enzymes, specifically the pairing of pro-protein convertases PCSK1 and PCSK2 (**Figure 6.8 G-G' and H-H'**, respectively), and the classic calpains CAPN1 and CAPN2 (**Figure 6.8 A-A' and B-B'**, respectively). Even if the expression of an enzyme is not specifically confined to a particular area (**Figure 6.9-6.12**), it does not preclude the possibility of sub-regional restriction. The layer-specific restriction of these enzymes may be critical for ensuring the precise delivery of the appropriate peptide to its intended target cell population, such as post-mitotic neurons in the subplate and outer radial glia in the OSVZ. Importantly, this mechanism offers an energy-efficient strategy by transforming a single molecular factor, such as VGF, into multiple molecular factors.

The specificity of its effects within specific layers is not dictated by the physical location of factor secretion, which could be challenging due to diffusion or overlapping regions, particularly in younger and smaller brains. Instead, the specificity is determined by the selective encounter between the generic molecule, VGF, and the restricted repertoire of enzymes responsible for its cleavage into functional peptides. Yet, this hypothesis requires further support, such as: (i) functional assays to assess the product of full-size VGF cleavage by these layer-restricted enzymes, similarly to Quinn's work on Calpain-1 and Cathepsin S (Quinn *et al.* 2023); (ii) analysis of the specific effects of the resulting peptides on the target cortical cell populations. Differential interactions of distinct VGF peptides with mitotic progenitors and post-mitotic neurons could strongly support this hypothesis.

CHAPTER 7

General discussion and future perspectives of the study

7.1 General discussion on the study

In my thesis I investigated the intricate spatiotemporal dynamics governing the initial interactions between thalamic axons and the developing cortex within the human fetal brain. Central to my inquiry was the evaluation of the interactions between these axons and the cortical progenitors and subplate neurons in the developing human brain. My work provided evidence of anatomical overlap between TCA and germinal compartments, most notably the OSVZ (Zunic Isasegi *et al.* 2018). A similar result was obtained at correspondent developmental stages in monkey by Carney in the Molnár and Kennedy laboratories (Carney *et al.* 2004). Both studies unveiled an unprecedented pattern of innervation in macaque and human, with thalamocortical axons projecting toward the OSVZ - a phenomenon that has never been observed in any other extensively studied species (Molnar *et al.* 1998; Molnar *et al.* 2003).

General discussion on the main results of the study

I confirmed that thalamocortical projections arrive to the cortex at very early stages of neurogenesis in human, in alignment with existing literature (Alzu'bi *et al.* 2019), and from initial stages they maintain a tight anatomical relationship with the germinal compartments. This anatomical proximity establishes a basis for direct interactions with progenitor cells, as evidenced by instances of trans neuronally labelled radial glial cells (RGCs) in both the 13 post-conceptional week (PCW) stage (**Figures 3.13 and 3.14**) and the 17 PCW stage (**Figure 3.27 and 3.29**). Notably, the interaction was specific to the basal processes of the outer RGC (oRGC) populating the OSVZ and did not label progenitors with endfeet reaching the ventricular surface. In fact, DiI-labelled vRGC soma were not detected in the VZ/ISVZ in both ages, which would be expected if the labelling were merely induced by nonspecific transfer of the dye from the tangentially oriented TCA and the radially-oriented basal processes of RGC crossing their path. It is worth highlighting that at the time of Carney's study on fetal

monkeys, the oRGC had not yet been identified as a separate progenitor population (Hansen *et al.* 2010). Consequently, it was assumed as possible that transneuronal labelling of cell bodies in the OSVZ were byproducts of the extended incubation period with lipid soluble carbocyanine dye. It would be interesting to revisit these experiments in the fetal monkey brain considering the current knowledge on the oRGC, as well as the availability of specific molecular markers for these precursors (Pollen *et al.* 2015) .

Despite the clear cases of transneuronal labelling of oRGC (**Figures 3.27 and 3.29**), I also gathered evidence for DiI-labelled thalamocortical fibres in the OSVZ. These labelled fibres correspond to anterogradely labelled TCA, end in growthcones and they do not contain DAPI stained nuclei (**Figure 3.30**). In fact, they appeared remarkably like the axons extending in the subplate (SP), that were characterized extensively (Ghosh *et al.* 1993; Catalano *et al.* 1998; Hanganu *et al.* 2002; Anton-Bolanos *et al.* 2018). DiI-labelled radially oriented fibres were at proximity with both Tbr1-positive subplate neurons (**Figure 3.25**) and HOPX-positive progenitors (**Figures 3.28 and 3.29**).

While SP neurons are known to establish synaptic contacts with the thalamic axons from initial stages (Moore *et al.* 2011; Kostovic *et al.* 2015), both cell populations could be influenced by secreted molecules that are produced by thalamic neurons and transported to the cortex via their axonal projections, that release them in the extracellular environment. A paracrine mode of interaction lends itself as a plausible explanation for the presence of projections within the OSVZ. Given the extraordinary expansion of this compartment over evolution (Rakic 1972; Smart *et al.* 2002; Zecevic *et al.* 2006; Kelley *et al.* 2022), the readjustment of thalamic axons within the transient cortical compartments in the human brain is an adaptation to exert paracrine influence on progenitor cells. In fact, for a thalamus-derived secreted molecule to be effective on human RGC, it should diffuse over a considerable distance from the intermediate zone (IZ) where it is released by the thalamic axons. It is possible that thalamic axons might have evolutionarily adapted by extending collateral projections directly into the OSVZ, a mechanism that could efficiently provide extrinsic molecular cues to cortical progenitors within primate brains where the OSVZ is substantially expanded. Support for the effects of thalamus-derived paracrine molecules in modulating cortical progenitors come from mouse studies,

where they show the pivotal role played by TCA in instructing precursor cells on their fate commitment, leading to the generation of layer 4 cortical neurons at the expense of upper layer neurons. In rodents, the arrival of thalamic axons in the cortex coincides with layer 4 neurogenesis (Monko *et al.* 2022). In human, where thalamic axons were observed in the OSVZ, the effect of paracrine molecules secreted by TCA might affect corticogenesis differently. Specifically, the progenitors of the OSVZ are responsible for the production of upper layer (i.e. supragranular) cortical neurons. An evolutionary adaptation of the TCA to reach these precursor cells effectively and specifically might underly a key role played by extrinsic paracrine cues to modulate the generation of these cortical cells. This would provide a mechanistic explanation of the thalamic influence on important processes such as tangential cortical expansion and gyrification, that have been linked to these cortical cells in human (Reillo *et al.* 2011). Moreover, the reduced thalamic influence on these progenitors might explain the changes in brain folding observed in the enucleation model by Rakic and Dehay as reviewed in the introduction in **Figure 1.12** (Rakic 1988; Dehay *et al.* 1996). The close thalamocortical and oRG interaction that I observed in human and the previous observations in fetal monkey both occurred at the time of the switch between deep and upper layer cortical neurogenesis.

My TCA tracing results supported my hypothesis of a role played by thalamic axons in modulating the intrinsic developmental programmes of human corticogenesis, I then sought to investigate the molecular pathway underlying such interaction. Two primary strategies can be adopted when seeking a molecular candidate for these interactions:

1. **Reviewing existing datasets and literature** to identify a paracrine factor with promising attributes for the envisaged role, yet to be validated in humans.
2. Employing an **unbiased, data-driven approach** to screen for novel candidate molecules that could potentially mediate the thalamic extrinsic modulatory impacts within the human cortex. Such molecules may have evaded prior identification due to the predominant use of animal models in previous studies.

For the scope of my thesis, I followed the first approach, while the second approach is discussed later amongst the future directions of the study (Section 7.2). In the current work, I focused on VGF, a molecule that has been previously associated with the extrinsic modulation exerted by thalamic axons during neocortical development in rodents (Sato *et al.* 2012; Monko *et al.* 2022; Sato *et al.* 2022). Despite these studies indicate that this effect is confined to primary sensory systems, I did not consider this a constraining factor in my selection of VGF as a candidate. In fact, it is plausible that evolutionarily conserved molecules, such as VGF, undergo repurposing to serve new roles in distinct species, according to the overall evolution of the systems they participate in. This phenomenon is evident not only at the molecular level, but also at anatomical and cellular levels. For instance, recent research demonstrated that certain classes of inhibitory interneurons, although originally conserved across mammalian brains, underwent repurposing in primates. These neurons, referred to as peristriatal *straitum laureatum* neurons, shifted from their initial role in the small olfactory bulb of rodents to contribute to the expanded striatum and cortex in primates (Schmitz *et al.* 2022). In a comparable manner, it is reasonable that a conserved growth factor, like VGF, has been channelled to fulfil its pivotal functions in an evolutionary more recent context such as the case of associative regions in the human brain. This hypothesis was supported by evidence from studies that linked VGF to human conditions related to disruption of prefrontal connectivity, such as neurodevelopmental disorders in human (Thakker-Varia *et al.* 2010; Bartolomucci *et al.* 2011; Busse *et al.* 2012; Quinn *et al.* 2021). However, these previous studies have not directly investigated thalamocortical system development. I based my selection on the fact that VGF was correlated to the very same conditions where the thalamocortical connectivity appeared to play a role, as well as the two cortical transient compartments that I identified as their initial target in human, namely the subplate and the OSVZ. A peculiar aspect of VGF is its conversion into multiple peptides, recognized for their significant effects on cellular populations that can be analogous of either subplate neurons (post-mitotic functionally active neurons) (Sato *et al.* 2012; Behnke *et al.* 2017) or OSVZ progenitors (actively mitotic neural progenitors) (Thakker-Varia *et al.* 2014; Monko *et al.* 2022). The effects of VGF and its derived peptides have yet to be explored within the developing thalamocortical system of humans. Therefore, the potential to

elicit the predicted effects in these specific cell populations remained to be assessed. This is what I started investigating in the *in vitro* studies presented in Chapter 6.

Critical assessment of the results contradicting the working hypothesis of the current study

It is crucial to acknowledge that not all the data presented in this study align with my initial working hypothesis, positing that VGF is a crucial thalamic molecule contributing to cortical specification through paracrine mechanisms. A few of my own observations directly contradict this perspective, although representing a minority of cases, and thus not leading me to completely discard my hypothesis. For instance, the Brainspan LMD microarray data (**Figures 4.5 and 4.6**) revealed the presence of Vgf mRNA within the cortical intermediate zone (IZ), This observation is in contrast with the first criterium I set to evaluate my working hypothesis, whereby VGF mRNA should not be expressed endogenously by the cortex, but rather being preferentially produced at thalamic level. One plausible explanation for this finding could involve the active transport of VGF mRNA through thalamocortical axons to axon terminals, where it could undergo translation by free ribosomes within the synaptic terminals. This rationale aligns with VGF's nature as a synaptic protein, many of which are notably translated within synaptic terminals rather than the cell body. However, this hypothesis requires further scrutiny and investigation. Interestingly, there is limited literature exploring this potential pathway for VGF, and the available information appears to be contradictory. Notably, one study confirms a specific activity-dependent transcription-independent upregulation of VGF (Lin *et al.* 2021), while conflicting results can be found elsewhere in the literature (Glock *et al.* 2021). The lack of additional supporting evidence leaves the presence of VGF mRNA within the cortical IZ unexplained and, in itself, contrasting my working hypothesis. Further research is needed to elucidate the mechanisms underlying this unexpected observation. A similarly contrasting observation against criterium #1 of my working hypothesis derived from the results of immunohistochemistry (IHC) conducted on the frontal cortex. The pattern of VGF protein distribution in the 13 and 17 PCW human cortex (**Figures 5.6 and 5.7**, respectively) resembled the palisade organization of the radial glia basal processes and could suggest an endogenous production of the protein by the cortical progenitors of the frontal cortex. This would also be the most obvious

interpretation of the IHC results, if considered by themselves. However, when interpreting these data, I also considered the parallel mRNA expression profiling previously that I conducted in the human frontal cortex and presented in Chapter 4. Given the absence of any observed endogenous expression of VGF by the frontal cortex in both qPCR (**Figure 4.13**) and single-cell transcriptomics analyses (**Figure 4.12**), I opted to provide an alternative explanation for the pattern of VGF protein distribution at this level, which was more in line with my working hypothesis. However, additional experiments might be needed to confirm either one or the other explanation with confidence. A plausible alternative explanation for this discrepancy could be the orientation of the cutting plane in this anterior-most brain slab. In fact, the significant expansion of the human frontal lobe led to a considerate "invagination" of this region, resulting in a slightly different orientation of the thalamocortical axons (TCA) in these frontal sections compared to the parietal slices depicted in **Figures 5.8** (16 PCW) **and 5.9** (17 PCW).

Finally, the insular cortex presents a unique case as it stands out from the general observation of VGF being expressed at exceptionally low levels in the cortex (**Figure 4.13**). This deviation is not a result of technical artifacts in the experimental analyses presented in my Thesis, as it has been recapitulated by spatial transcriptomics in similar human fetal samples (unpublished observation from the laboratory of Professor Chiaki Ohtaka-Maruyama, Tokyo Metropolitan Institute of Medical Science, Japan). This finding directly contradicts my working hypothesis. It is crucial to note that VGF can exert its influence both in a paracrine and autocrine fashion, and the two mechanisms can co-exist. However, for the specific focus of this study on the paracrine modulation of human cortical development, I introduced criterium #1 to eliminate the possibility of effects induced by an autocrine mechanism. The presence of high endogenous VGF expression in the insula suggests that, in this region, VGF might primarily act as an autocrine factor, with underlying developmental programs differing from those in other cortices. This intriguing aspect should be subjected to further investigation in separate studies. For the purpose of this Thesis, given this exception in the insula, I chose to concentrate on other cortical areas where my criterion was met, directing my interest away from this specific cortical region.

7.2 Future perspectives of the study

A second approach that can be used to identify relevant candidate paracrine factors like VGF (Sato *et al.* 2012), as well as molecules mediating cell-cell direct contact like EFNA5/EPHA4 (Gerstmann *et al.* 2015), is by using a **bioinformatic data-driven search.** For instance, the single cell transcriptomic datasets used for VGF expression profiling in the human thalamus and cortex in Chapter 4 can be used as an input for this search. These datasets hold the advantage of offering single-cell resolution, allowing for *post hoc* marker analyses of the cell clusters present in the dataset similarly to what I have done to identify the VGF-expressing thalamic cells as mature projecting neurons (**Figures 4.7 and 4.8**). Since my data suggest that SPN and oRGC are the earliest cell populations contacted by the thalamic axons within the human developing cortex, a similar marker analysis can be performed to identify the clusters that correspond to these cell population within specific cortical datasets. By sub setting them, an unbiased search can be done by using recently developed tools such as LIgand-receptor ANalysis framework (LIANA, https://saezlab.github.io/liana/) (Dimitrov *et al.* 2022) that integrates existing methods (https://www.cellphonedb.org/) (Vento-Tormo *et al.* 2018) to identify interacting ligand-receptor pairs in single-cell, spatially resolved, and multi-modal omics data. The thalamocortical projecting neurons (cluster #2 in the thalamus dataset, **Figures 4.7 and 4.8**) can be used as the source of ligands, while the clusters identified by marker gene analysis as subplate neurons and/or oRGC in the cortical datasets (**Figures 4.9-4.12**) can serve as source of "receptors". From the resultant list of ligand-receptor interactions, further refinement can be done based on the relevance and specificity of these interactions (p-values) and on the nature of the molecules involved (for example, paracrine vs membrane-bounded). Further refinement can depend on the aims of the study: a comparison can be made across cortical cell targets (i.e. receptors in SPN vs oRGC), or across cortical areas (for example, prefrontal associative cortex and primary sensorial areas). However, in the second instance, better spatial resolution would be needed also at thalamic level, as one should match projecting neurons from specific nuclei of the thalamus to those dinstinct cortical areas. Spatial transcriptomics might be further implemented in this specific case. Finally, cross-species comparisons could be also perfomed, when similar datasets are available for other developing species (i.e. Allen Brain resource for mouse and

monkey). This is an interesting avenue that I aim to explore in the future and can complement this study by taking a different approach to the same research questions.

Despite this approach might provide a new fresh prospective on the topic, it is not without limitations. For instance, one necessary assumption for the identification of a pair of ligand-receptor is that both molecules have been previously characterized and determined as interacting in a pathway. This information typically stems from rodent studies; therefore, it is possible that the interaction does not occur the human brain. Moreover, cases such as VGF would be excluded from the results, as its specific receptors remain unidentified, while the receptors proposed often are related to VGF peptides that cannot be included as independent entries ("ligands") in transcriptomic analyses since they share the same mRNA as VGF itself. Regardless the specific approach taken to identify a molecular candidate, it is imperative to bare the specific limitations, and manually select based on relevant literature available.

Besides its action as a full-size protein, VGF can also encounter specific proteases in the extracellular space, that can recognize this molecule and cleave it into neuroactive peptides (Ferri *et al.* 1996; Levi *et al.* 2004; Mishiro-Sato *et al.* 2010; Quinn *et al.* 2021). Importantly, VGF peptides have been more extensively at functional level. In fact, most of the functions associated to this molecule derive from studies on its peptides, including the potential effects on cortical progenitors and neurons that I considered key features for the initial section of VGF for this study. A more extensive investigation of the peptide distribution, effects, and cell-specific responsiveness should be added to the *in vitro* validation of VGF, as discussed in Chapter 6. To extend this consideration, plans have been made to improve the reliability and overall validation of VGF effects on human cortical neurons and progenitor cells. First and foremost, it would be beneficial to repeat the preliminary assessment of VGF effects with sufficient power in both *in vitro* 2D cultures and 3D organotypic slices. Besides increasing the number of technical replicates, I also plan to test VGF application at various stages of the culture protocol (cell cultures) or at different ages of human development (organotypic slices). Taking advantage of these *in vitro* platform for screening effects in an unbiased manner, I also intend to directly

test recombinant VGF peptides, rather than solely the full-size protein. This might yield more comprehensive results on VGF mechanisms and functional effects.

To gain further insights into these proteoforms, future studies should also include an analysis on the proteases cleaving VGF, and especially their potential regional, laminar, and cell-specific patterns of expression in the developing human brain. The example of prohormone convertases (PC or PCSK), the most characterized enzymes for VGF cleavage, demonstrates that adult human data may not always reflect prenatal stages. This aspect must be carefully considered in any study in developmental neurobiology.

Finally, an optimized strategy for future validation of the current study would be the use of **thalamic explants in co-culture** with cortical slices. This model has proven highly valuable in rodent studies (Yamamoto *et al.* 1989; Yamamoto *et al.* 1992; Blakey *et al.* 2012; Matsumoto *et al.* 2016; Matsumoto *et al.* 2018). Dr. McLeod and Dr. Clowry at Newcastle University have recently started optimizing the human thalamo-cortical co-culture system, and it would be extremely interesting to replicate some of the analyses conducted in this study in such model. For instance, TCA tracing could be perfomed, either by carbocyanine dyes or other axonal tracers (i.e rabies retrograde tracing; fluorescent genetic tracers), to confirm the results gathered in *post-mortem* tissues (Chapter 3) and assess whether thalamic axons have affinity to both OSVZ and SP in a similar pattern as *in vivo*. Furthermore, I would be able to investigate the expression, transport, secretion and effects of VGF in a more physiological context, alongside the presence of VGF cleaving proteases that are included into the secretory granules with it.

This approach might shed lights into the mechanisms underlying the handshake between thalamic and cortical projections in human, and the details of the interactions between thalamic axons and cortical cell populations, to complement the seminal studies conducted in rodents (Molnar *et al.* 1991; Higashi *et al.* 2002; Molnar *et al.* 2003; Yamamoto *et al.* 1989; Yamamoto *et al.* 1992; Matsumoto *et al.* 2018).

7.3 Other future directions

Finally, what emerged from my study is that the expression of a molecule does not translate inequivocably into its presence as active protein *in situ*. This process involves numerous factors such as translation, post-translational processing, and axonal transport, all of which must be considered. Recent progress in the field of transcriptomics has led to a shift towards identifying novel markers or molecular candidates within the newly available datasets. Recent advancement in the field of transcriptomics led to a shift toward seeking for novel markers and/or molecular candidate to study within the newly available datasets, often overlooking the importance of these factors.

This is well exemplified by the lack of comprehensive proteomic datasets to complement the numerous transcriptomic datasets generated for the developing human brain, with only a handful of research groups beginning to venture into such investigations recently (Nascimento *et al.* 2019; Wang *et al.* 2023). Recognizing this gap in the literature, I initiated a collaborative endeavor with Dr. Helle Bogetofte and Prof. Martin Røssel Larsen (University of Southern Denmark) to establish an extensive proteomic survey of the 20 PCW human brain, using one of the samples analysed in this work. As highlighted by the case study of VGF, post-translational events are also crucial when interpreting the function of a specific molecule. Since technical advancements in the field allow for the investigation of post-translational modifications (PTMs) in proteomic studies (Zhao *et al.* 2009; Doll *et al.* 2015; Aebersold *et al.* 2018), we will also include this approach in the analysis. Notably, PTMs can have a significant impact in the physiological events of human brain development, as well as in neurodevelopmental and neuropsychiatric conditions (Mueller *et al.* 2020; Murtaza *et al.* 2020; Grubisha *et al.* 2021; Smith *et al.* 2022). The dataset would complement available transcriptomic data, allowing for candidate validation as well as identification of novel targets of interest for future studies in the context of human cortical development.

7.4 Limitations of the study

A crucial aspect to consider while interpreting the data is the **inter-individual variability** observed throughout this study. This variability was particularly notable when comparing two samples from the same age, as evident in the comparison between 20 PCW brain #1 and #2 (qPCR and Western Blot analyses, in Chapters 4 and 5, respectively). A similar consideration applies to any comparison between the results I presented in this study, and other data obtained in similar human studies by other researchers, even when the same Tissue Bank sourced the samples, or the same gestational age is analysed. Such variability is inherently linked to working with human samples and dealing with small sample sizes. While differences between samples are beyond control, they should not be considered as merely negative factors *per se*. In fact, inter-individual variability exists, and as such should be regarded as physiological, an aspect that is very often disregarded and rather avoided in animal studies. Another important and related limit is the **lack of statistical relevance**. Although a statistical test would be more informative on the significance of the results described, the experimental design of this study does not allow for any to be applied. For example, to compare molecular data obtained in different brain regions between two developmental timepoints, a paired t-test could be applied. However, this test would require the assumption of normal distribution of the data, that cannot be assumed if only one observation is available for each brain region. Even if other tests, such as Wilcoxon signed-rank test, overcome the requirement for normal distribution of the, these are also limited by the small sample size used in this study, and were in fact inapplicabile in the analyses presented.

Additional limitations are imposed by the **choice of specific datasets** used in this work. For instance, the way samples were collected in different studies, the subsequent processing, and protocols applied to obtain different transcriptomic and proteomic datasets vary substantially, and this might mislead the interpretation of some results. This is well exemplified by the case of the LMD microarray (Brainspan) used in this work to evaluate the layer-specific expression of VGF (Chapter 4), as well as VGF enzymes (Chapter 6). Calpain 5 (CAPN5) appeared to have an inversion of the trend of expression within the cortical plate, with high levels in the motor cortex and low levels in the somatosensory cortex at 15 PCW, and an opposite areal expressionat 21 PCW. (**Figure 6.8 C-C'**). However, the dataset lacks

any areal information for all the other cortical layers, as the sampling approach was not the same across layers of the cortex. Therefore, drawing the conclusion of a layer-restricted phenomenon might not be appropriate in this example, and must be eventually confirmed by experimental validation. Similarly, data on VGF expression levels are not available for the transient cortical layers across areas (VZ, SVZ, IZ, SP) (Table 4.2), but only for the CP (Table 4.3).

Conclusive remarks

In conclusion, my thesis resides at the heart of an enduring discourse, wherein fundamental questions about intrinsic and extrinsic determinants of cortical development and specification were articulated more than three decades ago, initiating the protomap-protocortex debate (Rakic 1988; O'Leary 1989). Despite considerable effort in the field, the mechanistic details of these events in human remain far from clear. The advent of sophisticated methods for monitoring cell-cell interactions, imaging, alongside spacial transcriptomics and proteomics innovations holds great promise for future investigation on the evolution and development of the most fascinating human feature – the cerebral cortex.

References

Ackman, J. B. and M. C. Crair (2014). "Role of emergent neural activity in visual map development." Curr Opin Neurobiol **24**(1): 166-175.

Adorjan, I., T. Tyler, A. Bhaduri, S. Demharter, C. K. Finszter, M. Bako, O. M. Sebok, T. J. Nowakowski, K. Khodosevich, K. Mollgard, A. R. Kriegstein, L. Shi, A. Hoerder-Suabedissen, O. Ansorge and Z. Molnar (2019). "Neuroserpin expression during human brain development and in adult brain revealed by immunohistochemistry and single cell RNA sequencing." J Anat **235**(3): 543-554.

Aebersold, R., J. N. Agar, I. J. Amster, M. S. Baker, C. R. Bertozzi, E. S. Boja, C. E. Costello, B. F. Cravatt, C. Fenselau, B. A. Garcia, Y. Ge, J. Gunawardena, R. C. Hendrickson, P. J. Hergenrother, C. G. Huber, A. R. Ivanov, O. N. Jensen, M. C. Jewett, N. L. Kelleher, L. L. Kiessling, N. J. Krogan, M. R. Larsen, J. A. Loo, R. R. Ogorzalek Loo, E. Lundberg, M. J. MacCoss, P. Mallick, V. K. Mootha, M. Mrksich, T. W. Muir, S. M. Patrie, J. J. Pesavento, S. J. Pitteri, H. Rodriguez, A. Saghatelian, W. Sandoval, H. Schlüter, S. Sechi, S. A. Slavoff, L. M. Smith, M. P. Snyder, P. M. Thomas, M. Uhlén, J. E. Van Eyk, M. Vidal, D. R. Walt, F. M. White, E. R. Williams, T. Wohlschlager, V. H. Wysocki, N. A. Yates, N. L. Young and B. Zhang (2018). "How many human proteoforms are there?" Nature Chemical Biology **14**(3): 206-214.

Akbarian, S., J. J. Kim, S. G. Potkin, J. O. Hagman, A. Tafazzoli, W. E. Bunney, Jr. and E. G. Jones (1995). "Gene expression for glutamic acid decarboxylase is reduced without loss of neurons in prefrontal cortex of schizophrenics." Arch Gen Psychiatry **52**(4): 258-266.

Akerman, C. J., D. Smyth and I. D. Thompson (2002). "Visual experience before eye-opening and the development of the retinogeniculate pathway." Neuron **36**(5): 869-879.

Akhter, M. S. and J. Arif (2018). "The Pathways Involved in TLQP-62 Mediated Biological Functions: A Review." JOURNAL OF ADVANCES IN BIOTECHNOLOGY **7**: 953 - 966.

Akhter, S., S. Chakraborty, D. Moutinho, E. Alvarez-Coiradas, I. Rosa, J. Vinuela, E. Dominguez, A. Garcia and J. R. Requena (2017). "The human VGF-derived bioactive peptide TLQP-21 binds heat shock 71 kDa protein 8 (HSPA8)on the surface of SH-SY5Y cells." PLoS One **12**(9): e0185176.

Alder, J., S. Thakker-Varia, D. A. Bangasser, M. Kuroiwa, M. R. Plummer, T. J. Shors and I. B. Black (2003). "Brain-Derived Neurotrophic Factor-Induced Gene Expression Reveals Novel Actions of VGF in Hippocampal Synaptic Plasticity." The Journal of Neuroscience **23**(34): 10800-10808.

Allendoerfer, K. L. and C. J. Shatz (1994). "The subplate, a transient neocortical structure: its role in the development of connections between thalamus and cortex." Annu Rev Neurosci **17**: 185-218.

Alqarni, S. and M. Alsebai (2022). "Could VGF and/or its derived peptide act as biomarkers for the diagnosis of neurodegenerative diseases: A systematic review." Front Endocrinol (Lausanne) **13**: 1032192.

Alvarez-Medina, R., G. Le Dreau, M. Ros and E. Marti (2009). "Hedgehog activation is required upstream of Wnt signalling to control neural progenitor proliferation." Development **136**(19): 3301-3309.

Alzu'bi, A., J. Homman-Ludiye, J. A. Bourne and G. J. Clowry (2019). "Thalamocortical Afferents Innervate the Cortical Subplate much Earlier in Development in Primate than in Rodent." Cereb Cortex **29**(4): 1706-1718.

Anderson, M. L. and B. L. Finlay (2014). "Allocating structure to function: the strong links between neuroplasticity and natural selection." Front Hum Neurosci **7**: 918.

Andescavage, N., A. duPlessis, M. Metzler, D. Bulas, G. Vezina, M. Jacobs, S. N. Iqbal, A. Baschat and C. Limperopoulos (2017). "In vivo assessment of placental and brain volumes in growth-restricted fetuses with and without fetal Doppler changes using quantitative 3D MRI." J Perinatol **37**(12): 1278-1284.

Andreasen, N. C. (1997). "The role of the thalamus in schizophrenia." Can J Psychiatry **42**(1): 27-33.

Angevine, J. B., Jr. and R. L. Sidman (1961). "Autoradiographic study of cell migration during histogenesis of cerebral cortex in the mouse." Nature **192**: 766-768.

Anticevic, A., M. W. Cole, G. Repovs, J. D. Murray, M. S. Brumbaugh, A. M. Winkler, A. Savic, J. H. Krystal, G. D. Pearlson and D. C. Glahn (2014). "Characterizing thalamo-cortical disturbances in schizophrenia and bipolar illness." Cereb Cortex **24**(12): 3116-3130.

Anton-Bolanos, N., A. Espinosa and G. Lopez-Bendito (2018). "Developmental interactions between thalamus and cortex: a true love reciprocal story." Curr Opin Neurobiol **52**: 33-41.

Anton-Bolanos, N., A. Sempere-Ferrandez, T. Guillamon-Vivancos, F. J. Martini, L. Perez-Saiz, H. Gezelius, A. Filipchuk, M. Valdeolmillos and G. Lopez-Bendito (2019). "Prenatal activity from thalamic neurons governs the emergence of functional cortical maps in mice." Science **364**(6444): 987-990.

Arias, M. S., J. Baratta, J. Yu and R. T. Robertson (2002). "Absence of selectivity in the loss of neurons from the developing cortical subplate of the rat." Brain Res Dev Brain Res **139**(2): 331-335.

Armentano, M., S. J. Chou, G. S. Tomassy, A. Leingartner, D. D. O'Leary and M. Studer (2007). "COUP-TFI regulates the balance of cortical patterning between frontal/motor and sensory areas." Nat Neurosci **10**(10): 1277-1286.

Arshad, A., L. R. Vose, G. Vinukonda, F. Hu, K. Yoshikawa, A. Csiszar, J. C. Brumberg and P. Ballabh (2016). "Extended Production of Cortical Interneurons into the Third Trimester of Human Gestation." Cereb Cortex **26**(5): 2242-2256.

Assimacopoulos, S., T. Kao, N. P. Issa and E. A. Grove (2012). "Fibroblast growth factor 8 organizes the neocortical area map and regulates sensory map topography." J Neurosci **32**(21): 7191-7201.

Augustyniak, J., H. Kozlowska and L. Buzanska (2023). "Genes Involved in DNA Repair and Mitophagy Protect Embryoid Bodies from the Toxic Effect of Methylmercury Chloride under Physioxia Conditions." Cells **12**(3).

Auladell, C., P. Perez-Sust, H. Super and E. Soriano (2000). "The early development of thalamocortical and corticothalamic projections in the mouse." Anat Embryol (Berl) **201**(3): 169-179.

Back, S. A., N. L. Luo, N. S. Borenstein, J. M. Levine, J. J. Volpe and H. C. Kinney (2001). "Late oligodendrocyte progenitors coincide with the developmental window of vulnerability for human perinatal white matter injury." J Neurosci **21**(4): 1302-1312.

Bai, B., X. Wang, Y. Li, P. C. Chen, K. Yu, K. K. Dey, J. M. Yarbro, X. Han, B. M. Lutz, S. Rao, Y. Jiao, J. M. Sifford, J. Han, M. Wang, H. Tan, T. I. Shaw, J. H. Cho, S. Zhou, H. Wang, M. Niu, A. Mancieri, K. A. Messler, X. Sun, Z. Wu, V. Pagala, A. A. High, W. Bi, H. Zhang, H. Chi, V. Haroutunian, B. Zhang, T. G. Beach, G. Yu and J. Peng (2020). "Deep Multilayer Brain Proteomics Identifies Molecular Networks in Alzheimer's Disease Progression." Neuron **106**(4): 700.

Bandiera, S. and Z. Molnár (2022). Development of the Thalamocortical Systems. The Thalamus. M. M. Halassa. Cambridge, Cambridge University Press**:** 139-162.

Bandiera, S. a. (2022). "Characterisation of the earliest thalamocortical interactions in the human fetal brain." Journal of Anatomy **240**(4): 775-819.

Bartolomucci, A., G. La Corte, R. Possenti, V. Locatelli, A. E. Rigamonti, A. Torsello, E. Bresciani, I. Bulgarelli, R. Rizzi, F. Pavone, F. R. D'Amato, C. Severini, G. Mignogna, A. Giorgi, M. E. Schinina, G. Elia, C. Brancia, G. L. Ferri, R. Conti, B. Ciani, T. Pascucci, G. Dell'Omo, E. E. Muller, A. Levi and A. Moles (2006). "TLQP-21, a VGF-derived peptide, increases energy expenditure and prevents the early phase of diet-induced obesity." Proc Natl Acad Sci U S A **103**(39): 14584-14589.

Bartolomucci, A., R. Possenti, S. K. Mahata, R. Fischer-Colbrie, Y. P. Loh and S. R. Salton (2011). "The extended granin family: structure, function, and biomedical implications." Endocr Rev **32**(6): 755-797.

Bathina, S. and U. N. Das (2015). "Brain-derived neurotrophic factor and its clinical implications." Arch Med Sci **11**(6): 1164-1178.

Baudry, M. and X. Bi (2016). "Calpain-1 and Calpain-2: The Yin and Yang of Synaptic Plasticity and Neurodegeneration." Trends Neurosci **39**(4): 235-245.

Baudry, M., G. Zhu, Y. Liu, Y. Wang, V. Briz and X. Bi (2015). "Multiple cellular cascades participate in long-term potentiation and in hippocampus-dependent learning." Brain Res **1621**: 73-81.

Bayatti, N., J. A. Moss, L. Sun, P. Ambrose, J. F. Ward, S. Lindsay and G. J. Clowry (2008). "A molecular neuroanatomical study of the developing human neocortex from 8 to 17 postconceptional weeks revealing the early differentiation of the subplate and subventricular zone." Cereb Cortex **18**(7): 1536-1548.

Bayer, S. A. and J. Altman (2005). The human brain during the second trimester, CRC Press.

Beckmann, N. D., W. J. Lin, M. Wang, A. T. Cohain, A. W. Charney, P. Wang, W. Ma, Y. C. Wang, C. Jiang, M. Audrain, P. H. Comella, A. K. Fakira, S. P. Hariharan, G. M. Belbin, K. Girdhar, A. I. Levey, N. T. Seyfried, E. B. Dammer, D. Duong, J. J. Lah, J. V. Haure-Mirande, B. Shackleton, T. Fanutza, R. Blitzer, E. Kenny, J. Zhu, V. Haroutunian, P. Katsel, S. Gandy, Z. Tu, M. E. Ehrlich, B. Zhang, S. R. Salton and E. E. Schadt (2020). "Multiscale causal networks identify VGF as a key regulator of Alzheimer's disease." Nat Commun **11**(1): 3942.

Behnke, J., A. Cheedalla, V. Bhatt, M. Bhat, S. Teng, A. Palmieri, C. C. Windon, S. Thakker-Varia and J. Alder (2017). "Neuropeptide VGF Promotes Maturation of Hippocampal Dendrites That Is Reduced by Single Nucleotide Polymorphisms." Int J Mol Sci **18**(3).

Berton, O., C. A. McClung, R. J. Dileone, V. Krishnan, W. Renthal, S. J. Russo, D. Graham, N. M. Tsankova, C. A. Bolanos, M. Rios, L. M. Monteggia, D. W. Self and E. J. Nestler (2006). "Essential role of BDNF in the mesolimbic dopamine pathway in social defeat stress." Science **311**(5762): 864-868.

Bishop, K. M., G. Goudreau and D. D. O'Leary (2000). "Regulation of area identity in the mammalian neocortex by Emx2 and Pax6." Science **288**(5464): 344-349.

Blakey, D., M. C. Wilson and Z. Molnar (2012). "Termination and initial branch formation of SNAP-25-deficient thalamocortical fibres in heterochronic organotypic co-cultures." Eur J Neurosci **35**(10): 1586-1594.

Boecker, C. A., J. Goldsmith, D. Dou, G. G. Cajka and E. L. F. Holzbaur (2021). "Increased LRRK2 kinase activity alters neuronal autophagy by disrupting the axonal transport of autophagosomes." Current Biology **31**(10): 2140-2154.e2146.

Boecker, C. A., M. A. Olenick, E. R. Gallagher, M. E. Ward and E. L. F. Holzbaur (2020). "ToolBox: Live Imaging of intracellular organelle transport in induced pluripotent stem cell-derived neurons." Traffic **21**(1): 138-155.

Bonni, A., D. D. Ginty, H. Dudek and M. E. Greenberg (1995). "Serine 133-phosphorylated CREB induces transcription via a cooperative mechanism that may confer specificity to neurotrophin signals." Mol Cell Neurosci **6**(2): 168-183.

Boyd, J. L., S. L. Skove, J. P. Rouanet, L. J. Pilaz, T. Bepler, R. Gordan, G. A. Wray and D. L. Silver (2015). "Human-chimpanzee differences in a FZD8 enhancer alter cell-cycle dynamics in the developing neocortex." Curr Biol **25**(6): 772-779.

Bozdagi, O., E. Rich, S. Tronel, M. Sadahiro, K. Patterson, M. L. Shapiro, C. M. Alberini, G. W. Huntley and S. R. J. Salton (2008). "The Neurotrophin-Inducible Gene Vgf Regulates Hippocampal Function and Behavior through a Brain-Derived Neurotrophic Factor-Dependent Mechanism." The Journal of Neuroscience **28**(39): 9857-9869.

Bresciani, E., R. Possenti, S. Coco, L. Rizzi, R. Meanti, L. Molteni, V. Locatelli and A. Torsello (2019). "TLQP-21, A VGF-Derived Peptide Endowed of Endocrine and Extraendocrine Properties: Focus on In Vitro Calcium Signaling." Int J Mol Sci **21**(1).

Buckner, R. L. and F. M. Krienen (2013). "The evolution of distributed association networks in the human brain." Trends Cogn Sci **17**(12): 648-665.

Budday, S., C. Raybaud and E. Kuhl (2014). "A mechanical model predicts morphological abnormalities in the developing human brain." Sci Rep **4**: 5644.

Bulfone, A., S. M. Smiga, K. Shimamura, A. Peterson, L. Puelles and J. L. Rubenstein (1995). "T-brain-1: a homolog of Brachyury whose expression defines molecularly distinct domains within the cerebral cortex." Neuron **15**(1): 63-78.

Busse, S., H. G. Bernstein, M. Busse, H. Bielau, R. Brisch, C. Mawrin, S. Muller, Z. Sarnyai, T. Gos, B. Bogerts and J. Steiner (2012). "Reduced density of hypothalamic VGF-immunoreactive neurons in schizophrenia: a potential link to impaired growth factor signaling and energy homeostasis." Eur Arch Psychiatry Clin Neurosci **262**(5): 365-374.

Butler, A., P. Hoffman, P. Smibert, E. Papalexi and R. Satija (2018). "Integrating single-cell transcriptomic data across different conditions, technologies, and species." Nature Biotechnology **36**(5): 411-420.

Bystron, I., C. Blakemore and P. Rakic (2008). "Development of the human cerebral cortex: Boulder Committee revisited." Nat Rev Neurosci **9**(2): 110-122.

Cadwell, C. R., A. Bhaduri, M. A. Mostajo-Radji, M. G. Keefe and T. J. Nowakowski (2019). "Development and Arealization of the Cerebral Cortex." Neuron **103**(6): 980-1004.

Cannon, T. D., T. G. van Erp, I. M. Rosso, M. Huttunen, J. Lonnqvist, T. Pirkola, O. Salonen, L. Valanne, V. P. Poutanen and C. G. Standertskjold-Nordenstam (2002). "Fetal hypoxia and structural brain abnormalities in schizophrenic patients, their siblings, and controls." Arch Gen Psychiatry **59**(1): 35-41.

Canu, N., R. Possenti, A. M. Rinaldi, E. Trani and A. Levi (1997). "Molecular cloning and characterization of the human VGF promoter region." J Neurochem **68**(4): 1390-1399.

Carlyle, B. C., R. R. Kitchen, J. E. Kanyo, E. Z. Voss, M. Pletikos, A. M. M. Sousa, T. T. Lam, M. B. Gerstein, N. Sestan and A. C. Nairn (2017). "A multiregional proteomic survey of the postnatal human brain." Nat Neurosci **20**(12): 1787-1795.

Carney, R. S., I. Bystron, G. Lopez-Bendito and Z. Molnar (2007). "Comparative analysis of extra-ventricular mitoses at early stages of cortical development in rat and human." Brain Struct Funct **212**(1): 37-54.

Carney, R. S. and Z. Molnar (2004). Thalamocortical Development and Cell Proliferation in Fetal Primate and Rodent Cortex. M. S. D. University of Oxford. Radcliffe Science Library MS. D.Phil. c. 18625 (Box B000001031119).

Caronia-Brown, G., M. Yoshida, F. Gulden, S. Assimacopoulos and E. A. Grove (2014). "The cortical hem regulates the size and patterning of neocortex." Development **141**(14): 2855-2865.

Castillo-Paterna, M., V. Moreno-Juan, A. Filipchuk, L. Rodriguez-Malmierca, R. Susin and G. Lopez-Bendito (2015). "DCC functions as an accelerator of thalamocortical axonal growth downstream of spontaneous thalamic activity." EMBO Rep **16**(7): 851-862.

Catalano, S. M. and C. J. Shatz (1998). "Activity-dependent cortical target selection by thalamic axons." Science **281**(5376): 559-562.

Caviness, V. S., Jr. and P. Rakic (1978). "Mechanisms of cortical development: a view from mutations in mice." Annu Rev Neurosci **1**: 297-326.

Cera, I., L. Whitton, G. Donohoe, D. W. Morris, G. Dechant and G. Apostolova (2019). "Genes encoding SATB2-interacting proteins in adult cerebral cortex contribute to human cognitive ability." PLoS Genet **15**(2): e1007890.

Cero, C., V. V. Vostrikov, R. Verardi, C. Severini, T. Gopinath, P. D. Braun, M. F. Sassano, A. Gurney, B. L. Roth, L. Vulchanova, R. Possenti, G. Veglia and A. Bartolomucci (2014). "The TLQP-21 peptide activates the G-protein-coupled receptor C3aR1 via a folding-upon-binding mechanism." Structure **22**(12): 1744-1753.

Chatterjee, M. and J. Y. Li (2012). "Patterning and compartment formation in the diencephalon." Front Neurosci **6**: 66.

Chen, Y., D. Magnani, T. Theil, T. Pratt and D. J. Price (2012). "Evidence that descending cortical axons are essential for thalamocortical axons to cross the pallial-subpallial boundary in the embryonic forebrain." PLoS One **7**(3): e33105.

Chen, Y. C., A. Pristera, M. Ayub, R. S. Swanwick, K. Karu, Y. Hamada, A. S. Rice and K. Okuse (2013). "Identification of a receptor for neuropeptide VGF and its role in neuropathic pain." J Biol Chem **288**(48): 34638-34646.

Chenn, A. and C. A. Walsh (2002). "Regulation of cerebral cortical size by control of cell cycle exit in neural precursors." Science **297**(5580): 365-369.

Chini, M. and I. L. Hanganu-Opatz (2021). "Prefrontal Cortex Development in Health and Disease: Lessons from Rodents and Humans." Trends Neurosci **44**(3): 227-240.

Choi, B. H. (1986). "Glial fibrillary acidic protein in radial glia of early human fetal cerebrum: a light and electron microscopic immunoperoxidase study." J Neuropathol Exp Neurol **45**(4): 408-418.

Cholfin, J. A. and J. L. Rubenstein (2007). "Patterning of frontal cortex subdivisions by Fgf17." Proc Natl Acad Sci U S A **104**(18): 7652-7657.

Cholfin, J. A. and J. L. Rubenstein (2008). "Frontal cortex subdivision patterning is coordinately regulated by Fgf8, Fgf17, and Emx2." J Comp Neurol **509**(2): 144-155.

Chou, S. J., Z. Babot, A. Leingartner, M. Studer, Y. Nakagawa and D. D. O'Leary (2013). "Geniculocortical input drives genetic distinctions between primary and higher-order visual areas." Science **340**(6137): 1239-1242.

Clasca, F., A. Angelucci and M. Sur (1995). "Layer-specific programs of development in neocortical projection neurons." Proc Natl Acad Sci U S A **92**(24): 11145-11149.

Clowry, G. J., A. Alzu'bi, L. F. Harkin, S. Sarma, J. Kerwin and S. J. Lindsay (2018). "Charting the protomap of the human telencephalon." Semin Cell Dev Biol **76**: 3-14.

Clowry, G. J., A. Alzu'bi, L. F. Harkin, S. Sarma, J. Kerwin and S. J. Lindsay (2018). "Charting the protomap of the human telencephalon." Seminars in Cell & Developmental Biology **76**: 3-14.

Cocco, C., F. D'Amato, B. Noli, A. Ledda, C. Brancia, P. Bongioanni and G. L. Ferri (2010). "Distribution of VGF peptides in the human cortex and their selective changes in Parkinson's and Alzheimer's diseases." J Anat **217**(6): 683-693.

Crair, M. C., D. C. Gillespie and M. P. Stryker (1998). "The role of visual experience in the development of columns in cat visual cortex." Science **279**(5350): 566-570.

Crowley, J. C. and L. C. Katz (2000). "Early development of ocular dominance columns." Science **290**(5495): 1321-1324.

Daviaud, N., C. Chevalier, R. H. Friedel and H. Zou (2019). "Distinct Vulnerability and Resilience of Human Neuroprogenitor Subtypes in Cerebral Organoid Model of Prenatal Hypoxic Injury." Front Cell Neurosci **13**: 336.

De Carlos, J. A. and D. D. O'Leary (1992). "Growth and targeting of subplate axons and establishment of major cortical pathways." J Neurosci **12**(4): 1194-1211.

deAzevedo, L. C., C. Fallet, V. Moura-Neto, C. Daumas-Duport, C. Hedin-Pereira and R. Lent (2003). "Cortical radial glial cells in human fetuses: depth-correlated transformation into astrocytes." J Neurobiol **55**(3): 288-298.

Deck, M., L. Lokmane, S. Chauvet, C. Mailhes, M. Keita, M. Niquille, M. Yoshida, Y. Yoshida, C. Lebrand, F. Mann, E. A. Grove and S. Garel (2013). "Pathfinding of corticothalamic axons relies on a rendezvous with thalamic projections." Neuron **77**(3): 472-484.

Dehay, C., P. Giroud, M. Berland, H. Killackey and H. Kennedy (1996). "Contribution of thalamic input to the specification of cytoarchitectonic cortical fields in the primate: effects of bilateral enucleation in the fetal monkey on the boundaries, dimensions, and gyrification of striate and extrastriate cortex." J Comp Neurol **367**(1): 70-89.

Dehay, C., G. Horsburgh, M. Berland, H. Killackey and H. Kennedy (1989). "Maturation and connectivity of the visual cortex in monkey is altered by prenatal removal of retinal input." Nature **337**(6204): 265-267.

Dehay, C. and H. Kennedy (2007). "Cell-cycle control and cortical development." Nat Rev Neurosci **8**(6): 438-450.

Dehay, C., H. Kennedy and K. S. Kosik (2015). "The outer subventricular zone and primate-specific cortical complexification." Neuron **85**(4): 683-694.

Dehay, C., P. Savatier, V. Cortay and H. Kennedy (2001). "Cell-cycle kinetics of neocortical precursors are influenced by embryonic thalamic axons." J Neurosci **21**(1): 201-214.

Delgado, R. N., D. E. Allen, M. G. Keefe, W. R. Mancia Leon, R. S. Ziffra, E. E. Crouch, A. Alvarez-Buylla and T. J. Nowakowski (2022). "Individual human cortical progenitors can produce excitatory and inhibitory neurons." Nature **601**(7893): 397-403.

Di Lullo, E. and A. R. Kriegstein (2017). "The use of brain organoids to investigate neural development and disease." Nat Rev Neurosci **18**(10): 573-584.

Dimitrov, D., D. Türei, M. Garrido-Rodriguez, P. L. Burmedi, J. S. Nagai, C. Boys, R. O. Ramirez Flores, H. Kim, B. Szalai, I. G. Costa, A. Valdeolivas, A. Dugourd and J. Saez-Rodriguez (2022). "Comparison of methods and resources for cell-cell communication inference from single-cell RNA-Seq data." Nature Communications **13**(1): 3224.

Doll, S. and A. L. Burlingame (2015). "Mass Spectrometry-Based Detection and Assignment of Protein Posttranslational Modifications." ACS Chemical Biology **10**(1): 63-71.

Dorph-Petersen, K. A. and D. A. Lewis (2017). "Postmortem structural studies of the thalamus in schizophrenia." Schizophr Res **180**: 28-35.

Doyle, D. Z., M. M. Lam, A. Qalieh, Y. Qalieh, A. Sorel, O. H. Funk and K. Y. Kwan (2021). "Chromatin remodeler Arid1a regulates subplate neuron identity and wiring of cortical connectivity." Proc Natl Acad Sci U S A **118**(21).

Dupont, E., I. L. Hanganu, W. Kilb, S. Hirsch and H. J. Luhmann (2006). "Rapid developmental switch in the mechanisms driving early cortical columnar networks." Nature **439**(7072): 79-83.

Duque, A., Z. Krsnik, I. Kostovic and P. Rakic (2016). "Secondary expansion of the transient subplate zone in the developing cerebrum of human and nonhuman primates." Proc Natl Acad Sci U S A **113**(35): 9892-9897.

Duquette, P. M. and N. Lamarche-Vane (2020). "The calcium-activated protease calpain regulates netrin-1 receptor deleted in colorectal cancer-induced axon outgrowth in cortical neurons." Journal of Neurochemistry **152**(3): 315-332.

duVerle, D., I. Takigawa, Y. Ono, H. Sorimachi and H. Mamitsuka (2010). "CaMPDB: a resource for calpain and modulatory proteolysis." Genome Inform **22**: 202-213.

duVerle, D. A. and H. Mamitsuka (2019). "CalCleaveMKL: a Tool for Calpain Cleavage Prediction." Methods Mol Biol **1915**: 121-147.

DuVerle, D. A., Y. Ono, H. Sorimachi and H. Mamitsuka (2011). "Calpain cleavage prediction using multiple kernel learning." PLoS One **6**(5): e19035.

El Gaamouch, F., M. Audrain, W. J. Lin, N. Beckmann, C. Jiang, S. Hariharan, P. S. Heeger, E. E. Schadt, S. Gandy, M. E. Ehrlich and S. R. Salton (2020). "VGF-derived peptide TLQP-21 modulates microglial function through C3aR1 signaling pathways and reduces neuropathology in 5xFAD mice." Mol Neurodegener **15**(1): 4.

Elmadany, N., F. de Almeida Sassi, S. Wendt, F. Logiacco, J. Visser, V. Haage, D. P. Hernandez, P. Mertins, D. Hambardzumyan, S. Wolf, H. Kettenmann and M. Semtner (2020). "The VGF-derived Peptide TLQP21 Impairs Purinergic Control of Chemotaxis and Phagocytosis in Mouse Microglia." J Neurosci **40**(17): 3320-3331.

Elston, G. N., A. Elston, V. Casagrande and J. H. Kaas (2005). "Pyramidal neurons of granular prefrontal cortex of the galago: complexity in evolution of the psychic cell in primates." Anat Rec A Discov Mol Cell Evol Biol **285**(1): 610-618.

Erzurumlu, R. S. and P. Gaspar (2012). "Development and critical period plasticity of the barrel cortex." Eur J Neurosci **35**(10): 1540-1553.

Ethell, I. M. and D. W. Ethell (2007). "Matrix metalloproteinases in brain development and remodeling: synaptic functions and targets." J Neurosci Res **85**(13): 2813-2823.

Failor, S., V. Nguyen, D. P. Darcy, J. Cang, M. F. Wendland, M. P. Stryker and P. S. McQuillen (2010). "Neonatal cerebral hypoxia-ischemia impairs plasticity in rat visual cortex." J Neurosci **30**(1): 81-92.

Fargali, S., A. L. Garcia, M. Sadahiro, C. Jiang, W. G. Janssen, W. J. Lin, V. Cogliani, A. Elste, S. Mortillo, C. Cero, B. Veitenheimer, G. Graiani, G. M. Pasinetti, S. K. Mahata, J. W. Osborn, G. W. Huntley, G. R. Phillips, D. L. Benson, A. Bartolomucci and S. R. Salton (2014). "The granin VGF promotes genesis of secretory vesicles, and regulates circulating catecholamine levels and blood pressure." FASEB J **28**(5): 2120-2133.

Ferrarelli, F. and G. Tononi (2011). "The thalamic reticular nucleus and schizophrenia." Schizophr Bull **37**(2): 306-315.

Ferri, G. L. and R. Possenti (1996). "vgf A neurotrophin-inducible gene expressed in neuroendocrine tissues." Trends Endocrinol Metab **7**(7): 233-239.

Fietz, S. A., I. Kelava, J. Vogt, M. Wilsch-Brauninger, D. Stenzel, J. L. Fish, D. Corbeil, A. Riehn, W. Distler, R. Nitsch and W. B. Huttner (2010). "OSVZ progenitors of human and ferret neocortex are epithelial-like and expand by integrin signaling." Nat Neurosci **13**(6): 690-699.

Filipovic, R. and N. Zecevic (2008). "The effect of CXCL1 on human fetal oligodendrocyte progenitor cells." Glia **56**(1): 1-15.

Florio, M., M. Albert, E. Taverna, T. Namba, H. Brandl, E. Lewitus, C. Haffner, A. Sykes, F. K. Wong, J. Peters, E. Guhr, S. Klemroth, K. Prufer, J. Kelso, R. Naumann, I. Nusslein, A. Dahl, R. Lachmann, S. Paabo and W. B. Huttner (2015). "Human-specific gene ARHGAP11B promotes basal progenitor amplification and neocortex expansion." Science **347**(6229): 1465-1470.

Frantz, G. D. and S. K. McConnell (1996). "Restriction of late cerebral cortical progenitors to an upper-layer fate." Neuron **17**(1): 55-61.

Fred, S. M., L. Laukkanen, C. A. Brunello, L. Vesa, H. Göös, I. Cardon, R. Moliner, T. Maritzen, M. Varjosalo, P. C. Casarotto and E. Castrén (2019). "Pharmacologically diverse antidepressants facilitate TRKB receptor activation by disrupting its interaction with the endocytic adaptor complex AP-2." Journal of Biological Chemistry **294**(48): 18150-18161.

Fukuchi-Shimogori, T. and E. A. Grove (2001). "Neocortex patterning by the secreted signaling molecule FGF8." Science **294**(5544): 1071-1074.

Funahashi, S. (2013). "Thalamic mediodorsal nucleus and its participation in spatial working memory processes: comparison with the prefrontal cortex." Front Syst Neurosci **7**: 36.

Garcia-Moreno, F., E. Anderton, M. Jankowska, J. Begbie, J. M. Encinas, M. Irimia and Z. Molnar (2018). "Absence of Tangentially Migrating Glutamatergic Neurons in the Developing Avian Brain." Cell Rep **22**(1): 96-109.

Garcia-Moreno, F., N. A. Vasistha, N. Trevia, J. A. Bourne and Z. Molnar (2012). "Compartmentalization of cerebral cortical germinal zones in a lissencephalic primate and gyrencephalic rodent." Cereb Cortex **22**(2): 482-492.

Garcia, A. L., S. K. Han, W. G. Janssen, Z. Z. Khaing, T. Ito, M. J. Glucksman, D. L. Benson and S. R. Salton (2005). "A prohormone convertase cleavage site within a predicted alpha-helix mediates sorting of the neuronal and endocrine polypeptide VGF into the regulated secretory pathway." J Biol Chem **280**(50): 41595-41608.

Gerstmann, K., D. Pensold, J. Symmank, M. Khundadze, C. A. Hubner, J. Bolz and G. Zimmer (2015). "Thalamic afferents influence cortical progenitors via ephrin A5-EphA4 interactions." Development **142**(1): 140-150.

Geschwind, D. H. and P. Levitt (2007). "Autism spectrum disorders: developmental disconnection syndromes." Curr Opin Neurobiol **17**(1): 103-111.

Geschwind, D. H. and P. Rakic (2013). "Cortical evolution: judge the brain by its cover." Neuron **80**(3): 633-647.

Gezelius, H. and G. Lopez-Bendito (2017). "Thalamic neuronal specification and early circuit formation." Dev Neurobiol **77**(7): 830-843.

Ghosh, A., A. Antonini, S. K. McConnell and C. J. Shatz (1990). "Requirement for subplate neurons in the formation of thalamocortical connections." Nature **347**(6289): 179-181.

Ghosh, A. and C. J. Shatz (1993). "A role for subplate neurons in the patterning of connections from thalamus to neocortex." Development **117**(3): 1031-1047.

Gillentine, M. A., J. Yin, A. Bajic, P. Zhang, S. Cummock, J. J. Kim and C. P. Schaaf (2017). "Functional Consequences of CHRNA7 Copy-Number Alterations in Induced Pluripotent Stem Cells and Neural Progenitor Cells." Am J Hum Genet **101**(6): 874-887.

Glock, C., A. Biever, G. Tushev, B. Nassim-Assir, A. Kao, I. Bartnik, S. Tom Dieck and E. M. Schuman (2021). "The translatome of neuronal cell bodies, dendrites, and axons." Proc Natl Acad Sci U S A **118**(43).

Godement, P., J. Vanselow, S. Thanos and F. Bonhoeffer (1987). "A study in developing visual systems with a new method of staining neurones and their processes in fixed tissue." Development **101**(4): 697-713.

Gonzalez-Gomez, M. and G. Meyer (2014). "Dynamic expression of calretinin in embryonic and early fetal human cortex." Front Neuroanat **8**: 41.

Goo, M. S., L. Sancho, N. Slepak, D. Boassa, T. J. Deerinck, M. H. Ellisman, B. L. Bloodgood and G. N. Patrick (2017). "Activity-dependent trafficking of lysosomes in dendrites and dendritic spines." J Cell Biol **216**(8): 2499-2513.

Grant, E., A. Hoerder-Suabedissen and Z. Molnar (2012). "Development of the corticothalamic projections." Front Neurosci **6**: 53.

Grove, E. A., S. Tole, J. Limon, L. Yip and C. W. Ragsdale (1998). "The hem of the embryonic cerebral cortex is defined by the expression of multiple Wnt genes and is compromised in Gli3-deficient mice." Development **125**(12): 2315-2325.

Grubisha, M. J., R. A. Sweet and M. L. MacDonald (2021). "Investigating Post-translational Modifications in Neuropsychiatric Disease: The Next Frontier in Human Post-mortem Brain Research." Front Mol Neurosci **14**: 689495.

Gutierrez-Fernandez, F., M. Pinto-Gonzalez and O. Gonzalez-Perez (2014). "Neuro-immune interactions in the postnatal ventricular-subventricular zone." J Stem Cells **9**(1): 53-64.

Hanashima, C., Z. Molnar and G. Fishell (2006). "Building bridges to the cortex." Cell **125**(1): 24-27.

Hanganu, I. L., W. Kilb and H. J. Luhmann (2001). "Spontaneous synaptic activity of subplate neurons in neonatal rat somatosensory cortex." Cereb Cortex **11**(5): 400-410.

Hanganu, I. L., W. Kilb and H. J. Luhmann (2002). "Functional synaptic projections onto subplate neurons in neonatal rat somatosensory cortex." J Neurosci **22**(16): 7165-7176.

Hanganu, I. L., A. Okabe, V. Lessmann and H. J. Luhmann (2008). "Cellular Mechanisms of Subplate-Driven and Cholinergic Input-Dependent Network Activity in the Neonatal Rat Somatosensory Cortex." Cerebral Cortex **19**(1): 89-105.

Hannedouche, S., V. Beck, J. Leighton-Davies, M. Beibel, G. Roma, E. J. Oakeley, V. Lannoy, J. Bernard, J. Hamon, S. Barbieri, I. Preuss, M. C. Lasbennes, A. W. Sailer, T. Suply, K. Seuwen, C. N. Parker and F. Bassilana (2013). "Identification of the C3a receptor (C3AR1) as the target of the VGF-derived peptide TLQP-21 in rodent cells." J Biol Chem **288**(38): 27434-27443.

Hansen, D. V., J. H. Lui, P. R. Parker and A. R. Kriegstein (2010). "Neurogenic radial glia in the outer subventricular zone of human neocortex." Nature **464**(7288): 554-561.

Hao, Y., S. Hao, E. Andersen-Nissen, W. M. Mauck, 3rd, S. Zheng, A. Butler, M. J. Lee, A. J. Wilk, C. Darby, M. Zager, P. Hoffman, M. Stoeckius, E. Papalexi, E. P. Mimitou, J. Jain, A. Srivastava, T. Stuart, L. M. Fleming, B. Yeung, A. J. Rogers, J. M. McElrath, C. A. Blish, R. Gottardo, P. Smibert and R. Satija (2021). "Integrated analysis of multimodal single-cell data." Cell **184**(13): 3573-3587 e3529.

Harkin, L. F., S. J. Lindsay, Y. Xu, A. Alzu'bi, A. Ferrara, E. A. Gullon, O. G. James and G. J. Clowry (2017). "Neurexins 1-3 Each Have a Distinct Pattern of Expression in the Early Developing Human Cerebral Cortex." Cereb Cortex **27**(1): 216-232.

Hawley, R. J., R. J. Scheibe and J. A. Wagner (1992). "NGF induces the expression of the VGF gene through a cAMP response element." J Neurosci **12**(7): 2573-2581.

Haydar, T. F., C. Y. Kuan, R. A. Flavell and P. Rakic (1999). "The role of cell death in regulating the size and shape of the mammalian forebrain." Cereb Cortex **9**(6): 621-626.

Hebert, J. M., Y. Mishina and S. K. McConnell (2002). "BMP signaling is required locally to pattern the dorsal telencephalic midline." Neuron **35**(6): 1029-1041.

Helle, K. B. (2004). "The granin family of uniquely acidic proteins of the diffuse neuroendocrine system: comparative and functional aspects." Biol Rev Camb Philos Soc **79**(4): 769-794.

Hensch, T. K. (2004). "Critical period regulation." Annu Rev Neurosci **27**: 549-579.

Herrmann, K., A. Antonini and C. J. Shatz (1994). "Ultrastructural Evidence for Synaptic Interactions between Thalamocortical Axons and Subplate Neurons." European Journal of Neuroscience **6**(11): 1729-1742.

Hevner, R. F., L. Shi, N. Justice, Y. Hsueh, M. Sheng, S. Smiga, A. Bulfone, A. M. Goffinet, A. T. Campagnoni and J. L. Rubenstein (2001). "Tbr1 regulates differentiation of the preplate and layer 6." Neuron **29**(2): 353-366.

Higashi, K., A. Fujita, A. Inanobe, M. Tanemoto, K. Doi, T. Kubo and Y. Kurachi (2001). "An inwardly rectifying K(+) channel, Kir4.1, expressed in astrocytes surrounds synapses and blood vessels in brain." Am J Physiol Cell Physiol **281**(3): C922-931.

Higashi, S., K. Hioki, T. Kurotani, N. Kasim and Z. Molnar (2005). "Functional thalamocortical synapse reorganization from subplate to layer IV during postnatal development in the reeler-like mutant rat (shaking rat Kawasaki)." J Neurosci **25**(6): 1395-1406.

Higashi, S., Z. Molnar, T. Kurotani and K. Toyama (2002). "Prenatal development of neural excitation in rat thalamocortical projections studied by optical recording." Neuroscience **115**(4): 1231-1246.

Hoerder-Suabedissen, A. and Z. Molnar (2015). "Development, evolution and pathology of neocortical subplate neurons." Nat Rev Neurosci **16**(3): 133-146.

Howard, B. M., M. Zhicheng, R. Filipovic, A. R. Moore, S. D. Antic and N. Zecevic (2008). "Radial glia cells in the developing human brain." Neuroscientist **14**(5): 459-473.

Huang, H. (2010). "Delineating neural structures of developmental human brains with diffusion tensor imaging." ScientificWorldJournal **10**: 135-144.

Huang, J. T., F. M. Leweke, D. Oxley, L. Wang, N. Harris, D. Koethe, C. W. Gerth, B. M. Nolden, S. Gross, D. Schreiber, B. Reed and S. Bahn (2006). "Disease biomarkers in cerebrospinal fluid of patients with first-onset psychosis." PLoS Med **3**(11): e428.

Huang, J. T., F. M. Leweke, T. M. Tsang, D. Koethe, L. Kranaster, C. W. Gerth, S. Gross, D. Schreiber, S. Ruhrmann, F. Schultze-Lutter, J. Klosterkotter, E. Holmes and S. Bahn (2007). "CSF metabolic and proteomic profiles in patients prodromal for psychosis." PLoS One **2**(8): e756.

Huang, Y., N. N. Song, W. Lan, L. Hu, C. J. Su, Y. Q. Ding and L. Zhang (2013). "Expression of transcription factor Satb2 in adult mouse brain." Anat Rec (Hoboken) **296**(3): 452-461.

Hunsberger, J. G., S. S. Newton, A. H. Bennett, C. H. Duman, D. S. Russell, S. R. Salton and R. S. Duman (2007). "Antidepressant actions of the exercise-regulated gene VGF." Nat Med **13**(12): 1476-1482.

Jakovcevski, I., N. Mayer and N. Zecevic (2011). "Multiple origins of human neocortical interneurons are supported by distinct expression of transcription factors." Cereb Cortex **21**(8): 1771-1782.

Jakovcevski, I. and N. Zecevic (2005). "Olig transcription factors are expressed in oligodendrocyte and neuronal cells in human fetal CNS." J Neurosci **25**(44): 10064-10073.

Jensen, K. F. and H. P. Killackey (1987). "Terminal arbors of axons projecting to the somatosensory cortex of the adult rat. II. The altered morphology of thalamocortical afferents following neonatal infraorbital nerve cut." J Neurosci **7**(11): 3544-3553.

Jiang, C., W. J. Lin, B. Labonte, C. A. Tamminga, G. Turecki, E. J. Nestler, S. J. Russo and S. R. Salton (2019). "VGF and its C-terminal peptide TLQP-62 in ventromedial prefrontal cortex regulate depression-related behaviors and the response to ketamine." Neuropsychopharmacology **44**(5): 971-981.

Jiang, C., W. J. Lin and S. R. Salton (2019). "Role of a VGF/BDNF/TrkB Autoregulatory Feedback Loop in Rapid-Acting Antidepressant Efficacy." J Mol Neurosci **68**(3): 504-509.

Jiang, M., J. Meng, F. Zeng, H. Qing, G. Hook, V. Hook, Z. Wu and J. Ni (2020). "Cathepsin B inhibition blocks neurite outgrowth in cultured neurons by regulating lysosomal trafficking and remodeling." J Neurochem **155**(3): 300-312.

Jones, E. G. (1985). Transmitters, Receptors, and Related Compounds in the Thalamus. The Thalamus. E. G. Jones. Boston, MA, Springer US**:** 225-256.

Ju, X. C., Q. Q. Hou, A. L. Sheng, K. Y. Wu, Y. Zhou, Y. Jin, T. Wen, Z. Yang, X. Wang and Z. G. Luo (2016). "The hominoid-specific gene TBC1D3 promotes generation of basal neural progenitors and induces cortical folding in mice." Elife **5**.

Judas, M., G. Sedmak and I. Kostovic (2013). "The significance of the subplate for evolution and developmental plasticity of the human brain." Front Hum Neurosci **7**: 423.

Judas, M., G. Sedmak, M. Pletikos and N. Jovanov-Milosevic (2010). "Populations of subplate and interstitial neurons in fetal and adult human telencephalon." J Anat **217**(4): 381-399.

Kadoshima, T., H. Sakaguchi, T. Nakano, M. Soen, S. Ando, M. Eiraku and Y. Sasai (2013). "Self-organization of axial polarity, inside-out layer pattern, and species-specific progenitor dynamics in human ES cell–derived neocortex." Proceedings of the National Academy of Sciences **110**(50): 20284-20289.

Kahn, D. M. and L. Krubitzer (2002). "Massive cross-modal cortical plasticity and the emergence of a new cortical area in developmentally blind mammals." Proc Natl Acad Sci U S A **99**(17): 11429-11434.

Kang, H. J., Y. I. Kawasawa, F. Cheng, Y. Zhu, X. Xu, M. Li, A. M. M. Sousa, M. Pletikos, K. A. Meyer, G. Sedmak, T. Guennel, Y. Shin, M. B. Johnson, Ž. Krsnik, S. Mayer, S. Fertuzinhos, S. Umlauf, S. N. Lisgo, A. Vortmeyer, D. R. Weinberger, S. Mane, T. M. Hyde, A. Huttner, M. Reimers, J. E. Kleinman and N. Šestan (2011). "Spatio-temporal transcriptome of the human brain." Nature **478**(7370): 483-489.

Kanold, P. O., P. Kara, R. C. Reid and C. J. Shatz (2003). "Role of subplate neurons in functional maturation of visual cortical columns." Science **301**(5632): 521-525.

Kanold, P. O. and H. J. Luhmann (2010). "The subplate and early cortical circuits." Annu Rev Neurosci **33**: 23-48.

Katz, L. C. and C. J. Shatz (1996). "Synaptic activity and the construction of cortical circuits." Science **274**(5290): 1133-1138.

Keller, A., A. Westenberger, M. J. Sobrido, M. Garcia-Murias, A. Domingo, R. L. Sears, R. R. Lemos, A. Ordonez-Ugalde, G. Nicolas, J. E. da Cunha, E. J. Rushing, M. Hugelshofer, M. C. Wurnig, A. Kaech, R. Reimann, K. Lohmann, V. Dobricic, A. Carracedo, I. Petrovic, J. M. Miyasaki, I. Abakumova, M. A. Mae, E. Raschperger, M. Zatz, K. Zschiedrich, J. Klepper, E. Spiteri, J. M. Prieto, I. Navas, M. Preuss, C. Dering, M. Jankovic, M. Paucar, P. Svenningsson, K. Saliminejad, H. R. Khorshid, I. Novakovic, A. Aguzzi, A. Boss, I. Le Ber, G. Defer, D. Hannequin, V. S. Kostic, D. Campion, D. H. Geschwind, G. Coppola, C. Betsholtz, C. Klein and J. R. Oliveira (2013). "Mutations

in the gene encoding PDGF-B cause brain calcifications in humans and mice." Nat Genet **45**(9): 1077-1082.

Kelley, K. W. and S. P. Pasca (2022). "Human brain organogenesis: Toward a cellular understanding of development and disease." Cell **185**(1): 42-61.

Kerschensteiner, D. (2014). "Spontaneous Network Activity and Synaptic Development." Neuroscientist **20**(3): 272-290.

Klingler, E., A. De la Rossa, S. Fièvre, K. Devaraju, P. Abe and D. Jabaudon (2019). "A translaminar genetic logic for the circuit identity of intracortically projecting neurons." Current Biology **29**(2): 332-339. e335.

Knable, M. B. (1999). "Schizophrenia and bipolar disorder: findings from studies of the Stanley Foundation Brain Collection." Schizophr Res **39**(2): 149-152; discussion 163.

Knopp, R. C., A. Jastaniah, O. Dubrovskyi, I. Gaisina, L. Tai and G. R. J. Thatcher (2021). "Extending the Calpain-Cathepsin Hypothesis to the Neurovasculature: Protection of Brain Endothelial Cells and Mice from Neurotrauma." ACS Pharmacol Transl Sci **4**(1): 372-385.

Kondo, S., H. Al-Hasani, A. Hoerder-Suabedissen, W. Z. Wang and Z. Molnar (2015). "Secretory function in subplate neurons during cortical development." Front Neurosci **9**: 100.

Kopić, J., A. Junaković, I. Salamon, M.-R. Rasin, I. Kostović and Ž. Krsnik (2023). "Early Regional Patterning in the Human Prefrontal Cortex Revealed by Laminar Dynamics of Deep Projection Neuron Markers." Cells **12**(2): 231.

Kostovic, I., I. Z. Isasegi and Z. Krsnik (2019). "Sublaminar organization of the human subplate: developmental changes in the distribution of neurons, glia, growing axons and extracellular matrix." J Anat **235**(3): 481-506.

Kostovic, I., N. Jovanov-Milosevic, M. Rados, G. Sedmak, V. Benjak, M. Kostovic-Srzentic, L. Vasung, M. Culjat, M. Rados, P. Huppi and M. Judas (2014). "Perinatal and early postnatal reorganization of the subplate and related cellular compartments in the human cerebral wall as revealed by histological and MRI approaches." Brain Struct Funct **219**(1): 231-253.

Kostovic, I. and M. Judas (2002). "Correlation between the sequential ingrowth of afferents and transient patterns of cortical lamination in preterm infants." Anat Rec **267**(1): 1-6.

Kostovic, I. and M. Judas (2007). "Transient patterns of cortical lamination during prenatal life: do they have implications for treatment?" Neurosci Biobehav Rev **31**(8): 1157-1168.

Kostovic, I. and M. Judas (2010). "The development of the subplate and thalamocortical connections in the human foetal brain." Acta Paediatr **99**(8): 1119-1127.

Kostovic, I., M. Judas and G. Sedmak (2011). "Developmental history of the subplate zone, subplate neurons and interstitial white matter neurons: relevance for schizophrenia." Int J Dev Neurosci **29**(3): 193-205.

Kostovic, I., M. Kostovic-Srzentic, V. Benjak, N. Jovanov-Milosevic and M. Rados (2014). "Developmental dynamics of radial vulnerability in the cerebral compartments in preterm infants and neonates." Front Neurol **5**: 139.

Kostovic, I. and P. Rakic (1980). "Cytology and time of origin of interstitial neurons in the white matter in infant and adult human and monkey telencephalon." J Neurocytol **9**(2): 219-242.

Kostovic, I. and P. Rakic (1984). "Development of prestriate visual projections in the monkey and human fetal cerebrum revealed by transient cholinesterase staining." J Neurosci **4**(1): 25-42.

Kostovic, I. and P. Rakic (1990). "Developmental history of the transient subplate zone in the visual and somatosensory cortex of the macaque monkey and human brain." J Comp Neurol **297**(3): 441-470.

Kostovic, I., G. Sedmak and M. Judas (2019). "Neural histology and neurogenesis of the human fetal and infant brain." Neuroimage **188**: 743-773.

Kostovic, I., G. Sedmak, M. Vuksic and M. Judas (2015). "The relevance of human fetal subplate zone for developmental neuropathology of neuronal migration disorders and cortical dysplasia." CNS Neurosci Ther **21**(2): 74-82.

Krettek, J. E. and J. L. Price (1977). "The cortical projections of the mediodorsal nucleus and adjacent thalamic nuclei in the rat." J Comp Neurol **171**(2): 157-191.

Kriegstein, A., S. Noctor and V. Martinez-Cerdeno (2006). "Patterns of neural stem and progenitor cell division may underlie evolutionary cortical expansion." Nat Rev Neurosci **7**(11): 883-890.

Krsnik, Z., V. Majic, L. Vasung, H. Huang and I. Kostovic (2017). "Growth of Thalamocortical Fibers to the Somatosensory Cortex in the Human Fetal Brain." Front Neurosci **11**: 233.

Krubitzer, L. A. and T. J. Prescott (2018). "The Combinatorial Creature: Cortical Phenotypes within and across Lifetimes." Trends Neurosci **41**(10): 744-762.

Kuburovic, V., J. D. Marshall, G. B. Collin, K. Nykamp, N. Kuburovic, T. Milenkovic, S. Rakic, M. Djuric, J. Jecmenica, S. Milenkovic and J. K. Naggert (2013). "Differences in the clinical spectrum of two adolescent male patients with Alstrom syndrome." Clin Dysmorphol **22**(1): 7-12.

Kwan, K. Y., N. Sestan and E. S. Anton (2012). "Transcriptional co-regulation of neuronal migration and laminar identity in the neocortex." Development **139**(9): 1535-1546.

La Manno, G., R. Soldatov, A. Zeisel, E. Braun, H. Hochgerner, V. Petukhov, K. Lidschreiber, M. E. Kastriti, P. Lönnerberg, A. Furlan, J. Fan, L. E. Borm, Z. Liu, D. van Bruggen, J. Guo, X. He, R. Barker, E. Sundström, G. Castelo-Branco, P. Cramer, I. Adameyko, S. Linnarsson and P. V. Kharchenko (2018). "RNA velocity of single cells." Nature **560**(7719): 494-498.

Lancaster, M. A., M. Renner, C.-A. Martin, D. Wenzel, L. S. Bicknell, M. E. Hurles, T. Homfray, J. M. Penninger, A. P. Jackson and J. A. Knoblich (2013). "Cerebral organoids model human brain development and microcephaly." Nature **501**(7467): 373-379.

Leal, G., D. Comprido, P. de Luca, E. Morais, L. Rodrigues, M. Mele, A. R. Santos, R. O. Costa, M. J. Pinto, S. Patil, B. Berentsen, P. Afonso, L. Carreto, K. W. Li, P. Pinheiro, R. D. Almeida, M. A. S. Santos, C. R. Bramham and C. B. Duarte (2017). "The RNA-Binding Protein hnRNP K Mediates the Effect of BDNF on Dendritic mRNA Metabolism and Regulates Synaptic NMDA Receptors in Hippocampal Neurons." eNeuro **4**(6).

Leclerc, C., I. Néant and M. Moreau (2012). "The calcium: an early signal that initiates the formation of the nervous system during embryogenesis." Front Mol Neurosci **5**: 3.

Leonard, C. M. (1969). "The prefrontal cortex of the rat. I. Cortical projection of the mediodorsal nucleus. II. Efferent connections." Brain Res **12**(2): 321-343.

Letinic, K., R. Zoncu and P. Rakic (2002). "Origin of GABAergic neurons in the human neocortex." Nature **417**(6889): 645-649.

Levi, A., J. D. Eldridge and B. M. Paterson (1985). "Molecular cloning of a gene sequence regulated by nerve growth factor." Science **229**(4711): 393-395.

Levi, A., G. L. Ferri, E. Watson, R. Possenti and S. R. Salton (2004). "Processing, distribution, and function of VGF, a neuronal and endocrine peptide precursor." Cell Mol Neurobiol **24**(4): 517-533.

Lewis, D. A., A. A. Curley, J. R. Glausier and D. W. Volk (2012). "Cortical parvalbumin interneurons and cognitive dysfunction in schizophrenia." Trends Neurosci **35**(1): 57-67.

Lewis, J. E., J. M. Brameld and P. H. Jethwa (2015). "Neuroendocrine Role for VGF." Front Endocrinol (Lausanne) **6**: 3.

Li, C., M. Li, H. Yu, X. Shen, J. Wang, X. Sun, Q. Wang and C. Wang (2017). "Neuropeptide VGF C-Terminal Peptide TLQP-62 Alleviates Lipopolysaccharide-Induced Memory Deficits and Anxiety-like and Depression-like Behaviors in Mice: The Role of BDNF/TrkB Signaling." ACS Chem Neurosci **8**(9): 2005-2018.

Li, H., S. Fertuzinhos, E. Mohns, T. S. Hnasko, M. Verhage, R. Edwards, N. Sestan and M. C. Crair (2013). "Laminar and columnar development of barrel cortex relies on thalamocortical neurotransmission." Neuron **79**(5): 970-986.

Li, J., S. Yang and G. Zhu (2017). "Postnatal calpain inhibition elicits cerebellar cell death and motor dysfunction." Oncotarget **8**(50): 87997-88007.

Li, X. X., J. D. Lee, H. S. Lee, R. J. Clark and T. M. Woodruff (2023). "TLQP-21 is a low potency partial C3aR activator on human primary macrophages." Frontiers in Immunology **14**.

Li, Y., V. Bondada, A. Joshi and J. W. Geddes (2009). "Calpain 1 and Calpastatin expression is developmentally regulated in rat brain." Exp Neurol **220**(2): 316-319.

Lin, W.-J., Y. Zhao, Z. Li, S. Zheng, J.-l. Zou, N. A. Warren, P. Bali, J. Wu, M. Xing, C. Jiang, Y. Tang, S. R. Salton and X. Ye (2021). "An increase in VGF expression through a rapid, transcription-independent, autofeedback mechanism improves cognitive function." Translational Psychiatry **11**(1): 383.

Lin, W. J., C. Jiang, M. Sadahiro, O. Bozdagi, L. Vulchanova, C. M. Alberini and S. R. Salton (2015). "VGF and Its C-Terminal Peptide TLQP-62 Regulate Memory Formation in Hippocampus via a BDNF-TrkB-Dependent Mechanism." J Neurosci **35**(28): 10343-10356.

Liu, Z.-X., K. Yu, J. Dong, L. Zhao, Z. Liu, Q. Zhang, S. Li, Y. Du and H. Cheng (2019). "Precise Prediction of Calpain Cleavage Sites and Their Aberrance Caused by Mutations in Cancer." Frontiers in Genetics **10**.

Lombardo, A., S. A. Rabacchi, F. Cremisi, T. Pizzorusso, M. C. Cenni, R. Possenti, G. Barsacchi and L. Maffei (1995). "A developmentally regulated nerve growth factor-induced gene, VGF, is expressed in geniculocortical afferents during synaptogenesis." Neuroscience **65**(4): 997-1008.

Lopez-Bendito, G., A. Cautinat, J. A. Sanchez, F. Bielle, N. Flames, A. N. Garratt, D. A. Talmage, L. W. Role, P. Charnay, O. Marin and S. Garel (2006). "Tangential neuronal migration controls axon guidance: a role for neuregulin-1 in thalamocortical axon navigation." Cell **125**(1): 127-142.

Lopez-Bendito, G. and Z. Molnar (2003). "Thalamocortical development: how are we going to get there?" Nat Rev Neurosci **4**(4): 276-289.

Lu, Q. R., D. Yuk, J. A. Alberta, Z. Zhu, I. Pawlitzky, J. Chan, A. P. McMahon, C. D. Stiles and D. H. Rowitch (2000). "Sonic hedgehog--regulated oligodendrocyte lineage genes encoding bHLH proteins in the mammalian central nervous system." Neuron **25**(2): 317-329.

Luhmann, H. J., A. Sinning, J. W. Yang, V. Reyes-Puerta, M. C. Stuttgen, S. Kirischuk and W. Kilb (2016). "Spontaneous Neuronal Activity in Developing Neocortical Networks: From Single Cells to Large-Scale Interactions." Front Neural Circuits **10**: 40.

Lui, J. H., D. V. Hansen and A. R. Kriegstein (2011). "Development and evolution of the human neocortex." Cell **146**(1): 18-36.

Lui, J. H., T. J. Nowakowski, A. A. Pollen, A. Javaherian, A. R. Kriegstein and M. C. Oldham (2014). "Radial glia require PDGFD-PDGFRbeta signalling in human but not mouse neocortex." Nature **515**(7526): 264-268.

Lukaszewicz, A., P. Savatier, V. Cortay, P. Giroud, C. Huissoud, M. Berland, H. Kennedy and C. Dehay (2005). "G1 phase regulation, area-specific cell cycle control, and cytoarchitectonics in the primate cortex." Neuron **47**(3): 353-364.

Luskin, M. B. and C. J. Shatz (1985). "Neurogenesis of the cat's primary visual cortex." J Comp Neurol **242**(4): 611-631.

Luskin, M. B. and C. J. Shatz (1985). "Studies of the earliest generated cells of the cat's visual cortex: cogeneration of subplate and marginal zones." J Neurosci **5**(4): 1062-1075.

Ma, T., C. Wang, L. Wang, X. Zhou, M. Tian, Q. Zhang, Y. Zhang, J. Li, Z. Liu, Y. Cai, F. Liu, Y. You, C. Chen, K. Campbell, H. Song, L. Ma, J. L. Rubenstein and Z. Yang (2013). "Subcortical origins of human and monkey neocortical interneurons." Nat Neurosci **16**(11): 1588-1597.

Maguire, J. A., F. L. Cardenas-Diaz, P. Gadue and D. L. French (2019). "Highly Efficient CRISPR-Cas9-Mediated Genome Editing in Human Pluripotent Stem Cells." Curr Protoc Stem Cell Biol **48**(1): e64.

Malik, S., G. Vinukonda, L. R. Vose, D. Diamond, B. B. Bhimavarapu, F. Hu, M. T. Zia, R. Hevner, N. Zecevic and P. Ballabh (2013). "Neurogenesis continues in the third trimester of pregnancy and is suppressed by premature birth." J Neurosci **33**(2): 411-423.

Mallamaci, A., L. Muzio, C. H. Chan, J. Parnavelas and E. Boncinelli (2000). "Area identity shifts in the early cerebral cortex of Emx2-/- mutant mice." Nat Neurosci **3**(7): 679-686.

Marcos-Mondejar, P., S. Peregrin, J. Y. Li, L. Carlsson, S. Tole and G. Lopez-Bendito (2012). "The lhx2 transcription factor controls thalamocortical axonal guidance by specific regulation of robo1 and robo2 receptors." J Neurosci **32**(13): 4372-4385.

Marin-Padilla, M. (1995). "Prenatal development of fibrous (white matter), protoplasmic (gray matter), and layer I astrocytes in the human cerebral cortex: a Golgi study." J Comp Neurol **357**(4): 554-572.

Marin-Padilla, M. (2014). "The mammalian neocortex new pyramidal neuron: a new conception." Front Neuroanat **7**: 51.

Marin, O. and J. L. Rubenstein (2001). "A long, remarkable journey: tangential migration in the telencephalon." Nat Rev Neurosci **2**(11): 780-790.

Martinez-Cerdeno, V., C. L. Cunningham, J. Camacho, J. L. Antczak, A. N. Prakash, M. E. Cziep, A. I. Walker and S. C. Noctor (2012). "Comparative analysis of the subventricular zone in rat, ferret and macaque: evidence for an outer subventricular zone in rodents." PLoS One **7**(1): e30178.

Martini, F. J., V. Moreno-Juan, A. Filipchuk, M. Valdeolmillos and G. Lopez-Bendito (2018). "Impact of thalamocortical input on barrel cortex development." Neuroscience **368**: 246-255.

Marx, M., G. Qi, I. L. Hanganu-Opatz, W. Kilb, H. J. Luhmann and D. Feldmeyer (2017). "Neocortical Layer 6B as a Remnant of the Subplate - A Morphological Comparison." Cereb Cortex **27**(2): 1011-1026.

Matsumoto, N., M. Hoshiko, N. Sugo, Y. Fukazawa and N. Yamamoto (2016). "Synapse-dependent and independent mechanisms of thalamocortical axon branching are regulated by neuronal activity." Dev Neurobiol **76**(3): 323-336.

Matsumoto, N. and N. Yamamoto (2018). "Visualization of Thalamocortical Axon Branching and Synapse Formation in Organotypic Cocultures." J Vis Exp(133).

McConnell, S. K., A. Ghosh and C. J. Shatz (1994). "Subplate pioneers and the formation of descending connections from cerebral cortex." J Neurosci **14**(4): 1892-1907.

McConnell, S. K. and C. E. Kaznowski (1991). "Cell cycle dependence of laminar determination in developing neocortex." Science **254**(5029): 282-285.

McLeod, F., A. Dimtsi, A. C. Marshall, D. Lewis-Smith, R. Thomas, G. J. Clowry and A. J. Trevelyan (2023). "Altered synaptic connectivity in an in vitro human model of STXBP1 encephalopathy." Brain **146**(3): 850-857.

McQuillen, P. S. and D. M. Ferriero (2005). "Perinatal subplate neuron injury: implications for cortical development and plasticity." Brain Pathol **15**(3): 250-260.

McQuillen, P. S., R. A. Sheldon, C. J. Shatz and D. M. Ferriero (2003). "Selective vulnerability of subplate neurons after early neonatal hypoxia-ischemia." J Neurosci **23**(8): 3308-3315.

McVea, D. A., M. H. Mohajerani and T. H. Murphy (2012). "Voltage-sensitive dye imaging reveals dynamic spatiotemporal properties of cortical activity after spontaneous muscle twitches in the newborn rat." J Neurosci **32**(32): 10982-10994.

Merighi, A. (2018). "Costorage of High Molecular Weight Neurotransmitters in Large Dense Core Vesicles of Mammalian Neurons." Front Cell Neurosci **12**: 272.

Merve Cikili, U. (2018). Development Period of Prefrontal Cortex. Prefrontal Cortex. S. Ana and F. Branislav. Rijeka, IntechOpen**:** Ch. 1.

Metin, C. and P. Godement (1996). "The ganglionic eminence may be an intermediate target for corticofugal and thalamocortical axons." J Neurosci **16**(10): 3219-3235.

Meyer, G. (2007). "Genetic control of neuronal migrations in human cortical development." Adv Anat Embryol Cell Biol **189**: 1 p preceding 1, 1-111.

Meyer, G., J. P. Schaaps, L. Moreau and A. M. Goffinet (2000). "Embryonic and early fetal development of the human neocortex." J Neurosci **20**(5): 1858-1868.

Meyer, G., P. Wahle, A. Castaneyra-Perdomo and R. Ferres-Torres (1992). "Morphology of neurons in the white matter of the adult human neocortex." Exp Brain Res **88**(1): 204-212.

Miller, J. A., S. L. Ding, S. M. Sunkin, K. A. Smith, L. Ng, A. Szafer, A. Ebbert, Z. L. Riley, J. J. Royall, K. Aiona, J. M. Arnold, C. Bennet, D. Bertagnolli, K. Brouner, S. Butler, S. Caldejon, A. Carey, C. Cuhaciyan, R. A. Dalley, N. Dee, T. A. Dolbeare, B. A. Facer, D. Feng, T. P. Fliss, G. Gee, J. Goldy, L. Gourley, B. W. Gregor, G. Gu, R. E. Howard, J. M. Jochim, C. L. Kuan, C. Lau, C. K. Lee, F. Lee, T. A. Lemon, P. Lesnar, B. McMurray, N. Mastan, N. Mosqueda, T. Naluai-Cecchini, N. K. Ngo, J. Nyhus, A. Oldre, E. Olson, J. Parente, P. D. Parker, S. E. Parry, A. Stevens, M. Pletikos, M. Reding, K. Roll, D. Sandman, M. Sarreal, S. Shapouri, N. V. Shapovalova, E. H. Shen, N. Sjoquist, C. R. Slaughterbeck, M. Smith, A. J. Sodt, D. Williams, L. Zollei, B. Fischl, M. B. Gerstein, D. H. Geschwind, I. A. Glass, M. J. Hawrylycz, R. F. Hevner, H. Huang, A. R. Jones, J. A. Knowles, P. Levitt, J. W. Phillips, N. Sestan, P. Wohnoutka, C. Dang, A. Bernard, J. G. Hohmann and E. S. Lein (2014). "Transcriptional landscape of the prenatal human brain." Nature **508**(7495): 199-206.

Minlebaev, M., M. Colonnese, T. Tsintsadze, A. Sirota and R. Khazipov (2011). "Early gamma oscillations synchronize developing thalamus and cortex." Science **334**(6053): 226-229.

Minzenberg, M. J. and C. S. Carter (2012). "Developing treatments for impaired cognition in schizophrenia." Trends Cogn Sci **16**(1): 35-42.

Mire, E., C. Mezzera, E. Leyva-Diaz, A. V. Paternain, P. Squarzoni, L. Bluy, M. Castillo-Paterna, M. J. Lopez, S. Peregrin, M. Tessier-Lavigne, S. Garel, J. Galceran, J. Lerma and G. Lopez-Bendito (2012). "Spontaneous activity regulates Robo1 transcription to mediate a switch in thalamocortical axon growth." Nat Neurosci **15**(8): 1134-1143.

Mishiro-Sato, E., K. Sasaki, T. Matsuo, H. Kageyama, H. Yamaguchi, Y. Date, M. Matsubara, T. Ishizu, K. Yoshizawa-Kumagaye, Y. Satomi, T. Takao, S. Shioda, M. Nakazato and N. Minamino (2010). "Distribution of neuroendocrine regulatory peptide-1 and -2, and proteolytic processing of their precursor VGF protein in the rat." J Neurochem **114**(4): 1097-1106.

Miyashita-Lin, E. M., R. Hevner, K. M. Wassarman, S. Martinez and J. L. Rubenstein (1999). "Early neocortical regionalization in the absence of thalamic innervation." Science **285**(5429): 906-909.

Mizoguchi, T., H. Minakuchi, M. Ishisaka, K. Tsuruma, M. Shimazawa and H. Hara (2018). "Author Correction: Behavioral abnormalities with disruption of brain structure in mice overexpressing VGF." Sci Rep **8**(1): 17326.

Mizoguchi, T., M. Shimazawa, K. Ohuchi, Y. Kuse, S. Nakamura and H. Hara (2019). "Impaired Cerebellar Development in Mice Overexpressing VGF." Neurochem Res **44**(2): 374-387.

Molliver, M. E., I. Kostovic and H. van der Loos (1973). "The development of synapses in cerebral cortex of the human fetus." Brain Res **50**(2): 403-407.

Molnár, Z. (1998). Development of thalamocortical connections. Oxford, Springer.

Molnar, Z., R. Adams and C. Blakemore (1998). "Mechanisms underlying the early establishment of thalamocortical connections in the rat." J Neurosci **18**(15): 5723-5745.

Molnar, Z. and C. Blakemore (1991). "Lack of regional specificity for connections formed between thalamus and cortex in coculture." Nature **351**(6326): 475-477.

Molnar, Z. and C. Blakemore (1995). "How do thalamic axons find their way to the cortex?" Trends Neurosci **18**(9): 389-397.

Molnár, Z., D. Blakey, I. Bystron and R. S. E. Carney (2006). Tract-Tracing in Developing Systems and in Postmortem Human Material Using Carbocyanine Dyes. Neuroanatomical Tract-Tracing 3:

Molecules, Neurons, and Systems. L. Zaborszky, F. G. Wouterlood and J. L. Lanciego. Boston, MA, Springer US**:** 366-393.

Molnar, Z. and G. Clowry (2012). "Cerebral cortical development in rodents and primates." Prog Brain Res **195**: 45-70.

Molnar, Z. and P. Cordery (1999). "Connections between cells of the internal capsule, thalamus, and cerebral cortex in embryonic rat." J Comp Neurol **413**(1): 1-25.

Molnar, Z., S. Garel, G. Lopez-Bendito, P. Maness and D. J. Price (2012). "Mechanisms controlling the guidance of thalamocortical axons through the embryonic forebrain." Eur J Neurosci **35**(10): 1573-1585.

Molnar, Z., T. Kurotani, S. Higashi, N. Yamamoto and K. Toyama (2003). "Development of functional thalamocortical synapses studied with current source-density analysis in whole forebrain slices in the rat." Brain Res Bull **60**(4): 355-371.

Molnar, Z., H. J. Luhmann and P. O. Kanold (2020). "Transient cortical circuits match spontaneous and sensory-driven activity during development." Science **370**(6514).

Molnar, Z., C. Metin, A. Stoykova, V. Tarabykin, D. J. Price, F. Francis, G. Meyer, C. Dehay and H. Kennedy (2006). "Comparative aspects of cerebral cortical development." Eur J Neurosci **23**(4): 921-934.

Molyneaux, B. J., P. Arlotta, J. R. Menezes and J. D. Macklis (2007). "Neuronal subtype specification in the cerebral cortex." Nat Rev Neurosci **8**(6): 427-437.

Monko, T., J. Rebertus, J. Stolley, S. R. Salton and Y. Nakagawa (2022). "Thalamocortical axons regulate neurogenesis and laminar fates in the early sensory cortex." Proc Natl Acad Sci U S A **119**(22): e2201355119.

Moon, H. Y., A. Becke, D. Berron, B. Becker, N. Sah, G. Benoni, E. Janke, S. T. Lubejko, N. H. Greig, J. A. Mattison, E. Duzel and H. van Praag (2016). "Running-Induced Systemic Cathepsin B Secretion Is Associated with Memory Function." Cell Metab **24**(2): 332-340.

Moore, A. R., W. L. Zhou, I. Jakovcevski, N. Zecevic and S. D. Antic (2011). "Spontaneous electrical activity in the human fetal cortex in vitro." J Neurosci **31**(7): 2391-2398.

Moreno-Juan, V., A. Filipchuk, N. Anton-Bolanos, C. Mezzera, H. Gezelius, B. Andres, L. Rodriguez-Malmierca, R. Susin, O. Schaad, T. Iwasato, R. Schule, M. Rutlin, S. Nelson, S. Ducret, M. Valdeolmillos, F. M. Rijli and G. Lopez-Bendito (2017). "Prenatal thalamic waves regulate cortical area size prior to sensory processing." Nat Commun **8**: 14172.

Mountcastle, V. B. (1997). "The columnar organization of the neocortex." Brain **120 (Pt 4)**: 701-722.

Mrzljak, L., H. B. Uylings, I. Kostovic and C. G. van Eden (1992). "Prenatal development of neurons in the human prefrontal cortex. II. A quantitative Golgi study." J Comp Neurol **316**(4): 485-496.

Mueller, T. M. and J. H. Meador-Woodruff (2020). "Post-translational protein modifications in schizophrenia." npj Schizophrenia **6**(1): 5.

Mundinano, I. C., W. C. Kwan and J. A. Bourne (2015). "Mapping the mosaic sequence of primate visual cortical development." Front Neuroanat **9**: 132.

Munji, R. N., Y. Choe, G. Li, J. A. Siegenthaler and S. J. Pleasure (2011). "Wnt signaling regulates neuronal differentiation of cortical intermediate progenitors." J Neurosci **31**(5): 1676-1687.

Murray, K. D., P. V. Choudary and E. G. Jones (2007). "Nucleus- and cell-specific gene expression in monkey thalamus." Proc Natl Acad Sci U S A **104**(6): 1989-1994.

Murtaza, N., J. Uy and K. K. Singh (2020). "Emerging proteomic approaches to identify the underlying pathophysiology of neurodevelopmental and neurodegenerative disorders." Molecular Autism **11**(1): 27.

Nadarajah, B., P. Alifragis, R. O. Wong and J. G. Parnavelas (2003). "Neuronal migration in the developing cerebral cortex: observations based on real-time imaging." Cereb Cortex **13**(6): 607-611.

Nagalski, A., L. Puelles, M. Dabrowski, T. Wegierski, J. Kuznicki and M. B. Wisniewska (2016). "Molecular anatomy of the thalamic complex and the underlying transcription factors." Brain Structure and Function **221**(5): 2493-2510.

Nakagawa, Y., J. E. Johnson and D. D. O'Leary (1999). "Graded and areal expression patterns of regulatory genes and cadherins in embryonic neocortex independent of thalamocortical input." J Neurosci **19**(24): 10877-10885.

Nakatsu, T., C. Uwabe and K. Shiota (2000). "Neural tube closure in humans initiates at multiple sites: evidence from human embryos and implications for the pathogenesis of neural tube defects." Anat Embryol (Berl) **201**(6): 455-466.

Nascimento, J. M., V. M. Saia-Cereda, R. C. Sartore, R. M. da Costa, C. S. Schitine, H. R. Freitas, M. Murgu, R. A. de Melo Reis, S. K. Rehen and D. Martins-de-Souza (2019). "Human Cerebral Organoids and Fetal Brain Tissue Share Proteomic Similarities." Front Cell Dev Biol **7**: 303.

Nobin, A. and A. Bjorklund (1973). "Topography of the monoamine neuron systems in the human brain as revealed in fetuses." Acta Physiol Scand Suppl **388**: 1-40.

Noctor, S. C., V. Martinez-Cerdeno, L. Ivic and A. R. Kriegstein (2004). "Cortical neurons arise in symmetric and asymmetric division zones and migrate through specific phases." Nat Neurosci **7**(2): 136-144.

Noda, Y., M. Shimazawa, H. Tanaka, S. Tamura, T. Inoue, K. Tsuruma and H. Hara (2015). "VGF and striatal cell damage in in vitro and in vivo models of Huntington's disease." Pharmacol Res Perspect **3**(3): e00140.

Noda, Y., M. Tanaka, S. Nakamura, J. Ito, A. Kakita, H. Hara and M. Shimazawa (2020). "Identification of VGF nerve growth factor inducible-producing cells in human spinal cords and expression change in patients with amyotrophic lateral sclerosis." Int J Med Sci **17**(4): 480-489.

Nowakowski, T. J., A. Bhaduri, A. A. Pollen, B. Alvarado, M. A. Mostajo-Radji, E. Di Lullo, M. Haeussler, C. Sandoval-Espinosa, S. J. Liu, D. Velmeshev, J. R. Ounadjela, J. Shuga, X. Wang, D. A. Lim, J. A. West, A. A. Leyrat, W. J. Kent and A. R. Kriegstein (2017). "Spatiotemporal gene expression trajectories reveal developmental hierarchies of the human cortex." Science **358**(6368): 1318-1323.

Nowakowski, T. J., A. A. Pollen, C. Sandoval-Espinosa and A. R. Kriegstein (2016). "Transformation of the Radial Glia Scaffold Demarcates Two Stages of Human Cerebral Cortex Development." Neuron **91**(6): 1219-1227.

O'Leary, D. D. (1989). "Do cortical areas emerge from a protocortex?" Trends Neurosci **12**(10): 400-406.

O'Leary, D. D. and Y. Nakagawa (2002). "Patterning centers, regulatory genes and extrinsic mechanisms controlling arealization of the neocortex." Curr Opin Neurobiol **12**(1): 14-25.

Ohtaka-Maruyama, C., M. Okamoto, K. Endo, M. Oshima, N. Kaneko, K. Yura, H. Okado, T. Miyata and N. Maeda (2018). "Synaptic transmission from subplate neurons controls radial migration of neocortical neurons." Science **360**(6386): 313-317.

Ortega, J. A., F. Memi, N. Radonjic, R. Filipovic, I. Bagasrawala, N. Zecevic and I. Jakovcevski (2018). "The Subventricular Zone: A Key Player in Human Neocortical Development." Neuroscientist **24**(2): 156-170.

Ortega, J. A., N. V. Radonjic and N. Zecevic (2013). "Sonic hedgehog promotes generation and maintenance of human forebrain Olig2 progenitors." Front Cell Neurosci **7**: 254.

Ortega, J. A., C. L. Sirois, F. Memi, N. Glidden and N. Zecevic (2017). "Oxygen Levels Regulate the Development of Human Cortical Radial Glia Cells." Cereb Cortex **27**(7): 3736-3751.

Ostrem, B., E. Di Lullo and A. Kriegstein (2017). "oRGs and mitotic somal translocation - a role in development and disease." Curr Opin Neurobiol **42**: 61-67.

Ouhaz, Z., H. Fleming and A. S. Mitchell (2018). "Cognitive Functions and Neurodevelopmental Disorders Involving the Prefrontal Cortex and Mediodorsal Thalamus." Front Neurosci **12**: 33.

Ozair, M. Z., C. Kirst, B. L. van den Berg, A. Ruzo, T. Rito and A. H. Brivanlou (2018). "hPSC Modeling Reveals that Fate Selection of Cortical Deep Projection Neurons Occurs in the Subplate." Cell Stem Cell **23**(1): 60-73 e66.

Padamsey, Z., L. McGuinness, S. J. Bardo, M. Reinhart, R. Tong, A. Hedegaard, M. L. Hart and N. J. Emptage (2017). "Activity-Dependent Exocytosis of Lysosomes Regulates the Structural Plasticity of Dendritic Spines." Neuron **93**(1): 132-146.

Palaniyappan, L., P. Mallikarjun, V. Joseph, T. P. White and P. F. Liddle (2011). "Folding of the prefrontal cortex in schizophrenia: regional differences in gyrification." Biol Psychiatry **69**(10): 974-979.

Pan, H., F. Y. Che, B. Peng, D. F. Steiner, J. E. Pintar and L. D. Fricker (2006). "The role of prohormone convertase-2 in hypothalamic neuropeptide processing: a quantitative neuropeptidomic study." J Neurochem **98**(6): 1763-1777.

Pan, H., D. Nanno, F. Y. Che, X. Zhu, S. R. Salton, D. F. Steiner, L. D. Fricker and L. A. Devi (2005). "Neuropeptide processing profile in mice lacking prohormone convertase-1." Biochemistry **44**(12): 4939-4948.

Parnavelas, J. G. (2000). "The origin and migration of cortical neurones: new vistas." Trends Neurosci **23**(3): 126-131.

Patel, S., A. Homaei, H. R. El-Seedi and N. Akhtar (2018). "Cathepsins: Proteases that are vital for survival but can also be fatal." Biomed Pharmacother **105**: 526-532.

Pedrero-Prieto, C. M., S. Garcia-Carpintero, J. Frontinan-Rubio, E. Llanos-Gonzalez, C. Aguilera Garcia, F. J. Alcain, I. Lindberg, M. Duran-Prado, J. R. Peinado and Y. Rabanal-Ruiz (2020). "A comprehensive systematic review of CSF proteins and peptides that define Alzheimer's disease." Clin Proteomics **17**: 21.

Perkins, L., E. Hughes, L. Srinivasan, J. Allsop, A. Glover, S. Kumar, N. Fisk and M. Rutherford (2008). "Exploring cortical subplate evolution using magnetic resonance imaging of the fetal brain." Dev Neurosci **30**(1-3): 211-220.

Pollen, A. A., T. J. Nowakowski, J. Chen, H. Retallack, C. Sandoval-Espinosa, C. R. Nicholas, J. Shuga, S. J. Liu, M. C. Oldham, A. Diaz, D. A. Lim, A. A. Leyrat, J. A. West and A. R. Kriegstein (2015). "Molecular identity of human outer radial glia during cortical development." Cell **163**(1): 55-67.

Polleux, F., C. Dehay, A. Goffinet and H. Kennedy (2001). "Pre- and post-mitotic events contribute to the progressive acquisition of area-specific connectional fate in the neocortex." Cereb Cortex **11**(11): 1027-1039.

Possenti, R., J. D. Eldridge, B. M. Paterson, A. Grasso and A. Levi (1989). "A protein induced by NGF in PC12 cells is stored in secretory vesicles and released through the regulated pathway." EMBO J **8**(8): 2217-2223.

Pouchelon, G., F. Gambino, C. Bellone, L. Telley, I. Vitali, C. Luscher, A. Holtmaat and D. Jabaudon (2014). "Modality-specific thalamocortical inputs instruct the identity of postsynaptic L4 neurons." Nature **511**(7510): 471-474.

Price, D. J., S. Aslam, L. Tasker and K. Gillies (1997). "Fates of the earliest generated cells in the developing murine neocortex." J Comp Neurol **377**(3): 414-422.

Qian, X., H. N. Nguyen, M. M. Song, C. Hadiono, S. C. Ogden, C. Hammack, B. Yao, G. R. Hamersky, F. Jacob, C. Zhong, K. J. Yoon, W. Jeang, L. Lin, Y. Li, J. Thakor, D. A. Berg, C. Zhang, E. Kang, M. Chickering, D. Nauen, C. Y. Ho, Z. Wen, K. M. Christian, P. Y. Shi, B. J. Maher, H. Wu, P. Jin, H. Tang, H. Song and G. L. Ming (2016). "Brain-Region-Specific Organoids Using Mini-bioreactors for Modeling ZIKV Exposure." Cell **165**(5): 1238-1254.

Quinn, J. P., E. C. Ethier, A. Novielli, A. Malone, C. E. Ramirez, L. Salloum, B. A. Trombetta, P. Kivisäkk, M. Bremang, S. Selzer, M. Fournier, S. Das, Y. Xing, S. E. Arnold and B. C. Carlyle (2023). "Cerebrospinal Fluid and Brain Proteoforms of the Granin Neuropeptide Family in Alzheimer's Disease." J Am Soc Mass Spectrom **34**(4): 649-667.

Quinn, J. P., S. E. Kandigian, B. A. Trombetta, S. E. Arnold and B. C. Carlyle (2021). "VGF as a biomarker and therapeutic target in neurodegenerative and psychiatric diseases." Brain Commun **3**(4): fcab261.

Radonjic, N. V., A. E. Ayoub, F. Memi, X. Yu, A. Maroof, I. Jakovcevski, S. A. Anderson, P. Rakic and N. Zecevic (2014). "Diversity of cortical interneurons in primates: the role of the dorsal proliferative niche." Cell Rep **9**(6): 2139-2151.

Radonjic, N. V., F. Memi, J. A. Ortega, N. Glidden, H. Zhan and N. Zecevic (2016). "The Role of Sonic Hedgehog in the Specification of Human Cortical Progenitors In Vitro." Cereb Cortex **26**(1): 131-143.

Radonjic, N. V., J. A. Ortega, F. Memi, K. Dionne, I. Jakovcevski and N. Zecevic (2014). "The complexity of the calretinin-expressing progenitors in the human cerebral cortex." Front Neuroanat **8**: 82.

Rajkumar, A. P., G. Bidkhori, S. Shoaie, E. Clarke, H. Morrin, A. Hye, G. Williams, C. Ballard, P. Francis and D. Aarsland (2020). "Postmortem Cortical Transcriptomics of Lewy Body Dementia Reveal Mitochondrial Dysfunction and Lack of Neuroinflammation." Am J Geriatr Psychiatry **28**(1): 75-86.

Rakic, P. (1972). "Mode of cell migration to the superficial layers of fetal monkey neocortex." J Comp Neurol **145**(1): 61-83.

Rakic, P. (1974). "Neurons in rhesus monkey visual cortex: systematic relation between time of origin and eventual disposition." Science **183**(4123): 425-427.

Rakic, P. (1976). "Prenatal genesis of connections subserving ocular dominance in the rhesus monkey." Nature **261**(5560): 467-471.

Rakic, P. (1988). "Specification of cerebral cortical areas." Science **241**(4862): 170-176.

Rakic, P. (1991). "Experimental manipulation of cerebral cortical areas in primates." Philos Trans R Soc Lond B Biol Sci **331**(1261): 291-294.

Rakic, P. (2009). "Evolution of the neocortex: a perspective from developmental biology." Nat Rev Neurosci **10**(10): 724-735.

Rakic, P., A. E. Ayoub, J. J. Breunig and M. H. Dominguez (2009). "Decision by division: making cortical maps." Trends Neurosci **32**(5): 291-301.

Rakic, P. and R. L. Sidman (1968). "Supravital DNA synthesis in the developing human and mouse brain." J Neuropathol Exp Neurol **27**(2): 246-276.

Rakic, P., I. Suner and R. W. Williams (1991). "A novel cytoarchitectonic area induced experimentally within the primate visual cortex." Proc Natl Acad Sci U S A **88**(6): 2083-2087.

Ramsay, I. S. (2019). "An Activation Likelihood Estimate Meta-analysis of Thalamocortical Dysconnectivity in Psychosis." Biol Psychiatry Cogn Neurosci Neuroimaging **4**(10): 859-869.

Rash, B. G., S. Tomasi, H. D. Lim, C. Y. Suh and F. M. Vaccarino (2013). "Cortical gyrification induced by fibroblast growth factor 2 in the mouse brain." J Neurosci **33**(26): 10802-10814.

Reep, R. L. (2000). "Cortical layer VII and persistent subplate cells in mammalian brains." Brain Behav Evol **56**(4): 212-234.

Reillo, I., C. de Juan Romero, M. A. Garcia-Cabezas and V. Borrell (2011). "A role for intermediate radial glia in the tangential expansion of the mammalian cerebral cortex." Cereb Cortex **21**(7): 1674-1694.

Reilly, S. K., J. Yin, A. E. Ayoub, D. Emera, J. Leng, J. Cotney, R. Sarro, P. Rakic and J. P. Noonan (2015). "Evolutionary genomics. Evolutionary changes in promoter and enhancer activity during human corticogenesis." Science **347**(6226): 1155-1159.

Rezaie, P., N. Ulfig and D. Male (2003). "Distribution and morphology of GFAP-positive astrocytes in the human fetal brain at second trimester." Neuroembryology and Aging **2**(2): 50-63.

Richman, D. P., R. M. Stewart, J. W. Hutchinson and V. S. Caviness, Jr. (1975). "Mechanical model of brain convolutional development." Science **189**(4196): 18-21.

Rouille, Y., S. J. Duguay, K. Lund, M. Furuta, Q. Gong, G. Lipkind, A. A. Oliva, Jr., S. J. Chan and D. F. Steiner (1995). "Proteolytic processing mechanisms in the biosynthesis of neuroendocrine peptides: the subtilisin-like proprotein convertases." Front Neuroendocrinol **16**(4): 322-361.

Rubenstein, J. L., S. Anderson, L. Shi, E. Miyashita-Lin, A. Bulfone and R. Hevner (1999). "Genetic control of cortical regionalization and connectivity." Cereb Cortex **9**(6): 524-532.

Ruetschi, U., H. Zetterberg, V. N. Podust, J. Gottfries, S. Li, A. Hviid Simonsen, J. McGuire, M. Karlsson, L. Rymo, H. Davies, L. Minthon and K. Blennow (2005). "Identification of CSF biomarkers for frontotemporal dementia using SELDI-TOF." Exp Neurol **196**(2): 273-281.

Saito, K., K. Mizuguchi, T. Horiike, T. A. Dinh Duong, Y. Shinmyo and H. Kawasaki (2019). "Characterization of the Inner and Outer Fiber Layers in the Developing Cerebral Cortex of Gyrencephalic Ferrets." Cereb Cortex **29**(10): 4303-4311.

Salgado-Pineda, P., A. Caclin, I. Baeza, C. Junqué, M. Bernardo, O. Blin and P. Fonlupt (2007). "Schizophrenia and frontal cortex: Where does it fail?" Schizophrenia Research **91**(1): 73-81.

Salton, S. R. (1991). "Nucleotide sequence and regulatory studies of VGF, a nervous system-specific mRNA that is rapidly and relatively selectively induced by nerve growth factor." J Neurochem **57**(3): 991-996.

Salton, S. R., G. L. Ferri, S. Hahm, S. E. Snyder, A. J. Wilson, R. Possenti and A. Levi (2000). "VGF: a novel role for this neuronal and neuroendocrine polypeptide in the regulation of energy balance." Front Neuroendocrinol **21**(3): 199-219.

Salton, S. R., D. J. Fischberg and K. W. Dong (1991). "Structure of the gene encoding VGF, a nervous system-specific mRNA that is rapidly and selectively induced by nerve growth factor in PC12 cells." Mol Cell Biol **11**(5): 2335-2349.

Sanai, N., T. Nguyen, R. A. Ihrie, Z. Mirzadeh, H. H. Tsai, M. Wong, N. Gupta, M. S. Berger, E. Huang, J. M. Garcia-Verdugo, D. H. Rowitch and A. Alvarez-Buylla (2011). "Corridors of migrating neurons in the human brain and their decline during infancy." Nature **478**(7369): 382-386.

Satija, R., J. A. Farrell, D. Gennert, A. F. Schier and A. Regev (2015). "Spatial reconstruction of single-cell gene expression data." Nature Biotechnology **33**(5): 495-502.

Sato, H., Y. Fukutani, Y. Yamamoto, E. Tatara, M. Takemoto, K. Shimamura and N. Yamamoto (2012). "Thalamus-derived molecules promote survival and dendritic growth of developing cortical neurons." J Neurosci **32**(44): 15388-15402.

Sato, H., J. Hatakeyama, T. Iwasato, K. Araki, N. Yamamoto and K. Shimamura (2022). "Thalamocortical axons control the cytoarchitecture of neocortical layers by area-specific supply of VGF." Elife **11**.

Scarisbrick, I. A., R. Linbo, A. G. Vandell, M. Keegan, S. I. Blaber, M. Blaber, D. Sneve, C. F. Lucchinetti, M. Rodriguez and E. P. Diamandis (2008). "Kallikreins are associated with secondary progressive multiple sclerosis and promote neurodegeneration." Biol Chem **389**(6): 739-745.

Schlaepfer, T. E., G. J. Harris, A. Y. Tien, L. W. Peng, S. Lee, E. B. Federman, G. A. Chase, P. E. Barta and G. D. Pearlson (1994). "Decreased regional cortical gray matter volume in schizophrenia." Am J Psychiatry **151**(6): 842-848.

Schmitz, M. T., K. Sandoval, C. P. Chen, M. A. Mostajo-Radji, W. W. Seeley, T. J. Nowakowski, C. J. Ye, M. F. Paredes and A. A. Pollen (2022). "The development and evolution of inhibitory neurons in primate cerebrum." Nature **603**(7903): 871-877.

Seidah, N. G. and M. Chretien (1999). "Proprotein and prohormone convertases: a family of subtilases generating diverse bioactive polypeptides." Brain Res **848**(1-2): 45-62.

Selemon, L. D. and N. Zecevic (2015). "Schizophrenia: a tale of two critical periods for prefrontal cortical development." Translational Psychiatry **5**(8): e623-e623.

Selten, M., C. Bernard, F. Hamid, A. Hanusz-Godoy, F. Oozeer, C. Zimmer and O. Marín (2023). "Regulation of parvalbumin interneuron plasticity by neuropeptide-encoding genes." bioRxiv: 2023.2002.2003.527010.

Severini, C., M. T. Ciotti, L. Biondini, S. Quaresima, A. M. Rinaldi, A. Levi, C. Frank and R. Possenti (2008). "TLQP-21, a neuroendocrine VGF-derived peptide, prevents cerebellar granule cells death induced by serum and potassium deprivation." J Neurochem **104**(2): 534-544.

Shatz, C. J., A. Ghosh, S. K. McConnell, K. L. Allendoerfer, E. Friauf and A. Antonini (1990). "Pioneer neurons and target selection in cerebral cortical development." Cold Spring Harb Symp Quant Biol **55**: 469-480.

Shatz, C. J. and M. B. Luskin (1986). "The relationship between the geniculocortical afferents and their cortical target cells during development of the cat's primary visual cortex." J Neurosci **6**(12): 3655-3668.

Shatz, C. J. and P. Rakic (1981). "The genesis of efferent connections from the visual cortex of the fetal rhesus monkey." J Comp Neurol **196**(2): 287-307.

Sheikh, A., X. Meng, J. Liu, A. Mikhailova, J. P. Y. Kao, P. S. McQuillen and P. O. Kanold (2019). "Neonatal Hypoxia-Ischemia Causes Functional Circuit Changes in Subplate Neurons." Cereb Cortex **29**(2): 765-776.

Sheikh, A. M., X. Li, G. Wen, Z. Tauqeer, W. T. Brown and M. Malik (2010). "Cathepsin D and apoptosis related proteins are elevated in the brain of autistic subjects." Neuroscience **165**(2): 363-370.

Shi, W., A. Xianyu, Z. Han, X. Tang, Z. Li, H. Zhong, T. Mao, K. Huang and S. H. Shi (2017). "Ontogenetic establishment of order-specific nuclear organization in the mammalian thalamus." Nat Neurosci **20**(4): 516-528.

Sidman, R. L. and P. Rakic (1973). "Neuronal migration, with special reference to developing human brain: a review." Brain Res **62**(1): 1-35.

Singh, M. B., J. A. White, E. J. McKimm, M. M. Milosevic and S. D. Antic (2019). "Mechanisms of Spontaneous Electrical Activity in the Developing Cerebral Cortex-Mouse Subplate Zone." Cereb Cortex **29**(8): 3363-3379.

Singh, R., M. K. Brewer, C. B. Mashburn, D. Lou, V. Bondada, B. Graham and J. W. Geddes (2014). "Calpain 5 is highly expressed in the central nervous system (CNS), carries dual nuclear localization signals, and is associated with nuclear promyelocytic leukemia protein bodies." J Biol Chem **289**(28): 19383-19394.

Small, C. D. and B. D. Crawford (2016). "Matrix metalloproteinases in neural development: a phylogenetically diverse perspective." Neural Regen Res **11**(3): 357-362.

Smart, I. H., C. Dehay, P. Giroud, M. Berland and H. Kennedy (2002). "Unique morphological features of the proliferative zones and postmitotic compartments of the neural epithelium giving rise to striate and extrastriate cortex in the monkey." Cereb Cortex **12**(1): 37-53.

Smith, B. J. and V. C. Carregari (2022). "Post-Translational Modifications During Brain Development." Adv Exp Med Biol **1382**: 29-38.

Snyder, S. E., H. W. Cheng, K. D. Murray, P. J. Isackson, T. H. McNeill and S. R. J. Salton (1997). "The messenger RNA encoding VGF, a neuronal peptide precursor, is rapidly regulated in the rat central nervous system by neuronal activity, seizure and lesion." Neuroscience **82**(1): 7-19.

Snyder, S. E., J. E. Pintar and S. R. Salton (1998). "Developmental expression of VGF mRNA in the prenatal and postnatal rat." J Comp Neurol **394**(1): 64-90.

Sorimachi, H., S. Hata and Y. Ono (2011). "Calpain chronicle--an enzyme family under multidisciplinary characterization." Proc Jpn Acad Ser B Phys Biol Sci **87**(6): 287-327.

Sorimachi, H., H. Mamitsuka and Y. Ono (2012). "Understanding the substrate specificity of conventional calpains." Biol Chem **393**(9): 853-871.

Spadory, T., A. Duque and L. D. Selemon (2022). "Spatial-temporal topography in neurogenesis of the macaque thalamus." Brain Struct Funct **227**(5): 1673-1682.

Speir, M. L., A. Bhaduri, N. S. Markov, P. Moreno, T. J. Nowakowski, I. Papatheodorou, A. A. Pollen, B. J. Raney, L. Seninge, W. J. Kent and M. Haeussler (2021). "UCSC Cell Browser: visualize your single-cell data." Bioinformatics **37**(23): 4578-4580.

Steullet, P. (2020). "Thalamus-related anomalies as candidate mechanism-based biomarkers for psychosis." Schizophr Res **226**: 147-157.

Stuart, T., A. Butler, P. Hoffman, C. Hafemeister, E. Papalexi, W. M. Mauck, 3rd, Y. Hao, M. Stoeckius, P. Smibert and R. Satija (2019). "Comprehensive Integration of Single-Cell Data." Cell **177**(7): 1888-1902.e1821.

Subramanian, L., M. E. Calcagnotto and M. F. Paredes (2019). "Cortical Malformations: Lessons in Human Brain Development." Front Cell Neurosci **13**: 576.

Suzuki, S. C., T. Inoue, Y. Kimura, T. Tanaka and M. Takeichi (1997). "Neuronal circuits are subdivided by differential expression of type-II classic cadherins in postnatal mouse brains." Mol Cell Neurosci **9**(5-6): 433-447.

Takahashi, E., R. D. Folkerth, A. M. Galaburda and P. E. Grant (2012). "Emerging cerebral connectivity in the human fetal brain: an MR tractography study." Cereb Cortex **22**(2): 455-464.

Tamamaki, N., K. E. Fujimori and R. Takauji (1997). "Origin and route of tangentially migrating neurons in the developing neocortical intermediate zone." J Neurosci **17**(21): 8313-8323.

Thacker, J. S., D. Andersen, S. Liang, N. Zieniewicz, J. S. Trivino-Paredes, P. C. Nahirney and B. R. Christie (2021). "Unlocking the brain: A new method for Western blot protein detection from fixed brain tissue." J Neurosci Methods **348**: 108995.

Thakker-Varia, S., J. Behnke, D. Doobin, V. Dalal, K. Thakkar, F. Khadim, E. Wilson, A. Palmieri, H. Antila, T. Rantamaki and J. Alder (2014). "VGF (TLQP-62)-induced neurogenesis targets early phase neural progenitor cells in the adult hippocampus and requires glutamate and BDNF signaling." Stem Cell Res **12**(3): 762-777.

Thakker-Varia, S., Y. Y. Jean, P. Parikh, C. F. Sizer, J. Jernstedt Ayer, A. Parikh, T. M. Hyde, S. Buyske and J. Alder (2010). "The neuropeptide VGF is reduced in human bipolar postmortem brain and contributes to some of the behavioral and molecular effects of lithium." J Neurosci **30**(28): 9368-9380.

Thakker-Varia, S., J. J. Krol, J. Nettleton, P. M. Bilimoria, D. A. Bangasser, T. J. Shors, I. B. Black and J. Alder (2007). "The neuropeptide VGF produces antidepressant-like behavioral effects and enhances proliferation in the hippocampus." J Neurosci **27**(45): 12156-12167.

Toda, T., Y. Shinmyo, T. A. Dinh Duong, K. Masuda and H. Kawasaki (2016). "An essential role of SVZ progenitors in cortical folding in gyrencephalic mammals." Sci Rep **6**: 29578.

Tohda, C. and M. Tohda (2017). "Extracellular cathepsin L stimulates axonal growth in neurons." BMC Res Notes **10**(1): 613.

Tolner, E. A., A. Sheikh, A. Y. Yukin, K. Kaila and P. O. Kanold (2012). "Subplate neurons promote spindle bursts and thalamocortical patterning in the neonatal rat somatosensory cortex." J Neurosci **32**(2): 692-702.

Toma, K., T. Kumamoto and C. Hanashima (2014). "The timing of upper-layer neurogenesis is conferred by sequential derepression and negative feedback from deep-layer neurons." J Neurosci **34**(39): 13259-13276.

Tran, A. P. and J. Silver (2021). "Cathepsins in neuronal plasticity." Neural Regen Res **16**(1): 26-35.

Trani, E., T. Ciotti, A. M. Rinaldi, N. Canu, G. L. Ferri, A. Levi and R. Possenti (1995). "Tissue-specific processing of the neuroendocrine protein VGF." J Neurochem **65**(6): 2441-2449.

Trani, E., A. Giorgi, N. Canu, G. Amadoro, A. M. Rinaldi, P. A. Halban, G. L. Ferri, R. Possenti, M. E. Schinina and A. Levi (2002). "Isolation and characterization of VGF peptides in rat brain. Role of PC1/3 and PC2 in the maturation of VGF precursor." J Neurochem **81**(3): 565-574.

Tuttle, R., Y. Nakagawa, J. E. Johnson and D. D. O'Leary (1999). "Defects in thalamocortical axon pathfinding correlate with altered cell domains in Mash-1-deficient mice." Development **126**(9): 1903-1916.

Uesaka, N., Y. Hayano, A. Yamada and N. Yamamoto (2007). "Interplay between laminar specificity and activity-dependent mechanisms of thalamocortical axon branching." J Neurosci **27**(19): 5215-5223.

Ulfig, N. (2000). "The ganglionic eminence--new vistas." Trends Neurosci **23**(11): 530.

Vaccarino, F. M., M. L. Schwartz, R. Raballo, J. Nilsen, J. Rhee, M. Zhou, T. Doetschman, J. D. Coffin, J. J. Wyland and Y. T. Hung (1999). "Changes in cerebral cortex size are governed by fibroblast growth factor during embryogenesis." Nat Neurosci **2**(9): 848.

van den Pol, A. N., K. Bina, C. Decavel and P. Ghosh (1994). "VGF expression in the brain." J Comp Neurol **347**(3): 455-469.

Van der Loos, H. and T. A. Woolsey (1973). "Somatosensory cortex: structural alterations following early injury to sense organs." Science **179**(4071): 395-398.

Vanhatalo, S. and K. Kaila (2006). "Development of neonatal EEG activity: from phenomenology to physiology." Semin Fetal Neonatal Med **11**(6): 471-478.

Vanhatalo, S., J. M. Palva, S. Andersson, C. Rivera, J. Voipio and K. Kaila (2005). "Slow endogenous activity transients and developmental expression of K+-Cl- cotransporter 2 in the immature human cortex." Eur J Neurosci **22**(11): 2799-2804.

Vasung, L., H. Huang, N. Jovanov-Milosevic, M. Pletikos, S. Mori and I. Kostovic (2010). "Development of axonal pathways in the human fetal fronto-limbic brain: histochemical characterization and diffusion tensor imaging." J Anat **217**(4): 400-417.

Vasung, L., C. Lepage, M. Rados, M. Pletikos, J. S. Goldman, J. Richiardi, M. Raguz, E. Fischi-Gomez, S. Karama, P. S. Huppi, A. C. Evans and I. Kostovic (2016). "Quantitative and Qualitative Analysis of Transient Fetal Compartments during Prenatal Human Brain Development." Front Neuroanat **10**: 11.

Vasung, L., M. Raguz, I. Kostovic and E. Takahashi (2017). "Spatiotemporal Relationship of Brain Pathways during Human Fetal Development Using High-Angular Resolution Diffusion MR Imaging and Histology." Front Neurosci **11**: 348.

Velez, G., Y. J. Sun, S. Khan, J. Yang, J. Herrmann, T. Chemudupati, R. E. MacLaren, L. Gakhar, S. Wakatsuki, A. G. Bassuk and V. B. Mahajan (2020). "Structural Insights into the Unique Activation Mechanisms of a Non-classical Calpain and Its Disease-Causing Variants." Cell Rep **30**(3): 881-892.e885.

Vento-Tormo, R., M. Efremova, R. A. Botting, M. Y. Turco, M. Vento-Tormo, K. B. Meyer, J.-E. Park, E. Stephenson, K. Polański, A. Goncalves, L. Gardner, S. Holmqvist, J. Henriksson, A. Zou, A. M. Sharkey, B. Millar, B. Innes, L. Wood, A. Wilbrey-Clark, R. P. Payne, M. A. Ivarsson, S. Lisgo, A. Filby, D. H. Rowitch, J. N. Bulmer, G. J. Wright, M. J. T. Stubbington, M. Haniffa, A. Moffett and S. A. Teichmann (2018). "Single-cell reconstruction of the early maternal–fetal interface in humans." Nature **563**(7731): 347-353.

Vitner, E. B., H. Dekel, H. Zigdon, T. Shachar, T. Farfel-Becker, R. Eilam, S. Karlsson and A. H. Futerman (2010). "Altered expression and distribution of cathepsins in neuronopathic forms of Gaucher disease and in other sphingolipidoses." Human Molecular Genetics **19**(18): 3583-3590.

Wallace, G. L., B. Robustelli, N. Dankner, L. Kenworthy, J. N. Giedd and A. Martin (2013). "Increased gyrification, but comparable surface area in adolescents with autism spectrum disorders." Brain **136**(Pt 6): 1956-1967.

Wang, C., M. E. Ward, R. Chen, K. Liu, T. E. Tracy, X. Chen, M. Xie, P. D. Sohn, C. Ludwig, A. Meyer-Franke, C. M. Karch, S. Ding and L. Gan (2017). "Scalable Production of iPSC-Derived Human Neurons to Identify Tau-Lowering Compounds by High-Content Screening." Stem Cell Reports **9**(4): 1221-1233.

Wang, I. E., S. W. Lapan, M. L. Scimone, T. R. Clandinin and P. W. Reddien (2016). "Hedgehog signaling regulates gene expression in planarian glia." Elife **5**.

Wang, L., K. Pang, L. Zhou, A. Cebrián-Silla, S. González-Granero, S. Wang, Q. Bi, M. L. White, B. Ho, J. Li, T. Li, Y. Perez, E. J. Huang, E. A. Winkler, M. F. Paredes, R. Kovner, N. Sestan, A. A. Pollen, P. Liu, J. Li, X. Piao, J. M. García-Verdugo, A. Alvarez-Buylla, Z. Liu and A. R. Kriegstein (2023). "A cross-species proteomic map reveals neoteny of human synapse development." bioRxiv: 2022.2010.2024.513541.

Wang, W. Z., A. Hoerder-Suabedissen, F. M. Oeschger, N. Bayatti, B. K. Ip, S. Lindsay, V. Supramaniam, L. Srinivasan, M. Rutherford, K. Mollgard, G. J. Clowry and Z. Molnar (2010). "Subplate in the developing cortex of mouse and human." J Anat **217**(4): 368-380.

Wang, Y., V. Briz, A. Chishti, X. Bi and M. Baudry (2013). "Distinct roles for mu-calpain and m-calpain in synaptic NMDAR-mediated neuroprotection and extrasynaptic NMDAR-mediated neurodegeneration." J Neurosci **33**(48): 18880-18892.

Wang, Y., J. Hersheson, D. Lopez, M. Hammer, Y. Liu, K. H. Lee, V. Pinto, J. Seinfeld, S. Wiethoff, J. Sun, R. Amouri, F. Hentati, N. Baudry, J. Tran, A. B. Singleton, M. Coutelier, A. Brice, G. Stevanin, A. Durr, X. Bi, H. Houlden and M. Baudry (2016). "Defects in the CAPN1 Gene Result in Alterations in Cerebellar Development and Cerebellar Ataxia in Mice and Humans." Cell Rep **16**(1): 79-91.

Wang, Y., Y. Liu, X. Bi and M. Baudry (2020). "Calpain-1 and Calpain-2 in the Brain: New Evidence for a Critical Role of Calpain-2 in Neuronal Death." Cells **9**(12).

Watanabe, N., R. Kageyama and T. Ohtsuka (2015). "Hbp1 regulates the timing of neuronal differentiation during cortical development by controlling cell cycle progression." Development **142**(13): 2278-2290.

Wegrzyn, J. L., S. J. Bark, L. Funkelstein, C. Mosier, A. Yap, P. Kazemi-Esfarjani, A. R. La Spada, C. Sigurdson, D. T. O'Connor and V. Hook (2010). "Proteomics of dense core secretory vesicles reveal distinct protein categories for secretion of neuroeffectors for cell-cell communication." J Proteome Res **9**(10): 5002-5024.

Wible, C. G., J. Anderson, M. E. Shenton, A. Kricun, Y. Hirayasu, S. Tanaka, J. J. Levitt, B. F. O'Donnell, R. Kikinis, F. A. Jolesz and R. W. McCarley (2001). "Prefrontal cortex, negative symptoms, and schizophrenia: an MRI study." Psychiatry Res **108**(2): 65-78.

Woodward, N. D., H. Karbasforoushan and S. Heckers (2012). "Thalamocortical dysconnectivity in schizophrenia." Am J Psychiatry **169**(10): 1092-1099.

Workman, A. D., C. J. Charvet, B. Clancy, R. B. Darlington and B. L. Finlay (2013). "Modeling Transformations of Neurodevelopmental Sequences across Mammalian Species." The Journal of Neuroscience **33**(17): 7368-7383.

Yadati, T., T. Houben, A. Bitorina and R. Shiri-Sverdlov (2020). "The Ins and Outs of Cathepsins: Physiological Function and Role in Disease Management." Cells **9**(7).

Yamamoto, N., T. Kurotani and K. Toyama (1989). "Neural Connections Between the Lateral Geniculate Nucleus and Visual Cortex in Vitro." Science **245**(4914): 192-194.

Yamamoto, N., K. Yamada, T. Kurotani and K. Toyama (1992). "Laminar specificity of extrinsic cortical connections studied in coculture preparations." Neuron **9**(2): 217-228.

Yamashima, T. (2016). "Can 'calpain-cathepsin hypothesis' explain Alzheimer neuronal death?" Ageing Research Reviews **32**: 169-179.

Yang, J. W., W. Kilb, S. Kirischuk, P. Unichenko, M. C. Stuttgen and H. J. Luhmann (2018). "Development of the whisker-to-barrel cortex system." Curr Opin Neurobiol **53**: 29-34.

Yu, L., V. A. Petyuk, K. P. Lopes, S. Tasaki, V. Menon, Y. Wang, J. A. Schneider, P. L. De Jager and D. A. Bennett (2023). "Associations of VGF with Neuropathologies and Cognitive Health in Older Adults." Ann Neurol **94**(2): 232-244.

Yuste, R., A. Peinado and L. C. Katz (1992). "Neuronal Domains in Developing Neocortex." Science **257**(5070): 665-669.

Zecevic, N. (2004). "Specific characteristic of radial glia in the human fetal telencephalon." Glia **48**(1): 27-35.

Zecevic, N., Y. Chen and R. Filipovic (2005). "Contributions of cortical subventricular zone to the development of the human cerebral cortex." J Comp Neurol **491**(2): 109-122.

Zecevic, N., F. Hu and I. Jakovcevski (2011). "Interneurons in the developing human neocortex." Dev Neurobiol **71**(1): 18-33.

Zecevic, N., S. Rakic, I. Jakovcevski and R. Filipovic (2006). Contributions of the Neocortical Svz to Human Brain Development. Mammalian Subventricular Zones: Their Roles in Brain Development, Cell Replacement and Disease. S. W. Levison. Boston, MA, Springer US**:** 117-158.

Zhang, X., H. Pan, B. Peng, D. F. Steiner, J. E. Pintar and L. D. Fricker (2010). "Neuropeptidomic analysis establishes a major role for prohormone convertase-2 in neuropeptide biosynthesis." J Neurochem **112**(5): 1168-1179.

Zhao, Y. and O. N. Jensen (2009). "Modification-specific proteomics: strategies for characterization of post-translational modifications using enrichment techniques." Proteomics **9**(20): 4632-4641.

Zhou, C., S. Y. Tsai and M. J. Tsai (2001). "COUP-TFI: an intrinsic factor for early regionalization of the neocortex." Genes Dev **15**(16): 2054-2059.

Zipursky, R. B., K. O. Lim, E. V. Sullivan, B. W. Brown and A. Pfefferbaum (1992). "Widespread cerebral gray matter volume deficits in schizophrenia." Arch Gen Psychiatry **49**(3): 195-205.

Zunic Isasegi, I., M. Rados, Z. Krsnik, M. Rados, V. Benjak and I. Kostovic (2018). "Interactive histogenesis of axonal strata and proliferative zones in the human fetal cerebral wall." Brain Struct Funct **223**(9): 3919-3943.

Supplementary Material

DPhil Thesis

Sara Bandiera

Figure S1 [Supplementary to Chapter 3]

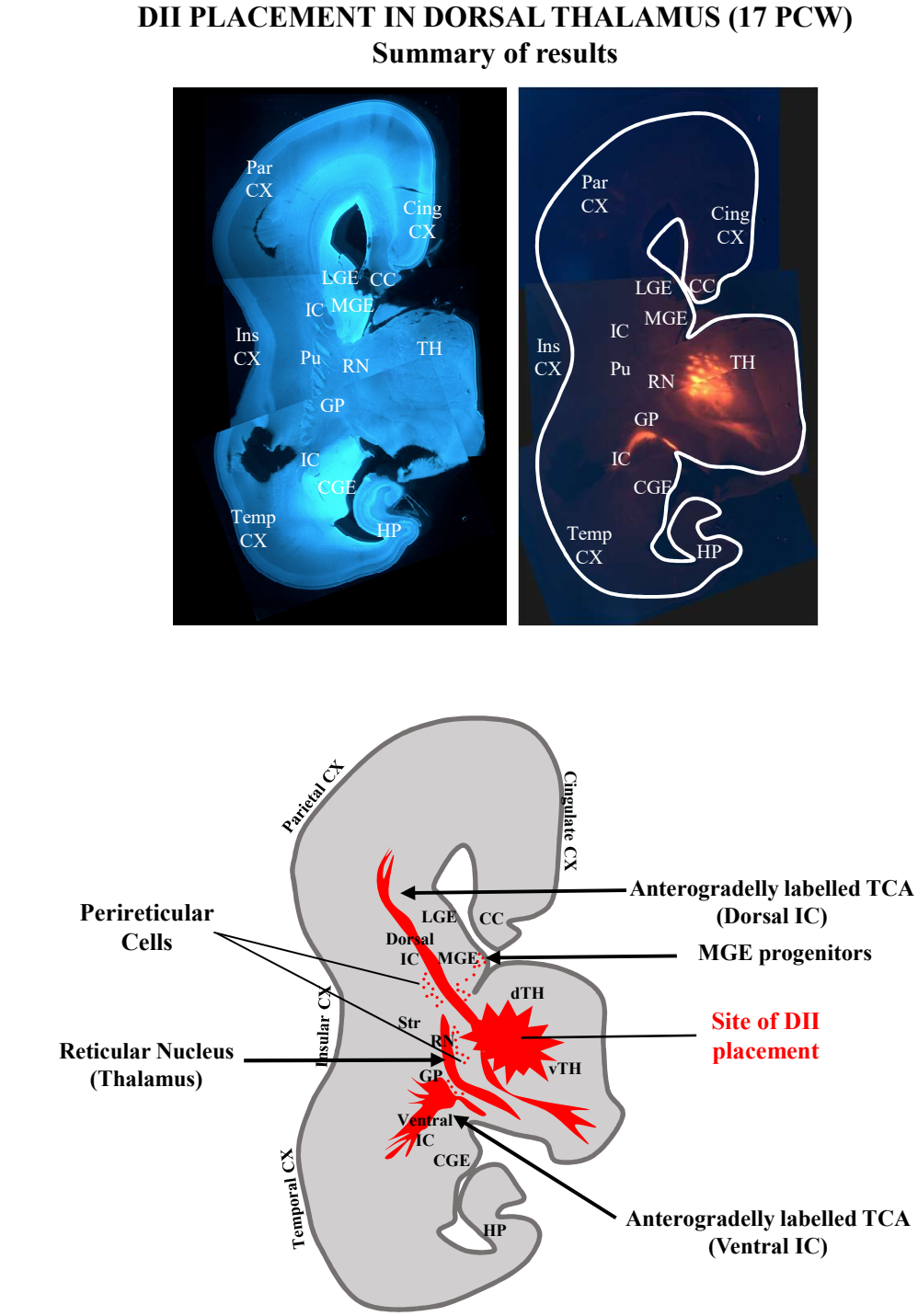

Figure S1: Summary of the results from axon tracing by DiI crystal placement in the dorsal thalamus of the 17 PCW human brain (slab #6).

(**A**) DAPI nuclear staining reveals the main anatomical structures in the coronal sections analysed. (**B**) DiI-positive signal detected in the coronal sections and schematized in detail in (C). (**C**) Schematic representation of the coronal sections from slab #6, indicating the site of DiI crystal placement in the dorsal aspect of the thalamus. The pattern of labelling obtained shows anterograde labelling of the dorsal and ventral branches of the internal capsule (IC), the DiI-positive signal in the reticular nucleus (RN), the surrounding perireticular cells, and the progenitor cells of the medial ganglionic eminence (MGE).

Figure S2 [Supplementary to Chapter 3]

Reticular Nucleus and Perireticular Cells

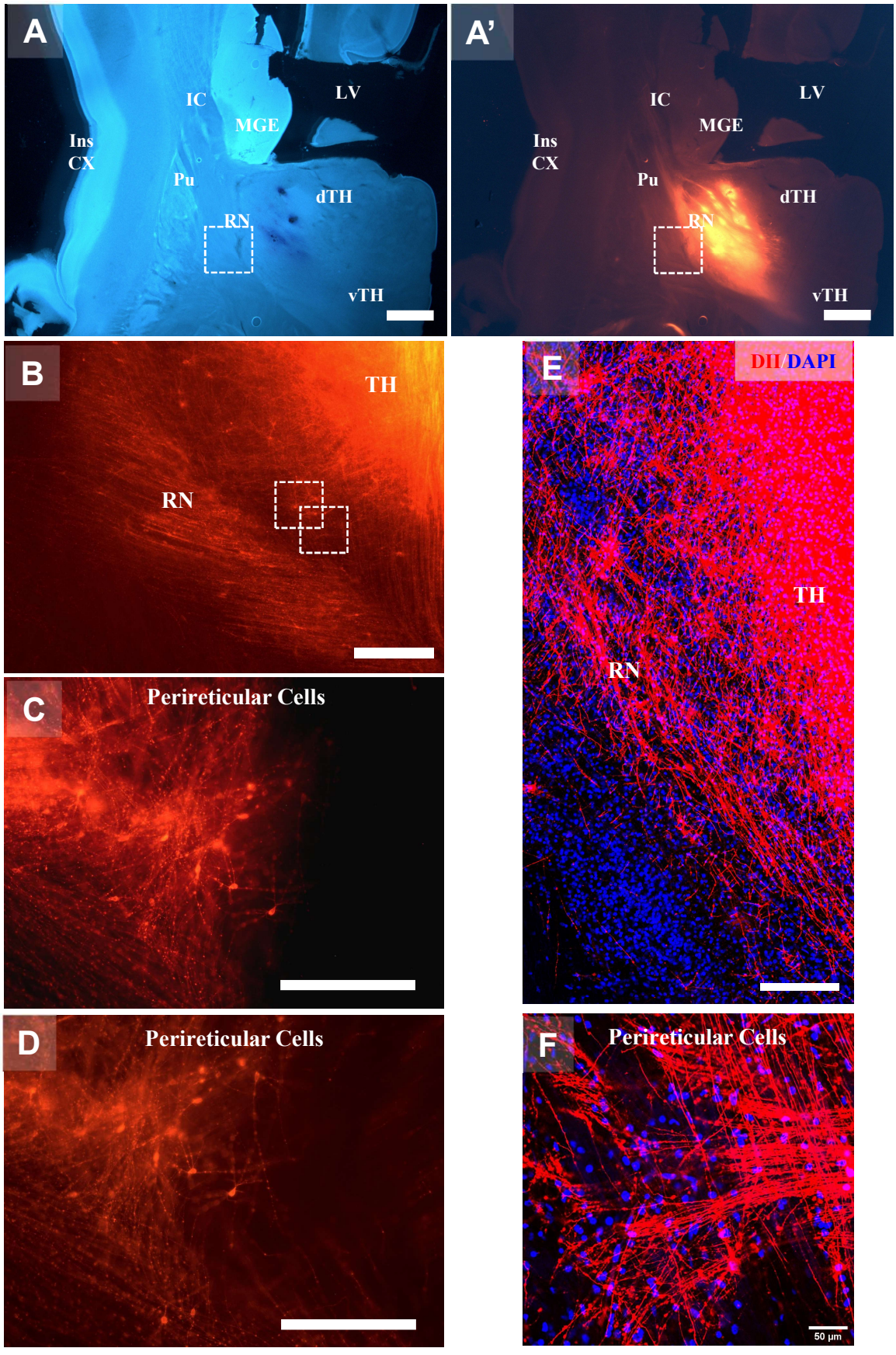

Figure S2: DiI crystal placement in the dorsal thalamus reveals labelling of the thalamic area, the surrounding reticular nucleus (RN), and the perireticular cells scattered in the area between the thalamus and the internal capsule (IC) in the 17 PCW human brain.

(**A, A'**) Epifluorescence imaging of the entire coronal section highlighting the anatomical structures with DAPI nuclear staining (A) and the site of DiI placement in the thalamus (A'). Epifluorescence (**B**) and confocal imaging (**E**) showing strong labelling of the reticular nucleus surrounding the thalamus, that was clearly distinguishable by DAPI staining in several sections. The reticular nucleus represents an important intermediate station for both thalamocortical and corticothalamic axons en route to their respective targets (Mitrofanis et al. 1993). Therefore, the signal detected at this level was expected. Adjacent to the reticular nucleus (**C, D**), and close to the initial segment of the dorsal internal capsule medially to the ganglionic eminence (**F**), I also detected a group of neuronal cell bodies scattered throughout the area and visibly labelled by DiI. These represented what has been described as "transient cells of the IC" by Letinic and Kostovic (Letinić *et al.* 1996), and are also referred to as **perireticular cells or perireticular nucleus** (Mitrofanis *et al.* 1993). Perireticular cells also represent an important developmental structure connecting the cortex with the thalamus, alongside with the reticular nucleus that is anatomically and developmentally associated with them. These neurons have not been observed in the 17 PCW human brain in previous studies that mostly concentrated on much earlier or later developmental stages (Tulay et al. 2004; Bystron et al. 2005). However, as they represent an intermediate station for the TCA and the eventually retrogradely labelled CTA, this was also an expected result. Scale bars = 2000 μm (A, A'); 500 μm (B, E); 50 μm (F).

Figure S3 [Supplementary to Chapter 3]

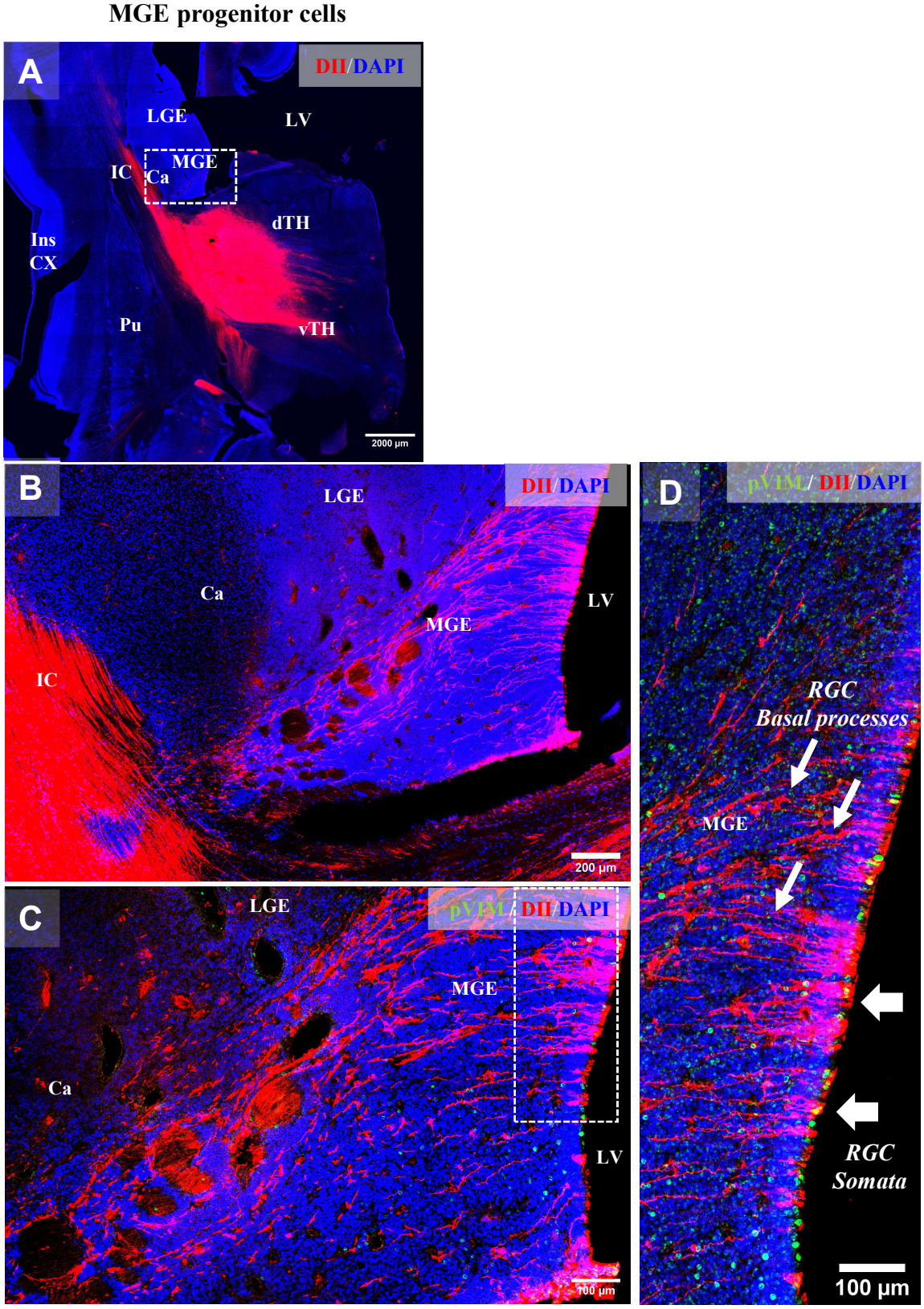

Figure S3: DiI crystal placement in the dorsal thalamus reveals radial glial cells (RGC) of the medial ganglionic eminence (MGE) throughout their processes up to their cell bodies, immunoreactive for phosphor-Vimentin (pVim) in the ventricular side in the 17 PCW human brain.

(**A, B**) Tiled scans of the area of the brain where the DiI-positive signal stains the basal processes of the MGE progenitors. The processes, perpendicular to the thalamocortical axons, extended from the vicinity of the internal capsule near the site of DiI injection, up to the ventricular side of the MGE. This phenomenon was observed exclusively in the MGE, and all DiI-labelled processes in fact avoided the adjacent LGE. Progenitors of the LGE would not extend through the area were the DiI crystals were placed, but rather extend from a more dorsal location closer to the boundary with the cortex. Therefore, a similar labelling of progenitors of the LGE would be more unlikely, as supported by the absence of any DiI-positive process in this region.

(**C, D**) Staining for phospho-Vimentin (pVim) (green), a marker of neuronal progenitors, revealed the location of precursor cells lining the ventricular zone (VZ) of the MGE, as well as some cell bodies located farther away from the ventricle, representing basal progenitors of the ganglionic eminence (thick arrows). Both ventricular and subventricular pVim-progenitors populations appeared to be back-labelled by DiI, likely at the intersection between their basal processes and the the tangentially oriented axons of the internal capsule (IC). Since the MGE territory is considered as non-permissive for TCA (Lopez-Bendito et al. 2006), therefore the possibility that these processes represented collaterals of thalamic axons was excluded.

Scale bars = 2000 µm (A); 200 µm (B); 100 µm (C, D).

Figure S4 [Supplementary to Chapter 3]

Dorsal and Ventral Internal Capsule

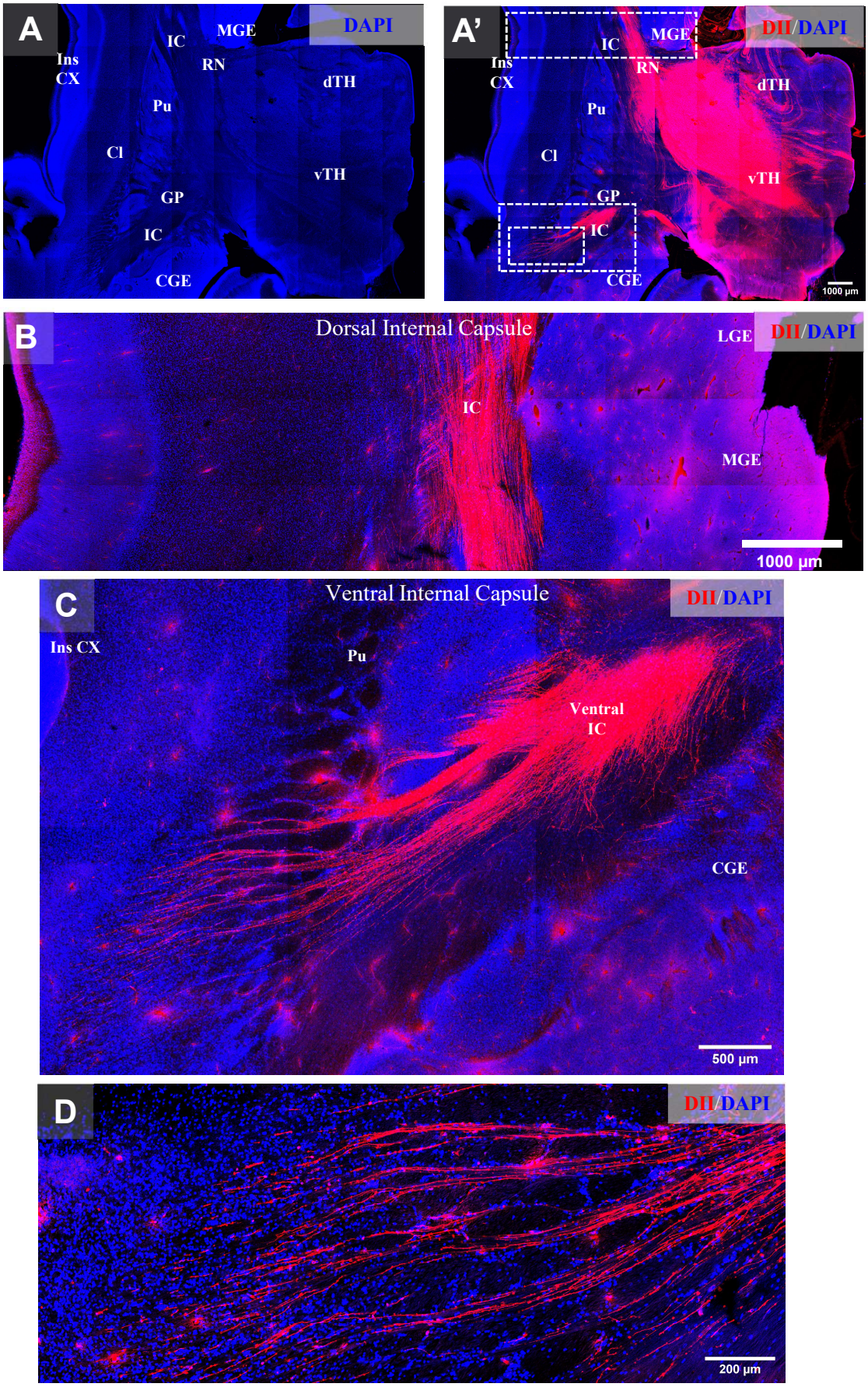

Figure S4: DiI crystal placement into the dorsal thalamus reveals labelling of both dorsal and ventral branches of the internal capsule (IC) in the 17 PCW human brain . (A, A') Tiled confocal scans of the coronal section showing DiI-labelled dorsal and ventral IC imaged in the other panels. Confocal scans of the dorsal (**B**) and ventral (**C, D**) segments of the IC departing from the area next to the crystal placement in the dorsal thalamus and projecting toward the prospective parietal and insular/temporal cortices, respectively.
Scale bars = 1000 μm (A-B); 500 μm (C); 100 μm (D).

Figure S5 [Supplementary to Chapter 3]

Internal Capsule, Perireticular Cells

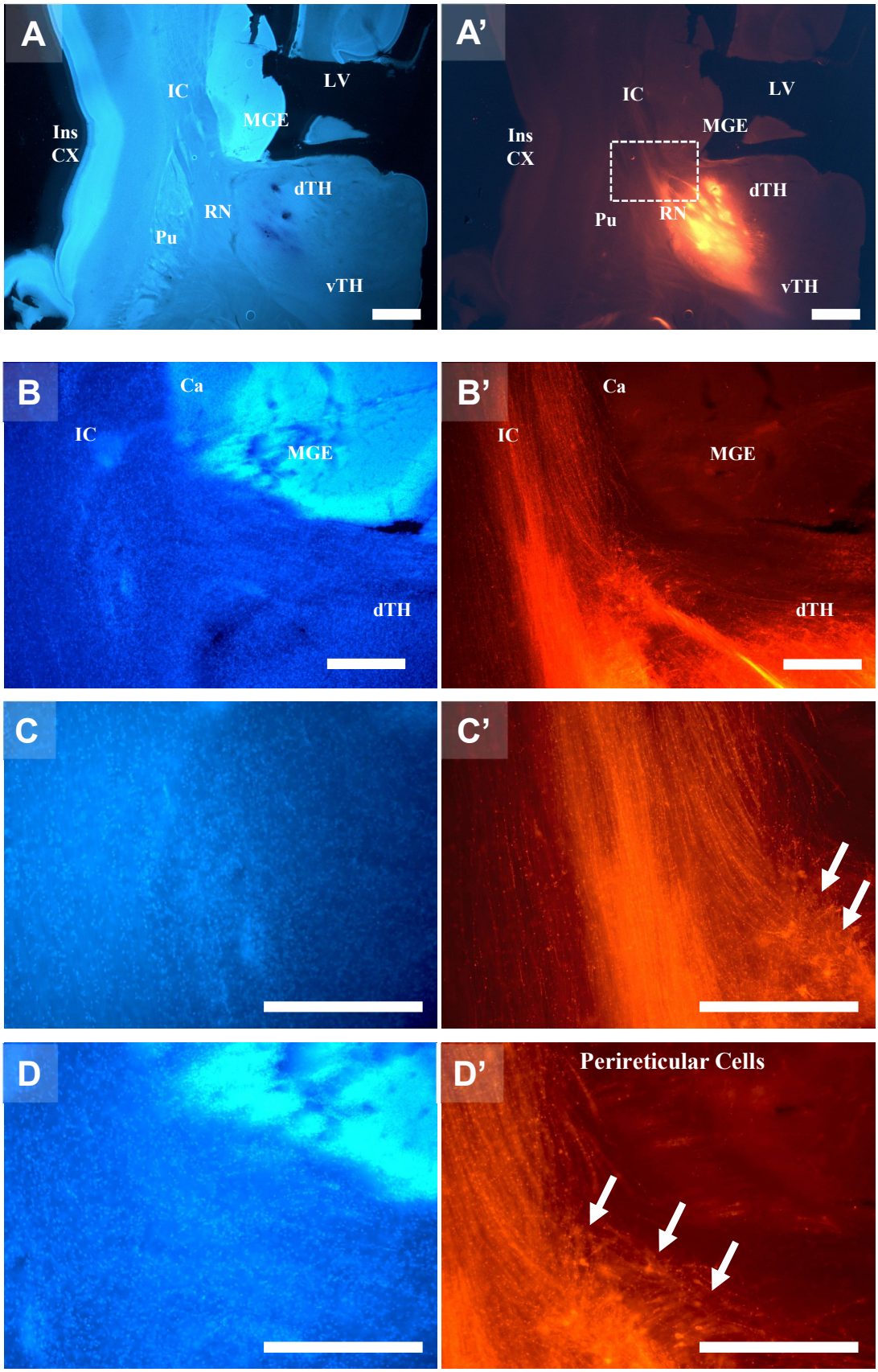

Figure S5 [Supplementary to Chapter 3]

Axonal Fasciculation

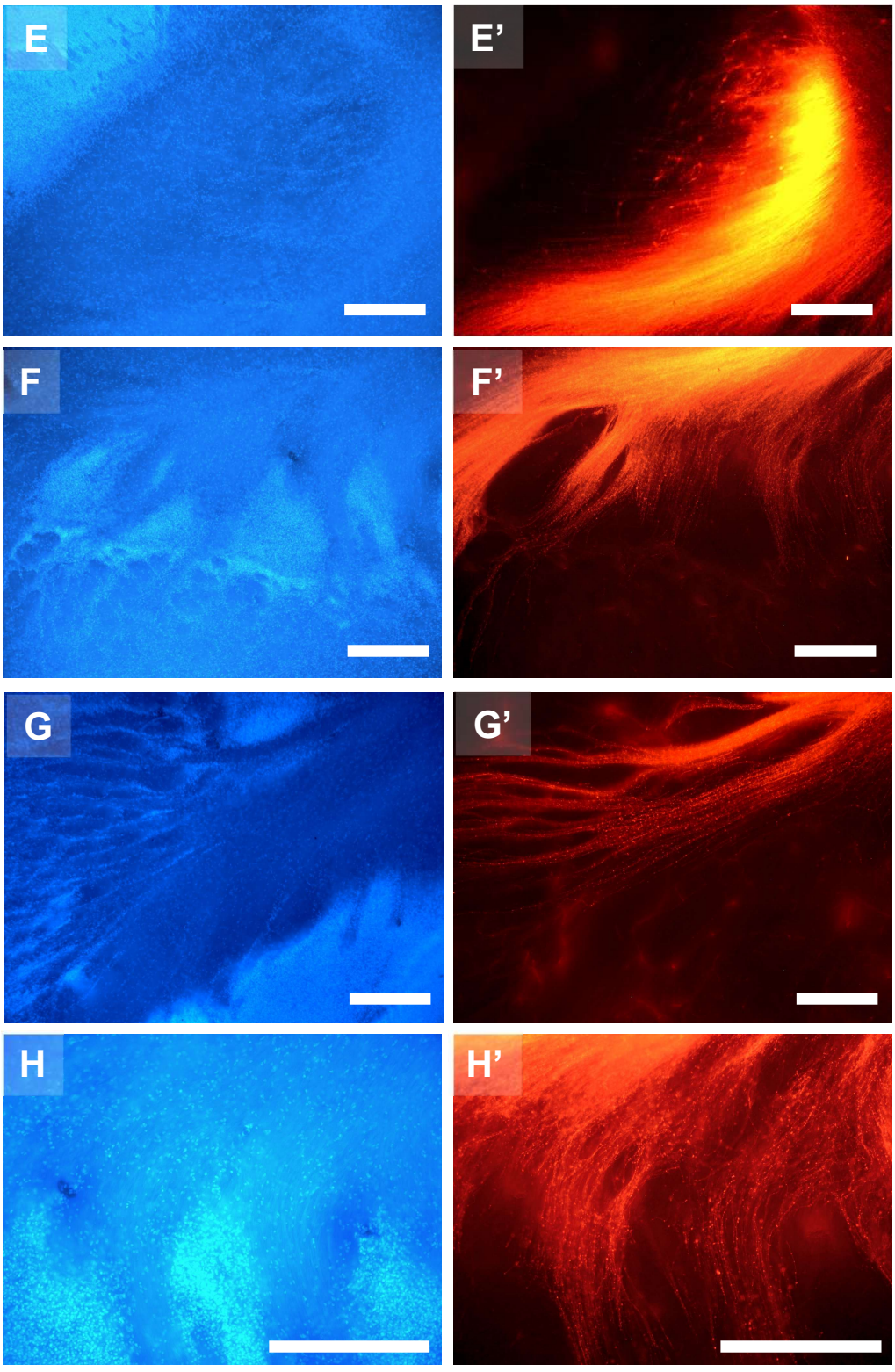

Figure S5: DiI crystal placement in the dorsal thalamus reveals labelling of both dorsal and ventral branches of the internal capsule (IC) in the 17 PCW human brain (epifluorescence imaging). (A, A') Low power epifluorescence images of the coronal section. **(B-D')** Epifluorescence images of the initial segment of the dorsal IC departing from the dorsal thalamus where DiI crystals were placed and projecting toward the prospective parietal cortex. Arrows in C', D' highlight some perireticular cells, also labelled by DiI, and located close to the IC. (**E-H'**) Epifluorescence images of the ventral portion of the IC departing projecting toward the prospective insular and temporal cortices. The panels **E', F', G', H'** highlight the fasciculation of the axonal tract upon reaching the cortical areas, and following the anatomical structures revealed by DAPI staining (**E, F, G, H**). Scale bars = 500 μm.

Figure S6 [Supplementary to Chapter 4]

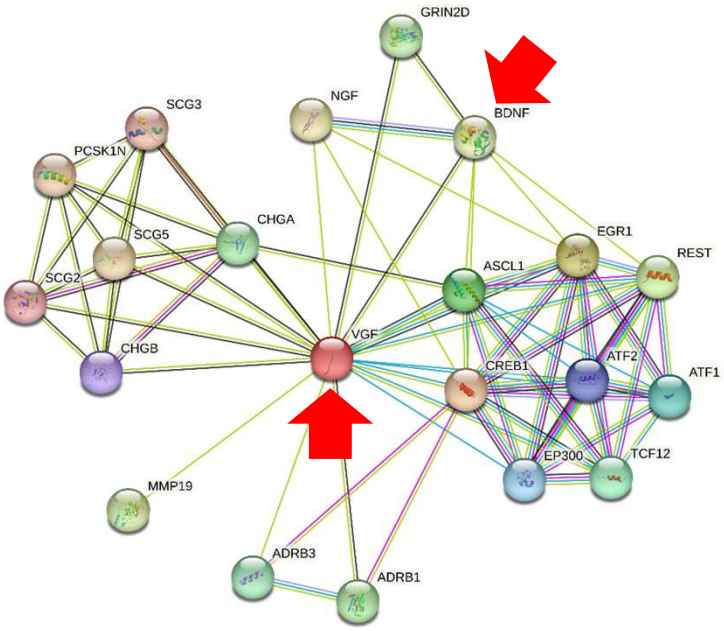

Figure S6: Representative illustration of VGF protein-protein interaction (PPI) network in homo sapiens. Network obtain by STRING version 11.5, selecting VGF as a central node and showing maximum 20 interactions (first shell only). Nodes represent genes in the network, edges represent the type of evidence of the interaction (i.e. interaction sources: Textmining; Experiments; Databases; Co-expression; Neighborhood; Gene Fusion; Co-occurrence). The level of confidence is set at 0.400 (Medium).

The PPI Network shows BDNF as one of the VGF-interacting molecules (Red thick arrows), alongside other genes with important roles in neuronal differentiation. These includes other neurotrophins, like Nerve Growth Factor (NGF) responsible for the induction of VGF mRNA transcription via activation of TrkB receptor (Salton et al. 1995); transcription factors, such as Cyclic AMP-responsive element-binding protein 1 (CREB1), that is selectively activated by phosphorylation upon stimulation of neuronal cells with neurotrophins, such as NGF and BDNF, which it ultimately upregulates in turns (Wang et al. 2022); neurotransmitter receptor-encoding gene Glutamate receptor ionotropic, NMDA 2D (GRIN2D), and other members of the granin family, Secretogranin 2 (SCG2), Secretogranin 3 (SCG3), Secretogranin 5 (SCG5), Chromogranin-A (CHGA), and Chromogranin-B (CHGB).

Figure S7 [Supplementary to Chapter 4]

A

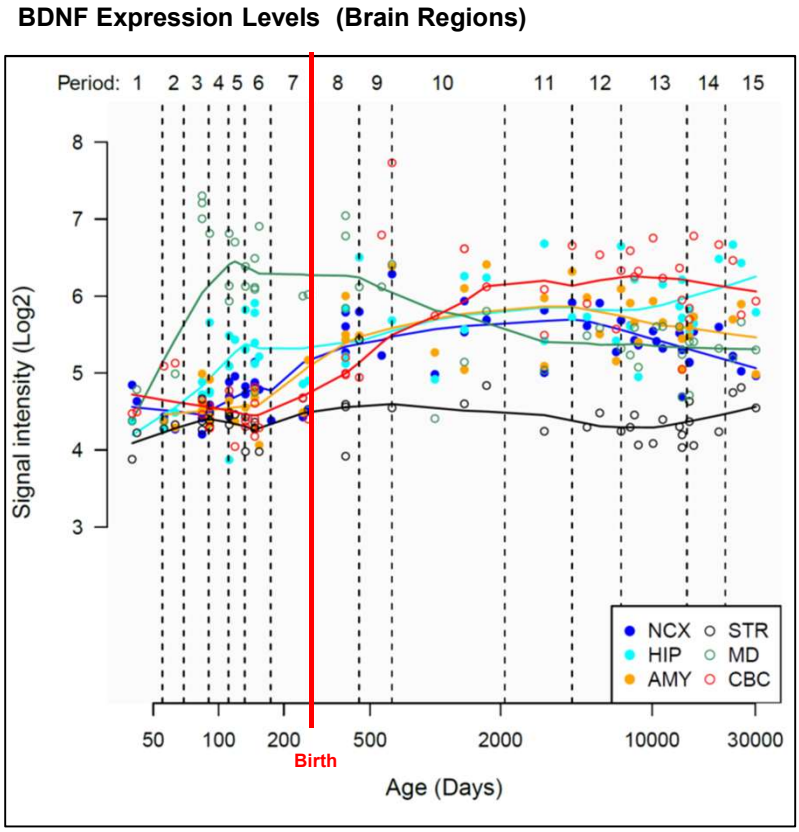

B

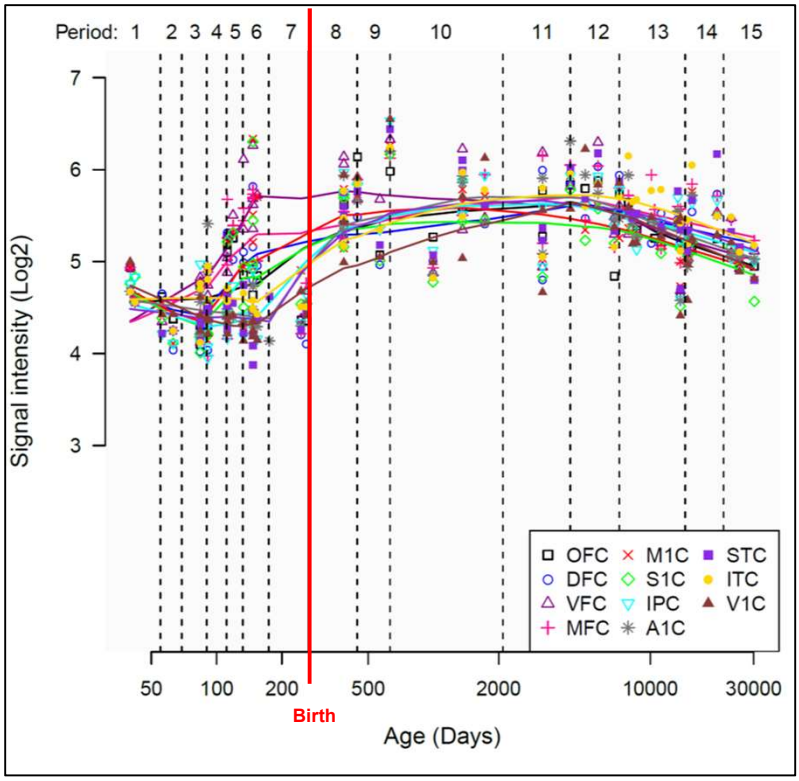

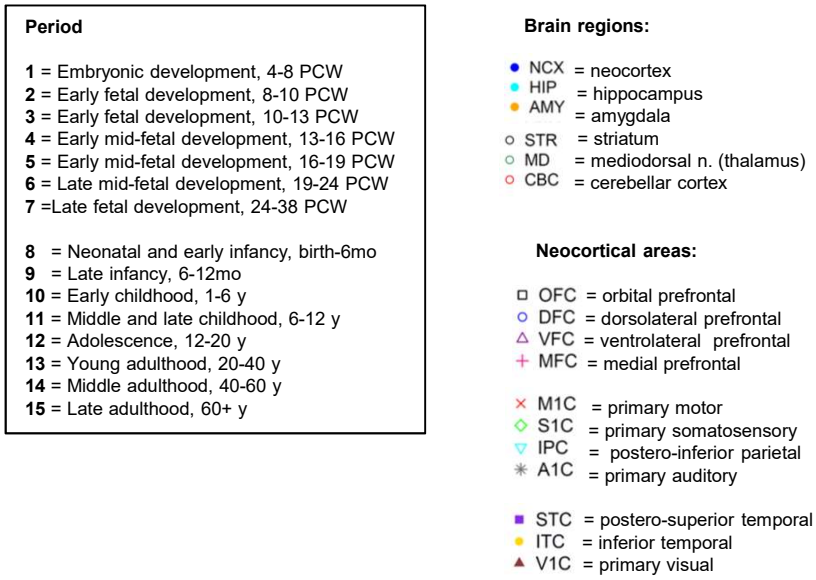

Figure S7: Line chart graphs of BDGF expression levels in the human brain regions (A) and neocortical areas (B) from embryonic development to adulthood.

Expression levels are represented by log2 signal intensity (y-axis), and ages are expressed in day (x-axis). A red line highlights birth, dividing prenatal and postnatal periods. (**A**) Surprisingly, BDNF expression levels in the prenatal human brain range between log2 values of 4-5 before midgestation (period 4; 13-16 PCW) and increasing slightly in the hippocampal region between 16 and 24 PCW (periods 5-6). These values appear to be lower than VGF (all log2 signal intensity > 5). A major exception is the mediodorsal nucleus of the thalamus (MD, green line), with values peaking to >7 at midgestation. This is in line with the significantly greater VGF expression levels in this region as compared to all other brain areas samples, as previously discussed (see **Figure 4.6**). (**B**) Although BDNF seems to have relatively similar expression patterns across the human prenatal brain regions as the one of VGF (see **Figure 4.6**), this is not the case when looking at different neocortical areas (NCX). In fact, if VGF shows a similar trend of expression regulation within the 11 neocortices analysed in the study BDNF appears significantly more abundant in the frontal areas, with gradually decreasing levels in the antero-posterior axis. This observation suggests that the two growth factors, despite sharing some molecular pathways, differ in their regulation in the neocortex, possibly due to different roles that they play in the development and specification of those areas.

Data from Kuang et al., 2011, and downloaded from hbatlas.org.

Figure S8 [Supplementary to Chapter 4]

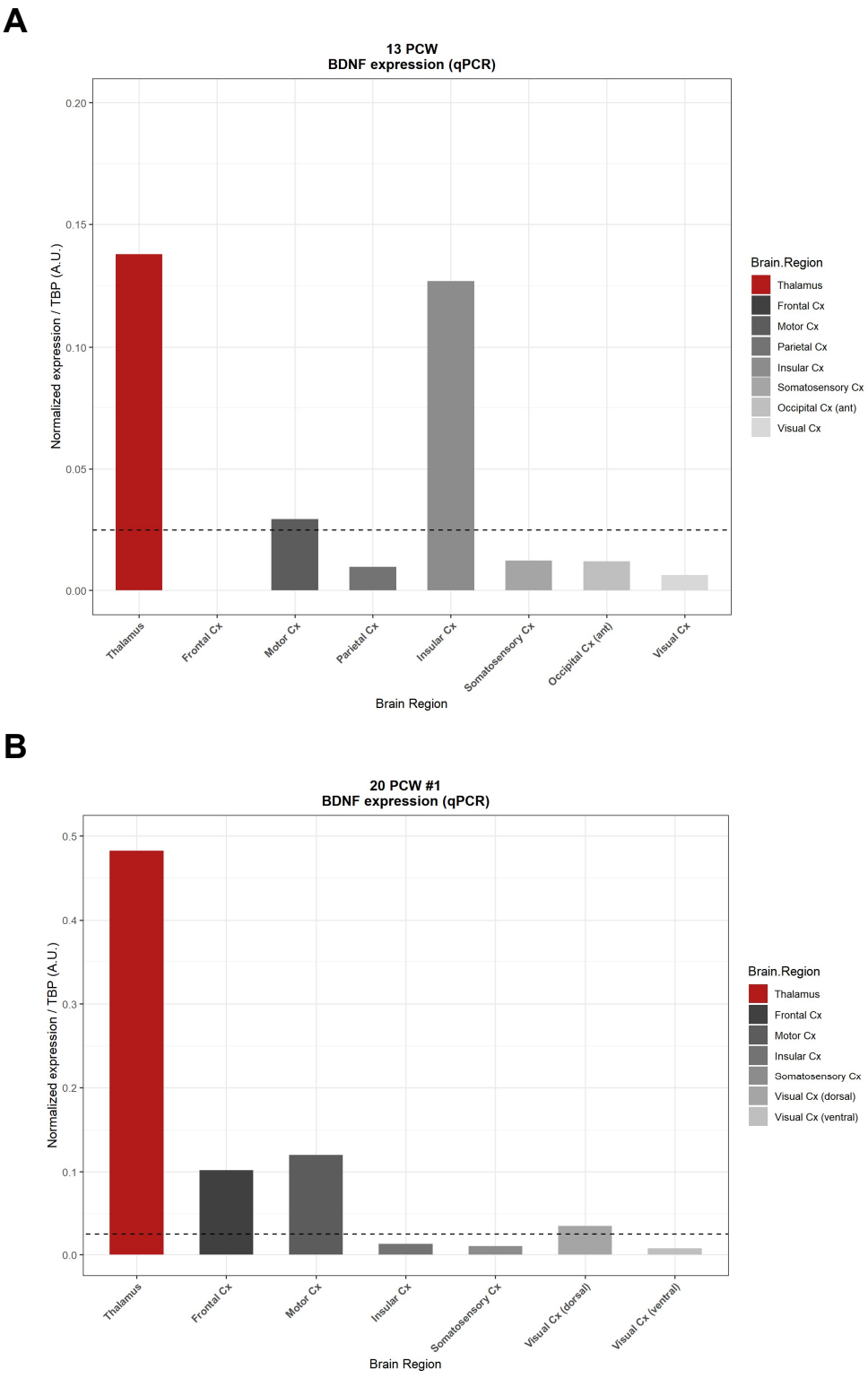

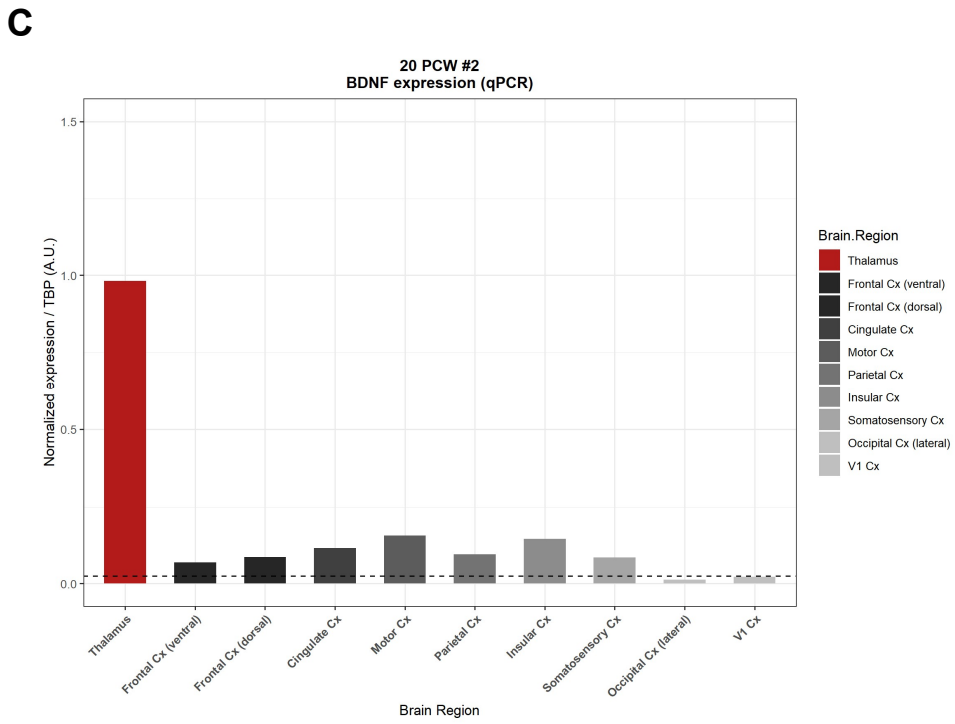

Figure S8: Quantification of BDNF expression levels in the 13 PCW (A) and 20 PCW (B, C) human thalamus and neocortical areas evaluated with qPCR. Gene expression values are normalized relative to the housekeeping gene TBP. Values are absolute arbitrary units (A.U.) calculated with the DCt method. Statistics does not apply due to the small sample size.

(**A**) At 13 PCW, BDNF is virtually absent in the frontal cortex, whereas VGF is already endogenously expressed in this region. Conversely, BDNF appears to be slightly higher in the motor cortex, where VGF is extremely low (see **Figure 4.13 A** for VGF data).

(**B,C**) On the other hand, at 20 PCW expression levels of BDNF in the frontal areas appear relatively increased as compared to the 13 PCW brain, in both individuals. The motor cortex remains the region with the highest BDNF expression amongst neocortical areas. This is again in contrast with VGF expression patterns, which are kept extremely low in the motor areas (see **Figure 4.13 B, C** for VGF data).

Although VGF and BDNF appear to share a similar trend in their expression pattern (high expression in thalamus, low expression in cortex), BDNF cortical levels, on the other hand, seem to fluctuate more extensively, not only between two different time points, but also across individuals.

Figure S9 [Supplementary to Chapter 5]

A

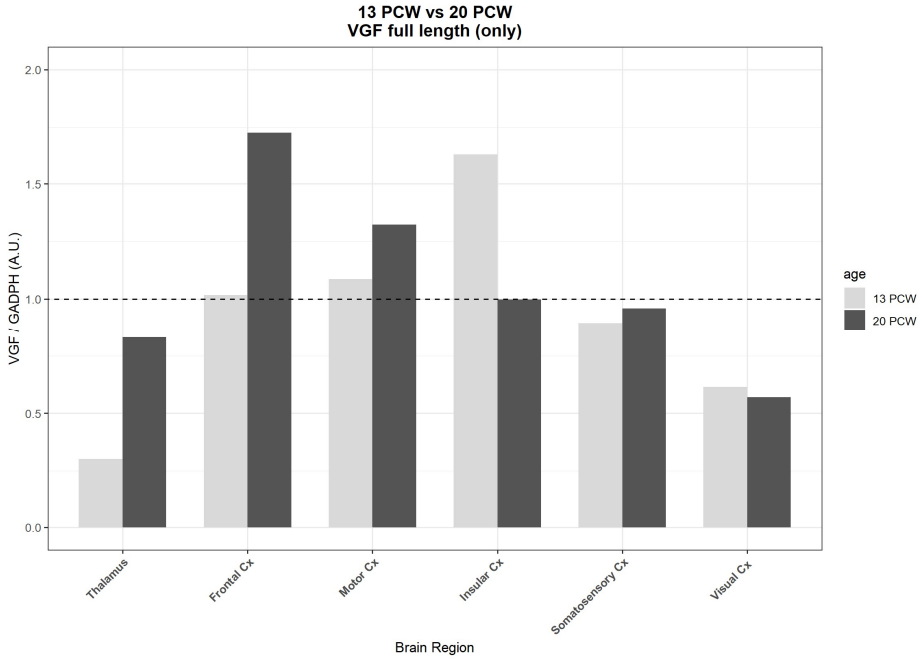

B

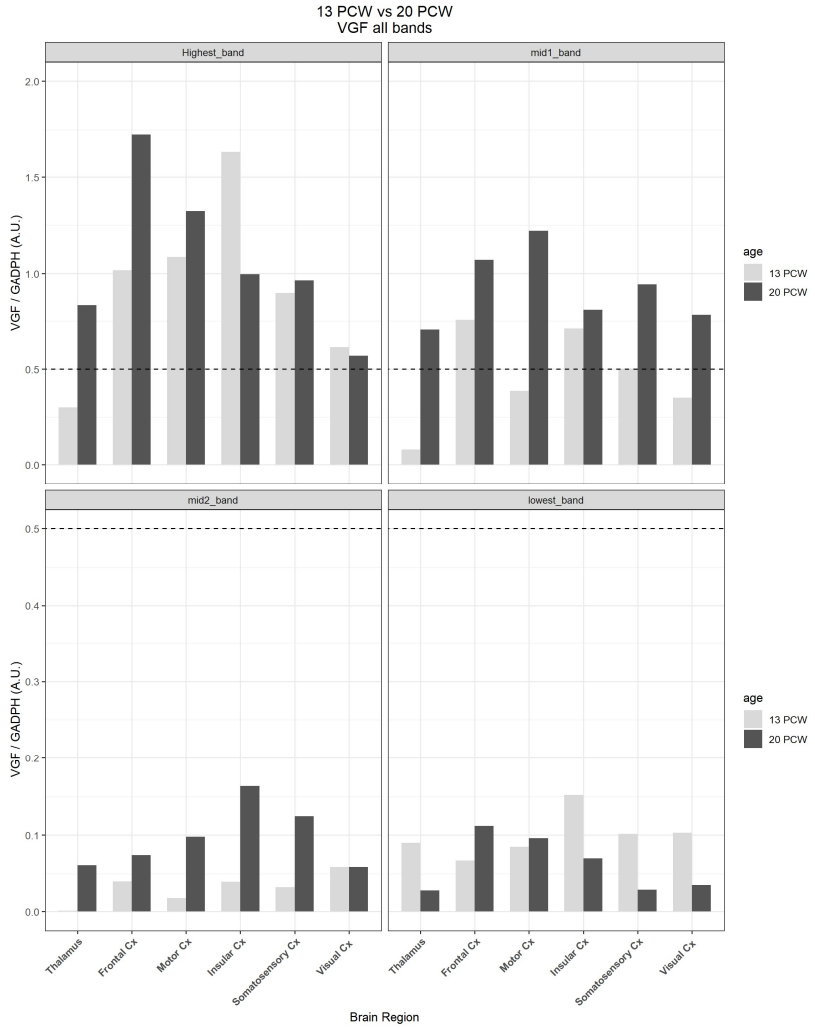

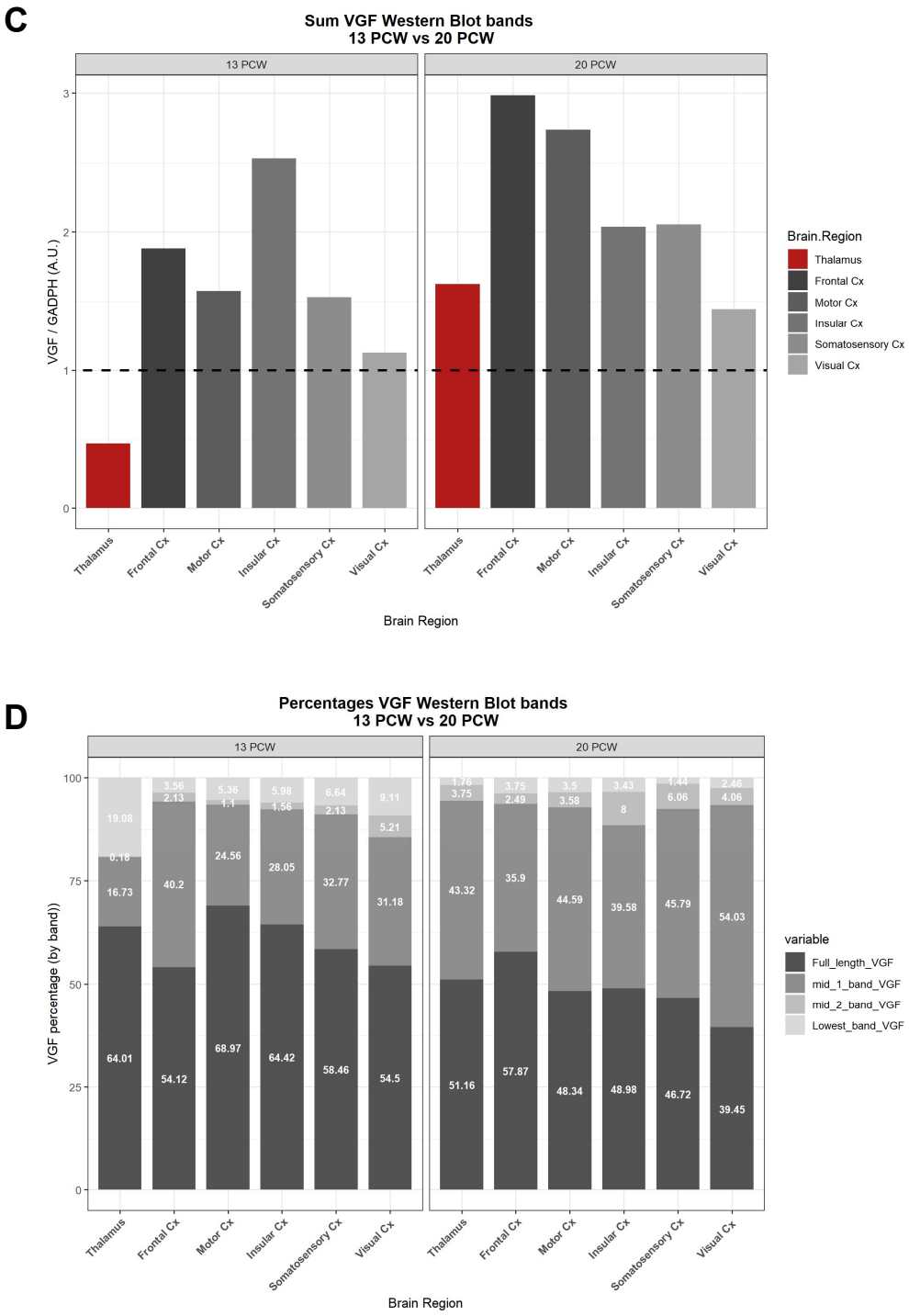

Figure S9: **Comparison of VGF protein levels between 13 and 20 PCW human brains**. (**A**) VGF densitometric measurement performed by including only the full size VGF, detected as a single band at 75 kDa. A dashed line intercepts the y-axis at 1 for comparison. Colour coded by donor age. (**B**) Densitometric measurement of each VGF proteoform performed individually. A dashed line intercepts the y-axis at 1 for comparison. Colour coded by donor age. (**C**) Comparison of VGF protein quantification in the 13 and 20 PCW human brains, performed by including all the 4 proteoforms detected by Western Blotting. Data are represented by absolute values of the normalized measurement. A dashed line intercepts the y-axis at 0.5 for comparison. Colour coded by brain region. (**D**) Relative percentage of each proteoform of VGF in the total amount of protein quantified in D. Color-coded by VGF Western Blot band (i.e. proteoform).

Figure S10 [Supplementary to Chapter 5]

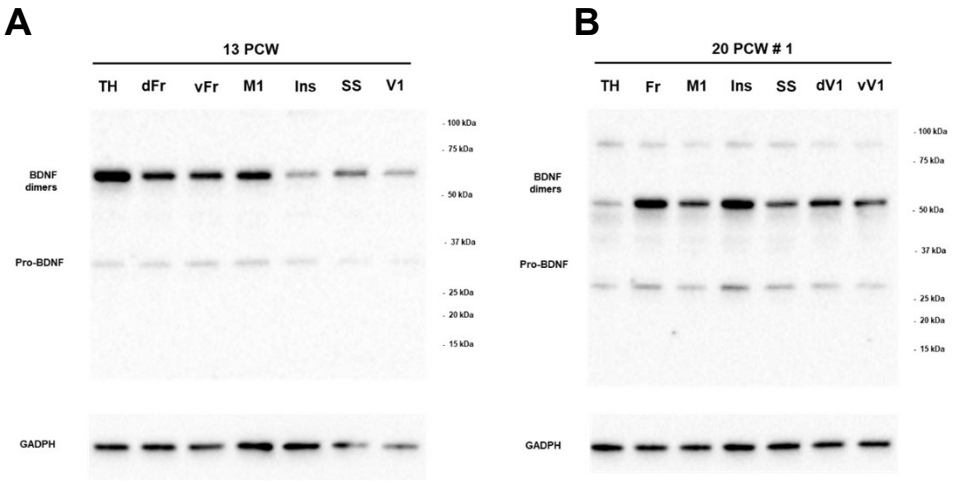

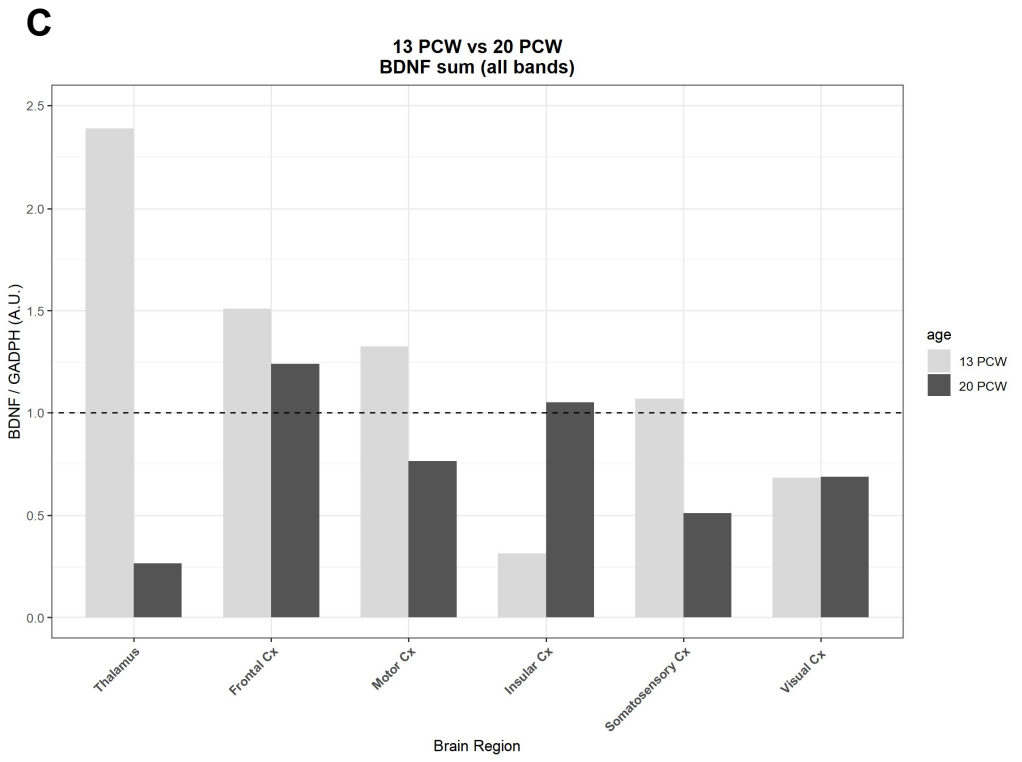

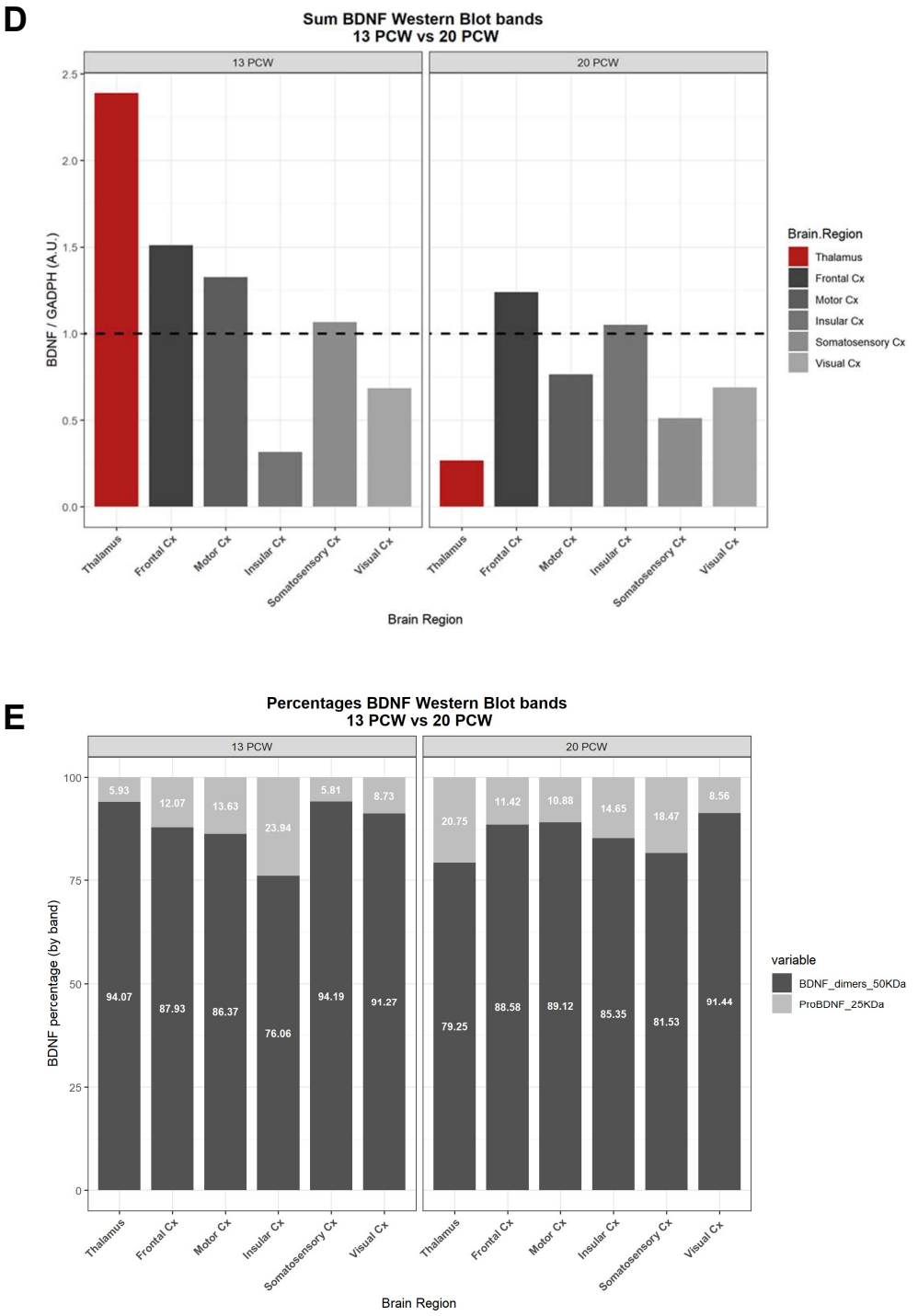

Figure S10: **Comparison of BDNF protein levels between 13 and 20 PCW human brains. (A-B)**. Representative blots of BDNF in the 13 and 20 PCW human brain. (**C**) Densitometric quantification of BDNF signal detected by Western Blot. BDNF is considered as the sum of the two forms detected in the membrane (i.e. Dimeric form 50kDa; Pro-BDNF 25kDa). A dashed line intercepts the y-axis at 1 for comparison. Colour coded by donor age. (**D**) Same quantification of C colour coded by brain region. (**E**) Relative percentage of the two BDNF forms detected in the total amount of protein quantified in C-D. Colour coded by protein band.

Figure S11 [Supplementary to Chapter 6]

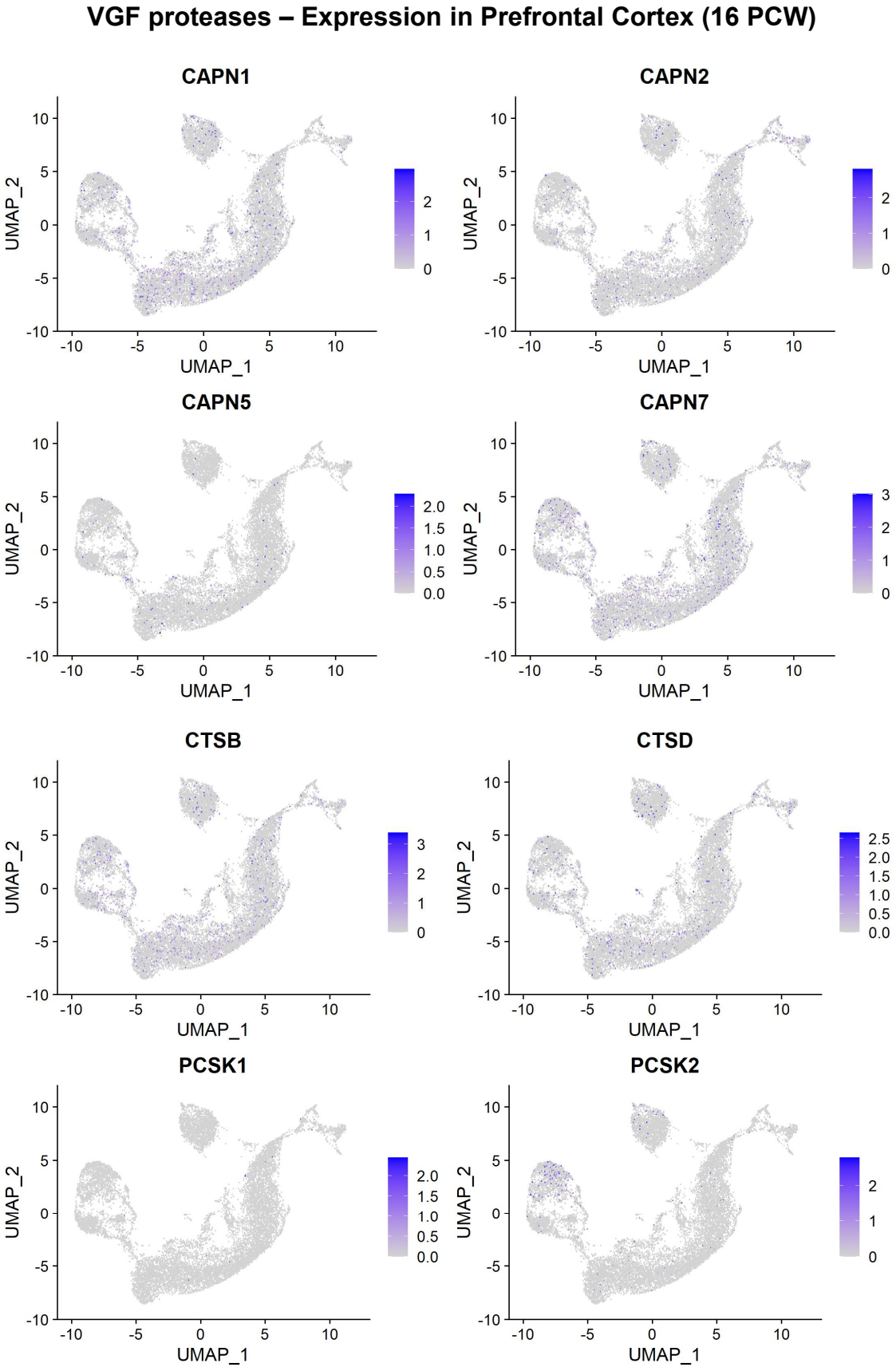

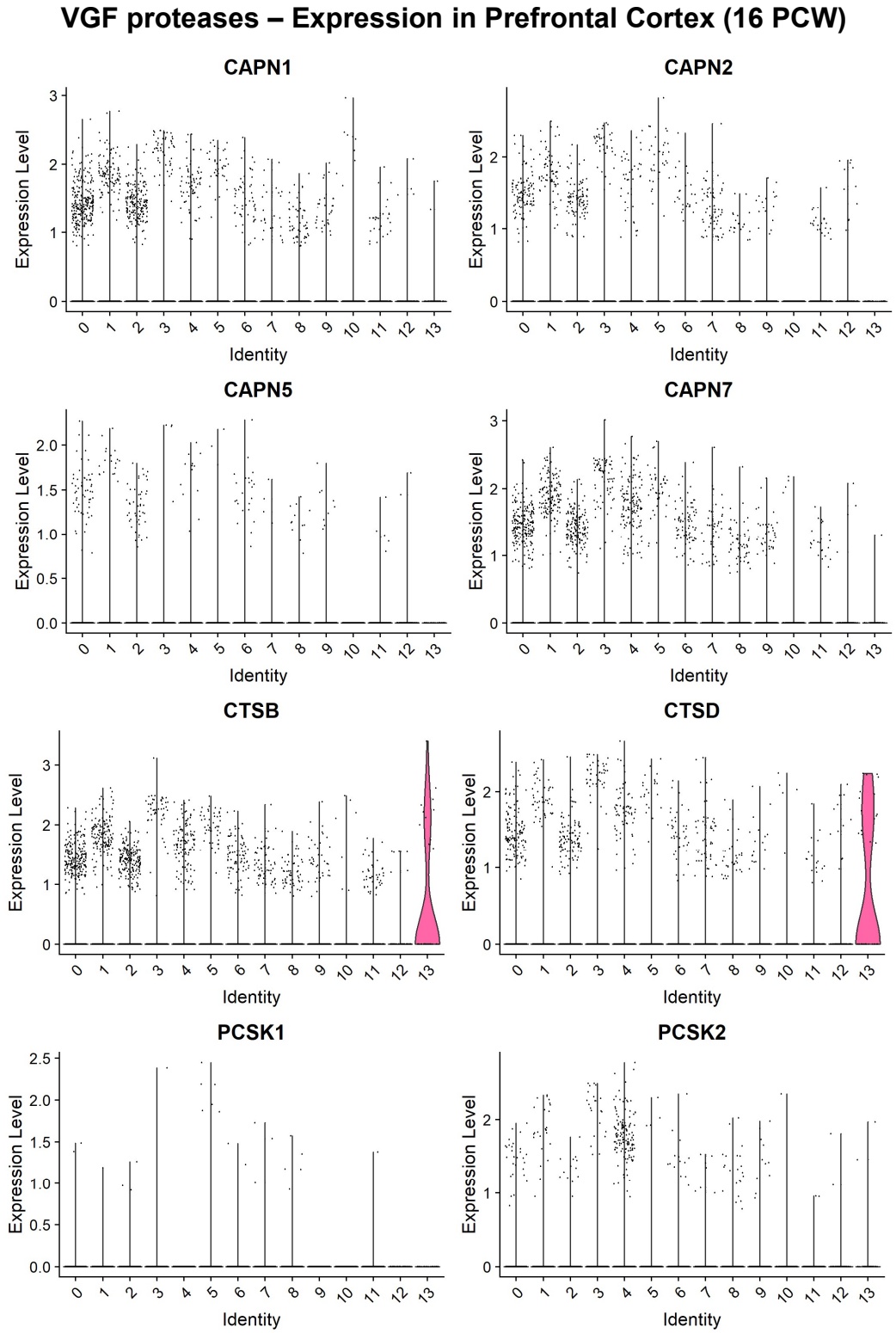

Figure S11: Single-cell transcriptomic profiling of the expression of VGF-cleaving proteases in the 16 PCW human prefrontal cortex.

(**A**) Scatter Plots of 15,060 cells where data are represented in the UMAP space. A gradient of violet is used to show expression, from lowest levels (light) to highest ones (dark). (**B**) Violin Plots with the cluster identity in the x-axis, and the expression levels of each marker in the y-axis. The colours are relative to the cluster identity (depicted in Chapter 4, Figure 4.12 A). VGF proteases selected in this study (Chapter 6, Section 6.2) are: Calpain (CAPN) 1, 2, 5 and 7; Cathepsin (CTS) B and D; pro-protein convertases (PCSK) 1 and 2.

Figure S12 [Supplementary to Chapter 6]

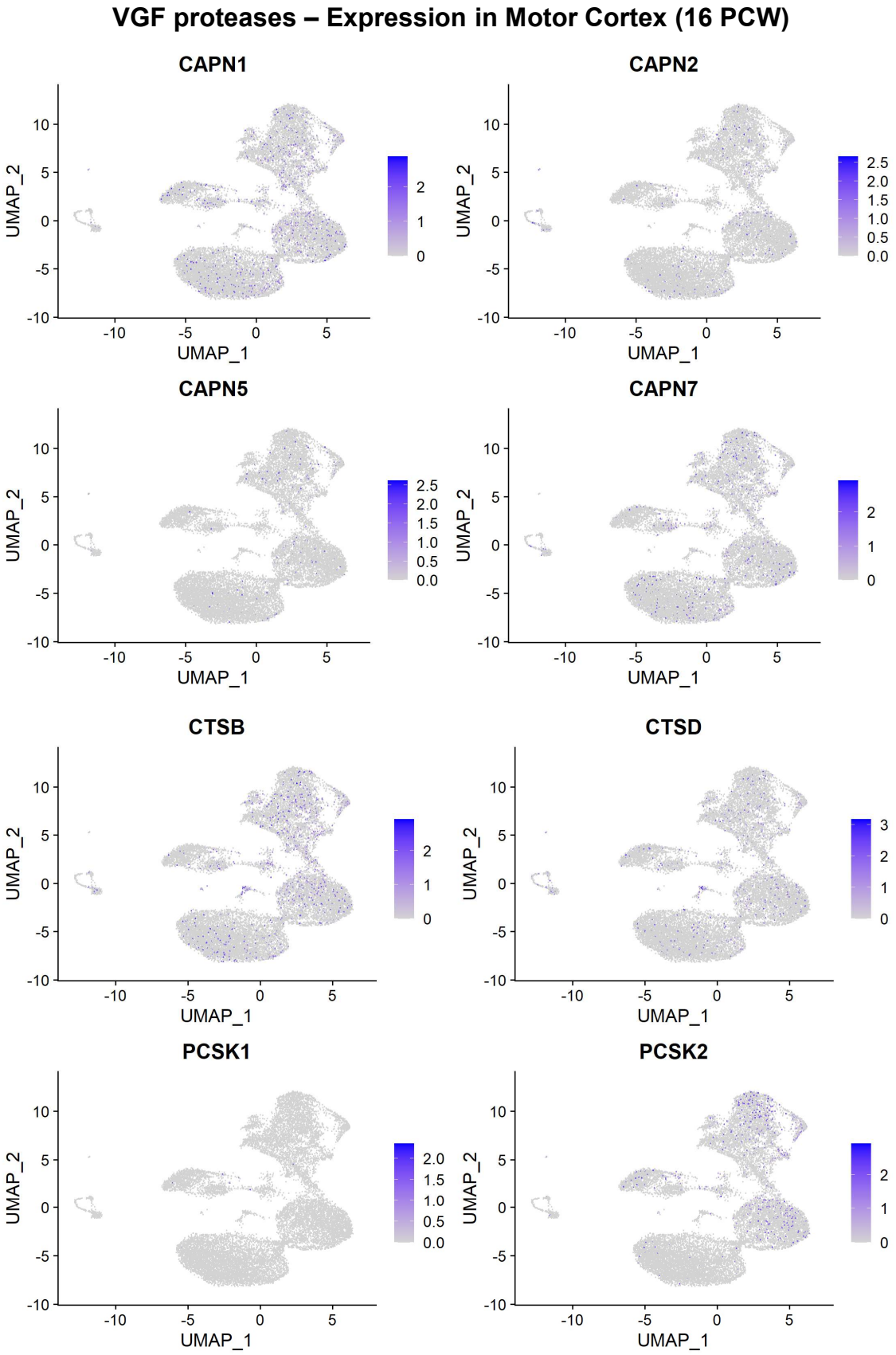

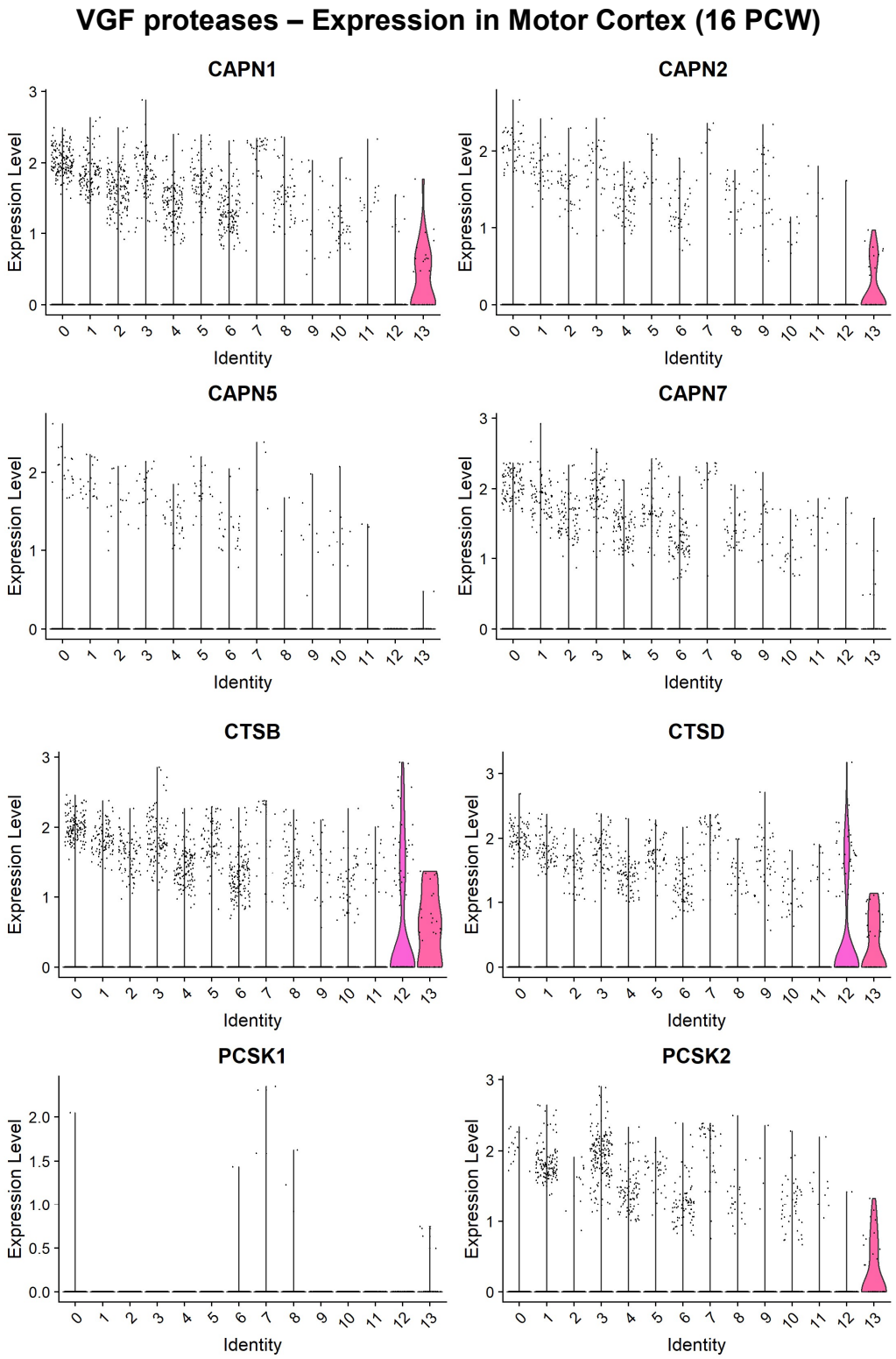

Figure S12: Single-cell transcriptomic profiling of the expression of VGF-cleaving proteases in the 16 PCW human motor cortex.

(**A**) Scatter Plots of 16,883 cells where data are represented in the UMAP space. A gradient of violet is used to show expression, from lowest levels (light) to highest ones (dark). (**B**) Violin Plots with the cluster identity in the x-axis, and the expression levels of each marker in the y-axis. The colours are relative to the cluster identity (depicted in Chapter 4, Figure 4.11 A). VGF proteases selected in this study (Chapter 6, Section 6.2) are: Calpain (CAPN) 1, 2, 5 and 7; Cathepsin (CTS) B and D; pro-protein convertases (PCSK) 1 and 2.

Figure S13 [Supplementary to Chapter 6]

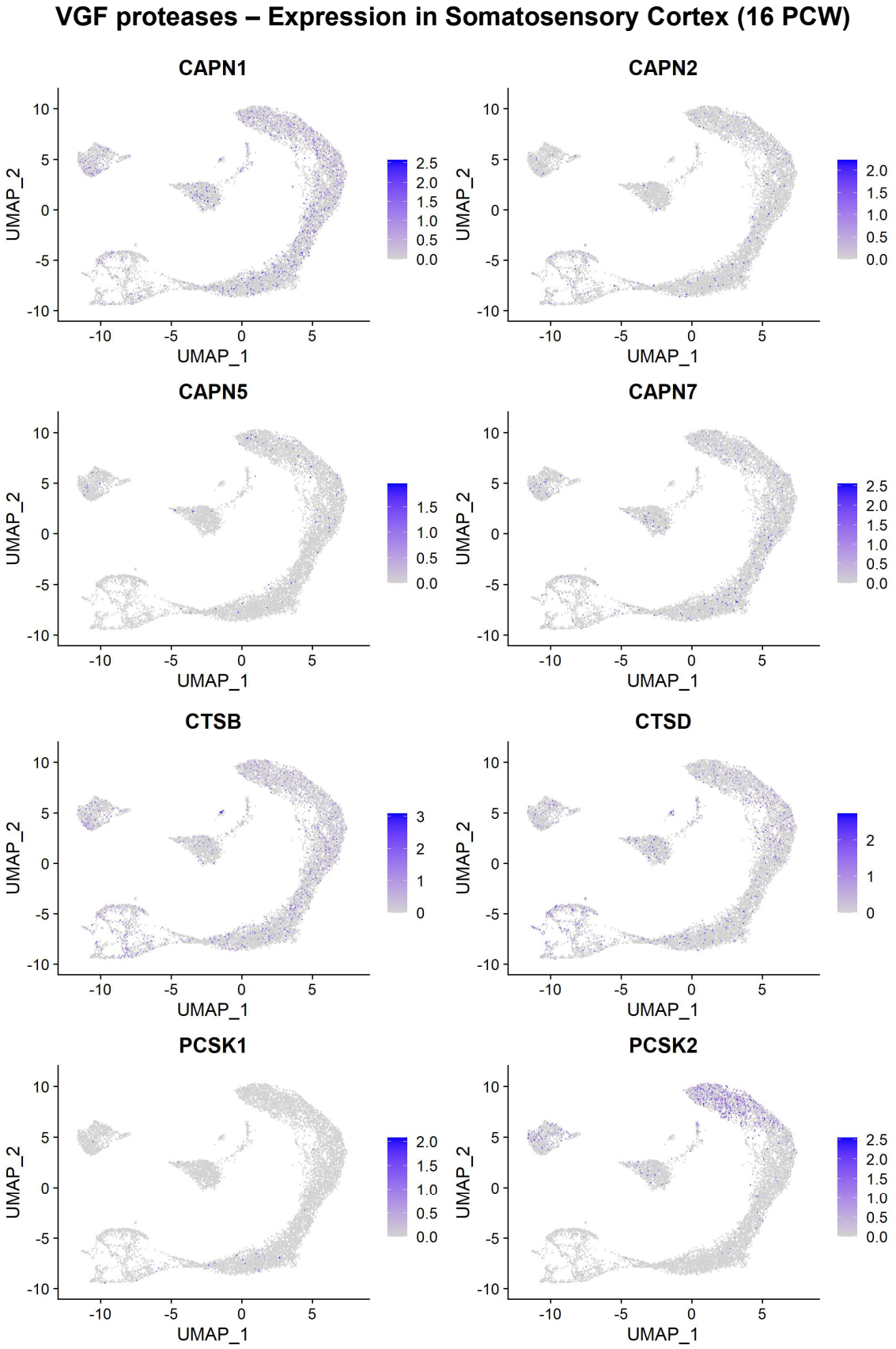

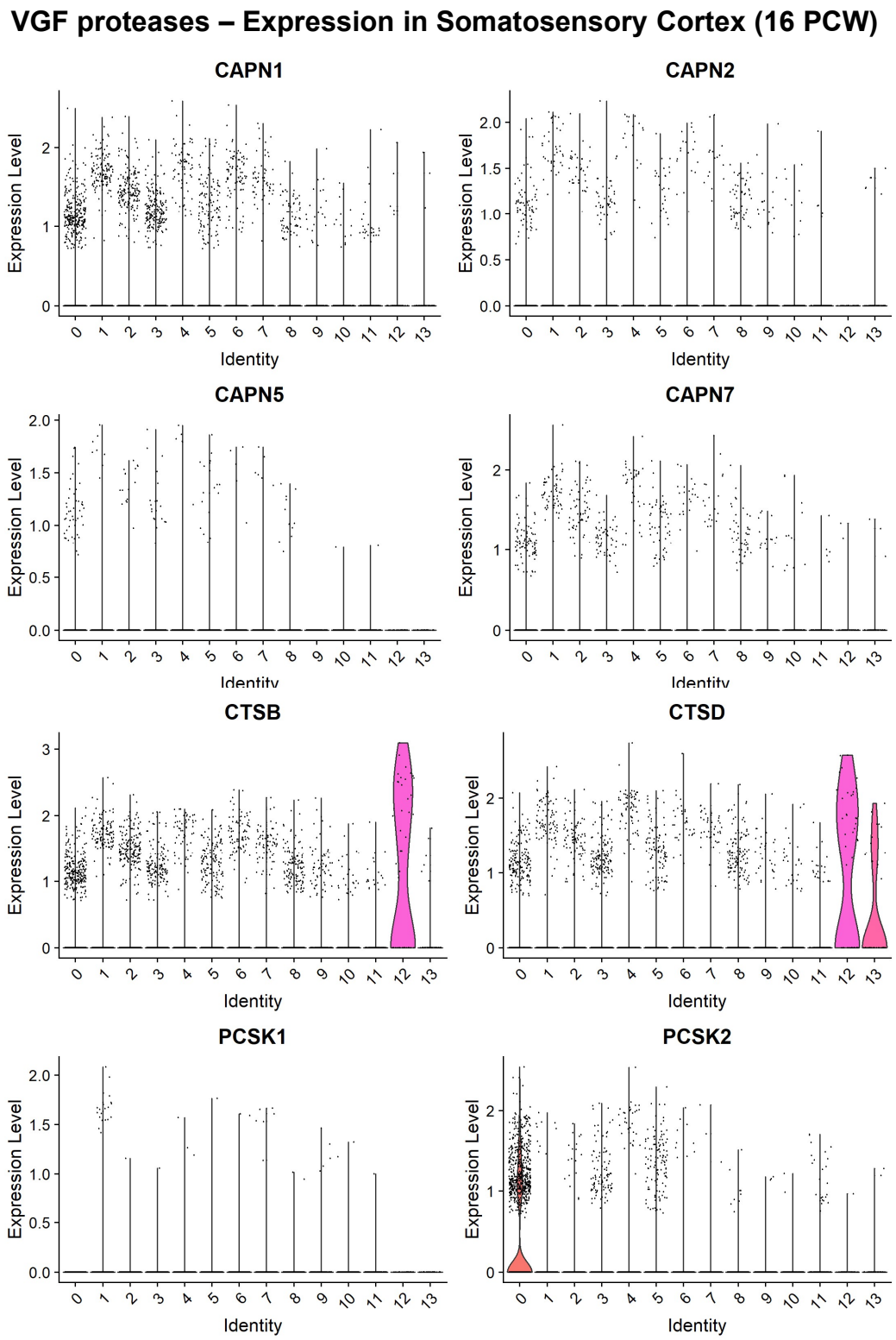

Figure S13: Single-cell transcriptomic profiling of the expression of VGF-cleaving proteases in the 16 PCW human somatosensory cortex.

(**A**) Scatter Plots of 10,915 cells where data are represented in the UMAP space. A gradient of violet is used to show expression, from lowest levels (light) to highest ones (dark). (**B**) Violin Plots with the cluster identity in the x-axis, and the expression levels of each marker in the y-axis. The colours are relative to the cluster identity (depicted in Chapter 4, Figure 4.9 A). VGF proteases selected in this study (Chapter 6, Section 6.2) are: Calpain (CAPN) 1, 2, 5 and 7; Cathepsin (CTS) B and D; pro-protein convertases (PCSK) 1 and 2.

Figure S14 [Supplementary to Chapter 6]

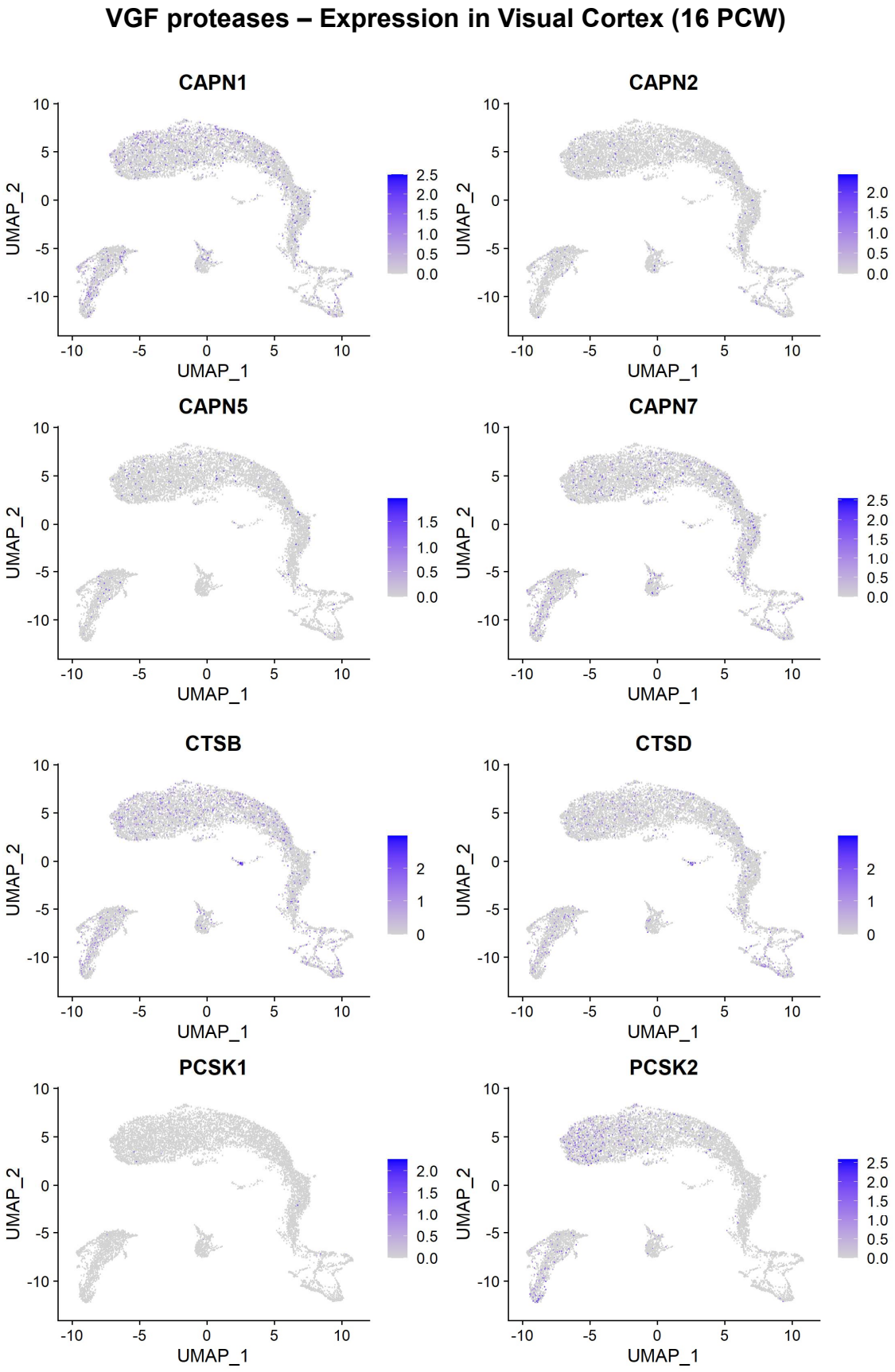

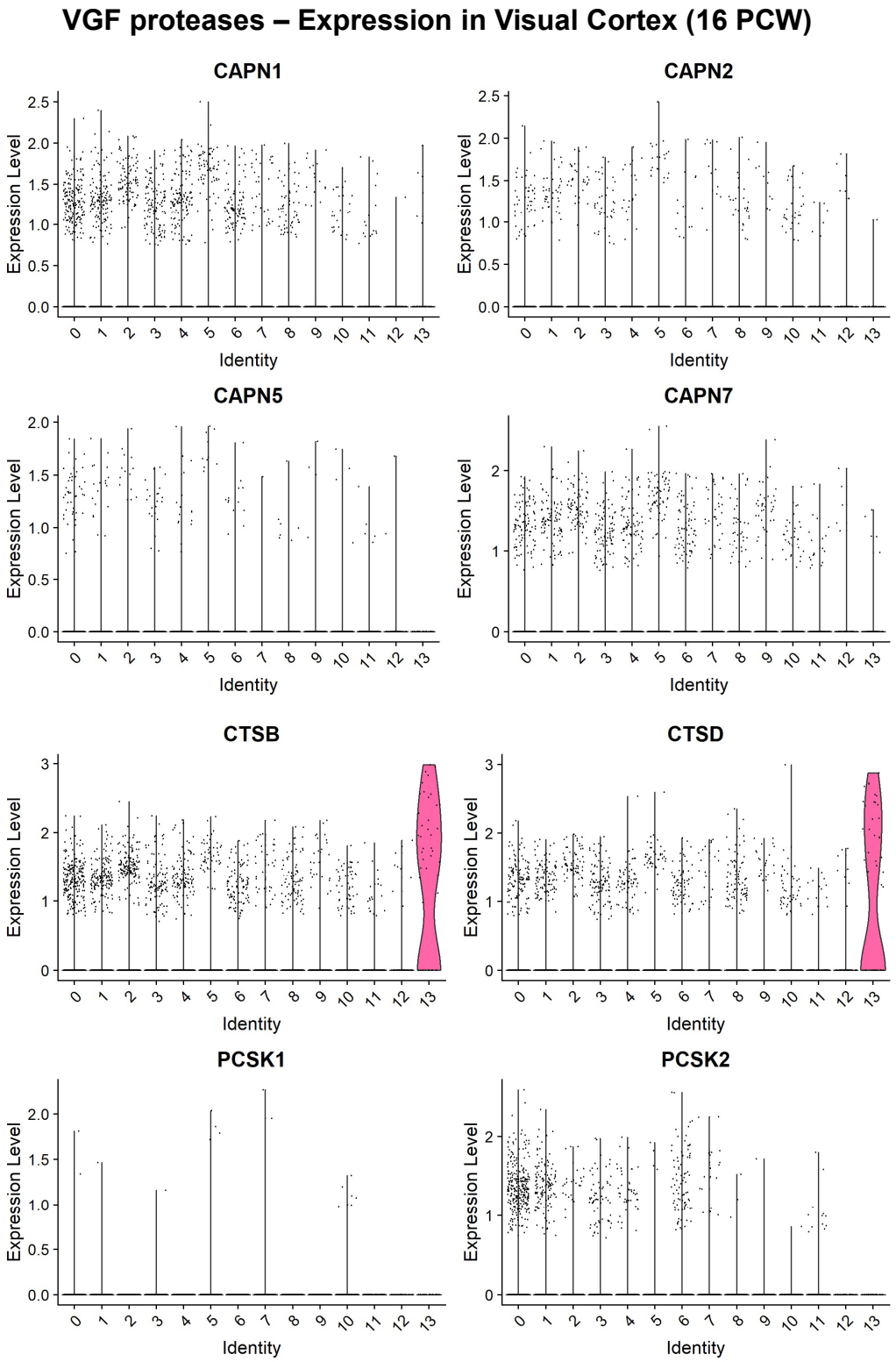

Figure S14: Single-cell transcriptomic profiling of the expression of VGF-cleaving proteases in the 16 PCW human visual cortex.

(**A**) Scatter Plots of 10,541 cells where data are represented in the UMAP space. A gradient of violet is used to show expression, from lowest levels (light) to highest ones (dark). (**B**) Violin Plots with the cluster identity in the x-axis, and the expression levels of each marker in the y-axis. The colours are relative to the cluster identity (depicted in Chapter 4, Figure 4.10 A). VGF proteases selected in this study (Chapter 6, Section 6.2) are: Calpain (CAPN) 1, 2, 5 and 7; Cathepsin (CTS) B and D; pro-protein convertases (PCSK) 1 and 2.

Figure S15 [Supplementary to Chapter 6]

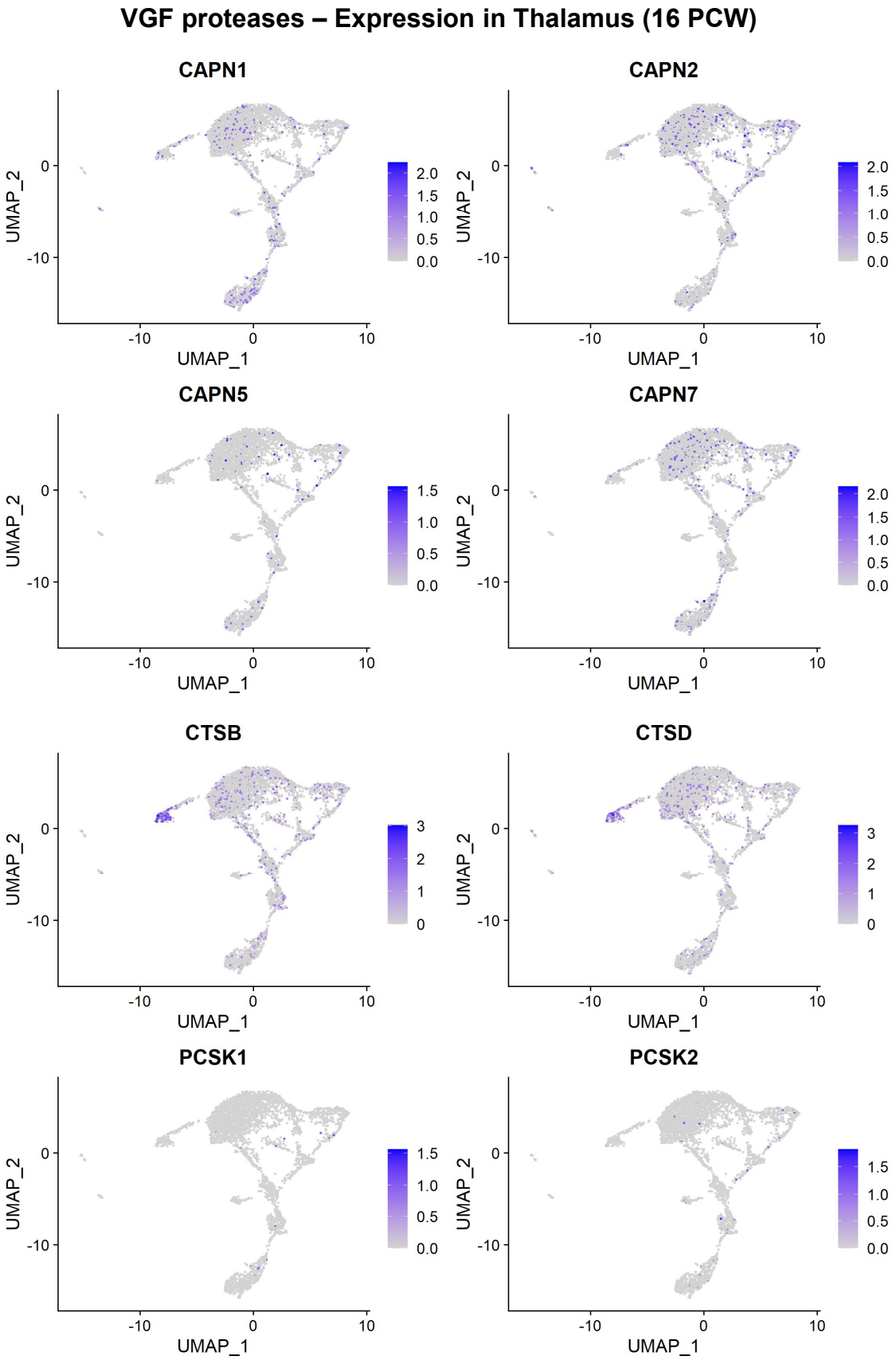

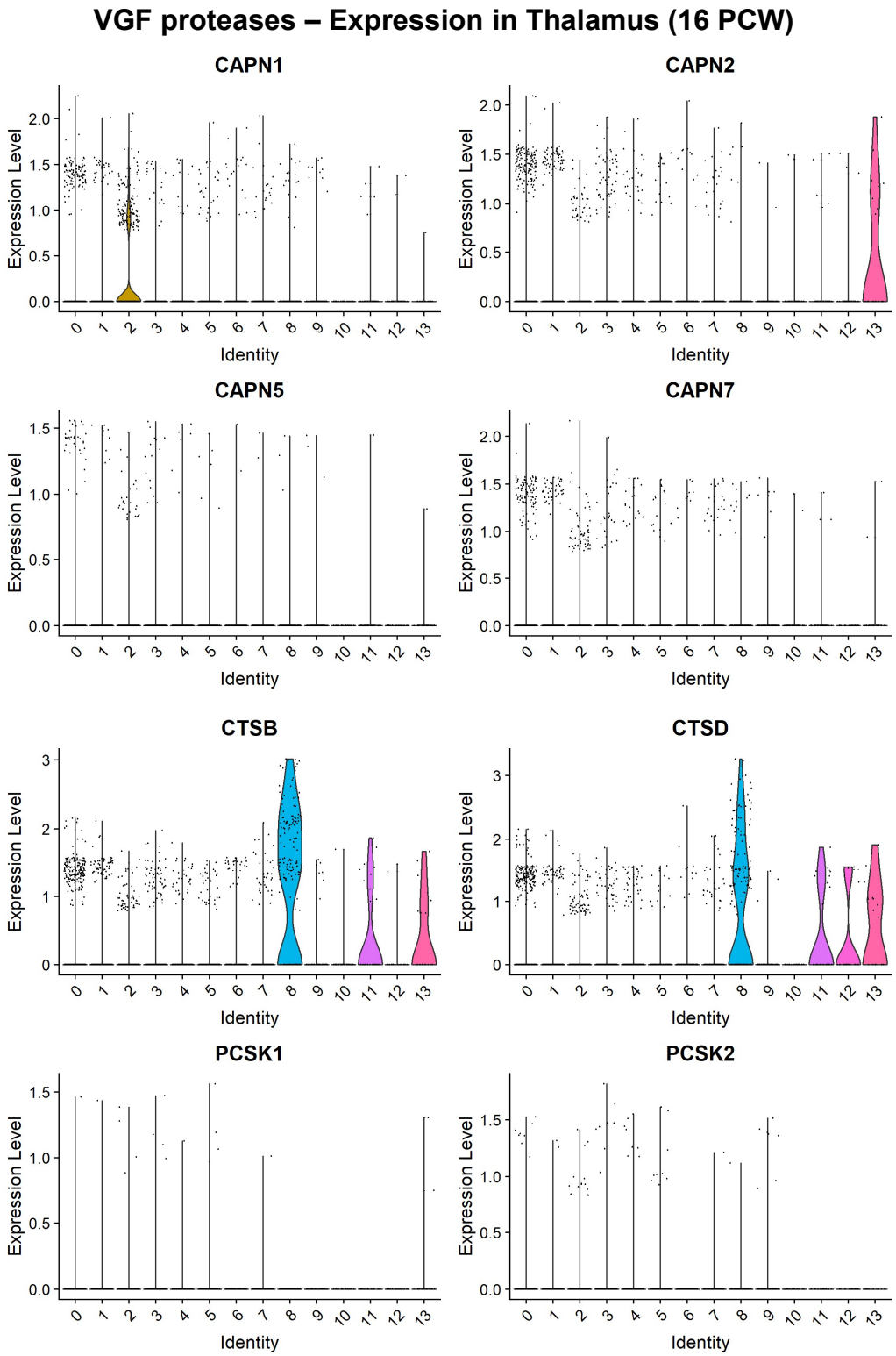

Figure S15: Single-cell transcriptomic profiling of the expression of VGF-cleaving proteases in the 16 PCW human thalamus.

(**A**) Scatter Plots of 4,076 cells where data are represented in the UMAP space. A gradient of violet is used to show expression, from lowest levels (light) to highest ones (dark). (**B**) Violin Plots with the cluster identity in the x-axis, and the expression levels of each marker in the y-axis. The colours are relative to the cluster identity (depicted in Chapter 4, Figure 4.7 A). VGF proteases selected in this study (Chapter 6, Section 6.2) are: Calpain (CAPN) 1, 2, 5 and 7; Cathepsin (CTS) B and D; pro-protein convertases (PCSK) 1 and 2.

Supplementary Table S1

Table S1: Number of significantly over-represented terms for each Gene Ontology category after GO Enrichment analysis of proteomics analysis of the 20 PCW human cortex

CATEGORY	#SIGNIFICANT TERMS (p-value < 0.001)	CATEGORY	#SIGNIFICANT TERMS (p-value < 0.001)
GO Molecular Function	159	TISSUES	144
GO Biological Process	1072	DISEASES	33
GO Cellular Component	244	COMPARTMENTS	218
Reactome Pathways	398	UniProt Keywords	90
KEGG Pathways	89	Pfam	14
WikiPathways	79	InterPro Domains	39

Significantly over-represented in the human fetal cortical dataset with a p-value <0.001. Data from the GO Enrichment analysis of the proteomic dataset obtained by a 2-hour long run of LC-MS/MS of the 20 PCW human cortex (from Chapter 5.3.1).